

**Palacký University**  
**Faculty of Science, Department of Organic Chemistry**



**Synthesis of Novel Potential Antituberculotics**  
**Syntéza Nových Potenciálních Antituberkulotik**  
**Doctoral thesis**

**Mgr. Veronika Šlachtová**

**Supervisor: RNDr. Lucie Brulíková, Ph.D.**

**Consultant: Dr. Yvan Six**

**Olomouc, 2021**

## Bibliographic entry

**Author:** Mgr. Veronika Šlachtová  
Faculty of Science, Palacký University  
Department of Organic Chemistry

**Title of the Thesis:** Synthesis of Novel Potential Antituberculotics

**Degree program:** Chemistry

**Field of Study:** Organic Chemistry

**Supervisor:** RNDr. Lucie Brulíková, Ph.D.

**Consultant:** Dr. Yvan Six

**Academic Year:** 2020/2021

**Number of pages:** 248 + 157 pages of appendices

**Keywords:** tuberculosis, mycobacterial virulence factors, mycobacterial ATP synthase, benzoxazoles, phenotypic screening, thiazolidinedione

**Declaration:**

I declare hereby, with my signature, that the abovementioned thesis is my original work. Moreover, I confirm that I have referenced in accordance with departmental requirements.

Olomouc, 28.06.2021

Mgr. Veronika Šlachtová

## Acknowledgements

Firstly, I would like to thank Dr. Lucie Brulíková for the opportunity to work in her group. I am grateful for her guidance, care and friendly working environment provided. I also appreciate her readiness to help me and the unique possibility of 2 research visits in France. Many thanks go to other members of the Brulikova group. It was a pleasure to work with all of you!

Secondly, I would like to thank Dr. Yvan Six for supervision on my research visits at École Polytechnique (FR) for 3 and 2 months, respectively. I admire his endless patience, support and concern for his students. It was a great honor and scientific experience to work in the Six group.

Among so many amazing people met on my PhD journey, I would like to emphasize Assoc. Prof. Jiří Pospíšil for his first-class help with my internship arrangement and Assoc. Prof. Milan Urban for TOP cooperation on as much as two reviews. Furthermore, I owe a big thank to KOCH analytic team for NMR and HRMS measurements. I would also like to express my gratitude for important financial support (IGA\_PrF\_2020\_012, JG\_2019\_002).

Finally, I want to thank my loving family. Indeed, their endless support was/is/ever will be invaluable for me.



## Abstract

My Ph.D. thesis is dedicated to the design and synthesis of novel potential antitubercular agents. The **Theoretical part** covers the current state of all the antitubercular problematic including molecular targets at *Mtb* or the host level and selected anti-TB drug discovery approaches. Those molecular targets and approaches also inspired the division of the thesis into three main sections: mycobacterial virulence factors inhibition, ATP synthase inhibition and phenotypic screening.

The first section of **Results and discussion** is devoted to the synthesis of mycobacterial virulence factors zinc metalloprotease 1 (Zmp1) and mycobacterial protein tyrosine phosphatase B (MptpB) inhibitors resulting in two generations of hydroxamate-based Zmp1 inhibitors and *N*-fused polycycles as potential MptpB inhibitors including the evaluation of their biological potential. The second section is focused on a synthetic methodology development toward aminobenzoxazoles as a preferable structural motive in novel potential squaramide-based mycobacterial ATP synthase inhibitors. The last section describes combinatorial approach toward thiazolidinedione-derived heterocyclic conjugates for phenotypic screening yielding two chemical libraries of thiazolidinedione-pyrimidines and thiazolidinedione-triazoles designed, synthesized and biologically tested to reveal their antitubercular activity.

## Abstrakt

Má disertační práce je zasvěcena návrhu a syntéze nových potenciálních antituberkulotik za účelem studia jejich biologických vlastností. Teoretická část předložené práce pokrývá současný stav problematiky tuberkulózy a její terapie včetně molekulárních cílů na úrovni *Mtb* nebo hostitele a vybraných přístupů k vývoji antituberkulotik. Tyto molekulární cíle a přístupy rovněž inspirovaly rozdělení celé disertační práce na tři hlavní sekce: inhibice mykobakteriálních virulentních faktorů, inhibice mykobakteriální ATP syntázy a fenotypové testování.

První část **Výsledků a diskuse** je zasvěcena syntéze inhibitorů mykobakteriálních virulentních faktorů zinečnaté metaloproteázy 1 (Zmp1) a mykobakteriální proteinové tyrosin fosfatázy B (MptpB), která vyústila do dvou generací Zmp1 inhibitorů odvozených od kyseliny hydroxamové a *N*-fúzovaných polycyklických potenciálních inhibitorů MptpB včetně hodnocení jejich biologických vlastností. Druhá část se soustředí na vývoj metody syntézy aminobenzoxazolů jako klíčového strukturního motivu nových potenciálních squaramidových inhibitorů mykobakteriální ATP syntázy. Poslední sekce popisuje kombinatoriální přístup k heterocyklickým konjugátům thiazolidindionu pro fenotypové testování včetně výsledného designu a syntézy dvou chemických knihoven thiazolidindion-pyrimidinů a thiazolidindion-triazolů, které byly podrobeny biologickému testování za účelem studia jejich antituberkulotické aktivity.

## List of abbreviations

Ac	acetate
aq	aqueous
AIDS	acquired immunodeficiency syndrome
Akt	protein kinase B
All	allyl
Ar	aryl
ATP	adenosine triphosphate
BIOS	biology-oriented synthesis
Bn	benzyl
Boc	<i>tert</i> -butyloxycarbonyl
COVID-19	coronavirus disease of 2019
DBU	1,8-diazabicyclo[5.4.0]undec-7-ene
DCM	dichloromethane
DHAP	dihydroxyacetone phosphate
DIAD	diisopropyl azodicarboxylate
DIC	<i>N,N'</i> -diisopropylcarbodiimide
DIPEA	<i>N,N</i> -diisopropylethylamine
DMAP	(4-dimethylamino)pyridine
DMF	<i>N,N</i> -dimethylformamide
DMSO	dimethylsulfoxide
DNA	deoxyribonucleic acid
ECE-1	endothelin-converting enzyme 1
EDC	1-ethyl-3-(3-dimethylaminopropyl)carbodiimide
EMA	European Medicines Agency
equiv	equivalent(s)
ESI	electrospray ionization
FDA	Food and Drug Administration
Fmoc	9-fluorenylmethoxycarbonyl
HDT	host-directed therapy
Hex	hexane
HIV	human immunodeficiency virus

HMBA	hydroxy methylene benzoic acid
HOBt	1-hydroxybenzotriazole
HMDS	bis(trimethylsilyl)amine
HRMS	high-resolution mass spectrometry
IC <sub>50</sub>	half maximal inhibitory concentration
IL	interleukin
KOH	potassium hydroxide
LC-MS	liquid chromatography-mass spectrometry
LORA	low oxygen recovery assay
LTBI	latent tuberculosis infection
MABA	microplate alamar Blue assay
MAPK	mitogen-activated protein kinase
MALDI-TOF MS	matrix-assisted laser desorption/ionization-time of flight mass spectrometry
Me	methyl
MIC	minimum inhibitory concentration
MDR	multi-drug resistant
<i>Mtb</i>	<i>Mycobacterium tuberculosis</i>
MptpB	mycobacterial protein tyrosine phosphatase B
MW	microwave
NCTS	<i>N</i> -cyano- <i>N</i> -phenyl- <i>p</i> -toluenesulfonamide
NEP	neprilysin
NF	nuclear factor
NMM	<i>N</i> -methylmorpholine
NMR	nuclear magnetic resonance
NRL	NOD-like receptors
OMTS	(oxylamino-methylene)-thiophene sulfonamide
on	overnight
PET	petroleum ether
Ph	phenyl
PTP	protein tyrosine phosphatase
R <sub>f</sub>	retention factor
RNA	ribonucleic acid
rt	room temperature

SAR	structure-activity relationship
SFC	supercritical fluid chromatography
TB	tuberculosis
TFA	trifluoroacetic acid
Tf	trifluoromethanesulfonyl
THF	tetrahydrofuran
TLC	thin layer chromatography
Ts	<i>p</i> -toluenesulfonyl
TZD	thiazolidinedione
WHO	World Health Organization
XDR	extensively drug-resistant
ZBG	zinc-binding group
Zmp1	zinc metalloprotease 1

## Foreword

The main objective of the thesis is the synthesis of novel compounds with potential antitubercular activity. The design of particular compounds then reflects molecular targets at *Mtb* or the host level and selected drug discovery approaches. The overall thesis is divided in accordance with those molecular targets and approaches into three main sections dedicated to mycobacterial virulence factors inhibition, ATP synthase inhibition and phenotypic screening. Such a division corresponds with the three main approaches taken toward anti-TB drug design. All the three main sections are further divided in accordance with included research projects. In this context, the first section is focused on inhibition of two mycobacterial virulence factors zinc metalloprotease 1 (Zmp1) and mycobacterial protein tyrosine phosphatase B (MptpB). The following part is dedicated to ATP synthase inhibition including 2-aminobenzoxazoles synthesis for novel potential squaramide-aminobenzoxazole ATP synthase inhibitors. Finally, the last section includes phenotypic screening of thiazolidinedione (TZD)-pyrimidines and TZD-triazoles. Covering a broad spectrum of organic and medicinal chemistry issues, the **Theoretical part** is meant to introduce background on particular projects rather than provide detailed review upon such diverse studied areas.

The following parts: **Results and discussion** and **Experimental part** are divided into chapters, which content correspond to the described projects/published papers. Each chapter serves as a comprehensive overview of the related project, including a short introduction into studied compounds, an actual discussion about unsuccessful/unpublished results, and synthetic pathways and final compounds achieved and characterized. Considering the characterization of all the intermediates, there are presented analytical data on all the new compounds not yet reported in the literature. All the mentioned publications are included in the **Appendix** section. **Supporting information** is attached as an electronic file containing relevant spectral data.

---

# Table of content

1	Aims of the thesis .....	1
1.1	Synthesis of mycobacterial virulence factors inhibitors .....	1
1.2	Synthesis of mycobacterial ATP synthase inhibitors .....	2
1.3	Synthesis of thiazolidinedione hybrids for phenotypic screening .....	2
2	Introduction .....	4
3	Theoretical part .....	8
3.1	Hydroxamate-based Zmp1 inhibitors .....	8
3.1.1	Functional characterization of mycobacterial Zmp1 .....	8
3.1.2	State of the art for Zmp1 inhibitors development .....	10
3.1.3	Synthesis of current Zmp1 inhibitors .....	11
3.2	Polycyclic MptpB inhibitors <i>via gem</i> -dihaloaminocyclopropanes .....	12
3.2.1	Functional characterization of mycobacterial protein tyrosine phosphatases .....	12
3.2.2	State of the art for fused polycyclic MptpB inhibitors development .....	14
3.2.3	Synthetic approaches toward izidines .....	15
3.2.4	Reactivity of <i>gem</i> -dihaloaminocyclopropanes toward izidines .....	17
3.3	2-Aminobenzoxazoles preparation for mycobacterial ATP synthase inhibitors .....	19
3.3.1	Functional characterization of mycobacterial ATP synthase .....	19
3.3.2	State of the art for selected ATP synthase inhibitors development .....	21
3.4	Phenotypic screening of thiazolidinedione-based conjugates .....	23
3.4.1	Phenotypic screening in antitubercular research .....	23
3.4.2	Thiazolidinedione as privileged anti-TB structure .....	24
3.4.3	Antitubercular potential of pyrimidines and triazoles .....	25

4	Results and Discussion.....	27
4.1	Hydroxamate-based mycobacterial Zmp1 inhibitors.....	27
4.1.1	Design and synthesis of TZD-hydroxamates.....	27
4.1.2	Biological activity of TZD-hydroxamates.....	30
4.1.3	Design and synthesis of pyrrole/indole-hydroxamates.....	31
4.1.4	Biological activity of pyrrole/indole-hydroxamates.....	34
4.1.5	Conclusive remark 1.....	35
4.2	Polycyclic MptpB inhibitors <i>via gem</i> -dihaloaminocyclopropanes.....	35
4.2.1	Proposed pathway toward <i>N</i> -fused polycycles.....	35
4.2.2	Synthesis of starting <i>gem</i> -dihalocyclopropane amides.....	36
4.2.3	Deprotection and ring expansion of <i>gem</i> -dihalocyclopropane amides.....	40
4.2.4	Acid-mediated cyclization to final polycycles.....	48
4.2.5	Conclusive remark 2.....	55
4.3	2-Aminobenzoxazoles preparation for mycobacterial ATP synthase inhibitors.....	55
4.3.1	Design of squaramide-based ATP synthase inhibitors and proposed pathway toward 2-aminobenzoxazoles.....	55
4.3.2	NCTS-mediated cyclization to 2-aminobenzoxazoles.....	57
4.3.3	The Smiles rearrangement approach to <i>N</i> -substituted 2-aminobenzoxazoles.....	60
4.3.4	Conclusive remark 3.....	66
4.4	Thiazolidinedione-based conjugates for phenotypic screening.....	67
4.4.1	Design and solid phase synthesis of the TZD-pyrimidines.....	67
4.4.2	Biological activity of TZD-pyrimidines.....	70
4.4.3	Design and combinatorial synthesis of TZD-triazoles.....	71
4.4.4	Conclusive remark 4.....	74
5	General conclusions and outlook.....	76
6	Experimental Part.....	78



6.1	General information .....	78
6.2	Synthesis of TZD-hydroxamates .....	80
6.3	Synthesis of indole/pyrrole-hydroxamates .....	89
6.4	Synthesis of starting <i>gem</i> -dihalocyclopropane amides.....	107
6.5	Synthesis of dihydroazepines .....	115
6.6	Synthesis of dihydropyridines.....	119
6.7	Cyclization to <i>N</i> -fused polycycles .....	121
6.8	NCTS-mediated cyclization to 2-aminobenzoxazoles.....	128
6.9	The Smiles rearrangement approach to <i>N</i> -substituted 2-aminobenzoxazoles	131
6.10	Synthesis of TZD-pyrimidines .....	140
6.11	Synthesis of TZD-triazoles.....	151
7	References .....	159
8	Appendix .....	165
8.1	List of Publications .....	165

---

# 1 Aims of the thesis

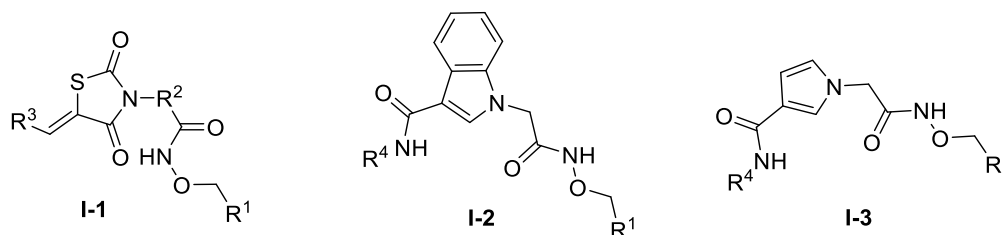
The ultimate goal of the thesis was the synthesis of novel chemical entities with potential antitubercular activity. The design of particular compounds then reflected molecular targets at *Mtb* or the host level and selected drug discovery approaches. Consequently, the whole thesis is divided in accordance with all the aforementioned molecular targets and approaches into the following sections:

## 1.1 Synthesis of mycobacterial virulence factors inhibitors

Antivirulence as an alternative antitubercular strategy inspired us to the synthesis of inhibitors of two mycobacterial virulence factors: zinc metalloprotease 1 and protein tyrosine phosphatase B resulting in two corresponding approaches taken:

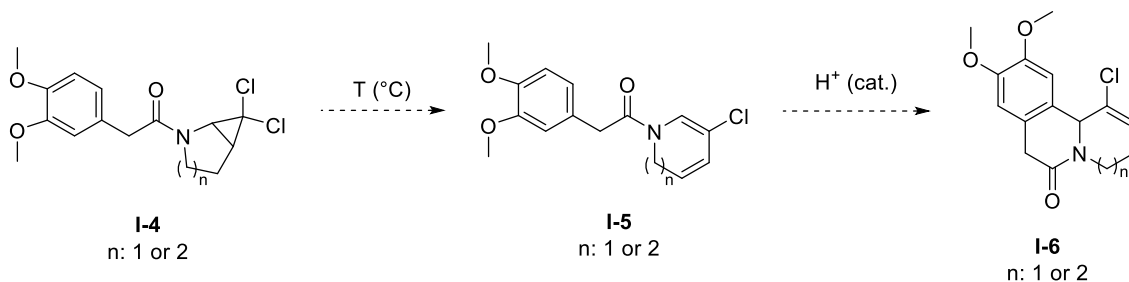
### 1.1.1 Design and synthesis of two generations of hydroxamate-based mycobacterial Zmp1 inhibitors

The initial effort was taken to access various heterocyclic compounds **I-1**, **I-2**, and **I-3** with hydroxamate zinc-binding group (ZBG) and test their Zmp1 inhibitory potential.



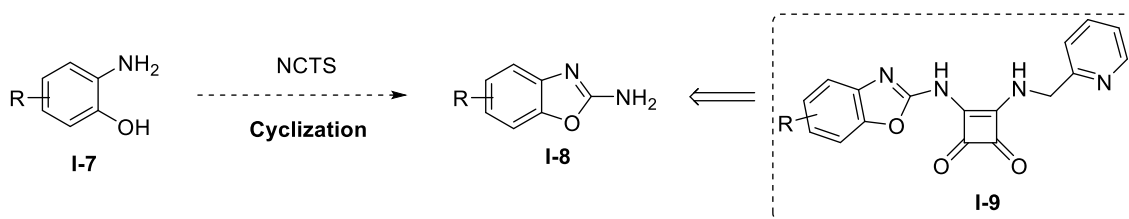
### 1.1.2 Study of ring expansion/cyclization tandem process to access MptpB inhibitors

The subsequent interest was focused on *N*-fused polycycles **I-6** as novel potential MptpB inhibitors. An expansion/cyclization tandem synthetic pathway was proposed and developed to follow the objective, taking advantage of *gem*-dihaloaminocyclopropanes **I-4**.



## 1.2 Synthesis of mycobacterial ATP synthase inhibitors

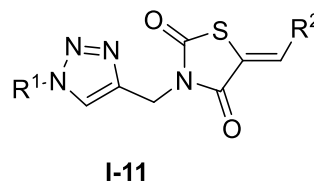
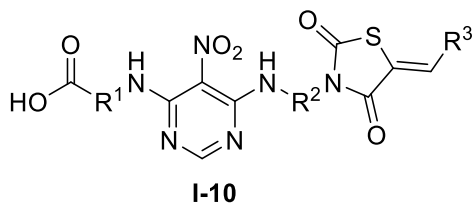
Mycobacterial ATP synthase is a druggable molecular target within *Mtb* electron transport chain involved in energy production *via* oxidative phosphorylation. Based on the biological relevance of squaramide-based inhibitors, we made a particular effort on squaramide derivatization. To enable the synthesis of squaramide-benzoxazoles **I-9** as mycobacterial ATP synthase inhibitors, a straightforward way to aminobenzoxazoles as the building blocks **I-8** was required. To fulfill such a requirement, we decided to provide a feasible approach toward 2-aminobenzoxazoles and their *N*-substituted analogues. To access 2-aminobenzoxazoles efficiently, firstly, we studied *N*-cyano-*N*-phenyl-*p*-toluenesulfonamide (NCTS)-mediated cyclization of various *o*-aminophenols **I-7**. Secondly, the Smiles rearrangement was utilized for the desired functionalization of heteroaromatic rings leading to diverse *N*-substituted 2-aminobenzoxazoles.



## 1.3 Synthesis of thiazolidinedione hybrids for phenotypic screening

The combination of two pharmacophores was envisioned as a well-established approach to novel more potent anti-TB compounds. From a synthetic perspective, the combinatorial approach is a valuable technique to produce large chemical libraries from abundant and economic building blocks with minimal synthetic operations in a time and resource-

effective manner. Finally, phenotypic screening of such diverse chemical libraries can result in the identification of novel chemical entities with remarkable anti-TB potential. Herein, the pharmacologically relevant thiazolidinedione (TZD) core inspired us to design and synthesize two chemical libraries comprising TZD-pyrimidine and TZD-triazole hybrids **I-10** and **I-11** for phenotypic screening.



---

## 2 Introduction

Tuberculosis is a communicable disease caused mainly by the bacillus *Mycobacterium tuberculosis*. In 2019, WHO reported 10 million new TB cases and about 1.4 million TB deaths.<sup>1</sup> With approximately a quarter of the world's population infected by *M. tuberculosis*, TB remains among the top 10 lethal diseases worldwide.<sup>1</sup> Moreover, such an epidemic is exacerbated by the current HIV/AIDS and COVID-19 pandemic as well as ever-increasing drug-resistant TB occurrence.<sup>2</sup> On a general basis, drug resistance development is induced by long-term exposure to antibiotics in low enough concentrations. The leading causes of drug resistance on the molecular level are mutations in genes coding the drug target or drug-activating enzymes.<sup>3</sup> The resulting resistant bacterial strains currently represent a severe public health problem. Especially multidrug resistant (MDR) and extensively resistant (XDR) TB is a notable threat.<sup>4</sup> To define *Mtb* resistance, MDR-TB is resistant to the two most potent anti-TB agents rifampicin and isoniazid. XDR-TB is MDR-TB with additional resistance to a fluoroquinolone and an injectable agent. DR-TB treatment remains relatively limited and usually requires multiple drugs and thus suffers from a compromised success rate. Such drugs are typically more expensive, toxic and less efficient than those for drug-susceptible TB.<sup>1,5</sup> Furthermore, 1.7 billion people are estimated to have latent TB infection (LTBI). LTBI is defined as the persistent immune response to stimulation by *Mtb* antigens without any clinical manifestation. Considering an extreme reactivation risk, LTBI-affected people possess a vast reservoir for new, active TB cases.<sup>6</sup> Therefore, the inadequate control over TB disease still represents a severe public health problem and research on new anti-TB compounds with a novel mechanism of action.

Current anti-TB treatment is based on WHO classification of anti-TB agents into 5 groups.<sup>7</sup> The first group includes isoniazid **II-1**, pyrazinamide **II-2**, rifampicin **II-3** and ethambutol **II-4** (Figure 1) interfering with fatty acid production, intracellular pH, RNA synthesis and cell wall construction, respectively. These agents are the most effective essential components of any short-course (usually 6 months) therapeutic regimen to treat susceptible TB. Short-course therapeutic regimen includes 2 months of isoniazid,

rifampicin, pyrazinamide and ethambutol therapy followed by additional 4 months of isoniazid and rifampicin treatment.<sup>8</sup>

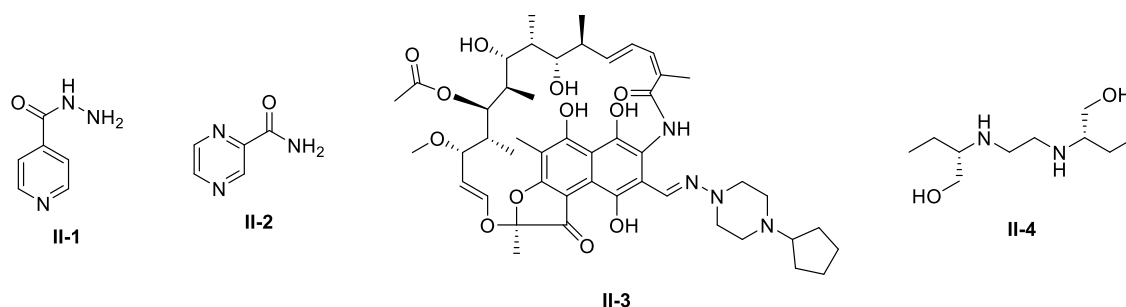


**Figure 1** First group of anti-TB agents.

On the other hand, the remaining A-D groups of anti-TB agents are only used to treat DR TB together with first-line antitubercular drugs in combined drug regimens (Table 1). Treatment of DR TB is more complicated, involves at least five anti-TB agents used for 8 months of intensive therapy and accomplished by one-year course. Ideally, it should be based on pyrazinamide, one anti-TB agent from each A and B group and two ones from C group. Unfortunately, these anti-TB agents are clinically much less effective and provoke severe side reactions more frequently. For this reason, they should be used under the supervision of an experienced doctor. To summarize their mechanism of action, DNA replication, RNA translation (protein synthesis), cell-wall biosynthesis and/or maintenance, interference with iron acquisition, respectively are included.<sup>8</sup> Treatment of DR TB is more complicated, involves at least five anti-TB agents and its overall duration is up to 20 months.

**Table 1** A-D Groups of anti-TB agents for DR TB treatment

Group	Anti-TB agents
A: Fluoroquinolones	Levofloxacin
	Moxifloxacin
	Gatifloxacin
B: Injectable drugs	Amikacin
	Capreomycin
	Kanamycin
C: Other second-line anti-TB agents	Ethionamide/Prothionamide
	Cycloserine/Terizidone

	Linezolid
	Clofazimine
D: Additional anti-TB agents	Bedaquiline
	Delamanid
	<i>p</i> -Aminosalicylic acid
	Imipenem-cilastin
	Meropenem
	Amoxicillin-clavulonate

Within recent years, several novel antitubercular compounds were discovered. Three significant drugs represent these anti-TB compounds, namely bedaquiline **II-5**, delamanid **II-6** and pretomanid **II-7** (Figure 2). Regarding their mechanism of action, ATP synthase inhibition, mycolic acid and protein synthesis disruption are supposed to be involved, respectively. Unfortunately, TB treatment is still lengthy and complicated by numerous side effects. Despite some novel potent entities in (pre-)clinical evaluation, only three new medications recently appeared on the market: bedaquiline **II-5** and pretomanid **II-6** approved by FDA in 2012 and 2019, respectively, and delamanid **II-7** firstly approved by EMA in 2014 (Figure 2).<sup>9</sup>

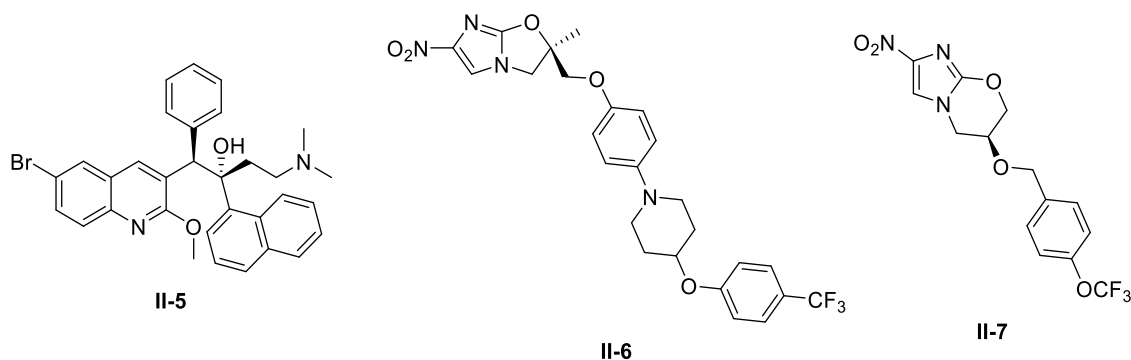


**Figure 2** Selected novel anti-TB agents.

Therefore, new anti-TB regimens that would shorten and simplify the therapy of active disease that would be effective against MDR and XDR TB as well as suitable for coadministration with antiretroviral agents remain urgently needed. Exploring novel mycobacterial drug targets is inevitable to address all the criteria mentioned above and increase TB control. The development of novel anti-TB compounds with a novel mechanism of action can provide an alternative treatment strategy for LTBI and/or DR

TB, mainly in combination with existing antitubercular drugs. On the other hand, non-lethal molecules directed toward virulence factors possess synergistic effects and thus make *Mtb* generally more susceptible to existing anti-TB chemotherapy. For this reason, the non-lethal approach provides similar overall therapeutical outcome.<sup>5</sup>

Along the way, many (non-)lethal drug targets within *Mtb* have been revealed comprising cell wall biosynthesis, redox homeostasis, DNA replication and protein synthesis, oxidative phosphorylation, toxin-antitoxin system and phagosome-lysosome fusion (Figure 3). Also, several processes at the level of the host such as autophagy, granuloma formation and inflammatory responses were identified as suitable drug targets (Figure 3).<sup>5</sup>

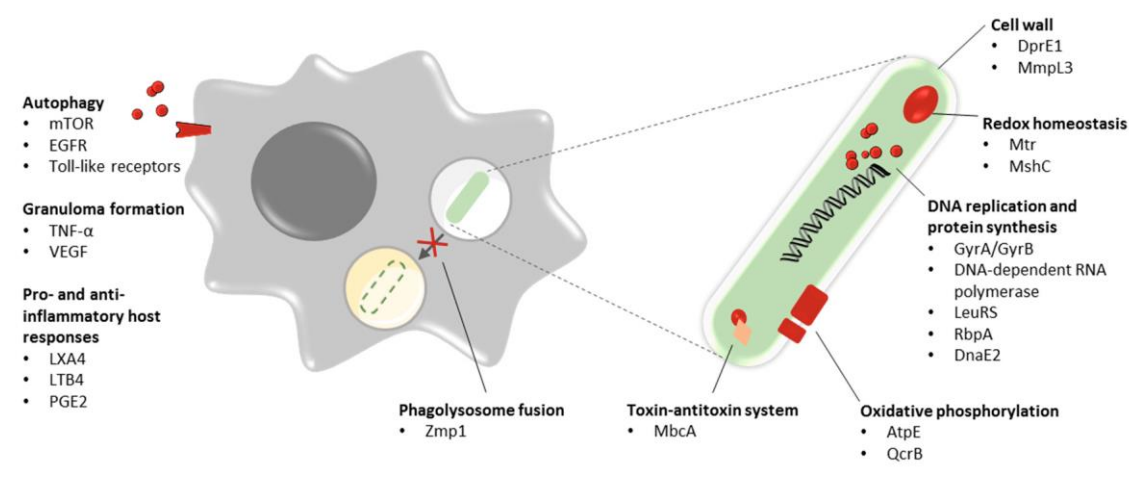


**Figure 3** Overview of the emerging mycobacterial targets and host-directed therapies addressed.<sup>5</sup>

Based on the aforementioned knowledge, the first part of the thesis is focused on the inhibition of two mycobacterial virulence factors: Zmp1 and MptpB. The second part of the thesis is inspired by targeting mycobacterial energy metabolism. In particular, mycobacterial ATP synthase, a crucial druggable molecular target within the electron transport chain-mediated energy production, was chosen for the design and synthesis of the following potent anti-TB candidates. Since the current trend in “empirical drug discovery” emphasizes the inherent complementarity of phenotypic and target-based approaches, the last part of the thesis is dedicated to new anti-TB entities for whole-cell phenotypic screening. To obtain two chemical libraries of eligible hybrid entities, a well-established combinatorial approach was proposed.



---

## 3 Theoretical part

This theoretical part is divided in accordance with mycobacterial molecular targets and drug discovery approaches into three main sections dedicated to mycobacterial virulence factors inhibition, ATP synthase inhibition and phenotypic screening. Such a division corresponds with the three main approaches taken toward anti-TB drug design. All the three main sections are further divided in accordance with included research projects focused on inhibition of two mycobacterial virulence factors zinc metalloprotease 1 (Zmp1) and mycobacterial protein tyrosine phosphatase B (MptpB), ATP synthase inhibition including 2-aminobenzoxazoles synthesis for novel potential squaramide-aminobenzoxazole ATP synthase inhibitors and phenotypic screening of thiazolidinedione (TZD)-pyrimidines and TZD-triazoles.

### 3.1 Hydroxamate-based Zmp1 inhibitors

#### 3.1.1 Functional characterization of mycobacterial Zmp1

The enzyme Zmp1 is a zinc-containing peptidase essential for *Mtb* pathogenicity.<sup>2</sup> In 2008, Master et al. proved Zmp1 to interfere with the macrophage phagosome maturation *via* suppressing of inflammasome activation and subsequent phagolysosome formation.<sup>10</sup> Typical inflammasome includes cytosolic immune sensors: so-called NOD-like receptors (NLRs), a subset of pattern recognition receptors essential for detecting invading pathogens and initiating the innate immune response. Certain NLRs, namely NLRP1, NLRP3 and NLRC4 oligomerize to form multiprotein inflammasome complexes. Such an inflammasome oligomerization leads to the cleavage and activation of caspase-1, which promotes the processing and secretion of IL-1 $\beta$  and IL-18 proinflammatory cytokines.<sup>11</sup> IL-1 $\beta$  subsequently binds to IL-1 receptor and activates the phagosome fusion with intracellular lysosomes and the early inflammatory response. As an overall result of Zmp1-mediated inhibition of the inflammasome activation pathways, the enzyme prevents full clearance of the invalid pathogens (Figure 4). However, the entire action mechanism of Zmp1 remains not fully elucidated. There is only evidence of Zmp1-

mediated disruption of the caspase-1-dependent activation of interleukin-1 $\beta$  secretion.<sup>12</sup> Suppression of the inflammasome activation signaling pathway is also confirmed to ultimately inhibit phagolysosome formation as well as *Mtb* clearance. Mycobacterial zinc metallopeptidases are widely distributed virulence factors localized outside the impenetrable mycobacterial cell wall and represent significant pharmacological targets.<sup>12</sup>

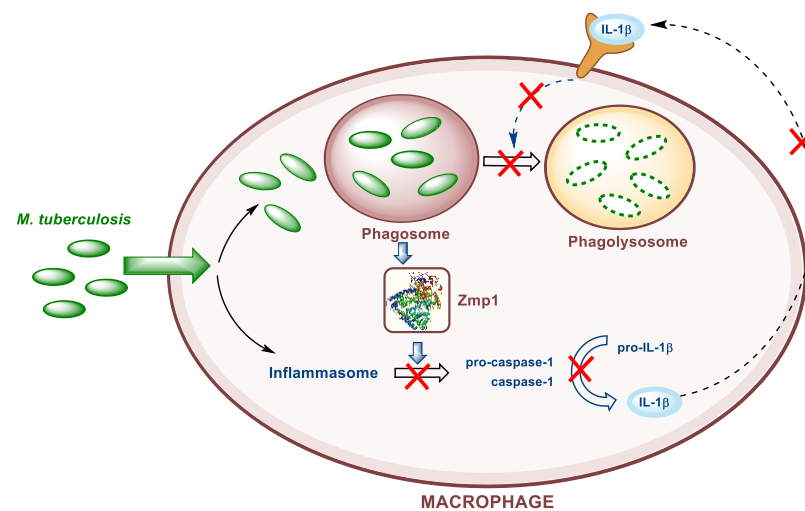


**Figure 4** Mycobacterial Zmp1-mediated inhibition of the phagosome maturation (adopted from Ferraris and Rizzi).<sup>13</sup>

The molecular structure of the mycobacterial Zmp1 comprises two  $\alpha$ -helical lobes interconnected by loops located over the protein equatorial line. The enzyme catalytic active site is located between the two lobes and contains a catalytic zinc ion in tetrahedral coordination. Due to the hydrophobic residues present, peptide substrates with a large hydrophobic P1' side chain such as PHE, LEU or ILE are well accommodated. The catalytic active site also possesses a secondary binding pocket containing ARG residues. Zmp1 shares 31% identity and 48% similarity with both human neprilysin (NEP) (Figure 5) and endothelin-converting enzyme-1 (ECE-1) onto which it can be superimposed with a root mean square deviation (rmsd) of 1.87 Å and 1.73 Å, respectively.<sup>2,13</sup> Computational DNA sequence analysis indicated a remarkably close structural similarity with both the abovementioned human zinc metalloproteases NEP and ECE-1 and thus identified Zmp1 as a member of M13 Zn-dependent metalloproteases.<sup>14</sup>

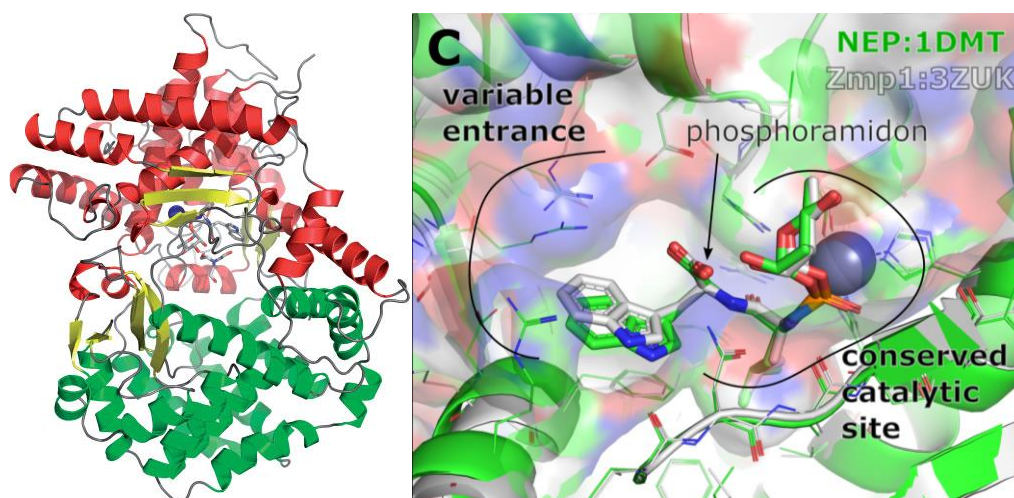


**Figure 5** Ribbon representation of Zmp1 structure.<sup>13</sup> A comparison of the binding of phosphoramidon in the cavity of Zmp1 (PDB ID: 3ZUK) and neprilysin (NEP; PDB ID: 1DMT).

### 3.1.2 State of the art for Zmp1 inhibitors development

To date, the number of known Zmp1 inhibitors remains very limited.<sup>15,16</sup> In 2014, the Botta group synthesized and identified the first selective *Mtb* Zmp1 inhibitor based on the available X-ray structure of Zmp1/ligand complex.<sup>15</sup> Their most potent competitive inhibitor ZTB23(R) **III-1** showed  $K_i$  of 94 nM and SI > 250 with respect to the human NEP (Figure 6). Extensive SAR was coupled with molecular modeling to highlight structural determinants for Zmp1 inhibition. In the docking-based binding mode of **III-1**, the rhodanine performs a H-bond with ASN452 and the benzoic acid moiety is well inserted in the large S2' sub-site to interact with THR606. Moreover, favorable H-bonds with GLU494 and HIS622 reinforce the inhibitory affinity toward Zmp1.<sup>15</sup> Subsequently, several rhodanine-derived Zmp1 inhibitors such as tetrazoloquinoline-rhodanines **III-2** (MIC (*Mtb H37Ra*) up to 4.5  $\mu\text{g/mL}$ ), quinolidene-rhodanines **III-3** (MIC *Mtb H37Ra* = 3.5-19.9  $\mu\text{g/mL}$ ) and 3-(carboxymethyl)rhodanines **III-4** (Zmp1 inhibition with  $\text{IC}_{50}$  = 1.3-43.9  $\mu\text{M}$ ) were described and thus confirmed rhodanine as a preferred structural feature of Zmp1 inhibitors (Figure 6).<sup>17-20</sup> The synthesized tetrazoloquinoline-rhodanines **III-2** have exhibited good binding energies with Zmp1 enzyme as -37.07 to -58.44 kcal/mol.<sup>20</sup> With the minimum energy for the formation of ligand-receptor complex ranging from -42.06 to -26.20 kcal/mol, quinolidene-rhodanines **III-3** showed a high affinity toward Zmp1 active site with Van der Waals interactions surpassing the electrostatic ones.<sup>19</sup> Finally, the amino acid carboxylic functionality of 3-(carboxymethyl)rhodanine **III-4** coordinates the catalytic Zn(II) ion while possesses H-bonding to key Glu494 and His622 residues.<sup>18</sup> In 2018, Paolino et al. revealed 8-

hydroxyquinolines bearing hydroxamate ZBG potent Zmp1 inhibitors.<sup>16</sup> Namely *N*-(benzyloxy)-8-hydroxyquinoline-2-carboxamide **III-5** with Zmp1 inhibitory activity IC<sub>50</sub> value of 0.011±0.002 μM is the best inhibitor known so far with the carbonyl group accommodated at a suitable distance of 2.2 Å for a metal-coordination to Zn(II) and with the remaining heteroatoms form productive interactions with neighboring residues in the active site pocket. Its estimated ligand binding energy corresponds to -77.53 kcal/mol.<sup>16</sup>

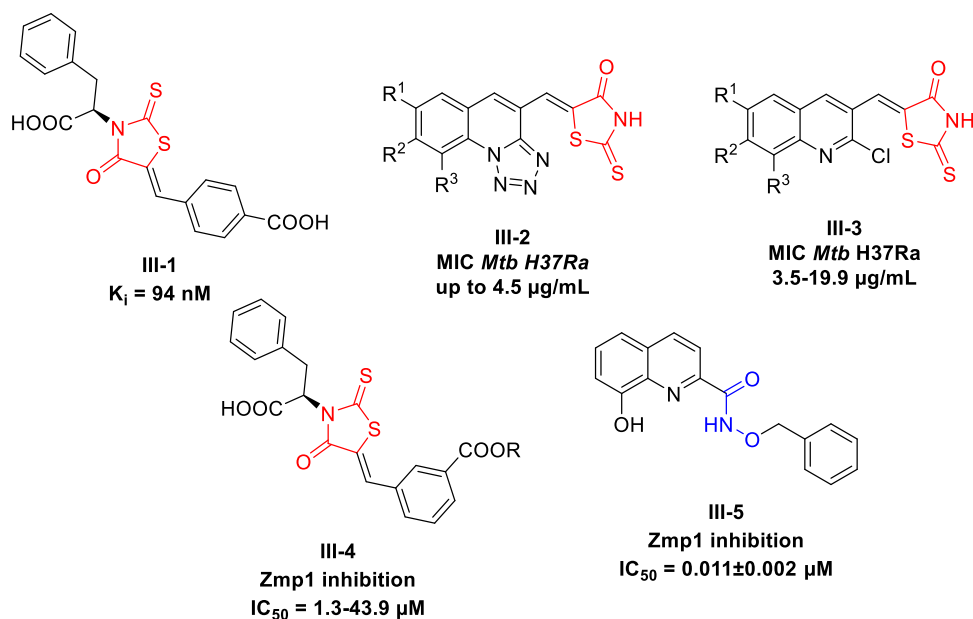
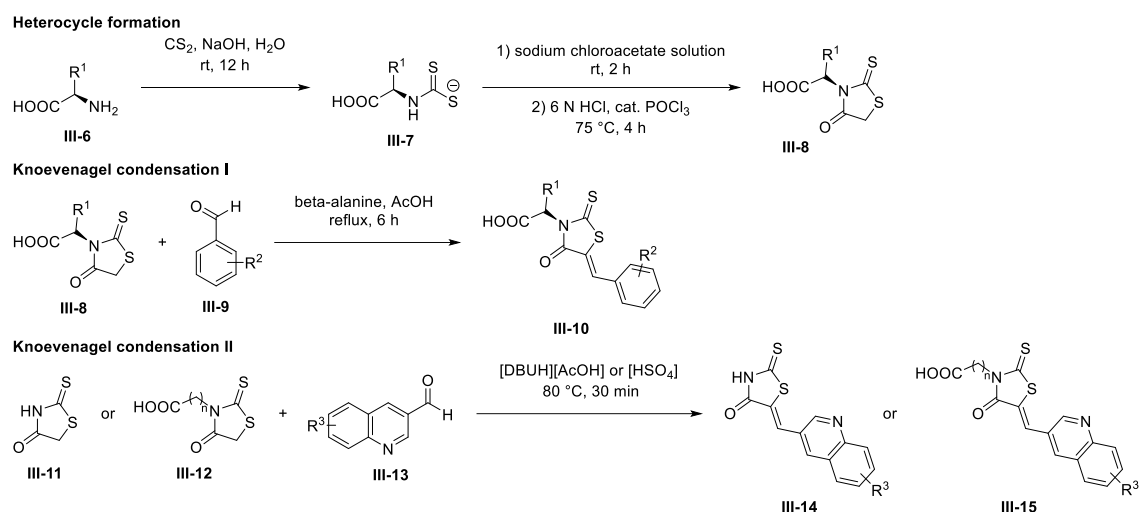


**Figure 6** Current Zmp1 inhibitors.

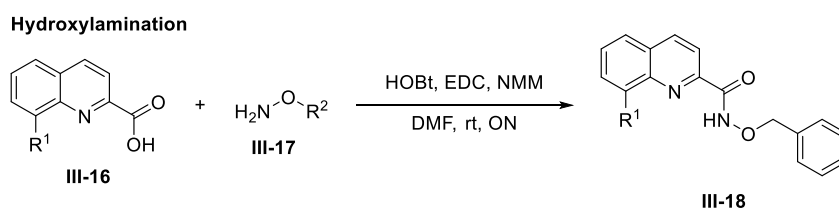
### 3.1.3 Synthesis of current Zmp1 inhibitors

The synthetic approach toward known Zmp1 inhibitors is relatively straightforward. From the synthetic perspective, all their structural modifications can be divided into three main sections: heterocycle formation, *N*-alkylation, Knoevenagel condensation and hydroxylamination. The first known Zmp1 inhibitors, 3-(carboxymethyl)rhodanines **III-10**, were synthesized within three simple steps (Scheme 1).<sup>18</sup> *N*-alkylated rhodanine intermediates **III-8** were formed from β-amino acids **III-6** treated with CS<sub>2</sub> in H<sub>2</sub>O and resulting intermediates **III-7** reacted firstly with sodium chloroacetate and subsequently cyclized in an acidic environment (Scheme 1). The following Knoevenagel condensation of rhodanines **III-8** with aromatic aldehydes **III-9** was accomplished in refluxing acetic acid. Modified Knoevenagel condensation based on solvent-free procedure with 20 mol% of DBU acetate/sulfate yielded various rhodanine-quinolidenes **III-14** or **III-15** (Scheme 1).<sup>19,20</sup>



**Scheme 1** Key synthetic modifications to access rhodanine-based Zmp1 inhibitors.

The last relevant modification to mention is hydroxylation. Concerning the known Zmp1 inhibitors, hydroxylation was employed in the synthesis of 8-hydroxyquinoline-2-hydroxamates **III-18** (Scheme 2). Hydroxylation is typically achieved by standard coupling between the corresponding carboxylic acids **III-16** and *O*-alkylhydroxylamines **III-17**, leading to the desired hydroxamates **III-18**.<sup>16</sup>



**Scheme 2** Key synthetic modifications to access quinoline-based Zmp1 inhibitors.

## 3.2 Polycyclic MptpB inhibitors *via gem-dihaloaminocyclopropanes*

### 3.2.1 Functional characterization of mycobacterial protein tyrosine phosphatases

Both the enzymes mycobacterial protein tyrosine phosphatases (MptpA, MptpB) modulate host-cell signaling by proteins dephosphorylation in interferon- $\gamma$ -signalling pathways (Figure 7).<sup>21</sup> Mycobacterial inhibition of these pathways impairs phagosomes

maturation into phagolysosomes, modulates host-cell apoptosis and suppresses the host immune response.<sup>22</sup> As an overall result, pathogenic mycobacteria can escape the bactericidal action of macrophages. While MtpA interferes with phagosome acidification, MtpB disrupts signal transduction cascades, thereby causing immune response subversion. Since MtpA is comparatively less explored than MtpB and potential inhibitors are usually unselective against human protein tyrosine phosphatases, MtpA is not further discussed within the thesis. Biochemical observations revealed that MtpB attenuates signalling pathways related to mitogen-activated protein kinase (MAPK), Ser/Thr protein kinase involved in a stimulation of cell growth and proliferation, and nuclear factor- $\kappa$ B (NF- $\kappa$ B), a pivotal mediator of inflammatory responses. Such an attenuation is leading to reduced secretion of inflammatory cytokines IL-1 $\beta$  and IL-6, critical factors for the upregulation of microbicidal activity, and initiates the host immune response to *Mtb* infection.<sup>23,24</sup> There is strong evidence showing that MtpB promotes infected macrophage survival *via* augmenting Akt phosphorylation and suppressing caspase 3.<sup>25</sup> On the contrary, non-pathogenic or dead *Mtb* activate host-cell signalization and thus induces antibacterial responses as well as phagosome maturation.<sup>26</sup> Considering their central role in cellular signalization, mycobacterial protein tyrosine phosphatases were identified as an attractive antitubercular target.

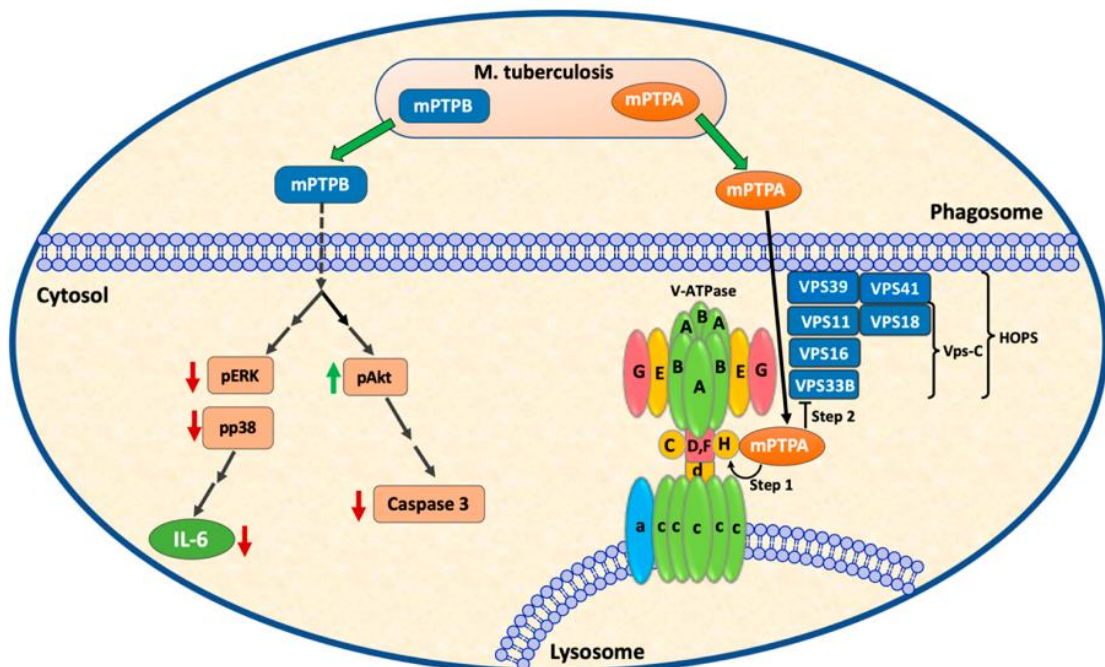


**Figure 7** Roles of MtpA and MtpB in mediating pathogen-host interactions.<sup>23</sup>



In recent year, an extensive amount of structural data has been published on pathogenic protein tyrosine phosphatases. All the data contributed to the elucidation of their physiological functions as well as the molecular basis for substrate binding (Figure 8).<sup>27</sup> MtpB is a 30kDa protein with an unusual fold, resembling the human myotubularin MTMR deviated from the classic PTP fold.<sup>28</sup> MtpB displays a huge active site, unlike the narrow and deep PTP cleft, which is consistent with its phosphoinositide activity.<sup>29</sup> The P-loop signature contains an extra basic ARG residue like other lipid phosphatases. On the other hand, MtpB possesses the catalytic ASP in the P loop rather than in the distant WPD loop of typical PTPs.<sup>30</sup>

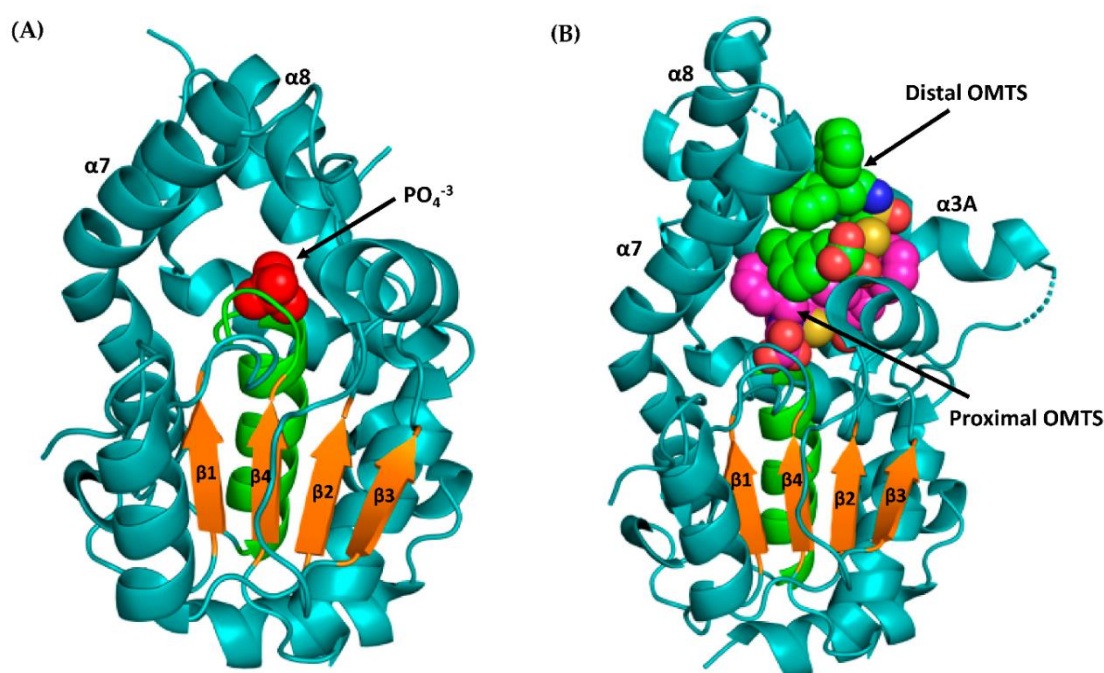


**Figure 8** X-ray crystal structures of MtpB. (A) X-ray structure of phosphate bound MtpB in the flexible lid closed form. (B) X-ray structure of OMTS ((oxalylamino-methylene)-thiophene sulphonamide) bound MtpB in open form.<sup>23</sup>

### 3.2.2 State of the art for fused polycyclic MtpB inhibitors development

In general, many MtpB inhibitors have been identified. However, their promising pharmacological qualities require further improvement in terms of selectivity and bioavailability.<sup>31,32</sup> Within an infinite number of known potent MtpB inhibitors,<sup>33,34</sup> diverse fused polycycles seem to be favored scaffolds and therefore attracted our attention. The first paper relevant to inhibition of MtpB appeared in 2012 reporting

various indolizidine and quinolizidine iminocyclitols **III-19** (Figure 9). Although all the compounds **III-19** inhibit glycoprocessing enzymes such as  $\alpha$ -L-rhamnosidase, they lack any significant anti-TB activity.<sup>35</sup> More importantly, Waldmann et al. accessed a wide variety of substituted indolo[2,3-a]quinolizidines. The resulting Yohimbane-derived quinolizidines **III-20** showed remarkable MptpB inhibition with  $IC_{50}$  less than 10  $\mu$ M (Figure 9).<sup>21</sup> Subsequently, Asperterpenoid A **III-21**, a novel member of sesterpenoid family, was recently isolated from a mangrove endophytic fungus *Aspergillus* sp. (Figure 9). Further pharmacological studies proved that Asperterpenoid A **III-21** is a potent inhibitor of MptpB with an  $IC_{50}$  value of 2.2  $\mu$ M.<sup>36</sup> Ongoing research of Waldman and co-workers yielded another significant MptpB inhibitor **III-22** ( $IC_{50}$  = 0.36  $\mu$ M).<sup>21</sup> Finally, fragment-based optimization of  $\alpha$ -sulfophenylacetic amide led to excellent MptpB inhibitor **III-23**. Compound **III-23** demonstrated  $IC_{50}$  of 18 nM,  $K_i$  of 7.9 nM and >10000-fold selectivity against another phosphatases.<sup>37</sup>

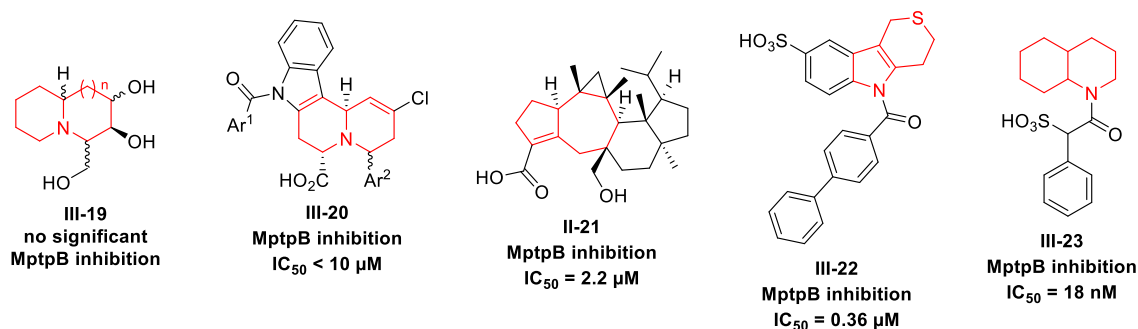


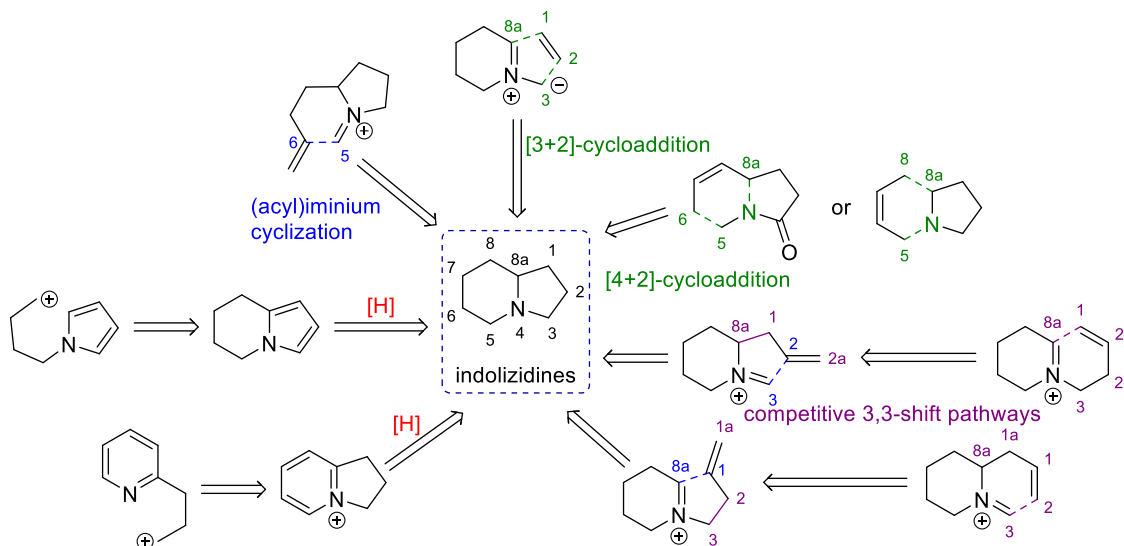
**Figure 9** Known fused polycyclic MptpB inhibitors.

### 3.2.3 Synthetic approaches toward izidines

Typical synthetic approaches toward izidines concerning azabicycles formation include hydrogenation of corresponding heteroaromatic cores, condensation of carbonyls, cycloadditions, sigmatropic shifts, transition metal-mediated cyclizations and radical processes (Scheme 3).<sup>38</sup> The most abundant methods for the synthesis of indolizidines comprise various manipulation with peripheral substituents of the bicyclic core, as well as intramolecular alkylation, acylation and reductive amination, which close the second ring in terms of N-C<sub>(3/5)</sub> disconnection. However, their syntheses usually require many steps or reagents, complex intermediates preparation, suffer from severe substrate limit and/or harsh reaction conditions. Therefore, a widely applicable synthetic strategy to obtain these heterocycles in short high-yielding reaction sequences remains a desirable

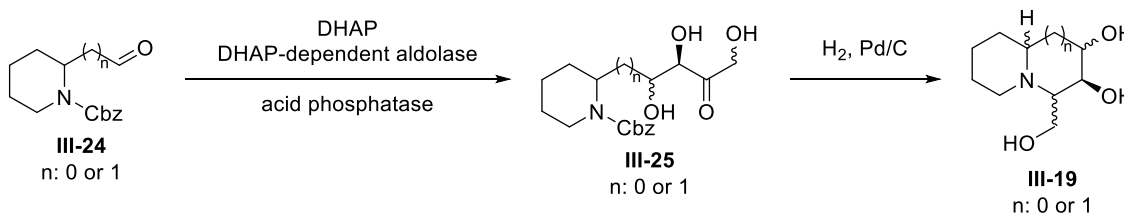


unmet challenge. In the abovementioned context, domino reaction sequences are gaining general interest as plausible reliable, efficient and environmentally friendly alternatives from readily available starting materials.<sup>39</sup>



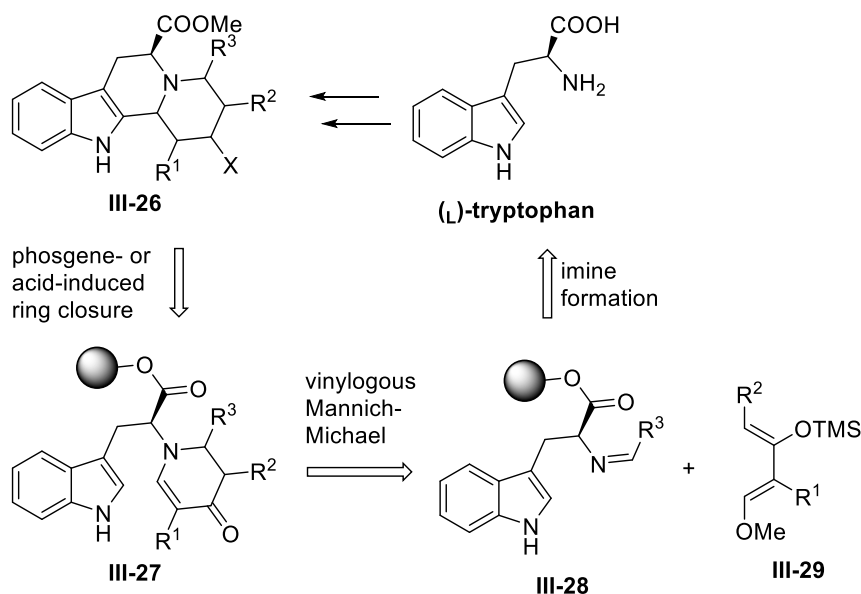
**Scheme 3** Overview of synthetic approaches toward indolizidines.

Attempts to build up a full retrosynthetic scheme to summarize all the strategic approaches for the indolizidines preparation would provide too complex picture. For this reason, only particular synthetic pathways toward selected MtpB inhibitors will be detailed within the chapter to further demonstrate the versatility of *N*-fused polycyclic preparation. Moreover, the overview of synthetic approaches will thus be extended from 5+6 izidines (Scheme 3) to their larger 6+6 *N*-fused polycyclic analogues. The first synthetic pathway describes chemoenzymatic synthesis of indolizidine and quinolizidine iminocyclitols **III-19** (Scheme 4).<sup>35</sup> The initial step comprises the aldol addition of dihydroacetone phosphate (DHAP) to *N*-Cbz-piperidine carbaldehydes **III-24** catalyzed by L-rhamnulose-1-phosphate aldolase affording key intermediates **III-25**. The subsequent reductive amination enables the cyclization to the final izidine iminocyclitols **III-19**.



**Scheme 4** Chemoenzymatic synthesis of izidine iminocyclitols.

The second relevant synthetic approach is based on solid-supported biology-oriented synthesis (BIOS), which integrates computational and synthetic tools for the generation of compound collections for biological applications, yielding indolo[2,3-a]quinolizidines **III-26** (Scheme 5).<sup>21</sup> Because of the multistep overall sequence, which is beyond the scope of the chapter, the main retrosynthetic disconnections are illustrated. From the retrosynthetic perspective, the indolo[2,3-a]quinolizidine core was traced back to pyridione precursor **III-27** with a carboxylate function chosen for attachment to the solid support. The pyridine precursor **III-27** was available by vinylogous Mannich-Michael reaction between imine **III-28** and diverse electron-rich silyloxydienes **III-29**. All the sequence was accomplished by two different cyclization modes possible. Firstly, phosgene-mediated ring closure performed on the Wang linker provided tetracyclic vinyl chlorides **III-26** where X is Cl. Secondly acid-mediated cyclization on the hydroxy methylene benzoic acid (HMBA) linker gave tetracyclic ketones **III-26** where X is =O.

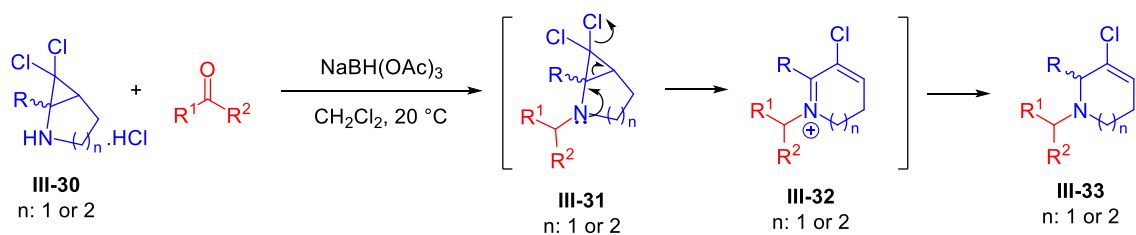


**Scheme 5** Retrosynthetic analysis of highly substituted indolo[2,3-a]quinolizidines.

### 3.2.4 Reactivity of *gem*-dihaloaminocyclopropanes toward izidines

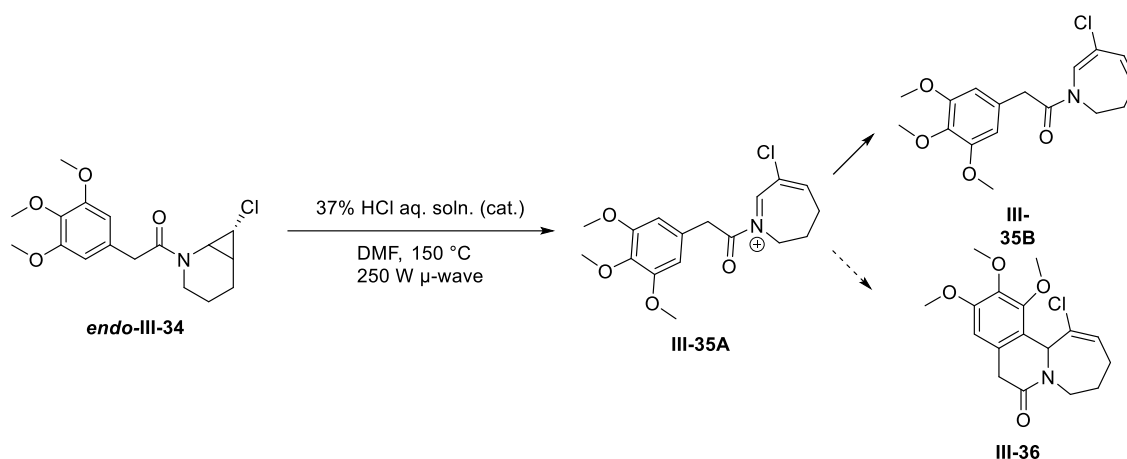
Fused bicyclic aminocyclopropanes represent a readily available reservoir for valuable transformations into nitrogen-containing polycyclic systems. All the methods include cyclopropane compounds activated just through the amino group.<sup>40,41</sup> Of exceptional value are transformations of halocyclopropanes usually proceeding *via* thermal ring-

opening with a concomitant halide ion departure to generate allyl cation intermediates.<sup>42,43</sup> Nevertheless, the corresponding reactivity of nitrogen-substituted *gem*-dihalocyclopropanes remains underexplored. Such ring-openings require heating and/or activation by silver salts and are often low-yielding.<sup>44,45</sup> On the other hand, amines were from time to time mentioned as more reactive due to better stabilization of the allyl cation intermediate.<sup>46,47</sup> Therefore, Six et al. envisioned the enhanced reactivity of dihalogenated cyclopropylamines **III-31**, generated from ammonium salts **III-30**. Functionalized azepanes and piperidines **III-33** could thus be obtained by reductive amination and ring expansion (Scheme 6).<sup>48</sup> Indeed, aldehydes and ketones were reacted with 2,2-dihaloaminocyclopropane salts **III-30** using NaBH(OAc)<sub>3</sub>, to provide the thermally unstable dihalogenated aminocyclopropanes **III-31**. The transformation not only enabled functionalization but also triggered the cyclopropane ring cleavage to access the nitrogen-containing final products **III-33**.<sup>48</sup>



**Scheme 6** Ring enlargement of *gem*-dihaloaminocyclopropane salts upon reductive amination.

Moreover, the successful reaction between an acyl chloride and an *endo* monochlorocyclopropylammonium salt successfully provided the amide *endo*-**III-34** under Schotten-Baumann conditions. Such a transformation was fast enough to trap the free secondary amine even before cyclopropane-ring cleavage. However, upon microwave irradiation, only the ring-expanded dihydroazepine **III-35B** was formed *via* deprotonation of the intermediate iminium species **III-35A** (Scheme 7). Unfortunately, this deprotonation proceeded faster than the desired cyclization onto the electron-rich aromatic ring. As a result, the overall reactivity disabled the cyclization toward a fused polycycle **III-36**.<sup>48</sup>



**Scheme 7** Ring enlargement of monochlorocyclopropane amide.

### 3.3 2-Aminobenzoxazoles preparation for mycobacterial ATP synthase inhibitors

#### 3.3.1 Functional characterization of mycobacterial ATP synthase

ATP synthase is a ubiquitous enzyme involved in cellular energy metabolism. Resembling a turbine, ATP synthase contains two components: a rotor ( $F_0$ ) and a stator ( $F_1$ ) connected through a central stalk, reversibly coupling proton flow to either ATP formation or hydrolysis (Figure 10).<sup>49</sup> The overall oxidative phosphorylation is an essential energy source driving ATP synthase to convert the electrochemical potential energy into chemical energy produced *via* ADP and inorganic phosphate ( $P_i$ ) reaction.<sup>50,51</sup> Furthermore, mycobacterial ATP synthase is essential also in the dormant state under nonreplicating conditions such as oxygen insufficiency, nutrient limitation or acidic pH.<sup>52</sup>

As a result, mycobacterial ATP synthase possesses several idiosyncratic functional adaptations. Firstly, mycobacterial ATP synthase lacks the ATP hydrolysis function to prevent the unwanted waste of ATP. The hydrolytic activity is usually suppressed by inhibitory binding of Mg-ADP, subunit  $\epsilon$  dysregulation, or inhibitory protein subunit  $\zeta$ .<sup>53</sup> The next specific feature to mention is the possibility to produce ATP even under low proton motive force ( $-110$  mV) closely related to the subunit  $c$  structure. A large  $c$  oligomer increases  $H^+$ /ATP turnover leading to promoted ATP formation. Finally, a

remarkable stiffness of the stator stalk, as well as highly lipophilic cytoplasmatic membrane, are believed to speed up ATP synthesis.<sup>54,55</sup>

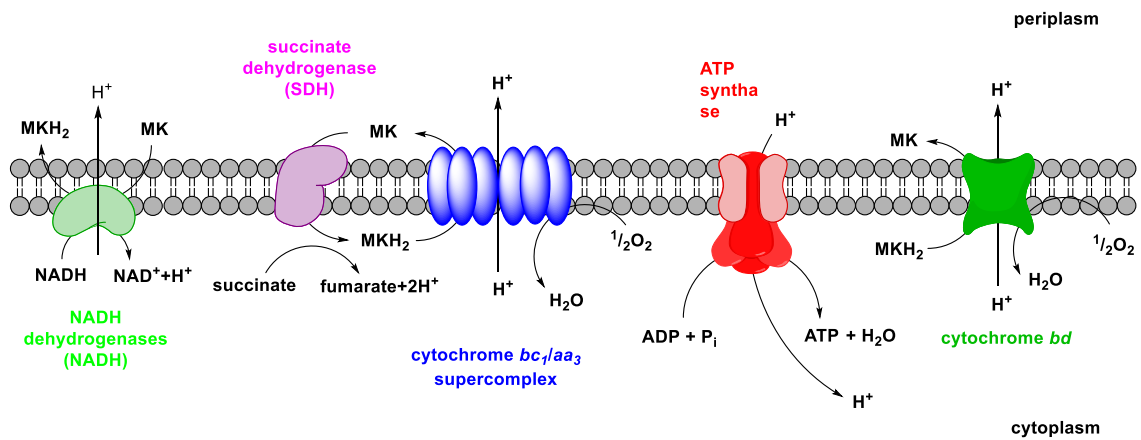


**Figure 10** Mycobacterial oxidative phosphorylation (drawn according to Bald and Koul).<sup>56</sup>

From the structural point of view, mycobacterial ATP synthase (Figure 11) contains three  $\alpha$  and three  $\beta$  subunits alternate to form hydrophilic stator ( $F_1$ ) extending into the cytoplasm. The membrane-embedded rotor ( $F_0$ ) includes one  $a$ , two  $b$  and a ring of more than ten  $c$  subunits. Rotor and stator connection *via* the central stalk composed from  $\gamma$ ,  $\delta$  and  $\epsilon$  subunits has a characteristic fusion between one  $b$  and one  $\delta$  subunit.<sup>57</sup> The resulting  $b/\delta$  fusion protein facilitates the bonding interaction between ATP precursors and the  $\alpha_3\beta_3$  hexamer, while the free  $b$  subunit enhances power transmission within the ATP synthase complex. Therefore, the two diverse  $b$  subunits present tend to improve their overall mutual interaction.<sup>58</sup> Indeed, the comprehensive rotor and stator connection is needed to avoid unproductive rotation during catalysis.

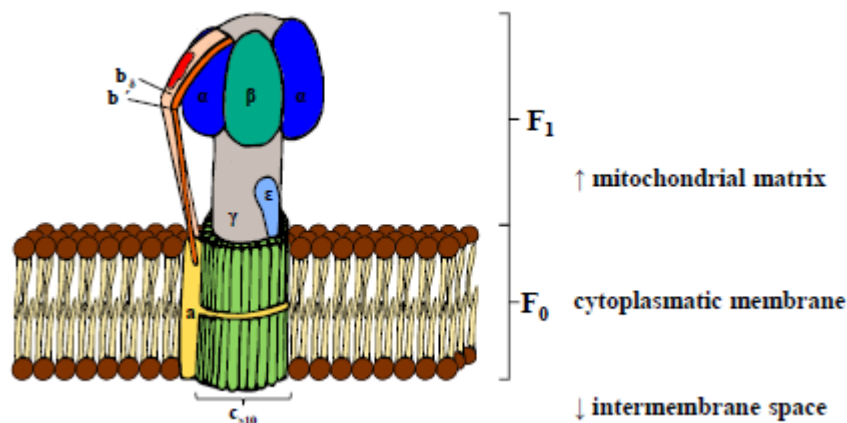


**Figure 11** Mycobacterial ATP synthase (drawn according to Lu and Bald).<sup>54</sup>

### 3.3.2 State of the art for selected ATP synthase inhibitors development

Mycobacterial ATP synthase is well known to carry idiosyncratic features enabling remarkably efficient ATP production. A better insight into the functional and structural characterization of ATP synthase may provide essential input for the rational development of its inhibitors as novel anti-TB agents. In addition, selective mycobacterial ATP synthase inhibitors can be accessed due to crucial differences compared to human ATP synthase. There have already been two (pre)clinical candidates discovered among mycobacterial ATP synthase inhibitors to highlight the importance of targeting mycobacterial oxidative phosphorylation.<sup>59</sup> The first anti-TB compound to interfere with *Mtb* ATP synthase, especially its subunit *c*, was bedaquiline **III-37** (Figure 12). The diarylquinoline lead compound turned out active against MDR *Mtb* and was developed by Jansen Pharmaceuticals into phase 3 of clinical investigation.<sup>60</sup> The most potent mycobacterial ATP synthase inhibitors **III-38** and **III-39** were derived from bedaquiline **III-37** and reported by Palmer et al.<sup>61</sup> The naphthalene subunit was replaced with substituted pyridine heterocycles to reduce cardiotoxicity, lipophilicity and half-life. Both the pyridyl analogues **III-38** and **III-39** inhibit *Mtb* H37Rv growth under MABA, with MIC<sub>90</sub> of 0.01 and 0.02 µg/mL, as well as LORA conditions, with MIC<sub>90</sub> of 0.06 and 0.02 µg/mL, respectively.<sup>61</sup> Finally, an extensive SAR study of squaramides revealed derivative **III-40** as the most promising one within the series (*Mtb* H37Rv MIC = 0.43 µM), currently standing for the preclinical drug candidate.<sup>62</sup> Membrane-based biochemical assay (Myc\_ATPS IC<sub>50</sub> 0.03 µM) supported ATP synthase as a plausible molecular target. Finally,  $\pi$ - $\pi$  interactions and H-bonds between the pyridine nitrogen of **III-40**, and ARG186 of subunit *a*, as well as H-bonds between the morpholine oxygen and PHE69 of subunit *c* were identified as essential for the binding mode.<sup>63</sup>

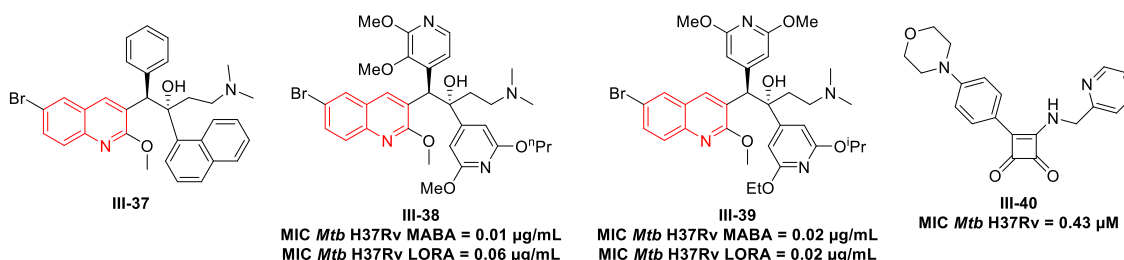
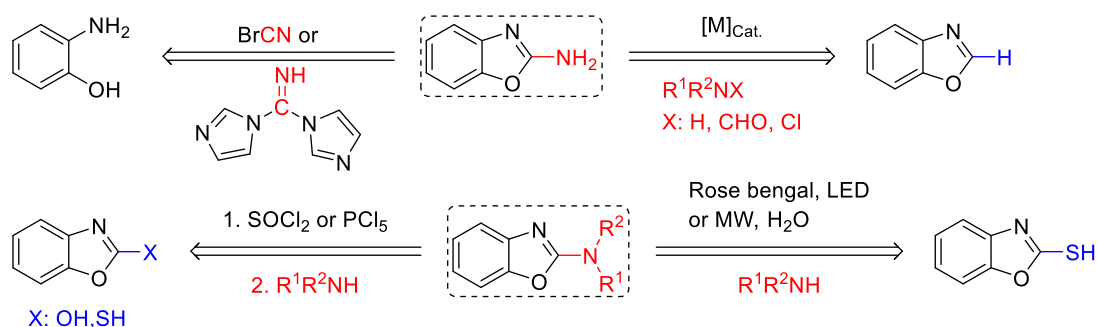


**Figure 12** The most potent ATP synthase inhibitors.

Authors of compound **III-40** performed the extensive SAR study focused on the both parts of the squaramide ring. A wide range of right-hand part variation confirmed the

importance of the pyridine moiety. On the other hand, the diversification of the left-hand part of the molecule **IV-40** was comparatively underexplored enabling further modification. Together with the notable pharmacological potential of benzoxazole moieties, squaramide-benzoxazole structures were indicated as interesting potential ATP synthase inhibitors. For this reason, the particular objective of my work within such a complex research project was the improvement of a synthetic pathway toward 2-aminobenzoxazole moiety and this part of the presented thesis is focused on synthetic approaches toward 2-aminobenzoxazoles (Scheme 8). Despite the numerous synthetic protocols reported, aminobenzoxazoles synthesis still suffers from many remaining drawbacks.<sup>64–66</sup> The most common synthetic strategy is based on the cyclization of 2-aminophenols with highly toxic cyanating reagent BrCN.<sup>67,68</sup> The following approach is direct 2C amination of benzoxazoles, unfortunately, limited by potentially expensive and/or difficult-to-remove transition metal catalysts, high temperatures, the necessity to use an inert atmosphere and/or co-oxidants.<sup>69,70</sup>

Over the past years, multiple methods have been developed to access *N*-substituted aminobenzoxazoles (Scheme 8).<sup>71–73</sup> However, most of them suffer from low yields or involve toxic precursors and/or expensive reagents. Firstly, *N*-substituted aminobenzoxazoles are often formed in two steps by halogenation of the corresponding hydroxyl/thiol precursors, followed by the amination.<sup>74</sup> Secondly, more specialized procedures such as Rose Bengal-catalyzed photochemical amination or microwave-enhanced on-water amination of 2-mercaptobenzoxazoles were introduced.<sup>72,73</sup> Both methods are complicated by long reaction time, and the elevated temperature needed, respectively. Hence, new, safer, efficient synthetic protocols relying on inexpensive precursors are very desirable to expand the number of building blocks for squaramide-benzoxazoles as potential mycobacterial ATP synthase inhibitors.



**Scheme 8** Synthetic approaches toward aminobenzoxazoles.

Apart from our interest in novel potent ATP synthase inhibitors, benzoxazole moieties attracted our attention due to their widespread pharmacological potential.<sup>75</sup> Considering anti-TB research, the benzoxazole moiety has already been successfully combined with a wide variety of other potent antitubercular heterocycles. However, none of the reviewed benzoxazoles reached nanomolar inhibitory concentrations or has entered preclinical hit-to-lead optimization as anti-TB compounds. To the best of our knowledge, only a few benzoxazole-derived conjugates have micromolar potency and are worth mentioning (Figure 13). The selected candidates with MICs against *Mtb* R37Rv ranging from 0.63 to 8  $\mu\text{g}/\text{mL}$  are 2-quinolin-4-ylacetamide **III-41**, pyrazoline-benzoxazoles **III-42** or **III-43** and 5-amino-2-(4-substituted phenyl/benzy) benzoxazole **III-44**.<sup>76-78</sup>

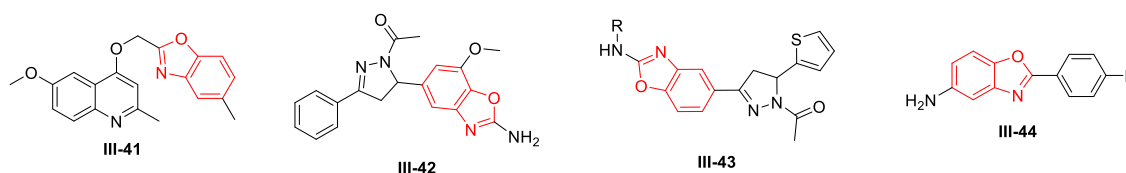


**Figure 13** Selected anti-TB benzoxazole-derived conjugates.

### 3.4 Phenotypic screening of thiazolidinedione-based conjugates

#### 3.4.1 Phenotypic screening in antitubercular research

In terms of drug discovery, phenotypic screening is the nascent method to evaluate pharmacological effects of novel chemical entities. Over the past three decades, drug discovery has shifted toward molecular target-based strategies using rational drug design. To compare their main differences, target-based methodologies use simple *in vitro* biochemical readouts, whereas phenotypic screening requires more elaborate whole cell- or/and tissue-based readouts.<sup>79</sup> Nonetheless, rapidly evolving biotechnologies and some more complex diseases changed the *status quo* and thus phenotypic screens are surpassing target-based approaches in the production of first-in-class scaffolds.<sup>80</sup>

Despite a wide range of active compounds identified through phenotypic screens, the conversion of hits into clinical candidates is threatened by lacking the particular target(s)



and/or the decreased efficacy within difficult-to-penetrate host compartments.<sup>81</sup> Therefore, carefully selected compounds with promising IC<sub>50</sub> values are subjected to further investigation to expand their structure-activity relationships and elucidate binding interactions.<sup>82</sup>

From a synthetic perspective, combinatorial chemistry is a valuable technique to produce focused chemical libraries, designed with respect to a certain chemotype or privileged structure, in a time and resource-effective manner. The fundamental combinatorial principle resides in easy access to unique structural variations from abundant and economic building blocks with minimal synthetic operations.<sup>83</sup> In conclusion, phenotypic screening of diverse chemical libraries can result in the identification of novel chemical entities with remarkable anti-TB potential.

### 3.4.2 Thiazolidinedione as privileged anti-TB structure

Introduced for the treatment of type 2 diabetes mellitus, the thiazolidine-2,4-diones (glitazones) are important pharmacophores with broad pharmacological potential that can be for example antimicrobial, antidiabetic or antiviral.<sup>84-87</sup> Certain TZDs were also found to possess significant anti-TB activity against *Mtb* R37Rv, indicating their potential in antitubercular drug development (Figure 14). For example, Kumar et al. synthesized promising arylidene-thiazolidinedione hybrids **III-45** with MIC values < 50 μM.<sup>88</sup> Following hit-to-lead development resulted in excellent anti-TB candidate **III-46** probably targeting *Mtb* ATP synthase (MIC = 1.4 μM).<sup>82</sup>

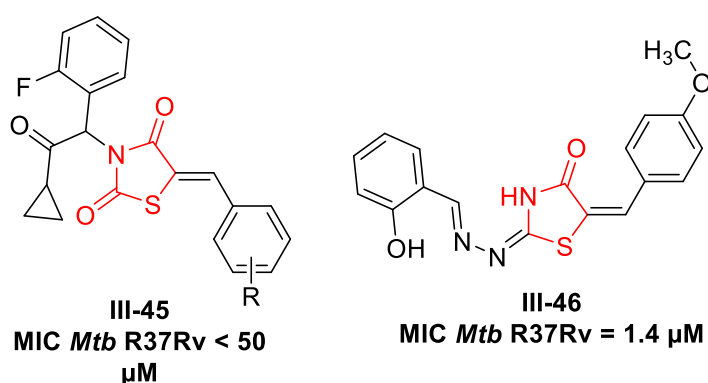


**Figure 14** Selected thiazolidinedione anti-TB entities.

### 3.4.3 Antitubercular potential of pyrimidines and triazoles

As well as many other nitrogen heterocyclic compounds, the pyrimidine pharmacophore is also an essential component of many antimicrobial substances.<sup>89</sup> Owing to their appreciated antitubercular properties, the use of pyrimidines as templates for the addition of versatile substituents into various positions frequently resulted in new pharmacologically active structural frames (Figure 15).<sup>90,91</sup> Consequently, several hybrid pyrimidine-containing structures, for example benzocoumarins **III-47** or sulfonamide **III-48**, possessed remarkable potential against *Mtb* H37Rv with MIC values of 0.05-2.81  $\mu\text{g/mL}$  and 0.02  $\mu\text{g/mL}$ , respectively, and low cytotoxicity against VERO cells (Figure 15).<sup>92,93</sup>

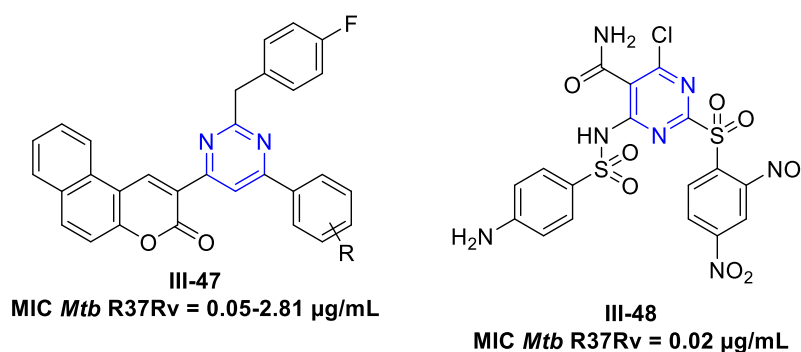
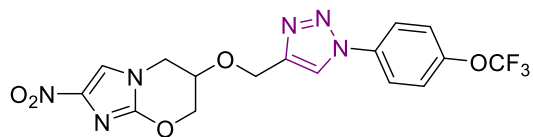
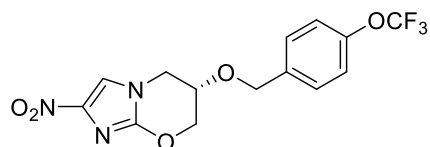


**Figure 15** Selected pyrimidine anti-TB entities.

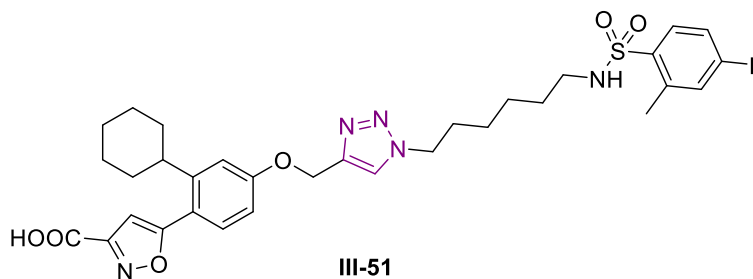
Unique achievements have also been acquired within the research in triazole-derived medicines. Furthermore, the triazole ring is a valuable linker to combine a wide range of pharmacophoric moieties into innovative bifunctional molecules. Typically, 1,2,3-triazole is introduced to anti-TB compounds to moderate dipole character and rigidity as a favorable passive linker. Triazole compound **III-49**, synthesized upon introducing of a 1,2,3-triazole into the structure of the marketed antitubercular drug PA-824 **III-50**, showed up to 7-fold increased potency against replicating *Mtb* under MABA (MIC =  $0.075 \pm 0.015 \mu\text{M}$ ) and LORA ( $3.3 \pm 0.2 \mu\text{M}$ ) conditions and better solubility than the parent molecule (Figure 16).<sup>94,95</sup> An additional antitubercular triazole that is worth mentioning is compound **III-51**. With a  $K_i$  as low as  $0.15 \mu\text{M}$ , triazole hybrid **III-51** remains the best MptpB inhibitor known up to now.<sup>96</sup>



**III-49**  
MIC *Mtb* MABA =  $0.075 \pm 0.015 \mu\text{M}$   
MIC *Mtb* LORA =  $3.3 \pm 0.2 \mu\text{M}$



**III-50**



**III-51**  
MptpB inhibition  
 $K_i = 0.15 \mu\text{M}$

**Figure 16** Selected triazole-related anti-TB entities.

---

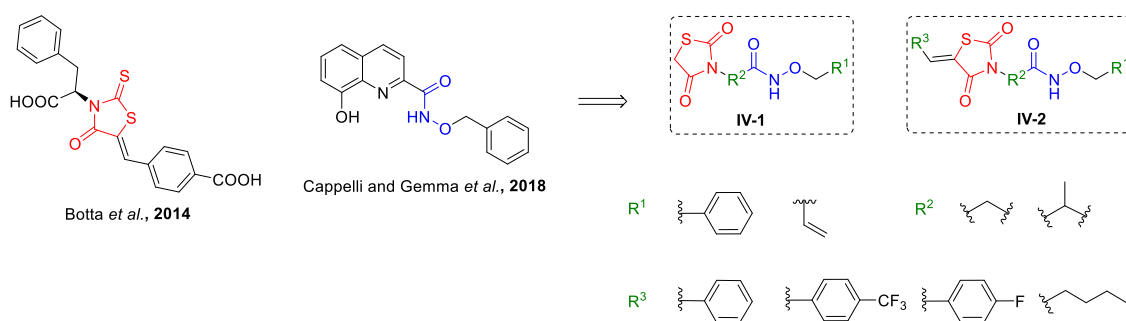
## 4 Results and Discussion

The **Results and discussion** part is divided into chapters with contents corresponding to the described projects/published papers focused on inhibition of two mycobacterial virulence factors zinc metalloprotease 1 (Zmp1) and mycobacterial protein tyrosine phosphatase B (MptpB), ATP synthase inhibition including 2-aminobenzoxazoles synthesis for novel potential squaramide-aminobenzoxazole ATP synthase inhibitors and phenotypic screening of thiazolidinedione (TZD)-pyrimidines and TZD-triazoles. Each chapter serves as a comprehensive overview of the related project, including a short introduction onto the studied compounds, an actual discussion about unsuccessful/unpublished results, and synthetic pathways and final compounds achieved.

### 4.1 Hydroxamate-based mycobacterial Zmp1 inhibitors

#### 4.1.1 Design and synthesis of TZD-hydroxamates

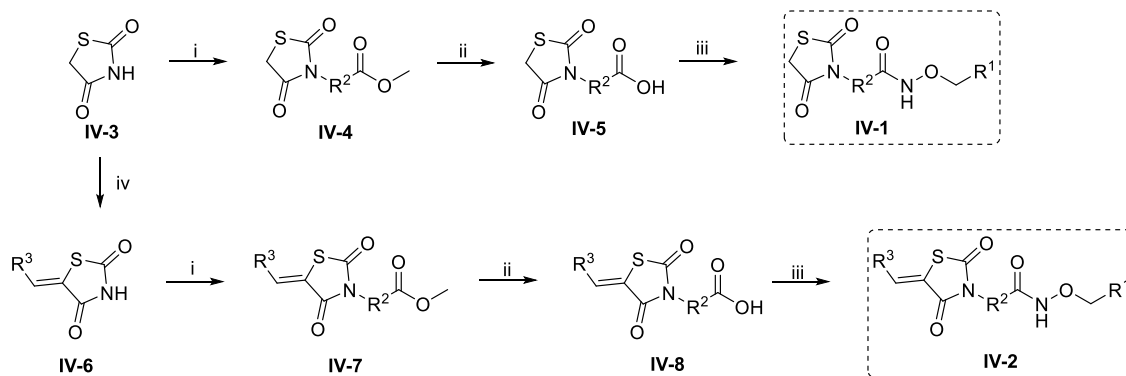
Our first attempt to achieve the discovery of new potential anti-TB compounds was based on mycobacterial virulence factor Zmp1 inhibition. Privileged scaffolds within known Zmp1 inhibitors were hence employed to design Zmp1-targeting chemical library.<sup>15,16</sup> The pharmacological relevance of thiazolidinedione core<sup>97</sup> and well-established hydroxamate-based ZBG<sup>98</sup> inspired the design of a novel series of TZD-hydroxamates **IV-1** and **IV-2** (Scheme 9). For the initial study, two medicinally useful lipophilic hydroxamates were chosen.<sup>99</sup> In regards of, two simple linkers R<sup>2</sup> were selected to connect TZD and hydroxamate scaffolds. Furthermore, several benzylidene or alkylidene-based TZD modifications were envisioned according to known pharmacophores. The outcome of this strategy was the design of the first generation of our TZD-hydroxamate Zmp1 inhibitors **IV-1** and **IV-2** (Scheme 9).<sup>2,100</sup>



**Scheme 9** Design of TZD-hydroxamates.

To obtain the desired TZD-hydroxamates, we developed a straightforward synthetic procedure (Scheme 10). In the beginning, TZD-unsubstituted hydroxamates **IV-1** were formed. The starting TZD **IV-3** was prepared easily from thiourea and chloroacetic acid.<sup>101</sup> The overall yields varied from 57 % to 65 % and thus corresponded to the literature precedent. With TZD **IV-3** in hand, *N*-alkylation with either methyl bromoacetate or methyl 2-bromopropionate was performed. The esters **IV-4** obtained were subjected to acidic hydrolysis providing free acids **IV-5**. Both the acids were coupled with substituted *O*-alkyl hydroxylamine hydrochlorides to give TZD-hydroxamates **IV-1** in moderate yields (Figure 17).

On the other hand, synthesis of TZD-hydroxamates **IV-2** started with Knoevenagel condensation (Scheme 10). Despite well-optimized high-yielding TZD-benzylidene formation, synthetic approach toward TZD-alkylidenes was less documented and more troublesome.<sup>102</sup> Indeed, due to presumed decomposition on silica, we isolated just 40 % of TZD-pentylidene compared to 67-97 % of aromatic analogues. The residual sequence included analogous *N*-alkylation, acidic hydrolysis and coupling with *O*-alkyl hydroxylamine hydrochlorides to achieve substituted TZD-hydroxamates **IV-2** in reasonable yields (Figure 17). Regardless of the particular structure, all the studied compounds exhibited similar reactivity. Occasionally observed compromised yields were caused by lower purity of the crude products and following losses during column chromatography.



**Scheme 10** Synthesis of TZD-hydroxamates.<sup>a</sup>

<sup>a</sup> Reagents and conditions: (i): methyl bromoacetate/methyl 2-bromopropionate, NaH, DMF dry, rt, on (24 h); (ii): HBr (40%), reflux, 5 h; (iii): *O*-allylhydroxylamine.HCl/*O*-benzylhydroxylamine.HCl, EDC.HCl, H<sub>2</sub>O, rt, 2 h; (iv): aldehyde, piperidine, EtOH, reflux, on (16-20 h).

Concerning the geometrical *E/Z* isomerism, the stereochemical outcome of the Knoevenagel condensation was assessed. Both possible isomers may be distinguished by <sup>1</sup>H NMR spectral measurement.<sup>103</sup> The obtained NMR data confirmed the *Z* configuration for all our products, with the benzyldiene proton shifted approximately to 7.90 ppm. Finally, the racemic nature of the present stereogenic centre was revealed by SFC analysis.

The abovementioned synthetic pathway resulted in a novel series of TZD-hydroxamates conjugates **IV-1** and **IV-2** (Figure 17). Desired TZD-hydroxamates **IV-1** and **IV-2** were hence obtained in a straightforward manner in 31-75% yields (Figure 17).

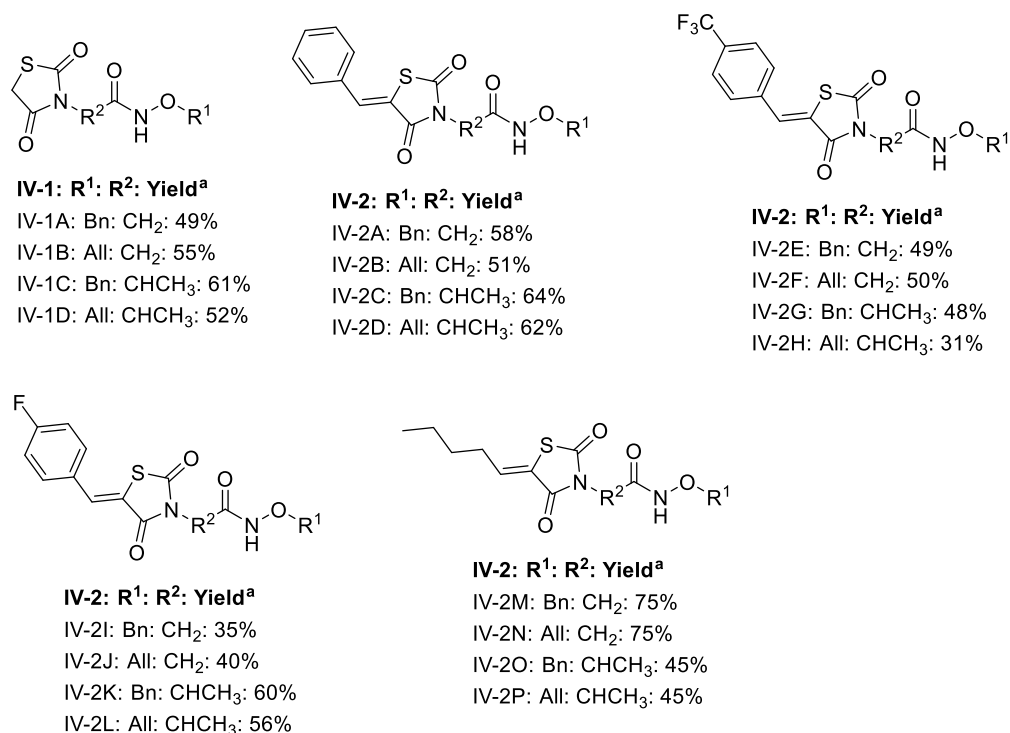


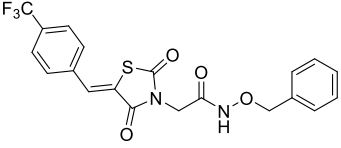
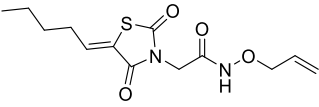
**Figure 17** Overview of obtained TZD-hydroxamates.

<sup>a</sup> Isolated yield.

### 4.1.2 Biological activity of TZD-hydroxamates

Finally, the chemical library was biologically tested (Table 2). The biological investigation started with *in silico* prediction of drug-likeness properties. Herein, software tools<sup>104</sup> identified all the TZD-hydroxamates to possess druggable behavior. Then the Zmp1 inhibition was analyzed by MALDI-TOF MS. All our compounds inhibited the enzymatic reaction and their inhibitory strength depended on the structure. Based on the experimental IC<sub>50</sub> values, TZD-hydroxamates **IV-2E** and **IV-2N** were revealed medium-efficient and high-efficient inhibitors, respectively. Furthermore, with a MIC value of 61.8 μM, conjugate **IV-2N** exhibited the best extracellular anti-*Mtb* potency. In contrast, **IV-2E** features unique 48.8% inhibition of intracellular *Mtb* H37Ra even at 10 μM concentration while **IV-2N** was active at the relatively high 100-μM concentration. To summarize the biological outcome, hybrid **IV-2N** was proved the most optimal anti-TB candidate based on the overall results including *in silico* predictions and enzymatic assays.

**Table 2** Biological characterization of the most potent TZD-hydroxamates

Entry	IC <sub>50</sub> (μM) <sup>a</sup>	MIC (μM) <sup>b</sup>	Percentage inhibition (%) <sup>c</sup>
 IV-2E	38	>64	48.8
 IV-2N	18	61.8	-

<sup>a</sup> Fifty percent Zmp1 inhibitory concentration. <sup>b</sup> Minimum inhibitory concentration against extracellular *Mtb* H37Ra. <sup>c</sup> Percentage inhibition of intracellular *Mtb* H37Ra at 10 μM concentration.

### 4.1.3 Design and synthesis of pyrrole/indole-hydroxamates

Encouraged by the promising results within our first series of TZD-hydroxamates, the improved hydroxamate-based Zmp1 inhibitors were proposed. Herein, we were inspired by *in silico* molecular docking combined with the best anti-TB candidate **IV-2N** obtained within the first series of TZD-hydroxamates (Table 2). Docking investigation of the first generation showed that the TZD-hydroxamates occupy just the entrance to the central cavity, located 7 Å apart from the Zn catalytic site. Therefore, longer peptide chains R<sup>2</sup> bearing a terminal ZBG were supposed to better reach the Zmp1 active site. Often reported as pan-assay interfering compounds (PAINS),<sup>105</sup> TZDs can complicate drug-like molecules development. For this reason, we tend to replace the central TZD with either pyrrole or indole moiety using scaffold hopping to propose hydroxamates **IV-9** or **IV-10**, respectively (Figure 18).<sup>106,107</sup> Considering the dipeptide motif R<sup>2</sup>, four readily accessible aliphatic amino acids were picked up for the initial anti-TB screening. Finally, the simplest methylene linker was selected to connect both the pharmacophores. Two lipophilic hydroxamates R<sup>1</sup> were maintained following the previous series of Zmp1 inhibitors.



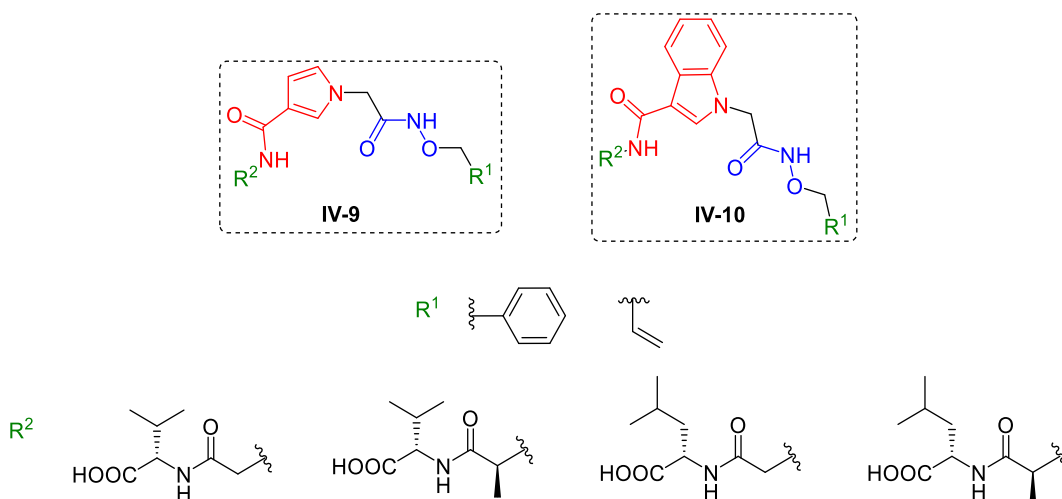
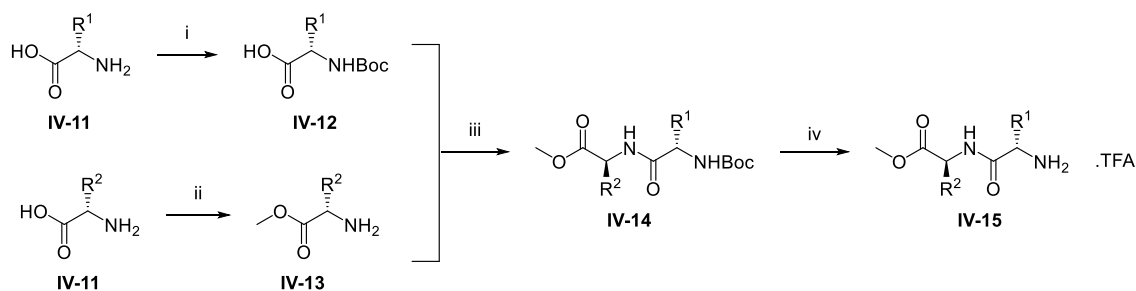


**Figure 18** Proposed structures of pyrrole/indole-hydroxamates.

Despite some structural similarity with TZD-hydroxamates, a notably different synthetic pathway toward pyrrole/indole-hydroxamates was needed (Schemes 11, 12). Our synthetic effort started with construction of dipeptide side chains (Scheme 11). Firstly, standard protecting groups were used for pre-modification of GLY/ALA and VAL/LEU **IV-11**.<sup>108,109</sup> Once protected, the pre-modified amino acids **IV-12** and **IV-13** underwent HOBt/EDC amide coupling to achieve *N*-Boc dipeptides **IV-14**. The dipeptide preparation was finished upon Boc removal and quantitatively provided four NH<sub>2</sub>-dipeptides **IV-15** as their trifluoroacetates.<sup>110</sup>

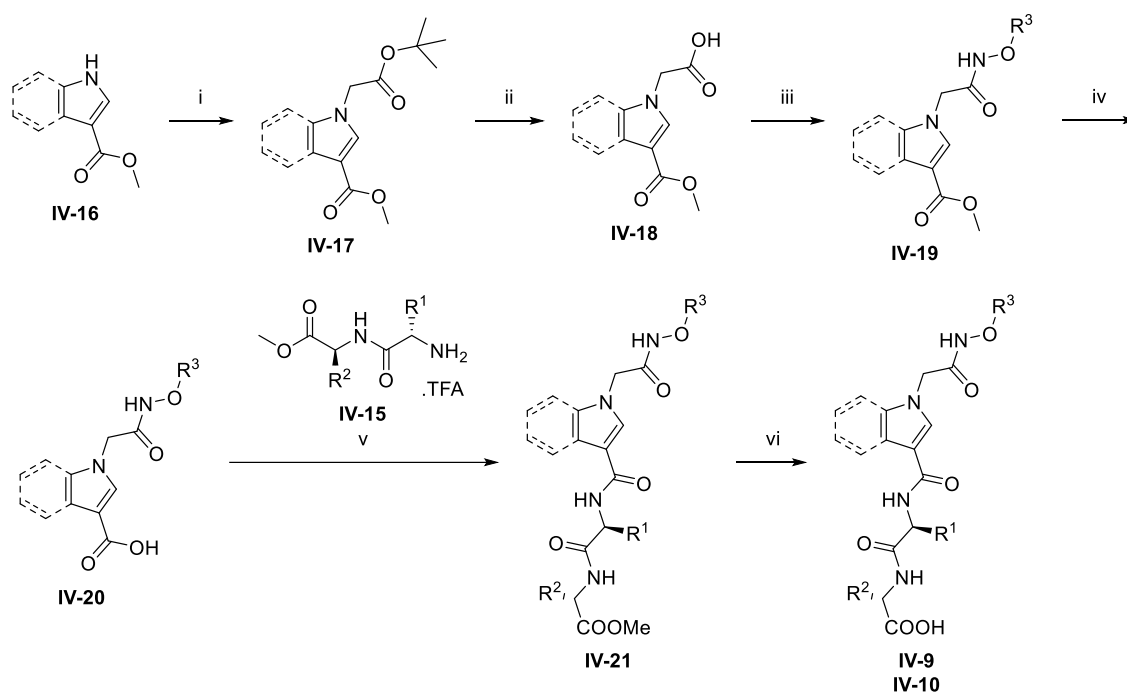


**Scheme 11** Synthesis of dipeptides.<sup>a</sup>

<sup>a</sup> Reagents and conditions: (i): Boc<sub>2</sub>O, NaOH, H<sub>2</sub>O/dioxane (1:1), rt, on (16 h); (ii): SOCl<sub>2</sub>, MeOH, 0 °C to reflux, 2 h; (iii): EDC.HCl, HOBt, DIPEA, CH<sub>2</sub>Cl<sub>2</sub>, 0 °C to rt, on (16 h); (iv): TFA, CH<sub>2</sub>Cl<sub>2</sub>, 0 °C to rt, 5 h.

The subsequent formation of heterocyclic cores proceeded smoothly (Scheme 12). Being commercially available, methyl pyrrole- or indole-3-carboxylates **IV-16** were chosen as starting materials. The reaction sequence started with their *N*-alkylation using *tert*-butyl bromoacetate. Selective *tert*-butyl removal from diesters **IV-17** provided intermediates

**IV-18** in an acidic environment. The desired heterocyclic hydroxamates **IV-19** resulted from coupling of intermediate acids **IV-18** with *O*-alkyl hydroxylamines hydrochlorides, and consequent basic methyl ester hydrolysis yielded the free acids **IV-20**. Achieved heterocyclic-hydroxamates **IV-20** were involved in following conjugation with pre-modified dipeptides **IV-15**. Unfortunately, the conjugation turned out to be the most complicated step within the whole sequence. Regardless of the well-proven HOBt/EDC technique,<sup>111</sup> quite complex mixtures were isolated, and their further purification often failed. Since all the esters **IV-21** were intermediates excluded from the biological investigation, no additional optimization was pursued. For this reason, slightly impure conjugates **IV-21** were excluded from the **Experimental part** and engaged in the final step without any further purification. Formation of the target pyrrole/indole-hydroxamates **IV-9** and **IV-10** was accomplished by base-mediated methyl ester cleavage. The synthetic procedure was finished by multiple co-distillation to eliminate residual solvents and H<sub>2</sub>O.



**Scheme 12** Synthesis of pyrrole/indole-hydroxamates.<sup>a</sup>

<sup>a</sup> Reagents and conditions: (i): K<sub>2</sub>CO<sub>3</sub>, *t*-butyl bromoacetate, MeCN, reflux, on (16 h); (ii): TFA, CH<sub>2</sub>Cl<sub>2</sub>, rt, 2 h; (iii): *O*-allylhydroxylamine.HCl/*O*-benzylhydroxylamine.HCl, EDC.HCl, H<sub>2</sub>O, rt, 2 h; (iv): 2 M aq. LiOH, THF, 60 °C, 2 h; (v): EDC.HCl, HOBt, DIPEA, DMF, rt, on (16 h); (vi): LiOH.H<sub>2</sub>O, H<sub>2</sub>O, MeOH, rt, 2 h.

Our synthetic protocol thus yielded two series of heterocyclic hydroxamates **IV-9** and **IV-10** (Figure 19). The desired pyrrole/indole-hydroxamates **IV-9** and **IV-10** were isolated in lower yields varying from 2 to 60 % over two steps (Figure 19). In this regards, pyrrole-hydroxamates **IV-10** behaved comparatively worse than their indole analogues **IV-9**. Mainly pyrrole-hydroxamate **IV-10B**, achieved in unsatisfactory 2% yield, turned out hard-to-handle. Due to a certain level of instability in solution, we were unable to remove residual impurities from the **IV-10B** sample. For the reason, compound **IV-10B** was not involved in biological assays.

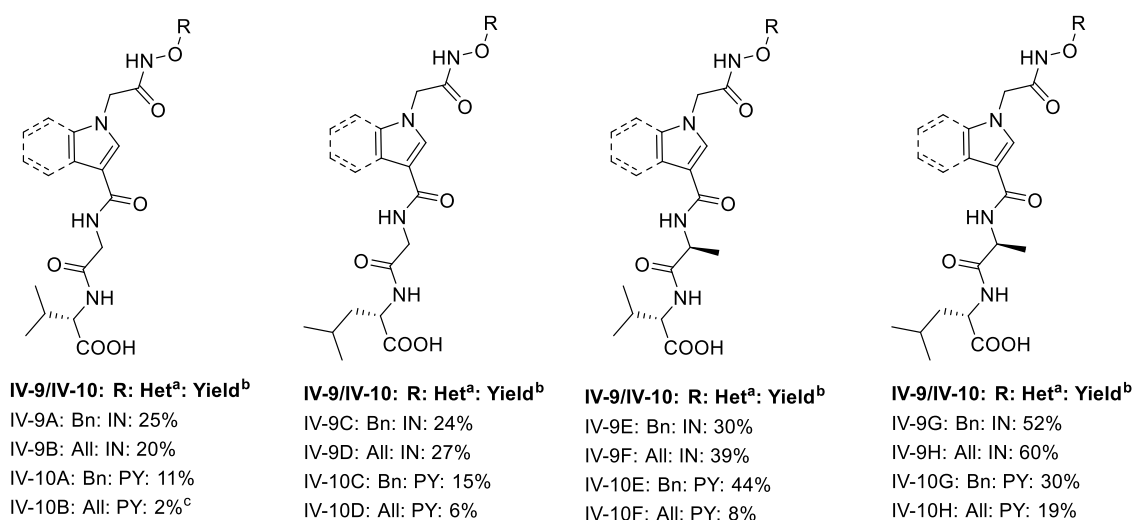


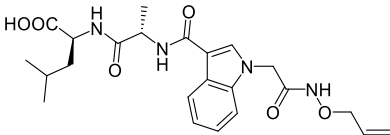
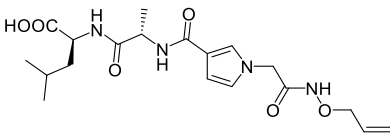
**Figure 19** Overview of obtained pyrrole/indole-hydroxamates.

<sup>a</sup> IN: indole; PY: pyrrole. <sup>b</sup> Isolated yields over 2 steps. <sup>c</sup> Residual impurities contained.

#### 4.1.4 Biological activity of pyrrole/indole-hydroxamates

All the pyrrole/indole-hydroxamates **IV-9** and **IV-10** are currently under biological investigation. Their Zmp1 inhibition was only analyzed by MALDI-TOF MS so far (Table 3). Considering the experimental IC<sub>50</sub> values, indole-hydroxamate **IV-9H** and pyrrole-hydroxamate **IV-10H** turned out similarly efficient inhibitors (IC<sub>50</sub> ≤ 20 μM) compared to the first generation of TZD-hydroxamates.

**Table 3** Zmp1 inhibition of the most potent pyrrole/indole-hydroxamates

Entry	IC <sub>50</sub> (μM) <sup>a</sup>
 IV-9H	20
 IV-10H	17

<sup>a</sup> Fifty percent Zmp1 inhibitory concentration.

### 4.1.5 Conclusive remark 1

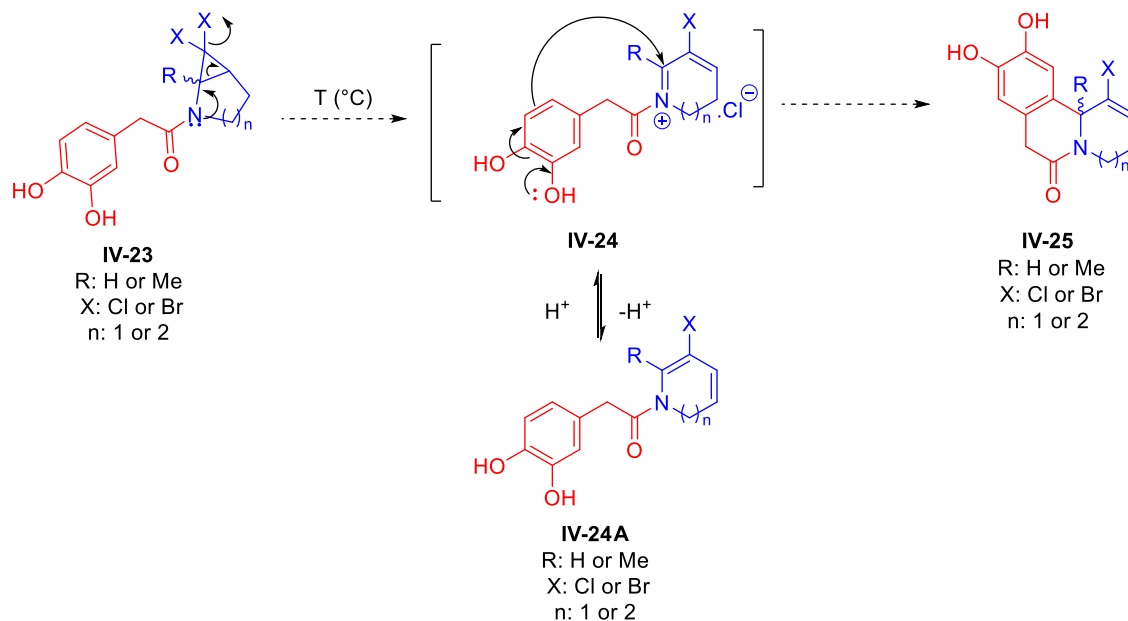
This chapter is dedicated to the design and synthesis of mycobacterial Zmp1 inhibitors. Encouraged by our initial promising results achieved with TZD-hydroxamates, our extended effort resulted in pyrrole/indole-hydroxamates analogues. Two different series of heterocyclic hydroxamates were thus successfully designed and synthesized and all the final products were provided for biological investigation, which indicated their notable micromolar Zmp1 inhibitory and promising anti-TB potency. Based on the abovementioned findings, further optimizations reflecting *in silico* studies can be the subject of future work.

## 4.2 Polycyclic MptpB inhibitors via *gem*-dihaloaminocyclopropanes

### 4.2.1 Proposed pathway toward *N*-fused polycycles

To extend the known reactivity of *gem*-dihaloaminocyclopropanes **IV-23**, we designed a general procedure based on their ring expansion and cyclization to prepare various functionalized *N*-fused tricyclic compounds **IV-25** (Scheme 13). Taking the preceding ring enlargement results reported by Six et al. as a starting point,<sup>48</sup> we proposed thermally mediated ring expansion of the starting *gem*-dihalocyclopropane amides **IV-23** to the corresponding dihydropyridinium or dihydroazepinium species **IV-24** to be the plausible first step (Scheme 18). Following the unsuccessful attempt for the direct cyclization, acid-mediated regeneration of the iminium **IV-24** from deprotonated intermediate

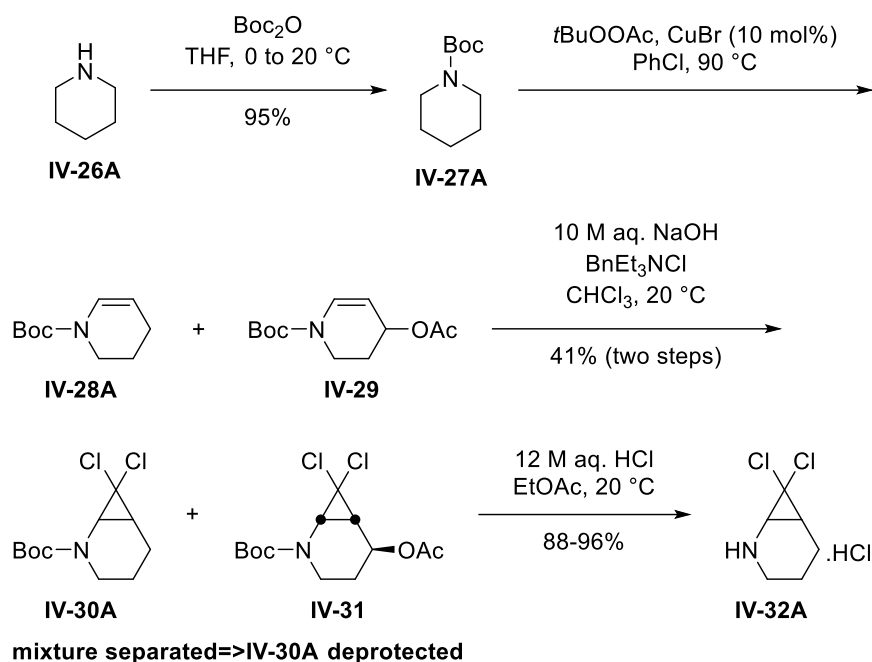
dihydroazepines and dihydropyridines was then supposed crucial for the successful key cyclization onto diverse electron-rich aromatic rings to achieve the desired functionalized *N*-fused tricyclic compounds **IV-25** (Scheme 13). Keeping the earlier reported uncontrolled iminium deprotonation under heating in mind, we intended to explore more promising potential of acid-mediated procedure.<sup>39</sup>



**Scheme 13** Strategy for the production of *N*-fused polycycles from *gem*-dihaloaminocyclopropanes.

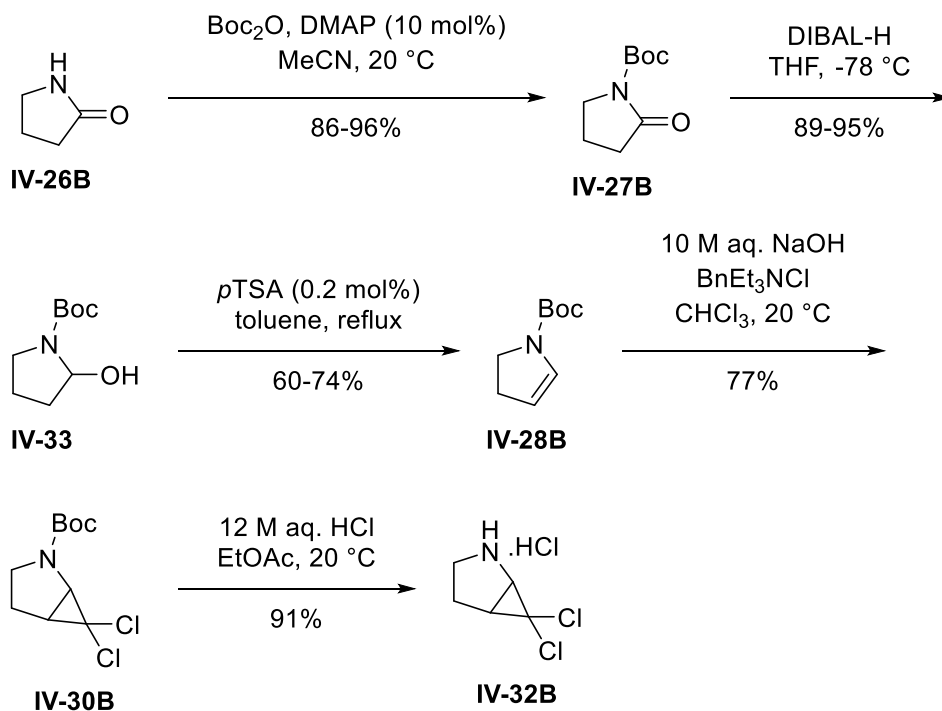
#### 4.2.2 Synthesis of starting *gem*-dihaloacyclopropane amides

Our initial synthetic effort was focused on the preparation of the key precursors: *gem*-dihaloacyclopropane amides **IV-23**. Inspired by the previous experience of Six et al.,<sup>48</sup> the acylation reaction between aminocyclopropane hydrochlorides **IV-32** and acyl chlorides **IV-34** was supposed to be the most feasible transformation to acquire the desired amide precursors **IV-23**. All the starting aminocyclopropane hydrochloride salts **IV-32** were synthesized according to the literature precedent.<sup>48</sup> Herein, two complementary synthetic approaches were employed. The first one, based on a Kharasch-Sosnovsky reaction, was applied onto *N*-Boc piperidine **IV-26A** leading to azabicyclo[4.1.0]heptane substrate **IV-32A** (Scheme 14).



**Scheme 14** A Kharash-Sosnovsky approach toward cyclopropylammonium salts.

The second one comprises functional group transformation from lactams **IV-26B** yielding azabicyclo[3.1.0]hexanes **IV-32B** (Scheme 15).

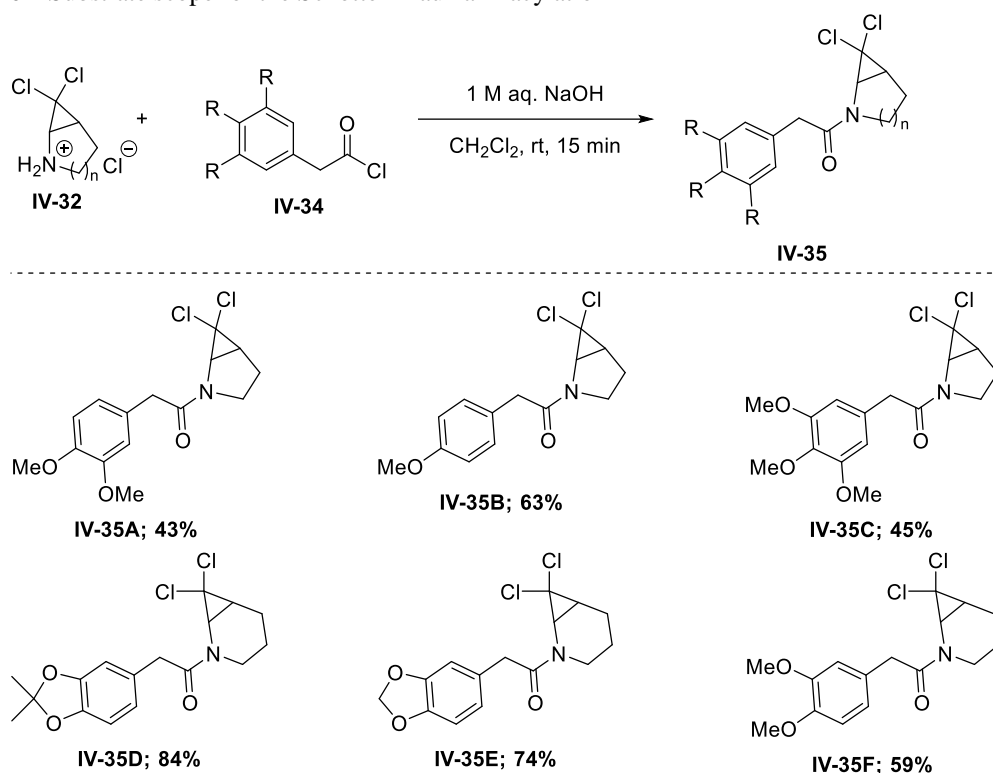


**Scheme 15** Functional group transformation toward cyclopropylammonium salts.

Additional starting compounds, acyl chlorides **IV-34** were obtained quite easily from the corresponding acids using standard chlorination protocols.<sup>112,113</sup> Both aforementioned

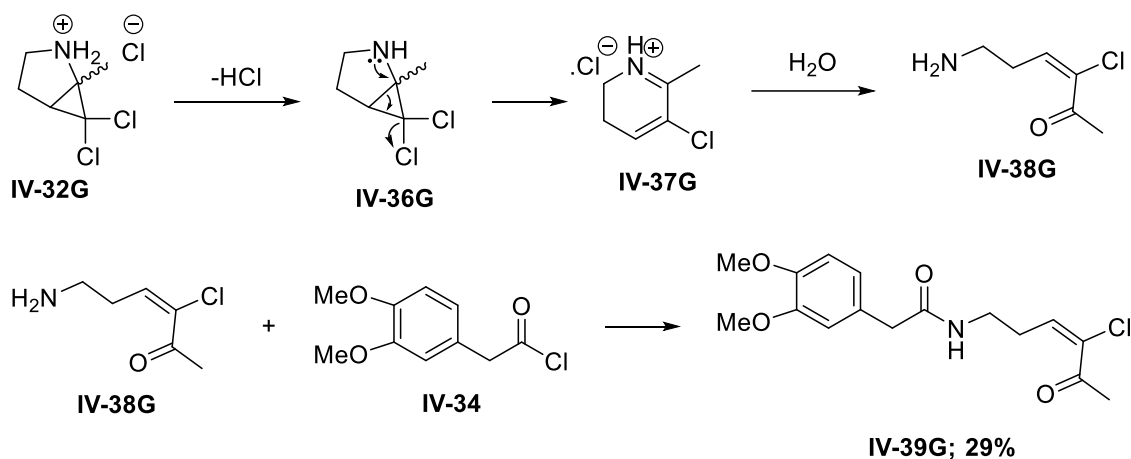
entities were then transformed into six desired cyclopropane amides **IV-35A-F** under Schotten-Baumann conditions and isolated in satisfactory yields ranging from 43 to 84 % (Table 4). Compared to the acylation conditions reported by Six et al., there was only minor optimization needed: the concentration of the reaction mixture was increased from 0.025 mol/L of aminocyclopropane hydrochloride **IV-32** in DCM up to 0.65 mol/L to speed up the acylation and prevent any unwanted hydrolytic side reactions and premature ring-opening.

**Table 4** Substrate scope for the Schotten-Baumann acylation<sup>a</sup>



<sup>a</sup> Reaction conditions correspond to the general procedure provided in the experimental section. Isolated yield.

However, following substrate scope extension to the methylated aminocyclopropane hydrochloride **IV-32G** brought complication related to a slower acylation rate caused by the presence of the methyl substituent. Since increased steric hindrance probably facilitated amine **IV-36G** ring-opening, the Schotten-Baumann acylation was notably compromised. For this reason, the free amine **IV-36G** did not undergo the expected conversion and yielded the corresponding ring-opened amide **IV-39G** (Scheme 16).

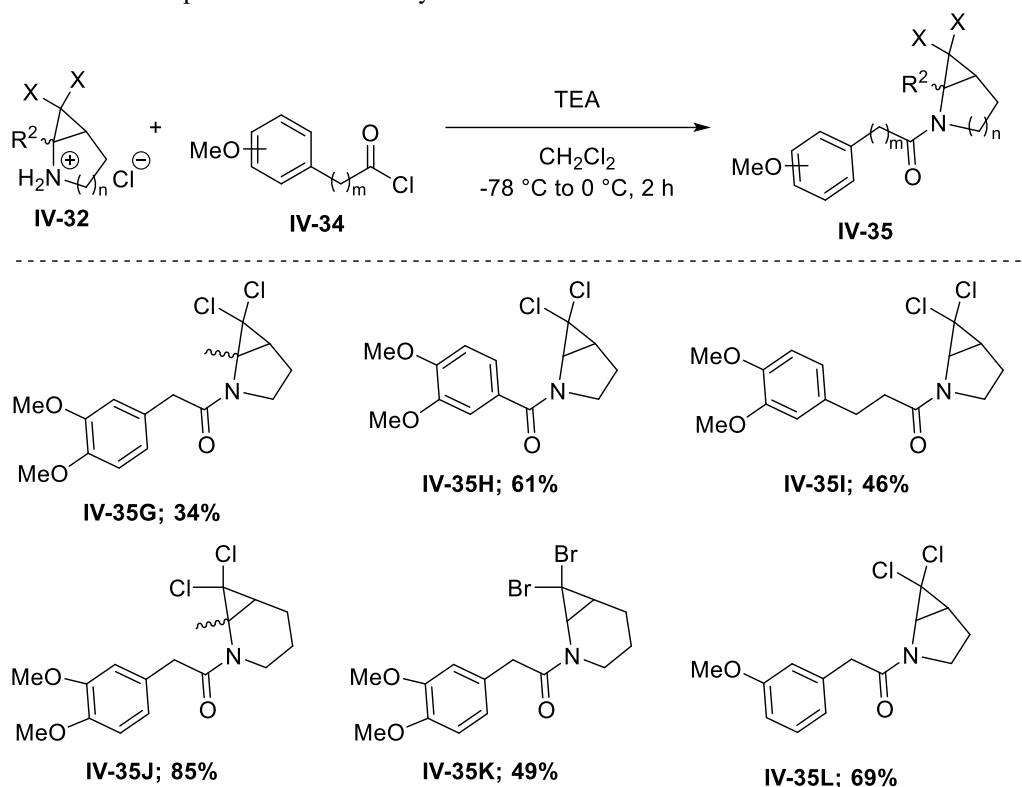


**Scheme 16** Plausible mechanism for the unexpected ring-opened ketone formation.

Therefore, more suitable acylation conditions were proposed and tested. To prevent the premature ring opening and subsequent hydrolysis, we decided to lower the reaction temperature and to exclude water potentially harmful in terms of an acyl chloride hydrolysis. Finally, 2.2 equiv of TEA were revealed optimal to liberate the amine and neutralize the released HCl. The reaction mixture was allowed to warm up gradually from  $-78$  to  $0$  °C to slow down the transformation. Indeed, improved acylation conditions were successfully applied to all the remaining aminocyclopropane hydrochlorides **IV-32G-L** and yielded six new *gem*-dihalocyclopropane amides **IV-35G-L** in a wide range of isolated yields varying from 27 to 85 % (Table 5).



**Table 5** Substrate scope for the modified acylation<sup>a</sup>



<sup>a</sup> Reaction conditions correspond to the general procedure provided in the experimental section. Isolated yield.

To summarize all the achievements reached within the synthesis of *gem*-dihaloaminocyclopropane amides, two acylation procedures were successfully developed. The first procedure involved Schotten-Baumann conditions and provided 6 novel amide precursors **IV-35A-F**, not yet reported in the literature, in lower to good isolated yields of 43-84 % (Table 4). Subsequently, anhydrous conditions used to suppress competing ring-opening of the free amines afforded lower to good isolated yields of six remaining *gem*-dihaloaminocyclopropanes **IV-35G-L** ranging from 27 to 85 % (Table 5).

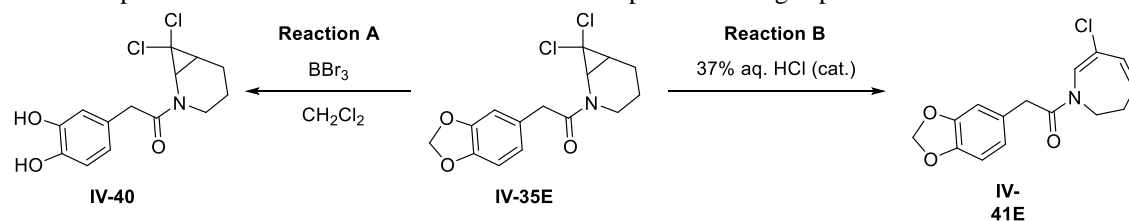
### 4.2.3 Deprotection and ring expansion of *gem*-dihalocyclopropane amides

The subsequent part of the studied reaction sequence involved deprotection and ring expansion of amides precursors to obtain dihydroazepines and dihydropyridines suitable for the final cyclization. Based on the different ring-size and reactivity of the expected

intermediates, this chapter is divided into dihydroazepine and dihydropyridine sections, respectively.

#### 4.2.3.1 Synthesis of dihydroazepines

Encouraged by preliminary results from the Six group, our initial investigation was focused on 6-membered amide precursors. Particularly, we started with finding the most appropriate amide precursor in terms of protecting group. Combining the commercial and synthetic availability, methylenedioxy-protected amide precursor **IV-35E** was chosen as a primary substrate. Firstly, we tried to deprotect the amide precursor **IV-35E** to release hydroxy groups. The resulting catechol derivative can be deprotonated to become more powerful nucleophiles and thus facilitate the final cyclization. To deprotect the substrate, common Lewis acidic conditions were applied (Table 6, Reaction A, Entry 1, 2).<sup>114</sup> Unfortunately, the deprotection of our dihalocyclopropane amide **IV-35E** completely failed (Table 6, Entry 1). Allowing the reaction mixture to warm to rt, TLC analysis showed at least low conversion to the deprotected amide **IV-40** (Table 6, Entry 2). Finally, the catechol **IV-40** was isolated only in negligible yield of 12 % and the amide precursor **IV-35E** was found out inappropriate for further investigation. To utilize the remaining protected amide **IV-35E**, we decided to test the acid catalyzed ring expansion (Table 6, Reaction B, Entry 3, 4). In accordance with analogous transformation of *endo*-monohalocyclopropanes reported by Six et al., verified acidic conditions were tried (Table 6, Entry 3). However, *gem*-dihaloaminocyclopropanes showed slower kinetic of the ring opening and we isolated dihydroazepine **IV-41E** in poor 11% yield with 52 % of **IV-35E** recovered. To drive the ring expansion forward, we switched to *o*-dichlorobenzene and elevated temperature of 180 °C with catalytic *tert*-butanol to reversibly trap the iminium intermediate to provide it more time to cyclise (Table 6, Entry 4). Indeed, the reaction outcome was improved up to 37 % of isolated dihydroazepine **IV-41E**. Our results thus clearly confirmed a temperature dependence of the ring enlargement.

**Table 6** Optimization of the reaction conditions for the deprotection/ring expansion of **IV-35E**<sup>a</sup>

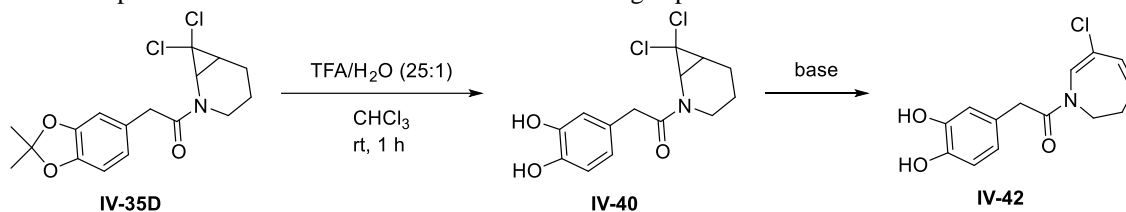
Entry	Reaction	Additive (equiv)	Solvent	T (°C)	Yield (%) <sup>b</sup>
1	A	-	$\text{CH}_2\text{Cl}_2$	0	-
2	A	-	$\text{CH}_2\text{Cl}_2$	0 to rt	12
3	B	-	DMF	150 (MW)	11
4	B	<i>t</i> -BuOH (cat.)	<i>o</i> - $\text{C}_6\text{H}_4\text{Cl}_2$	180 (MW)	40

<sup>a</sup> Reaction conditions A: **IV-35E** (0.23 mmol, 75 mg),  $\text{BBr}_3$ : 1.0 M in hexanes (0.34 mmol, 347  $\mu\text{L}$ ), solvent (0.5 mL), 6 h. Reaction conditions B: **IV-35E** (64.6  $\mu\text{mol}$ , 21 mg), solvent (1.0 mL), 30 min. <sup>b</sup> Isolated yield. The residual reaction mixture contained unreacted **IV-35E**.

Our initial results indicated that a more labile protecting group had to be employed. Therefore, we decided to continue our investigation with amide precursor **IV-35D** protected with a dimethylated methylenedioxy bridge (Table 7). Amide **IV-35D** was deprotected quite easily in acidic environment in accordance with a literature protocol<sup>115</sup> furnishing the free catechol **IV-40**. With the desired dihydroxy-substituted amide **IV-40** in hand, we moved on to the following ring expansion. Discouraged by the diminished reactivity observed under acid catalysis, we switched to basic conditions. We took advantage of the results described by Six et al. and started with catalytic collidine in chlorobenzene under microwave irradiation. However, LCMS analysis indicated only unsatisfactory 37% conversion to the product **IV-42** (Table 7, Entry 1). On the other hand, the reaction mixture heated to 180 °C in *o*-dichlorobenzene verified the aforementioned temperature dependence of the ring expansion and afforded 71% conversion of the deprotected amide **IV-40** to dihydroazepine **IV-42** (Table 7, Entry 2). Finally, increased amount of collidine then drove the reaction to completion (Table 7, Entry 3). Despite the full conversion, dihydroazepine **IV-42** was isolated in rather disappointing yield of 22 %. Herein, enhanced polarity of the dihydroxy-substituted product was suspected to complicate the isolation and notably compromise the overall yield. Neither the subsequent replacement of collidine with stronger base DBU was not useful and resulted in more

complex mixture including also the starting amide **IV-40** and the ring enlarged product **IV-42** (Table 7, Entry 4).

**Table 7** Optimization of the reaction conditions for the ring expansion of **IV-35D**<sup>a</sup>



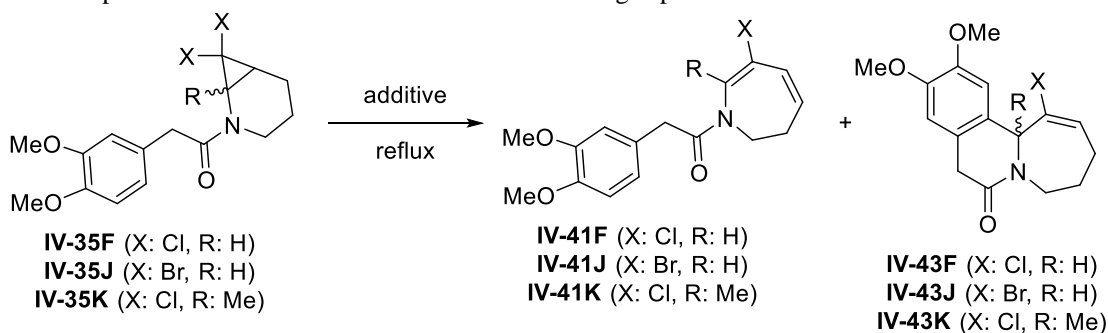
Entry	Base (equiv)	Solvent	T (°C)	Time (min)	Ratio of IV-40:IV-42 (%) <sup>b</sup>
1	2,4,6-collidine (cat.)	PhCl	150 (MW)	30	63:37
2	2,4,6-collidine (cat.)	<i>o</i> -C <sub>6</sub> H <sub>4</sub> Cl <sub>2</sub>	180 (MW)	15	29:71
<b>3</b>	<b>2,4,6-collidine (1)</b>	<b><i>o</i>-C<sub>6</sub>H<sub>4</sub>Cl<sub>2</sub></b>	<b>180 (MW)</b>	<b>15</b>	<b>0:100</b>
4	DBU (cat.)	<i>o</i> -C <sub>6</sub> H <sub>4</sub> Cl <sub>2</sub>	180 (MW)	15	59:41 <sup>c</sup>

<sup>a</sup> Reaction conditions: **IV-40** (0.23 mmol, 72 mg), solvent (1.0 mL). <sup>b</sup> Estimated from LC-MS at 210-500 nm. <sup>c</sup> Complex mixture observed.

Because of higher polarity of the ring enlarged catechol **IV-40** and resulting problematic isolation, we abandoned the deprotection and started to wonder whether the dimethoxy-substituted *gem*-dihalocyclopropane amides **IV-35F**, **J**, **K** (Table 8) may be a better alternative. Lone pairs-bearing methoxy substituents were hypothesized to retain the electron donating power while decreasing the overall polarity and thus make the isolation easier. To confirm our hypothesis, amide precursor **IV-35F** was tested as model substrate (Table 8). At the beginning, our initial experiment was settled under the conditions inspired by Craig et al. using excess K<sub>2</sub>CO<sub>3</sub> in refluxing toluene (Table 8, Entry 1).<sup>116</sup> Because of lacking reactivity and known temperature-dependence of the ring enlargement, we decided to use refluxing chlorobenzene instead (Table 8, Entry 2). There were traces of ring-opened dihydroazepine **IV-41F** formed with approximately 10% conversion estimated. For this reason, an even harsher procedure based on additive-free refluxing *o*-dichlorobenzene was tested (Table 8, Entry 3, 4). Surprisingly, we reached 64% and 98% transformation to 7-membered compound **IV-41F** after 30 minutes and one hour, respectively.

On the contrary, our next substrate, brominated *gem*-dihalocyclopropane amide **IV-35J**, reacted more readily. In accordance with the literature, hydrogen bromide was eliminated easier to trigger the ring expansion already in refluxing chlorobenzene to give brominated dihydroazepine **IV-41J** (Table 8, Entry 6). Despite such a feasible reactivity of brominated derivative **IV-35J**, the lower temperature of refluxing acetonitrile turned out insufficient to complete the reaction, compared to full conversion achieved in refluxing chlorobenzene (Table 8, Entry 5). Finally, methylated analogue **IV-35K** was the last example engaged. This amide precursor was the hardest to open, probably due to steric hindrance. Herein, no reaction proceeded neither in well-proven refluxing *o*-dichlorobenzene (Table 8, Entry 7). Stoichiometric silver salts are well-known to bind to halogen atoms and thus facilitate the carbon-halogen C-X bond cleavage.<sup>117</sup> Therefore, 2.0 equiv of silver salt AgBF<sub>4</sub> were added to access methylated dihydroazepine **IV-41K** (Table 8, Entry 8). More interestingly, the use of the silver salt also forced the subsequent cyclization leading to notable traces of polycyclic compound **IV-43K** present in the crude mixture. Such an unexpected activation of the dihydroazepine intermediate **IV-41K** was presumably caused *via* coordination of AgBF<sub>4</sub> to the halogen-substituted double bond or regeneration of the iminium intermediate mediated by a stronger acid HBF<sub>4</sub> formed during the transformation.

**Table 8** Optimization of the reaction conditions for the ring expansion of **IV-35F/J/K**<sup>a</sup>



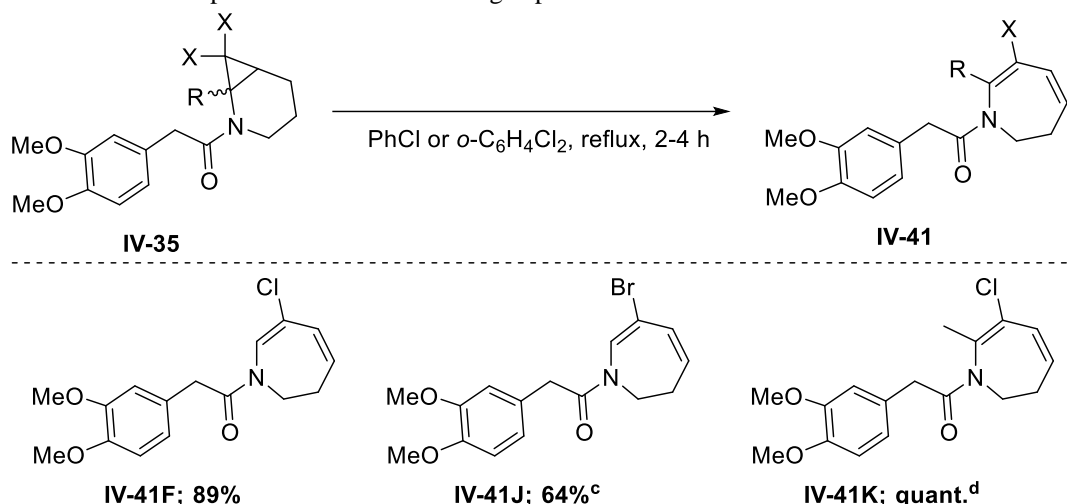
Entry	R	X	Solvent	Additive (equiv)	Time (h)	Ratio of IV-35:4-41:IV-43 (%) <sup>b</sup>
1	H	Cl	toluene	K <sub>2</sub> CO <sub>3</sub> (2)	ON	100:0:0
2	H	Cl	PhCl	K <sub>2</sub> CO <sub>3</sub> (2)	ON	90:10:0
3	H	Cl	<i>o</i> -C <sub>6</sub> H <sub>4</sub> Cl <sub>2</sub>	-	½	36:64:0

<b>4</b>	<b>H</b>	<b>Cl</b>	<i>o</i> -C <sub>6</sub> H <sub>4</sub> Cl <sub>2</sub>	-	<b>1</b>	<b>2:98:0</b>
5	H	Br	MeCN	-	2	100:0:0
<b>6</b>	<b>H</b>	<b>Br</b>	<b>PhCl</b>	-	<b>3</b>	<b>2:98:0</b>
7	Me	Cl	<i>o</i> -C <sub>6</sub> H <sub>4</sub> Cl <sub>2</sub>	-	2	100:0:0
<b>8</b>	<b>Me</b>	<b>Cl</b>	<i>o</i> -C <sub>6</sub> H <sub>4</sub> Cl <sub>2</sub>	<b>AgBF<sub>4</sub> (2)</b>	<b>4</b>	<b>9:45:46</b>

<sup>a</sup> Reaction conditions: **IV-35F/J/K** (0.12 mmol, 40 mg), solvent (0.5 mL), reflux. <sup>b</sup> Estimated from <sup>1</sup>H NMR.

Optimized conditions reached for each of the 6-membered amide precursors **IV-35F/J/K** enabled the synthesis of three corresponding dihydroazepines **IV-41F/J/K** (Table 9). Despite the harsh reaction conditions, all the 7-membered intermediates **IV-41F/J/K** were prepared in satisfactory yields ranging from 64% to quantitative and immediately consumed in following transformation without any further purification.

**Table 9** Substrate scope for the 6-membered ring expansion<sup>a</sup>



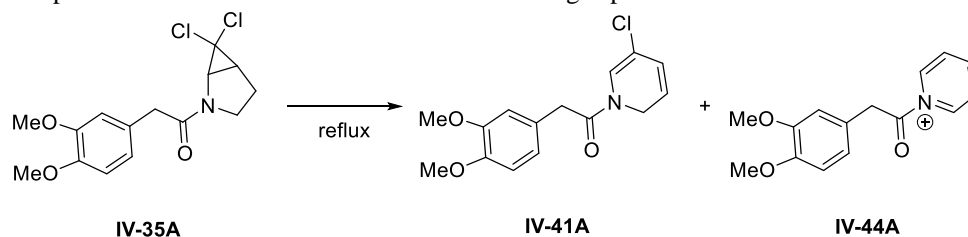
<sup>a</sup> Reaction conditions correspond to the general procedure detailed in the experimental section. Yield for crude product. <sup>b</sup> Mixture of **IV-41J** and unknown (probably regioisomeric) side product. <sup>c</sup> Mixture of **IV-41K** and cyclized compound in 50:50 ratio estimated by <sup>1</sup>H NMR. <sup>d</sup> AgBF<sub>4</sub> (2.0 equiv) used to access **IV-41K**.

#### 4.2.3.2 Synthesis of dihydropyridines

All the effort made on the ring expansion of 6-membered cyclopropane amides was subsequently extended to their 5-membered analogues. Their higher ring strain compared to the 6-membered compounds was expected to ease their ring enlargement into functionalized pyridines. Our experimental observation met such an expectation and the optimization procedure was more straightforward (Table 10). In accordance with our

experience in treating 6-membered amide precursors, we skipped the deprotection and started directly with methoxy-protected 5-membered amide **IV-35A** as a model substrate. Regarding the comparable behavior of 6-membered analogues, refluxing chlorobenzene stood for our first optimization attempt (Table 10, Entry 1). Since the reaction proceeded smoothly with 91% conversion to the desired dihydropyridine **IV-41A**, we wondered if milder conditions could provide the same reaction outcome. Therefore, the next experiment was carried out in refluxing toluene (Table 10, Entry 2). Despite the prolonged reaction time, slightly worse 83% ring opening was observed. Based on mechanistic considerations, we suspected polar solvents to speed up the reaction *via* stabilization of the developing positive charge in the transition state. For this reason, impact of refluxing acetonitrile was tested (Table 10, Entry 3, 4). In true, faster conversion was achieved. However, the overall reaction outcome differed notably in dependence on the fate of HCl released upon the cyclopropane cleavage. Once present in the reaction mixture, HCl forced the protonation of **IV-41A** and following HCl elimination resulting in 32% transformation into unexpected side-product **IV-44A** (Table 10, Entry 3). On the other hand, decent nitrogen flow enabled gaseous HCl to escape and afforded 95% transformation to the targeted dihydropyridine **IV-41A** within 30 minutes (Table 10, Entry 4).

**Table 10** Optimization of the reaction conditions for the ring expansion of **IV-35A**<sup>a</sup>

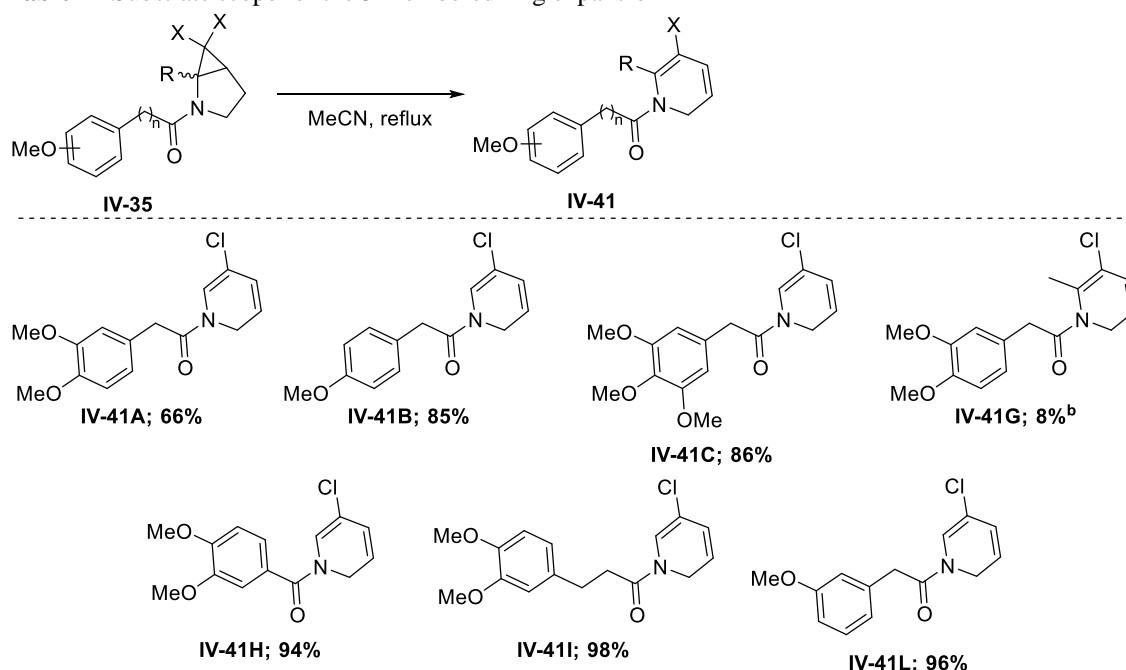


Entry	Solvent	Time (h)	Specific conditions	Ratio of IV-35A:IV-41A:IV-44A (%) <sup>b</sup>
1	PhCl	1	-	9:91:0
2	toluene	3	N <sub>2</sub> flow <sup>c</sup>	17:83:0
3	MeCN	¼	Sealed vial	23:45:32
4	MeCN	½	N <sub>2</sub> flow <sup>c</sup>	<b>5:95:0</b>

<sup>a</sup> Reaction conditions: **IV-35A** (0.12 mmol, 40 mg), solvent (2.0 mL), reflux. <sup>b</sup> Estimated from <sup>1</sup>H NMR. <sup>c</sup> Nitrogen flow at the top of the reflux condenser.

With optimized conditions developed, we set out to investigate the scope of the 5-membered ring enlargement (Table 11). The first substrate scope extension relied on the diversification of the aromatic substitution pattern. As a result, tri-, di- and mono-methoxylated derivatives **IV-41A/B/C/L** were successfully obtained in satisfactory 66-96% yields based on the weight of the crude products. Varying the length of the linker between the aromatic and cyclopropane-containing units was the following objective pursued. Herein, the ring enlargement of the corresponding amide **IV-35H** and **IV-35I** proceeded almost quantitatively. The last example included ring opening of methyl-substituted compound **IV-35G**. In analogy with the methylated 6-membered *gem*-dihalocyclopropane amide **IV-35K**, steric hindrance made the ring expansion more difficult again. For this reason, increased temperature of refluxing chlorobenzene was needed to trigger the transformation. The resulting complexity of the crude product made further purification inevitable affording a poor 8% isolated yield of the intermediate dihydropyridine **IV-41G**. Therefore, the particular transformation requires additional optimization.

**Table 11** Substrate scope for the 5-membered ring expansion<sup>a</sup>



<sup>a</sup> Reaction conditions correspond to the general procedure detailed in the experimental section. Yield based on the weight of the crude product. <sup>b</sup> Isolated yield.

After an extensive study of reactivity within three differently protected 6-membered amide precursors, we found suitable conditions for their deprotection as well as the



following ring expansion. Regarding the deprotection, methylated methylenedioxy-protected amide **IV-35D** turned out the most appropriate substrate and delivered a quantitative yield of the deprotected catechol **IV-40** in acidic environment. However, subsequent base-mediated ring enlargement proved fruitless, probably due to polarity-related isolation issues. On the other hand, more straightforward ring enlargement pathway from dimethoxy-protected amides furnished all the proposed dimethoxy-substituted dihydroazepines and dihydropyridines **IV-41** in good to quantitative yields. Despite a little bit diverse reactivity within the series of 6-membered amides, elevated temperature was revealed universal to induce ring opening across the whole spectrum of studied *gem*-dihalocyclopropane amides.

#### 4.2.4 Acid-mediated cyclization to final polycycles

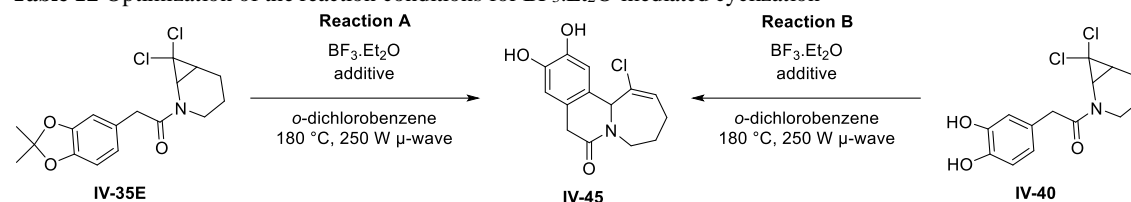
To accomplish the proposed synthetic pathway and deliver *N*-fused polycycles as potential MptpB inhibitors, cyclization of ring-enlarged intermediates was the final transformation to pursue. Following all the results of the preceding ring expansion experiments, we tested one-pot procedures on deprotected amide precursors as well as tandem ring enlargement/cyclization sequences on dimethoxy-substituted dihalocyclopropanes, which is reflected also in the division of this chapter.

##### 4.2.4.1 One-pot procedure toward catechol-containing polycycles

The compromised isolation of catechol-containing dihydroazepines (Chapter 4.2.3.1) excited our interest in a one-pot procedure to improve the overall reaction outcome (Table 12, Reaction A, Entry 1, 2). Based on the relevant literature, Lewis acid  $\text{BF}_3 \cdot \text{Et}_2\text{O}$  was expected to remove the protecting group as well as, perhaps, force the final cyclization *via* the formation of a dioxaborole intermediate. For this reason,  $\text{BF}_3 \cdot \text{Et}_2\text{O}$  was the reagent of choice for such a one-pot procedure. Moreover, addition of 2,4,6-collidine was supposed useful to neutralize HCl released during the ring opening and thus prevent hydrolysis of the dioxaborole intermediate. On small scale (0.20 mmol), these reagents completed all the cyclization sequence, however, with rather low 30% isolated yield (Table 12, Entry 1). On somewhat larger scale (0.33 mmol), the crude mixture still contained 44 % of the unreacted protected amide precursor **IV-35E** and the cyclized product was isolated only in moderate 36% yield (Table 12, Entry 2). To eliminate any deprotection issues, we decided for stepwise approach from catechol species **IV-40**

(Table 12, Reaction B, Entry 3, 4). Herein, the initial base-free cyclization experiment disproved our primary acidic hydrolysis-related hypothesis and afforded similar level of cyclization compared to analogous base-mediated reactions (Table 12, Entry 3). Oppositely, slightly higher isolated yield of 39 % indicated acidic environment more appropriate to avoid a formation of unwanted salts and ease the isolation of the desired polycycle **IV-45**. The last control experiment with equimolar H<sub>3</sub>BO<sub>3</sub> additive and comparatively lower amount of Lewis acid confirmed the presumed dioxaborole formation giving almost identical crude mixture as in both previous cases (Table 12, Entry 4). On the other hand, the isolated yield of cyclized product **IV-45** again dropped to 31 %.

**Table 12** Optimization of the reaction conditions for BF<sub>3</sub>.Et<sub>2</sub>O-mediated cyclization<sup>a,b,c</sup>



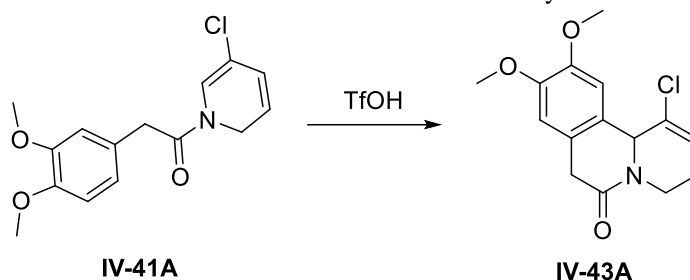
Entry	Reaction	Additive (equiv)	BF <sub>3</sub> .Et <sub>2</sub> O (equiv)	Time (min)	Ratio of	Yield of
					IV- 35E:IV- 40:IV-45 <sup>d</sup>	IV-45 (IV-40) (%) <sup>e</sup>
1 <sup>a</sup>	A	2,4,6-collidine (1)	1	30	0:0:100	30
2 <sup>b</sup>	A	2,4,6-collidine (1)	1	40	44:0:56	36 (28)
3 <sup>c</sup>	B	-	2.50	2 × 30	0:49:51	39 (37)
4 <sup>c</sup>	B	H <sub>3</sub> BO <sub>3</sub> (1.25)	1.25	2 × 30	0:54:46	29 (25)

<sup>a</sup> Reaction conditions: **IV-35E** (0.20 mmol, 71 mg), *o*-dichlorobenzene (1.5 mL), MW: 180 °C. <sup>b</sup> Reaction conditions: **IV-35E** (0.33 mmol, 118 mg), *o*-dichlorobenzene (1.0 mL), MW: 180 °C. <sup>c</sup> Reaction conditions: **IV-40** (0.16 mmol, 50 mg), *o*-dichlorobenzene (1.0 mL), MW: 180 °C. <sup>d</sup> Estimated by <sup>1</sup>H NMR. <sup>e</sup> Isolated yield.

All of our cyclization effort toward catechol polycycles **IV-45** thus brought numerous complications and unsatisfactory results. To overcome such a difficulty, we decided to follow successful ring expansion of dimethoxy-protected ring enlarged species. In this context, we took an inspiration from Sánchez et al.<sup>39</sup> and chose super acidic TfOH to

regenerate the iminium and accomplish the desired cyclization. At the beginning, 30% isolated yield of the polycycle **IV-43A** was obtained after 30 min using catalytic TfOH in microwave-irradiated (100 °C) dichlorobenzene (Table 13, Entry 1). Chasing as mild and efficient conditions as possible, we continued with conventional heating at 90 °C in toluene (Table 13, Entry 2). After prolonged reaction time of 3 h, these conditions improved the isolated yield up to 53 %. Contrarily, polar solvents such as MeCN were revealed inappropriate leading to more complex mixture and thus lowering the isolated yield to 25 % (Table 13, Entry 3). Finally, the best conditions found (see Table 13, Entry 2) were used to scale up the cyclization procedure (Table 13, Entry 4). Unfortunately, we faced up an unexpectedly diminished reactivity reflected in dominant side products. After an additional effort, stoichiometric TfOH was proved inevitable for smooth transformation to the polycycle **IV-43A** in 49% isolated yield (Table 13, Entry 5).

**Table 13** Optimization of the reaction conditions for TfOH-mediated cyclization<sup>a,b</sup>



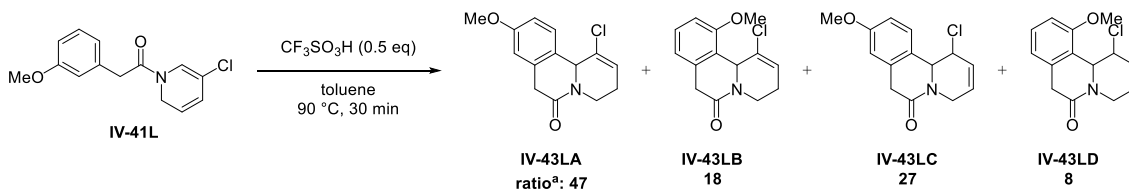
Entry	TfOH (equiv)	Solvent	T (°C)	Time (h)	Yield of IV-43A (%) <sup>c</sup>
1 <sup>a</sup>	Cat.	PhCl	MW: 100	½	30
2 <sup>a</sup>	Cat.	toluene	90	3	53
3 <sup>a</sup>	Cat.	MeCN	RT	1	25 <sup>d</sup>
4 <sup>b</sup>	Cat.	toluene	90	¾	- <sup>d</sup>
<b>5<sup>b</sup></b>	<b>0.50</b>	<b>toluene</b>	<b>90</b>	¾	<b>49</b>

<sup>a</sup> Reaction conditions: **IV-41A** (0.10 mmol, 30 mg), solvent (0.5 mL). <sup>b</sup> Reaction conditions: **IV-41A** (0.34 mmol, 100 mg), solvent (3.0 mL). <sup>c</sup> Isolated yield. <sup>d</sup> Complex mixture obtained.

Once arrived at the optimized conditions, we set out to develop the scope and limitations of the TfOH-mediated cyclization (Table 14). Our first achievement included the cyclization of dimethoxy-substituted model substrates **IV-41A/F** to synthesize polycycles of tetrahydropyridine **IV-43A** and tetrahydroazepine **IV-43F** type in moderate 49% and

44% yield, respectively. Herein, the reaction outcome clearly reflected the different ring expansion rate associated with varying ring strain of the corresponding 5- or 6-membered amide precursors.

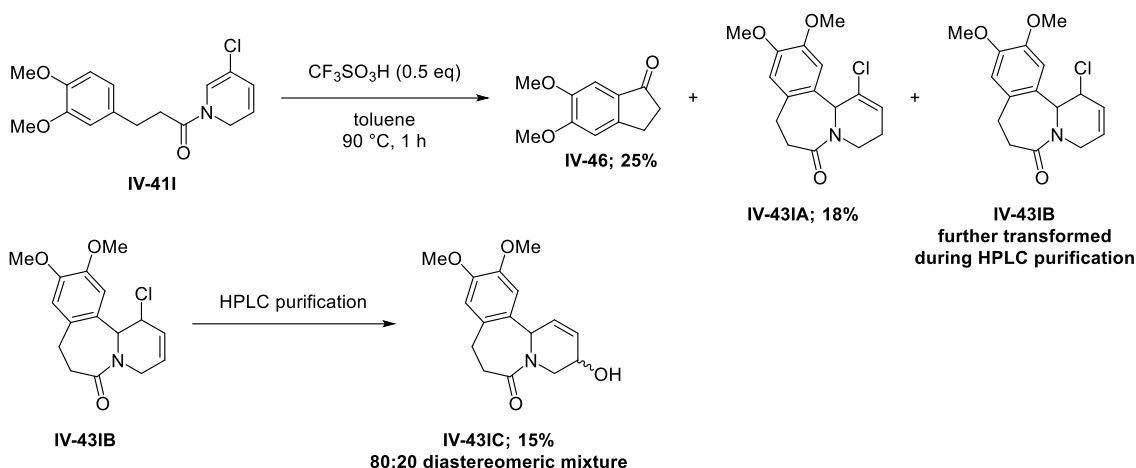
Next, we explored an influence of the aromatic substitution pattern. Electron rich trimethoxy-containing dihydropyridine cyclized readily giving 52% yield of the desired polycycle **IV-43C**. Subsequently, electron poorer *m*-monomethoxy-substituted analogue was employed. Its lower reactivity enabled numerous competitive isomerization processes resulting in a complex <sup>1</sup>H NMR spectrum of the crude product containing 2 regioisomers **IV-43LA** and **IV-43LB**, as well as their 2 counterparts **IV-43LC** and **IV-43LD** with translocated double bond in 47:18:27:8 ratio, respectively (Scheme 17). However, only the unexpected isomer **IV-43LC** was isolated in appropriate purity for structural confirmation and full characterization. Comparatively, *p*-monomethoxy-substituted analogue failed to cyclize at all, and the complexity of the resulting mixture clearly indicates that the presence of a *m*-EDG is essential for the cyclization.



**Scheme 17** Unexpected isomerisation observed upon cyclization of **IV-41L**

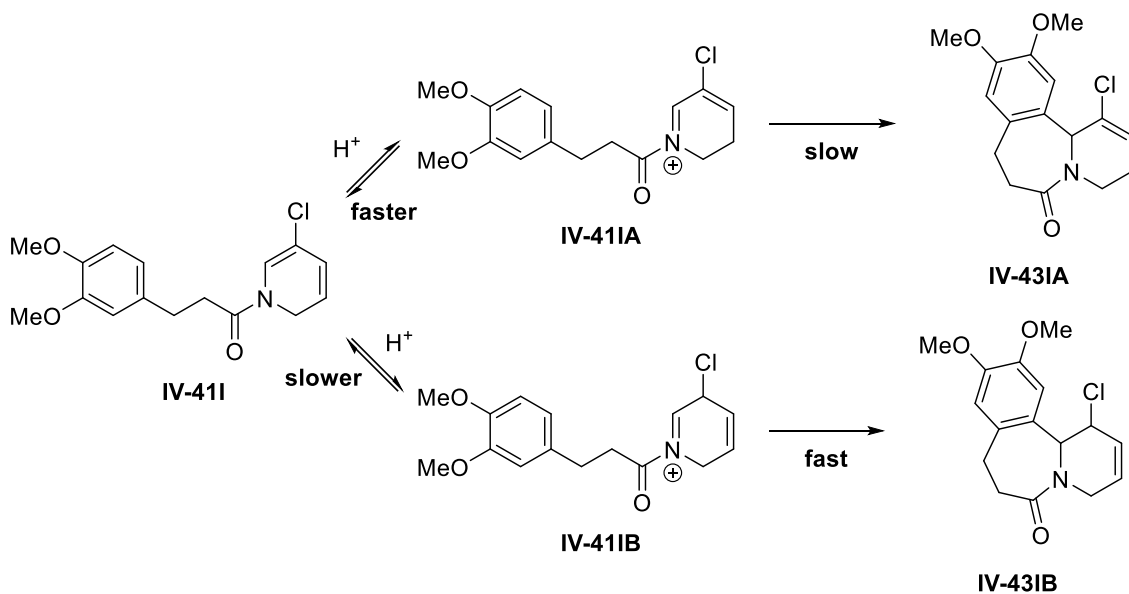
<sup>a</sup> Estimated from <sup>1</sup>H NMR.

To further extend the substrate scope, we varied the size of the middle ring. For this reason, we used dihydropyridine precursors with modified linkers. Herein, homologue **IV-41I** having a longer chain reacted smoothly, however, yielded a mixture of three products (Scheme 18).



**Scheme 18** Unexpected transformations observed upon cyclization of **IV-41I**.

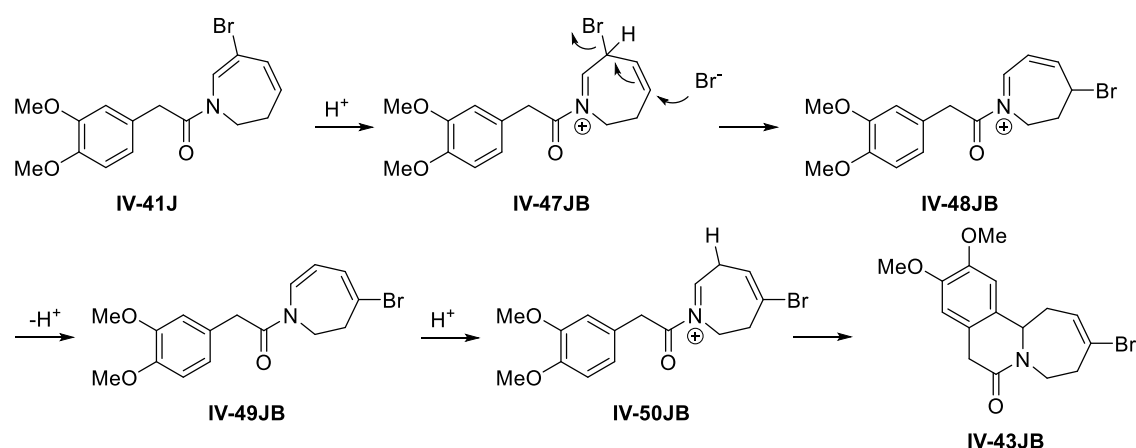
Outside the desired cyclized compound **IV-43IB**, we were also faced with 2,3-dihydro-1*H*-inden-1-one **IV-46** formation. The third compound was probably the isomer **IV-43IB** with a differently located double bond. Firstly, the protonation of **IV-41I** can provide two possible carbocations (Scheme 19). Secondly, the first carbocation **IV-41IA** which leads to the expected polycycle **IV-43IA**, is more stable and easier to form, however, less reactive. On the other hand, the second carbocation **IV-41IB**, providing the surprising polycycle **IV-43IB**, is more difficult to access but more reactive. Subsequently, unstable isomer **IV-43IB** underwent further transformation upon HPLC purification leading to the nucleophilic substitution product **IV-43IC** isolated as an 80:20 diastereomeric mixture.



**Scheme 19** Formation of two possible carbocations.

On the other hand, the shorter-linked homologue reacted rapidly, but its susceptibility to decomposition resulted in a complex crude mixture. For this reason, *N*-fused polycycle **IV-43H** was isolated in slightly lower quality and quantity so far. Therefore, further optimizations, perhaps lowering the temperature and/or concentration of the reaction solution, remain inevitable. The last substrate proposed for the cyclization toward tetrahydropyridine-based *N*-fused polycycles was a methylated analogue. Unfortunately, sterically demanding preceding ring enlargement gave the intermediate dihydropyridine in unsatisfactory quantity of 58.5  $\mu\text{mol}$ . Despite of such a low quantity, the final cyclization proceeded in an acceptable way, however, affording a mixture of the desired polycycle **IV-43G** and its double bond-shifted isomer, that we were not able to separate.

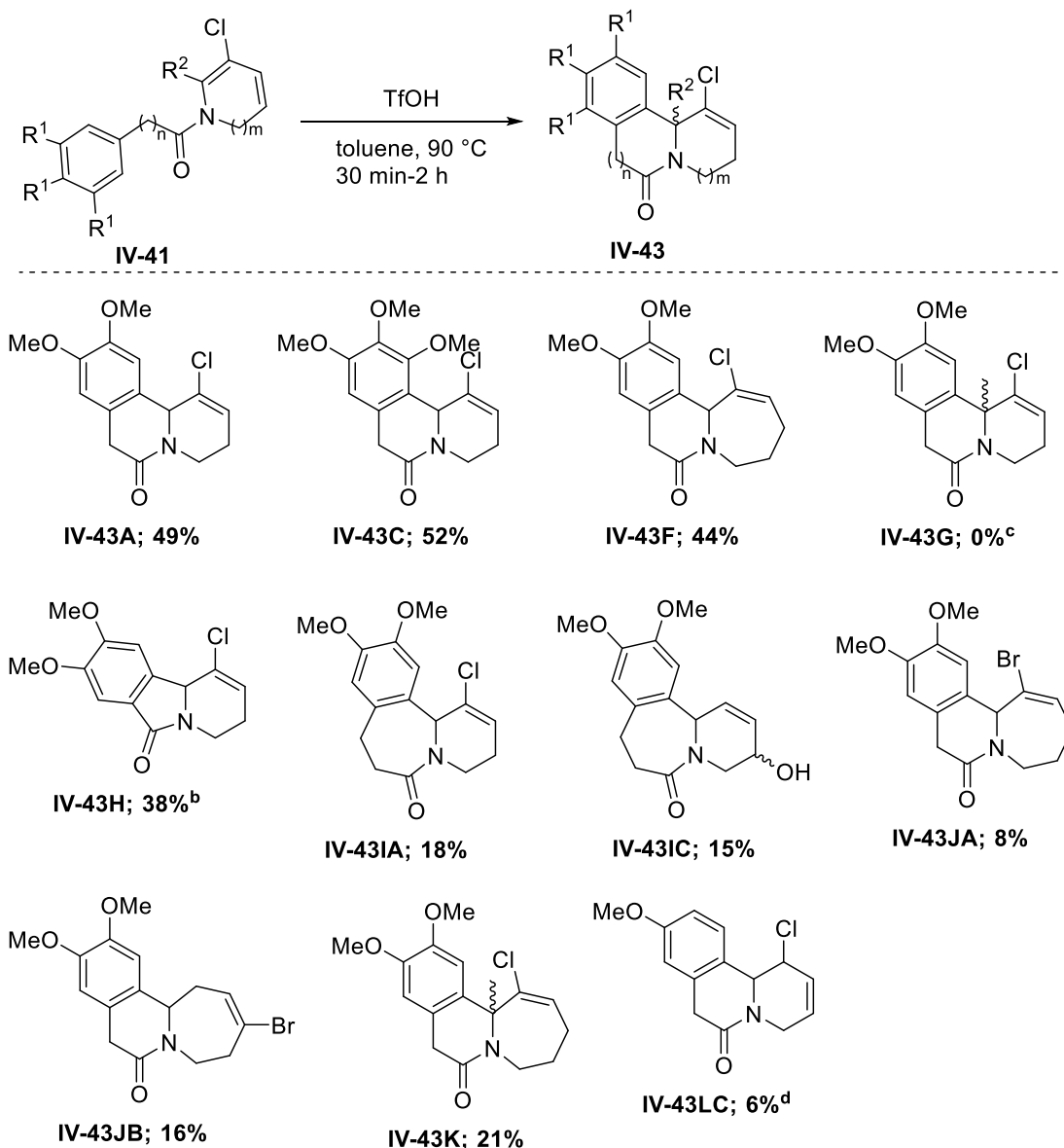
Regarding dihydroazepine intermediates, brominated analogue **IV-41J** underwent less selective cyclization and afforded even two regioisomeric polycycles **IV-43JA** and **IV-43JB** in correspondingly decreased yield of 8 % and 16 %, respectively. To account for the unexpected polycycle **IV-43JB**, we suppose a mechanistic pathway as follows (Scheme 20). After an initial iminium regeneration, a bromide anion as a soft nucleophile attacks the resulting allylic bromide moiety according to an  $\text{S}_{\text{N}}2'$  process. The intermediate regioisomeric iminium **IV-48JB** then rearranges to the iminium species **IV-50JB**, to eventually form the final brominated regioisomer **IV-43JB**.



**Scheme 20** Plausible mechanism for the unexpected brominated polycycle **IV-43JB** formation.

Opposingly, the corresponding methylated dihydroazepine cyclized smoothly giving the final tricycle **IV-43K** in 21% yield lowered by the sterically demanding preceding reaction step.

**Table 14** Substrate scope for the TfOH-mediated cyclization<sup>a</sup>



<sup>a</sup> Reaction conditions correspond to the general procedure detailed in the experimental section. Isolated yields over two steps. <sup>b</sup> Residual impurities contained. <sup>c</sup> Entirely remained in mixture with its double bond-shifted isomer impossible to separate. <sup>d</sup> Partly remained in mixture with its isomers impossible to separate.

To summarize the cyclization studies, our initial Lewis acid-mediated one-pot procedure toward catechol-containing polycycle **IV-45** brought unsatisfactory results in terms of reproducibility and an overall reaction outcome. Such complications were assigned to incomplete deprotection step and plausible formation of undesirable salts during the workup, respectively. On the other hand, additional effort on dimethoxy-substituted intermediate dihydroazepines and dihydropyridines **IV-41** yielded more satisfactory results. Following substrate scope exploration of TfOH-mediated cyclization resulted in a series of 10 *N*-fused polycycles **IV-43** as novel potential MptpB inhibitors in variable

isolated yields ranging from 6 to 52 %. Among them, three unexpected isomers were produced due to wide structural variation leading to diverse reactivity within the whole series.

#### **4.2.5 Conclusive remark 2**

This chapter describes a straightforward tandem ring expansion/cyclization pathway from *gem*-dihaloaminocyclopropanes toward novel *N*-fused polycycles as potential mycobacterial virulence factor MptpB inhibitors. Wide structural diversity and unexpected reactivity of the prepared *gem*-dihaloaminocyclopropanes furnished ten novel *N*-fused tricycles and, additionally, several isomerized counterparts. We thus extended the synthetic utility of dihalocyclopropanes in terms of cyclization and accessed unprecedented halogenated polycycles in a straightforward manner. Finally, antitubercular potential of all the achieved polycycles is currently under biological investigation.

### **4.3 2-Aminobenzoxazoles preparation for mycobacterial ATP synthase inhibitors<sup>1</sup>**

#### **4.3.1 Design of squaramide-based ATP synthase inhibitors and proposed pathway toward 2-aminobenzoxazoles**

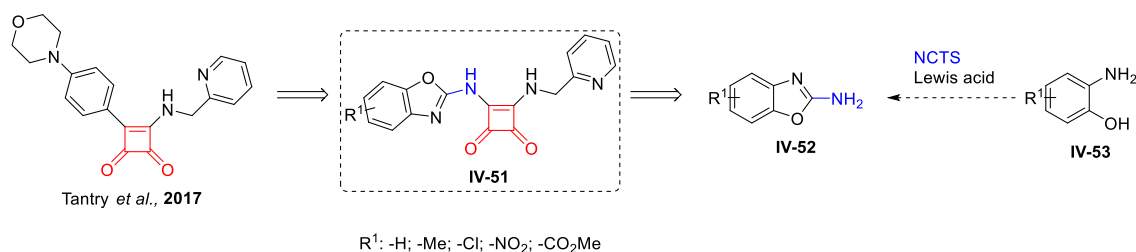
Our following approach toward novel anti-TB compounds consisted of mycobacterial ATP synthase inhibition. In this context, Tantry et al. published a very informative paper on squaramide-mediated inhibition of mycobacterial ATP-synthesis, which became an invaluable source of inspiration for the whole project.<sup>63</sup> Inspired by Tantry et al., numerous modified squaramides **IV-51** were designed (Scheme 21). To summarize the main idea behind the whole squaramide-based chemical library, a wide variety of aromatic, aliphatic and heterocyclic substituents attached *via* amine linker to the squaramide core were predicted to offer extended possibilities of free rotation and H-bonding, reinforcing their ATP synthase binding mode. Moreover, benzoxazole-

---

<sup>1</sup> As the main topic of his bachelor thesis, the synthesis of squaramides was performed by Jan Chasak (Chasak, J. **2020**, *Synthesis of novel squaramides as potent mycobacterial ATP synthase inhibitors*, UPOL, Olomouc).

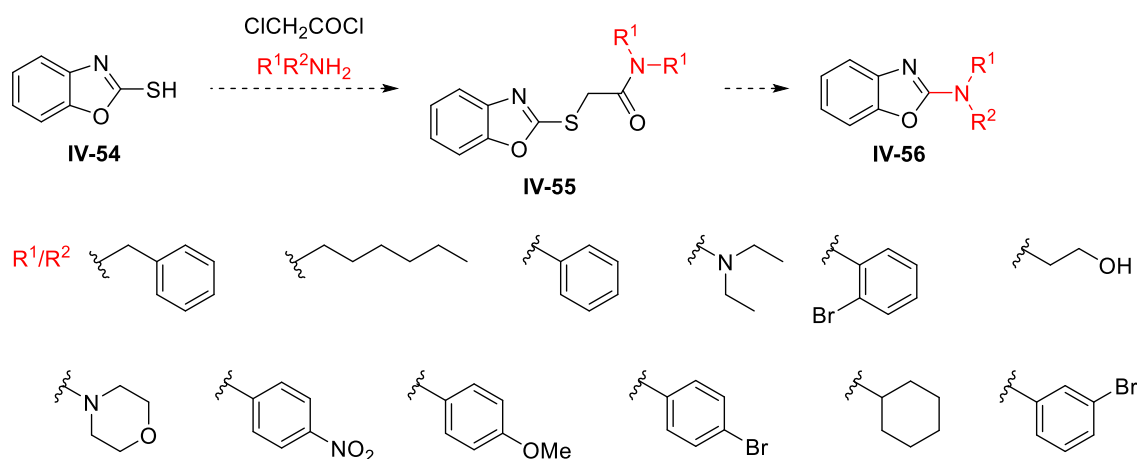


containing squaramides **IV-51** exhibited better binding energy than  $-7.7$  kcal/mol measured for the parent compound arising from *in silico* molecular docking to mycobacterial ATP synthase (Scheme 21). To synthesize all the proposed benzoxazole-squaramides, we needed a straightforward pathway to various 2-aminobenzoxazoles **IV-52** as privileged building blocks. Taking inspiration from the relevant precedent in literature,<sup>118,119</sup> the plausible synthetic strategy toward 2-aminobenzoxazoles **IV-52** was based on a reaction between substituted *o*-aminophenols **IV-53** and NCTS as a beneficial nonhazardous electrophilic cyanating agent under Lewis acid catalysis (Scheme 20).<sup>120</sup>



**Scheme 21** Design and plausible access toward aminobenzoxazole-containing ATP synthase inhibitors.

Additionally, a complementary synthetic approach to their *N*-substituted counterparts was suggested (Scheme 22). The Smiles rearrangement, an intramolecular nucleophilic aromatic substitution reaction, has received our attention to achieve the desired *N*-substituted analogues. In 2011, Zuo et al. published an inspiring synthesis of *N*-aryl-2-aminobenzoxazoles from substituted benzoxazole-2-thiol and *in situ* formed 2-chloro-*N*-arylacetamides in a Cs<sub>2</sub>CO<sub>3</sub>-DMF system. However, it was limited only to aromatic substrates.<sup>121</sup> Such a capability of the Smiles rearrangement combined with economic precursor benzoxazole-2-thiol **IV-54** enabled us to predict its functionalization by different amines upon chloroacetyl chloride-mediated activation to reach various *N*-derivatized benzoxazoles **IV-56** (Scheme 22).<sup>120</sup>

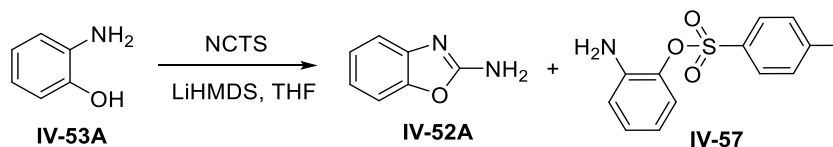


**Scheme 22** Proposed approach to *N*-substituted aminobenzoxazoles via Smiles rearrangement.

### 4.3.2 NCTS-mediated cyclization to 2-aminobenzoxazoles

Our first intention consisted of using *N*-cyano-*N*-phenyl-*p*-toluenesulfonamide as a benign electrophilic cyanating agent.<sup>122</sup> With Kurzer's method employed, NCTS was easy-to-synthesize from inexpensive phenylurea and *p*-toluenesulfonyl chloride.<sup>123</sup> Indeed, this dehydrative tosylation in pyridine provided NCTS in satisfactory yields varying from 55 % to 69 % after recrystallization. Once we had NCTS available, we tried to reproduce the reaction conditions reported by Kasthuri et al. (Table 15).<sup>118</sup> To follow their synthetic protocol, we started with equimolar LiHMDS and NCTS (Table 15, Entry 1). However, we observed only 9% conversion. Determined to optimize the procedure, we increased NCTS and/or LiHMDS (Table 15, Entry 2-4). Unfortunately, the conversion remained unchanged. Finally, a higher temperature of 60 °C afforded 11% conversion (Table 15, Entry 5). Despite our effort, compound **IV-57** always predominated in the reaction mixture over the desired 2-aminobenzoxazole **IV-52A**.

**Table 15** Optimization of the reaction conditions for the LiHMDS-mediated cyclization<sup>a</sup>

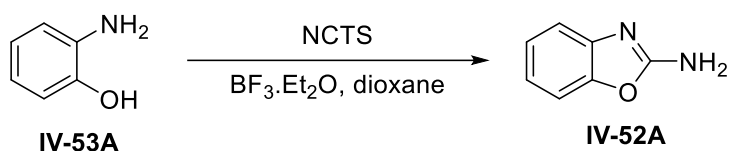


Entry	NCTS (equiv)	LiHMDS (equiv)	T (°C)	Yield of IV-52A (%) <sup>b</sup>
1	1	1	0 to rt	9
2	1	3	0 to rt	9
3	1.2	1	0 to rt	6
4	1.2	3	0 to rt	9

<sup>a</sup> Reaction conditions: *o*-aminophenol (0.18 mmol, 20 mg), NCTS, LiHMDS, THF (1 mL), 2 h. <sup>b</sup> Conversion estimated from LC-MS at 210-500 nm.

Consequently, we switched to the Lewis acid-mediated procedure. In fact, Lewis acids were suggested to activate the cyano group of NCTS toward a nucleophilic attack of the aniline group and thus facilitate the cyclization.<sup>118</sup> Indeed, the proposed hypothesis met our expectations and after careful optimization (Table 16), 2-aminobenzoxazole **IV-52A** was obtained in suitable isolated yield of 60%. To summarize the optimization procedure, we started with an excess of both reagents in refluxing dioxane (Table 16, Entry 1). Firstly, notable temperature dependence was observed from poor 39% conversion below 100 °C while refluxing dioxane enabled comparatively increased 86% transformation to the desired 2-aminobenzoxazole **IV-52A** (Table 16, Entry 1, 2). Secondly, 1.5 equiv of NCTS turned out the most appropriate amount to use without compromising the overall conversion (Table 16, Entry 3, 4). Finally, we were able to decrease the required amount of BF<sub>3</sub>·Et<sub>2</sub>O to 2 equiv (Table 16, Entry 5, 6). It should be noted that no reaction appeared in different solvents such as toluene, anisole, diphenyl ether or DMF. Only 2-methyltetrahydrofuran gave similar reaction outcome as reported in Entry 5.

**Table 16** Optimization of the reaction conditions for the Lewis acid-mediated cyclization<sup>a</sup>

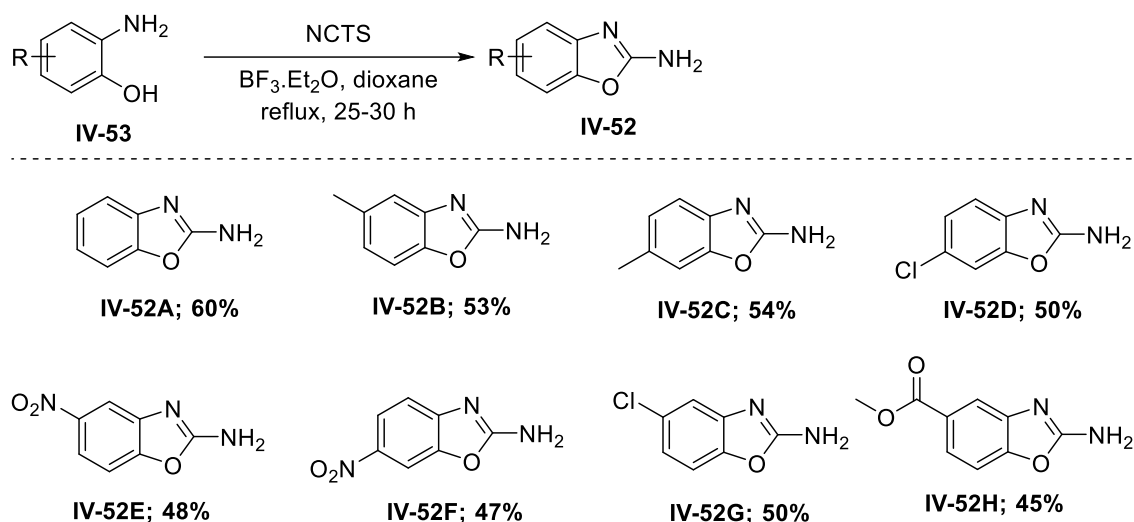


Entry	BF <sub>3</sub> ·Et <sub>2</sub> O (equiv)	NCTS (equiv)	T (°C)	Yield of <b>IV-52A</b> (%) <sup>c</sup>
1	3	3	reflux	86
2	3	3	100 <sup>b</sup>	39
3	3	1.5	reflux	87
4	3	1.2	reflux	54
<b>5</b>	<b>2</b>	<b>1.5</b>	<b>reflux</b>	<b>90</b>
6	1	1.5	reflux	71

<sup>a</sup> Reaction conditions: *o*-aminophenol (0.18 mmol, 20 mg), NCTS, BF<sub>3</sub>·Et<sub>2</sub>O, 1,4-dioxane (1 mL), 30 h. <sup>b</sup> External temperature of the bath. <sup>c</sup> Conversion estimated from LC-MS at 210-500 nm.

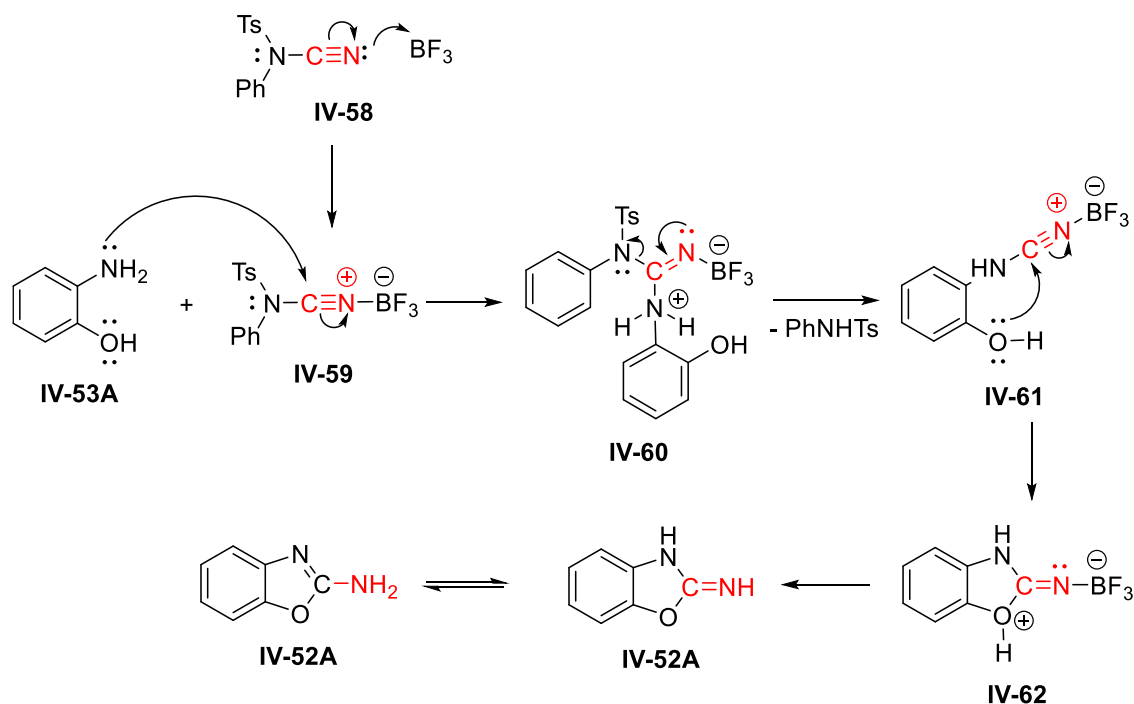
With optimal reaction conditions, the scope and limitations of the cyclization were examined (Table 17). Both EWG- and EDG-bearing *o*-aminophenols **IV-53** showed similar reactivity. Neither the position of substituent on the aromatic ring influenced the reaction. All the corresponding 2-aminobenzoxazoles **IV-52** were thus accessed in moderate yields of 45-60 %. Concerning satisfactory LC-MS conversion, the multistep isolation/purification is estimated to lower the yields.

**Table 17** Substrate scope for the Lewis acid-mediated cyclization<sup>a</sup>



<sup>a</sup> Reaction conditions correspond to the general procedure detailed in the experimental section. Isolated yields.

Considering our observation and prevalent literature, the following reaction mechanism is proposed (Scheme 23).<sup>118</sup> With its cyano group coordinated to  $\text{BF}_3 \cdot \text{Et}_2\text{O}$ , NCTS **IV-58** is more prone to the subsequent nucleophilic attack of the amine accompanied by the sulfonamide elimination. Within the proposed intermediate **IV-61**, the ring closure is completed by the hydroxyl group attacking the electron-poor carbon atom and the desired 2-aminobenzoxazole **IV-52A** is released after the basic workup. Finally, LC-MS analysis clearly showed  $m/z$  of 246  $[\text{M} - \text{H}]$  and experimentally confirmed the assumed sulfonamide elimination.

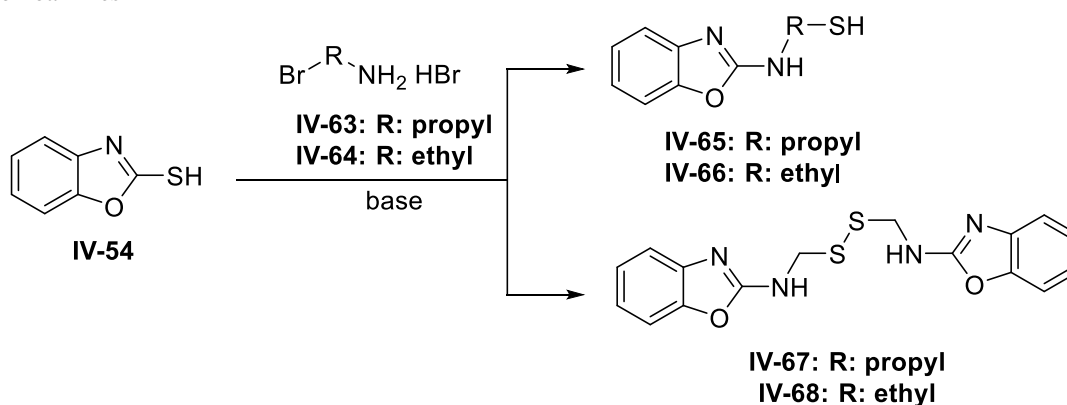


**Scheme 23** Proposed mechanism for the Lewis acid-mediated cyclization.

### 4.3.3 The Smiles rearrangement approach to *N*-substituted 2-aminobenzoxazoles

Following our interest in the catalyst-free synthesis of *N*-substituted 2-aminobenzoxazoles, we focused on the Smiles rearrangement. For this reason, the treatment of benzoxazole-2-thiol **IV-54** with various aliphatic bromoamines was studied. Unexpected reactivity of 3-bromopropylamine.HBr **IV-63** as well as 2-bromoethylamine.HBr **IV-64** yielded a mixture of corresponding thiol **IV-65** or **IV-66** and disulfide **IV-67** or **IV-68** (Table 18). We started with conditions adapted from Abdelazeem et al.<sup>124</sup> and applied them to 3-bromopropylamine.HBr **IV-64** which selectively yielded disulfide **IV-67** *via* a radical pathway (Table 18, Entry 1). Even a lower amine concentration did not influence the reaction outcome (Table 18, Entry 2). However, a less basic environment enabled a selective formation of the desired compound **IV-65** (Table 18, Entry 3-5). On the other hand, 2-bromoethylamine.HBr **IV-64** showed different behavior (Table 18, Entry 6). An increased temperature of 120 °C was needed to reach disulfide **IV-68** selectively (Table 18, Entry 7). While the altered amount of K<sub>2</sub>CO<sub>3</sub> turned out useless, switching to 1 equiv of Et<sub>3</sub>N afforded compound **IV-66** selectively (Table 18, Entry 8-10).

**Table 18** Optimization of the reaction conditions for the Smiles rearrangement with shorter aliphatic bromoamines<sup>a</sup>



Entry	Amine (equiv)	Base (equiv)	T (°C)	Ratio of IV-65:IV-67 (%) <sup>b</sup>
1	IV-63 (2)	K <sub>2</sub> CO <sub>3</sub> (3)	70	0:95
2	<b>IV-63 (1)</b>	<b>K<sub>2</sub>CO<sub>3</sub> (3)</b>	<b>70</b>	<b>0:95</b>
3	IV-63 (1)	K <sub>2</sub> CO <sub>3</sub> (2)	70	38:38
4	<b>IV-63 (2)</b>	<b>K<sub>2</sub>CO<sub>3</sub> (2)</b>	<b>70</b>	<b>80:7</b>
5	IV-63 (4)	K <sub>2</sub> CO <sub>3</sub> (2)	70	80:5

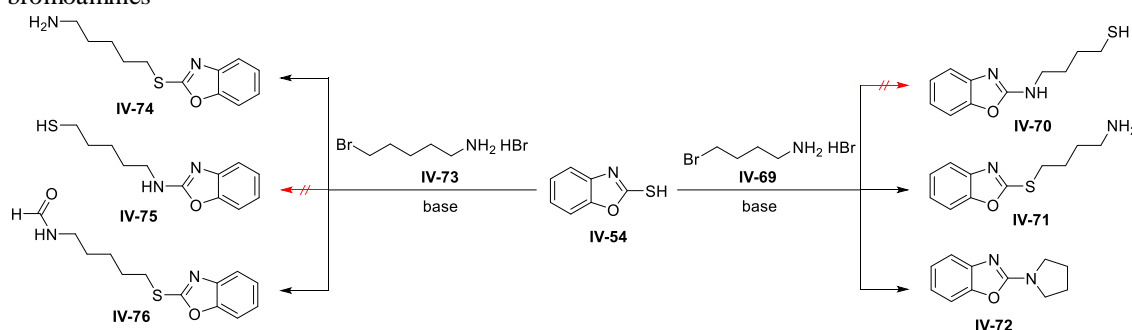
Entry	Amine (equiv)	Base (equiv)	T (°C)	Ratio of IV-66:IV-68 (%) <sup>b</sup>
6	IV-64 (2)	K <sub>2</sub> CO <sub>3</sub> (3)	70	50:33
7	<b>IV-64 (2)</b>	<b>K<sub>2</sub>CO<sub>3</sub> (3)</b>	<b>120</b>	<b>5:80</b>
8	IV-64 (2)	K <sub>2</sub> CO <sub>3</sub> (2)	70	33:30
9	IV-64 (2)	K <sub>2</sub> CO <sub>3</sub> (4)	70	20:60
<b>10</b>	<b>IV-64 (2)</b>	<b>Et<sub>3</sub>N (1)</b>	<b>70</b>	<b>94:4</b>

<sup>a</sup> Reaction conditions: benzoxazole-2-thiol (0.16 mmol, 25 mg), 3-bromopropylamine.HBr/2-bromoethylamine.HBr, base, DMF (1 mL), 2 h. <sup>b</sup> Estimated from LC-MS at 210-500 nm. The rest of the crude mixture contained unknown impurities and (or) by-products.

Also, two longer bromoamines **IV-69** and **IV-73** were subjected to our Smiles rearrangement exploration (Table 19). Herein, both the bromoamines were synthesized from commercial aminoalcohols according to the literature precedent using ionex workup.<sup>125</sup> In the case of 4-bromobutylamine.HBr **IV-69**, preferential 5-membered ring closure always resulted in pyrrolidine **IV-72** as the main product. Facilitated by negligible ring strain and minimal entropy change, ring closure was observed with inconsiderable dependence on the reaction conditions (Table 19, Entry 1-3). Lower temperature only

decreased the reaction rate (Table 19, Entry 4). In the context of the abovementioned results, 2 equiv of the amine **IV-69** and 2 equiv of Et<sub>3</sub>N in refluxing toluene seemed to be the most efficient conditions. Finally, 5-bromopentylamine **IV-73** substituted the starting benzoxazole-2-thiol smoothly, leading to compound **IV-74**. Herein, 2 equiv of the amine **IV-73** and 2 equiv of Et<sub>3</sub>N in refluxing toluene were found to be useful again (Table 19, Entry 7). To force the rearrangement, harsher conditions were applied directly onto the amine **IV-74** (Table 19, Entry 8, 9). Instead of the expected rearrangement, just undesired formylation, confirmed by NMR spectroscopy, occurred to give formamide **IV-76**.

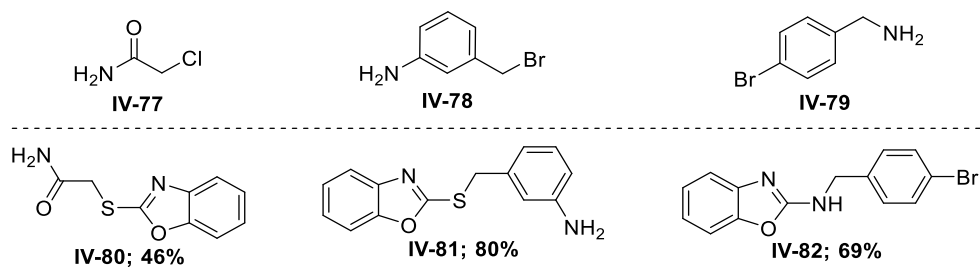
**Table 19** Optimization of the reaction conditions for the Smiles rearrangement with larger aliphatic bromoamines<sup>a</sup>



Entry	Base	Solvent	T (°C)	Time (h)	Ratio of IV-71:IV-72 (%) <sup>b</sup>
1	NaH	toluene	reflux	26	0:92
2	Et <sub>3</sub> N	toluene	reflux	4	<b>0:95</b>
3	Et <sub>3</sub> N	DMF	120	22	0:16
4	Et <sub>3</sub> N	toluene	80	22	26:9
Entry	Base	Solvent	T (°C)	Time (h)	Ratio of IV-74:IV-76 (%) <sup>b</sup>
5	NaH	DMF	120 (MW)	½	24:48
6	Et <sub>3</sub> N	DMF	120 (MW)	½	42:11
7	Et <sub>3</sub> N	toluene	reflux	2	<b>99:0</b>
8 <sup>c</sup>	Et <sub>3</sub> N	DMF	120 (MW)	½	54:44
9 <sup>c</sup>	Et <sub>3</sub> N	DMF	120 (MW)	2	<b>0:98</b>

<sup>a</sup> Reaction conditions: benzoxazole-2-thiol (0.06 mmol, 10 mg), 4-bromobutylamine.HBr/5-bromopentylamine.HBr (0.12 mmol), base (0.12 mmol), solvent (0.5 mL). <sup>b</sup> Estimated from LC-MS at 210-500 nm. The rest of the crude mixture contained unknown impurities and (or) by-products. <sup>c</sup> Compound **IV-74** used as starting material.

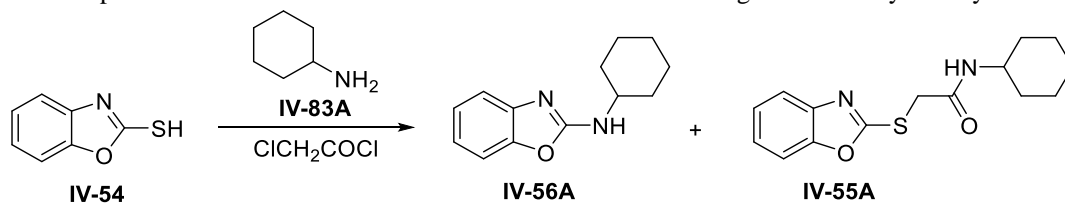
Later on, some more challenging substrates such as 2-chloroacetamide **IV-77**, 3-(bromomethyl)aniline **IV-78**, 4-bromobenzylamine **IV-79** were also employed in the Smiles rearrangement (Figure 20). Presumably compromised by sterically and energetically demanding transition states, all the substrates failed in term of the Smiles rearrangement, and only the corresponding nucleophilic substitution products **IV-80**, **IV-81**, **IV-82** were isolated regardless of the reaction conditions (Figure 20).



**Figure 20** Extended substrate scope with resulting nucleophilic substitution products. Isolated yields included.

Motivated by the abovementioned observations, we needed a universal method to widen the substrate scope. To meet rather ambitious expectation, Smiles rearrangement was performed (Table 20). The initial reaction conditions were adopted from Tian et al.<sup>121</sup> and tested on cyclohexylamine **IV-83A** as a model substrate (Table 20, Entry 1). Conventional heating at 160 °C provided similar conversion compared to microwave irradiation (Table 20, Entry 2). On the other hand, the change of stoichiometry, solvent or reaction time had no positive influence on the reaction outcome (Table 20, Entry 3-6). Different bases than Cs<sub>2</sub>CO<sub>3</sub> completely suppressed the rearrangement leading to the substitution product **IV-55A** (Table 20, Entry 7, 8).



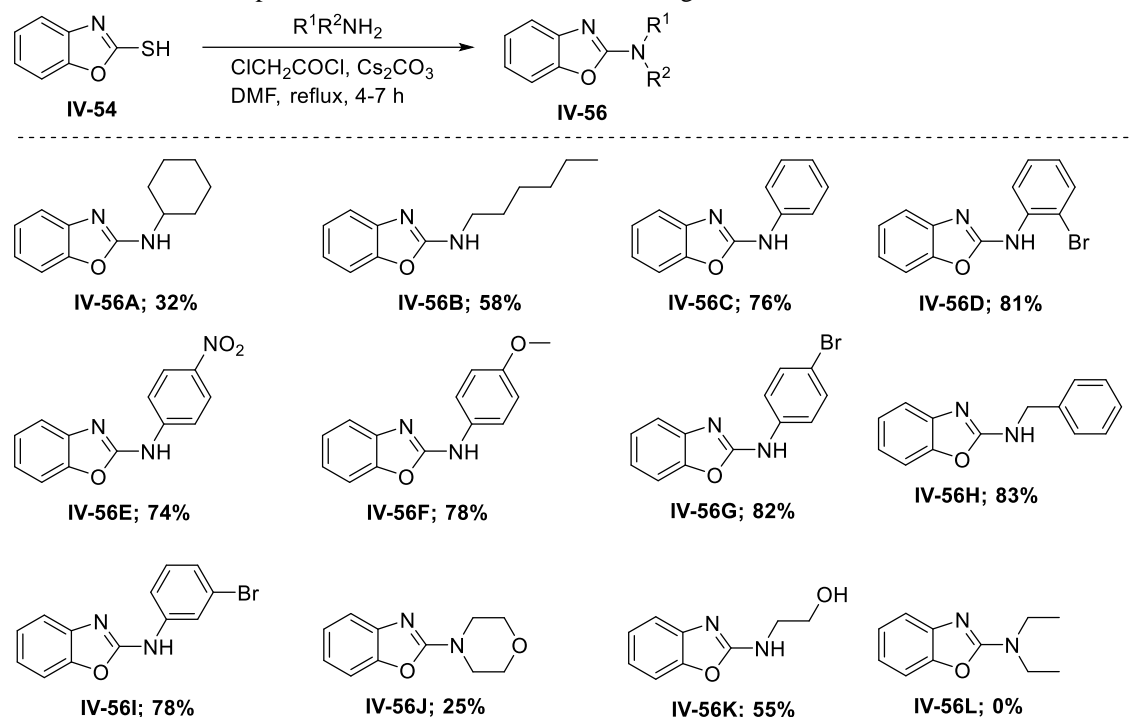
**Table 20** Optimization of the reaction conditions for the Smiles rearrangement with cyclohexylamine<sup>a</sup>

Entry	Chlorid		T (°C)	Time (h)	Solvent	Ratio of IV-56A:IV-55A (%) <sup>b</sup>
	e	Base (equiv)				
1	1.2	Cs <sub>2</sub> CO <sub>3</sub> (3.2)	160 (MW)	½	DMF	57:0
2	<b>1.2</b>	<b>Cs<sub>2</sub>CO<sub>3</sub> (3.2)</b>	<b>160</b>	<b>8</b>	<b>DMF</b>	<b>58:0</b>
3	1.7	Cs <sub>2</sub> CO <sub>3</sub> (3.2)	160 (MW)	½	DMF	31:0
4	1.2	Cs <sub>2</sub> CO <sub>3</sub> (3.7)	160 (MW)	½	DMF	48:0
5	1.2	Cs <sub>2</sub> CO <sub>3</sub> (3.2)	160 (MW)	½	<i>N,N</i> -DMA	25:0
6	1.2	Cs <sub>2</sub> CO <sub>3</sub> (3.2)	160 (MW)	2	DMF	42:0
7	1.2	NaH (3.2)	150	2	<i>N,N</i> -DMA	0:42
8	1.2	DBU (3.2)	reflux	2	MeCN	0:95

<sup>a</sup> Reaction conditions: benzoxazole-2-thiol (0.16 mmol, 25 mg), cyclohexylamine (0.16 mmol), base, CICH<sub>2</sub>COCl, solvent (1 mL). <sup>b</sup> Estimated from LC-MS at 210-500 nm. The rest of the crude mixture contained unknown impurities and (or) by-products.

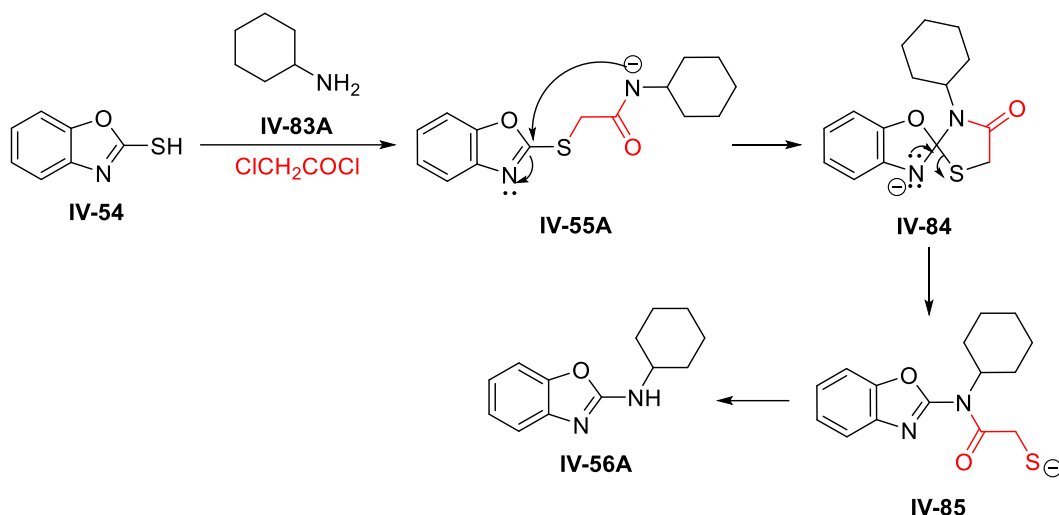
Having the optimized reaction conditions in hand, we set out to explore the scope of the Smiles rearrangement (Table 21). A broad scope of primary and secondary aromatic, aliphatic, alicyclic amines and bisnucleophilic ethanolamine was tested. Considering the aromatic and primary amines, there was no influence of the electron effects or substitution patterns recognized, and the corresponding *N*-substituted aminobenzoxazoles **IV-56B-I** and **IV-56K** were isolated in good yields of 55-83%. In contrast, bulkier amines exhibited comparatively worse reactivity reflected in decreased yield of **IV-56A** (32%) and **IV-56J** (25%). The rearrangement with diethylamine ultimately failed.

**Table 21** Substrate scope for the intramolecular Smiles rearrangement<sup>a</sup>



<sup>a</sup> Reaction conditions correspond to the general procedure detailed in the experimental section. Isolated yields.

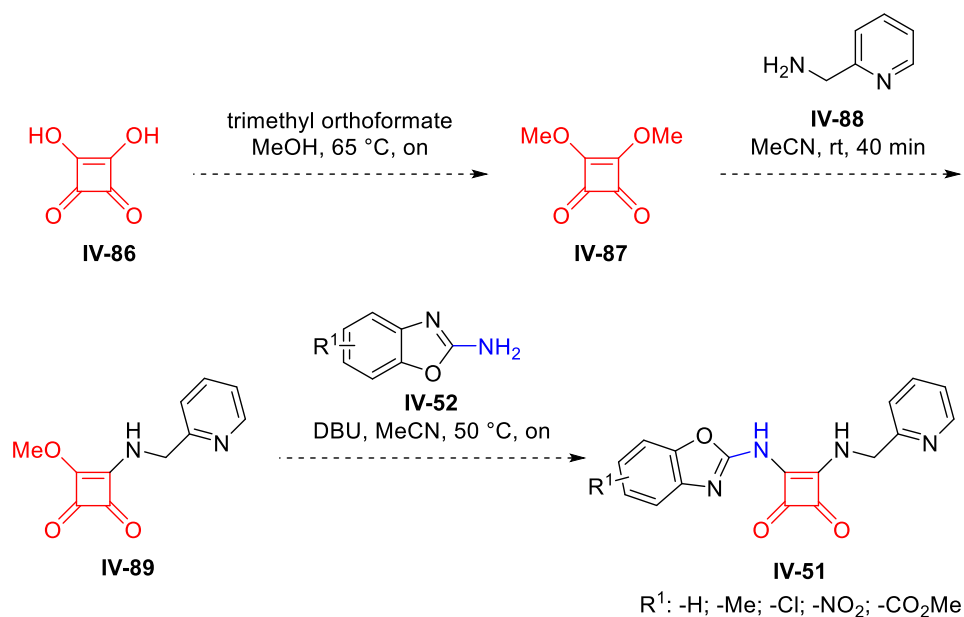
The mechanistic proposal has been made concerning the experimental observations and the existing literature (Scheme 24). After the initial *S*-alkylation, the Smiles rearrangement is driven forward *via* intermediate **IV-55A** by the nitrogen's nucleophilic attack at the electron-deficient benzoxazole carbon. The process is accompanied by a new C-N bond formation to give spiro compound **IV-84**. The conclusive rearomatization and Cs<sub>2</sub>CO<sub>3</sub>-mediated alkaline hydrolysis furnishes the desired *N*-substituted benzoxazole **IV-56A**.



**Scheme 24** Proposed mechanism for the intramolecular Smiles rearrangement.

#### 4.3.4 Conclusive remark 3

This chapter outlines two novel synthetic approaches toward 2-aminobenzoxazoles and their *N*-substituted analogues from safe and readily available starting materials. Both achieved synthetic protocols are widely applicable, provide the target aminobenzoxazoles in moderate to excellent yields, and use nontoxic, inexpensive precursors. Moreover, the cyclization protocol was successfully utilized within our group to prepare squaramide-benzoxazoles **IV-51** as potential mycobacterial ATP synthase inhibitors (Scheme 25). Most of the squaramide-benzoxazoles exhibited promising preliminary results against extracellular *Mtb* R37Ra and their mechanism of action is currently under elucidation.



**Scheme 25** Synthetic pathway toward the target squaramide-benzoxazoles.

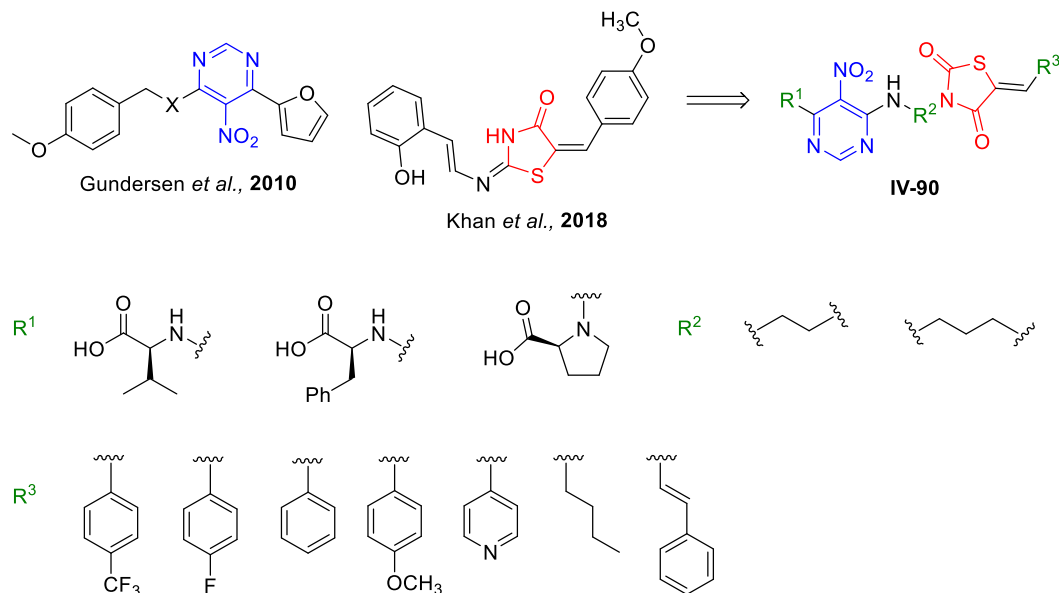
## 4.4 Thiazolidinedione-based conjugates for phenotypic screening

### 4.4.1 Design and solid phase synthesis of the TZD-pyrimidines

Over many years, combining two pharmacophores became a well-established approach for designing more potent drugs with enhanced pharmacotherapeutic activity. The resulting hybrid molecules aimed at manifold targets are considered better drug candidates with more predictable pharmacological behavior and extend patient compliance.

Encouraged by all the aforementioned findings, especially by the reported relevance of TZD and 5-nitropyrimidine heterocycles in anti-TB research, we decided to combine these two attractive pharmacophores to reach novel promising anti-TB TZD-pyrimidine hybrids **IV-90** (Scheme 26).<sup>86,126</sup> The central heterocycles were connected by an appropriate linker. Herein, ethylenediamine and propylenediamine were selected for primary screening.<sup>127</sup> Because we envisioned the polymer-supported synthetic protocol as the most suitable approach to the desired library of TZD-pyrimidines, the whole system was built on Wang resin *via* immobilization of lipophilic amino acids to optimize the overall drug-likeness of final hybrids.<sup>128</sup> Three amino acids, namely valine, phenylalanine

and proline, were incorporated in compounds **IV-90** to evaluate their influence on the resulting biological qualities. The last modification yielded from typical benzylidene or alkylidene substitution pattern engaged to diversify the TZD core.<sup>88</sup>

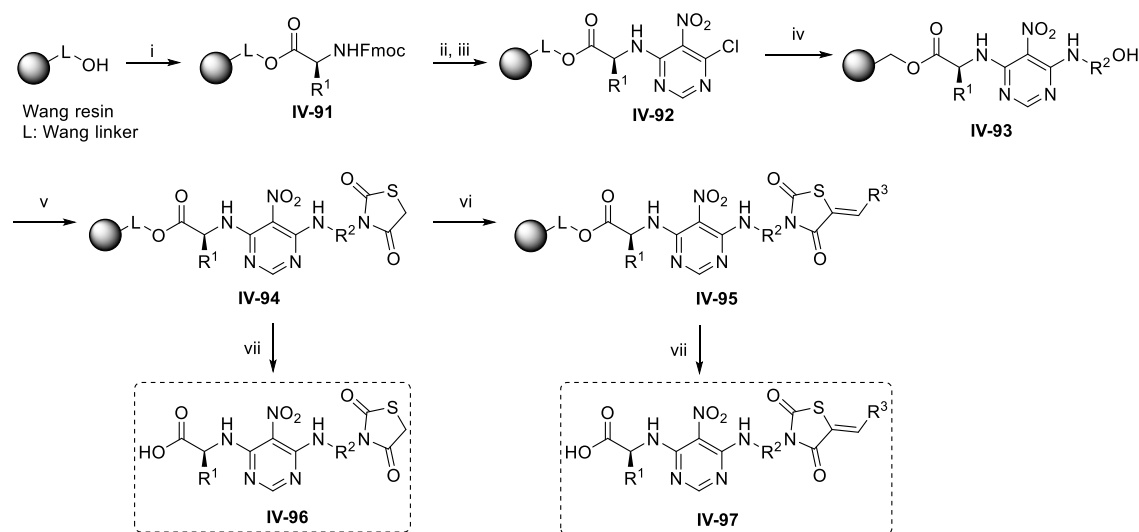


**Scheme 26** Design of anti-TB TZD-pyrimidines.

For the conjugation of TZD with 5-nitropyrimidine, the polymer-supported synthetic protocol was introduced (Scheme 27). To emphasize our synthetic procedure's main advantages in general comparison with typical medicinal chemistry synthetic protocols, it does not require multiple isolation/purification and proceeds from relatively inexpensive precursors. Furthermore, our method includes minimal synthetic operations to reach structural diversity from feasible building blocks. The solid phase synthesis started with amino acid immobilization on Wang resin. Such a modified resin **IV-91** underwent Fmoc deprotection and substitution with 4,6-dichloro-5-nitropyrimidine to provide resin **IV-92**. The resulting chlorine atom was reported to be prone to hydrolysis.<sup>129</sup> That is why resin **IV-92** was immediately treated with aminoethanol or aminopropanol resulting in resin **IV-93**. Fukuyama-Mitsunobu transformation then yielded the key polymer-supported intermediate **IV-94**. Herein, shorten reaction time turned out useful to increase the purity of the resin-bound intermediate **IV-94** with quantitative conversion observed after 1 h. The TZD was again obtained in 57% yield from thiourea and chloroacetic acid by reproduction of the literature precedent.<sup>84</sup> Later on, Knoevenagel condensation of resin **IV-94** with various aldehydes resulted in conjugate **IV-95**. After several published protocols tested, the most suitable conditions were found to include piperidine, DMF, 70

°C, on (16 h).<sup>130</sup> All the desired TZD-pyrimidines **IV-96** and **IV-97** were finally isolated by standard acidic cleavage and subsequent HPLC purification.

As already stated in Chapter 4.1.1, Knoevenagel condensation gave rise to *E/Z* geometrical isomers. Both the isomers may be differentiated by <sup>1</sup>H NMR shifts.<sup>102,131,132</sup> Based on the method, all our final products **IV-96** and **IV-97** were confirmed as *Z* isomers with characteristic vinylic proton shifted above 7.90 ppm, deshielded by the adjacent C=O.



**Scheme 27** Solid-phase synthesis of TZD-pyrimidines.<sup>a</sup>

<sup>a</sup> Reagents and conditions: (i): Fmoc-amino acid, HOBt, DMAP, DIC, DMF/CH<sub>2</sub>Cl<sub>2</sub> (1:1), rt, on; (ii): 50% piperidine, DMF, rt, 15 min; (iii): 4,6-dichloro-5-nitropyrimidine, DIPEA, DMF, rt, 2 h; (iv): amino alcohol, DIPEA, DMF, rt, 2 h; (v): thiazolidine-2,4-dione, PPh<sub>3</sub>, DIAD, THF, rt, 1 h; (vi): aldehyde, piperidine, DMF, 70 °C, on; (vii): 50% TFA in CH<sub>2</sub>Cl<sub>2</sub>, rt, 1 h.

The introduced solid-phase protocol yielded a novel chemical library of TZD-pyrimidines **IV-96** and **IV-97** (Figure 22). The reaction sequence was successfully applied on aromatic aldehydes with electron-withdrawing and electron-donating substitution pattern and aliphatic aldehydes. All the proposed TZD-pyrimidines **IV-96** and **IV-97** were synthesized in acceptable crude purity from 58 to 91 %. Their isolated yields varied between 29 and 63 %, sometimes lowered by HPLC purification.

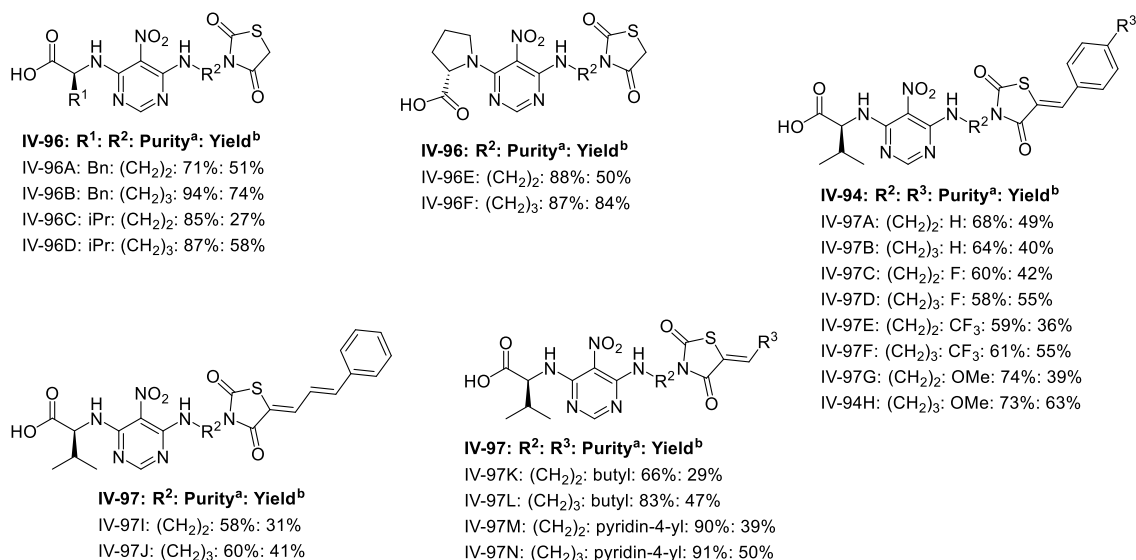


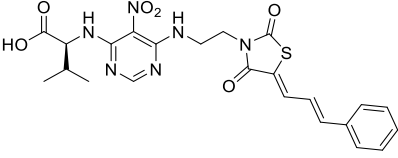
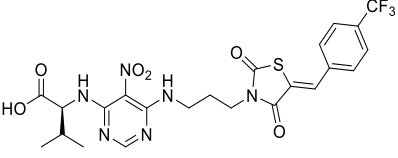
**Figure 21** Overview of obtained TZD-pyrimidines.

<sup>a</sup> Crude purity estimated from LC-MS at 210-500 nm. <sup>b</sup> Isolated yield after HPLC purification.

#### 4.4.2 Biological activity of TZD-pyrimidines

The chemical library was consequently tested for antitubercular and antimicrobial activity (Table 22). Regarding their antitubercular potential against *Mtb* H37Rv, conjugate **IV-97F** possessed MIC = 256 µg/mL while TZD-pyrimidine **IV-97I** exhibited bacteriostatic effect on *Mtb* H37Rv. Subsequently, reference Gram-positive as well as Gram-negative bacterial strains (*S. aureus* CCM 3953, *P. aeruginosa* CCM 3955, *E. coli* CCM 3954, *E. faecalis* CCM 4224), two fungal strains (*C. albicans* ATCC 90028, *A. niger* CCM 8189) were employed. Unfortunately, TZD-pyrimidines **IV-96** turned out completely inactive. On the contrary, conjugates **IV-97** were more potent. Namely compound **IV-97F** expressed the best inhibition of *S. aureus* CCM 3953 with MIC = 128 µg/mL. Concerning the structure-activity relationship, the propylene diamine linker between the pharmacophores enhanced antimicrobial potential compared to corresponding ethylenediamine-containing analogues.

**Table 22** Biological characterization of the most active TZD-pyrimidines

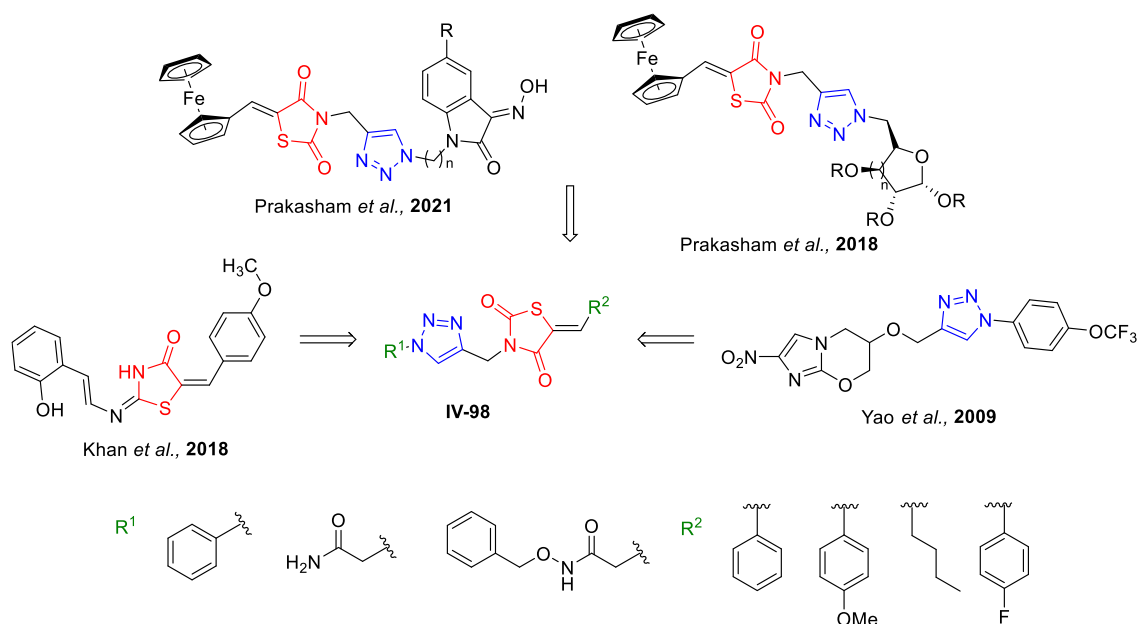
Entry	<i>M. tuberculosis</i> <sup>a</sup>	<i>S. aureus</i> <sup>a</sup>	<i>E. faecalis</i> <sup>a</sup>
 IV-94I	1024	256	256
 IV-94F	256	128	256

<sup>a</sup> Minimum inhibitory concentration (MIC;  $\mu\text{g/mL}$ ).

#### 4.4.3 Design and combinatorial synthesis of TZD-triazoles

We decided to further continue with the TZD-based combinatorial approach to extend phenotypic screening. This time, our research relied on the unique anti-TB potential of triazole moiety and its role as a linker between two bioactive functionalities.<sup>94</sup> The construction of bioconjugates *via* triazoles is thus an appealing synthetic methodology. Namely 1,2,3-triazoles were of our interest, and their combination with TZD thus resulted in design of novel TZD-triazole hybrids **IV-98** (Scheme 28). Our interest in such a combination was further enhanced by recently reported promising pharmacological properties of the TZD-triazole hybrids such as isatin (oxime)-triazole-TZD ferrocenes and ferrocenyl sugar-triazole conjugates (Scheme 28).<sup>133,134</sup> To enable the combinatorial synthesis while keeping the synthetic protocol as straightforward as possible, click transformation was engaged to connect both the pharmacophores.<sup>135,136</sup> In this context, we took an advantage of the Cu<sup>I</sup> catalyzed azide-alkyne cycloaddition.<sup>137</sup> For this reason, corresponding azide and alkyne building blocks were proposed. Herein, three simple azide-substituted residues R<sup>1</sup> were chosen for the initial investigation to reveal any possible consequences of the triazole ring modification. On the other hand, further diversification of the TZD core by various benzylidenes or alkylidenes was proposed according to the prevalent literature.<sup>88</sup>



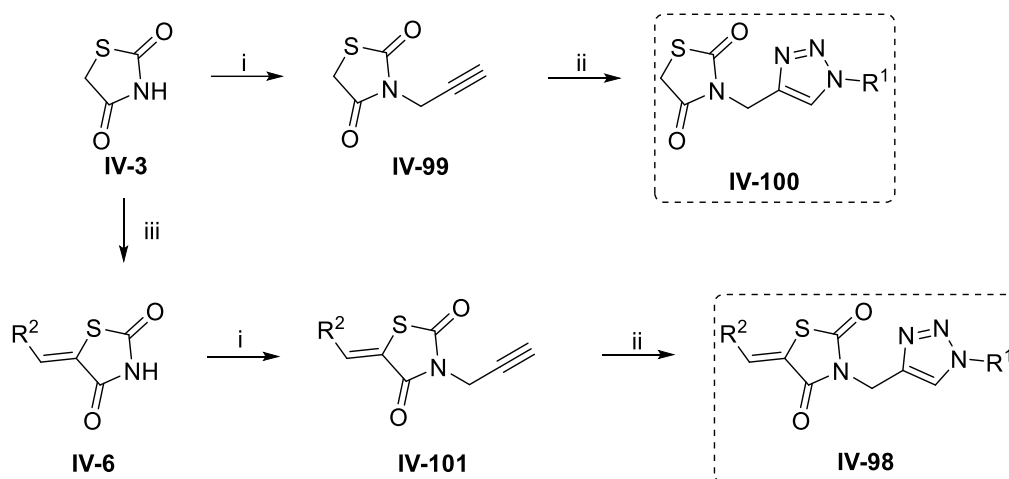


**Scheme 28** Design of anti-TB TZD-triazoles.

To access all the proposed TZD-triazoles, we developed a straightforward synthetic protocol based on 2 or 3 simple steps (Scheme 29). We started with formation of simpler TZD-unsubstituted conjugates **IV-100**. As reported in the Chapter 4.1.1, TZD precursor **IV-3** was synthesized easily from thiourea and chloroacetic acid.<sup>101</sup> The overall yields varied from 57 % to 65 % and thus corresponded to the literature precedent. Once TZD **IV-3** was obtained, *N*-alkylation with propargyl bromide followed under standard conditions using  $K_2CO_3$  in refluxing acetone.<sup>138</sup> The resulting *N*-alkylated TZD **IV-99** was then isolated in a moderate 48% yield. Subsequently, all the necessary azides were prepared. Both the aliphatic azides were accessed by nucleophilic substitution from appropriate bromides in accordance with literature precedents.<sup>139,140</sup> On the other hand, azidobenzene was formed by diazotation. Achieved TZD-alkyne **IV-99** then underwent  $Cu^I$  catalyzed azide-alkyne cycloaddition resulting in the desired TZD-triazoles **IV-100** in low to moderate isolated yields of 13-58 % (Figure 23). Concerning the Huisgen cycloaddition, typical conditions with  $CuSO_4 \cdot 5H_2O$  reduced by sodium ascorbate for *in situ* generation of  $Cu^I$  were involved.<sup>141</sup>

The following synthesis of TZD-triazoles **IV-98** started with Knoevenagel condensation (Scheme 29). Herein, we observed a similar trend in reactivity as reported during analogous TZD-hydroxamates synthesis in Chapter 4.1.1. Contrary to well-optimized high-yielding TZD-benzylidene formation, TZD-pentylidene turned out more problematic.<sup>102</sup> Presumed decomposition on silica lowered the isolated yield of TZD-

pentylidene to 43 % while all the aromatic counterparts were obtained in satisfactory 64-97% isolated yields. The sequence continued with *N*-alkylation providing TZD-alkynes **IV-101** in excellent 50-97% isolated yields. All the desired TZD-triazoles **IV-98** were formed by Huisgen cycloaddition with various azides (Figure 23). Regardless of the substitution pattern, all the studied compounds exhibited comparable reactivity. To generalize the reaction outcome within the series, pentylidene-substituted hybrids were finally isolated in compromised quantity compared to benzylidene-bearing conjugates.



**Scheme 29** Synthesis of TZD-triazoles.<sup>a</sup>

<sup>a</sup> Reagents and conditions: (i): propargyl bromide,  $K_2CO_3$ , acetone, reflux, on (16 h); (ii): azide, sodium ascorbate,  $CuSO_4 \cdot 5H_2O$ , DMF, rt, 5 h; (iii): aldehyde, piperidine, EtOH, reflux, on, (16-20 h).

To determine the stereochemical outcome of the Knoevenagel condensation reactions, the geometrical *E/Z* isomerism was questioned again. As stated in Chapter 4.1.1, both possible isomers are known to be distinguishable by  $^1H$  NMR spectral measurement.<sup>103</sup> Concerning all the final TZD-triazoles **IV-98**, the benzylidene proton was found out shifted approximately to 7.90 ppm, and thus, *Z* configuration was proposed. Due to the comparatively lesser deshielding effect of sulphur, a vinylic proton in *E*-isomers should resonate at lower frequency values.<sup>142,143</sup>

The developed synthetic protocol provided us with a chemical library of novel TZD-triazoles **IV-100** and **IV-98** (Figure 23). All the reaction sequence was successfully applied on unsubstituted TZD-alkynes, as well as on their substituted analogues containing aromatic aldehydes having electron-withdrawing or electron-donating functional groups and aliphatic aldehydes treated with various azides. The desired TZD-

triazole hybrids **IV-100** and **IV-98** were isolated in quite variable yields ranging from 13 to 90 %.

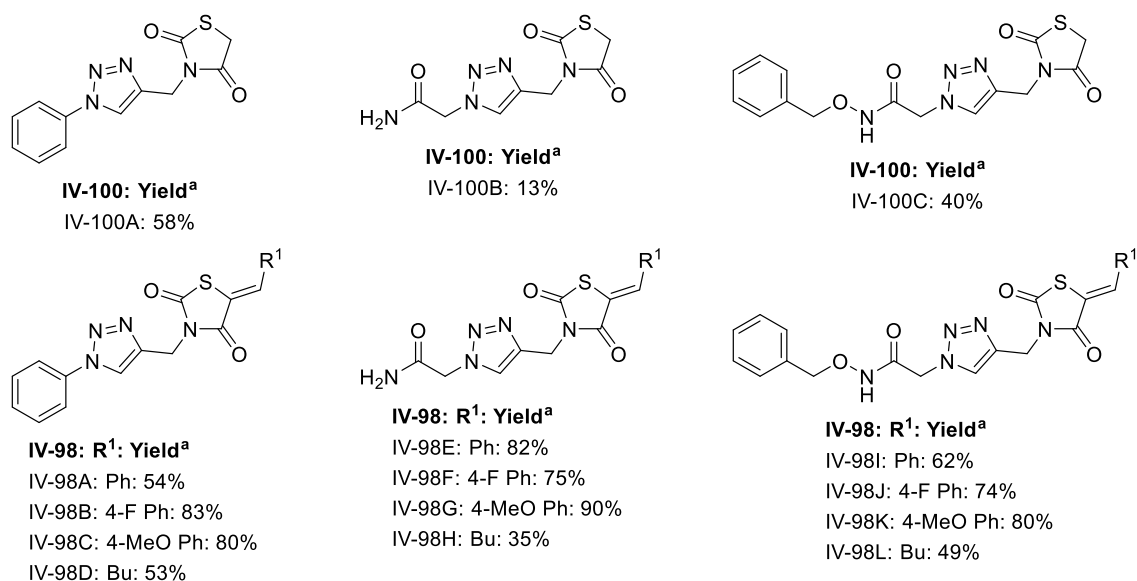


**Figure 22** Overview of obtained TZD-triazoles.

<sup>a</sup> Isolated yield.

Once we obtained the chemical library of TZD-triazoles, their antitubercular activity against *Mtb* R37Ra was tested. However, none of the conjugates exhibited any significant anti-TB potential. After all, the antimicrobial properties of the chemical library were explored. For this purpose, selected Gram-positive and Gram-negative bacterial strains (*S. aureus* CCM 3953, *E. coli* CCM 3954) and one fungal strain (*C. albicans* ATCC 90028) were employed. Unfortunately, all the TZD-triazoles **IV-100** as well as **IV-98** were found to be completely inactive.

#### 4.4.4 Conclusive remark 4

Two chemical libraries of novel TZD-based hybrids were reported in this chapter. Herein, wide structural diversity needed for phenotypic screening was accessed *in* a combinatorial synthetic approach. Firstly, 20 novel TZD-pyrimidines **IV-96** and **IV-97** were prepared using an efficient solid-phase protocol. We thus explored various building blocks in terms of their reactivity as well as influence on antimicrobial activity. Despite their moderate antibacterial potential, our compact synthetic method can be further successfully combined with sophisticated *in silico*-supported drug design.

Secondly, we synthesized 15 new TZD-triazole **IV-100** and **IV-98** hybrids in a combinatorial manner. In accordance with the previously accessed TZD-pyrimidines, diverse building blocks were used to extend the investigation of their reactivity as well as biological properties. Despite their insignificant antimicrobial activity, they exhibited promising antileishmanial properties undergoing an extensive biological study.

---

## 5 General conclusions and outlook

The ultimate goal of the thesis was the synthesis of novel chemical entities with potential antitubercular activity. We have envisioned that mycobacterial virulence factors inhibition, ATP synthase inhibition and phenotypic screening may be attractive approaches for development of promising anti-TB candidates.

Firstly, we focused on inhibition of two mycobacterial virulence factors Zmp1 and MptpB. To access potential mycobacterial Zmp1 inhibitors, we designed and synthesized two generations of heterocyclic compounds with hydroxamate-based zinc binding group. Herein, our initial effort resulted in the first generation of 20 TZD-hydroxamates with the most efficient *Mtb* H37Ra inhibitor possessing IC<sub>50</sub> of 18 μM. Such an encouraging result inspired the following work on the second generation of pyrrole- and indole-hydroxamates leading to another 16 potential Zmp1 inhibitors which are currently under biological investigation. Subsequently, our synthetic effort on tandem ring expansion/cyclization enabled preparation of 10 novel *N*-fused polycycles presumed to inhibit MptpB. Moreover, we extended the reactivity of *gem*-dihaloaminocyclopropanes in terms of their thermic ring enlargement followed by TfOH-mediated cyclization and accounted for unexpected competitive pathways. Finally, all the achieved *N*-fused polycycles are undergoing biological investigation.

The second research area included inhibition of mycobacterial ATP synthase. Within a complex research project comprising design and synthesis of squaramide-benzoxazoles as potential mycobacterial ATP synthase inhibitors, the development of widely applicable synthetic approach toward 2-aminobenzoxazole moiety from nonhazardous and inexpensive precursors was the partial objective of the thesis. Indeed, all the careful study of cyclization and Smiles rearrangement yielded two novel synthetic procedures affording 2-aminobenzoxazoles and their *N*-substituted analogues from nonhazardous, inexpensive precursors. Such a straightforward pathway toward 2-aminobenzoxazoles enabled synthesis of the target squaramide-benzoxazoles as potential mycobacterial ATP synthase inhibitors. Most of the squaramide-benzoxazoles exhibited promising preliminary results

against extracellular *Mtb* R37Ra and their mechanism of action is currently under elucidation.

Our last anti-TB drug discovery approach taken was phenotypic screening. Wide structural diversity required for phenotypic screening was accessed *via* the combinatorial technique and yielded two novel chemical libraries of TZD-based hybrids. Firstly, 20 novel TZD-pyrimidines were prepared using an efficient solid-phase protocol. Despite their moderate antibacterial potential, our compact synthetic method can be further successfully combined with sophisticated *in silico*-supported drug design. Secondly, we synthesized 15 new TZD-triazole hybrids in a combinatorial manner. Regardless of their negligible antimicrobial activity, obtained TZD-triazoles showed notable antileishmanial potential.

In summary, three selected molecular targets and drug discovery approaches yielded 5 series of novel potential anti-TB compounds and thus fulfilled the main goal of the thesis. Moreover, the valuable preliminary results obtained from their biological evaluation may be of scientific value for further extensive antitubercular research.

---

## 6 Experimental Part

### 6.1 General information

Solvents and chemicals were purchased from Sigma-Aldrich ([www.sigmaaldrich.com](http://www.sigmaaldrich.com)) and Fluorochem ([www.fluorochem.co.uk](http://www.fluorochem.co.uk)). All reactions were carried out at ambient temperature (21 °C) unless stated otherwise. Analytical thin-layer chromatography (TLC) was performed using aluminum plates precoated with silica gel (silica gel 60 F254).

The LC-MS analyses were carried out on UHPLC-MS system (Waters, Santa Clara, USA). This system consists of UHPLC chromatograph Acquity with photodiode array detector and single quadrupole mass spectrometer and uses XSelect C18 column (dimensions 1.8  $\mu\text{m}$ , 2.1  $\times$  50 mm at 30 °C and a flow rate of 600  $\mu\text{L}/\text{min}$ . The mobile phase was (A) 10 mM ammonium acetate in HPLC grade water, and (B) HPLC grade acetonitrile. A gradient was formed from 10% A to 80% B over 2.5 min; kept for 1.5 min. The column was re-equilibrated with a 10% solution of B for 1 min. The ESI source operated at a discharge current of 5  $\mu\text{A}$ , vaporizer temperature of 350 °C and a capillary temperature of 200 °C.

NMR  $^1\text{H}/^{13}\text{C}$  spectra were recorded on JEOL ECX-500SS (500 MHz) or JEOL ECA400II (400 MHz) or AVANCE 400 Bruker (400 MHz) spectrometers at magnetic field strengths of 11.75 T (with operating frequencies 500.16 MHz for  $^1\text{H}$  and 125.77 MHz for  $^{13}\text{C}$ ) and 9.39 T (with operating frequencies 399.78 MHz for  $^1\text{H}$  and 100.53 MHz for  $^{13}\text{C}$ ) at ambient temperature ( $\sim 21$  °C). Chemical shifts ( $\delta$ ) are reported in parts per million (ppm) and coupling constants ( $J$ ) are reported in Hertz (Hz). NMR spectra were recorded at ambient temperature (21 °C) in  $\text{DMSO-}d_6$  or  $\text{CDCl}_3$  and referenced to the resonance signals of  $\text{CDCl}_3$  (7.26 ppm for  $^1\text{H}$  and 77.16 ppm for  $^{13}\text{C}$ ) and  $\text{DMSO-}d_6$  (2.50 ppm for  $^1\text{H}$  and 39.51 ppm for  $^{13}\text{C}$ ). Abbreviations in NMR spectra: app: apparent, br s: broad singlet, s: singlet, d: doublet, t: triplet, q: quartet, q: quintet, h: hextet, m: multiplet.

HRMS analysis was performed with LC-MS and an Orbitrap high-resolution mass spectrometer (Dionex, Ultimate 3000, Thermo Exactive plus, MA, USA) operating in positive full scan mode in the range of 80-1200  $m/z$ . The settings for electrospray ionization were as follows: 150 °C oven temperature and 3.6 kV source voltage. The acquired data were internally calibrated with phthalate as a contaminant in methanol ( $m/z$  297.15909). Samples were diluted to a final concentration of 0.1 mg/mL in a solution of water and acetonitrile (50:50, v/v). The samples were injected into the mass spectrometer following HPLC separation on a Kinetex C18 column (2.6  $\mu$ m, 100 Å, 50  $\times$  3.0 mm) using an isocratic mobile phase of 0.01M MeCN/ammonium acetate (80/20) at a flow rate of 0.3 mL/min.

All reactions carried out under microwave irradiation were performed with a CEM Discover® SP microwave synthesizer, using the Dynamic mode with the following settings: maximum amount of microwave power (150 W), premixing time (1 minute), and stirring speed (high). Simultaneous cooling of the reaction vessel provided by compressed air (24 psi) was applied during the entire experiment (PowerMax option "ON"). All 0.5 mmol scale reactions were performed in a 10 mL borosilicate glass reaction vessel closed with a disposable silicon cap and equipped with a Teflon coated egg-shaped magnetic stir bar. The temperature was monitored by an external infrared sensor.

Solid phase synthesis was carried out on Domino Blocks in disposable polypropylene reaction vessels (Torviq, Niles, MI). The resulting crude products were purified on C18 column 19  $\times$  100 mm for 5  $\mu$ m particles; gradient was formed from 10 mM aqueous ammonium acetate and acetonitrile with a flow rate 15mL/min. For lyophilization of residual solvents at -110 °C SanVac Coolsafe 110-4 was used.

Considering the characterization of all the synthesized compounds, there are presented analytical data on all the new final compounds as well as their precursors not yet reported in the literature. **Supporting information** is attached as an electronic file containing NMR spectra.



## 6.2 Synthesis of TZD-hydroxamates

### General procedure for Knoevenagel condensation reactions

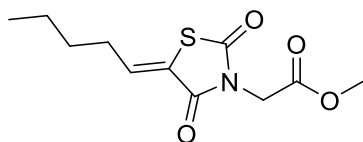
A mixture of thiazolidinedione **IV-3**, aldehyde (1.0 eq), piperidine (0.8 eq) and EtOH (0.1 M) was refluxed on for 16-20 h and worked up according to *method A* or *B*.

*Method A*: The reaction mixture was poured into H<sub>2</sub>O, acidified with AcOH (pH ≈ 1) and filtered.

*Method B*: The product was concentrated *in vacuum* and purified by column chromatography (Hex/EtOAc, isocratic 25 %).

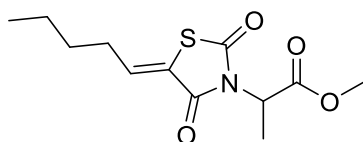
### General procedure for reactions with bromoesters

Thiazolidinedione **IV-3** or **IV-6** was dissolved in dry DMF (0.8 M). NaH (1.0 eq) was slowly added to the reaction mixture followed by stirring at rt for 10 min. The bromoester (1.0 eq) was added dropwise. After stirring for 24 h, the reaction mixture was diluted with water. The product was extracted with DCM, organic layers were washed with 5% aq. HCl, brine, dried over Na<sub>2</sub>SO<sub>4</sub> and concentrated *in vacuum*.



### Methyl (Z)-2-(2,4-dioxo-5-pentylidenethiazolidin-3-yl)acetate **IV-7A**

Orange oil. Yield: 81 % (822 mg). <sup>1</sup>H NMR (500 MHz, DMSO-*d*<sub>6</sub>): δ 7.12 (t, *J* = 7.7 Hz, 1H), 4.44 (s, 2H), 3.70 (s, 3H), 2.28 – 2.23 (m, 2H), 1.53 – 1.47 (m, 2H), 1.35 – 1.30 (m, 2H), 0.89 (t, *J* = 7.3 Hz, 3H). <sup>13</sup>C NMR (126 MHz, DMSO-*d*<sub>6</sub>): δ 167.2, 166.6, 163.6, 140.1, 123.9, 52.6, 41.8, 31.0, 29.2, 21.7, 13.6. HRMS: *m/z*: calcd for C<sub>11</sub>H<sub>15</sub>NO<sub>4</sub>S: 258.0795 [M+H]<sup>+</sup>; found: 258.0796.



### Methyl (Z)-2-(2,4-dioxo-5-pentylidenethiazolidin-3-yl)propanoate **IV-7B**

The crude product was purified by column chromatography (DCM/MeOH, isocratic 2 %). Brown solid. Yield: 44 % (467 mg). <sup>1</sup>H NMR (500 MHz, DMSO-*d*<sub>6</sub>): δ 7.10 (t, *J* =

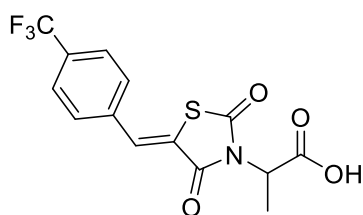
7.7 Hz, 1H), 5.07 (q,  $J = 7.1$  Hz, 1H), 3.65 (s, 3H), 2.27 – 2.22 (m, 2H), 1.51 – 1.46 (m, 2H), 1.47 (d,  $J = 7.7$  Hz, 2H), 1.35 – 1.30 (m, 2H), 0.89 (d,  $J = 7.3$  Hz, 3H).  $^{13}\text{C}$  NMR (126 MHz,  $\text{DMSO-}d_6$ ):  $\delta$  169.0, 166.4, 163.4, 140.1, 123.8, 52.6, 49.98, 31.0, 29.2, 21.8, 14.0, 13.6. HRMS:  $m/z$ : calcd for  $\text{C}_{12}\text{H}_{17}\text{NO}_4\text{S}$ : 272.0951  $[\text{M}+\text{H}]^+$ ; found: 272.0952.

### Ester hydrolysis

Methyl ester **IV-5** or **IV-7** (1.0 eq) was dissolved in 40% aq. HBr (0.6 M) and refluxed for 5 h. The mixture was cooled down to rt and diluted with  $\text{H}_2\text{O}$  and worked up according to *method A* or *B*.

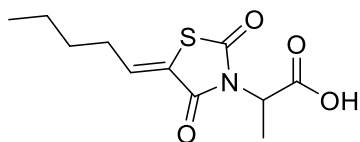
*Method A*: The resulting suspension was filtered, washed with  $\text{H}_2\text{O}$  (10 mL) and the solid was lyophilized overnight.

*Method B*: The product was extracted with EtOAc ( $3 \times 10$  mL), washed with brine (10 mL), dried over  $\text{Na}_2\text{SO}_4$  and concentrated *in vacuo*.



### (*Z*)-2-(2,4-Dioxo-5-(4-trifluoromethyl)benzylidene)thiazolidin-3-yl)propanoic acid **IV-8A**

*Method A*. Brown solid. Yield: 55 % (734 mg).  $^1\text{H}$  NMR (500 MHz,  $\text{DMSO-}d_6$ ):  $\delta$  13.28 (s, 1H), 8.06 (s, 1H), 7.91 (d,  $J = 8.3$  Hz, 2H), 7.86 (d,  $J = 8.3$  Hz, 2H), 5.03 (q,  $J = 7.2$  Hz, 1H), 1.52 (d,  $J = 7.2$  Hz, 3H).  $^{13}\text{C}$  NMR (126 MHz,  $\text{DMSO-}d_6$ ):  $\delta$  169.9, 166.3, 164.6, 136.8, 131.9, 130.6, 130.0 (q,  $J = 32.7$  Hz), 126.1, 123.8 (q,  $J = 272.1$  Hz), 123.7, 50.5, 13.9. HRMS:  $m/z$ : calcd for  $\text{C}_{14}\text{H}_{10}\text{F}_3\text{NO}_4\text{S}$ : 346.0355  $[\text{M}+\text{H}]^+$ ; found: 346.0358.



### (*Z*)-2-(2,4-Dioxo-5-pentylidenethiazolidin-3-yl)propanoic acid **IV-8B**

*Method B*. Brown solid. Yield: 83 % (415 mg).  $^1\text{H}$  NMR (500 MHz,  $\text{DMSO-}d_6$ ):  $\delta$  13.16 (s, 1H), 7.08 (t,  $J = 7.7$  Hz, 1H), 4.93 (q,  $J = 7.2$  Hz, 1H), 2.24 – 2.21 (m, 2H), 1.51 – 1.45 (m, 2H), 1.46 (d,  $J = 7.7$  Hz, 3H), 1.35 – 1.29 (m, 2H), 0.89 (t,  $J = 7.3$  Hz, 3H).  $^{13}\text{C}$  NMR

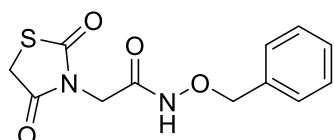
(126 MHz, DMSO-*d*<sub>6</sub>):  $\delta$  170.0, 166.5, 163.6, 139.6, 123.9, 50.1, 31.0, 29.3, 21.8, 13.9, 13.6. HRMS: *m/z*: calcd for C<sub>11</sub>H<sub>15</sub>NO<sub>4</sub>S: 258.0795 [M+H]<sup>+</sup>; found: 258.0795.

### Reaction with hydroxylamine.HCl

Carboxylic acid (1.0 eq) **IV-5** or **IV-8** was suspended in water (0.05 M). Hydroxylamine.HCl (1.5 eq) was dissolved in water (0.05 M). The amine solution was added to the acid suspension and the pH was adjusted to 4.5 with 1 M aq. NaOH. THF was added until a homogeneous solution was obtained. EDC.HCl (3.0 eq) was dissolved in water (0.1 M) and added in aliquots (4 mL/1 min) to the reaction mixture. The reaction was stirred for 2 h and worked up according to the *method A* or *B*.

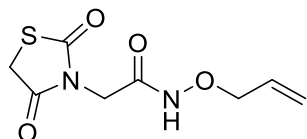
*Method A*: The reaction was filtered and the solid was lyophilized overnight.

*Method B*: The product was extracted with EtOAc (3 × 30 mL), washed with saturated aq. NaHCO<sub>3</sub> (30 mL), brine (30 mL), dried over Na<sub>2</sub>SO<sub>4</sub> and concentrated *in vacuo*.



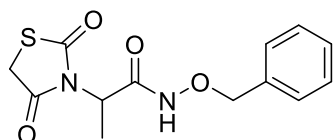
### *N*-(benzyloxy)-2-(2,4-dioxothiazolidin-3-yl)acetamide **IV-1A**

*Method A*. Mobile phase: DCM/MeOH, isocratic 10 %. White solid. Yield: 49 % (277 mg). <sup>1</sup>H NMR (500 MHz, DMSO-*d*<sub>6</sub>):  $\delta$  11.22 (s, 1H), 7.42 – 7.35 (m, 5H), 4.82 (s, 2H), 4.25 (s, 2H), 4.10 (s, 2H). <sup>13</sup>C NMR (126 MHz, DMSO-*d*<sub>6</sub>):  $\delta$  171.8, 171.5, 162.7, 135.7, 128.9, 128.3, 77.1, 41.1, 34.0. HRMS: *m/z*: calcd for C<sub>12</sub>H<sub>12</sub>N<sub>2</sub>O<sub>4</sub>S: 281.0591 [M+H]<sup>+</sup>; found: 281.0592.



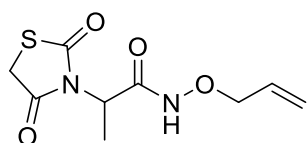
### *N*-(allyloxy)-2-(2,4-dioxothiazolidin-3-yl)acetamide **IV-1B**

*Method B*. Mobile phase: CHCl<sub>3</sub>/MeOH, isocratic 10 %. Yellow oil. Yield: 55 % (257 mg). <sup>1</sup>H NMR (500 MHz, DMSO-*d*<sub>6</sub>):  $\delta$  11.35 (s, 1H), 5.95 – 5.87 (ddt, *J* = 17.3, 10.4, 6.0 Hz, 1H), 5.31 (d, *J* = 17.3 Hz, 1H), 5.26 (d, *J* = 10.4 Hz, 1H), 4.27 (app br s, 4H), 4.03 (s, 2H). <sup>13</sup>C NMR (126 MHz, DMSO-*d*<sub>6</sub>):  $\delta$  171.8, 171.4, 162.5, 132.7, 119.5, 76.1, 41.1, 34.0. HRMS: *m/z*: calcd for C<sub>8</sub>H<sub>10</sub>N<sub>2</sub>O<sub>4</sub>S: 231.0434 [M+H]<sup>+</sup>; found: 231.0435.



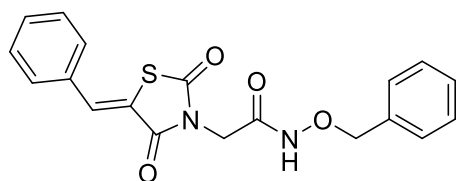
***N*-(benzyloxy)-2-(2,4-dioxothiazolidin-3-yl)propanamide IV-1C**

*Method B.* Mobile phase: DCM/MeOH, isocratic 10 %. Yellow oil. Yield: 61 % (342 mg). <sup>1</sup>H NMR (500 MHz, DMSO-*d*<sub>6</sub>): δ 11.35 (s, 1H), 7.40 – 7.38 (m, 4H), 7.37 – 7.36 (m, 1H), 4.75 (AB system, δ<sub>A</sub> 4.74, δ<sub>B</sub> 4.76, *J*<sub>AB</sub> = 10.7, 2H), 4.68 (q, *J* = 7.1 Hz, 1H), 4.16 (s, 2H), 1.40 (d, *J* = 7.1 Hz, 3H). <sup>13</sup>C NMR (126 MHz, DMSO-*d*<sub>6</sub>): δ 171.7, 171.3, 165.1, 135.7, 128.9, 128.3, 76.9, 49.4, 34.0, 13.6. HRMS: *m/z*: calcd for C<sub>13</sub>H<sub>14</sub>N<sub>2</sub>O<sub>4</sub>S: 295.0747 [M+H]<sup>+</sup>; found: 295.0749.



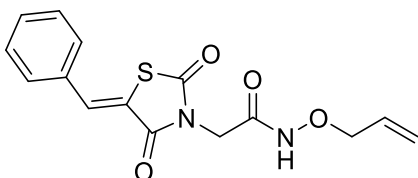
***N*-(allyloxy)-2-(2,4-dioxothiazolidin-3-yl)propanamide IV-1D**

*Method B.* Mobile phase: CHCl<sub>3</sub>/MeOH, isocratic 10 %. Yellow oil. Yield: 52 % (240 mg). <sup>1</sup>H NMR (500 MHz, DMSO-*d*<sub>6</sub>): δ 11.24 (s, 1H), 5.94 – 5.86 (m, 1H), 5.30 (dd, *J* = 17.3, 1.6 Hz, 1H), 5.24 (d, *J* = 10.5 Hz, 1H), 4.65 (q, *J* = 7.1 Hz, 1H), 4.25 – 4.23 (m, 2H), 4.16 (s, 2H), 1.38 (d, *J* = 7.1 Hz, 3H). <sup>13</sup>C NMR (126 MHz, DMSO-*d*<sub>6</sub>): δ 171.66, 171.29, 164.87, 132.80, 119.24, 75.83, 49.33, 34.02, 13.59. HRMS: *m/z*: calcd for C<sub>9</sub>H<sub>12</sub>N<sub>2</sub>O<sub>4</sub>S: 245.0591 [M+H]<sup>+</sup>; found: 245.0593.



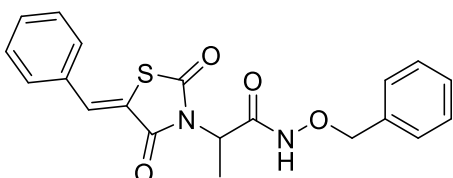
**(*Z*)-2-(5-benzylidene-2,4-dioxothiazolidin-3-yl)-*N*-(benzyloxy)acetamide IV-2A**

*Method A.* White solid. Yield: 58 % (451 mg). <sup>1</sup>H NMR (500 MHz, DMSO-*d*<sub>6</sub>): δ 11.34 (s, 1H), 7.96 (s, 1H), 7.65 (d, *J* = 7.3 Hz, 2H), 7.56 (t, *J* = 7.3 Hz, 2H), 7.52 (d, *J* = 7.1 Hz, 1H), 7.42 – 7.37 (m, 5H), 4.84 (s, 2H), 4.28 (s, 2H). <sup>13</sup>C NMR (126 MHz, DMSO-*d*<sub>6</sub>): δ 166.96, 165.15, 162.54, 135.64, 133.50, 132.83, 130.77, 130.15, 129.39, 128.91, 128.33, 121.00, 77.10, 41.50. HRMS: *m/z*: calcd for C<sub>19</sub>H<sub>16</sub>N<sub>2</sub>O<sub>4</sub>S: 369.0904 [M+H]<sup>+</sup>; found: 369.0907.



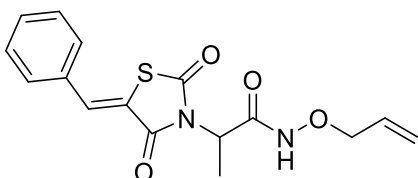
**(Z)-N-(allyloxy)-2-(5-benzylidene-2,4-dioxothiazolidin-3-yl)acetamide IV-2B**

*Method A.* White solid. Yield: 51 % (339 mg).  $^1\text{H}$  NMR (500 MHz,  $\text{DMSO-}d_6$ ):  $\delta$  11.26 (s, 1H), 7.96 (s, 1H), 7.64 (d,  $J = 6.0$  Hz, 2H), 7.58 – 7.51 (m, 3H), 5.96 (s, 1H), 5.35 (d,  $J = 17.2$  Hz, 1H), 5.28 (d,  $J = 9.2$  Hz, 1H), 4.30 (app br s, 4H).  $^{13}\text{C}$  NMR (126 MHz,  $\text{DMSO-}d_6$ ):  $\delta$  166.94, 165.13, 162.38, 133.48, 132.82, 132.69, 130.77, 130.14, 129.39, 120.99, 119.54, 76.09, 41.46. HRMS:  $m/z$ : calcd for  $\text{C}_{15}\text{H}_{14}\text{N}_2\text{O}_4\text{S}$ : 319.0747  $[\text{M}+\text{H}]^+$ ; found: 319.0749.



**(Z)-2-(5-benzylidene-2,4-dioxothiazolidin-3-yl)-N-(benzyloxy)propanamide IV-2C**

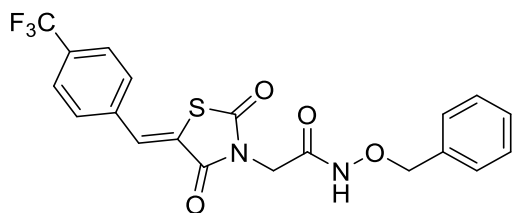
*Method B.* Mobile phase: DCM/MeOH, isocratic 2 %. Yellow solid. Yield: 64 % (373 mg).  $^1\text{H}$  NMR (500 MHz,  $\text{DMSO-}d_6$ ):  $\delta$  11.46 (s, 1H), 7.94 (s, 1H), 7.65 (d,  $J = 7.4$  Hz, 2H), 7.58 – 7.50 (m, 3H), 7.40 – 7.34 (m, 5H), 4.87 (q,  $J = 7.1$  Hz, 1H), 4.77 (AB system,  $\delta_A$  4.75,  $\delta_B$  4.79,  $J_{AB} = 10.7$ , 2H), 1.50 (d,  $J = 7.1$  Hz, 3H).  $^{13}\text{C}$  NMR (126 MHz,  $\text{DMSO-}d_6$ ):  $\delta$  166.75, 164.99, 164.90, 135.69, 132.96, 130.63, 130.05, 129.40, 128.97, 128.27, 121.36, 76.92, 49.85, 13.86. HRMS:  $m/z$ : calcd for  $\text{C}_{20}\text{H}_{18}\text{N}_2\text{O}_4\text{S}$ : 383.1060  $[\text{M}+\text{H}]^+$ ; found: 383.1058.



**(Z)-N-(allyloxy)-2-(5-benzylidene-2,4-dioxothiazolidin-3-yl)propanamide IV-2D**

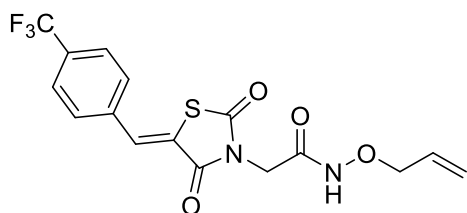
*Method B.* Mobile phase: DCM/MeOH, isocratic 2 %. Yellow solid. Yield: 62 % (314 mg).  $^1\text{H}$  NMR (500 MHz,  $\text{DMSO-}d_6$ ):  $\delta$  11.36 (s, 1H), 7.94 (s, 1H), 7.64 (d,  $J = 7.4$  Hz, 2H), 7.58 – 7.51 (m, 3H), 5.91 (ddt,  $J = 17.3, 11.7, 6.1$  Hz, 1H), 5.31 (d,  $J = 17.3$  Hz, 1H), 5.24 (d,  $J = 11.7$  Hz, 1H), 4.85 (q,  $J = 7.1$  Hz, 1H), 4.29 – 4.24 (m, 2H), 1.48 (d,  $J = 7.1$  Hz, 3H).  $^{13}\text{C}$  NMR (126 MHz,  $\text{DMSO-}d_6$ ):  $\delta$  166.72, 164.98, 164.70, 132.95, 132.82,

130.63, 130.05, 129.39, 121.36, 119.30, 75.87, 49.81, 13.85. HRMS: m/z: calcd for C<sub>16</sub>H<sub>16</sub>N<sub>2</sub>O<sub>4</sub>S: 333.0904 [M+H]<sup>+</sup>; found: 333.0905.



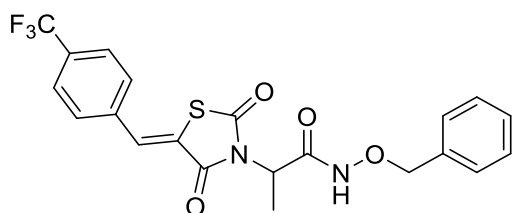
**(Z)-N-(benzyloxy)-2-(2,4-dioxo-5-(4-trifluoromethyl)benzylidene)thiazolidin-3-yl)acetamide IV-2E**

*Method A.* White solid. Yield: 49 % (298 mg). <sup>1</sup>H NMR (500 MHz, DMSO-*d*<sub>6</sub>): δ 11.35 (s, 1H), 8.04 (s, 1H), 7.90 – 7.85 (m, 4H), 7.43 – 7.37 (m, 5H), 4.85 (s, 2H), 4.29 (s, 2H). <sup>13</sup>C NMR (126 MHz, DMSO-*d*<sub>6</sub>): δ 166.6, 164.9, 162.5, 136.8, 135.63, 131.7, 130.0 (q, *J* = 31.5 Hz), 128.9, 128.3, 126.1, 124.0, 123.8 (q, *J* = 273.4 Hz), 77.1, 41.6. HRMS: m/z: calcd for C<sub>20</sub>H<sub>15</sub>F<sub>3</sub>N<sub>2</sub>O<sub>4</sub>S: 437.0777 [M+H]<sup>+</sup>; found: 437.0775.



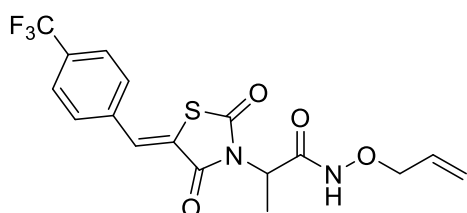
**(Z)-N-(allyloxy)-2-(2,4-dioxo-5-(4-trifluoromethyl)benzylidene)thiazolidin-3-yl)acetamide IV-2F**

*Method A.* Yellow solid. Yield: 50 % (289 mg). <sup>1</sup>H NMR (500 MHz, DMSO-*d*<sub>6</sub>): δ 11.27 (s, 1H), 8.03 (s, 1H), 7.89 (d, *J* = 8.4 Hz, 2H), 7.85 (d, *J* = 8.4 Hz, 2H), 6.00 – 5.91 (m, 1H), 5.35 (d, *J* = 17.2 Hz, 1H), 5.28 (d, *J* = 10.1 Hz, 1H), 4.33 (app br s, 4H). <sup>13</sup>C NMR (126 MHz, DMSO-*d*<sub>6</sub>): δ 166.6, 164.9, 162.3, 136.8, 132.7, 131.7, 130.6, 130.0 (q, *J* = 31.5 Hz), 126.2, 124.0, 123.8 (q, *J* = 272.1 Hz), 119.6, 76.1, 41.6. HRMS: m/z: calcd for C<sub>16</sub>H<sub>13</sub>F<sub>3</sub>N<sub>2</sub>O<sub>4</sub>S: 387.0621 [M+H]<sup>+</sup>; found: 387.0621.



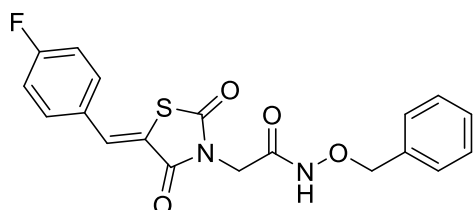
**(Z)-N-(benzyloxy)-2-(2,4-dioxo-5-(4-trifluoromethyl)benzylidene)thiazolidin-3-yl)propanamide IV-2G**

*Method B.* Mobile phase: DCM/MeOH, isocratic 5 %. White solid. Yield: 48 % (126 mg). <sup>1</sup>H NMR (500 MHz, DMSO-*d*<sub>6</sub>): δ 11.47 (s, 1H), 8.03 (s, 1H), 7.91 (d, *J* = 8.1 Hz, 2H), 7.86 (d, *J* = 8.1 Hz, 2H), 7.41 – 7.34 (m, 5H), 4.88 (q, *J* = 7.0 Hz, 1H), 4.77 (AB system, δ<sub>A</sub> 4.75, δ<sub>B</sub> 4.79, *J*<sub>AB</sub> = 10.7, 2H), 1.50 (d, *J* = 7.0 Hz, 3H). <sup>13</sup>C NMR (126 MHz, DMSO-*d*<sub>6</sub>): δ 166.4, 164.8, 164.8, 136.9, 135.7, 131.1, 130.5, 129.9 (q, *J* = 32.7), 129.0, 128.3, 126.2, 124.4, 123.8 (q, *J* = 273.4 Hz), 50.0, 13.8. HRMS: *m/z*: calcd for C<sub>21</sub>H<sub>17</sub>F<sub>3</sub>N<sub>2</sub>O<sub>4</sub>S: 451.0934 [M+H]<sup>+</sup>; found: 451.0934.



**(Z)-N-(allyloxy)-2-(2,4-dioxo-5-(4-trifluoromethyl)benzylidene)thiazolidin-3-yl)propanamide IV-2H**

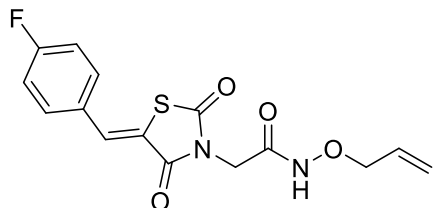
*Method B.* Mobile phase: DCM/MeOH, isocratic 2 %. White solid. Yield: 31 % (127 mg). <sup>1</sup>H NMR (500 MHz, DMSO-*d*<sub>6</sub>): δ 11.37 (s, 1H), 8.02 (s, 1H), 7.91 (d, *J* = 8.2 Hz, 2H), 7.85 (d, *J* = 8.2 Hz, 2H), 5.91 (ddt, *J* = 17.3, 11.8, 6.1 Hz, 1H), 5.31 (d, *J* = 17.3 Hz, 1H), 5.24 (d, *J* = 10.4 Hz, 1H), 4.86 (q, *J* = 7.0 Hz, 1H), 4.28 – 4.25 (m, 2H), 1.49 (d, *J* = 7.0 Hz, 3H). <sup>13</sup>C NMR (126 MHz, DMSO-*d*<sub>6</sub>): δ 166.4, 164.8, 164.6, 136.9, 132.8, 131.0, 130.5, 129.9 (q, *J* = 31.5 Hz), 126.2, 124.4, 123.8 (q, *J* = 272.1 Hz), 119.3, 75.9, 49.9, 13.8. HRMS: *m/z*: calcd for C<sub>17</sub>H<sub>15</sub>F<sub>3</sub>N<sub>2</sub>O<sub>4</sub>S: 401.0777 [M+H]<sup>+</sup>; found: 401.0775.



**(Z)-N-(benzyloxy)-2-(5-(4-fluorobenzylidene)-2,4-dioxothiazolidin-3-yl)acetamide IV-2I**

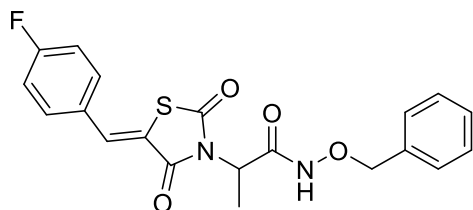
*Method A.* Yellow solid. Yield: 75 % (617 mg). <sup>1</sup>H NMR (500 MHz, DMSO-*d*<sub>6</sub>): δ 11.33 (s, 1H), 7.98 – 7.96 (m, 1H), 7.71 (dd, *J* = 12.5, 6.7 Hz, 2H), 7.42 – 7.36 (m, 7H), 4.84 (s, 2H), 4.27 (s, 2H). <sup>13</sup>C NMR (126 MHz, DMSO-*d*<sub>6</sub>): δ 165.5 (d, *J* = 218.4 Hz), 164.06,

162.5, 162.1, 135.6, 132.7 (m), 132.5 (d,  $J = 7.0$  Hz), 129.5, 128.9 (d,  $J = 22.1$  Hz), 128.3 (d,  $J = 22.1$  Hz), 120.7, 116.6 (m), 116.6, 77.1, 41.5. HRMS:  $m/z$ : calcd for  $C_{19}H_{15}FN_2O_4S$ : 387.0809  $[M+H]^+$ ; found: 387.0813.



**(Z)-N-(allyloxy)-2-(5-(4-fluorobenzylidene)-2,4-dioxothiazolidin-3-yl)acetamide IV-2J**

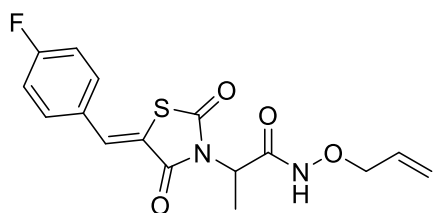
*Method A.* Yellow solid. Yield: 75 % (432 mg).  $^1H$  NMR (500 MHz,  $DMSO-d_6$ ):  $\delta$  11.25 (s, 1H), 7.97 (s, 1H), 7.74 – 7.69 (m, 2H), 7.38 (t,  $J = 8.4$  Hz, 2H), 6.00 – 5.91 (m, 1H), 5.35 (d,  $J = 17.1$  Hz, 2H), 5.28 (d,  $J = 9.5$  Hz, 2H), 4.32 (app br s, 4H).  $^{13}C$  NMR (126 MHz,  $DMSO-d_6$ ):  $\delta$  166.0 (d,  $J = 216.7$  Hz), 162.4, 162.1, 132.7 (d,  $J = 9.3$  Hz), 132.4, 129.5, 120.7, 119.5, 116.6 (d,  $J = 21.5$  Hz), 116.6, 116.4, 76.1, 41.5. HRMS:  $m/z$ : calcd for  $C_{15}H_{13}FN_2O_4S$ : 337.0653  $[M+H]^+$ ; found: 337.0653.



**(Z)-N-(benzyloxy)-2-(5-(4-fluorobenzylidene)-2,4-dioxothiazolidin-3-yl)propanamide IV-2K**

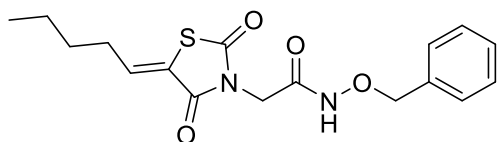
*Method B.* Mobile phase: DCM/MeOH, isocratic 2 %. Green solid. Yield: 45 % (62 mg).  $^1H$  NMR (500 MHz,  $DMSO-d_6$ ):  $\delta$  11.46 (s, 1H), 7.96 (s, 1H), 7.72 (dd,  $J = 8.5, 5.5$  Hz, 2H), 7.43 – 7.34 (m, 7H), 4.87 (q,  $J = 7.1$  Hz, 1H), 4.77 (AB system,  $\delta_A$  4.75,  $\delta_B$  4.79,  $J_{AB} = 10.7$ , 2H), 1.49 (d,  $J = 7.1$  Hz, 3H).  $^{13}C$  NMR (126 MHz,  $DMSO-d_6$ ):  $\delta$  165.8 (d,  $J = 210.3$  Hz), 164.9, 164.0, 162.0, 135.7, 132.6 (d,  $J = 8.8$  Hz), 131.9, 129.6, 129.0, 128.3, 128.3, 121.1, 116.6 (d,  $J = 22.6$  Hz), 76.9, 49.9, 13.9. HRMS:  $m/z$ : calcd for  $C_{20}H_{17}FN_2O_4S$ : 401.0966  $[M+H]^+$ ; found: 401.0968.





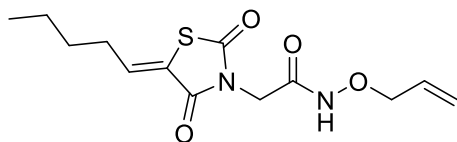
**(Z)-N-(allyloxy)-2-(5-(4-fluorobenzylidene)-2,4-dioxothiazolidin-3-yl)propanamide  
IV-2L**

*Method B.* Mobile phase: DCM/MeOH, isocratic 5 %. Green solid. Yield: 45 % (54 mg).  $^1\text{H}$  NMR (500 MHz, DMSO- $d_6$ ):  $\delta$  11.35 (s, 1H), 7.95 (s, 1H), 7.72 (dd,  $J = 8.7, 5.4$  Hz, 2H), 7.41 (t,  $J = 8.7$  Hz, 2H), 5.95 – 5.87 (m, 1H), 5.30 (d,  $J = 16.0$  Hz, 1H), 5.24 (d,  $J = 10.4$  Hz, 1H), 4.84 (q,  $J = 7.1$  Hz, 1H), 4.28 – 4.25 (m, 2H), 1.48 (d,  $J = 7.1$  Hz, 3H).  $^{13}\text{C}$  NMR (126 MHz, DMSO- $d_6$ ):  $\delta$  165.8 (d,  $J = 208.6$  Hz), 164.7, 162.0, 132.8, 132.6 (d,  $J = 8.8$  Hz), 131.9, 129.6, 129.6, 121.1, 119.3, 116.6 (d,  $J = 22.2$  Hz), 75.88, 49.84, 13.84. HRMS:  $m/z$ : calcd for  $\text{C}_{16}\text{H}_{15}\text{FN}_2\text{O}_4\text{S}$ : 351.0809  $[\text{M}+\text{H}]^+$ ; found: 351.0811.



**(Z)-N-(benzyloxy)-2-(2,4-dioxo-5-pentylidenethiazolidin-3-yl)acetamide IV-2M**

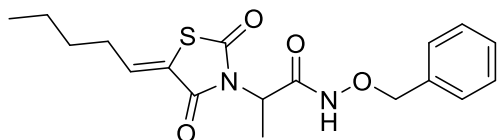
*Method B.* Brown solid. Yield: 35 % (174 mg).  $^1\text{H}$  NMR (500 MHz, DMSO- $d_6$ ):  $\delta$  11.29 (s, 1H), 7.43 – 7.37 (m, 5H), 7.12 – 7.06 (m, 1H), 4.85 – 4.81 (m, 2H), 4.21 (s, 2H), 2.31 – 2.24 (m, 2H), 1.56 – 1.50 (m, 2H), 1.40 – 1.32 (m, 2H), 0.95 – 0.89 (m, 3H).  $^{13}\text{C}$  NMR (126 MHz, DMSO- $d_6$ ):  $\delta$  166.8, 163.9, 162.6, 139.3, 135.6, 128.9, 128.3, 128.3, 124.3, 77.1, 41.2, 31.0, 29.3, 21.8, 13.6. HRMS:  $m/z$ : calcd for  $\text{C}_{17}\text{H}_{20}\text{N}_2\text{O}_4\text{S}$ : 349.1217  $[\text{M}+\text{H}]^+$ ; found: 349.1217.



**(Z)-N-(allyloxy)-2-(2,4-dioxo-5-pentylidenethiazolidin-3-yl)acetamide IV-2N**

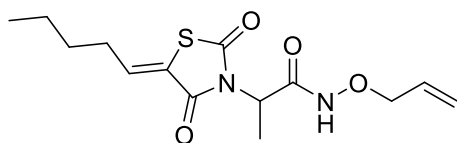
*Method B.* Mobile phase: Hex/EtOAc, isocratic 40 %. Yellow solid. Yield: 40 % (178 mg).  $^1\text{H}$  NMR (500 MHz, DMSO- $d_6$ ):  $\delta$  11.40 (s, 1H), 7.08 (t,  $J = 7.7$  Hz, 1H), 5.91 (ddt,  $J = 17.3, 10.4, 6.0$  Hz, 1H), 5.32 (d,  $J = 17.3$  Hz, 1H), 5.26 (d,  $J = 10.4$  Hz, 1H), 4.35 – 4.13 (m, 4H), 2.27 – 2.22 (m, 2H), 1.50 (q,  $J = 7.4$  Hz, 2H), 1.32 (h,  $J = 7.4$  Hz, 2H), 0.89

(t,  $J = 7.3$  Hz, 3H).  $^{13}\text{C}$  NMR (126 MHz, DMSO- $d_6$ ):  $\delta$  166.76, 163.9, 162.4, 139.3, 132.7, 124.3, 119.5, 76.1, 41.2, 30.9, 29.3, 21.7, 13.6. HRMS:  $m/z$ : calcd for  $\text{C}_{13}\text{H}_{18}\text{N}_2\text{O}_4\text{S}$ : 299.1060  $[\text{M}+\text{H}]^+$ ; found: 299.1060.



**(Z)-N-(benzyloxy)-2-(2,4-dioxo-5-pentylidenethiazolidin-3-yl)propanamide IV-2O**

*Method B.* Mobile phase: DCM/MeOH, isocratic 5 %. Yellow oil. Yield: 60 % (160 mg).  $^1\text{H}$  NMR (500 MHz, DMSO- $d_6$ ):  $\delta$  11.41 (s, 1H), 7.39 – 7.34 (m, 5H), 7.04 (app t,  $J = 7.7$  Hz, 1H), 4.79 – 4.74 (m, 3H), 2.23 (q,  $J = 7.3$  Hz, 2H), 1.51 – 1.48 (m, 2H), 1.45 (d,  $J = 7.3$  Hz, 3H), 1.35 – 1.30 (m, 2H), 0.89 (t,  $J = 7.3$  Hz, 3H).  $^{13}\text{C}$  NMR (126 MHz, DMSO- $d_6$ ):  $\delta$  166.6, 164.9, 163.7, 138.6, 135.7, 129.0, 128.3, 124.5, 76.9, 49.6, 30.9, 29.3, 21.8, 13.9, 13.6. HRMS:  $m/z$ : calcd for  $\text{C}_{18}\text{H}_{22}\text{N}_2\text{O}_4\text{S}$ : 363.1373  $[\text{M}+\text{H}]^+$ ; found: 363.1372.



**(Z)-N-(allyloxy)-2-(2,4-dioxo-5-pentylidenethiazolidin-3-yl)propanamide IV-2P**

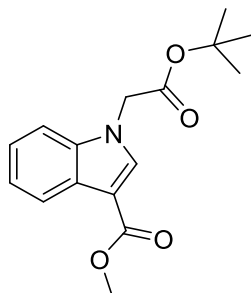
*Method B.* Mobile phase: DCM/MeOH, isocratic 15 %. Yellow oil. Yield: 56 % (129 mg).  $^1\text{H}$  NMR (500 MHz, DMSO- $d_6$ ):  $\delta$  11.31 (s, 1H), 7.04 (t,  $J = 7.7$ , 1H), 5.91 (ddt,  $J = 17.0, 11.2, 5.9$  Hz, 1H), 5.32 – 5.27 (m, 1H), 5.25 – 5.22 (m, 1H), 4.76 (q,  $J = 7.1$  Hz, 1H), 4.26 – 4.23 (m, 2H), 2.25 – 2.20 (m, 2H), 1.51 – 1.47 (m, 2H), 1.43 (d,  $J = 7.1$  Hz, 3H), 1.33 (h,  $J = 7.4$  Hz, 2H), 0.89 (t,  $J = 7.3$  Hz, 3H).  $^{13}\text{C}$  NMR (126 MHz, DMSO- $d_6$ ):  $\delta$  166.5, 164.7, 163.7, 138.6, 132.8, 124.5, 119.3, 75.8, 49.6, 30.9, 29.3, 21.8, 13.8, 13.6. HRMS:  $m/z$ : calcd for  $\text{C}_{14}\text{H}_{20}\text{N}_2\text{O}_4\text{S}$ : 313.1217  $[\text{M}+\text{H}]^+$ ; found: 313.1215.

## 6.3 Synthesis of indole/pyrrole-hydroxamates

### Typical procedure for *N*-alkylation

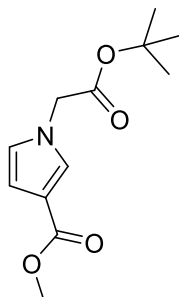
To a suspension of methyl 1*H*-indole-3-carboxylate **IV-16A** (1.0 eq, 10 mmol) and anhydrous  $\text{K}_2\text{CO}_3$  (2.3 eq, 23 mmol) in MeCN (50 mL) was added *tert*-butyl bromoacetate (1.4 eq, 14 mmol) and the reaction mixture was refluxed overnight. The mixture was cooled to rt, diluted with  $\text{H}_2\text{O}$  (100 mL) and extracted with EtOAc ( $3 \times 100$

mL). The combined organic layers were dried over Na<sub>2</sub>SO<sub>4</sub> and concentrated *in vacuum*. The residue was purified by column chromatography (PE/EtOAc, isocratic 20 %). The same procedure applied on methyl 1*H*-pyrrole-3-carboxylate **IV-16B** (1.0 eq, 20 mmol).



#### Methyl 1-(2-(*tert*-butoxy)-2-oxoethyl)-1*H*-indole-3-carboxylate **IV-17A**

Light orange amorphous solid. Yield: 90 % (2.62 g). <sup>1</sup>H NMR (400 MHz, CDCl<sub>3</sub>): δ 8.19 (m, 1H), 7.82 (s, 1H), 7.31 – 7.27 (m, 3H), 7.27 – 7.25 (m, 1H), 4.76 (s, 2H), 3.91 (s, 3H), 1.44 (s, 9H). <sup>13</sup>C NMR (101 MHz, CDCl<sub>3</sub>): δ 166.9, 165.5, 137.1, 135.2, 126.7, 123.3, 122.3, 122.0, 109.6, 108.3, 83.4, 51.2, 49.2, 28.1. HRMS: m/z: calcd for C<sub>16</sub>H<sub>19</sub>NO<sub>4</sub>: 290.1387 [M+H]<sup>+</sup>; found: 290.1385.



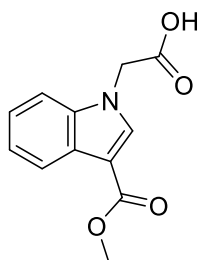
#### Methyl 1-(2-(*tert*-butoxy)-2-oxoethyl)-1*H*-pyrrole-3-carboxylate **IV-17B**

Yellow oil. Yield: 83 % (3.98 g). <sup>1</sup>H NMR (400 MHz, CDCl<sub>3</sub>): δ 7.30 – 7.27 (m, 1H), 6.64 – 6.57 (m, 2H), 4.51 (s, 2H), 3.79 (s, 3H), 1.47 (s, 9H). <sup>13</sup>C NMR (101 MHz, CDCl<sub>3</sub>): δ 167.0, 165.1, 127.1, 122.8, 116.7, 110.6, 83.1, 52.0, 51.1, 28.0. HRMS: m/z: calcd for C<sub>12</sub>H<sub>17</sub>NO<sub>4</sub>: 240.1230 [M+H]<sup>+</sup>; found: 240.1232.

#### Typical procedure for *tert*-butyl ester hydrolysis

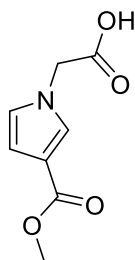
*Tert*-butyl ester **IV-17A** (1.0 eq, 9.1 mmol) was dissolved in CH<sub>2</sub>Cl<sub>2</sub> (27 mL), TFA (15.0 eq, 136 mmol) was added and the solution was stirred at rt for 2 h. The crude mixture was concentrated *in vacuum*.

The same procedure applied on *tert*-butyl ester **IV-17B** (1.0 eq, 16.6 mmol).



#### 2-(3-(Methoxycarbonyl)-1H-indol-1-yl)acetic acid **IV-18A**

Red amorphous solid. Yield: 95 % (2.00 g). <sup>1</sup>H NMR (400 MHz, DMSO-*d*<sub>6</sub>): δ 13.17 (br s, 1H), 8.13 (s, 1H), 8.04 – 7.98 (m, 1H), 7.55 – 7.45 (m, 1H), 7.29 – 7.19 (m, 2H), 5.13 (s, 2H), 3.81 (s, 3H). <sup>13</sup>C NMR (101 MHz, DMSO-*d*<sub>6</sub>): δ 169.7, 164.4, 136.9, 136.4, 125.8, 122.6, 121.6, 120.5, 110.8, 105.9, 50.7, 47.3. HRMS: *m/z*: calcd for C<sub>12</sub>H<sub>11</sub>NO<sub>4</sub>: 234.0761 [M+H]<sup>+</sup>; found: 234.0762.



#### 2-(3-(Methoxycarbonyl)-1H-pyrrol-1-yl)acetic acid **IV-18B**

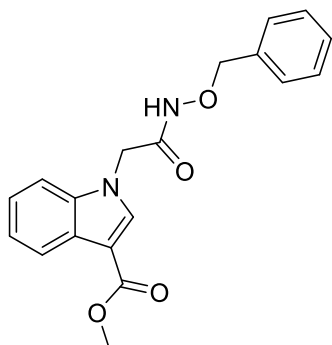
Light yellow amorphous solid. Yield: 98 % (3.01 mg). <sup>1</sup>H NMR (400 MHz, DMSO-*d*<sub>6</sub>): δ 12.99 (br s, 1H), 7.43 (dd, *J* = 2.2, 1.7 Hz, 1H), 6.80 (dd, *J* = 2.8, 2.2 Hz, 1H), 6.38 (dd, *J* = 2.8, 1.7 Hz, 1H), 4.80 (s, 2H), 3.69 (s, 3H). <sup>13</sup>C NMR (101 MHz, DMSO-*d*<sub>6</sub>): δ 170.0, 164.3, 127.8, 123.7, 114.6, 108.9, 50.6, 50.2. HRMS: *m/z*: calcd for C<sub>8</sub>H<sub>9</sub>NO<sub>4</sub>: 184.0604 [M+H]<sup>+</sup>; found: 184.0605.

#### General procedure for reaction with hydroxylamine.HCl

Carboxylic acid **IV-18A** (1.0 eq, 4.3 mmol) was suspended in water (12 mL). Hydroxylamine.HCl (1.5 eq, 6.4 mmol) was dissolved in water (20 mL). The hydroxylamine aq. solution was added to the acid suspension and the pH was adjusted to 4.5 with 1 M aq. NaOH. THF was added until a homogeneous solution was obtained. EDC.HCl (3.0 eq, 12.9 mmol) was dissolved in water (40 mL) and added in aliquots (12 mL every min) to the reaction mixture. The reaction was stirred for 4 h. The mixture was

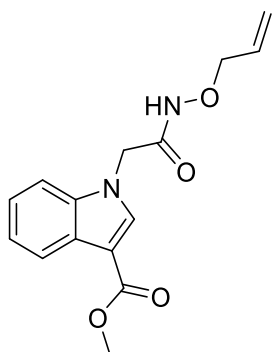
extracted with EtOAc (3 × 100 mL), washed with saturated aq. NaHCO<sub>3</sub> (150 mL), brine (150 mL), dried over MgSO<sub>4</sub> and concentrated *in vacuo*. The residue was purified by column chromatography (PE/EtOAc, isocratic 60 %).

The same procedure applied on carboxylic acid **IV-18B** (1.0 eq, 8.2 mmol).



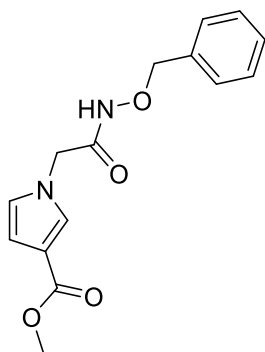
**Methyl 1-(2-((benzyloxy)amino)-2-oxoethyl)-1H-indole-3-carboxylate IV-19A**

White amorphous solid. Yield: 84 % (1222 mg). <sup>1</sup>H NMR (400 MHz, DMSO-*d*<sub>6</sub>): δ 11.31 (br s, 1H), 8.09 – 7.99 (m, 2H), 7.49 – 7.30 (m, 6H), 7.29 – 7.18 (m, 2H), 4.98 – 4.97 (m, 4H), 3.84 (s, 3H). <sup>13</sup>C NMR (101 MHz, DMSO-*d*<sub>6</sub>): δ 164.3, 163.8, 136.6; 136.6, 135.7, 128.9, 128.4, 128.3, 126.0, 122.6, 121.7, 120.6, 110.7, 105.8, 77.0, 50.7, 46.7. HRMS: m/z: calcd for C<sub>19</sub>H<sub>18</sub>N<sub>2</sub>O<sub>4</sub>: 337.1183 [M-H]<sup>+</sup>; found: 337.1186.



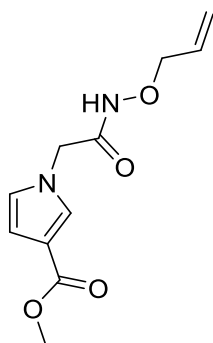
**Methyl 1-(2-((allyloxy)amino)-2-oxoethyl)-1H-indole-3-carboxylate IV-19B**

Orange amorphous solid. Yield: 83 % (1027 mg). <sup>1</sup>H NMR (400 MHz, DMSO-*d*<sub>6</sub>): δ 11.50 (br s, 1H), 8.11 (s, 1H), 8.06 – 7.97 (m, 1H), 7.50 – 7.40 (m, 1H), 7.32 – 7.18 (m, 2H), 6.17 – 5.82 (m, 1H), 5.36 – 5.18 (m, 2H), 4.86 (br s, 2H), 4.52 – 4.24 (m, 2H), 3.82 (s, 3H). <sup>13</sup>C NMR (101 MHz, DMSO-*d*<sub>6</sub>): δ 164.3, 163.7, 136.6, 136.6, 132.8, 126.0, 122.5, 121.7, 120.6, 119.6, 110.7, 105.8, 76.1, 50.7, 46.7. HRMS: m/z: calcd for C<sub>15</sub>H<sub>16</sub>N<sub>2</sub>O<sub>4</sub>: 287.1032 [M-H]<sup>+</sup>; found: 287.1035.



**Methyl 1-(2-((benzyloxy)amino)-2-oxoethyl)-1H-pyrrole-3-carboxylate IV-19C**

Yellow oil. Yield: 73 % (1738 mg).  $^1\text{H}$  NMR (400 MHz,  $\text{DMSO-}d_6$ ):  $\delta$  11.38 (br s, 1H), 7.50 – 7.29 (m, 6H), 6.81 – 6.60 (m, 1H), 6.46 – 6.28 (m, 1H), 4.90 (br s, 2H), 4.52 (s, 2H), 3.69 (s, 3H).  $^{13}\text{C}$  NMR (101 MHz,  $\text{DMSO-}d_6$ ):  $\delta$  164.2, 164.1, 135.7, 128.9, 128.3, 127.5, 123.4, 114.8, 109.2, 77.0, 50.6, 49.6. HRMS:  $m/z$ : calcd for  $\text{C}_{15}\text{H}_{16}\text{N}_2\text{O}_4$ : 289.1183  $[\text{M}+\text{H}]^+$ ; found: 289.1179.



**Methyl 1-(2-((allyloxy)amino)-2-oxoethyl)-1H-pyrrole-3-carboxylate IV-19D**

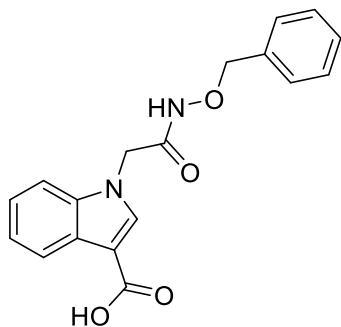
Light orange oil. Yield: 92 % (1818 mg).  $^1\text{H}$  NMR (400 MHz,  $\text{DMSO-}d_6$ ):  $\delta$  11.31 (br s, 1H), 7.44 – 7.37 (m, 1H), 6.76 (m, 1H), 6.44 – 6.35 (m, 1H), 6.06 – 5.83 (m, 1H), 5.45 – 5.21 (m, 2H), 4.52 (s, 2H), 4.36 – 4.19 (m, 2H), 3.69 (s, 3H).  $^{13}\text{C}$  NMR (101 MHz,  $\text{DMSO-}d_6$ ):  $\delta$  164.2, 164.0, 132.8, 127.5, 123.3, 119.5, 114.8, 109.2, 76.1, 50.6, 49.5. HRMS:  $m/z$ : calcd for  $\text{C}_{11}\text{H}_{14}\text{N}_2\text{O}_4$ : 239.1026  $[\text{M}+\text{H}]^+$ ; found: 239.1029.

**Typical procedure for methyl ester hydrolysis**

Methyl ester **IV-19A** or **IV-19B** (1.0 eq, 3.6 mmol) was dissolved in THF (36 mL). 2 M aq. LiOH solution (7 mL/mmol of **IV-19A** or **IV-19B**) was added and the reaction mixture was refluxed overnight. After cooling, the mixture was acidified ( $\text{pH} \approx 2$ ) with 12 M aq. HCl and extracted with EtOAc ( $3 \times 70$  mL). The combined organic layers were dried over

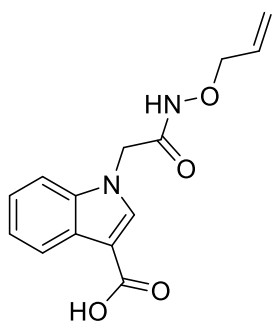
MgSO<sub>4</sub> and concentrated *in vacuum*. The residue was purified by column chromatography (PE/EtOAc, isocratic 60 %).

The same procedure applied on methyl ester **IV-19C** or **IV-19D** (1.0 eq, 6.0 mmol or 7.6 mmol respectively). **IV-20D** was synthesized at rt.



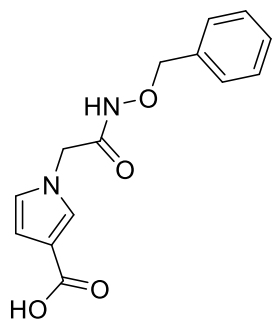
**1-(2-((Benzyloxy)amino)-2-oxoethyl)-1H-indole-3-carboxylic acid IV-20A**

Light pink amorphous solid. Yield: 88 % (1.03 g). <sup>1</sup>H NMR (400 MHz, DMSO-*d*<sub>6</sub>): δ 11.99 (br s, 1H), 11.56 (br s, 1H), 8.08 – 7.92 (m, 2H), 7.61 – 7.31 (m, 6H), 7.29 – 7.00 (m, 2H), 5.18 – 4.75 (m, 4H). <sup>13</sup>C NMR (101 MHz, DMSO-*d*<sub>6</sub>): δ 165.5, 163.9, 136.7, 136.5, 135.7, 128.9, 128.4, 128.3, 126.4, 122.3, 121.4, 120.8, 110.5, 106.9, 77.0, 46.7. HRMS: *m/z*: calcd for C<sub>18</sub>H<sub>16</sub>N<sub>2</sub>O<sub>4</sub>: 323.1026 [M-H]<sup>+</sup>; found: 323.1029.



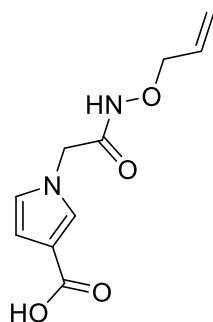
**1-(2-((Allyloxy)amino)-2-oxoethyl)-1H-indole-3-carboxylic acid IV-20B**

White amorphous solid. Yield: 56 % (548 mg). <sup>1</sup>H NMR (400 MHz, DMSO-*d*<sub>6</sub>): δ 11.80 (br s, 2H), 8.05 – 8.01 (m, 1H), 8.00 (s, 1H), 7.50 – 7.35 (m, 1H), 7.29 – 7.11 (m, 2H), 5.92 (ddt, *J* = 16.9, 11.6, 6.0 Hz, 1H), 5.49 – 5.20 (m, 2H), 4.84 (s, 2H), 4.63 – 4.20 (m, 2H). <sup>13</sup>C NMR (101 MHz, DMSO-*d*<sub>6</sub>): δ 165.5, 163.8, 136.7, 136.5, 132.8, 126.4, 122.3, 121.4, 120.8, 119.6, 110.5, 106.9, 76.1, 46.7. HRMS: *m/z*: calcd for C<sub>14</sub>H<sub>14</sub>N<sub>2</sub>O<sub>4</sub>: 275.1026 [M+H]<sup>+</sup>; found: 275.1026.



**1-(2-((Benzyloxy)amino)-2-oxoethyl)-1H-pyrrole-3-carboxylic acid IV-20C**

White amorphous solid. Yield: 98 % (1.62 g). <sup>1</sup>H NMR (400 MHz, DMSO-*d*<sub>6</sub>): δ 11.59 (br s, 2H), 7.45 – 7.29 (m, 6H), 6.77 – 6.62 (m, 1H), 6.41 – 6.29 (m, 1H), 4.81 (br s, 2H), 4.50 (s, 2H). <sup>13</sup>C NMR (101 MHz, DMSO-*d*<sub>6</sub>): δ 165.3, 164.1, 135.7, 128.9, 128.4, 127.3, 123.0, 116.0, 109.5, 77.0, 49.5. HRMS: *m/z*: calcd for C<sub>14</sub>H<sub>14</sub>N<sub>2</sub>O<sub>4</sub>: 275.1026 [M+H]<sup>+</sup>; found: 275.1026.



**1-(2-((Allyloxy)amino)-2-oxoethyl)-1H-pyrrole-3-carboxylic acid IV-20D**

Light orange amorphous solid. Yield: 83 % (1.42 g). <sup>1</sup>H NMR (400 MHz, DMSO-*d*<sub>6</sub>): δ 11.69 (br s, 1H), 11.34 (br s, 1H), 7.37 – 7.27 (m, 1H), 6.78 – 6.66 (m, 1H), 6.42 – 6.29 (m, 1H), 5.92 (ddt, *J* = 16.6, 11.3, 6.0 Hz, 1H), 5.47 – 5.17 (m, 2H), 4.50 (br s, 2H), 4.41 – 4.24 (m, 2H). <sup>13</sup>C NMR (101 MHz, DMSO-*d*<sub>6</sub>): δ 165.3, 164.0, 132.8, 127.3, 123.0, 119.5, 116.0, 109.5, 76.0, 49.5. HRMS: *m/z*: calcd for C<sub>10</sub>H<sub>12</sub>N<sub>2</sub>O<sub>4</sub>: 225.0870 [M+H]<sup>+</sup>; found: 225.0869.

**Typical procedure for amide bond formation**

Indole-derived carboxylic acid **IV-20A** and **IV-20B** (1.0 eq, 0.8 mmol and 0.5 mmol respectively) were dissolved in DMF (14 mL) and HOBt (1.1 eq, 0.9/0.6 mmol), DIPEA (3.0 eq, 2.4/1.5 mmol), EDC.HCl (1.2 eq, 0.9/0.6 mmol) and dipeptide trifluoroacetate **IV-15A-D** (1.0 eq, 0.8/0.5 mmol) were added. The reaction mixture was stirred at rt overnight. The mixture was diluted with EtOAc (100 mL) and washed with sulfate buffer

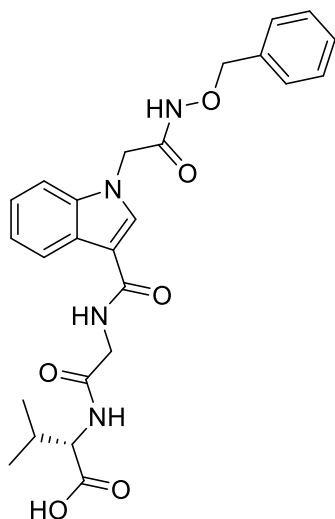


(100 mL), saturated aq. NaHCO<sub>3</sub> (100 mL) and brine (100 mL). The organic phase was dried over Na<sub>2</sub>SO<sub>4</sub> and concentrated *in vacuum*. The residue was purified by column chromatography (CH<sub>2</sub>Cl<sub>2</sub>/MeOH, gradient from 0 to 16 %) and used in the next step despite the residual impurities contained.

The same procedure was applied on pyrrole-derived carboxylic acids **IV-20C** and **IV-20D** (1.0 eq, 1.5 mmol and 1.6 mmol respectively).

### General procedure for final methyl ester hydrolysis

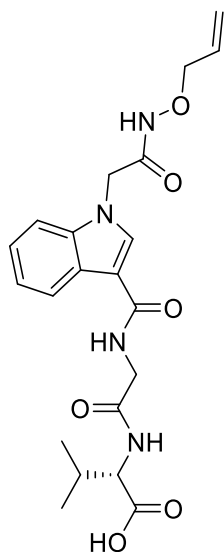
The intermediate methyl ester **IV-21** was dissolved in MeOH (0.7 M) and 3.3 M aq. LiOH.H<sub>2</sub>O (1.5 mL per mmol of **IV-21**) was added dropwise. The reaction mixture was stirred at rt for 1–5 h (monitored by TLC). The mixture was acidified (pH ≈ 2) with 1 M aq. HCl and extracted with EtOAc (3 × 20 mL). The combined organic phases were dried over Na<sub>2</sub>SO<sub>4</sub> and concentrated *in vacuum*. The crude product was purified by column chromatography (CH<sub>2</sub>Cl<sub>2</sub>/MeOH, acidified with AcOH (1 drop/50 mL), gradient from 0 to 16 %) followed by codistillation with Tol/MeOH, 9/1 (2 × 2 mL) and Et<sub>2</sub>O/MeOH, 1/1 (3 × 2 mL).



### (1-(2-((Benzyloxy)amino)-2-oxoethyl)-1H-indole-3-carbonyl)glycyl-L-valine **IV-9A**

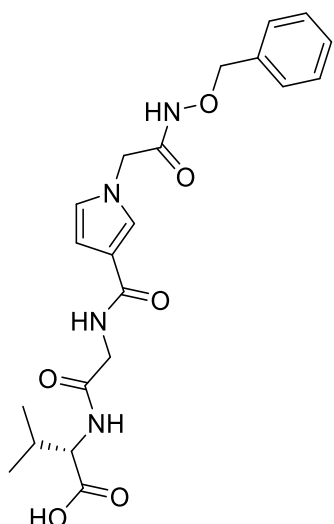
Yellow oil. Yield: 25 % over two steps (111 mg). <sup>1</sup>H NMR (400 MHz, DMSO-*d*<sub>6</sub>): δ 12.64 (br s, 1H), 11.57 (br s, 1H), 8.26 – 8.07 (m, 2H), 8.04 (s, 1H), 8.00 – 7.88 (m, 1H), 7.62 – 7.30 (m, 6H), 7.29 – 7.03 (m, 2H), 5.16 – 4.73 (m, 4H), 4.21 (dd, *J* = 8.6, 5.7 Hz, 1H), 4.03 – 3.89 (m, 2H), 2.14 – 2.00 (m, 1H), 0.90 (d, *J* = 6.7 Hz, 3H), 0.88 (d, *J* = 6.7 Hz, 3H). <sup>13</sup>C NMR (101 MHz, DMSO-*d*<sub>6</sub>): δ 172.9, 169.7, 164.4, 164.0, 136.5, 135.7,

132.4, 128.9, 128.4, 126.4, 122.1, 121.1, 120.9, 110.2, 110.0, 77.0, 57.0, 46.7, 41.8, 30.1, 19.1, 17.9. HRMS:  $m/z$ : calcd for  $C_{25}H_{28}N_4O_6$ : 481.2082  $[M+H]^+$ ; found: 481.2082.



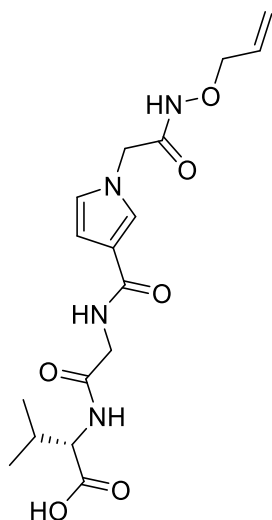
**(1-(2-((Allyloxy)amino)-2-oxoethyl)-1H-indole-3-carbonyl)glycyl-L-valine IV-9B**

White amorphous solid. Yield: 20 % over two steps (42 mg).  $^1H$  NMR (400 MHz,  $DMSO-d_6$ ):  $\delta$  12.64 (br s, 1H), 11.53 (br s, 1H), 8.23 – 8.16 (m, 1H), 8.16 – 8.10 (m, 1H), 8.03 (s, 1H), 7.99 – 7.91 (m, 1H), 7.49 – 7.38 (m, 1H), 7.25 – 7.19 (m, 1H), 7.18 – 7.13 (m, 1H), 6.15 – 5.86 (m, 1H), 5.50 – 5.19 (m, 2H), 5.14 – 4.72 (br s, 2H), 4.51 – 4.27 (m, 2H), 4.21 (dd,  $J = 8.6, 5.7$  Hz, 1H), 4.09 – 3.86 (m, 2H), 2.15 – 1.98 (m, 1H), 0.90 (d,  $J = 6.6$  Hz, 3H), 0.88 (d,  $J = 6.6$  Hz, 3H).  $^{13}C$  NMR (101 MHz,  $DMSO-d_6$ )  $\delta$  172.9, 169.7, 164.4, 163.9, 136.5, 132.8, 132.4, 126.4, 122.1, 121.3, 120.9, 119.7, 110.2, 110.0, 76.1, 57.0, 46.7, 41.8, 30.1, 19.1, 17.9. HRMS:  $m/z$ : calcd for  $C_{21}H_{26}N_4O_6$ : 431.1925  $[M+H]^+$ ; found: 431.1925.



**(1-(2-((Benzyloxy)amino)-2-oxoethyl)-1H-pyrrole-3-carbonyl)glycyl-L-valine IV-10A**

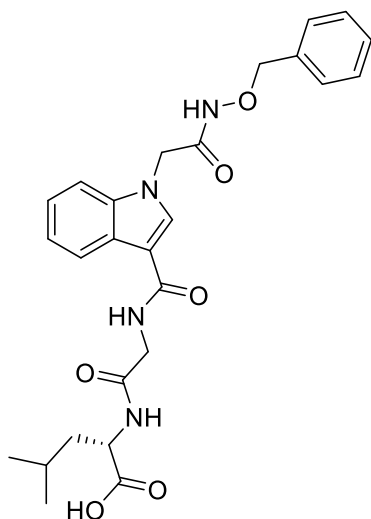
Colourless amorphous solid. Yield: 11 % over two steps (69 mg).  $^1\text{H}$  NMR (400 MHz,  $\text{DMSO-}d_6$ ):  $\delta$  12.52 (br s, 1H), 11.40 (br s, 1H), 8.11 – 7.94 (m, 1H), 7.93 – 7.77 (d,  $J = 8.5$  Hz, 1H), 7.38 (app br s, 5H), 7.32 – 7.17 (m, 1H), 6.76 – 6.57 (m, 1H), 6.56 – 6.28 (m, 1H), 4.81 (br s, 2H), 4.47 (s, 2H), 4.18 (dd,  $J = 8.6, 5.7$  Hz, 1H), 3.93 – 3.78 (m, 2H), 2.11 – 1.99 (m, 1H), 0.88 (d,  $J = 6.5$  Hz, H), 0.86 (d,  $J = 6.5$  Hz, 3H).  $^{13}\text{C}$  NMR (101 MHz,  $\text{DMSO-}d_6$ ):  $\delta$  172.9, 169.7, 164.3, 164.0, 135.7, 128.9, 128.4, 124.6, 122.5, 119.5, 107.8, 77.0, 57.0, 49.6, 41.9, 30.1, 19.1, 17.9. HRMS:  $m/z$ : calcd for  $\text{C}_{21}\text{H}_{26}\text{N}_4\text{O}_6$ : 431.1925  $[\text{M}+\text{H}]^+$ ; found: 431.1925.



**(1-(2-((Allyloxy)amino)-2-oxoethyl)-1H-pyrrole-3-carbonyl)glycyl-L-valine IV-10B**

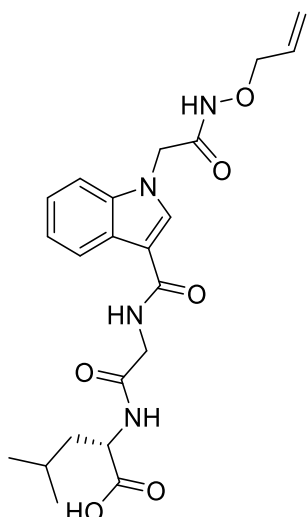
Pale orange oil. Yield: 2 % over two steps (9 mg). Note: Residual impurities contained. Assumed decomposition in solution.  $^1\text{H}$  NMR (400 MHz,  $\text{DMSO-}d_6$ ):  $\delta$  12.61 (s, 1H),

11.34 (br s, 1H), 8.07 – 7.96 (m, 1H), 7.95 – 7.78 (m, 1H), 7.33 – 7.22 (m, 1H), 6.76 – 6.64 (m, 1H), 6.51 – 6.39 (m, 1H), 5.92 (ddt,  $J = 16.5, 11.3, 6.0$  Hz, 1H), 5.46 – 5.20 (m, 2H), 4.47 (br s, 2H), 4.29 (d,  $J = 5.9$  Hz, 2H), 4.17 (dd,  $J = 8.6, 5.7$  Hz, 1H), 3.93 – 3.78 (m, 2H), 2.11 – 1.98 (m, 1H), 0.88 (d,  $J = 6.8$  Hz, 3H), 0.86 (d,  $J = 6.8$  Hz, 3H).  $^{13}\text{C}$  NMR (101 MHz, DMSO- $d_6$ ):  $\delta$  172.9, 169.6, 164.1, 163.9, 132.8, 124.5, 122.4, 119.5, 107.7, 76.0, 57.0, 49.6, 41.8, 30.0, 19.0, 17.9. HRMS:  $m/z$ : calcd for  $\text{C}_{17}\text{H}_{24}\text{N}_4\text{O}_6$ : 381.1769  $[\text{M}+\text{H}]^+$ ; found: 381.1769. HRMS:  $m/z$ : calcd for  $\text{C}_{17}\text{H}_{24}\text{N}_4\text{O}_6$ : 403.1588  $[\text{M}+\text{Na}]^+$ ; found: 403.1588.



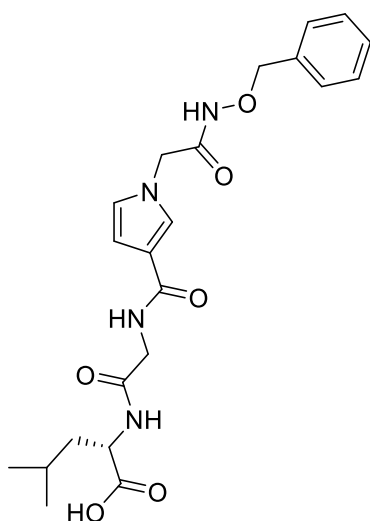
**(1-(2-((Benzyloxy)amino)-2-oxoethyl)-1H-indole-3-carbonyl)glycyl-L-leucine IV-9C**

Light red oil. Yield: 24 % over two steps (114 mg).  $^1\text{H}$  NMR (400 MHz, DMSO- $d_6$ ):  $\delta$  12.54 (br s, 1H), 11.57 (br s, 1H), 8.30 – 8.06 (m, 3H), 8.04 (s, 1H), 7.67 – 7.28 (m, 6H), 7.27 – 7.06 (m, 2H), 5.22 – 4.70 (m, 4H), 4.29 (td,  $J = 8.5, 6.0$  Hz, 1H), 4.06 – 3.80 (m, 2H), 1.75 – 1.60 (m, 1H), 1.60 – 1.46 (m, 2H), 0.90 (d,  $J = 6.5$  Hz, 3H), 0.86 (d,  $J = 6.5$  Hz, 3H).  $^{13}\text{C}$  NMR (101 MHz, DMSO- $d_6$ ):  $\delta$  174.0, 169.5, 164.3, 164.1, 136.5, 135.7, 132.4, 129.0, 128.4, 126.4, 122.1, 121.2, 120.9, 110.2, 110.0, 77.0, 50.2, 46.7, 41.6, 40.2, 24.3, 22.8, 21.5. HRMS:  $m/z$ : calcd for  $\text{C}_{26}\text{H}_{30}\text{N}_4\text{O}_6$ : 495.2238  $[\text{M}+\text{H}]^+$ ; found: 495.2239.



**(1-(2-((Allyloxy)amino)-2-oxoethyl)-1H-indole-3-carbonyl)glycyl-L-leucine IV-9D**

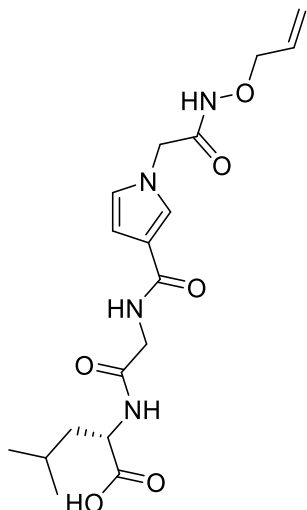
Light yellow amorphous solid. Yield: 27 % over two steps (61 mg).  $^1\text{H}$  NMR (400 MHz,  $\text{DMSO-}d_6$ ):  $\delta$  12.55 (br s, 1H), 11.53 (br s, 1H), 8.24 – 8.05 (m, 3H), 8.02 (s, 1H), 7.43 – 7.33 (m, 1H), 7.23 – 7.14 (m, 1H), 7.14 – 7.05 (m, 1H), 5.93 (ddt,  $J = 16.6, 11.4, 6.1$  Hz, 1H), 5.47 – 5.15 (m, 2H), 5.12 – 4.70 (m, 2H), 4.33 – 4.25 (m, 2H), 4.09 – 3.79 (m, 2H), 1.76 – 1.61 (m, 1H), 1.60 – 1.46 (m, 2H), 0.90 (d,  $J = 6.5$  Hz, 3H), 0.86 (d,  $J = 6.5$  Hz, 3H).  $^{13}\text{C}$  NMR (101 MHz,  $\text{DMSO-}d_6$ )  $\delta$  174.0, 169.5, 164.3, 163.9, 136.5, 132.8, 132.4, 126.4, 122.1, 121.2, 120.9, 119.7, 110.2, 110.0, 76.2, 50.2, 46.7, 41.6, 40.3, 24.3, 22.9, 21.5. HRMS:  $m/z$ : calcd for  $\text{C}_{22}\text{H}_{28}\text{N}_4\text{O}_6$ : 445.2082  $[\text{M}+\text{H}]^+$ ; found: 445.2081.



**(1-(2-((Benzyloxy)amino)-2-oxoethyl)-1H-pyrrole-3-carbonyl)glycyl-L-leucine IV-10C**

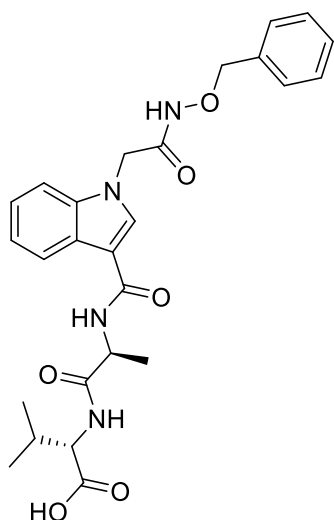
Light yellow amorphous solid. Yield: 15 % over two steps (98 mg).  $^1\text{H}$  NMR (400 MHz,  $\text{DMSO-}d_6$ ):  $\delta$  12.49 (br s, 1H), 11.39 (br s, 1H), 8.21 – 8.00 (m, 1H), 7.99 – 7.70 (m, 1H),

7.38 (app br s, 5H), 7.32 – 7.19 (m, 1H), 6.78 – 6.55 (m, 1H), 6.53 – 6.31 (m, 1H), 4.89 (br s, 2H), 4.47 (s, 2H), 4.26 (td,  $J = 8.4, 6.1$  Hz, 1H), 3.90 – 3.74 (m, 2H), 1.70 – 1.55 (m, 1H), 1.56 – 1.43 (m, 2H), 0.89 (d,  $J = 6.5$  Hz, 3H), 0.85 (d,  $J = 6.5$  Hz, 3H).  $^{13}\text{C}$  NMR (101 MHz, DMSO- $d_6$ )  $\delta$  174.0, 169.5, 164.2, 163.8, 135.7, 128.9, 128.4, 124.5, 122.4, 119.6, 107.8, 77.0, 50.2, 49.6, 41.6, 40.2, 24.3, 22.8, 21.4. HRMS:  $m/z$ : calcd for  $\text{C}_{22}\text{H}_{28}\text{N}_4\text{O}_6$ : 445.2081  $[\text{M}+\text{H}]^+$ ; found: 445.2082.



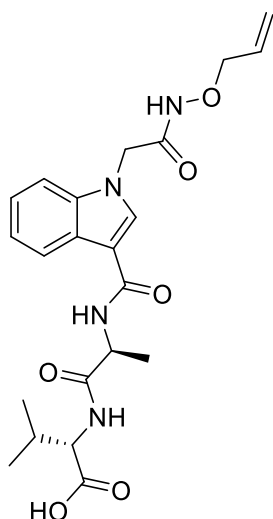
**(1-(2-((Allyloxy)amino)-2-oxoethyl)-1H-pyrrole-3-carbonyl)glycyl-L-leucine IV-10D**

White amorphous solid. Yield: 6 % over two steps (40 mg).  $^1\text{H}$  NMR (400 MHz, DMSO- $d_6$ ):  $\delta$  12.53 (br s, 1H), 11.37 (br s, 1H), 8.06 – 7.90 (m, 2H), 7.30 – 7.26 (m, 1H), 6.72 – 6.67 (m, 1H), 6.50 – 6.41 (m, 1H), 5.92 (ddt,  $J = 16.6, 11.4, 6.0$  Hz, 1H), 5.28 (m, 2H), 4.47 (br s, 2H), 4.29 (d,  $J = 6.1$  Hz, 2H), 4.27 – 4.21 (m, 1H), 3.89 – 3.75 (m, 2H), 1.69 – 1.57 (m, 1H), 1.57 – 1.45 (m, 2H), 0.89 (d,  $J = 6.5$  Hz, 3H), 0.85 (d,  $J = 6.5$  Hz, 3H).  $^{13}\text{C}$  NMR (101 MHz, DMSO- $d_6$ ):  $\delta$  175.2, 169.1, 164.0, 164.0, 132.9, 124.6, 122.5, 119.5, 107.8, 76.0, 51.2, 49.6, 42.0, 41.1, 24.3, 23.0, 21.8. HRMS:  $m/z$ : calcd for  $\text{C}_{18}\text{H}_{26}\text{N}_4\text{O}_6$ : 395.1925  $[\text{M}+\text{H}]^+$ ; found: 395.1925.



**(1-(2-((Benzyloxy)amino)-2-oxoethyl)-1*H*-indole-3-carbonyl)-L-alanyl-L-valine IV-9E**

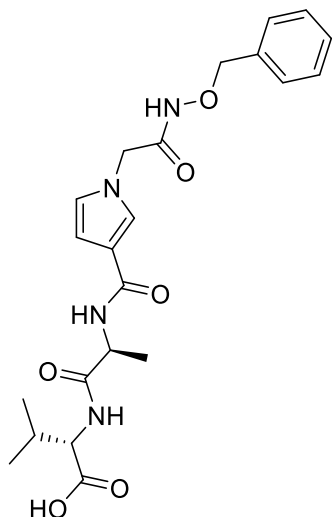
Yellow amorphous solid. Yield: 30 % over two steps (141 mg). <sup>1</sup>H NMR (400 MHz, DMSO-*d*<sub>6</sub>): δ 12.60 (br s, 1H), 11.58 (br s, 1H), 8.21 – 8.06 (m, 2H), 8.06 – 8.00 (m, 1H), 7.98 – 7.93 (m, 1H), 7.57 – 7.31 (m, 5H), 7.27 – 7.06 (m, 2H), 5.22 – 4.71 (m, 4H), 4.70 – 4.56 (m, 1H), 4.23 – 4.00 (m, 1H), 2.15 – 1.99 (m, 1H), 1.34 (d, *J* = 7.1 Hz, 3H), 0.90 (d, *J* = 6.6, Hz, 3H), 0.88 (d, *J* = 6.6, Hz, 3H). <sup>13</sup>C NMR (101 MHz, DMSO-*d*<sub>6</sub>) δ 173.0, 172.9, 164.0, 163.9, 136.5, 135.7, 132.5, 128.9, 128.4, 126.6, 122.1, 121.1, 120.9, 110.2, 109.8, 77.0, 57.0, 47.9, 46.7, 30.0, 19.1, 17.9, 17.9. HRMS: *m/z*: calcd for C<sub>26</sub>H<sub>30</sub>N<sub>4</sub>O<sub>6</sub>: 495.2238 [M+H]<sup>+</sup>; found: 495.2238.



**(1-(2-((Allyloxy)amino)-2-oxoethyl)-1*H*-indole-3-carbonyl)-L-alanyl-L-valine IV-9F**

White amorphous solid. Yield: 39 % over two steps (86 mg). <sup>1</sup>H NMR (400 MHz, DMSO-*d*<sub>6</sub>): δ 11.74 (br s, 1H), 8.24 – 8.10 (m, 2H), 8.10 – 8.00 (m, 1H), 7.91 – 7.64 (m, 1H),

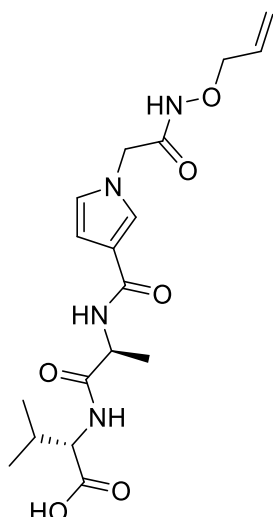
7.54 – 7.34 (m, 1H), 7.27 – 7.18 (m, 1H), 7.17 – 7.10 (m, 1H), 5.92 (ddt,  $J = 16.4, 11.5, 6.8$  Hz, 1H), 5.50 – 5.12 (m, 2H), 4.81 (br s, 2H), 4.67 – 4.52 (m, 1H), 4.52 – 4.22 (m, 2H), 4.17 – 4.03 (m, 1H), 2.16 – 1.96 (m, 1H), 1.33 (d,  $J = 7.1$  Hz, 3H), 1.00 – 0.75 (m, 6H).  $^{13}\text{C}$  NMR (101 MHz,  $\text{DMSO-}d_6$ )  $\delta$  173.7, 172.6, 164.0, 163.8, 136.5, 132.9, 132.6, 126.6, 122.1, 121.2, 120.9, 119.6, 110.3, 109.8, 76.1, 57.6, 48.1, 46.8, 30.4, 19.3, 18.0. HRMS:  $m/z$ : calcd for  $\text{C}_{22}\text{H}_{28}\text{N}_4\text{O}_6$ : 445.2082  $[\text{M}+\text{H}]^+$ ; found: 445.2082.



**(1-(2-((Benzyloxy)amino)-2-oxoethyl)-1H-pyrrole-3-carbonyl)-L-alanyl-L-valine IV-10E**

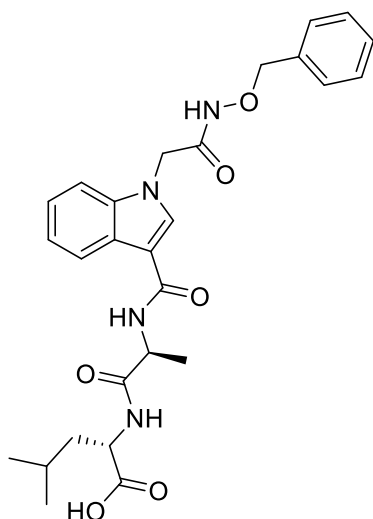
Light yellow amorphous solid. Yield: 44 % over two steps (289 mg).  $^1\text{H}$  NMR (400 MHz,  $\text{DMSO-}d_6$ ):  $\delta$  12.57 (br s, 1H), 11.39 (br s, 1H), 7.90 – 7.83 (m, 1H), 7.84 – 7.62 (m, 1H), 7.38 (app br s, 5H), 7.36 – 7.30 (m, 1H), 6.76 – 6.57 (m, 1H), 6.56 – 6.38 (m, 1H), 4.81 (br s, 2H), 4.67 – 4.48 (m, 1H), 4.47 (s, 2H), 4.15 (dd,  $J = 8.6, 5.7$  Hz, 1H), 2.11 – 1.98 (m, 1H), 1.28 (d,  $J = 7.1$  Hz, 3H), 0.88 (d,  $J = 6.8$  Hz, 3H), 0.86 (d,  $J = 6.8$  Hz, 3H).  $^{13}\text{C}$  NMR (101 MHz,  $\text{DMSO-}d_6$ )  $\delta$  173.0, 172.9, 164.2, 163.5, 135.7, 128.9, 128.4, 124.7, 122.4, 119.4, 107.9, 77.0, 57.0, 49.6, 47.9, 30.0, 19.1, 17.9, 17.8. HRMS:  $m/z$ : calcd for  $\text{C}_{22}\text{H}_{28}\text{N}_4\text{O}_6$ : 445.2082  $[\text{M}+\text{H}]^+$ ; found: 445.2082.





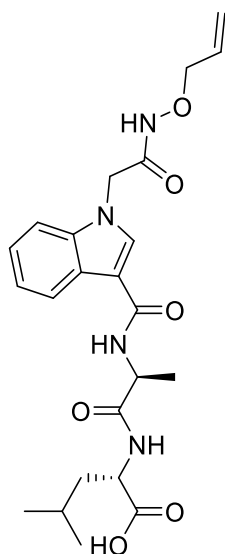
**(1-(2-((Allyloxy)amino)-2-oxoethyl)-1H-pyrrole-3-carbonyl)-L-alanyl-L-valine IV-10F**

Colourless amorphous solid. Yield: 8 % over two steps (52 mg).  $^1\text{H}$  NMR (400 MHz,  $\text{DMSO-}d_6$ ):  $\delta$  11.39 (s, 1H), 7.87 – 7.79 (m, 1H), 7.79 – 7.68 (m, 1H), 7.39 – 7.28 (m, 1H), 6.76 – 6.66 (m, 1H), 6.54 – 6.43 (m, 1H), 5.92 (ddt,  $J = 16.6, 11.3, 6.0$  Hz, 1H), 5.45 – 5.19 (m, 2H), 4.95 – 4.42 (m, 3H), 4.39 – 4.24 (m, 2H), 4.11 (dd,  $J = 8.2, 5.6$  Hz, 1H), 2.12 – 1.98 (m, 1H), 1.27 (d,  $J = 7.1$  Hz, 3H), 0.86 (br s, 3H), 0.85 (br s, 3H).  $^{13}\text{C}$  NMR (101 MHz,  $\text{DMSO-}d_6$ )  $\delta$  173.3, 172.8, 164.0, 163.5, 132.9, 124.7, 122.4, 119.4, 108.0, 76.0, 57.2, 49.6, 48.0, 30.2, 19.2, 17.9, 17.8. HRMS:  $m/z$ : calcd for  $\text{C}_{18}\text{H}_{26}\text{N}_4\text{O}_6$ : 395.1925  $[\text{M}+\text{H}]^+$ ; found: 395.1924.



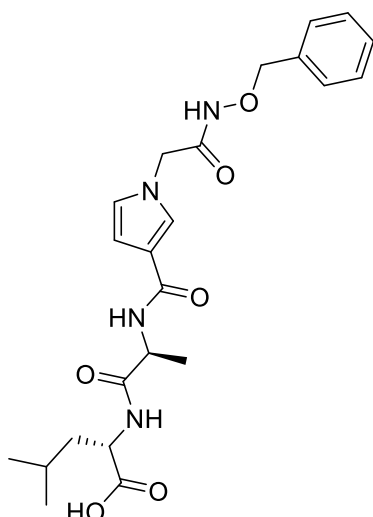
**(1-(2-((Benzyloxy)amino)-2-oxoethyl)-1H-indole-3-carbonyl)-L-alanyl-L-leucine IV-9G**

Light orange oil. Yield: 52 % over two steps (249 mg).  $^1\text{H}$  NMR (400 MHz,  $\text{DMSO-}d_6$ ):  $\delta$  12.50 (br s, 1H), 11.57 (br s, 1H), 8.23 – 8.03 (m, 3H), 8.00 – 7.88 (m, 1H), 7.49 – 7.33 (m, 5H), 7.25 – 7.10 (m, 2H), 5.11 – 4.71 (m, 4H), 4.64 – 4.52 (m, 1H), 4.30 – 4.21 (m, 1H), 1.75 – 1.63 (m, 1H), 1.62 – 1.47 (m, 2H), 1.33 (d,  $J = 7.1$  Hz, 3H), 0.90 (d,  $J = 6.5$  Hz, 3H), 0.85 (d,  $J = 6.5$  Hz, 3H).  $^{13}\text{C}$  NMR (101 MHz,  $\text{DMSO-}d_6$ )  $\delta$  174.0, 172.9, 164.0, 163.8, 136.5, 135.7, 132.6, 129.0, 128.4, 126.6, 122.1, 121.2, 120.9, 110.2, 109.9, 77.0, 50.3, 47.8, 46.8, 40.1, 24.3, 22.9, 21.5, 18.3. HRMS:  $m/z$ : calcd for  $\text{C}_{27}\text{H}_{32}\text{N}_4\text{O}_6$ : 509.2395  $[\text{M}+\text{H}]^+$ ; found: 509.2396.



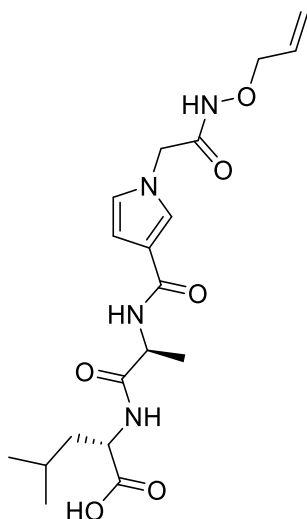
**(1-(2-((Allyloxy)amino)-2-oxoethyl)-1H-indole-3-carbonyl)-L-alanyl-L-leucine IV-9H**

White amorphous solid. Yield: 60 % over two steps (137 mg).  $^1\text{H}$  NMR (400 MHz,  $\text{DMSO-}d_6$ ):  $\delta$  12.49 (br s, 1H), 11.53 (br s, 1H), 8.20 – 8.10 (m, 2H), 8.10 – 8.05 (m, 1H), 8.01 – 7.84 (m, 1H), 7.49 – 7.35 (m, 1H), 7.25 – 7.18 (m, 1H), 7.18 – 7.11 (m, 1H), 5.93 (ddt,  $J = 16.6, 11.7, 6.0$  Hz, 1H), 5.49 – 5.15 (m, 2H), 4.79 (br s, 2H), 4.67 – 4.49 (m, 1H), 4.49 – 4.29 (m, 2H), 4.25 (td,  $J = 9.3, 5.6$  Hz, 1H), 1.78 – 1.63 (m, 1H), 1.62 – 1.47 (m, 2H), 1.33 (d,  $J = 7.1$  Hz, 3H), 0.90 (d,  $J = 6.5$  Hz, 3H), 0.85 (d,  $J = 6.5$  Hz, 3H).  $^{13}\text{C}$  NMR (101 MHz,  $\text{DMSO-}d_6$ )  $\delta$  174.0, 172.9, 163.9, 163.8, 136.4, 132.8, 132.5, 126.6, 122.1, 121.1, 120.8, 119.6, 110.1, 109.9, 76.1, 50.2, 47.8, 46.7, 40.1, 24.3, 22.8, 21.4, 18.2. HRMS:  $m/z$ : calcd for  $\text{C}_{23}\text{H}_{30}\text{N}_4\text{O}_6$ : 459.2238  $[\text{M}+\text{H}]^+$ ; found: 459.2239.



**(1-(2-((Benzyloxy)amino)-2-oxoethyl)-1*H*-pyrrole-3-carbonyl)-L-alanyl-L-leucine  
IV-10G**

Colourless amorphous solid. Yield: 30 % over two steps (206 mg). <sup>1</sup>H NMR (400 MHz, DMSO-*d*<sub>6</sub>): δ 12.46 (br s, 1H), 11.39 (br s, 1H), 8.09 – 7.90 (m, 1H), 7.78 – 7.63 (m, 1H), 7.38 (app br s, 5H), 7.35 – 7.29 (m, 1H), 6.77 – 6.56 (br s, 1H), 6.55 – 6.36 (m, 1H), 4.81 (br s, 2H), 4.57 – 4.37 (m, 3H), 4.22 (td, *J* = 8.7, 5.9 Hz, 1H), 1.70 – 1.59 (m, 1H), 1.59 – 1.46 (m, 2H), 1.28 (d, *J* = 7.1 Hz, 2H), 0.89 (d, *J* = 6.5 Hz, 3H), 0.84 (d, *J* = 6.5 Hz, 3H). <sup>13</sup>C NMR (101 MHz, DMSO-*d*<sub>6</sub>): δ 174.0, 172.8, 164.2, 163.3, 135.7, 128.9, 128.4, 124.6, 122.4, 119.5, 108.0, 77.0, 50.2, 49.6, 47.8, 40.1, 24.3, 22.8, 21.5, 18.1. HRMS: *m/z*: calcd for C<sub>23</sub>H<sub>30</sub>N<sub>4</sub>O<sub>6</sub>: 459.2238 [M+H]<sup>+</sup>; found: 459.2237.



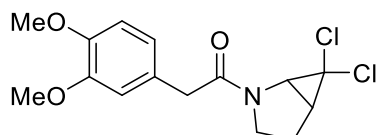
**(1-(2-((Allyloxy)amino)-2-oxoethyl)-1*H*-pyrrole-3-carbonyl)-L-alanyl-L-leucine IV-  
10H**

White amorphous solid. Yield: 19 % over two steps (121 mg).  $^1\text{H}$  NMR (400 MHz,  $\text{DMSO-}d_6$ ):  $\delta$  11.37 (s, 1H), 8.03 – 7.88 (m, 1H), 7.81 – 7.63 (m, 1H), 7.39 – 7.26 (m, 1H), 6.76 – 6.63 (m, 1H), 6.55 – 6.41 (m, 1H), 5.92 (ddt,  $J = 16.6, 11.5, 6.1$  Hz, 1H), 5.46 – 5.20 (m, 2H), 4.96 – 4.40 (m, 3H), 4.32 – 4.26 (m, 2H), 4.25 – 4.14 (m, 1H), 1.71 – 1.58 (m, 1H), 1.57 – 1.45 (m, 2H), 1.27 (d,  $J = 7.1$  Hz, 3H), 0.88 (d,  $J = 6.5$  Hz, 3H), 0.84 (d,  $J = 6.5$  Hz, 3H).  $^{13}\text{C}$  NMR (101 MHz,  $\text{DMSO-}d_6$ )  $\delta$  174.1, 172.8, 164.1, 163.3, 132.9, 124.6, 122.4, 119.5, 108.0, 76.0, 50.3, 49.6, 47.8, 40.2, 24.3, 22.9, 21.5, 18.1. HRMS:  $m/z$ : calcd for  $\text{C}_{19}\text{H}_{28}\text{N}_4\text{O}_6$ : 409.2082  $[\text{M}+\text{H}]^+$ ; found: 409.2080.

## 6.4 Synthesis of starting *gem*-dihalocyclopropane amides

### General acylation procedure A

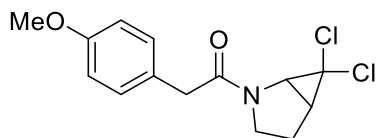
1 M aq. NaOH (0.3 M) was added to a solution of acyl chloride **IV-34** (1.4 eq) and aminocyclopropane salt **IV-32** (1.0 eq) in  $\text{CH}_2\text{Cl}_2$  (0.7 M). After 10 min of strong stirring, the mixture was diluted with  $\text{CH}_2\text{Cl}_2$  (20 mL) and  $\text{H}_2\text{O}$  (20 mL). The organic layer was separated and the aqueous phase was extracted with  $\text{CH}_2\text{Cl}_2$  ( $2 \times 20$  mL). The combined organic layers were dried over  $\text{MgSO}_4$  and concentrated *in vacuum*. The residue was purified by column chromatography (PET/EtOAc, gradient).



### 1-(6,6-Dichloro-2-azabicyclo[3.1.0]hexan-2-yl)-2-(3,4-dimethoxyphenyl)ethan-1-one **IV-35A**

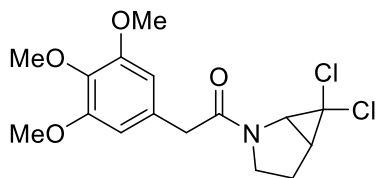
Orange oil. Yield: 43 % (375 mg).  $^1\text{H}$  NMR ( $\text{CDCl}_3$ , 400 MHz), 79 : 21 mixture of two rotamers. Major rotamer:  $\delta$  6.82–6.89 (m, 3H), 3.88 (s, 3H), 3.87 (s, 3H), 3.73 (AB system,  $\delta_A$  3.70,  $\delta_B$  3.76,  $J_{AB} = 15.0$ , 2H), 3.72 (ddd,  $J = 12.0, 10.5, 6.0$ , 1H), 3.69 (d,  $J = 8.0$ , 1H), 3.61 (ddd,  $J = 12.0, 9.5, 5.5$ , 1H), 2.46 (ddd,  $J = 8.0, 7.5, 1.0$ , 1H), 2.30 (dddd,  $J = 14.0, 10.5, 7.5, 5.5$ , 1H), 2.14 (dddd,  $J = 14.0, 9.5, 6.0, 1.0$ , 1H). Minor rotamer, characteristic signals:  $\delta$  6.78 (AB part of an ABX system,  $\delta_A$  6.76,  $\delta_B$  6.79,  $J_{AB} = 8.0$ ,  $J_{AX} = 2.0$ ,  $J_{BX} = 0.0$ , 2H), 4.17 (d,  $J = 7.0$ , 1H), 3.36 (ddd,  $J = 10.5, 9.5, 6.0$ , 1H), 2.40 (m, 1H), 2.24 (dddd,  $J = 14.0, 9.5, 4.5, 0.5$ , 1H).  $^{13}\text{C}$  NMR ( $\text{CDCl}_3$ , 100.6 MHz), 79 : 21 mixture of two rotamers. Major rotamer:  $\delta$  171.5, 149.1, 148.1, 126.4, 121.3, 112.1, 111.3, 65.1, 55.88, 55.85, 50.0, 49.0, 42.2, 37.3, 23.9. Minor rotamer:  $\delta$  170.9, 149.0, 148.0,

126.2, 121.0, 111.8, 111.1, 64.4, 55.88, 55.85, 49.3, 48.8, 41.9, 34.2, 25.8. HRMS:  $m/z$ : calcd for  $C_{15}H_{17}^{35}Cl_2NO_3$ : 330.0658  $[M+H]^+$ ; found: 330.0657, calcd for  $C_{15}H_{17}^{35}Cl^{37}ClNO_3$ : 332.0629  $[M+H]^+$ ; found: 332.0629, calcd for  $C_{15}H_{17}^{37}Cl_2NO_3$ : 334.0599  $[M+H]^+$ ; found: 334.0605.



**1-(6,6-dichloro-2-azabicyclo[3.1.0]hexan-2-yl)-2-(4-methoxyphenyl)ethan-1-one IV-35B**

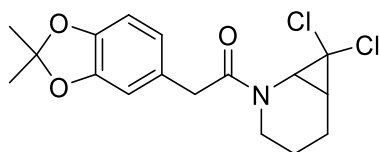
Orange oil. Yield: 63 % (163 mg).  $^1H$  NMR ( $CDCl_3$ , 400 MHz),  $\underline{77}$  : 23 mixture of two rotamers. Major rotamer:  $\delta$  7.24 (br d,  $J = 8.5$ , 2H), 6.88 (br d,  $J = 8.5$ , 2H), 3.80 (s, 3H), 3.72 (AB system,  $\delta_A$  3.70,  $\delta_B$  3.75,  $J_{AB} = 14.5$ , 2H), 3.71 (ddd,  $J = 12.0$ , 10.5, 6.0, 1H), 3.67 (d,  $J$  8.0, 1H), 3.61 (ddd,  $J = 12.0$ , 10.0, 5.5, 1H), 2.46 (ddd,  $J = 8.0$ , 7.5, 1.0, 1H), 2.30 (dddd,  $J = 14.0$ , 10.5, 7.5, 5.5, 1H), 2.14 (dddd,  $J = 14.0$ , 10.0, 6.0, 1.0, 1H). Minor rotamer, characteristic signals:  $\delta$  7.18 (br d,  $J = 8.5$ , 2H), 6.85 (br d,  $J = 8.5$ , 2H), 4.16 (d,  $J = 7.5$ , 1H), 3.37 (ddd,  $J = 10.0$ , 9.5, 6.0, 1H), 2.38 (dddd,  $J = 14.0$ , 7.0, 6.0, 4.0, 1H), 2.24 (dddd,  $J = 14.0$ , 9.5, 4.5, 0.5, 1H).  $^{13}C$  NMR ( $CDCl_3$ , 100.6 MHz),  $\underline{77}$  : 23 mixture of two rotamers. Major rotamer:  $\delta$  171.6, 158.7, 130.2, 126.1, 114.2, 65.1, 52.3, 49.9, 49.0, 41.6, 37.4, 23.9. Minor rotamer, characteristic signals:  $\delta$  171.1, 158.6, 129.9, 125.8, 64.4, 41.4, 34.2, 25.8. HRMS:  $m/z$ : calcd for  $C_{14}H_{15}^{35}Cl_2NO_2$ : 300.0553  $[M+H]^+$ ; found: 300.0556, calcd for  $C_{14}H_{15}^{35}Cl^{37}ClNO_2$ : 302.0523  $[M+H]^+$ ; found: 302.0524, calcd for  $C_{14}H_{15}^{37}Cl_2NO_2$ : 304.0494  $[M+H]^+$ ; found: 304.0493.



**1-(6,6-Dichloro-2-azabicyclo[3.1.0]hexan-2-yl)-2-(3,4,5-trimethoxyphenyl)ethan-1-one IV-35C**

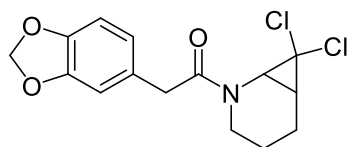
Orange oil. Yield: 45 % (185 mg).  $^1H$  NMR ( $CDCl_3$ , 400 MHz), 76 : 24 mixture of two rotamers. Major rotamer:  $\delta$  6.54 (s, 2H), 3.86 (s, 6H), 3.83 (s, 3H), 3.74 (ddd,  $J = 12.0$ , 10.5, 6.0, 1H), 3.72 (AB system,  $\delta_A$  3.69,  $\delta_B$  3.76,  $J_{AB} = 14.5$ , 2H), 3.70 (d,  $J = 8.0$ , 1H), 3.61 (ddd,  $J$  12.0, 9.5, 5.5, 1H), 2.48 (ddd,  $J = 8.0$ , 7.5, 1.0, 1H), 2.31 (dddd,  $J = 14.0$ ,

10.5, 7.5, 5.5, 1H), 2.15 (dddd,  $J = 14.0, 9.5, 6.0, 1.0$ , 1H). Minor rotamer, characteristic signals:  $\delta$  6.48 (s, 2H), 4.18 (d,  $J = 7.5$ , 1H), 3.37 (ddd,  $J = 10.5, 9.5, 6.0$ , 1H), 2.26 (dddd,  $J = 14.0, 9.5, 4.5, 0.5$ , 1H).  $^{13}\text{C}$  NMR ( $\text{CDCl}_3$ , 100.6 MHz),  $\underline{76}$  : 24 mixture of two rotamers. Major rotamer:  $\delta$  171.1, 153.4, 137.2, 129.6, 106.3, 65.2, 60.8, 56.1, 50.1, 49.1, 43.0, 37.4, 23.9. Minor rotamer, characteristic signals:  $\delta$  105.9, 49.3, 42.4, 34.2, 25.8. HRMS:  $m/z$ : calcd for  $\text{C}_{16}\text{H}_{19}^{35}\text{Cl}_2\text{NO}_4$ : 360.0764  $[\text{M}+\text{H}]^+$ ; found: 360.0767, calcd for  $\text{C}_{16}\text{H}_{19}^{35}\text{Cl}^{37}\text{ClNO}_4$ : 362.0734  $[\text{M}+\text{H}]^+$ ; found: 362.0735, calcd for  $\text{C}_{16}\text{H}_{19}^{37}\text{Cl}_2\text{NO}_4$ : 364.0705  $[\text{M}+\text{H}]^+$ ; found: 364.0701.



**1-(7,7-Dichloro-2-azabicyclo[4.1.0]heptan-2-yl)-2-(2,2-dimethylbenzo[d][1,3]dioxol-5-yl)ethan-1-one IV-35D**

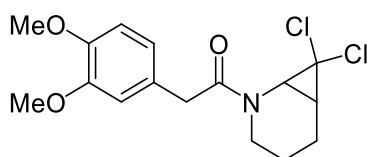
Yellow oil. Yield: 84 % (256 mg).  $^1\text{H}$  NMR ( $\text{CDCl}_3$ , 400 MHz):  $\delta$  6.77 (d,  $J = 1.5$ , 1H), 6.71 (AB part of an ABX system,  $\delta_A$  6.67,  $\delta_B$  6.75,  $J_{AB} = 8.0$ ,  $J_{AX} = 0.0$ ,  $J_{BX} = 1.5$ , 2H), 3.85 (ddd,  $J = 13.0, 7.0, 4.0$ , 1H), 3.73 (AB system,  $\delta_A$  3.72,  $\delta_B$  3.74,  $J_{AB} = 14.5$ , 2H), 3.35 (d,  $J = 9.5$ , 1H), 2.76 (ddd,  $J = 13.0, 9.0, 3.5$ , 1H), 2.09 (ddd,  $J = 9.5, 9.0, 2.5$ , 1H), 2.04 (dddd,  $J = 14.0, 9.0, 8.5, 6.0$ , 1H), 1.76 (dddd,  $J = 14.0, 6.0, 5.0, 2.5$ , 1H), 1.66 (s, 6H), 1.65 (dddd,  $J = 13.5, 9.0, 8.5, 5.0, 4.0$ , 1H), 1.49 (ddtd,  $J = 13.5, 7.0, 6.0, 3.5$ , 1H).  $^{13}\text{C}$  NMR ( $\text{CDCl}_3$ , 100.6 MHz):  $\delta$  173.4, 147.7, 146.5, 127.0, 121.8, 117.9, 109.5, 108.1, 63.3, 41.0, 40.6, 39.3, 28.8, 25.9, 20.7, 17.2. HRMS:  $m/z$ : calcd for  $\text{C}_{17}\text{H}_{19}^{35}\text{Cl}_2\text{NO}_3$ : 356.0815  $[\text{M}+\text{H}]^+$ ; found: 356.0813, calcd for  $\text{C}_{17}\text{H}_{19}^{35}\text{Cl}^{37}\text{ClNO}_3$ : 358.0785  $[\text{M}+\text{H}]^+$ ; found: 358.0781, calcd for  $\text{C}_{17}\text{H}_{19}^{37}\text{ClNO}_3$ : 360.0756  $[\text{M}+\text{H}]^+$ ; found: 360.0746.



**2-(Benzo[d][1,3]dioxol-5-yl)-1-(7,7-dichloro-2-azabicyclo[4.1.0]heptan-2-yl)ethan-1-one IV-35E**

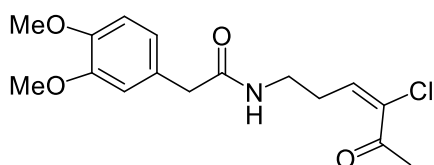
Pale yellow solid. Yield: 74 % (220 mg).  $^1\text{H}$  NMR ( $\text{CDCl}_3$ , 400 MHz):  $\delta$  6.87 (dd,  $J = 1.5, 0.5$ , 1H), 6.79 (AB part of an ABX system,  $\delta_A$  6.78,  $\delta_B$  6.80,  $J_{AB} = 8.0$ ,  $J_{AX} = 0.5$ ,  $J_{BX} = 1.5$ , 2H), 5.95 (s, 2H), 3.85 (ddd,  $J = 13.0, 7.0, 4.0$ , 1H), 3.75 (AB system,  $\delta_A$  3.74,  $\delta_B$

3.76,  $J_{AB} = 15.5$ , H8), 3.32 (d,  $J = 9.5$ , 1H), 2.76 (ddd,  $J = 13.0, 9.0, 3.5$ , 1H), 2.08 (ddd,  $J = 9.5, 9.0, 2.5$ , 1H), 2.03 (dddd,  $J = 14.0, 9.0, 8.5, 6.0$ , 1H), 1.76 (dddd,  $J = 14.0, 6.0, 5.0, 2.5$ , 1H), 1.65 (dddd,  $J = 14.0, 9.0, 8.5, 5.0, 4.0$ , 1H), 1.48 (ddtd,  $J = 14.0, 7.0, 6.0, 3.5$ , 1H).  $^{13}\text{C}$  NMR ( $\text{CDCl}_3$ , 100.6 MHz):  $\delta$  173.2, 147.8, 146.6, 127.7, 122.5, 109.8, 108.3, 101.1, 63.3, 41.0, 40.6, 39.3, 28.8, 20.6, 17.2. HRMS:  $m/z$ : calcd for  $\text{C}_{15}\text{H}_{15}^{35}\text{Cl}_2\text{NO}_3$ : 328.0502  $[\text{M}+\text{H}]^+$ ; found: 328.0501, calcd for  $\text{C}_{15}\text{H}_{15}^{35}\text{Cl}^{37}\text{ClNO}_3$ : 330.0473  $[\text{M}+\text{H}]^+$ ; found: 330.0473.



**1-(7,7-Dichloro-2-azabicyclo[4.1.0]heptan-2-yl)-2-(3,4-dimethoxyphenyl)ethan-1-one IV-35F**

Pale yellow oil. Yield: 59 % (229 mg).  $^1\text{H}$  NMR ( $\text{CDCl}_3$ , 400 MHz), 91 : 9 mixture of two rotamers. Major rotamer:  $\delta$  6.93 (d,  $J = 2.0$ , 1H), 6.87 (AB part of an ABX system,  $\delta_A$  6.84,  $\delta_B$  6.90,  $J_{AB} = 8.0$ ,  $J_{AX} = 0.0$ ,  $J_{BX} = 2.0$ , 2H), 3.88 (s, 3H), 3.87 (s, 3H), 3.87 (ddd,  $J = 13.0, 7.0, 4.0$ , 1H), 3.79 (AB system,  $\delta_A$  3.77,  $\delta_B$  3.80,  $J_{AB} = 15.0$ , 2H), 3.33 (d,  $J = 9.5$ , 1H), 2.75 (ddd,  $J = 13.0, 9.0, 3.5$ , 1H), 2.09 (ddd,  $J = 9.5, 9.0, 2.5$ , 1H), 2.04 (dddd,  $J = 14.0, 9.0, 8.5, 6.0$ , 1H), 1.77 (dddd,  $J = 14.0, 6.0, 5.0, 2.5$ , 1H), 1.65 (dddd,  $J = 14.0, 9.0, 8.5, 5.0, 4.0$ , 1H), 1.49 (ddtd,  $J = 14.0, 7.0, 6.0, 3.5$ , 1H). Minor rotamer, characteristic signals:  $\delta$  3.53 (d,  $J = 9.5$ , 1H), 3.09 (ddd,  $J = 12.0, 8.5, 3.5$ , 1H).  $^{13}\text{C}$  NMR ( $\text{CDCl}_3$ , 100.6 MHz), 91 : 9 mixture of two rotamers. Major rotamer:  $\delta$  173.4, 149.1, 148.1, 126.5, 121.5, 112.5, 111.3, 63.4, 55.92, 55.88, 41.1, 40.6, 39.3, 28.8, 20.7, 17.2. Minor rotamer, characteristic signals:  $\delta$  172.8, 147.9, 126.7, 121.0, 111.9, 111.2, 62.6, 43.0, 40.8, 39.3, 28.0, 21.5, 16.9. HRMS:  $m/z$ : calcd for  $\text{C}_{16}\text{H}_{19}^{35}\text{Cl}_2\text{NO}_3$ : 344.0815  $[\text{M}+\text{H}]^+$ ; found: 344.0806, calcd for  $\text{C}_{16}\text{H}_{19}^{35}\text{Cl}^{37}\text{ClNO}_3$ : 346.0785  $[\text{M}+\text{H}]^+$ ; found: 346.0780, calcd for  $\text{C}_{16}\text{H}_{19}^{37}\text{Cl}_2\text{NO}_3$ : 348.0755  $[\text{M}+\text{H}]^+$ ; found: 348.0750.

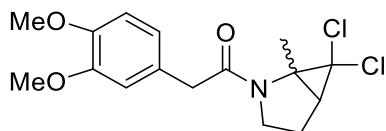


**(E)-N-(4-Chloro-5-oxohex-3-en-1-yl)-2-(3,4-dimethoxyphenyl)acetamide IV-39G**

Orange oil. Yield: 29 % (69 mg).  $^1\text{H}$  NMR ( $\text{CDCl}_3$ , 400 MHz):  $\delta$  6.79 (AB part of an ABX system,  $\delta_A$  6.76,  $\delta_B$  6.82,  $J_{AB} = 8.0$ ,  $J_{AX} = 2.0$ ,  $J_{BX} = 0.0$ , 2H), 6.73 (d,  $J = 2.0$ , 1H), 6.12 (t,  $J = 8.5$ , 1H), 5.92 (br s, 1H), 3.87 (br s, 6H), 3.48 (s, 2H), 3.35 (td,  $J = 6.5$ , 5.5, 2H), 2.56 (dt,  $J = 8.5$ , 6.5, 2H), 2.33 (s, 3H).  $^{13}\text{C}$  NMR ( $\text{CDCl}_3$ , 100.6 MHz):  $\delta$  195.9, 171.8, 149.2, 148.2, 138.0, 130.9, 127.2, 121.7, 112.5, 111.5, 55.85, 55.83, 43.4, 38.5, 29.0, 28.9. HRMS: m/z: calcd for  $\text{C}_{16}\text{H}_{20}^{35}\text{ClNO}_4$ : 326.1153  $[\text{M}+\text{H}]^+$ ; found: 326.1154, calcd for  $\text{C}_{16}\text{H}_{20}^{37}\text{ClNO}_4$ : 328.1124  $[\text{M}+\text{H}]^+$ ; found: 328.1122.

### General acylation procedure B

TEA (2.2 eq) was added dropwise, at  $-78$  °C, to a solution of acyl chloride **IV-29** (1.1 eq) and aminocyclopropane salt **IV-32** (1.0 eq) in dry  $\text{CH}_2\text{Cl}_2$  (0.3 M). The mixture was allowed to warm to 0 °C while stirring for 1 h. The resulting mixture was diluted with  $\text{CH}_2\text{Cl}_2$  (20 mL) and  $\text{H}_2\text{O}$  (30 mL). The organic layer was separated, and the aqueous phase was extracted with  $\text{CH}_2\text{Cl}_2$  ( $2 \times 20$  mL). The combined organic layers were dried over  $\text{MgSO}_4$  and concentrated *in vacuo*. The residue was purified by column chromatography (PET/EtOAc, gradient).

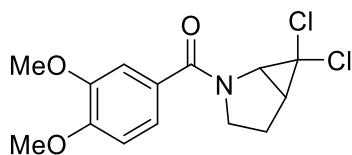


### 1-(6,6-Dichloro-1-methyl-2-azabicyclo[3.1.0]hexan-2-yl)-2-(3,4-dimethoxyphenyl)ethan-1-one **IV-35G**

Yellow oil. Yield: 34 % (66 mg).  $^1\text{H}$  NMR ( $\text{CDCl}_3$ , 400 MHz), 56 : 44 mixture of two rotamers: Major rotamer:  $\delta$  6.80–6.85 (m, 1H), 6.77 (AB part of an ABX system,  $\delta_A$  6.75,  $\delta_B$  6.79,  $J_{AB} = 8.0$ ,  $J_{AX} = 1.5$ ,  $J_{BX} = 0.0$ , 2H), 3.86 (s, 3H), 3.85 (s, 3H), 3.62–3.74 (m, 1H), 3.55 (AB system,  $\delta_A$  3.54,  $\delta_B$  3.56,  $J_{AB} = 15.0$ , 2H), 3.44 (ddd,  $J = 10.0$ , 9.5, 4.5, 1H), 2.29–2.39 (m, 1H), 2.06–2.20 (m, 1H), 1.90 (br d,  $J = 7.5$ , 1H), 1.85 (s, 3H). Minor rotamer:  $\delta$  6.89 (br s, 1H), 6.80–6.85 (m, 2H), 3.97 (ddd,  $J = 12.0$ , 9.5, 3.0, 1H), 3.87 (s, 3H), 3.86 (s, 3H), 3.67 (AB system,  $\delta_A$  3.61,  $\delta_B$  3.73,  $J_{AB} = 15.5$ , 2H), 3.62–3.74 (m, 1H), 2.29–2.39 (m, 1H), 2.15 (br d,  $J = 7.5$ , 1H), 2.06–2.20 (m, 1H), 1.86 (s, 3H).  $^{13}\text{C}$  NMR ( $\text{CDCl}_3$ , 100.6 MHz), 56 : 44 mixture of two rotamers. Major rotamer:  $\delta$  171.0, 149.0, 148.0, 126.6, 121.2, 112.0, 111.2, 69.8, 55.9, 54.2, 51.1, 42.8, 40.1, 25.0, 15.9. Minor rotamer:  $\delta$  172.1, 148.8, 148.0, 127.2, 121.6, 112.9, 111.2, 71.4, 55.9, 58.8, 52.3, 51.6, 43.5, 40.8, 24.5, 18.7. HRMS: m/z: calcd for  $\text{C}_{16}\text{H}_{19}^{35}\text{Cl}_2\text{NO}_3$ : 344.0815  $[\text{M}+\text{H}]^+$ ; found:

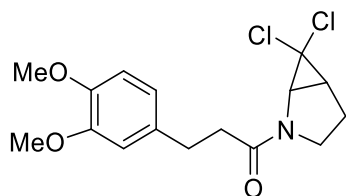


344.0815, calcd for  $C_{16}H_{19}^{35}Cl^{37}ClNO_3$ : 346.0785  $[M+H]^+$ ; found: 346.0783, calcd for  $C_{16}H_{19}^{37}Cl_2NO_3$ : 348.0756  $[M+H]^+$ ; found: 348.0749.



**(6,6-Dichloro-2-azabicyclo[3.1.0]hexan-2-yl)(3,4-dimethoxyphenyl)methanone IV-35H**

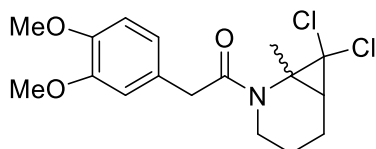
Colourless oil. Yield: 61 % (382 mg).  $^1H$  NMR ( $CDCl_3$ , 400 MHz),  $\delta$  7.32 (dd,  $J = 8.5$ , 1.5, 1H), 7.25 (d,  $J = 1.5$ , 1H), 6.94 (d,  $J = 8.5$ , 1H), 4.08 (ddd,  $J = 12.0$ , 11.0, 6.0, 1H), 3.96 (s, 3H), 3.93 (s, 3H), 3.71 (d,  $J = 7.5$ , 1H), 3.60 (ddd,  $J = 12.0$ , 10.0, 5.5, 1H), 2.53 (td,  $J = 7.5$ , 1.0, 1H), 2.40 (dddd,  $J = 14.0$ , 11.0, 7.5, 5.5, 1H), 2.26 (dddd,  $J = 14.0$ , 10.0, 6.0, 1.0, 1H).  $^{13}C$  NMR ( $CDCl_3$ , 100.6 MHz),  $\delta$  169.2, 151.1, 148.6, 127.8, 121.4, 110.9, 110.6, 65.4, 55.99, 55.97, 51.7, 50.3, 37.3, 23.8. HRMS:  $m/z$ : calcd for  $C_{14}H_{15}^{35}Cl_2NO_3$ : 316.0502  $[M+H]^+$ ; found: 316.0502, calcd for  $C_{14}H_{15}^{35}Cl^{37}ClNO_3$ : 318.0472  $[M+H]^+$ ; found: 318.0472, calcd for  $C_{14}H_{15}^{37}Cl_2NO_3$ : 320.0443  $[M+H]^+$ ; found: 320.0438.



**1-(6,6-Dichloro-2-azabicyclo[3.1.0]hexan-2-yl)-3-(3,4-dimethoxyphenyl)propan-1-one IV-35I**

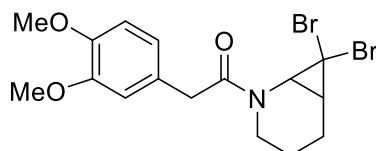
Colourless oil. Yield: 46 % (315 mg).  $^1H$  NMR ( $CDCl_3$ , 400 MHz),  $\delta$  7.8 : 2.2 mixture of two rotamers. Major rotamer:  $\delta$  6.72–6.82 (m, 3H), 3.88 (s, 3H), 3.86 (3 H, s, 3H), 3.70 (ddd,  $J = 12.0$ , 10.5, 6.0, 1H), 3.61 (ddd,  $J = 12.0$ , 9.5, 5.5, 1H), 3.57 (d,  $J = 8.0$ , 1H), 2.90–3.01 (m, 2H), 2.69–2.75 (m, 2H), 2.48 (ddd,  $J = 8.0$ , 7.5, 1.0, 1H), 2.32 (dddd,  $J = 14.0$ , 10.5, 7.5, 5.5, 1H), 2.16 (dddd,  $J = 14.0$ , 9.5, 6.0, 1.0, 1H). Minor rotamer, characteristic signals:  $\delta$  4.15 (d,  $J = 7.0$ , 1H), 3.86 (s, 3H), 3.85 (s, 3H), 3.33 (ddd,  $J = 10.0$ , 9.5, 6.0, 1H), 3.04–2.90 (m, 4H), 2.54 (ddd,  $J = 8.0$ , 7.5, 5.5, 1H), 2.40 (dddd,  $J = 13.5$ , 7.5, 6.0, 4.0, 1H), 2.26 (dddd,  $J = 13.5$ , 9.5, 5.5, 0.5, 1H).  $^{13}C$  NMR ( $CDCl_3$ , 100.6 MHz),  $\delta$  78 : 2.2 mixture of two rotamers. Major rotamer:  $\delta$  172.5, 149.0, 147.5, 133.7, 120.2, 111.9, 111.4, 65.1, 55.94, 55.85, 49.7, 49.0, 37.23, 37.18, 30.6, 24.0. Minor

rotamer:  $\delta$  172.0, 148.9, 147.5, 133.7, 120.2, 111.9, 111.4, 64.4, 55.94, 55.85, 49.1, 48.7, 36.8, 34.2, 30.4, 25.7. HRMS:  $m/z$ : calcd for  $C_{16}H_{19}^{35}Cl_2NO_3$ : 344.0815  $[M+H]^+$ ; found: 344.0815, calcd for  $C_{16}H_{19}^{35}Cl^{37}ClNO_3$ : 346.0785  $[M+H]^+$ ; found: 346.0783, calcd for  $C_{16}H_{19}^{37}Cl_2NO_3$ : 348.0756  $[M+H]^+$ ; found: 348.0750.



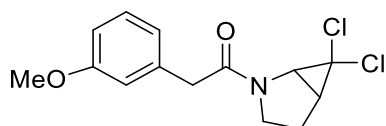
**1-(7,7-Dichloro-1-methyl-2-azabicyclo[4.1.0]heptan-2-yl)-2-(3,4-dimethoxyphenyl)ethan-1-one IV-35J**

Yellow oil. Yield: 85 % (371 mg).  $^1H$  NMR ( $CDCl_3$ , 400 MHz), 71 : 29 mixture of two rotamers. Major rotamer:  $\delta$  7.00 (d,  $J = 2.0$ , 1H), 6.86 (AB part of an ABX system,  $\delta_A$  6.82,  $\delta_B$  6.90,  $J_{AB}$  8.0,  $J_{AX} = 0.0$ ,  $J_{BX} = 2.0$ , 2H), 4.29 (ddd,  $J = 13.0$ , 4.5, 4.0, 1H), 3.89 (s, 3H), 3.86 (s, 3H), 3.76 (AB system,  $\delta_A$  3.70,  $\delta_B$  3.82,  $J_{AB} = 15.5$ , 2H), 2.48 (ddd,  $J = 13.0$ , 9.5, 4.5, 1H), 2.07 (dddd,  $J = 15.0$ , 9.5, 8.5, 8.0, 1H), 1.90 (dddd,  $J = 15.0$ , 5.5, 4.0, 2.0, 1H), 1.75 (s, 3H), 1.68 (dd,  $J = 8.5$ , 2.0, 1H), 1.49–1.59 (m, 2H). Minor rotamer, characteristic signals:  $\delta$  6.84 (d,  $J = 2.0$ , 1H), 6.77 (AB part of an ABX system,  $\delta_A$  6.76,  $\delta_B$  6.79,  $J_{AB} = 8.0$ ,  $J_{AX} = 2.0$ ,  $J_{BX} = 0.0$ , 2H), 3.66 (AB system,  $\delta_A$  3.65,  $\delta_B$  3.66,  $J_{AB} = 15.0$ , 2H), 3.52 (ddd,  $J = 13.0$ , 5.0, 4.0, 1H), 2.86 (ddd,  $J = 13.0$ , 10.0, 4.5, 1H), 1.69 (s, 3H).  $^{13}C$  NMR ( $CDCl_3$ , 100.6 MHz), 71 : 29 mixture of two rotamers. Major rotamer:  $\delta$  172.9, 148.9, 148.1, 127.9, 121.8, 113.2, 111.3, 69.4, 56.1, 56.0, 43.9, 39.9, 38.9, 34.8, 23.0, 20.1, 17.5. Minor rotamer, characteristic signals:  $\delta$  170.8, 149.2, 148.1, 127.1, 121.1, 112.1, 111.3, 68.3, 56.03, 56.02, 44.0, 42.9, 41.5, 33.7, 21.1, 19.4, 17.1. HRMS:  $m/z$ : calcd for  $C_{17}H_{21}^{35}Cl_2NO_3$ : 358.0971  $[M+H]^+$ ; found: 358.0970, calcd for  $C_{17}H_{21}^{35}Cl^{37}ClNO_3$ : 360.0942  $[M+H]^+$ ; found: 360.0939, calcd for  $C_{17}H_{21}^{37}Cl_2NO_3$ : 362.0912  $[M+H]^+$ ; found: 362.0920.



**1-(7,7-Dibromo-2-azabicyclo[4.1.0]heptan-2-yl)-2-(3,4-dimethoxyphenyl)ethan-1-one IV-35K**

Yellow oil. Yield: 49 % (198 mg).  $^1\text{H}$  NMR ( $\text{CDCl}_3$ , 400 MHz), 91 : 9 mixture of two rotamers. Major rotamer:  $\delta$ : 6.96 (d,  $J = 1.5$ , 2H), 6.89 (AB part of an ABX system,  $\delta_A$  6.84,  $\delta_B$  6.94,  $J_{AB} = 8.0$ ,  $J_{AX} = 0.0$ ,  $J_{BX} = 1.5$ , 2H), 3.88 (s, 3H), 3.87 (s, 3H), 3.81 (AB system,  $\delta_A$  3.80,  $\delta_B$  3.82,  $J_{AB} = 15.0$ , 2H), 3.73 (ddd,  $J = 13.0$ , 8.0, 4.0, 1H), 3.37 (d,  $J = 9.5$ , 1H), 2.87 (ddd,  $J = 13.0$ , 8.5, 4.0, 1H), 2.18 (ddd,  $J = 9.5$ , 8.5, 3.0, 1H), 2.12 (dddd,  $J = 13.5$ , 9.0, 8.5, 6.0, 1H), 1.73 (m, 1H), 1.64 (m, 1H), 1.45 (m, 1H). Minor rotamer, characteristic signals:  $\delta$  3.58 (d,  $J = 9.5$ , 1H), 3.16 (ddd,  $J = 12.0$ , 7.5, 4.0, 1H).  $^{13}\text{C}$  NMR ( $\text{CDCl}_3$ , 100.6 MHz), 91 : 9 mixture of two rotamers. Major rotamer:  $\delta$  173.6, 149.3, 148.3, 126.7, 121.6, 112.7, 111.5, 56.1, 41.4, 41.0, 39.8, 36.5, 30.1, 20.7, 19.4. Minor rotamer, characteristic signals:  $\delta$  121.4, 112.3, 111.3, 43.4, 40.6, 29.2, 21.7, 19.1. HRMS: m/z: calcd for  $\text{C}_{16}\text{H}_{19}^{79}\text{Br}_2\text{NO}_3$ : 431.9804  $[\text{M}+\text{H}]^+$ ; found: 431.9808, calcd for  $\text{C}_{16}\text{H}_{19}^{79}\text{Br}^{81}\text{BrNO}_3$ : 433.9784  $[\text{M}+\text{H}]^+$ ; found: 433.9786, calcd for  $\text{C}_{16}\text{H}_{19}^{81}\text{Br}_2\text{NO}_3$ : 435.9764  $[\text{M}+\text{H}]^+$ ; found: 435.9762.

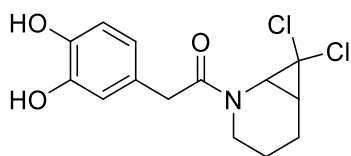


**1-(6,6-Dichloro-2-azabicyclo[3.1.0]hexan-2-yl)-2-(3-methoxyphenyl)ethan-1-one  
IV-35L**

Yellow oil. Yield: 69 % (410 mg).  $^1\text{H}$  NMR ( $\text{CDCl}_3$ , 400 MHz), 77 : 23 mixture of two rotamers. Major rotamer:  $\delta$  7.26 (dd,  $J = 8.5$ , 7.5, 1H), 6.80–6.93 (m, 3H), 3.81 (s, 3H), 3.77 (AB system,  $\delta_A$  3.74,  $\delta_B$  3.79,  $J_{AB} = 15.0$ , 2H), 3.73 (ddd,  $J = 12.0$ , 10.5, 6.0, 1H), 3.67 (d,  $J = 8.0$ , 1H), 3.61 (ddd,  $J = 12.0$ , 9.5, 5.0, 1H), 2.46 (ddd,  $J = 8.0$ , 7.5, 1.0, 1H), 2.30 (dddd,  $J = 14.0$ , 10.5, 7.5, 5.0, 1H), 2.14 (dddd,  $J = 14.0$ , 9.5, 6.0, 1.0, 1H). Minor rotamer, characteristic signals:  $\delta$  4.18 (d,  $J = 7.0$ , 1H), 3.80 (s, 3H), 3.37 (ddd,  $J = 10.5$ , 9.5, 6.0, 1H), 2.38 (dddd,  $J = 14.0$ , 7.0, 6.0, 4.0, 1H), 2.24 (dddd,  $J = 14.0$ , 9.5, 4.5, 0.5, 1H).  $^{13}\text{C}$  NMR ( $\text{CDCl}_3$ , 100.6 MHz), 77 : 23 mixture of two rotamers. Major rotamer:  $\delta$  171.2, 159.9, 135.4, 129.7, 121.5, 114.5, 112.8, 65.0, 55.2, 55.0, 49.0, 42.7, 37.3, 23.9. Minor rotamer:  $\delta$  170.7, 159.8, 135.3, 129.6, 121.3, 114.3, 112.7, 64.4, 55.16, 49.3, 48.9, 42.3, 34.2, 25.8. HRMS: m/z: calcd for  $\text{C}_{14}\text{H}_{15}^{35}\text{Cl}_2\text{NO}_2$ : 300.0553  $[\text{M}+\text{H}]^+$ ; found: 300.00554, calcd for  $\text{C}_{14}\text{H}_{15}^{35}\text{Cl}^{37}\text{ClNO}_2$ : 302.0523  $[\text{M}+\text{H}]^+$ ; found: 302.0521, calcd for  $\text{C}_{14}\text{H}_{15}^{37}\text{Cl}_2\text{NO}_2$ : 304.0494  $[\text{M}+\text{H}]^+$ ; found: 304.0490.

**Deprotection of *gem*-dihalocyclopropane amide IV-35E**

Boron tribromide (1.0 M in hexanes, 1.5 eq, 343  $\mu\text{mol}$ ) was added dropwise, at 0  $^{\circ}\text{C}$ , to a solution of 2-(benzo[*d*][1,3]dioxol-5-yl)-1-(7,7-dichloro-2-azabicyclo[4.1.0]heptan-2-yl)ethan-1-one **IV-35E** (1.0 eq, 229  $\mu\text{mol}$ ) in dry  $\text{CH}_2\text{Cl}_2$  (0.5 mL). After 2 h of stirring at rt, 1 M aq. HCl (15 mL) was added and the mixture was extracted with  $\text{CH}_2\text{Cl}_2$  ( $3 \times 10$  mL). The combined organic layers were dried over  $\text{MgSO}_4$  and concentrated *in vacuo*. The residue was purified by column chromatography (PET/EtOAc, gradient from 40 to 100 %) to afford pure 1-(7,7-dichloro-2-azabicyclo[4.1.0]heptan-2-yl)-2-(3,4-dihydroxyphenyl)ethan-1-one **IV-40** (9.0 mg, 28.5  $\mu\text{mol}$ , 12%) and recover 2-(benzo[*d*][1,3]dioxol-5-yl)-1-(7,7-dichloro-2-azabicyclo[4.1.0]heptan-2-yl)ethan-1-one **IV-35E** (24 mg, 73.1  $\mu\text{mol}$ , 32%).



**1-(7,7-Dichloro-2-azabicyclo[4.1.0]heptan-2-yl)-2-(3,4-dihydroxyphenyl)ethan-1-one **IV-40****

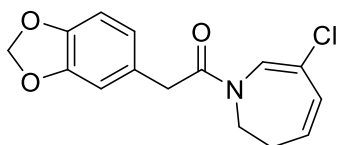
White crystals. Yield: 12 % (9.0 mg).  $^1\text{H}$  NMR ( $\text{CDCl}_3$ , 400 MHz):  $\delta$  8.27 (br s, 1H), 6.95 (d,  $J = 1.5$ , 1H), 6.73 (AB part of an ABX system,  $\delta_A$  6.69,  $\delta_B$  6.77,  $J_{AB} = 8.0$ ,  $J_{AX} = 1.5$ ,  $J_{BX} = 0.0$ , 2H), 6.19 (br s, 1H), 3.78 (ddd,  $J = 13.0$ , 7.5, 4.0, 1H), 3.74 (br s, 2H), 3.37 (d,  $J = 9.5$ , 1H), 2.84 (ddd,  $J = 13.0$ , 8.5, 4.0, 1H), 2.12 (ddd,  $J = 9.5$ , 9.0, 2.5, 1H), 2.07 (m, 1H), 1.72 (dddd,  $J = 14.0$ , 6.0, 5.0, 2.5, 1H), 1.66 (dtdd,  $J = 14.0$ , 8.5, 5.0, 4.0, 1H), 1.50 (m, 1H).  $^{13}\text{C}$  NMR ( $\text{CDCl}_3$ , 100.6 MHz):  $\delta$  175.4, 144.6, 144.0, 125.3, 121.9, 115.7, 115.1, 63.3, 41.0, 40.5, 40.0, 29.3, 20.7, 17.2. HRMS:  $m/z$ : calcd for  $\text{C}_{14}\text{H}_{15}^{35}\text{Cl}_2\text{NO}_3$ : 316.0502  $[\text{M}+\text{H}]^+$ ; found: 316.0491.

## 6.5 Synthesis of dihydroazepines

### Acid-mediated ring expansion of *gem*-dihalocyclopropane amide **IV-35E**

*Tert*-butanol (1 drop) was added, at 20  $^{\circ}\text{C}$ , to a solution of 2-(benzo[*d*][1,3]dioxol-5-yl)-1-(7,7-dichloro-2-azabicyclo[4.1.0]heptan-2-yl)ethan-1-one **IV-35E** (1.0 eq, 64.6  $\mu\text{mol}$ ) in *o*-dichlorobenzene (1.0 mL). The mixture was heated at 180  $^{\circ}\text{C}$  for 30 min with a  $\mu$ -wave reactor. After cooling,  $\text{H}_2\text{O}$  (10 mL) was added and the mixture was extracted with EtOAc ( $3 \times 10$  mL). The combined organic phases were dried over  $\text{MgSO}_4$ , filtered and

concentrated *in vacuo*. The residue was purified by column chromatography (PET/EtOAc, gradient from 5 to 50 %) to afford pure 2-(benzo[*d*][1,3]dioxol-5-yl)-1-(6-chloro-2,3-dihydro-1*H*-azepin-1-yl)ethan-1-one **IV-41E** (7.0 mg, 24.0  $\mu$ mol, 37%) and recover 2-(benzo[*d*][1,3]dioxol-5-yl)-1-(7,7-dichloro-2-azabicyclo[4.1.0]heptan-2-yl)ethan-1-one **IV-35E** (4.0 mg, 12.2  $\mu$ mol, 19%).

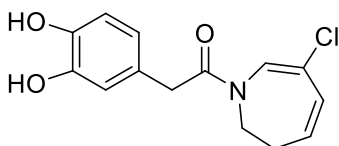


**2-(Benzo[*d*][1,3]dioxol-5-yl)-1-(6-chloro-2,3-dihydro-1*H*-azepin-1-yl)ethan-1-one  
IV-41E**

Pale yellow oil. Yield: 37 % (7.0 mg).  $^1\text{H}$  NMR ( $\text{CDCl}_3$ , 400 MHz):  $\delta$  6.87 (s, 1H), 6.76 (d,  $J = 8.0$ , 1H), 6.77 (d,  $J = 1.5$ , 1H), 6.67 (dd,  $J = 8.0, 1.5$ , 1H), 5.94 (s, 2H), 5.92–5.98 (m, 2H), 3.71 (t,  $J = 5.0$ , 2H), 3.68 (s, 2H), 2.52 (td,  $J = 5.0, 2.5$ , 2H).  $^{13}\text{C}$  NMR ( $\text{CDCl}_3$ , 100.6 MHz):  $\delta$  169.0, 147.0, 146.6, 134.2, 127.3, 127.2, 126.5, 122.1, 119.4, 109.3, 108.4, 101.0, 42.7, 41.3, 32.4. HRMS:  $m/z$ : calcd for  $\text{C}_{15}\text{H}_{14}^{35}\text{ClNO}_3$ : 292.0735  $[\text{M}+\text{H}]^+$ ; found: 292.0737, calcd for  $\text{C}_{15}\text{H}_{14}^{37}\text{ClNO}_3$ : 294.0705  $[\text{M}+\text{H}]^+$ ; found: 294.0710.

**Base-mediated ring expansion of *gem*-dihalocyclopropane amide IV-40**

2,4,6-Collidine (1.0 eq, 22.8  $\mu$ mol) was added dropwise, at 20  $^\circ\text{C}$ , to a solution of 1-(7,7-dichloro-2-azabicyclo[4.1.0]heptan-2-yl)-2-(3,4-dihydroxyphenyl)ethan-1-one **IV-40** (1.0 eq, 22.8  $\mu$ mol) in *o*-dichlorobenzene (1.0 mL). The mixture was heated at 180  $^\circ\text{C}$  for 15 min with a  $\mu$ -wave reactor. After cooling, 1 M aq. HCl (10 mL) was added and the mixture was extracted with EtOAc ( $3 \times 10$  mL). The combined organic phases were dried over  $\text{Na}_2\text{SO}_4$ , filtered and concentrated *in vacuo*. The residue was filtered through a pad of silica gel, washed with EtOAc ( $3 \times 6.0$  mL) and concentrated *in vacuo* to afford fairly pure 1-(6-chloro-2,3-dihydro-1*H*-azepin-1-yl)-2-(3,4-dihydroxyphenyl)ethan-1-one **IV-42**.

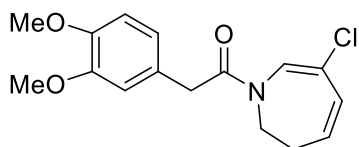


**1-(6-Chloro-2,3-dihydro-1H-azepin-1-yl)-2-(3,4-dihydroxyphenyl)ethan-1-one IV-42**

Orange oil. Yield: 22 % (14 mg). <sup>1</sup>H NMR (CDCl<sub>3</sub>, 400 MHz): δ 6.87 (s, 1H), 6.79 (d, *J* = 8.0, 1H), 6.77 (d, *J* = 2.0, 1H), 6.62 (dd, *J* = 8.0, 2.0, 1H), 5.91–6.01 (m, 2H), 3.72 (t, *J* = 5.0, 2H), 3.66 (s, 2H), 2.53 (td, *J* = 5.0, 3.0, 2H).

**Ring expansion of 6-membered *gem*-dihalocyclopropane amide IV-35G**

A solution of 1-(7,7-dichloro-2-azabicyclo[4.1.0]heptan-2-yl)-2-(3,4-dimethoxyphenyl)ethan-1-one **IV-35G** (1.0 eq, 505 μmol) in *o*-dichlorobenzene (4.0 mL) was heated at reflux for 1 h under a flow of nitrogen. The mixture was subsequently concentrated *in vacuo* to afford fairly pure 1-(6-chloro-2,3-dihydro-1H-azepin-1-yl)-2-(3,4-dimethoxyphenyl)ethan-1-one **IV-41G**.

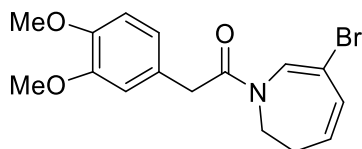


**1-(6-Chloro-2,3-dihydro-1H-azepin-1-yl)-2-(3,4-dimethoxyphenyl)ethan-1-one IV-41G**

Brown oil. Yield: 89 % (138 mg). <sup>1</sup>H NMR (CDCl<sub>3</sub>, 400 MHz): δ 6.90 (br s, 1H), 6.83 (d, *J* = 8.5, 1H), 6.76–6.79 (m, 2H), 5.91–5.99 (m, 2H), 3.87 (br s, 6H), 3.68–3.74 (m, 4H), 2.52 (td, *J* = 5.0, 3.0, 2H).

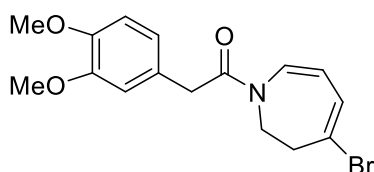
**Ring expansion of 6-membered *gem*-dihalocyclopropane amide IV-35J**

A solution of 1-(7,7-dibromo-2-azabicyclo[4.1.0]heptan-2-yl)-2-(3,4-dimethoxyphenyl)ethan-1-one **IV-35J** (1.00 eq, 543 μmol) in PhCl (4.0 mL) was heated at reflux for 3 h under a flow of nitrogen. After cooling, the solution was concentrated under reduced pressure to afford a mixture of at least two compounds, including 1-(6-bromo-2,3-dihydro-1H-azepin-1-yl)-2-(3,4-dimethoxyphenyl)ethan-1-one **IV-41JA** as a brown oil (122 mg, *i.e.* 346 μmol, 64%, if one assumes the other product(s) is (are) (an) isomer(s) of **IV-41JA**).



**1-(6-Bromo-2,3-dihydro-1H-azepin-1-yl)-2-(3,4-dimethoxyphenyl)ethan-1-one IV-41JA**

Brown oil. Yield: 64 % (122 mg).  $^1\text{H}$  NMR ( $\text{CDCl}_3$ , 400 MHz):  $\delta$  7.05 (br s, 1H), 6.73–6.85 (m, 3H), 6.08 (dtd,  $J = 12.0, 2.0, 1.0$ , 1H), 5.85 (dt,  $J = 12.0, 5.0$ , 1H), 3.87 (br s, 6H), 3.68–3.77 (m, 4H), 2.51 (qd,  $J = 5.0, 2.0$ , 2H). Note: This sample contained several contaminants, the major one having signals described for the compound below.



**1-(4-Bromo-2,3-dihydro-1H-azepin-1-yl)-2-(3,4-dimethoxyphenyl)ethan-1-one IV-41JB**

$^1\text{H}$  NMR ( $\text{CDCl}_3$ , 400 MHz), 74 : 26 mixture of two rotamers. Major rotamer, characteristic signals:  $\delta$  6.65 (br d,  $J = 9.0$ , 1H), 6.30 (br d,  $J = 8.0$ , 1H), 5.09 (dd,  $J = 9.0, 8.0$ , 1H), 2.94 (t,  $J = 5.0$ , 2H). Minor rotamer, characteristic signals:  $\delta$  6.62 (br d,  $J = 9.0$ , 1H), 5.27 (dd,  $J = 9.0, 8.0$ , 1H).

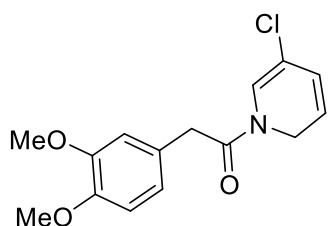
**Ring expansion of 6-membered *gem*-dihalocyclopropane amide IV-35K**

$\text{AgBF}_4$  (2.0 eq, 1.36 mmol) was added to a solution of 1-(7,7-dichloro-1-methyl-2-azabicyclo[4.1.0]heptan-2-yl)-2-(3,4-dimethoxyphenyl)ethan-1-one **IV-35K** (1.0 eq, 681  $\mu\text{mol}$ ) in *o*-dichlorobenzene (6.0 mL) and the resulting mixture was heated at reflux for 4 h under a flow of nitrogen. After cooling, the solution was filtered through a pad of celite, which was rinsed with  $\text{CHCl}_3$  ( $3 \times 6$  mL) and concentrated *in vacuo*. Analysis by  $^1\text{H}$  NMR spectroscopy showed that this crude product contained a 50:50 mixture of 1-(6-chloro-7-methyl-2,3-dihydro-1H-azepin-1-yl)-2-(3,4-dimethoxyphenyl)ethan-1-one **IV-41K** and 1-chloro-10,11-dimethoxy-12b-methyl-4,5,8,12b-tetrahydroazepino[2,1-*a*]isoquinolin-7(3*H*)-one **IV-43K** as a brown oil (239 mg).

## 6.6 Synthesis of dihydropyridines

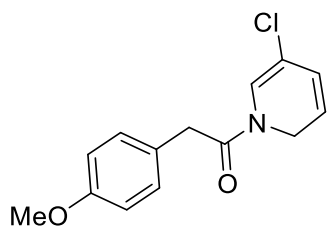
### General procedure for ring expansion of 5-membered *gem*-dihalocyclopropane amides

A solution of 5-membered *gem*-dihalocyclopropane amide **IV-35** in dry MeCN (0.2 M) was heated at reflux (monitored by TLC, ½-2 h) under a flow of nitrogen and concentrated *in vacuo* to afford fairly pure corresponding dihydropyridine **IV-41**.



#### 1-(5-Chloropyridin-1(2H)-yl)-2-(3,4-dimethoxyphenyl)ethan-1-one **IV-41A**

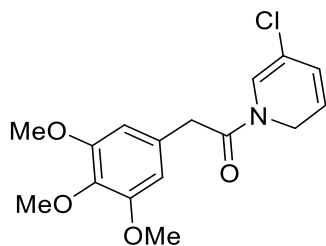
Orange oil. Yield: 80% (100 mg). <sup>1</sup>H NMR (CDCl<sub>3</sub>, 400 MHz), 80 : 20 mixture of two rotamers. Major rotamer:  $\delta$  6.72–6.86 (m, 3H), 6.74 (dd,  $J = 1.5, 1.0, 1\text{H}$ ), 5.87 (dtd,  $J = 10.0, 2.0, 1.5, 1\text{H}$ ), 5.73 (dtd,  $J = 10.0, 4.0, 1.0, 1\text{H}$ ), 4.42 (dd,  $J = 4.0, 2.0, 2\text{H}$ ), 3.87 (br s, 6H), 3.70 (s, 2H). Minor rotamer, characteristic signals:  $\delta$  5.89 (dtd,  $J = 10.0, 2.0, 1.5, 1\text{H}$ ), 5.57 (br dt,  $J = 10.0, 4.0, 1\text{H}$ ), 4.31 (dd,  $J = 4.0, 2.0, 2\text{H}$ ).



#### 1-(5-Chloropyridin-1(2H)-yl)-2-(4-methoxyphenyl)ethan-1-one **IV-41B**

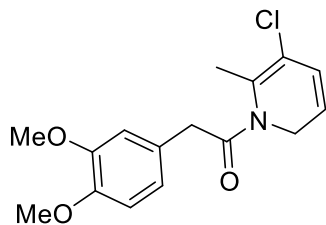
Orange oil. Yield: 85 % (121 mg). <sup>1</sup>H NMR (CDCl<sub>3</sub>, 400 MHz), 80 : 20 mixture of two rotamers. Major rotamer:  $\delta$  7.13 (br d,  $J = 8.0, 2\text{H}$ ), 6.86 (br d,  $J = 8.0, 2\text{H}$ ), 6.71 (s, 1H), 5.86 (dt,  $J = 10.0, 1.5, 1\text{H}$ ), 5.70 (dt,  $J = 10.0, 4.0, 1\text{H}$ ), 4.41 (dd,  $J = 4.0, 1.5, 2\text{H}$ ), 3.78 (s, 3H), 3.68 (br s, 2H). Minor rotamer, characteristic signals:  $\delta$  5.54 (dt,  $J = 10.0, 4.0, 1\text{H}$ ), 4.28 (dd,  $J = 4.0, 1.5, 2\text{H}$ ).





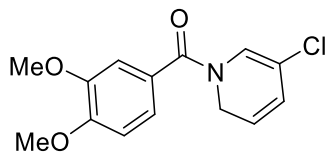
**1-(5-Chloropyridin-1(2H)-yl)-2-(3,4,5-trimethoxyphenyl)ethan-1-one IV-41C**

Orange oil. Yield: 86 % (139 mg). <sup>1</sup>H NMR (CDCl<sub>3</sub>, 400 MHz), 80 : 20 mixture of two rotamers. Major rotamer:  $\delta$  6.44 (s, 2H), 6.74 (dd,  $J = 1.5, 0.5$ , 1H), 5.88 (dtd,  $J = 10.0, 2.0, 1.5$ , 1H), 5.73 (dtd,  $J = 10.0, 4.0, 0.5$ , 1H), 4.42 (dd,  $J = 4.0, 2.0$ , 2H), 3.83 (s, 6H), 3.82 (s, 3H), 3.68 (s, 2H). Minor rotamer, characteristic signals:  $\delta$  5.58 (br dt,  $J = 10.0, 4.0$ , 1H), 4.31 (dd,  $J = 4.0, 2.0$ , 2H).



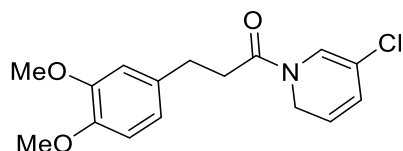
**1-(5-Chloro-6-methylpyridin-1(2H)-yl)-2-(3,4-dimethoxyphenyl)ethan-1-one IV-41G**

Purified by column chromatography (PET/EtOAc, gradient from 40 to 60 %). Colourless oil. Yield: 9 % (18 mg). <sup>1</sup>H NMR (CDCl<sub>3</sub>, 400 MHz):  $\delta$  6.78 (AB part of an ABX system,  $\delta_A$  6.75,  $\delta_B$  6.81,  $J_{AB} = 8.0$ ,  $J_{AX} = 2.0$ ,  $J_{BX} = 0.0$ , 2H), 6.77 (d,  $J = 2.0$ , 1H), 5.95 (br d,  $J = 9.5$ , 1H), 5.76 (br s, 1H), 4.16 (br s, 2H), 3.859 (s, 3H), 3.856 (s, 3H), 3.69 (s, 2H), 2.27 (s, 3H),



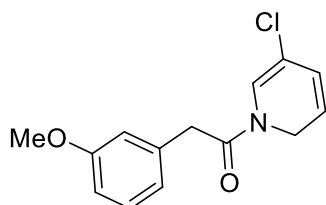
**(5-Chloropyridin-1(2H)-yl)(3,4-dimethoxyphenyl)methanone IV-41H**

Orange oil. Yield: 94 % (20 mg). <sup>1</sup>H NMR (CDCl<sub>3</sub>, 400 MHz):  $\delta$  7.10 (br dd,  $J = 8.0, 2.0$ , 1H), 7.08 (d,  $J = 2.0$ , 1H), 6.88 (br d,  $J = 8.0$ , 1H), 6.67 (br s, 1H), 5.95 (dtd,  $J = 10.0, 2.0, 1.5$ , 1H), 5.75 (dtd,  $J = 10.0, 4.0, 1.0$ , 1H), 4.47 (dd,  $J = 4.0, 2.0$ , 2H), 3.92 (s, 3H), 3.89 (s, 3H).



### 1-(5-chloropyridin-1(2H)-yl)-3-(3,4-dimethoxyphenyl)propan-1-one IV-41I

Orange oil. Yield: 96 % (206 mg). <sup>1</sup>H NMR (CDCl<sub>3</sub>, 400 MHz), 81 : 19 mixture of two rotamers. Major rotamer:  $\delta$  6.71–6.86 (m, 3H), 6.58 (dd,  $J = 1.5, 1.0$ , 1H), 5.86 (dtd,  $J = 10.0, 2.0, 1.5$ , 1H), 5.70 (dtd,  $J = 10.0, 4.0, 1.0$ , 1H), 4.40 (dd,  $J = 4.0, 2.0$ , 2H), 3.87 (br s, 3H), 3.85 (s, 3H), 2.93 (t,  $J = 7.5$ , 2H), 2.66 (t,  $J = 7.5$ , 2H). Minor rotamer, characteristic signals:  $\delta$  5.89 (dtd,  $J = 10.0, 2.0, 1.5$ , 1H), 5.55 (dtd,  $J = 10.0, 4.0, 1.0$ , 1H), 4.25 (dd,  $J = 4.0, 2.0$ , 2H).



### 1-(5-Chloropyridin-1(2H)-yl)-2-(3-methoxyphenyl)ethan-1-one IV-41L

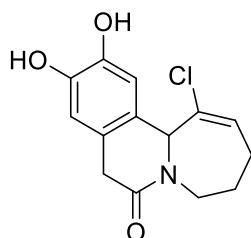
Orange oil. Yield: 95 % (172 mg). <sup>1</sup>H NMR (CDCl<sub>3</sub>, 400 MHz), 80 : 20 mixture of two rotamers. Major rotamer:  $\delta$  7.25 (dd,  $J = 8.5, 7.5$ , 1H), 6.76–6.84 (m, 3H), 6.70 (dd,  $J = 1.5, 0.5$ , 1H), 5.87 (dtd,  $J = 10.0, 2.0, 1.5$ , 1H), 5.72 (dtd,  $J = 10.0, 4.0, 1.0$ , 1H), 4.43 (dd,  $J = 4.0, 2.0$ , 2H), 3.79 (br s, 3H), 3.73 (br s, 2H). Minor rotamer, characteristic signals:  $\delta$  5.88 (dtd,  $J = 10.0, 2.0, 1.5$ , 1H), 5.55 (dtd,  $J = 10.0, 4.0, 0.5$ , 1H), 4.2 (dd,  $J = 4.0, 2.0$ , 2H), 3.79 (br s, 3H), 3.70 (s, 2H).

## 6.7 Cyclization to *N*-fused polycycles

### Lewis acid-mediated cyclization to catechol polycycle IV-45

Boron trifluoride diethyl etherate (1.0 eq, 200  $\mu$ mol) and 2,4,6-collidine (1.0 eq, 200  $\mu$ mol) were added, at 20 °C, to a solution of 1-(7,7-dichloro-2-azabicyclo[4.1.0]heptan-2-yl)-2-(2,2-dimethylbenzo[d][1,3]dioxol-5-yl)ethan-1-one **IV-35E** (1.0 eq, 200  $\mu$ mol) in *o*-dichlorobenzene (1.6 mL). The mixture was heated at 180 °C for 15 min with a  $\mu$ -wave reactor. After cooling, H<sub>2</sub>O (5.0 mL) was added and the mixture was extracted with CH<sub>2</sub>Cl<sub>2</sub> (3  $\times$  5.0 mL). The combined organic phases were dried over Na<sub>2</sub>SO<sub>4</sub> and

concentrated *in vacuum*. The residue was purified by column chromatography (CH<sub>2</sub>Cl<sub>2</sub>/MeOH, acidified with AcOH (1 drop/50 mL), gradient from 0 to 10 %) and gave pure 1-chloro-10,11-dihydroxy-4,5,8,12b-tetrahydroazepino[2,1-a]isoquinolin-7(3*H*)-one **IV-45**.

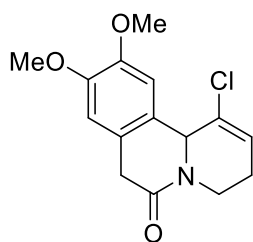


**1-Chloro-10,11-dihydroxy-4,5,8,12b-tetrahydroazepino[2,1-a]isoquinolin-7(3*H*)-one **IV-45****

Brown crystalline solid. Yield: 30 % (17 mg). <sup>1</sup>H NMR (DMSO-*d*<sub>6</sub>, 400 MHz): δ 8.94 (s, 1H), 1.68 (m, 1H), 8.88 (s, 1H), 6.69 (s, 1H), 6.57 (s, 1H), 6.13 (td, *J* = 6.5, 2.0, 1H), 5.51 (br s, 1H), 4.42 (dt, *J* = 13.5, 6.0, 1H), 3.29 (AB system, δ<sub>A</sub> 3.26, δ<sub>B</sub> 3.33, *J*<sub>AB</sub> = 18.5, 2H), 3.00 (ddd, *J* = 13.5, 7.0, 5.0, 1H), 2.33 (dddd, *J* = 15.5, 9.0, 7.5, 2.0, 1H), 2.11 (dddq, *J* = 15.5, 8.0, 6.5, 2.0, 1H), 1.83 (m, 1H). <sup>13</sup>C NMR (DMSO-*d*<sub>6</sub>, 100.6 MHz): δ 169.1, 145.0, 143.3, 134.2, 130.6, 124.3, 123.3, 114.9, 113.8, 62.1, 45.1, 36.7, 25.0, 24.9. HRMS: *m/z*: calcd for C<sub>14</sub>H<sub>14</sub><sup>35</sup>ClNO<sub>3</sub>: 280.0735 [M+H]<sup>+</sup>; found: 280.0733, calcd for C<sub>14</sub>H<sub>14</sub><sup>37</sup>ClNO<sub>3</sub>: 282.0705 [M+H]<sup>+</sup>; found: 282.0703.

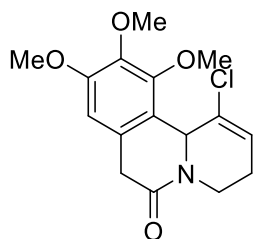
**General procedure for TfOH-mediated cyclization**

The crude dihydroazepine/dihydropyridine intermediate **IV-41** (1.0 eq) was dissolved in dry toluene (0.15 M). Trifluoromethanesulfonic acid (0.5 eq) was added and the mixture was heated at 90 °C (monitored by TLC, ½-2 h). After cooling, saturated aq. NaHCO<sub>3</sub> (20 mL) was added and the mixture was extracted with EtOAc (3 × 10 mL). The combined organic phases were dried over MgSO<sub>4</sub> and concentrated *in vacuum*. The residue was purified by column chromatography (PET/EtOAc, gradient). In case of residual impurities/inseparable isomers, column chromatography was followed by semipreparative HPLC (C18 reverse-phase column, gradient formed from 40 to 70 % or 30 to 60 % of 10 mM aq. AcNH<sub>4</sub> and MeCN).



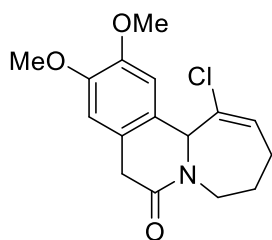
**1-Chloro-9,10-dimethoxy-3,4,7,11b-tetrahydro-6H-pyrido[2,1-a]isoquinolin-6-one  
IV-43A**

Yellow oil. Yield: 49 % over two steps (61 mg).  $^1\text{H}$  NMR ( $\text{CDCl}_3$ , 400 MHz):  $\delta$  6.94 (s, 1H), 6.64 (s, 1H), 6.16 (dt,  $J = 6.5, 2.0$ , 1H), 5.18 (br s, 1H), 4.64 (br dd,  $J = 13.0, 6.0$ , 1H), 3.89 (s, 3H), 3.88 (s, 3H), 3.57 (AB system,  $\delta_A$  3.55,  $\delta_B$  3.60,  $J_{AB} = 19.5$ , 2H), 2.96 (ddd,  $J = 13.0, 12.0, 4.5$ , 1H), 2.51 (dddd,  $J = 17.5, 12.0, 6.0, 3.0, 2.0$ , 1H), 2.19 (dddd,  $J = 17.5, 6.5, 4.5, 2.0, 1.5$ , 1H).  $^{13}\text{C}$  NMR ( $\text{CDCl}_3$ , 100.6 MHz):  $\delta$  170.2, 149.1, 147.2, 130.1, 126.7, 124.8, 123.1, 111.3, 109.9, 61.1, 56.2, 56.0, 40.7, 37.0, 25.2. HRMS:  $m/z$ : calcd for  $\text{C}_{15}\text{H}_{16}^{35}\text{ClNO}_3$ : 294.0891  $[\text{M}+\text{H}]^+$ ; found: 294.0893, calcd for  $\text{C}_{15}\text{H}_{16}^{37}\text{ClNO}_3$ : 296.0862  $[\text{M}+\text{H}]^+$ ; found: 296.0865.



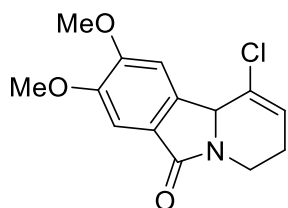
**1-Chloro-9,10,11-trimethoxy-3,4,7,11b-tetrahydro-6H-pyrido[2,1-a]isoquinolin-6-one  
IV-43C**

Yellow oil. Yield: 52 % over two steps (84 mg).  $^1\text{H}$  NMR ( $\text{CDCl}_3$ , 400 MHz):  $\delta$  6.39 (s, 1H), 5.93 (ddd,  $J = 5.0, 3.0, 2.5$ , 1H), 5.93 (ddd,  $J = 5.0, 3.0, 2.5$ , 1H), 5.59 (ddd,  $J = 3.5, 3.0, 2.5$ , 1H), 4.69 (br dd,  $J = 13.0, 7.0$ , 1H), 4.03 (s, 3H), 3.86 (s, 3H), 3.84 (s, 3H), 3.55 (AB part of an ABXY system,  $\delta_A$  3.51,  $\delta_B$  3.58,  $J_{AB} = 20.0$ ,  $J_{AX} = 0.0$ ,  $J_{AY} = 0.0$ ,  $J_{BX} = 1.5$ ,  $J_{BY} = 1.0$ , 2H), 3.08 (ddd,  $J = 13.0, 11.5, 5.5$ , 1H), 2.72 (dddd,  $J = 18.0, 11.5, 7.0, 3.5, 3.0$ , 1H), 2.14 (dddd,  $J = 18.0, 5.5, 5.0, 3.0, 0.5$ , 1H).  $^{13}\text{C}$  NMR ( $\text{CDCl}_3$ , 100.6 MHz):  $\delta$  170.8, 154.2, 151.1, 139.8, 131.6, 127.6, 125.1, 115.9, 105.0, 60.9, 60.7, 57.3, 56.0, 42.6, 36.7, 25.3. HRMS:  $m/z$ : calcd for  $\text{C}_{16}\text{H}_{18}^{35}\text{ClNO}_4$ : 324.0997  $[\text{M}+\text{H}]^+$ ; found: 324.0997, calcd for  $\text{C}_{16}\text{H}_{18}^{35}\text{ClNO}_4$ : 346.0817  $[\text{M}+\text{Na}]^+$ ; found: 346.0815.



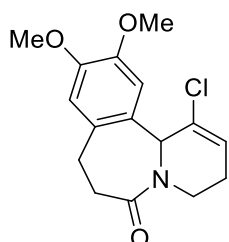
**1-Chloro-10,11-dimethoxy-4,5,8,12b-tetrahydroazepino [2,1-a]isoquinolin-7(3H)-one IV-43F**

Orange oil. Yield: 44 % over two steps (68 mg).  $^1\text{H}$  NMR ( $\text{CDCl}_3$ , 400 MHz):  $\delta$  6.76 (s, 1H), 1.82–1.99 (m, 2H), 6.64 (s, 1H), 6.14 (td,  $J = 6.5, 2.0$ , 1H), 5.26 (br s, 1H), 4.72 (dt,  $J = 13.5, 6.5$ , 1H), 3.873 (s, 3H), 3.869 (s, 3H), 3.54 (AB system,  $\delta_A$  3.47,  $\delta_B$  3.60,  $J_{AB} = 18.5$ , 2H), 2.98 (dt,  $J = 13.5, 6.5$ , 1H), 2.24–2.31 (m, 2H).  $^{13}\text{C}$  NMR ( $\text{CDCl}_3$ , 100.6 MHz):  $\delta$  169.7, 149.0, 147.4, 133.8, 130.9, 125.1, 110.9, 109.9, 64.0, 56.1, 56.0, 46.2, 37.2, 25.5, 25.4. HRMS:  $m/z$ : calcd for  $\text{C}_{16}\text{H}_{18}^{35}\text{ClNO}_3$ : 308.1048  $[\text{M}+\text{H}]^+$ ; found: 308.1048, calcd for  $\text{C}_{16}\text{H}_{18}^{37}\text{ClNO}_3$ : 310.1018  $[\text{M}+\text{H}]^+$ ; found: 310.1022.



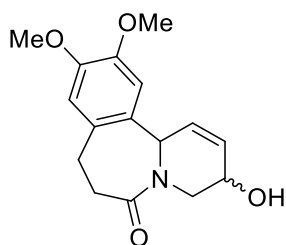
**1-Chloro-8,9-dimethoxy-3,10b-dihydropyrido[2,1-a]isoindol-6(4H)-one IV-43H**

Colourless oil. Yield: 38 % over two steps (8.0 mg). Residual impurities contained.  $^1\text{H}$  NMR ( $\text{CDCl}_3$ , 400 MHz):  $\delta$  7.39 (s, 1H), 7.32 (s, 1H), 2.19 (dddd,  $J = 17.5, 6.5, 4.5, 2.0, 1.0$ , 1H), 5.98 (dt,  $J = 6.5, 2.0$ , 1H), 5.05 (dt,  $J = 4.0, 2.0$ , 1H), 4.51 (ddd,  $J = 13.5, 6.0, 1.0$ , 1H), 3.98 (s, 3H), 3.94 (s, 3H), 3.16 (ddd,  $J = 13.5, 11.5, 4.5$ , 1H), 2.44 (dddd,  $J = 17.5, 11.5, 6.0, 4.0, 2.0$ , 1H), 2.19 (dddd,  $J = 17.5, 6.5, 4.5, 2.0, 1.0$ , 1H).  $^{13}\text{C}$  NMR ( $\text{CDCl}_3$ , 100.6 MHz):  $\delta$  168.8, 152.7, 150.6, 135.8, 129.2, 125.1, 124.8, 107.2, 105.4, 60.5, 56.5, 56.4, 37.0, 27.1. HRMS:  $m/z$ : calcd for  $\text{C}_{14}\text{H}_{14}^{35}\text{ClNO}_3$ : 280.0735  $[\text{M}+\text{H}]^+$ ; found: 280.0733, calcd for  $\text{C}_{14}\text{H}_{15}^{37}\text{ClNO}_3$ : 282.0705  $[\text{M}+\text{H}]^+$ ; found: 282.0703.



**1-Chloro-10,11-dimethoxy-3,7,8,12b-tetrahydrobenzo[c]pyrido[1,2-a]azepin-6(4H)-one IV-43IA**

Colourless oil. Yield: 18 % over two steps (38 mg). <sup>1</sup>H NMR (CDCl<sub>3</sub>, 400 MHz): δ 6.74 (s, 1H), 6.65 (s, 1H), 6.37 (dt, *J* = 5.5, 1.5, 1H), 5.62 (br s, 1H), 4.36 (br dd, *J* = 13.0, 6.0, 1H), 3.86 (s, 3H), 3.84 (s, 3H), 3.25–3.37 (m, 2H), 3.02 (m, 1H), 2.73 (m, 1H), 2.53 (ddd, *J* = 13.0, 11.5, 4.0, 1H), 2.39 (dddt, *J* = 17.5, 11.5, 5.5, 2.5, 1H), 2.26 (dddt, *J* = 17.5, 6.0, 4.0, 1.5, 1H). <sup>13</sup>C NMR (CDCl<sub>3</sub>, 100.6 MHz): δ 171.3, 148.9, 146.8, 129.7, 128.4, 127.9, 127.1, 114.2, 110.7, 58.6, 56.4, 56.1, 34.1, 33.7, 27.7, 25.9. HRMS: *m/z*: calcd for C<sub>16</sub>H<sub>18</sub><sup>35</sup>ClNO<sub>3</sub>: 308.1048 [M+H]<sup>+</sup>; found: 308.1041, calcd for C<sub>16</sub>H<sub>18</sub><sup>37</sup>ClNO<sub>3</sub>: 310.1018 [M+H]<sup>+</sup>; found: 310.1009.

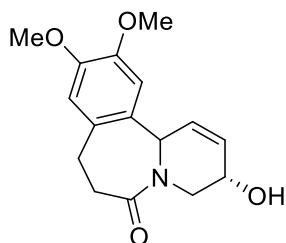


**3-Hydroxy-10,11-dimethoxy-3,7,8,12b-tetrahydrobenzo[c]pyrido[1,2-a]azepin-6(4H)-one IV-43IC**

80 : 20 mixture of two diastereoisomers.

White amorphous solid. Yield: 15 % over two steps (29 mg). HRMS: *m/z*: calcd for C<sub>16</sub>H<sub>19</sub>NO<sub>4</sub>: 290.1387 [M+H]<sup>+</sup>; found: 290.1386, calcd for C<sub>16</sub>H<sub>19</sub>NO<sub>4</sub>: 312.1207 [M+Na]<sup>+</sup>; found: 312.1203.

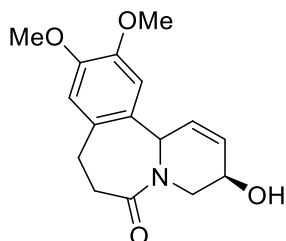
Major diastereoisomer:



<sup>1</sup>H NMR (DMSO-*d*<sub>6</sub>, 400 MHz): δ 6.79 (s, 1H), 6.60 (s, 1H), 6.22 (dddd, *J* = 10.0, 5.0, 2.0, 1.0, 1H), 6.08 (dd, *J* = 10.0, 4.0, 1H), 5.75 (dd, *J* = 4.0, 2.0, 1H), 4.13 (ddd, *J* = 13.5, 2.0, 1.0, 1H), 4.05 (ddd, *J* = 5.0, 3.0, 2.0, 1H), 3.71 (s, 3H), 3.68 (s, 3H), 3.43 (ddd, *J* = 14.0, 10.5, 9.0, 1H), 3.20 (ddd, *J* = 17.0, 9.0, 3.5, 1H), 2.90 (ddd, *J* = 17.0, 10.5, 8.0, 1H), 2.46 (dd, *J* = 13.5, 3.0, 1H), 2.43 (ddd, *J* = 14.0, 8.0, 3.5, 1H).

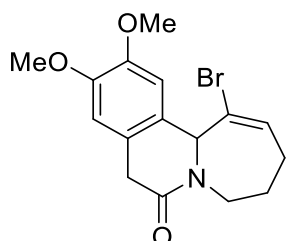
$^{13}\text{C}$  NMR (DMSO- $d_6$ , 100.6 MHz):  $\delta$  171.6, 148.1, 146.0, 129.8, 129.6, 126.9, 114.5, 110.7, 60.7, 55.7, 55.5, 52.1, 42.1, 33.4, 27.1.

Minor diastereoisomer:



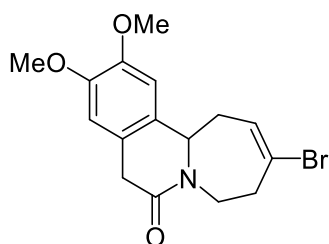
$^1\text{H}$  NMR (DMSO- $d_6$ , 400 MHz), characteristic signals:  $\delta$  6.79 (s, 1H), 6.69 (s, 1H), 6.10 (m, 1H), 5.99 (dd,  $J = 10.5, 3.5, 2.0$ , 1H), 5.67 (dt,  $J = 3.0, 2.5$ , 1H), 4.32 (ddd,  $J = 12.0, 6.0, 1.0$ , 1H), 4.04 (m, 1H), 3.72 (s, 3H), 2.02 (dd,  $J = 12.0, 10.0$ , 1H).

$^{13}\text{C}$  NMR (DMSO- $d_6$ , 100.6 MHz), characteristic signals:  $\delta$  171.0, 148.2, 146.0, 130.0, 124.7, 114.4, 111.0, 62.7, 55.8, 55.5, 52.1, 40.9, 32.8, 27.0.



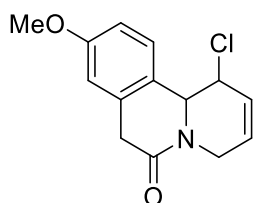
**1-Bromo-10,11-dimethoxy-4,5,8,12b-tetrahydroazepino[1,2-a]isoquinoline-7(3H)-one IV-43JA**

Yellow oil. Yield: 8 % over two steps (16 mg).  $^1\text{H}$  NMR (CDCl $_3$ , 400 MHz):  $\delta$  6.76 (s, 1H), 6.65 (s, 1H), 6.44 (td,  $J = 6.5, 2.0$ , 1H), 5.28 (dt,  $J = 2.0, 1.5$ , 1H), 4.75 (dt,  $J = 13.5, 6.0$ , 1H), 3.892 (s, 3H), 3.886 (s, 3H), 3.56 (AB system,  $\delta_A 3.48, \delta_B 3.63, J_{AB} = 18.5$ , 2H), 2.99 (dt,  $J = 13.5, 6.5$ , 1H), 2.26–2.33 (m, 2H), 1.87–1.95 (m, 2H).  $^{13}\text{C}$  NMR (CDCl $_3$ , 100.6 MHz):  $\delta$  169.8, 149.1, 147.4, 135.6, 126.6, 125.2, 125.1, 111.0, 109.8, 64.5, 56.2, 56.0, 46.4, 37.6, 27.4, 25.2. HRMS:  $m/z$ : calcd for C $_{16}$ H $_{18}^{79}\text{BrNO}_3$ : 352.0543 [M+H] $^+$ ; found: 352.0544, calcd for C $_{16}$ H $_{18}^{81}\text{BrNO}_3$ : 354.0522 [M+H] $^+$ ; found: 354.0522.



**3-Bromo-10,11-dimethoxy-4,5,8,12b-tetrahydroazepino[1,2-a]isoquinoline-7(1H)-one IV-43JB**

Orange oil. Yield: 12 % over two steps (23 mg).  $^1\text{H}$  NMR ( $\text{CDCl}_3$ , 400 MHz):  $\delta$  6.63 (s, 1H), 6.61 (s, 1H), 6.26 (ddd,  $J = 8.0, 3.5, 3.0$ , 1H), 4.55 (dt,  $J = 13.5, 4.0$ , 1H), 4.51 (dd,  $J = 10.5, 3.0$ , 1H), 3.869 (s, 3H), 3.868 (s, 3H), 3.58 (AB system,  $\delta_A 3.54, \delta_B 3.61, J_{AB} = 20.0$ , 2H), 3.18 (dddddd,  $J = 17.5, 11.5, 4.0, 3.0, 2.5, 1.0$ , 1H), 2.95 (ddd,  $J = 13.5, 11.5, 2.5$ , 1H), 2.80 (ddd,  $J = 17.5, 4.0, 2.5$ , 1H), 2.44 (dddd,  $J = 17.0, 8.0, 3.0, 1.0$ , 1H), 2.37 (dddd,  $J = 17.0, 10.5, 3.5, 2.5$ , 1H).  $^{13}\text{C}$  NMR ( $\text{CDCl}_3$ , 100.6 MHz):  $\delta$  168.1, 148.8, 148.1, 129.5, 127.0, 125.2, 123.2, 110.3, 108.5, 62.6, 56.2, 56.0, 45.7, 40.9, 39.6, 36.2. HRMS:  $m/z$ : calcd for  $\text{C}_{16}\text{H}_{18}^{79}\text{BrNO}_3$ : 352.0543  $[\text{M}+\text{H}]^+$ ; found: 352.0543, calcd for  $\text{C}_{16}\text{H}_{18}^{81}\text{BrNO}_3$ : 354.0522  $[\text{M}+\text{H}]^+$ ; found: 354.0522.



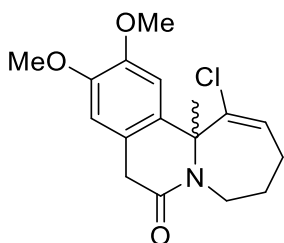
**1-Chloro-9-methoxy-1,4,7,11b-tetrahydro-6H-pyrido[2,1-a]isoquinolin-6-one IV-43LC**

Orange oil. Yield: 6 % over two steps (10 mg).  $^1\text{H}$  NMR ( $\text{CDCl}_3$ , 400 MHz):  $\delta$  7.44 (d,  $J = 8.5$  Hz, 1H), 6.83 (dd,  $J = 8.5, 2.5$  Hz, 1H), 6.68 (d,  $J = 2.5$  Hz, 1H), 5.94 (ddt,  $J = 10.1, 4.0, 1.5$  Hz, 1H), 5.89 (ddt,  $J = 10.0, 2.5, 1.5$  Hz, 1H), 5.12 (dddd,  $J = 18.0, 4.0, 2.0, 1.5$ , 1H), 4.54 (d,  $J = 10.0$  Hz, 1H), 4.41 (ddd,  $J = 10.0, 3.5, 2.0, 1.5$ , 1H), 3.82 (s, 3H), 3.65 (AB system,  $\delta_A 3.64, \delta_B 3.66, J_{AB} = 20.0$  Hz, 2H), 3.52 (dddd,  $J = 18.0, 3.5, 2.5, 1.5$ , 1H).  $^{13}\text{C}$  NMR ( $\text{CDCl}_3$ , 100.6 MHz):  $\delta$  167.5, 159.8, 132.8, 130.3, 129.0, 128.0, 122.1, 112.32, 112.25, 63.2, 58.0, 55.3, 42.3, 36.5. HRMS:  $m/z$ : calcd for  $\text{C}_{14}\text{H}_{15}^{35}\text{ClNO}_2$ : 264.0786  $[\text{M}+\text{H}]^+$ ; found: 264.0787, calcd for  $\text{C}_{14}\text{H}_{15}^{35}\text{ClNO}_2$ : 286.0605  $[\text{M}+\text{Na}]^+$ ; found: 286.0606.



### TfOH-mediated cyclization of 50:50 crude mixture of dihydroazepine IV-41K and N-fused polycycle IV-43K

Resulting from the preceding ring expansion, part of 50:50 crude mixture of dihydroazepine **IV-41K** and N-fused polycycle **IV-43K** (1.0 eq, assumed 482  $\mu\text{mol}$  of **IV-41K/IV-43K**, 169 mg) was dissolved in dry toluene (4.0 mL). Trifluoromethanesulfonic acid (0.5 eq, 263  $\mu\text{mol}$ , 23.3  $\mu\text{L}$ ) was added and the mixture was heated at 90 °C for 1 h. After cooling, saturated aq.  $\text{NaHCO}_3$  (20 mL) was added and the mixture was extracted with EtOAc (3  $\times$  15 mL). The combined organic phases were dried over  $\text{MgSO}_4$  and concentrated *in vacuo*. The crude product was purified by column chromatography (PET/EtOAc, gradient from 40 to 75 %).



### 1-Chloro-10,11-dimethoxy-12b-methyl-4,5,8,12b-tetrahydroazepino[2,1-a]isoquinolin-7(3H)-one IV-43K

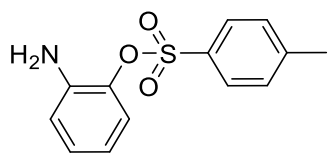
Orange oil. Yield: 34 % over two steps (52 mg).  $^1\text{H}$  NMR ( $\text{CDCl}_3$ , 400 MHz):  $\delta$  7.12 (s, 1H), 6.59 (s, 1H), 6.11 (dd,  $J = 9.5, 6.0$ , 1H), 4.56 (ddd,  $J = 14.0, 7.0, 4.5$ , 1H), 3.88 (s, 3H), 3.87 (s, 3H), 3.62 (br s, 2H), 3.18 (ddd,  $J = 14.0, 7.5, 7.0$ , 1H), 1.91–2.13 (m, 2H), 1.81 (s, 3H), 1.66 (m, 1H).  $^{13}\text{C}$  NMR ( $\text{CDCl}_3$ , 100.6 MHz):  $\delta$  169.8, 149.1, 147.8, 135.8, 130.4, 129.3, 110.0, 109.1, 68.2, 56.3, 56.1, 40.0, 37.3, 26.4, 24.3, 23.1. HRMS:  $m/z$ : calcd for  $\text{C}_{17}\text{H}_{20}^{35}\text{ClNO}_3$ : 322.1204  $[\text{M}+\text{H}]^+$ ; found: 322.1201, calcd for  $\text{C}_{17}\text{H}_{20}^{37}\text{ClNO}_3$ : 324.1175  $[\text{M}+\text{H}]^+$ ; found: 324.1169.

## 6.8 NCTS-mediated cyclization to 2-aminobenzoxazoles

### Cyclization of *o*-aminophenol IV-50A with LiHMDS

*O*-Aminophenol **IV-53A** (1.0 eq, 1.61 mmol) and NCTS were dissolved in THF dry (2.5 mL). The mixture was cooled down to 5 °C and LiHMDS (1.0 M in hexanes) (1.0 eq, 1.61 mmol) was added dropwise. It was stirred at 5 °C to rt for 1 h. Then the reaction mixture was poured into ice water (50 mL) and stirred for 15 min. It was followed by an extraction with EtOAc (3  $\times$  50 mL), the organic layers were washed with brine (50 mL),

dried over anhydrous Na<sub>2</sub>SO<sub>4</sub> and concentrated *in vacuo*. The residue was purified by column chromatography (Hex/EtOAc, gradient from 40 to 80 %).

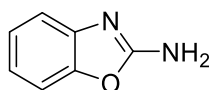


### 2-Aminophenyl-4-methylbenzenesulfonate IV-57

Brown solid. Yield: 35 % (148 mg). <sup>1</sup>H NMR (500 MHz, DMSO-*d*<sub>6</sub>): δ 9.28 (s, 2H), 7.63 (d, *J* = 8.2 Hz, 2H), 7.30 (d, *J* = 8.2 Hz, 2H), 7.13 (dd, *J* = 8.0, 1.6 Hz, 1H), 6.91 (td, *J* = 7.9, 1.6 Hz, 1H), 6.72 (dd, *J* = 8.0, 1.1 Hz, 1H), 6.68 (td, *J* = 7.9, 1.4 Hz, 1H), 2.33 (s, 3H). <sup>13</sup>C NMR (101 MHz, DMSO-*d*<sub>6</sub>): δ 150.2, 142.9, 137.8, 129.4, 126.9, 126.2, 124.4, 119.0, 115.6, 21.1. HRMS: *m/z*: calcd for C<sub>13</sub>H<sub>13</sub>NO<sub>3</sub>S: 264.0689 [M+H]<sup>+</sup>; found: 264.0689.

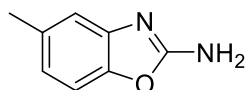
### General procedure for cyclization of aminophenols with NCTS

*O*-Aminophenol IV-53 (1.0 eq, 0.90 mmol) and NCTS (1.5 eq, 1.35 mmol) were dissolved in 1,4-dioxane (4.0 mL). BF<sub>3</sub>·Et<sub>2</sub>O (2.0 eq, 1.80 mmol) was added dropwise. The mixture was refluxed overnight (monitored by TLC, 24-30 h). After that, the cooled (rt) mixture was quenched with saturated aq. NaHCO<sub>3</sub> (pH ≈ 7), diluted with H<sub>2</sub>O (30 mL) and extracted with EtOAc (3 × 30 mL). Combined organic layers were dried over Na<sub>2</sub>SO<sub>4</sub> and concentrated *in vacuo*. The residue was purified by column chromatography (Hex/EtOAc, gradient from 40 to 80 %).



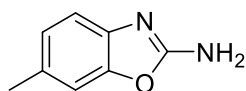
### Benzo[d]oxazol-2-amine IV-52A

Brown solid. Yield: 60 % (72 mg). <sup>1</sup>H NMR (400 MHz, DMSO-*d*<sub>6</sub>): δ 7.35 (s, 2H), 7.30 (d, *J* = 7.8 Hz, 1H), 7.19 (d, *J* = 7.3 Hz, 1H), 7.08 (t, *J* = 7.2 Hz, 1H), 6.95 (t, *J* = 7.2 Hz, 1H). <sup>13</sup>C NMR (101 MHz, DMSO-*d*<sub>6</sub>): δ 162.7, 147.9, 143.6, 123.5, 119.9, 115.3, 108.4. HRMS: *m/z*: calcd for C<sub>7</sub>H<sub>6</sub>N<sub>2</sub>O: 135.0553 [M+H]<sup>+</sup>; found: 135.0554.



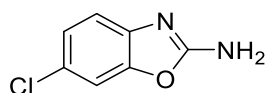
### 5-Methylbenzo[d]oxazol-2-amine IV-52B

Brown solid. Yield: 53 % (71 mg).  $^1\text{H}$  NMR (400 MHz,  $\text{DMSO-}d_6$ ):  $\delta$  7.29 (s, 2H), 7.16 (d,  $J = 8.0$  Hz, 1H), 7.00 (s, 1H), 6.75 (d,  $J = 7.9$  Hz, 1H), 2.30 (s, 3H).  $^{13}\text{C}$  NMR (101 MHz,  $\text{DMSO-}d_6$ ):  $\delta$  162.9, 146.1, 143.8, 132.5, 120.5, 115.69, 107.8, 21.1. HRMS:  $m/z$ : calcd for  $\text{C}_8\text{H}_8\text{N}_2\text{O}$ : 149.0709  $[\text{M}+\text{H}]^+$ ; found: 149.0709.



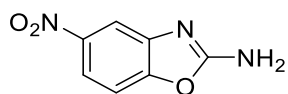
### 6-Methylbenzo[d]oxazol-2-amine IV-52C

Brown solid. Yield: 54 % (72 mg).  $^1\text{H}$  NMR (400 MHz,  $\text{DMSO-}d_6$ ):  $\delta$  7.29 (s, 2H), 7.14 (s, 1H), 7.06 (d,  $J = 7.9$  Hz, 1H), 6.90 (d,  $J = 7.6$  Hz, 1H), 2.32 (s, 3H).  $^{13}\text{C}$  NMR (101 MHz,  $\text{DMSO-}d_6$ ):  $\delta$  162.3, 148.1, 140.9, 129.4, 124.1, 114.7, 108.9, 21.0. HRMS:  $m/z$ : calcd for  $\text{C}_8\text{H}_8\text{N}_2\text{O}$ : 149.0709  $[\text{M}+\text{H}]^+$ ; found: 149.0710.



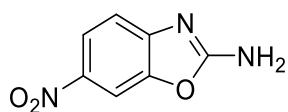
### 6-Chlorobenzo[d]oxazol-2-amine IV-52D

Red solid. Yield: 50 % (75 mg).  $^1\text{H}$  NMR (400 MHz,  $\text{DMSO-}d_6$ ):  $\delta$  7.52 (s, 2H), 7.48 (d,  $J = 1.8$  Hz, 1H), 7.17 (d,  $J = 8.3$  Hz, 1H), 7.12 (dd,  $J = 8.3, 2.0$  Hz, 1H).  $^{13}\text{C}$  NMR (101 MHz,  $\text{DMSO-}d_6$ ):  $\delta$  163.3, 148.3, 142.8, 123.7, 123.5, 115.9, 109.1. HRMS:  $m/z$ : calcd for  $\text{C}_7\text{H}_5\text{ClN}_2\text{O}$ : 169.0163  $[\text{M}+\text{H}]^+$ ; found: 169.0164.



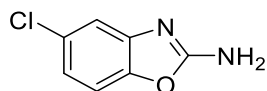
### 5-Nitrobenzo[d]oxazol-2-amine IV-52E

Yellow solid. Yield: 48 % (77 mg).  $^1\text{H}$  NMR (400 MHz,  $\text{DMSO-}d_6$ ):  $\delta$  7.97 (d,  $J = 2.3$  Hz, 1H), 7.96 – 7.87 (m, 3H), 7.56 (d,  $J = 8.7$  Hz, 1H).  $^{13}\text{C}$  NMR (101 MHz,  $\text{DMSO-}d_6$ ):  $\delta$  164.8, 152.3, 144.7, 144.4, 116.7, 110.0, 108.6. HRMS:  $m/z$ : calcd for  $\text{C}_7\text{H}_5\text{N}_3\text{O}_3$ : 178.0258  $[\text{M}+\text{H}]^+$ ; found: 178.0242.



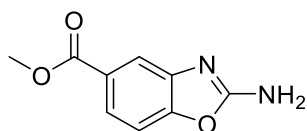
### 6-Nitrobenzo[d]oxazol-2-amine IV-52F

Yellow solid. Yield: 47 % (75 mg).  $^1\text{H}$  NMR (400 MHz,  $\text{DMSO-}d_6$ ):  $\delta$  8.29 – 8.17 (m, 3H), 8.10 (dd,  $J = 8.7, 2.3$  Hz, 1H), 7.32 (d,  $J = 8.7$  Hz, 1H).  $^{13}\text{C}$  NMR (101 MHz,  $\text{DMSO-}d_6$ ):  $\delta$  166.4, 151.0, 147.2, 140.3, 121.1, 114.1, 104.7. HRMS:  $m/z$ : calcd for  $\text{C}_7\text{H}_5\text{N}_3\text{O}_3$ : 178.0258  $[\text{M-H}]^+$ ; found: 178.0241.



#### 5-Chlorobenzo[d]oxazol-2-amine IV-52G

Brown solid. Yield: 50 % (76 mg).  $^1\text{H}$  NMR (400 MHz,  $\text{DMSO-}d_6$ ):  $\delta$  7.61 (s, 2H), 7.33 (d,  $J = 8.4$  Hz, 1H), 7.22 (d,  $J = 2.1$  Hz, 1H), 6.97 (dd,  $J = 8.4, 2.1$  Hz, 1H).  $^{13}\text{C}$  NMR (101 MHz,  $\text{DMSO-}d_6$ ):  $\delta$  163.9, 146.8, 145.3, 127.6, 119.5, 114.9, 109.56. HRMS:  $m/z$ : calcd for  $\text{C}_7\text{H}_5\text{ClN}_2\text{O}$ : 169.0163  $[\text{M+H}]^+$ ; found: 169.0165.



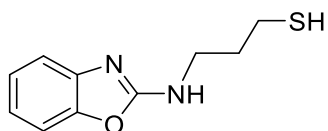
#### Methyl 2-aminobenzo[d]oxazol-5-carboxylate IV-52H

Yellow solid. Yield: 45 % (49 mg).  $^1\text{H}$  NMR (500 MHz,  $\text{DMSO-}d_6$ ):  $\delta$  7.72 (d,  $J = 1.7$  Hz, 1H), 7.65 (dd,  $J = 8.3, 1.7$  Hz, 1H), 7.63 (s, 2H), 7.43 (d,  $J = 8.3$  Hz, 1H), 3.84 (s, 3H).  $^{13}\text{C}$  NMR (101 MHz,  $\text{DMSO-}d_6$ ):  $\delta$  166.4, 163.7, 151.3, 144.0, 125.3, 122.2, 115.8, 108.5, 52.1. HRMS:  $m/z$ : calcd for  $\text{C}_9\text{H}_8\text{N}_2\text{O}_3$ : 193.0608  $[\text{M+H}]^+$ ; found: 193.0607.

## 6.9 The Smiles rearrangement approach to *N*-substituted 2-aminobenzoxazoles

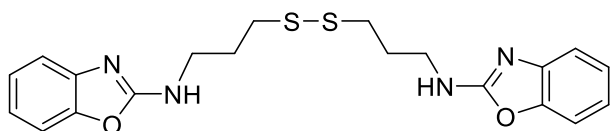
### The Smiles rearrangement with 3-bromopropylamine.HBr

Benzoxazole-2-thiol **IV-54** (1.0 eq, 1.6 mmol),  $\text{K}_2\text{CO}_3$  (2.0 eq, 3.2 mmol/3.0 eq, 4.8 mmol) and 3-bromopropylamine.HBr **IV-63** (2.0 eq, 3.2 mmol/1.0 eq, 1.6 mmol) were suspended in DMF (10 mL). The reaction mixture was stirred at 70 °C for 2 h. It was followed by dilution with  $\text{H}_2\text{O}$  (50 mL) and extraction with EtOAc ( $3 \times 50$  mL). Organic layers were washed with brine (50 mL), dried over  $\text{Na}_2\text{SO}_4$  and concentrated *in vacuo*. The residue was purified by column chromatography (Hex/EtOAc, gradient from 10 to 40 %).



### 3-(Benzo[d]oxazol-2-ylamino)propane-1-thiol IV-65

White solid. Yield: 67 % (222 mg).  $^1\text{H}$  NMR (500 MHz,  $\text{DMSO-}d_6$ ):  $\delta$  7.90 (t,  $J = 5.6$  Hz, 1H), 7.32 (d,  $J = 7.8$  Hz, 1H), 7.23 (d,  $J = 7.1$  Hz, 1H), 7.10 (td,  $J = 7.6, 1.0$  Hz, 1H), 6.96 (td,  $J = 7.7, 1.2$  Hz, 1H), 3.39 (dd,  $J = 12.6, 6.7$  Hz, 2H), 2.56 (dd,  $J = 13.8, 6.8$  Hz, 2H), 2.40 (t,  $J = 7.3$  Hz, 1H), 1.86 (p,  $J = 6.9$  Hz, 2H).  $^{13}\text{C}$  NMR (126 MHz,  $\text{DMSO-}d_6$ ):  $\delta$  162.3, 148.0, 143.2, 123.5, 120.0, 115.4, 108.4, 40.7, 33.0, 21.1. HRMS:  $m/z$ : calcd for  $\text{C}_{10}\text{H}_{12}\text{N}_2\text{OS}$ : 209.0743  $[\text{M}+\text{H}]^+$ ; found: 209.0743.

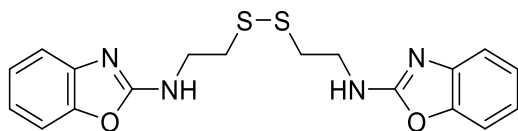


### *N,N'*-(Disulfanediy)bis(propane-3,1-diyl)bis(benzo[d]-oxazol-2-amine) IV-67

Yellow solid. Yield: 66 % (219 mg).  $^1\text{H}$  NMR (500 MHz,  $\text{DMSO-}d_6$ ):  $\delta$  7.94 (t,  $J = 5.6$  Hz, 2H), 7.31 (d,  $J = 7.8$  Hz, 2H), 7.23 (d,  $J = 7.4$  Hz, 2H), 7.09 (td,  $J = 7.7, 0.9$  Hz, 2H), 6.96 (td,  $J = 7.8, 1.1$  Hz, 2H), 3.39 (dd,  $J = 12.7, 6.6$  Hz, 4H), 2.81 (t,  $J = 7.1$  Hz, 4H), 2.03 – 1.90 (m, 4H).  $^{13}\text{C}$  NMR (126 MHz,  $\text{DMSO-}d_6$ ):  $\delta$  162.3, 148.0, 143.2, 123.51, 120.0, 115.4, 108.4, 40.9, 35.0, 28.4. HRMS:  $m/z$ : calcd for  $\text{C}_{20}\text{H}_{22}\text{N}_4\text{O}_2\text{S}_2$ : 415.1257  $[\text{M}+\text{H}]^+$ ; found: 415.1258

### The Smiles rearrangement with 2-bromoethylamine.HBr

Benzoxazole-2-thiol **IV-54** (1.0 eq, 1.6 mmol),  $\text{K}_2\text{CO}_3$  (3.0 eq, 4.8 mmol) and 2-bromoethylamine.HBr **IV-64** (2.0 eq, 3.2 mmol) were suspended in DMF (10 mL). The reaction mixture was stirred at 120 °C for 2 h. It was followed by dilution with  $\text{H}_2\text{O}$  (50 mL) and extraction with EtOAc ( $3 \times 50$  mL). Organic layers were washed with brine (50 mL), dried over  $\text{Na}_2\text{SO}_4$  and concentrated *in vacuo*. The residue was purified by column chromatography (Hex/EtOAc, gradient from 10 to 40 %).

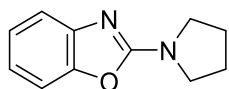


***N,N'*-(Disulfaneyldiylbis(ethane-2,1-diyl)bis(benzo[d]-oxazol-2-amine) IV-68**

White solid. Yield: 71 % (220 mg). <sup>1</sup>H NMR (400 MHz, DMSO-*d*<sub>6</sub>): δ 8.14 (t, *J* = 5.7 Hz, 2H), 7.33 (d, *J* = 7.8 Hz, 2H), 7.25 (d, *J* = 7.6 Hz, 2H), 7.10 (td, *J* = 7.5, 0.9 Hz, 2H), 6.97 (td, *J* = 7.7, 1.1 Hz, 2H), 3.61 (dd, *J* = 12.9, 6.4 Hz, 4H), 3.01 (t, *J* = 6.7 Hz, 4H). <sup>13</sup>C NMR (101 MHz, DMSO-*d*<sub>6</sub>): δ 162.0, 148.0, 143.1, 123.6, 120.2, 115.6, 108.6, 41.5, 36.9. HRMS: *m/z*: calcd for C<sub>18</sub>H<sub>18</sub>N<sub>4</sub>O<sub>2</sub>S<sub>2</sub>: 387.0944 [M+H]<sup>+</sup>; found: 387.0944.

**The Smiles rearrangement with 4-bromobutylamine.HBr**

Benzoxazole-2-thiol IV-54 (1.0 eq, 0.6 mmol) and Et<sub>3</sub>N (2.0 eq, 1.2 mmol) were dissolved in toluene (5.0 mL) and premixed at rt for 10 min. Subsequently, 4-bromobutylamine.HBr IV-69 (2.0 eq, 1.2 mmol) was added. The reaction mixture was refluxed for 4 h. It was cooled to rt, diluted with H<sub>2</sub>O (20 mL) and extracted with EtOAc (3 × 20 mL). Organic layers were dried over Na<sub>2</sub>SO<sub>4</sub> and concentrated *in vacuo*. The residue was purified by column chromatography (Hex/EtOAc, isocratic 20 %).

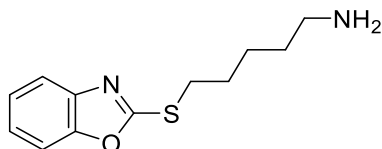


**2-(Pyrrolidin-1-yl)benzo[d]oxazole IV-72**

White solid. Yield: 54 % (60 mg). <sup>1</sup>H NMR (400 MHz, DMSO-*d*<sub>6</sub>): δ 7.37 (dd, *J* = 7.9, 0.5 Hz, 1H), 7.25 (dd, *J* = 7.8, 0.8 Hz, 1H), 7.12 (td, *J* = 7.7, 1.1 Hz, 1H), 6.97 (td, *J* = 7.7, 1.3 Hz, 1H), 3.54 (ddd, *J* = 6.7, 4.3, 2.6 Hz, 4H), 2.00 – 1.93 (m, 4H). <sup>13</sup>C NMR (101 MHz, DMSO-*d*<sub>6</sub>): δ 160.5, 148.5, 143.6, 123.7, 119.8, 115.4, 108.6, 47.2, 25.0. HRMS: *m/z*: calcd for C<sub>11</sub>H<sub>12</sub>N<sub>2</sub>O: 189.1022 [M+H]<sup>+</sup>; found: 189.1022.

**The Smiles rearrangement with 5-bromopentylamine.HBr**

Benzoxazole-2-thiol IV-54 (1.0 eq, 0.6 mmol) and Et<sub>3</sub>N (2.0 eq, 1.2 mmol) were dissolved in toluene (5.0 mL) and premixed at rt for 10 min. Subsequently, 5-bromopentylamine.HBr IV-73 (2.0 eq, 1.2 mmol) was added. The reaction mixture was refluxed for 4 h. It was cooled to rt, diluted with H<sub>2</sub>O (20 mL) and extracted with EtOAc (3 × 20 mL). Organic layers were dried over Na<sub>2</sub>SO<sub>4</sub> and concentrated *in vacuo*.

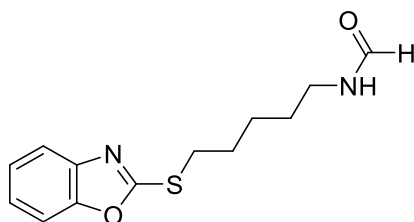


#### 5-(Benzo[d]oxazol-2-ylthio)pentan-1-amine.HBr **IV-74**

White solid. Yield: 95 % (134 mg).  $^1\text{H}$  NMR (400 MHz, DMSO- $d_6$ ):  $\delta$  7.68 – 7.59 (m, 2H), 7.37 – 7.28 (m, 2H), 3.54 (br s, 3H), 3.37 – 3.28 (m, 2H), 2.60 (t,  $J$  = 6.5 Hz, 2H), 1.85 – 1.71 (m, 2H), 1.53 – 1.35 (m, 4H).  $^{13}\text{C}$  NMR (101 MHz, DMSO- $d_6$ ):  $\delta$  164.5, 151.2, 141.3, 124.5, 124.1, 118.2, 110.1, 41.0, 31.8, 31.7, 28.8, 25.3. HRMS:  $m/z$ : calcd for  $\text{C}_{12}\text{H}_{16}\text{N}_2\text{OS}$ : 237.1056  $[\text{M}+\text{H}]^+$ ; found: 237.1056.

#### The Smiles rearrangement with **IV-74**

5-(Benzo[d]oxazol-2-ylthio)pentan-1-amine.HBr **IV-74** (1.0 eq, 0.42 mmol) and  $\text{Et}_3\text{N}$  (2.0 eq, 0.84 mmol) were dissolved in DMF (4.0 mL). The reaction mixture was stirred under microwave irradiation at 120 °C for 2 h. After that, it was cooled to rt, diluted with  $\text{H}_2\text{O}$  (20 mL) and extracted with EtOAc ( $3 \times 20$  mL). Organic layers were dried over  $\text{Na}_2\text{SO}_4$  and concentrated *in vacuo*. The residue was purified by column chromatography ( $\text{CHCl}_3/\text{MeOH}$ , isocratic 10 %).



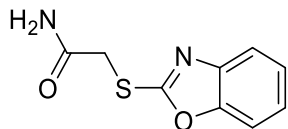
#### *N*-(5-(Benzo[d]oxazol-2-ylthio)pentyl)formamide **IV-76**

Brown oil. Yield: 58 % (64 mg).  $^1\text{H}$  NMR (400 MHz, DMSO- $d_6$ ):  $\delta$  7.99 (s, 1H), 7.97 (br s, 1H), 7.68 – 7.59 (m, 2H), 7.36 – 7.28 (m, 3H), 3.35 – 3.28 (m, 2H overlap with  $\text{H}_2\text{O}$ ), 3.09 (q,  $J$  = 6.3 Hz, 2H), 1.84 – 1.73 (m, 2H), 1.50 – 1.38 (m, 4H).  $^{13}\text{C}$  NMR (101 MHz, DMSO- $d_6$ ):  $\delta$  164.4, 160.9, 151.2, 141.3, 124.5, 124.1, 118.2, 110.1, 36.8, 31.6, 28.5, 28.4, 25.3. HRMS:  $m/z$ : calcd for  $\text{C}_{13}\text{H}_{16}\text{N}_2\text{O}_2\text{S}$ : 265.1005  $[\text{M}+\text{H}]^+$ ; found: 265.1006.

#### The Smiles rearrangement with 2-chloroacetamide

Benzoxazole-2-thiol **IV-54** (1.0 eq, 1.6 mmol),  $\text{K}_2\text{CO}_3$  (3 eq, 4.8 mmol) and 2-chloroacetamide **IV-77** (2.0 eq, 3.2 mmol) were suspended in DMF (10 mL). The reaction mixture was stirred at 70 °C for 4 h. It was cooled to rt, diluted with  $\text{H}_2\text{O}$  (50 mL) and

extracted with EtOAc (3 × 50 mL). Organic layers were washed with brine (50 mL), dried over Na<sub>2</sub>SO<sub>4</sub> and concentrated *in vacuum*. The residue was purified by column chromatography (Hex/EtOAc, gradient from 10 to 80 %).

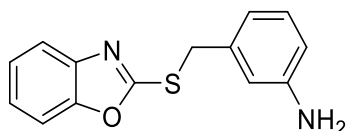


### 2-(Benzo[d]oxazol-2-ylthio)acetamide **IV-80**

Yellow solid. Yield: 46 % (152 mg). <sup>1</sup>H NMR (400 MHz, DMSO-*d*<sub>6</sub>): δ 7.75 (s, 1H), 7.63 (ddd, *J* = 7.0, 3.1, 1.2 Hz, 2H), 7.38 – 7.26 (m, 3H), 4.12 (s, 2H). <sup>13</sup>C NMR (101 MHz, DMSO-*d*<sub>6</sub>): δ 168.0, 164.1, 151.3, 141.3, 124.6, 124.3, 118.2, 110.2, 35.8. HRMS: *m/z*: calcd for C<sub>9</sub>H<sub>8</sub>N<sub>2</sub>O<sub>2</sub>S: 209.0379 [M+H]<sup>+</sup>; found: 209.0378.

### The Smiles rearrangement with 3-(bromomethyl)aniline

Benzoxazole-2-thiol **IV-54** (1.0 eq, 0.6 mmol), 3-(bromomethyl)aniline **IV-78** (2.0 eq, 1.2 mmol) and K<sub>2</sub>CO<sub>3</sub> (2.0 eq, 1.2 mmol) were suspended in DMF (5.0 mL). The reaction mixture was stirred at 70 °C for 2 h. It was cooled to rt, diluted with H<sub>2</sub>O (20 mL) and extracted with EtOAc (3 × 20 mL). Organic layers were dried over Na<sub>2</sub>SO<sub>4</sub> and concentrated *in vacuum*. The residue was purified by column chromatography (Hex/EtOAc, gradient from 30 to 60 %).



### 3-((Benzo[d]oxazol-2-ylthio)methyl)aniline **IV-81**

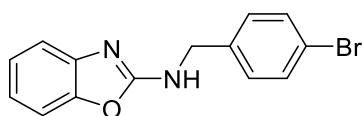
White solid. Yield: 80 % (123 mg). <sup>1</sup>H NMR (400 MHz, DMSO-*d*<sub>6</sub>): δ 7.65 (m, 2H), 7.37 – 7.29 (m, 2H), 6.97 (t, *J* = 7.7 Hz, 1H), 6.66 (t, *J* = 1.9 Hz, 1H), 6.59 (d, *J* = 7.5 Hz, 1H), 6.47 (m, 1H), 5.13 (br s, 2H), 4.47 (s, 2H). <sup>13</sup>C NMR (101 MHz, DMSO-*d*<sub>6</sub>): δ 164.0, 151.2, 148.9, 141.3, 136.5, 129.1, 124.6, 124.3, 118.3, 116.2, 114.0, 113.4, 110.2, 36.0. HRMS: *m/z*: calcd for C<sub>14</sub>H<sub>12</sub>N<sub>2</sub>OS: 257.0743 [M+H]<sup>+</sup>; found: 257.0742.

### The Smiles rearrangement with 4-bromobenzylamine

Benzoxazole-2-thiol **IV-54** (1.0 eq, 0.6 mmol) and Et<sub>3</sub>N (2.0 eq, 1.2 mmol) were dissolved in toluene (5.0 mL) and premixed at rt for 10 min. Subsequently, 4-



bromobenzylamine **IV-79** (2.0 eq, 1.2 mmol) was added. The reaction mixture was refluxed on (monitored by TLC, 18 h). It was cooled to rt, diluted with H<sub>2</sub>O (20 mL) and extracted with EtOAc (3 × 20 mL). Organic layers were dried over Na<sub>2</sub>SO<sub>4</sub> and concentrated *in vacuo*. The residue was purified by column chromatography (Hex/EtOAc, isocratic 20 %).

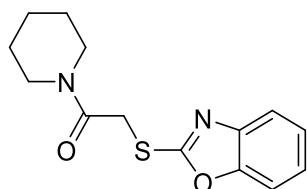


#### **N-(4-Bromobenzyl)benzo[d]oxazol-2-amine IV-82**

Brown solid. Yield: 69 % (125 mg). <sup>1</sup>H NMR (400 MHz, DMSO-*d*<sub>6</sub>): δ 8.48 (t, *J* = 6.1 Hz, 1H), 7.56 – 7.49 (m, 2H), 7.34 (d, *J* = 8.6 Hz, 3H), 7.24 (dd, *J* = 7.8, 0.6 Hz, 1H), 7.10 (td, *J* = 7.6, 1.0 Hz, 1H), 6.98 (td, *J* = 7.7, 1.2 Hz, 1H), 4.50 (d, *J* = 6.0 Hz, 2H). <sup>13</sup>C NMR (101 MHz, DMSO-*d*<sub>6</sub>): δ 162.3, 148.1, 143.0, 138.5, 131.2, 129.4, 123.6, 120.3, 120.0, 115.6, 108.6, 45.0. HRMS: *m/z*: calcd for C<sub>14</sub>H<sub>11</sub>BrN<sub>2</sub>O: 303.0128 [M+H]<sup>+</sup>; found: 303.0126.

#### **The substitution with cyclohexylamine**

To a stirred solution of cyclohexylamine **IV-83A** (1.0 eq, 0.48 mmol) and DBU (3.2 eq, 1.54 mmol) in MeCN (3.0 mL) cooled to -5 °C, were added chloroacetyl chloride (1.2 eq, 0.58 mmol) and benzoxazole-2-thiol **IV-54** (1.0 eq, 0.48 mmol). The reaction mixture was refluxed (monitored by TLC, 3 h). After that, cooled (rt) mixture was diluted by H<sub>2</sub>O (20 mL), extracted with CH<sub>2</sub>Cl<sub>2</sub> (3 × 30 mL) and washed with brine (50 mL). Combined organic layers were dried over Na<sub>2</sub>SO<sub>4</sub> and concentrated *in vacuo*. The residue was purified by column chromatography (Hex/EtOAc, gradient from 40 to 60 %).



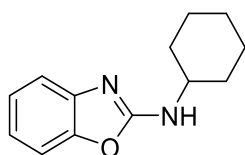
#### **2-(Benzo[d]oxazol-2-ylthio)-N-cyclohexylacetamide IV-55A**

White solid. Yield: 62 % (86 mg). <sup>1</sup>H NMR (400 MHz, DMSO-*d*<sub>6</sub>): δ 8.20 (d, *J* = 7.6 Hz, 1H), 7.68 – 7.57 (m, 2H), 7.37 – 7.28 (m, 2H), 4.11 (s, 2H), 3.55 (dt, *J* = 14.0, 8.4 Hz, 1H), 1.69 (m, 4H), 1.53 (m, 1H), 1.21 (m, 5H). <sup>13</sup>C NMR (101 MHz, DMSO-*d*<sub>6</sub>): δ 165.0,

163.9, 151.2, 141.2, 124.6, 124.2, 118.1, 110.1, 48.0, 35.8, 32.1, 25.1, 24.3. HRMS:  $m/z$ : calcd for  $C_{15}H_{18}N_2O_2S$ : 291.1162  $[M+H]^+$ ; found: 291.1161.

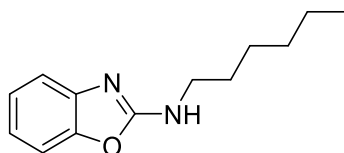
### General procedure for the Smiles rearrangement with amines

To a stirred solution of amine **IV-83** (1.0 eq, 0.48 mmol) and  $CS_2CO_3$  (3.2 eq, 1.54 mmol) in DMF (3.0 mL) cooled to  $-5\text{ }^\circ\text{C}$ , were added chloroacetyl chloride (1.2 eq, 0.58 mmol) and benzoxazole-2-thiol **IV-54** (1.0 eq, 0.48 mmol). The reaction mixture was refluxed (monitored by TLC, 4-7 h). After that, cooled (rt) mixture was diluted by  $H_2O$  (20 mL), extracted with  $CH_2Cl_2$  ( $3 \times 30$  mL) and washed with brine (50 mL). Combined organic layers were dried over  $Na_2SO_4$  and concentrated *in vacuo*. The residue was purified by column chromatography (Hex/EtOAc, gradient from 20 to 60 % or Tol/MeCN, isocratic 20 %).



### N-Cyclohexylbenzo[d]oxazol-2-amine IV-56A

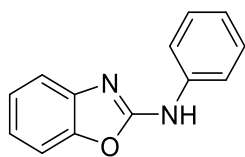
Orange solid. Yield: 33 % (34 mg).  $^1H$  NMR (400 MHz,  $DMSO-d_6$ ):  $\delta$  7.84 (d,  $J = 7.7$  Hz, 1H), 7.31 (d,  $J = 7.8$  Hz, 1H), 7.22 (d,  $J = 7.7$  Hz, 1H), 7.08 (t,  $J = 7.6$  Hz, 1H), 6.95 (t,  $J = 7.7$  Hz, 1H), 3.54 (br s, 1H), 1.96 (m, 2H), 1.73 (m, 2H), 1.59 (m, 1H), 1.36 – 1.23 (m, 4H), 1.21 – 1.10 (m, 1H).  $^{13}C$  NMR (101 MHz,  $DMSO-d_6$ ):  $\delta$  161.7, 147.9, 143.4, 123.5, 119.9, 115.3, 108.4, 51.6, 32.4, 25.2, 24.6. HRMS:  $m/z$ : calcd for  $C_{13}H_{16}N_2O$ : 217.1335  $[M+H]^+$ ; found: 217.1337.



### N-Hexylbenzo[d]oxazol-2-amine IV-56B

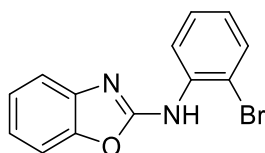
Orange solid. Yield: 58 % (60 mg).  $^1H$  NMR (400 MHz,  $DMSO-d_6$ ):  $\delta$  7.89 (t,  $J = 5.6$  Hz, 1H), 7.31 (d,  $J = 7.8$  Hz, 1H), 7.22 (d,  $J = 7.6$  Hz, 1H), 7.09 (t,  $J = 7.6$  Hz, 1H), 6.95 (td,  $J = 7.8, 0.9$  Hz, 1H), 3.28 (dd,  $J = 13.0, 6.8$  Hz, 2H), 1.62 – 1.51 (m, 2H), 1.35 – 1.25 (m, 6H), 0.86 (t,  $J = 6.7$  Hz, 3H).  $^{13}C$  NMR (101 MHz,  $DMSO-d_6$ ):  $\delta$  162.4, 148.0, 143.4,

123.5, 119.9, 115.3, 108.4, 42.3, 31.0, 28.9, 26.0, 22.1, 13.9. HRMS:  $m/z$ : calcd for  $C_{13}H_{18}N_2O$ : 219.1492  $[M+H]^+$ ; found: 219.1491



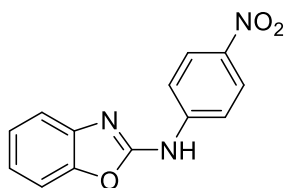
**N-Phenylbenzo[d]oxazol-2-amine IV-56C**

Yellow solid. Yield: 76 % (76 mg).  $^1H$  NMR (400 MHz,  $DMSO-d_6$ ):  $\delta$  10.61 (s, 1H), 7.76 (d,  $J = 7.8$  Hz, 2H), 7.47 (dd,  $J = 13.3, 7.7$  Hz, 2H), 7.37 (t,  $J = 7.9$  Hz, 2H), 7.22 (td,  $J = 7.7, 0.9$  Hz, 1H), 7.13 (td,  $J = 7.8, 1.2$  Hz, 1H), 7.03 (t,  $J = 7.4$  Hz, 1H).  $^{13}C$  NMR (101 MHz,  $DMSO-d_6$ ):  $\delta$  158.0, 147.0, 142.4, 138.7, 129.0, 124.0, 122.1, 121.7, 117.6, 116.6, 109.0. HRMS:  $m/z$ : calcd for  $C_{13}H_{10}N_2O$ : 211.0866  $[M+H]^+$ ; found: 211.0864



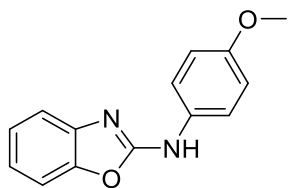
**N-(2-Bromophenyl)benzo[d]oxazol-2-amine IV-56D**

White solid. Yield: 81 % (112 mg).  $^1H$  NMR (400 MHz,  $DMSO-d_6$ ):  $\delta$  9.90 (s, 1H), 7.93 (d,  $J = 6.6$  Hz, 1H), 7.70 (dd,  $J = 7.9, 1.2$  Hz, 1H), 7.45 (t,  $J = 7.8$  Hz, 2H), 7.37 (d,  $J = 7.6$  Hz, 1H), 7.24 – 7.06 (m, 3H).  $^{13}C$  NMR (101 MHz,  $DMSO-d_6$ ):  $\delta$  133.0, 128.5, 126.5, 125.5, 124.1, 121.6, 117.2, 109.1. HRMS:  $m/z$ : calcd for  $C_{13}H_9BrN_2O$ : 288.9971  $[M+H]^+$ ; found: 288.9969.



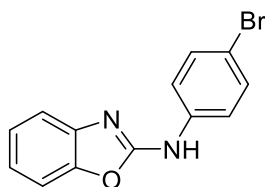
**N-(4-Nitrophenyl)benzo[d]oxazol-2-amine IV-56E**

Yellow solid. Yield: 74 % (90 mg).  $^1H$  NMR (400 MHz,  $DMSO-d_6$ ):  $\delta$  11.45 (s, 1H), 8.30 (d,  $J = 9.1$  Hz, 2H), 7.98 (d,  $J = 8.8$  Hz, 2H), 7.60 – 7.54 (m, 2H), 7.29 (t,  $J = 7.6$  Hz, 1H), 7.22 (t,  $J = 7.7$  Hz, 1H).  $^{13}C$  NMR (101 MHz,  $DMSO-d_6$ ):  $\delta$  156.9, 147.0, 144.9, 141.7, 141.3, 125.4, 124.4, 122.7, 117.3, 117.2, 109.4. HRMS:  $m/z$ : calcd for  $C_{13}H_9N_3O_3$ : 256.0717  $[M+H]^+$ ; found: 256.0719.



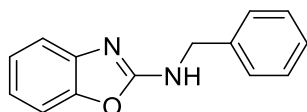
***N*-(4-Methoxyphenyl)benzo[d]oxazol-2-amine IV-56F**

Orange solid. Yield: 78 % (90 mg). <sup>1</sup>H NMR (500 MHz, DMSO-*d*<sub>6</sub>): δ 10.36 (s, 1H), 7.65 (d, *J* = 9.1 Hz, 2H), 7.45 (d, *J* = 7.8 Hz, 1H), 7.41 (d, *J* = 7.1 Hz, 1H), 7.19 (td, *J* = 7.6, 1.1 Hz, 1H), 7.09 (td, *J* = 7.7, 1.2 Hz, 1H), 6.96 (d, *J* = 9.1 Hz, 2H), 3.74 (s, 3H). <sup>13</sup>C NMR (101 MHz, DMSO-*d*<sub>6</sub>): δ 158.4, 154.7, 147.1, 142.6, 131.9, 123.9, 121.3, 119.2, 116.3, 114.2, 108.8, 55.3. HRMS: *m/z*: calcd for C<sub>14</sub>H<sub>12</sub>N<sub>2</sub>O<sub>2</sub>: 241.0972 [M+H]<sup>+</sup>; found: 241.0970.



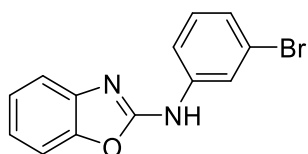
***N*-(4-Bromophenyl)benzo[d]oxazol-2-amine IV-56G**

Yellow solid. Yield: 82 % (113 mg). <sup>1</sup>H NMR (500 MHz, DMSO-*d*<sub>6</sub>): δ 10.77 (s, 1H), 7.74 (d, *J* = 8.9 Hz, 2H), 7.55 (d, *J* = 8.9 Hz, 2H), 7.48 (dd, *J* = 14.3, 7.7 Hz, 2H), 7.23 (td, *J* = 7.7, 1.0 Hz, 1H), 7.15 (td, *J* = 7.8, 1.2 Hz, 1H). <sup>13</sup>C NMR (101 MHz, DMSO-*d*<sub>6</sub>): δ 157.6, 147.0, 142.2, 138.1, 131.8, 124.1, 121.9, 119.5, 116.8, 113.6, 109.1. HRMS: *m/z*: calcd for C<sub>13</sub>H<sub>9</sub>BrN<sub>2</sub>O: 288.9971 [M+H]<sup>+</sup>; found: 288.9969.



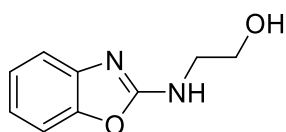
***N*-Benzylbenzo[d]oxazol-2-amine IV-56H**

Yellow solid. Yield: 83 % (89 mg). <sup>1</sup>H NMR (500 MHz, DMSO-*d*<sub>6</sub>): δ 8.45 (t, *J* = 6.1 Hz, 1H), 7.41 – 7.30 (m, 5H), 7.25 (dd, *J* = 15.1, 7.8 Hz, 2H), 7.10 (td, *J* = 7.7, 1.0 Hz, 1H), 6.98 (td, *J* = 7.8, 1.2 Hz, 1H), 4.52 (d, *J* = 6.2 Hz, 2H). <sup>13</sup>C NMR (101 MHz, DMSO-*d*<sub>6</sub>): δ 162.5, 148.1, 143.2, 139.1, 128.4, 127.2, 127.1, 123.6, 120.2, 115.5, 108.6, 45.7. HRMS: *m/z*: calcd for C<sub>9</sub>H<sub>12</sub>N<sub>2</sub>O<sub>4</sub>S: 225.1022 [M+H]<sup>+</sup>; found: 225.1023.



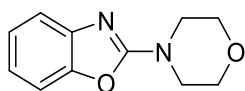
#### **N-(3-Bromophenyl)benzo[d]oxazol-2-amine IV-56I**

Yellow solid. Yield: 78 % (108 mg).  $^1\text{H}$  NMR (400 MHz,  $\text{DMSO-}d_6$ ):  $\delta$  10.82 (s, 1H), 8.11 (t,  $J = 1.9$  Hz, 1H), 7.67 (dd,  $J = 8.2, 1.2$  Hz, 1H), 7.51 (d,  $J = 8.9$  Hz, 2H), 7.33 (t,  $J = 8.1$  Hz, 1H), 7.23 (m, 2H), 7.16 (td,  $J = 7.6, 1.1$  Hz, 1H).  $^{13}\text{C}$  NMR (101 MHz,  $\text{DMSO-}d_6$ ):  $\delta$  157.4, 146.9, 142.1, 140.3, 131.0, 124.7, 124.2, 122.1, 121.9, 119.6, 116.9, 116.5, 109.1. HRMS:  $m/z$ : calcd for  $\text{C}_{13}\text{H}_9\text{BrN}_2\text{O}$ : 288.9971  $[\text{M}+\text{H}]^+$ ; found: 288.9971.



#### **2-(Benzo[d]oxazol-2-ylamino)ethan-1-ol IV-56J**

White solid. Yield: 55 % (47 mg).  $^1\text{H}$  NMR (400 MHz,  $\text{DMSO-}d_6$ ):  $\delta$  7.92 (t,  $J = 5.7$  Hz, 1H), 7.32 (d,  $J = 7.8$  Hz, 1H), 7.22 (d,  $J = 7.4$  Hz, 1H), 7.09 (td,  $J = 7.7, 0.8$  Hz, 1H), 6.96 (td,  $J = 7.7, 1.1$  Hz, 1H), 4.80 (t,  $J = 5.5$  Hz, 1H), 3.56 (q,  $J = 5.9$  Hz, 2H), 3.35 (q,  $J = 5.8$  Hz, 2H overlap with  $\text{H}_2\text{O}$ ).  $^{13}\text{C}$  NMR (101 MHz,  $\text{DMSO-}d_6$ ):  $\delta$  162.5, 148.0, 143.3, 123.6, 120.0, 115.3, 108.5, 59.4, 50.0. HRMS:  $m/z$ : calcd for  $\text{C}_9\text{H}_{10}\text{N}_2\text{O}_2$ : 179.0815  $[\text{M}+\text{H}]^+$ ; found: 179.0814.



#### **2-Morpholinobenzo[d]oxazole IV-56K**

White solid. Yield: 31 % (30 mg).  $^1\text{H}$  NMR (400 MHz,  $\text{DMSO-}d_6$ ):  $\delta$  7.41 (d,  $J = 7.8$  Hz, 1H), 7.31 (d,  $J = 7.7$  Hz, 1H), 7.16 (td,  $J = 7.7, 1.0$  Hz, 1H), 7.03 (td,  $J = 7.8, 1.2$  Hz, 1H), 3.76 – 3.69 (m, 4H), 3.63 – 3.56 (m, 4H).  $^{13}\text{C}$  NMR (101 MHz,  $\text{DMSO-}d_6$ ):  $\delta$  161.9, 148.3, 142.8, 124.0, 120.7, 116.0, 109.0, 65.4, 45.4. HRMS:  $m/z$ : calcd for  $\text{C}_{11}\text{H}_{12}\text{N}_2\text{O}_2$ : 205.0972  $[\text{M}+\text{H}]^+$ ; found: 205.0972.

## **6.10 Synthesis of TZD-pyrimidines**

### **General procedure of synthesis of resins IV-91**

Wang resin (loading 1.0 mmol/g, ~1 g) was washed three times with DCM. A solution consisting of Fmoc-amino acid (2.0 mmol), HOBt (2.0 mmol), DMAP (0.5 mmol) and DIC (2.0 mmol) in DMF/DCM (1:1, v/v, 10 mL) was added to the resin. The resin slurry was shaken at rt for 16 h. The resin was washed three times with DMF and three times with DCM.

**General procedure for reaction with 4,6-dichloro-5-nitropyrimidines (resins IV-92)**

Firstly, Fmoc protecting group of resins **IV-91** (~1 g) was removed by exposure to 50% piperidine in DMF (v/v 10 mL) for 15 min, and then, the resin was washed three times with DMF and three times with DCM. Further, resins were washed three times with dry DMF and reacted with a solution consisting of 4,6-dichloro-5-nitropyrimidine (5.0 mmol) and DIPEA (5.0 mmol) in dry DMF (10 mL) at rt for 2 h. The resin was washed five times with DMF and three times with DCM.

**General procedure for reaction with amino alcohols (resins IV-93)**

Resins **IV-92** (~500 mg) were each washed three times with dry DMF and reacted with a solution consisting of amino alcohol (2.5 mmol) and DIPEA (2.5 mmol) in dry DMF (5.0 mL) at rt for 2 h. The resin was washed three times with DMF and three times with DCM.

**General procedure for Fukuyama-Mitsunobu reaction with thiazolidinedione (resins IV-94)**

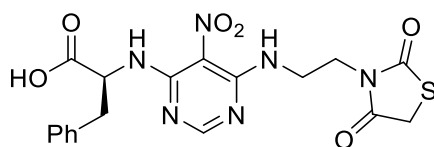
Resins **IV-93** (~500 mg) were each washed three times with dry THF. A solution consisting of thiazolidine-2,4-dione (1.25 mmol) and PPh<sub>3</sub> (1.25 mmol) in dry THF (5.0 mL) was added. The resin was stored in a freezer for 30 min followed by reaction with DIAD (1.25 mmol) at rt for 1 h. The resin was washed three times with THF and five times with DCM.

**General procedure for Knoevenagel condensation with aldehydes (resins IV-95)**

Resins **IV-94** (~250 mg) were each washed three times with DMF and reacted with a solution consisting of aldehyde (0.62 mmol) and piperidine (0.25 mmol) in DMF (2.5 mL) at 70 °C for 20 h. The resin was washed three times with DMF and three times with DCM.

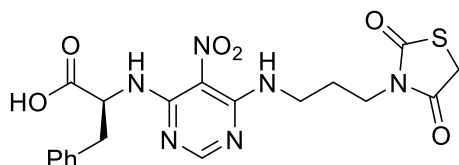
**General procedure for cleavage from resin with TFA (compounds IV-96 and IV-97)**

Resins **IV-94** and **IV-95** (~250 mg) were each treated with 2.0 mL of a solution consisting of TFA/DCM (1:1, v/v) for 1 h. The cleavage cocktail was collected, and the resin was washed three times with 50% TFA in DCM. The combined extracts were evaporated by a stream of nitrogen, and the crude products were purified by reversed-phase HPLC.



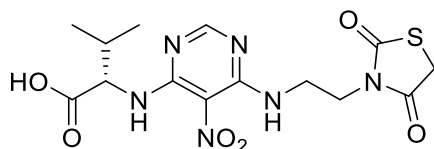
**(6-((2-(2,4-Dioxothiazolidin-3-yl)ethyl)amino)-5-nitropyrimidin-4-yl)-L-phenylalanine IV-96A**

Orange solid. Yield: 51%.  $^1\text{H}$  NMR (500 MHz,  $\text{DMSO-}d_6$ ):  $\delta$  9.59 (d,  $J = 6.7$  Hz, 1H), 9.47 (t,  $J = 5.1$  Hz, 1H), 8.07 (s, 1H), 7.21 (t,  $J = 7.2$  Hz, 2H), 7.15 (t,  $J = 7.2$  Hz, 1H), 7.10 (d,  $J = 6.9$  Hz, 2H), 4.75 (dd,  $J = 11.9, 5.5$  Hz, 1H), 4.07 (s, 2H), 3.75 (s, 4H), 3.28 (dd,  $J = 13.5, 5.4$  Hz, 1H), 3.18 (dd,  $J = 13.5, 5.4$  Hz, 1H).  $^{13}\text{C}$  NMR (126 MHz,  $\text{DMSO-}d_6$ ):  $\delta$  172.4, 172.1, 171.9, 159.2, 157.2, 155.4, 137.5, 129.4, 128.0, 126.2, 111.9, 56.3, 40.8, 38.7, 36.9, 33.8. HRMS:  $m/z$ : calcd for  $\text{C}_{18}\text{H}_{18}\text{N}_6\text{O}_6\text{S}$ : 447.1081  $[\text{M}+\text{H}]^+$ ; found: 447.1085.



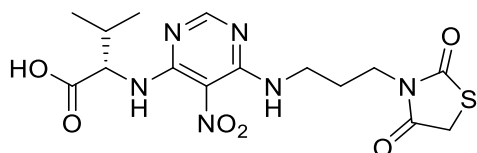
**(6-((3-(2,4-Dioxothiazolidin-3-yl)propyl)amino)-5-nitropyrimidin-4-yl)-L-phenylalanine IV-96B**

Brown solid. Yield: 74%.  $^1\text{H}$  NMR (500 MHz,  $\text{DMSO-}d_6$ ):  $\delta$  9.48 (dd,  $J = 14.1, 6.6$  Hz, 2H), 8.08 (s, 1H), 7.24 (t,  $J = 7.2$  Hz, 2H), 7.17 (dd,  $J = 17.5, 7.1$  Hz, 3H), 4.91 (dd,  $J = 12.3, 6.0$  Hz, 1H), 4.17 (s, 2H), 3.53 (dt,  $J = 11.1, 6.7$  Hz, 4H), 3.27 (dd,  $J = 13.7, 5.2$  Hz, 1H), 3.19 (dd,  $J = 13.7, 6.2$  Hz, 1H), 1.81 (p,  $J = 6.8$  Hz, 2H).  $^{13}\text{C}$  NMR (126 MHz,  $\text{DMSO-}d_6$ ):  $\delta$  172.6, 172.2, 171.9, 159.3, 156.6, 155.8, 137.0, 129.3, 128.1, 126.5, 112.1, 55.7, 38.8, 38.3, 36.7, 34.0, 26.8. HRMS:  $m/z$ : calcd for  $\text{C}_{19}\text{H}_{20}\text{N}_6\text{O}_6\text{S}$ : 461.1238  $[\text{M}+\text{H}]^+$ ; found: 461.1239.



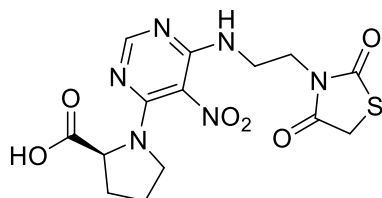
**(6-((2-(2,4-Dioxothiazolidin-3-yl)ethyl)amino)-5-nitropyrimidin-4-yl)-L-valine IV-96C**

Orange solid. Yield: 27%.  $^1\text{H}$  NMR (500 MHz,  $\text{DMSO-}d_6$ ):  $\delta$  9.64 (d,  $J = 7.7$  Hz, 1H), 9.52 (t,  $J = 4.9$  Hz, 1H), 8.06 (s, 1H), 4.63 (dd,  $J = 7.8, 4.3$  Hz, 1H), 4.08 (s, 2H), 3.75 (s, 4H), 2.28 – 2.22 (m, 1H), 0.97 (d,  $J = 6.9$  Hz, 3H), 0.90 (d,  $J = 6.9$  Hz, 3H).  $^{13}\text{C}$  NMR (126 MHz,  $\text{DMSO-}d_6$ ):  $\delta$  172.4, 172.0, 159.2, 157.1, 156.1, 112.1, 59.5, 40.7, 38.8, 33.8, 30.5, 18.8, 18.2. HRMS:  $m/z$ : calcd for  $\text{C}_{14}\text{H}_{18}\text{N}_6\text{O}_6\text{S}$ : 399.1081  $[\text{M}+\text{H}]^+$ ; found: 399.1085.



**(6-((3-(2,4-Dioxothiazolidin-3-yl)propyl)amino)-5-nitropyrimidin-4-yl)-L-valine IV-96D**

Orange solid. Yield: 58%.  $^1\text{H}$  NMR (500 MHz,  $\text{DMSO-}d_6$ ):  $\delta$  9.97 (d,  $J = 7.6$  Hz, 1H), 9.51 (t,  $J = 6.0$  Hz, 1H), 8.01 (s, 1H), 4.40 (dd,  $J = 7.6, 3.8$  Hz, 1H), 4.17 (s, 2H), 3.57 – 3.50 (m, 4H), 2.19 (qd,  $J = 10.8, 6.8$  Hz, 1H), 1.81 (p,  $J = 6.8$  Hz, 2H), 0.95 (d,  $J = 6.9$  Hz, 3H), 0.83 (d,  $J = 6.9$  Hz, 3H).  $^{13}\text{C}$  NMR (126 MHz,  $\text{DMSO-}d_6$ ):  $\delta$  172.6, 172.2, 159.4, 156.6, 156.4, 112.3, 59.0, 38.3, 30.3, 26.8, 18.7, 18.0. HRMS:  $m/z$ : calcd for  $\text{C}_{15}\text{H}_{20}\text{N}_6\text{O}_6\text{S}$ : 413.1238  $[\text{M}+\text{H}]^+$ ; found: 413.1241.

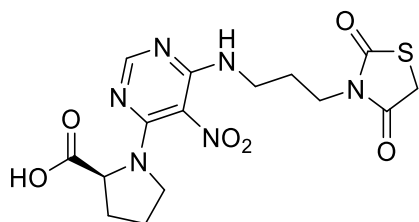


**(6-((2-(2,4-Dioxothiazolidin-3-yl)ethyl)amino)-5-nitropyrimidin-4-yl)-L-proline IV-96E**

Yellow solid. Yield: 50%.  $^1\text{H}$  NMR (500 MHz,  $\text{DMSO-}d_6$ ):  $\delta$  8.38 (t,  $J = 5.6$  Hz, 1H), 7.98 (s, 1H), 4.56 (s, 1H), 4.06 (s, 2H), 3.71 (s, 4H), 3.07 (d,  $J = 59.0$  Hz, 2H), 2.26 – 2.18 (m, 1H), 2.01 – 1.93 (m, 1H), 1.88 – 1.79 (m, 2H).  $^{13}\text{C}$  NMR (126 MHz,  $\text{DMSO-}$

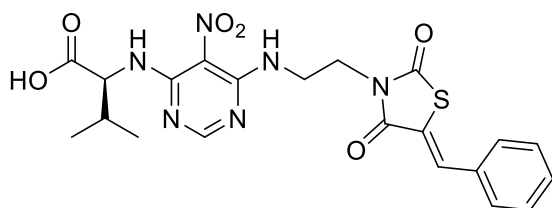


$d_6$ ):  $\delta$  173.0, 172.4, 172.1, 156.6, 156.0, 154.4, 113.8, 62.9, 50.0, 41.0, 38.63, 33.75, 24.46, 21.25. HRMS:  $m/z$ : calcd for  $C_{14}H_{16}N_6O_6S$ : 397.0925  $[M+H]^+$ ; found: 397.0928.



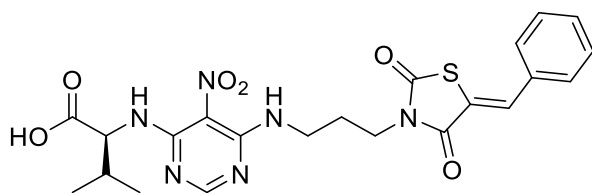
**(6-((3-(2,4-Dioxothiazolidin-3-yl)propyl)amino)-5-nitropyrimidin-4-yl)-L-proline  
IV-96F**

Yellow solid. Yield: 84%.  $^1H$  NMR (500 MHz,  $DMSO-d_6$ ):  $\delta$  8.40 (t,  $J = 6.0$  Hz, 1H), 7.98 (s, 1H), 4.57 (s, 1H), 4.18 (s, 2H), 3.53 (t,  $J = 6.8$  Hz, 2H), 3.46 (dt,  $J = 9.3, 6.8$  Hz, 2H), 3.15 (s, 1H), 3.03 (s, 1H), 2.28 – 2.18 (m, 1H), 2.02 – 1.92 (m, 1H), 1.91 – 1.83 (m, 2H), 1.82 – 1.75 (m, 2H).  $^{13}C$  NMR (126 MHz,  $DMSO-d_6$ ):  $\delta$  172.9, 172.6, 172.2, 156.8, 155.8, 154.7, 113.6, 63.0, 50.17, 38.9, 38.2, 34.0, 27.1. HRMS:  $m/z$ : calcd for  $C_{15}H_{18}N_6O_6S$ : 411.1081  $[M+H]^+$ ; found: 411.1084.



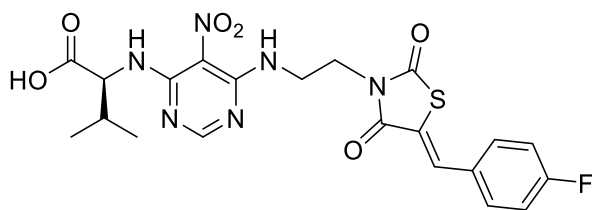
**(Z)-(6-((2-(5-Benzylidene-2,4-dioxothiazolidin-3-yl)ethyl)amino)-5-nitropyrimidin-4-yl)-L-valine IV-97A**

White solid. Yield: 49%.  $^1H$  NMR (500 MHz,  $DMSO-d_6$ ):  $\delta$  9.60 (t,  $J = 7.5$  Hz, 2H), 7.99 (s, 1H), 7.87 (s, 1H), 7.60 (d,  $J = 7.2$  Hz, 2H), 7.53 (t,  $J = 7.4$  Hz, 2H), 7.49 (t,  $J = 7.2$  Hz, 1H), 4.63 (dd,  $J = 7.8, 4.3$  Hz, 1H), 3.95 – 3.90 (m, 1H), 3.83 (ddd,  $J = 15.9, 8.3, 4.7$  Hz, 2H), 2.24 – 2.17 (m, 1H), 0.93 (d,  $J = 6.9$  Hz, 3H), 0.86 (d,  $J = 6.9$  Hz, 3H).  $^{13}C$  NMR (126 MHz,  $DMSO-d_6$ ):  $\delta$  171.9, 167.5, 165.8, 159.1, 157.1, 156.2, 133.0, 132.4, 130.5, 130.0, 129.3, 121.5, 112.1, 59.2, 41.1, 30.5, 18.7, 18.0. HRMS:  $m/z$ : calcd for  $C_{21}H_{22}N_6O_6S$ : 487.1394  $[M+H]^+$ ; found: 487.1399.



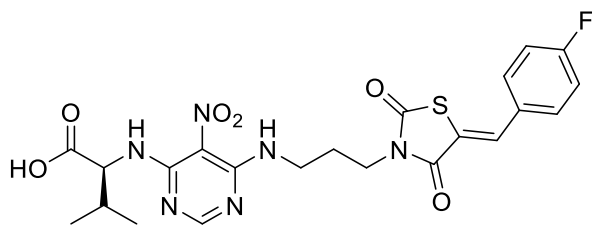
**(Z)-6-((3-(5-Benzylidene-2,4-dioxothiazolidin-3-yl)propyl)amino)-5-nitropyrimidin-4-yl-L-valine IV-97B**

White solid. Yield: 40%.  $^1\text{H}$  NMR (500 MHz,  $\text{DMSO-}d_6$ ):  $\delta$  9.67 (d,  $J = 7.8$  Hz, 1H), 9.54 (t,  $J = 6.0$  Hz, 1H), 8.04 (s, 1H), 7.92 (s, 1H), 7.62 (d,  $J = 7.2$  Hz, 2H), 7.54 (t,  $J = 7.4$  Hz, 2H), 7.49 (t,  $J = 7.2$  Hz, 1H), 4.63 (dd,  $J = 7.8, 4.3$  Hz, 1H), 3.72 (t,  $J = 6.7$  Hz, 2H), 3.58 (dt,  $J = 13.0, 6.7$  Hz, 2H), 2.28 – 2.21 (m, 1H), 1.96 – 1.89 (m, 2H), 0.95 (d,  $J = 6.9$  Hz, 3H), 0.89 (d,  $J = 6.9$  Hz, 3H).  $^{13}\text{C}$  NMR (126 MHz,  $\text{DMSO-}d_6$ ):  $\delta$  172.0, 167.6, 165.9, 159.4, 156.7, 156.2, 133.0, 132.8, 130.6, 130.1, 129.4, 121.4, 112.2, 59.4, 38.3, 30.5, 26.8, 18.7, 18.1. HRMS:  $m/z$ : calcd for  $\text{C}_{22}\text{H}_{24}\text{N}_6\text{O}_6\text{S}$ : 501.1551  $[\text{M}+\text{H}]^+$ ; found: 501.1553.



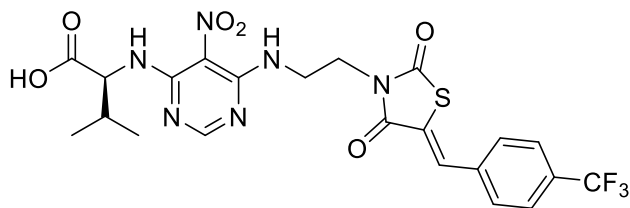
**(Z)-6-((2-(5-(4-Fluorobenzylidene)-2,4-dioxothiazolidin-3-yl)ethyl)amino)-5-nitropyrimidin-4-yl-L-valine IV-97C**

Brown solid. Yield: 42%.  $^1\text{H}$  NMR (500 MHz,  $\text{DMSO-}d_6$ ):  $\delta$  9.60 (t,  $J = 7.7$  Hz, 2H), 7.99 (s, 1H), 7.88 (s, 1H), 7.67 (dd,  $J = 8.8, 5.4$  Hz, 2H), 7.38 (t,  $J = 8.8$  Hz, 2H), 4.62 (dd,  $J = 7.8, 4.3$  Hz, 1H), 3.92 (ddd,  $J = 13.3, 6.4, 3.2$  Hz, 2H), 3.83 (ddd,  $J = 16.4, 8.4, 4.7$  Hz, 2H), 2.23 – 2.16 (m, 1H), 0.92 (d,  $J = 6.9$  Hz, 3H), 0.85 (d,  $J = 6.9$  Hz, 3H).  $^{13}\text{C}$  NMR (126 MHz,  $\text{DMSO-}d_6$ ):  $\delta$  171.98, 166.6 (d,  $J = 202.5$  Hz), 163.9, 161.9, 159.1, 157.1, 156.2, 132.5 (d,  $J = 9.5$  Hz), 131.4, 129.7, 121.2, 116.5 (d,  $J = 21.5$  Hz), 112.1, 59.3, 41.1, 30.5, 18.7, 18.0. HRMS:  $m/z$ : calcd for  $\text{C}_{21}\text{H}_{21}\text{FN}_6\text{O}_6\text{S}$ : 505.1300  $[\text{M}+\text{H}]^+$ ; found: 505.1302.



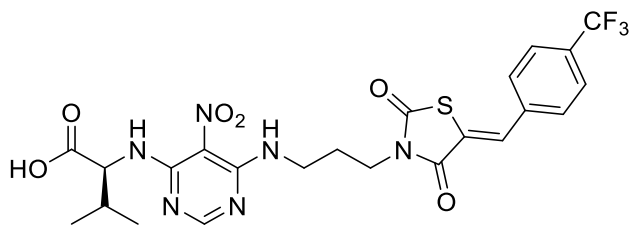
**(Z)-6-((3-(5-(4-Fluorobenzylidene)-2,4-dioxothiazolidin-3-yl)propyl)amino)-5-nitropyrimidin-4-yl)-L-valine IV-97D**

Yellow solid. Yield: 55%.  $^1\text{H}$  NMR (500 MHz,  $\text{DMSO-}d_6$ ):  $\delta$  9.90 (d,  $J = 7.7$  Hz, 1H), 9.54 (t,  $J = 6.0$  Hz, 1H), 8.00 (s, 1H), 7.93 (s, 1H), 7.69 (dd,  $J = 8.8, 5.4$  Hz, 2H), 7.38 (t,  $J = 8.8$  Hz, 2H), 4.44 (dd,  $J = 7.7, 3.9$  Hz, 1H), 3.71 (t,  $J = 6.6$  Hz, 2H), 3.56 (ddt,  $J = 19.7, 13.3, 6.5$  Hz, 2H), 2.24 – 2.15 (m, 1H), 1.95 – 1.89 (m, 2H), 0.94 (d,  $J = 6.9$  Hz, 3H), 0.84 (d,  $J = 6.9$  Hz, 3H).  $^{13}\text{C}$  NMR (126 MHz,  $\text{DMSO-}d_6$ ):  $\delta$  172.0, 166.6 (d,  $J = 203.5$  Hz), 163.9, 162.0, 159.3, 156.9, 155.6, 132.6 (d,  $J = 9.5$  Hz), 131.7, 129.7, 121.1, 116.5 (d,  $J = 22.5$  Hz), 112.0, 60.7, 38.2, 30.88, 26.9, 18.8, 18.6. HRMS:  $m/z$ : calcd for  $\text{C}_{22}\text{H}_{23}\text{FN}_6\text{O}_6\text{S}$ : 519.1457  $[\text{M}+\text{H}]^+$ ; found: 519.1457.



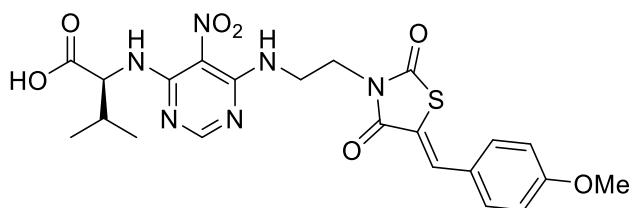
**(Z)-6-((2-(2,4-Dioxo-5-(4-(trifluoromethyl)benzylidene)thiazolidin-3-yl)ethyl)amino)-5-nitropyrimidin-4-yl)-L-valine IV-97E**

Brown solid. Yield: 36%.  $^1\text{H}$  NMR (500 MHz,  $\text{DMSO-}d_6$ ):  $\delta$  9.66 (d,  $J = 7.8$  Hz, 1H), 9.60 (t,  $J = 6.1$  Hz, 1H), 7.98 (s, 1H), 7.95 (s, 1H), 7.88 (d,  $J = 8.4$  Hz, 2H), 7.81 (d,  $J = 8.3$  Hz, 2H), 4.57 (dd,  $J = 7.8, 4.2$  Hz, 1H), 3.94 (ddd,  $J = 13.7, 6.4, 3.3$  Hz, 2H), 3.87 – 3.78 (m, 2H), 2.22 – 2.15 (m, 1H), 0.91 (d,  $J = 6.9$  Hz, 3H), 0.84 (d,  $J = 6.9$  Hz, 3H).  $^{13}\text{C}$  NMR (126 MHz,  $\text{DMSO-}d_6$ ):  $\delta$  172.0, 167.2, 165.6, 159.1, 157.2, 156.0, 137.0, 130.5, 130.48, 129.9 (q,  $J = 28.75$  Hz), 126.1, 126.1, 124.6, 123.8 (q,  $J = 271.25$  Hz), 112.1, 59.5, 41.3, 30.6, 18.7, 18.1. HRMS:  $m/z$ : calcd for  $\text{C}_{22}\text{H}_{21}\text{F}_3\text{N}_6\text{O}_6\text{S}$ : 555.1268  $[\text{M}+\text{H}]^+$ ; found: 555.1272.



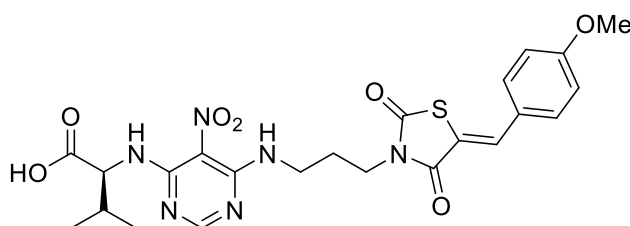
**(Z)-6-((3-(2,4-Dioxo-5-(4-(trifluoromethyl)benzylidene)thiazolidin-3-yl)propyl)amino)-5-nitropyrimidin-4-yl)-L-valine IV-97F**

Yellow solid. Yield: 55%.  $^1\text{H}$  NMR (500 MHz,  $\text{DMSO-}d_6$ ):  $\delta$  9.85 (d,  $J = 7.7$  Hz, 1H), 9.54 (t,  $J = 6.0$  Hz, 1H), 8.00 (d,  $J = 9.7$  Hz, 2H), 7.89 (d,  $J = 8.4$  Hz, 2H), 7.83 (d,  $J = 8.4$  Hz, 2H), 4.49 (dd,  $J = 7.7, 4.0$  Hz, 1H), 3.72 (t,  $J = 6.7$  Hz, 2H), 3.58 (dt,  $J = 16.2, 6.8$  Hz, 2H), 2.23 – 2.17 (m, 1H), 1.93 (t,  $J = 6.8$  Hz, 2H), 0.94 (d,  $J = 6.9$  Hz, 3H), 0.84 (d,  $J = 6.9$  Hz, 3H).  $^{13}\text{C}$  NMR (126 MHz,  $\text{DMSO-}d_6$ ):  $\delta$  172.1, 167.2, 165.6, 159.4, 156.9, 155.8, 137.0, 130.9, 130.5, 129.8 (q,  $J = 32.50$  Hz), 126.1, 126.1, 124.5, 123.8 (q,  $J = 271.25$  Hz), 112.0, 60.4, 38.3, 30.8, 26.8, 18.8, 18.508. HRMS:  $m/z$ : calcd for  $\text{C}_{23}\text{H}_{23}\text{F}_3\text{N}_6\text{O}_6\text{S}$ : 569.1425  $[\text{M}+\text{H}]^+$ ; found: 569.1440.



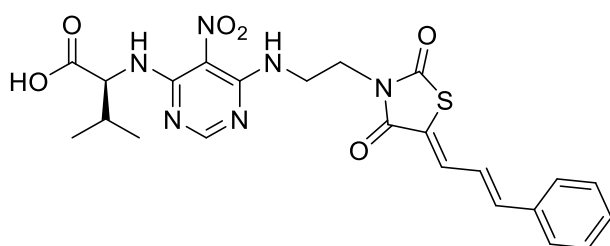
**(Z)-6-((2-(5-(4-Methoxybenzylidene)-2,4-dioxothiazolidin-3-yl)ethyl)amino)-5-nitropyrimidin-4-yl)-L-valine IV-97G**

White solid. Yield: 39%.  $^1\text{H}$  NMR (500 MHz,  $\text{DMSO-}d_6$ ):  $\delta$  9.59 (dd,  $J = 10.7, 5.0$  Hz, 2H), 7.99 (s, 1H), 7.82 (s, 1H), 7.56 (d,  $J = 8.8$  Hz, 2H), 7.10 (d,  $J = 8.9$  Hz, 2H), 4.64 (dd,  $J = 7.8, 4.3$  Hz, 1H), 3.94 – 3.88 (m, 2H), 3.88 – 3.79 (m, 5H), 2.24 – 2.18 (m, 1H), 0.93 (d,  $J = 6.9$  Hz, 3H), 0.87 (d,  $J = 6.9$  Hz, 3H).  $^{13}\text{C}$  NMR (126 MHz,  $\text{DMSO-}d_6$ ):  $\delta$  172.0, 167.6, 166.0, 161.07, 159.11, 157.10, 156.23, 132.46, 132.13, 125.48, 118.24, 114.94, 112.15, 59.11, 55.48, 41.0, 30.5, 18.7, 18.0. HRMS:  $m/z$ : calcd for  $\text{C}_{22}\text{H}_{24}\text{N}_6\text{O}_7\text{S}$ : 517.1500  $[\text{M}+\text{H}]^+$ ; found: 517.1500.



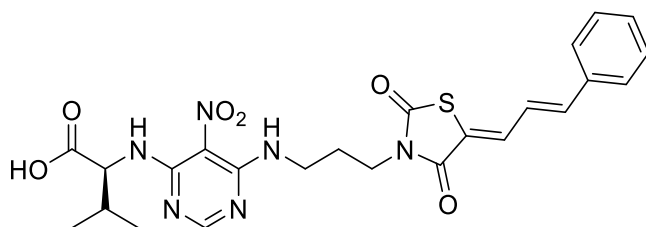
**(Z)-6-((3-(5-(4-Methoxybenzylidene)-2,4-dioxothiazolidin-3-yl)propyl)amino)-5-nitropyrimidin-4-yl)-L-valine IV-97H**

Yellow solid. Yield: 63%. <sup>1</sup>H NMR (500 MHz, DMSO-*d*<sub>6</sub>): δ 9.63 (d, *J* = 7.8 Hz, 1H), 9.54 (t, *J* = 6.0 Hz, 1H), 8.04 (s, 1H), 7.87 (s, 1H), 7.58 (d, *J* = 8.9 Hz, 2H), 7.10 (d, *J* = 8.9 Hz, 2H), 4.65 (dd, *J* = 7.8, 4.3 Hz, 1H), 3.83 (s, 3H), 3.70 (t, *J* = 6.6 Hz, 2H), 3.61 – 3.53 (m, 2H), 2.27 – 2.21 (m, 1H), 1.91 (p, *J* = 6.8 Hz, 2H), 0.96 (d, *J* = 6.9 Hz, 3H), 0.90 (d, *J* = 6.9 Hz, 3H). <sup>13</sup>C NMR (126 MHz, DMSO-*d*<sub>6</sub>): δ 172.0, 167.6, 166.0, 161.1, 159.4, 156.7, 156.3, 132.9, 132.2, 125.4, 118.0, 115.0, 112.2, 59.29, 55.5, 38.3, 30.5, 26.9, 18.7, 18.1. HRMS: *m/z*: calcd for C<sub>23</sub>H<sub>26</sub>N<sub>6</sub>O<sub>7</sub>S: 531.1656 [M+H]<sup>+</sup>; found: 531.1656.



**(Z)-6-((2-(2,4-Dioxo-5-(3-phenylallylidene)thiazolidin-3-yl)ethyl)amino)-5-nitropyrimidin-4-yl)-L-valine IV-97I**

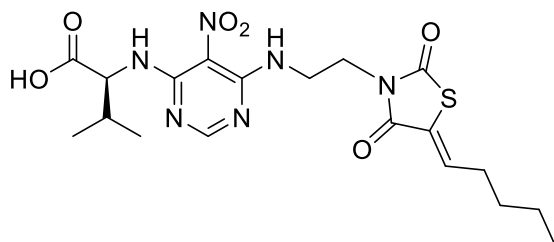
Yellow solid. Yield: 31%. <sup>1</sup>H NMR (500 MHz, DMSO-*d*<sub>6</sub>): δ 9.59 (t, *J* = 7.0 Hz, 2H), 8.01 (s, 1H), 7.66 (d, *J* = 7.0 Hz, 2H), 7.56 (d, *J* = 11.2 Hz, 1H), 7.45 – 7.36 (m, 3H), 7.30 (d, *J* = 15.2 Hz, 1H), 6.96 (dd, *J* = 15.2, 11.4 Hz, 1H), 4.66 (dd, *J* = 7.8, 4.3 Hz, 1H), 3.91 – 3.86 (m, 2H), 3.85 – 3.76 (m, 2H), 2.26 – 2.20 (m, 1H), 0.94 (d, *J* = 6.8 Hz, 3H), 0.89 (d, *J* = 6.8 Hz, 3H). <sup>13</sup>C NMR (126 MHz, DMSO-*d*<sub>6</sub>): δ 172.0, 167.3, 165.3, 159.1, 157.1, 156.3, 143.8, 135.5, 132.8, 129.8, 128.9, 127.8, 123.2, 122.7, 112.2, 59.1, 40.9, 30.5, 18.7, 18.0. HRMS: *m/z*: calcd for C<sub>23</sub>H<sub>24</sub>N<sub>6</sub>O<sub>6</sub>S: 513.1551 [M+H]<sup>+</sup>; found: 513.1555.



**(Z)-6-((3-(2,4-Dioxo-5-(3-phenylallylidene)thiazolidin-3-yl)propyl)amino)-5-nitropyrimidin-4-yl)-L-valine IV-97J**

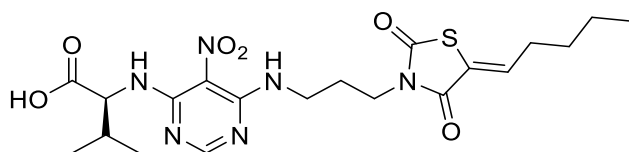
Yellow solid. Yield: 41%. <sup>1</sup>H NMR (500 MHz, DMSO-*d*<sub>6</sub>): δ 9.54 (d, *J* = 7.2 Hz, 2H), 8.06 (s, 1H), 7.67 (d, *J* = 7.1 Hz, 2H), 7.61 (d, *J* = 11.4 Hz, 1H), 7.46 – 7.36 (m, 3H), 7.33

(d,  $J = 15.2$  Hz, 1H), 6.99 (dd,  $J = 15.2, 11.4$  Hz, 1H), 4.72 (dd,  $J = 7.7, 4.5$  Hz, 1H), 3.68 (t,  $J = 6.5$  Hz, 2H), 3.57 (dt,  $J = 9.9, 6.8$  Hz, 2H, overlapped with H<sub>2</sub>O), 2.26 (dd,  $J = 11.4, 6.8$  Hz, 1H), 1.90 (t,  $J = 6.6$  Hz, 2H), 0.96 (d,  $J = 6.9$  Hz, 3H), 0.93 (d,  $J = 6.8$  Hz, 3H). <sup>13</sup>C NMR (126 MHz, DMSO-*d*<sub>6</sub>):  $\delta$  172.0, 167.4, 165.3, 159.4, 156.6, 156.6, 144.0, 135.5, 133.2, 129.8, 128.9, 127.9, 123.2, 122.5, 112.4, 58.8, 38.4, 30.3, 26.9, 18.7, 17.9. HRMS: *m/z*: calcd for C<sub>24</sub>H<sub>26</sub>N<sub>6</sub>O<sub>6</sub>S: 527.1707 [M+H]<sup>+</sup>; found: 527.1706.



**(Z)-6-((2-(2,4-Dioxo-5-pentylidene-thiazolidin-3-yl)ethyl)amino)-5-nitropyrimidin-4-yl)-L-valine IV-97K**

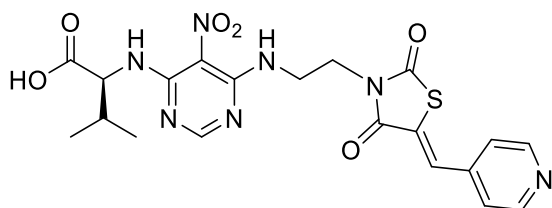
White solid. Yield: 29%. <sup>1</sup>H NMR (500 MHz, DMSO-*d*<sub>6</sub>):  $\delta$  9.57 (t,  $J = 5.9$  Hz, 1H), 9.51 (d,  $J = 7.8$  Hz, 1H), 7.99 (s, 1H), 6.96 (t,  $J = 7.7$  Hz, 1H), 4.72 (dd,  $J = 7.8, 4.4$  Hz, 1H), 3.85 (d,  $J = 5.0$  Hz, 2H), 3.82 – 3.76 (m, 2H), 2.29 – 2.24 (m, 1H), 2.17 (q,  $J = 7.4$  Hz, 2H), 1.49 – 1.42 (m, 2H), 1.30 (dt,  $J = 14.7, 7.3$  Hz, 2H), 0.97 (d,  $J = 6.9$  Hz, 3H), 0.93 (d,  $J = 6.8$  Hz, 3H), 0.87 (t,  $J = 7.3$  Hz, 3H). <sup>13</sup>C NMR (126 MHz, DMSO-*d*<sub>6</sub>):  $\delta$  172.0, 167.4, 164.5, 159.1, 157.0, 156.4, 138.0, 124.8, 112.2, 58.8, 40.9, 30.8, 30.4, 29.3, 21.7, 18.7, 17.9, 13.6. HRMS: *m/z*: calcd for C<sub>19</sub>H<sub>26</sub>N<sub>6</sub>O<sub>6</sub>S: 467.1707 [M+H]<sup>+</sup>; found: 467.1706.



**(Z)-6-((3-(2,4-Dioxo-5-pentylidene-thiazolidin-3-yl)propyl)amino)-5-nitropyrimidin-4-yl)-L-valine IV-97L**

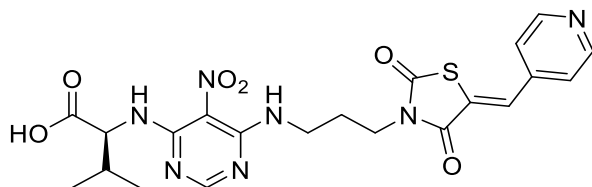
Yellow solid. Yield: 47%. <sup>1</sup>H NMR (500 MHz, DMSO-*d*<sub>6</sub>):  $\delta$  9.62 (d,  $J = 7.8$  Hz, 1H), 9.51 (t,  $J = 6.0$  Hz, 1H), 8.04 (s, 1H), 7.02 (t,  $J = 7.7$  Hz, 1H), 4.68 (dd,  $J = 7.8, 4.3$  Hz, 1H), 3.64 (t,  $J = 6.7$  Hz, 2H), 3.54 (dt,  $J = 10.5, 6.7$  Hz, 2H), 2.29 – 2.23 (m, 1H), 2.21 (dd,  $J = 14.8, 7.4$  Hz, 2H), 1.87 (p,  $J = 6.7$  Hz, 2H), 1.48 (dt,  $J = 14.9, 7.4$  Hz, 2H), 1.31 (dq,  $J = 14.4, 7.3$  Hz, 2H), 0.97 (d,  $J = 6.9$  Hz, 3H), 0.92 (d,  $J = 6.9$  Hz, 3H), 0.88 (t,  $J = 7.3$  Hz, 3H). <sup>13</sup>C NMR (126 MHz, DMSO-*d*<sub>6</sub>):  $\delta$  172.0, 167.3, 164.6, 159.4, 156.6, 156.4,

138.5, 124.6, 112.3, 59.2, 38.4, 30.9, 30.4, 29.3, 26.8, 21.7, 18.7, 18.0, 13.6. HRMS:  $m/z$ : calcd for  $C_{20}H_{28}N_6O_6S$ : 481.1864  $[M+H]^+$ ; found: 481.1867.



**(Z)-(6-((2-(2,4-Dioxo-5-(pyridin-4-ylmethylene)thiazolidin-3-yl)ethyl)amino)-5-nitropyrimidin-4-yl)-L-valine IV-97M**

Orange solid. Yield: 39%.  $^1H$  NMR (500 MHz,  $DMSO-d_6$ ):  $\delta$  9.60 (dd,  $J = 12.3, 6.9$  Hz, 2H), 8.72 (d,  $J = 6.1$  Hz, 2H), 7.99 (s, 1H), 7.84 (s, 1H), 7.53 (d,  $J = 6.1$  Hz, 2H), 4.61 (dd,  $J = 7.8, 4.3$  Hz, 1H), 3.99 – 3.90 (m, 2H), 3.87 – 3.77 (m, 2H), 2.25 – 2.17 (m, 1H), 0.92 (d,  $J = 6.9$  Hz, 3H), 0.85 (d,  $J = 6.9$  Hz, 3H).  $^{13}C$  NMR (126 MHz,  $DMSO-d_6$ ):  $\delta$  172.1, 166.9, 165.5, 159.2, 157.1, 156.2, 150.6, 140.0, 129.4, 126.6, 123.3, 112.1, 59.3, 41.3, 30.5, 18.7, 18.1. HRMS:  $m/z$ : calcd for  $C_{20}H_{21}N_7O_6S$ : 488.1347  $[M+H]^+$ ; found: 488.1350.



**(Z)-(6-((3-(2,4-Dioxo-5-(pyridin-4-ylmethylene)thiazolidin-3-yl)propyl)amino)-5-nitropyrimidin-4-yl)-L-valine IV-97N**

Brown solid. Yield: 50%.  $^1H$  NMR (500 MHz,  $DMSO-d_6$ ):  $\delta$  9.54 (dd,  $J = 14.1, 7.0$  Hz, 2H), 8.73 (d,  $J = 6.1$  Hz, 2H), 8.06 (s, 1H), 7.87 (s, 1H), 7.55 (d,  $J = 6.1$  Hz, 2H), 4.69 (dd,  $J = 7.8, 4.4$  Hz, 1H), 3.72 (t,  $J = 6.6$  Hz, 2H), 3.59 (dd,  $J = 13.6, 6.8$  Hz, 2H), 2.30 – 2.22 (m, 1H), 1.93 (dt,  $J = 12.0, 5.9$  Hz, 2H), 0.96 (d,  $J = 6.9$  Hz, 3H), 0.91 (d,  $J = 6.9$  Hz, 3H).  $^{13}C$  NMR (126 MHz,  $DMSO-d_6$ ):  $\delta$  172.0, 167.0, 165.5, 159.4, 156.6, 156.50, 150.6, 140.0, 129.8, 126.5, 123.3, 112.3, 59.0, 38.4, 30.3, 26.7, 18.7, 18.0. HRMS:  $m/z$ : calcd for  $C_{21}H_{23}N_7O_6S$ : 502.1503  $[M+H]^+$ ; found: 502.1503.

## 6.11 Synthesis of TZD-triazoles

### General procedure for Knoevenagel condensation

A mixture of thiazolidinedione **IV-3**, aldehyde (1.0 eq), piperidine (0.8 eq) and EtOH (0.1 M) were refluxed on (16-20 h) and worked up according to *method A* or *B*.

*Method A:* The reaction mixture was poured into H<sub>2</sub>O, acidified with AcOH (pH ≈ 1) and filtered.

*Method B:* The product was concentrated *in vacuum* and purified by column chromatography (Hex/EtOAc, isocratic 25 %).

### General procedure for N-alkylation

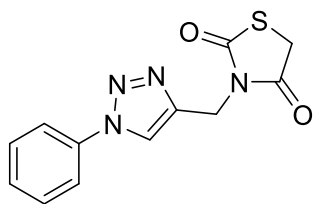
A mixture of thiazolidinedione **IV-3** or **IV-6** (1.0 eq, 7.73 mmol), propargyl bromide (80% w/w in toluene, 2.0 eq, 15.5 mmol) and anhydrous K<sub>2</sub>CO<sub>3</sub> (3.0 eq, 23.2 mmol) was refluxed in acetone (70 mL) for 16 h. After cooling to rt, the resulting mixture was filtered and concentrated *in vacuum*.

### General procedure for Husigen cycloaddition

In a typical procedure, alkyne **IV-99** or **IV-101** (1.0 eq) was dissolved in DMF (0.09 M). After formation of a clear solution, CuSO<sub>4</sub>·5H<sub>2</sub>O (10 mol %) was added. After formation of a blue solution, sodium ascorbate (0.5 eq) followed by the corresponding azide (1.0 eq) was added. The reaction mixture was stirred at rt (monitored by TLC, 4-6 h). The reaction mixture was poured into H<sub>2</sub>O (40 mL) and worked up according to *method A* or *B*.

*Method A:* The resulting suspension was filtered and washed with H<sub>2</sub>O (10 mL). The filter cake was lyophilized overnight.

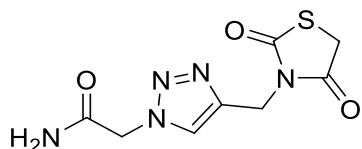
*Method B:* The product was extracted with EtOAc (3 × 40 mL), washed with brine (40 mL), dried over Na<sub>2</sub>SO<sub>4</sub>, concentrated *in vacuum* and purified by column chromatography (DCM/MeOH, gradient from 0 to 4 %).





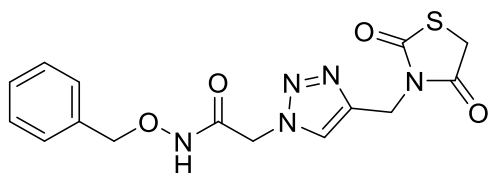
### 3-((1-phenyl-1*H*-1,2,3-triazol-4-yl)methyl)thiazolidine-2,4-dione IV-100A

*Method B.* White solid. Yield: 58 % (195 mg). <sup>1</sup>H NMR (500 MHz, DMSO-*d*<sub>6</sub>): δ 8.72 (s, 1H), 7.90 – 7.84 (m, 2H), 7.62 – 7.56 (m, 2H), 7.51 – 7.47 (m, 1H), 4.83 (s, 2H), 4.26 (s, 2H). <sup>13</sup>C NMR (126 MHz, DMSO-*d*<sub>6</sub>): δ 171.9, 171.5, 142.5, 136.5, 129.9, 128.7, 121.7, 120.1, 36.3, 34.0. HRMS: *m/z*: calcd for C<sub>12</sub>H<sub>10</sub>N<sub>4</sub>O<sub>2</sub>S: 275.0597 [M+H]<sup>+</sup>; found: 275.0596. HRMS: *m/z*: calcd for C<sub>12</sub>H<sub>10</sub>N<sub>4</sub>O<sub>2</sub>S: 297.0417 [M+Na]<sup>+</sup>; found: 297.0414.



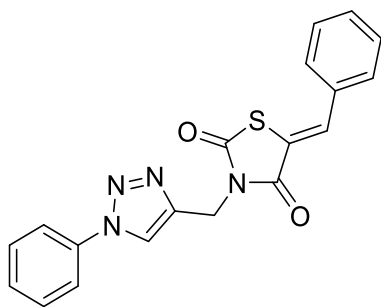
### 2-(4-((2,4-dioxothiazolidin-3-yl)methyl)-1*H*-1,2,3-triazol-1-yl)acetamide IV-100B

*Method B.* Brown solid. Yield: 13 % (39 mg). <sup>1</sup>H NMR (500 MHz, DMSO-*d*<sub>6</sub>): δ 7.96 (s, 1H), 7.69 (br s, 1H), 7.35 (br s, 1H), 5.02 (s, 2H), 4.74 (s, 2H), 4.25 (s, 2H). <sup>13</sup>C NMR (126 MHz, DMSO-*d*<sub>6</sub>): δ 171.9, 171.5, 167.2, 140.8, 125.1, 51.4, 36.3, 34.0. HRMS: *m/z*: calcd for C<sub>8</sub>H<sub>9</sub>N<sub>5</sub>O<sub>3</sub>S: 256.0500 [M+H]<sup>+</sup>; found: 256.0499, calcd for C<sub>8</sub>H<sub>9</sub>N<sub>5</sub>O<sub>3</sub>S: 278.0318 [M+Na]<sup>+</sup>; found: 278.0318.



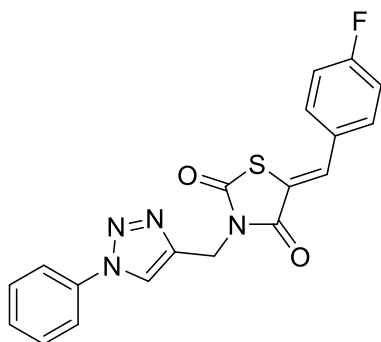
### (*Z*)-*N*-(benzyloxy)-2-(4-((2,4-dioxothiazolidin-3-yl)methyl)-1*H*-1,2,3-triazol-1-yl)acetamide IV-100C

*Method B.* Beige solid. Yield 40 % (174 mg). <sup>1</sup>H NMR (500 MHz, DMSO-*d*<sub>6</sub>): δ 11.34 (br s, 1H), 7.95 (s, 1H), 7.44 – 7.31 (m, 5H), 5.00 (br s, 2H), 4.85 (s, 2H), 4.77 (s, 2H), 4.24 (s, 2H). <sup>13</sup>C NMR (126 MHz, DMSO-*d*<sub>6</sub>): δ 171.9, 171.4, 162.5, 141.0, 135.6, 128.9, 128.4, 128.4, 125.0, 77.1, 49.5, 36.2, 34.0. HRMS: *m/z*: calcd for C<sub>15</sub>H<sub>15</sub>N<sub>5</sub>O<sub>4</sub>S: 362.0918 [M+H]<sup>+</sup>; found: 362.0916, calcd for C<sub>15</sub>H<sub>15</sub>N<sub>5</sub>O<sub>4</sub>S: 384.0737 [M+Na]<sup>+</sup>; found: 384.0734.



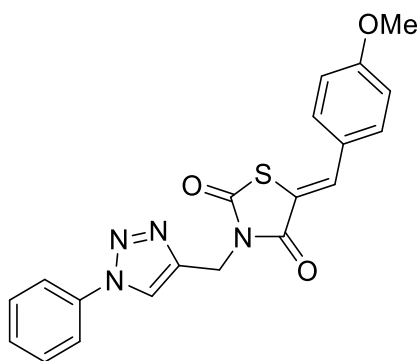
**(Z)-5-benzylidene-3-((1-phenyl-1H-1,2,3-triazol-4-yl)methyl)thiazolidine-2,4-dione  
IV-98A**

*Method A.* Yellow solid. Yield 54 % (215 mg).  $^1\text{H}$  NMR (500 MHz,  $\text{DMSO-}d_6$ ):  $\delta$  8.81 (s, 1H), 7.98 (s, 1H), 7.94 – 7.84 (m, 2H), 7.68 – 7.63 (m, 2H), 7.61 – 7.54 (m, 4H), 7.53 – 7.46 (m, 2H), 5.01 (s, 2H).  $^{13}\text{C}$  NMR (126 MHz,  $\text{DMSO-}d_6$ ):  $\delta$  167.0, 165.2, 142.3, 136.5, 133.3, 132.90, 130.7, 130.1, 129.8, 129.4, 128.7, 121.7, 121.2, 120.0, 36.7. HRMS:  $m/z$ : calcd for  $\text{C}_{19}\text{H}_{14}\text{N}_4\text{O}_2\text{S}$ : 363.0910  $[\text{M}+\text{H}]^+$ ; found: 363.0910.



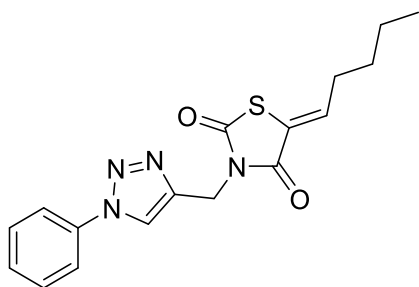
**(Z)-5-(4-fluorobenzylidene)-3-((1-phenyl-1H-1,2,3-triazol-4-yl)methyl)thiazolidine-  
2,4-dione IV-98B**

*Method A.* Beige solid. Yield: 83 % (350 mg).  $^1\text{H}$  NMR (500 MHz,  $\text{DMSO-}d_6$ ):  $\delta$  8.81 (s, 1H), 8.00 (s, 1H), 7.88 (d,  $J = 7.4$ , 2H), 7.73 (dd,  $J = 9.0, 5.3$  Hz, 2H), 7.63 – 7.55 (m, 2H), 7.53 – 7.46 (m, 1H), 7.45 – 7.37 (m, 2H), 5.00 (s, 2H).  $^{13}\text{C}$  NMR (101 MHz,  $\text{DMSO-}d_6$ ):  $\delta$  166.0 (d,  $J = 176.5$  Hz), 164.3, 161.8, 142.3, 136.5, 132.6 (d,  $J = 8.8$  Hz), 132.2, 129.9, 129.6 (d,  $J = 3.0$  Hz), 128.7, 121.7, 120.9, 120.0, 116.6 (d,  $J = 22.1$  Hz), 36.6. HRMS:  $m/z$ : calcd for  $\text{C}_{19}\text{H}_{13}\text{FN}_4\text{O}_2\text{S}$ : 381.0816  $[\text{M}+\text{H}]^+$ ; found: 381.0815.



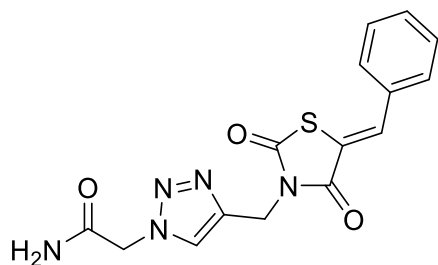
**(Z)-5-(4-methoxybenzylidene)-3-((1-phenyl-1H-1,2,3-triazol-4-yl)methyl)thiazolidine-2,4-dione IV-98C**

*Method A.* Yellow solid. Yield: 80 % (348 mg).  $^1\text{H}$  NMR (500 MHz,  $\text{DMSO-}d_6$ ):  $\delta$  8.80 (s, 1H), 7.94 (s, 1H), 7.88 (d,  $J = 8.3$  Hz, 2H), 7.65 – 7.61 (m, 2H), 7.61 – 7.56 (m, 2H), 7.52 – 7.45 (m, 1H), 7.16 – 7.08 (m, 2H), 4.99 (s, 2H), 3.84 (s, 3H).  $^{13}\text{C}$  NMR (126 MHz,  $\text{DMSO-}d_6$ ):  $\delta$  167.0, 165.3, 161.2, 142.4, 136.5, 133.3, 132.3, 129.8, 128.7, 125.4, 121.7, 120.0, 117.9, 115.0, 55.5, 36.6. HRMS:  $m/z$ : calcd for  $\text{C}_{20}\text{H}_{16}\text{N}_4\text{O}_3\text{S}$ : 393.1016  $[\text{M}+\text{H}]^+$ ; found: 393.1015.



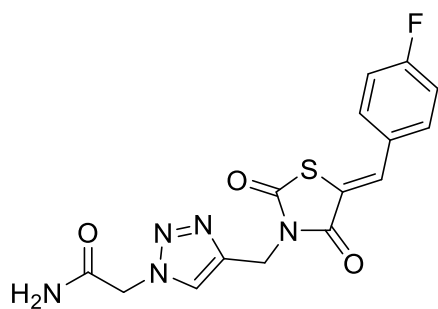
**(Z)-5-pentylidene-3-((1-phenyl-1H-1,2,3-triazol-4-yl)methyl)thiazolidine-2,4-dione IV-98D**

*Method B.* Yellow solid. Yield: 53 % (171 mg).  $^1\text{H}$  NMR (500 MHz,  $\text{DMSO-}d_6$ ):  $\delta$  8.77 (s, 1H), 7.90 – 7.85 (m, 2H), 7.62 – 7.56 (m, 2H), 7.52 – 7.46 (m, 1H), 7.09 (t,  $J = 7.5$  Hz, 1H), 4.93 (s, 2H), 2.24 (q,  $J = 7.2$  Hz, 2H), 1.49 (p,  $J = 7.2$  Hz, 2H), 1.32 (h,  $J = 7.2$  Hz, 2H), 0.88 (t,  $J = 7.2$  Hz, 3H).  $^{13}\text{C}$  NMR (126 MHz,  $\text{DMSO-}d_6$ ):  $\delta$  166.8, 163.9, 142.3, 139.1, 136.5, 129.8, 128.7, 124.5, 121.7, 120.1, 36.4, 31.0, 29.3, 21.7, 13.6. HRMS:  $m/z$ : calcd for  $\text{C}_{17}\text{H}_{18}\text{N}_4\text{O}_2\text{S}$ : 343.1223  $[\text{M}+\text{H}]^+$ ; found: 343.1224.



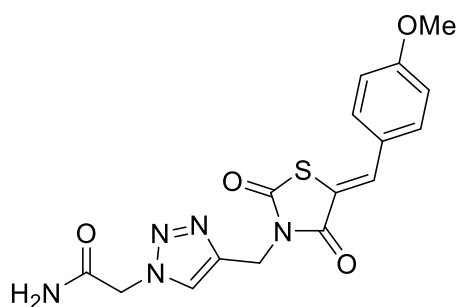
**(Z)-2-(4-((5-benzylidene-2,4-dioxothiazolidin-3-yl)methyl)-1H-1,2,3-triazol-1-yl)acetamide IV-98E**

*Method A.* Beige solid. Yield: 82 % (309 mg).  $^1\text{H}$  NMR (500 MHz,  $\text{DMSO-}d_6$ ):  $\delta$  8.05 (s, 1H), 7.97 (s, 1H), 7.68 (br s, 1H), 7.66 – 7.63 (m, 2H), 7.57 – 7.53 (m, 2H), 7.53 – 7.49 (m, 1H), 7.36 (br s, 1H), 5.04 (s, 2H), 4.92 (s, 2H).  $^{13}\text{C}$  NMR (126 MHz,  $\text{DMSO-}d_6$ ):  $\delta$  167.2, 166.9, 165.1, 140.7, 133.4, 132.9, 130.7, 130.1, 129.4, 125.1, 121.1, 51.4, 36.6. HRMS:  $m/z$ : calcd for  $\text{C}_{15}\text{H}_{13}\text{N}_5\text{O}_3\text{S}$ : 344.0812  $[\text{M}+\text{H}]^+$ ; found: 344.0812.



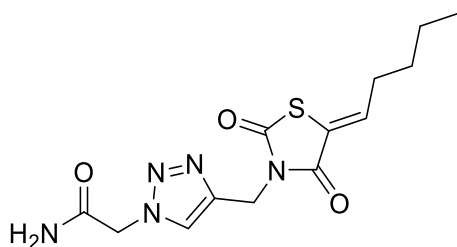
**(Z)-2-(4-((5-(4-fluorobenzylidene)-2,4-dioxothiazolidin-3-yl)methyl)-1H-1,2,3-triazol-1-yl)acetamide IV-98F**

*Method A.* Yellow solid. Yield: 75 % (299 mg).  $^1\text{H}$  NMR (500 MHz,  $\text{DMSO-}d_6$ ):  $\delta$  8.05 (s, 1H), 7.99 (s, 1H), 7.74 – 7.70 (m, 2H), 7.68 (br s, 1H), 7.42 – 7.38 (m, 2H), 7.36 (br s, 1H), 5.04 (s, 2H), 4.92 (s, 2H).  $^{13}\text{C}$  NMR (126 MHz,  $\text{DMSO-}d_6$ ):  $\delta$  167.1, 165.9 (d,  $J = 213.7$  Hz), 164.0, 162.0, 140.7, 132.6 (d,  $J = 8.9$  Hz), 132.3, 129.5 (d,  $J = 2.8$  Hz), 125.2, 120.8, 116.5 (d,  $J = 22.1$  Hz), 51.4, 36.6. HRMS:  $m/z$ : calcd for  $\text{C}_{15}\text{H}_{12}\text{FN}_5\text{O}_3\text{S}$ : 362.0718  $[\text{M}+\text{H}]^+$ ; found: 362.0717.



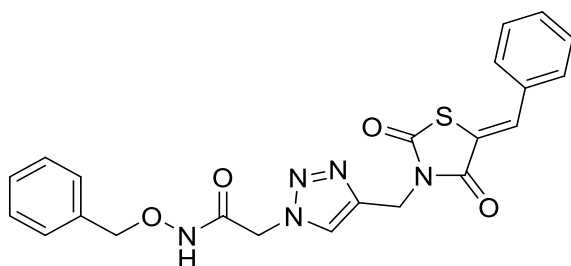
**(Z)-2-(4-((5-(4-methoxybenzylidene)-2,4-dioxothiazolidin-3-yl)methyl)-1H-1,2,3-triazol-1-yl)acetamide IV-98G**

*Method A.* Brown solid. Yield: 90 % (370 mg). <sup>1</sup>H NMR (500 MHz, DMSO-*d*<sub>6</sub>): δ 8.03 (s, 1H), 7.92 (s, 1H), 7.68 (br s, 1H), 7.61 (d, *J* = 8.9 Hz, 2H), 7.35 (br s, 1H), 7.12 (d, *J* = 8.9 Hz, 2H), 5.03 (s, 2H), 4.90 (s, 2H), 3.83 (s, 3H). <sup>13</sup>C NMR (126 MHz, DMSO-*d*<sub>6</sub>): δ 167.1, 166.9, 165.22, 161.2, 133.4, 132.3, 125.4, 125.1, 117.8, 115.0, 55.5, 51.4, 36.5. HRMS: *m/z*: calcd for C<sub>16</sub>H<sub>15</sub>N<sub>5</sub>O<sub>4</sub>S: 374.0918 [M+H]<sup>+</sup>; found: 374.0913.



**(Z)-2-(4-((5-butylidene-2,4-dioxothiazolidin-3-yl)methyl)-1H-1,2,3-triazol-1-yl)acetamide IV-98H**

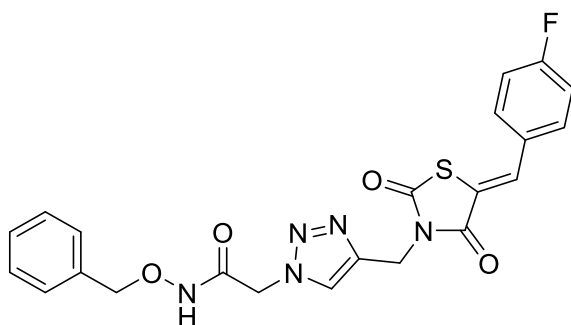
*Method B.* White solid. Yield: 35 % (104 mg). <sup>1</sup>H NMR (500 MHz, DMSO-*d*<sub>6</sub>): δ 8.00 (s, 1H), 7.68 (br s, 1H), 7.35 (br s, 1H), 7.08 (t, *J* = 7.5 Hz, 1H), 5.03 (s, 2H), 4.84 (s, 2H), 2.23 (q, *J* = 7.5 Hz, 2H), 1.49 (p, *J* = 7.5 Hz, 2H), 1.31 (h, *J* = 7.5 Hz, 2H), 0.88 (t, *J* = 7.5 Hz, 3H). <sup>13</sup>C NMR (126 MHz, DMSO-*d*<sub>6</sub>): δ 167.2, 166.7, 163.8, 140.7, 139.2, 125.1, 124.4, 51.4, 36.3, 30.9, 29.3, 21.7, 13.6. HRMS: *m/z*: calcd for C<sub>13</sub>H<sub>17</sub>N<sub>5</sub>O<sub>3</sub>S: 324.1125 [M+H]<sup>+</sup>; found: 324.1122.



**(Z)-2-(4-((5-benzylidene-2,4-dioxothiazolidin-3-yl)methyl)-1H-1,2,3-triazol-1-yl)-N-(benzyloxy)acetamide IV-98I**

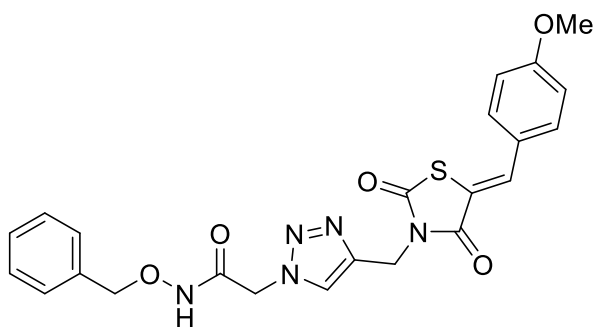
*Method A.* Beige solid. Yield: 62 % (307 mg). <sup>1</sup>H NMR (500 MHz, DMSO-*d*<sub>6</sub>): δ 11.57 (br s, 1H), 8.09 (s, 1H), 7.98 (s, 1H), 7.66 – 7.63 (m, 2H), 7.58 – 7.53 (m, 2H), 7.53 – 7.50 (m, 1H), 7.43 – 7.35 (m, 5H), 4.99 (s, 2H), 4.93 (s, 2H), 4.82 (s, 2H). <sup>13</sup>C NMR (126 MHz, DMSO-*d*<sub>6</sub>): δ 166.9, 165.1, 162.5, 140.9, 135.6, 133.4, 132.9, 130.7, 130.1, 129.4,

128.8, 128.3, 125.1, 121.1, 77.1, 49.5, 36.6. HRMS: m/z: calcd for C<sub>22</sub>H<sub>19</sub>N<sub>5</sub>O<sub>4</sub>S: 450.1231 [M+H]<sup>+</sup>; found: 450.1233.



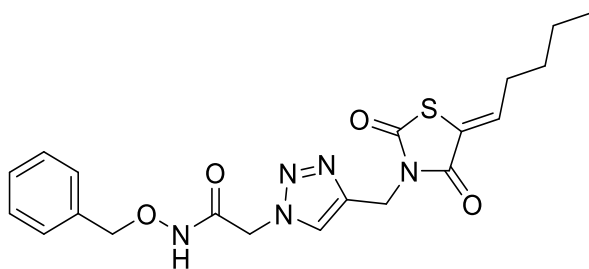
**(Z)-N-(benzyloxy)-2-(4-((5-(4-fluorobenzylidene)-2,4-dioxothiazolidin-3-yl)methyl)-1H-1,2,3-triazol-1-yl)acetamide IV-98J**

*Method A.* Yellow solid. Yield: 74 % (379 mg). <sup>1</sup>H NMR (500 MHz, DMSO-*d*<sub>6</sub>): δ 11.58 (br s, 1H), 8.09 (s, 1H), 7.99 (s, 1H), 7.75 – 7.69 (m, 2H), 7.43 – 7.36 (m, 7H), 4.99 (s, 2H), 4.93 (s, 2H), 4.82 (s, 2H). <sup>13</sup>C NMR (126 MHz, DMSO-*d*<sub>6</sub>): δ 166.8 (d, *J* = 215.0 Hz), 165.1, 163.0, 162.6, 140.9, 135.6, 132.6 (d, *J* = 8.0 Hz), 132.3, 129.6 (d, *J* = 3.2 Hz), 128.9, 128.3, 125.1, 120.8, 116.6 (d, *J* = 21.8 Hz), 77.1, 49.5, 36.6. HRMS: m/z: calcd for C<sub>22</sub>H<sub>18</sub>FN<sub>5</sub>O<sub>4</sub>S: 468.1136 [M+H]<sup>+</sup>; found: 468.1136.



**(Z)-N-(benzyloxy)-2-(4-((5-(4-methoxybenzylidene)-2,4-dioxothiazolidin-3-yl)methyl)-1H-1,2,3-triazol-1-yl)acetamide IV-98K**

*Method A.* Brown solid. Yield: 80 % (423 mg). <sup>1</sup>H NMR (500 MHz, DMSO-*d*<sub>6</sub>): δ 11.57 (br s, 1H), 8.08 (s, 1H), 7.93 (s, 1H), 7.61 (d, *J* = 8.9 Hz, 2H), 7.50 – 7.30 (m, 5H), 7.12 (d, *J* = 8.9 Hz, 2H), 4.99 (s, 2H), 4.92 (s, 2H), 4.82 (s, 2H), 3.84 (s, 3H). <sup>13</sup>C NMR (126 MHz, DMSO-*d*<sub>6</sub>): δ 167.0, 165.2, 162.6, 161.3, 141.0, 135.6, 133.4, 132.3, 128.9, 128.3, 125.4, 125.1, 117.8, 115.0, 77.1, 55.5, 49.5, 36.5. HRMS: m/z: calcd for C<sub>23</sub>H<sub>21</sub>N<sub>5</sub>O<sub>5</sub>S: 480.1336 [M+H]<sup>+</sup>; found: 480.1336.



**(Z)-N-(benzyloxy)-2-(4-((2,4-dioxo-5-pentylidenethiazolidin-3-yl)methyl)-1H-1,2,3-triazol-1-yl)acetamide IV-98L**

*Method B.* White solid. Yield: 49 % (196 mg).  $^1\text{H}$  NMR (500 MHz,  $\text{DMSO-}d_6$ ):  $\delta$  11.57 (br s, 1H), 8.04 (s, 1H), 7.45 – 7.32 (m, 5H), 7.08 (t,  $J = 7.3$  Hz, 1H), 4.98 (s, 2H), 4.85 (s, 2H), 4.82 (s, 2H), 2.23 (q,  $J = 7.3$  Hz, 2H), 1.49 (p,  $J = 7.3$  Hz, 2H), 1.31 (h,  $J = 7.3$  Hz, 2H), 0.88 (t,  $J = 7.3$  Hz, 3H).  $^{13}\text{C}$  NMR (126 MHz,  $\text{DMSO-}d_6$ ):  $\delta$  166.7, 163.8, 162.6, 140.9, 139.2, 135.6, 128.9, 128.3, 125.0, 124.4, 77.1, 49.5, 36.3, 31.0, 29.3, 21.7, 13.6. HRMS:  $m/z$ : calcd for  $\text{C}_{20}\text{H}_{23}\text{N}_5\text{O}_4\text{S}$ : 430.1544  $[\text{M}+\text{H}]^+$ ; found: 430.1543.

---

## 7 References

- (1) WHO *Global tuberculosis report 2020*. <https://www.who.int/teams/global-tuberculosis-programme/tb-reports>.
- (2) Šlachťová, V.; Šebela, M.; Torfs, E.; Oorts, L.; Cappoen, D.; Berka, K.; Bazgier, V.; Brulíková, L. *Eur. J. Med. Chem.* **2020**, *185*, 111812.
- (3) Dookie, N.; Rambaran, S.; Padayatchi, N.; Mahomed, S.; Naidoo, K. *J. Antimicrob. Chemother.* **2018**, *73* (5), 1138–1151.
- (4) Urban, M.; Šlachťová, V.; Brulíková, L. *Eur. J. Med. Chem.* **2020**, 113139.
- (5) Torfs, E.; Piller, T.; Cos, P.; Cappoen, D. *Int. J. Mol. Sci.* **2019**, *20* (12), 2868.
- (6) Kiazzyk, S.; Ball, T. B. *Canada Commun. Dis. Rep.* **2017**, *43* (3–4), 62.
- (7) Chang, K.-C.; Nuermberger, E.; Sotgiu, G.; Leung, C.-C. *Respirology* **2018**, *23* (11), 978–990.
- (8) Shi, R.; Itagaki, N.; Sugawara, I. *Mini Rev. Med. Chem.* **2007**, *7* (11), 1177–1185.
- (9) Appetecchia, F.; Consalvi, S.; Scarpecci, C.; Biava, M.; Poce, G. *Pharmaceuticals* **2020**, *13* (9), 227.
- (10) Master, S. S.; Rampini, S. K.; Davis, A. S.; Keller, C.; Ehlers, S.; Springer, B.; Timmins, G. S.; Sander, P.; Deretic, V. *Cell Host Microbe* **2008**, *3* (4), 224–232.
- (11) Lazarevic, V.; Martinon, F. *Cell Host Microbe* **2008**, *3* (4), 199–200.
- (12) Petrerá, A.; Amstutz, B.; Gioia, M.; Hahnlein, J.; Baici, A.; Selchow, P.; Ferraris, D. M.; Rizzi, M.; Sbardella, D.; Marini, S.; Coletta, M.; Sander, P. *Biol. Chem.* **2012**, *393* (7), 631–640.
- (13) Ferraris, D. M.; Rizzi, M. *Encycl. Inorg. Bioinorg. Chem.* **2011**, 1–7.
- (14) Ferraris, D. M.; Sbardella, D.; Petrerá, A.; Marini, S.; Amstutz, B.; Coletta, M.; Sander, P.; Rizzi, M. *J. Biol. Chem.* **2011**, *286* (37), 32475–32482, S32475/1-S32475/2.
- (15) Mori, M.; Moraca, F.; Deodato, D.; Ferraris, D. M.; Selchow, P.; Sander, P.; Rizzi, M.; Botta, M. *Bioorg. Med. Chem. Lett.* **2014**, *24* (11), 2508–2511.
- (16) Paolino, M.; Brindisi, M.; Vallone, A.; Butini, S.; Campiani, G.; Nannicini, C.; Giuliani, G.; Anzini, M.; Lamponi, S.; Giorgi, G.; Sbardella, D.; Ferraris, D. M.; Marini, S.; Coletta, M.; Palucci, I.; Minerva, M.; Delogu, G.; Pepponi, I.; Goletti, D.; Cappelli, A.; Gemma, S.; Brogi, S. *ChemMedChem* **2018**, *13* (5), 422–430.
- (17) Ferraris, D. M.; Sbardella, D.; Petrerá, A.; Marini, S.; Amstutz, B.; Coletta, M.; Sander, P.; Rizzi, M. *J. Biol. Chem.* **2011**, *286* (37), 32475–32482.
- (18) Mori, M.; Deodato, D.; Kasula, M.; Ferraris, D. M.; Sanna, A.; De Logu, A.; Rizzi, M.; Botta, M. *Bioorg. Med. Chem. Lett.* **2018**, *28* (4), 637–641.
- (19) Subhedar, D. D.; Shaikh, M. H.; Shingate, B. B.; Nawale, L.; Sarkar, D.; Khedkar, V. M.; Kalam Khan, F. A.; Sangshetti, J. N. *Eur. J. Med. Chem.* **2017**, *125*, 385–399.
- (20) Subhedar, D. D.; Shaikh, M. H.; Nawale, L.; Yeware, A.; Sarkar, D.; Kalam Khan, F. A.; Sangshetti, J. N.; Shingate, B. B. *Bioorg. Med. Chem. Lett.* **2016**, *26* (9), 2278–2283.
- (21) Corrêa Jr, I. R.; Nören-Müller, A.; Ambrosi, H.; Jakupovic, S.; Saxena, K.; Schwalbe, H.; Kaiser, M.; Waldmann, H. *Chem. Asian J.* **2007**, *2* (9), 1109–1126.



- (22) Koul, A.; Herget, T.; Klebl, B.; Ullrich, A. *Nat. Rev. Microbiol.* **2004**, *2* (3), 189–202.
- (23) Ruddraraju, K. V.; Aggarwal, D.; Zhang, Z.-Y. *Microorganisms* **2020**, *9* (1), 14.
- (24) Fan, L.; Wu, X.; Jin, C.; Li, F.; Xiong, S.; Dong, Y. *Front. Cell. Infect. Microbiol.* **2018**, *8*, 171.
- (25) Koul, A.; Choidas, A.; Treder, M.; Tyagi, A. K.; Drlica, K.; Singh, Y.; Ullrich, A. *J. Bacteriol.* **2000**, *182* (19), 5425–5432.
- (26) Zhou, B.; He, Y.; Zhang, X.; Xu, J.; Luo, Y.; Wang, Y.; Franzblau, S. G.; Yang, Z.; Chan, R. J.; Liu, Y.; Zheng, J.; Zhang, Z. Y. *Proc. Natl. Acad. Sci. U. S. A.* **2010**, *107* (10), 4573–4578.
- (27) Böhmer, F.; Szedlacsek, S.; Taberner, L.; Östman, A.; den Hertog, J. *FEBS J.* **2013**, *280* (2), 413–431.
- (28) Grundner, C.; Perrin, D.; Hooft van Huijsduijnen, R.; Swinnen, D.; Gonzalez, J.; Gee, C. L.; Wells, T. N.; Alber, T. *Structure* **2007**, *15* (4), 499–509.
- (29) Beresford, N.; Patel, S.; Armstrong, J.; Szöör, B.; Fordham-Skelton, A. P.; Taberner, L. *Biochem. J.* **2007**, *406* (1), 13–18.
- (30) Beresford, N. J.; Saville, C.; Bennett, H. J.; Roberts, I. S.; Taberner, L. *BMC Genomics* **2010**, *11* (1), 1–12.
- (31) Fanzani, L.; Porta, F.; Meneghetti, F.; Villa, S.; Gelain, A.; Lucarelli, A. P.; Parisini, E. *Curr. Med. Chem.* **2015**, *22* (27), 3110–3132.
- (32) Zhang, Z.-Y. *Acc. Chem. Res.* **2017**, *50* (1), 122–129.
- (33) Zeng, L. F.; Xu, J.; He, Y.; He, R.; Wu, L.; Gunawan, A. M.; Zhang, Z. Y. *ChemMedChem* **2013**, *8* (6), 904–908.
- (34) He, Y.; Xu, J.; Yu, Z. H.; Gunawan, A. M.; Wu, L.; Wang, L.; Zhang, Z. Y. *J. Med. Chem.* **2013**, *56* (3), 832–842.
- (35) Gómez, L.; Garrabou, X.; Joglar, J.; Bujons, J.; Parella, T.; Vilaplana, C.; Cardona, P. J.; Clapés, P. *Org. Biomol. Chem.* **2012**, *10* (31), 6309–6321.
- (36) Huang, X.; Huang, H.; Li, H.; Sun, X.; Huang, H.; Lu, Y.; Lin, Y.; Long, Y.; She, Z. *Org. Lett.* **2013**, *15* (4), 721–723.
- (37) He, R.; Yu, Z.-H.; Zhang, R.-Y.; Wu, L.; Gunawan, A. M.; Zhang, Z.-Y. *ACS Med. Chem. Lett.* **2015**, *6* (12), 1231–1235.
- (38) Ratmanova, N. K.; Andreev, I. A.; Leontiev, A. V.; Momotova, D.; Novoselov, A. M.; Ivanova, O. A.; Trushkov, I. V. *Tetrahedron* **2020**, *76* (14), 131031.
- (39) Quevedo-Acosta, Y.; Jurberg, I. D.; Gamba-Sánchez, D. *Org. Lett.* **2019**, *22* (1), 239–243.
- (40) Larquetoux, L.; Ouhamou, N.; Chiaroni, A.; Six, Y. *European J. Org. Chem.* **2005**, *2005* (21), 4654–4662.
- (41) Madelaine, C.; Buriez, O.; Crousse, B.; Florent, I.; Grellier, P.; Retailleau, P.; Six, Y. *Org. Biomol. Chem.* **2010**, *8* (24), 5591–5601.
- (42) Halton, B.; Harvey, J. *Synlett* **2006**, *2006* (13), 1975–2000.
- (43) Thankachan, A. P.; Sindhu, K. S.; Krishnan, K. K.; Anilkumar, G. *Org. Biomol. Chem.* **2015**, *13* (33), 8780–8802.
- (44) Xu, J.; Ahmed, E.; Xiao, B.; Lu, Q.; Wang, Y.; Yu, C.; Fu, Y. *Angew. Chemie* **2015**, *127* (28), 8349–8353.
- (45) Yuan, H.; Guo, Z.; Luo, T. *Org. Lett.* **2017**, *19* (3), 624–627.
- (46) Kubyshev, V.; Kheylik, Y.; Mykhailiuk, P. K. *J. Fluor. Chem.* **2015**, *175*, 73–83.
- (47) Castro, J. L.; Castedo, L.; Riguera, R. *Tetrahedron Lett.* **1985**, *26* (12), 1561–1564.
- (48) Chen, C.; Kattanguru, P.; Tomashenko, O. A.; Karpowicz, R.; Siemiaszko, G.; Bhattacharya, A.; Calasans, V.; Six, Y. *Org. Biomol. Chem.* **2017**, *15* (25), 5364–5372.

- (49) Alberts, B.; Alexander, J.; Lewis, J.; Raff, M.; Roberts, K.; Walter, P. *Molecular Biology of the Cell, 4th Edition.*; Wiley, 2004.
- (50) Black, P. A.; Warren, R. M.; Louw, G. E.; van Helden, P. D.; Victor, T. C.; Kana, B. D. *Antimicrob. Agents Chemother.* **2014**, *58* (5), 2491–2503, 14 pp.
- (51) Berney, M.; Cook, G. M. *Adv. Photosynth. Respir.* **2014**, *39* (Structural Basis of Biological Energy Generation), 277–293.
- (52) Koul, A.; Vranckx, L.; Dendouga, N.; Balemans, W.; Van den Wyngaert, I.; Vergauwen, K.; Goehlmann, H. W. H.; Willebrords, R.; Poncelet, A.; Guillemont, J.; Bald, D.; Andries, K. *J. Biol. Chem.* **2008**, *283* (37), 25273–25280.
- (53) Haagsma, A. C.; Driessen, N. N.; Hahn, M.-M.; Lill, H.; Bald, D. *FEMS Microbiol. Lett.* **2010**, *313* (1), 68–74.
- (54) Lu, P.; Lill, H.; Bald, D. *Biochim. Biophys. Acta, Bioenerg.* **2014**, *1837* (7), 1208–1218.
- (55) Berney, M.; Cook, G. M. *PLoS One* **2010**, *5* (1), No pp. given.
- (56) Bald, D.; Villellas, C.; Lu, P.; Koul, A. *MBio* **2017**, *8* (2), e00272-17/1-e00272-17/11.
- (57) Gajadeera, C. S.; Weber, J. *J. Biol. Chem.* **2013**, *288* (37), 26441–26447.
- (58) Del Rizzo, P. A.; Bi, Y.; Dunn, S. D. *J. Mol. Biol.* **2006**, *364* (4), 735–746.
- (59) Bald, D.; Koul, A. *FEMS Microbiol. Lett.* **2010**, *308* (1), 1–7.
- (60) Guo, H.; Courbon, G. M.; Bueler, S. A.; Mai, J.; Liu, J.; Rubinstein, J. L. *Nature* **2020**, 1–5.
- (61) Blaser, A.; Sutherland, H. S.; Tong, A. S. T.; Choi, P. J.; Conole, D.; Franzblau, S. G.; Cooper, C. B.; Upton, A. M.; Lotlikar, M.; Denny, W. A.; Palmer, B. D. *Bioorg. Med. Chem.* **2019**, *27* (7), 1283–1291.
- (62) Chasák, J.; Šlachtová, V.; Urban, M.; Brulíková, L. *Eur. J. Med. Chem.* **2020**, 112872.
- (63) Tantry, S. J.; Markad, S. D.; Shinde, V.; Bhat, J.; Balakrishnan, G.; Gupta, A. K.; Ambady, A.; Raichurkar, A.; Kedari, C.; Sharma, S.; Mudugal, N. V.; Narayan, A.; Naveen Kumar, C. N.; Nanduri, R.; Bharath, S.; Reddy, J.; Panduga, V.; Prabhakar, K. R.; Kandaswamy, K.; Saralaya, R.; Kaur, P.; Dinesh, N.; Guptha, S.; Rich, K.; Murray, D.; Plant, H.; Preston, M.; Ashton, H.; Plant, D.; Walsh, J.; Alcock, P.; Naylor, K.; Collier, M.; Whiteaker, J.; McLaughlin, R. E.; Mallya, M.; Panda, M.; Rudrapatna, S.; Ramachandran, V.; Shandil, R.; Sambandamurthy, V. K.; Mdluli, K.; Cooper, C. B.; Rubin, H.; Yano, T.; Iyer, P.; Narayanan, S.; Kavanagh, S.; Mukherjee, K.; Balasubramanian, V.; Hosagrahara, V. P.; Solapure, S.; Ravishankar, S.; Hameed P, S. *J. Med. Chem.* **2017**, *60* (4), 1379–1399.
- (64) Nagano, T.; Itoh, M.; Matsumura, K. *J. Am. Chem. Soc.* **1953**, *75*, 2770–2771.
- (65) Liu, J.; Hoover, J. M. *Org. Lett.* **2019**, *21* (12), 4510–4514.
- (66) Lee, S.; Lee, Y. *European J. Org. Chem.* **2019**, *2019* (19), 3045–3050.
- (67) Glotz, G.; Lebl, R.; Dallinger, D.; Kappe, C. O. *Angew. Chemie Int. Ed.* **2017**, *56* (44), 13786–13789.
- (68) Wu, Y.-Q.; Limburg, D. C.; Wilkinson, D. E.; Hamilton, G. S. *J. Heterocycl. Chem.* **2003**, *40* (1), 191–193.
- (69) Kim, J. Y.; Cho, S. H.; Joseph, J.; Chang, S. *Angew. Chemie, Int. Ed.* **2010**, *49* (51), 9899–9903, S9899/1-S9899/39.
- (70) Wang, J.; Hou, J.-T.; Wen, J.; Zhang, J.; Yu, X.-Q. *Chem. Commun.* **2011**, *47* (12), 3652–3654.
- (71) Liu, M.; Zeng, M.-T.; Xu, W.; Wu, L.; Dong, Z.-B. *Tetrahedron Lett.* **2017**, *58* (46), 4352–4356.
- (72) Rattanangkool, E.; Sukwattanasinitt, M.; Wacharasindhu, S. *J. Org. Chem.* **2017**,

- 82 (24), 13256–13262.
- (73) Tankam, T.; Srisa, J.; Sukwattanasinitt, M.; Wacharasindhu, S. *J. Org. Chem.* **2018**, *83* (19), 11936–11943.
- (74) Wang, G.; Peng, Z.; Wang, J.; Li, J.; Li, X. *Bioorg. Med. Chem.* **2016**, *24* (21), 5374–5379.
- (75) Šlachtová, V.; Brulíková, L. *ChemistrySelect* **2018**, *3* (17).
- (76) Pitta, E.; Rogacki, M. K.; Balabon, O.; Huss, S.; Cunningham, F.; Lopez-Roman, E. M.; Joossens, J.; Augustyns, K.; Ballell, L.; Bates, R. H. *J. Med. Chem.* **2016**, *59* (14), 6709–6728.
- (77) Soni, H. M.; Patel, P. K.; Chhabria, M. T.; Patel, A. K.; Rana, D. N.; Brahmkshatriya, P. S. *Int. J. Org. Chem.* **2016**, *6* (3), 157–176.
- (78) Ertan-Bolelli, T.; Yildiz, I.; Ozgen-Ozgarar, S. *Med. Chem. Res.* **2016**, *25* (4), 553–567.
- (79) Aulner, N.; Danckaert, A.; Ihm, J. E.; Shum, D.; Shorte, S. L. *Trends in Parasitology*. Elsevier Ltd July 1, 2019, pp 559–570.
- (80) Moffat, J. G.; Vincent, F.; Lee, J. A.; Eder, J.; Prunotto, M. *Nat. Rev. Drug Discov.* **2017**, *16* (8), 531–543.
- (81) Campaniço, A.; Moreira, R.; Lopes, F. *Eur. J. Med. Chem.* **2018**, *150*, 525–545.
- (82) Kumar, S.; Mehra, R.; Sharma, S.; Bokolia, N. P.; Raina, D.; Nargotra, A.; Singh, P. P.; Khan, I. A. *Tuberc. (Oxford, United Kingdom)* **2018**, *108*, 56–63.
- (83) Balkenhohl, F.; Von dem Bussche-Hünnefeld, C.; Lansky, A.; Zechel, C. *Angew. Chemie (International Ed. English)* **1996**, *35* (20), 2288–2337.
- (84) Parekh, N. M.; Juddhawal, K. V.; Rawal, B. M. *Med. Chem. Res.* **2013**, *22* (6), 2737–2745.
- (85) Desai, N. C.; Dodiya, A. M.; Shihora, P. N. *Med. Chem. Res.* **2012**, *21* (8), 1577–1586.
- (86) Sucheta; Tahlan, S.; Verma, P. K. *Chemistry Central Journal*. BioMed Central Ltd. December 8, 2017.
- (87) Barreca, M. L.; Chimirri, A.; De Luca, L.; Monforte, A.-M.; Monforte, P.; Rao, A.; Zappalà, M.; Balzarini, J.; De Clercq, E.; Pannecouque, C. *Bioorg. Med. Chem. Lett.* **2001**, *11* (13), 1793–1796.
- (88) Ponnuchamy, S.; Kanchithalaivan, S.; Ranjith Kumar, R.; Ashraf Ali, M.; Soo Choon, T. *Bioorganic Med. Chem. Lett.* **2014**, *24* (4), 1089–1093.
- (89) Rawat, D. S. *Med. Res. Rev.* **2013**, *33* (4), 693–764.
- (90) Verbitskiy, E. V.; Baskakova, S. A.; Kravchenko, M. A.; Skorniyakov, S. N.; Rusinov, G. L.; Chupakhin, O. N.; Charushin, V. N. *Bioorganic Med. Chem.* **2016**, *24* (16), 3771–3780.
- (91) Sura, M. R.; Peddiahgari, V. G. R.; Bhoomireddy, R. P. R.; Vadde, R. K. *J. Heterocycl. Chem.* **2013**, *50* (6), 1395–1399.
- (92) Reddy, D. S.; Hosamani, K. M.; Devarajegowda, H. C. *Eur. J. Med. Chem.* **2015**, *101*, 705–715.
- (93) Bhuva, N. H.; Talpara, P. K.; Singala, P. M.; Gothaliya, V. K.; Shah, V. H. *J. Saudi Chem. Soc.* **2017**, *21* (5), 517–527.
- (94) -H. Zhou, C.; Wang, Y. *Curr. Med. Chem.* **2012**, *19* (2), 239–280.
- (95) Sutherland, H. S.; Blaser, A.; Kmentova, I.; Franzblau, S. G.; Wan, B.; Wang, Y.; Ma, Z.; Palmer, B. D.; Denny, W. A.; Thompson, A. M. *J. Med. Chem.* **2010**, *53* (2), 855–866.
- (96) Tan, L. P.; Wu, H.; Yang, P.-Y.; Kalesh, K. A.; Zhang, X.; Hu, M.; Srinivasan, R.; Yao, S. Q. *Org. Lett.* **2009**, *11* (22), 5102–5105.
- (97) Patel, N. B.; Khan, I. H. *Indian J. Res. Pharm. Biotechnol.* **2014**, *2* (1), 993.

- (98) Majewski, M. W.; Cho, S.; Miller, P. A.; Franzblau, S. G.; Miller, M. J. *Bioorg. Med. Chem. Lett.* **2015**, *25* (21), 4933–4936.
- (99) Flipo, M.; Beghyn, T.; Charton, J.; Leroux, V. A.; Deprez, B. P.; Deprez-Poulain, R. F. *Bioorg. Med. Chem.* **2007**, *15* (1), 63–76.
- (100) Ponnuchamy, S.; Kanchithalaivan, S.; Ranjith Kumar, R.; Ashraf Ali, M.; Soo Choon, T. *Bioorg. Med. Chem. Lett.* **2014**, *24* (4), 1089–1093.
- (101) Kar, K.; Krithika, U.; Mithuna; Basu, P.; Santhosh Kumar, S.; Reji, A.; Prashantha Kumar, B. R. *Bioorg. Chem.* **2014**, *56*, 27–33.
- (102) Mohanty, S.; Roy, A. K.; Kumar, V. K. P.; Reddy, S. G.; Karmakar, A. C. *Tetrahedron Lett.* **2014**, *55* (33), 4585–4589.
- (103) Pratap, U. R.; Jawale, D. V.; Waghmare, R. A.; Lingampalle, D. L.; Mane, R. A. *New J. Chem.* **2011**, *35* (1), 49–51.
- (104) Mehra, R.; Khan, I. A.; Nargotra, A. *Eur. J. Pharm. Sci.* **2017**, *104*, 1–15.
- (105) Pouliot, M.; Jeanmart, S. *J. Med. Chem.* **2016**, *59* (2), 497–503.
- (106) Böhm, H.-J.; Flohr, A.; Stahl, M. *Drug Discov. today Technol.* **2004**, *1* (3), 217–224.
- (107) Sun, H.; Tawa, G.; Wallqvist, A. *Drug Discov. Today* **2012**, *17* (7–8), 310–324.
- (108) Gladysz, R.; Cleenewerck, M.; Joossens, J.; Lambeir, A.; Augustyns, K.; Van der Veken, P. *ChemBioChem* **2014**, *15* (15), 2238–2247.
- (109) Parveen, S.; Arjmand, F.; Mohapatra, D. K. *J. Photochem. Photobiol. B Biol.* **2013**, *126*, 78–86.
- (110) Chen, Y.; Guan, Z. *J. Am. Chem. Soc.* **2010**, *132* (13), 4577–4579.
- (111) Johansson, H.; Jørgensen, T. B.; Gloriam, D. E.; Bräuner-Osborne, H.; Pedersen, D. S. *RSC Adv.* **2013**, *3* (3), 945–960.
- (112) Higginson, C. J.; Malollari, K. G.; Xu, Y.; Kelleghan, A. V.; Ricipito, N. G.; Messersmith, P. B. *Angew. Chemie Int. Ed.* **2019**, *58* (35), 12271–12279.
- (113) Collins, S.; Hong, Y.; Hoover, G. J.; Veit, J. R. *J. Org. Chem.* **1990**, *55* (11), 3565–3568.
- (114) Elumalai, N.; Berg, A.; Natarajan, K.; Scharow, A.; Berg, T. *Angew. Chemie* **2015**, *127* (16), 4840–4845.
- (115) Geiseler, B.; Fruk, L. *J. Mater. Chem.* **2012**, *22* (2), 735–741.
- (116) Craig, D.; Spreadbury, S. R. J.; White, A. J. P. *Chem. Commun.* **2020**, *56* (68), 9803–9806.
- (117) Dhanak, D.; Kuroda, R.; Reese, C. B. *Tetrahedron Lett.* **1987**, *28* (16), 1827–1829.
- (118) Kasthuri, M.; Babu, H. S.; Kumar, K. S.; Sudhakar, C.; Kumar, P. V. N. *Synlett* **2015**, *26* (7), 897–900.
- (119) Grytsai, O.; Druzenko, T.; Demange, L.; Ronco, C.; Benhida, R. *Tetrahedron Lett.* **2018**, *59* (17), 1642–1645.
- (120) Šlachtová, V.; Chasák, J.; Brulíková, L. *ACS omega* **2019**, *4* (21), 19314–19323.
- (121) Tian, X.; Wu, R.-M.; Liu, G.; Li, Z.-B.; Wei, H.-L.; Yang, H.; Shin, D.-S.; Wang, L.-Y.; Zuo, H. *Ark. (Gainesville, FL, United States)* **2011**, No. 10, 118–126.
- (122) Mo, S. *Synlett* **2014**, *25* (09), 1337–1338.
- (123) Anbarasan, P.; Neumann, H.; Beller, M. *Chem. Eur. J.* **2011**, *17* (15), 4217–4222.
- (124) Abdelazeem, A. H.; Khan, S. I.; White, S. W.; Sufka, K. J.; McCurdy, C. R. *Bioorg. Med. Chem.* **2015**, *23* (13), 3248–3259.
- (125) Minin, P. L.; Walton, J. C. *J. Org. Chem.* **2003**, *68* (7), 2960–2963.
- (126) Read, M. L.; Brændvang, M.; Miranda, P. O.; Gundersen, L. L. *Bioorganic Med. Chem.* **2010**, *18* (11), 3885–3897.
- (127) Šlachtová, V.; Janovská, L.; Brulíková, L. *J. Mol. Struct.* **2019**, *1183*, 182–189.
- (128) Krylov, I. S.; Kashemirov, B. A.; Hilfinger, J. M.; McKenna, C. E. *Mol. Pharm.*

- 2013**, *10* (2), 445–458.
- (129) Brulikova, L.; Krupkova, S.; Labora, M.; Motyka, K.; Hradilova, L.; Mistrik, M.; Bartek, J.; Hlavac, J. *RSC Adv.* **2016**, *6* (28), 23242–23251.
- (130) Li, Y.; Giulianotti, M.; Houghten, R. A. *Tetrahedron Lett.* **2009**, *50* (42), 5857–5859.
- (131) Ramesh, V.; Rao, B. A.; Sharma, P.; Swarna, B.; Thummuri, D.; Srinivas, K.; Naidu, V. G. M.; Rao, V. J. *Eur. J. Med. Chem.* **2014**, *83*, 569–580.
- (132) Bruno, G.; Costantino, L.; Curinga, C.; Maccari, R.; Monforte, F.; Nicolo, F.; Ottana, R.; Vigorita, M. G. *Bioorg. Med. Chem.* **2002**, *10* (4), 1077–1084.
- (133) Yagnam, S.; Trivedi, R.; Krishna, S.; Giribabu, L.; Praveena, G.; Prakasham, R. S. *J. Organomet. Chem.* **2021**, 937, 121716.
- (134) Shinde, D. N.; Trivedi, R.; Vamsi Krishna, N.; Lingamallu, G.; Sridhar, B.; Khursade, P. S.; Reddy Shetty, P. *Eur. J. Inorg. Chem.* **2018**, *2018* (14), 1571–1580.
- (135) Le Droumaguet, C.; Wang, C.; Wang, Q. *Chem. Soc. Rev.* **2010**, *39* (4), 1233–1239.
- (136) Kolb, H. C.; Finn, M. G.; Sharpless, K. B. *Angew. Chemie Int. Ed.* **2001**, *40* (11), 2004–2021.
- (137) Rostovtsev, V. V.; Green, L. G.; Fokin, V. V.; Sharpless, K. B. *Angew. Chemie* **2002**, *114* (14), 2708–2711.
- (138) Marson, C. M.; Khan, A.; Porter, R. A. *J. Org. Chem.* **2001**, *66* (14), 4771–4775.
- (139) Fabre, B.; Pícha, J.; Vaněk, V.; Selicharová, I.; Chrudinová, M.; Collinsová, M.; Žáková, L.; Buděšínský, M.; Jiracek, J. *ACS Comb. Sci.* **2016**, *18* (12), 710–722.
- (140) Fernandez-Valparis, J.; Romea, P.; Urpí, F.; Font-Bardia, M. *Org. Lett.* **2017**, *19* (23), 6400–6403.
- (141) Tahir, M. N.; Lämmerhardt, N.; Mischnick, P. *Carbohydr. Polym.* **2012**, *88* (1), 154–164.
- (142) Momose, Y.; Meguro, K.; Ikeda, H.; Hatanaka, C.; Oi, S.; Sohda, T. *Chem. Pharm. Bull.* **1991**, *39* (6), 1440–1445.
- (143) Ispida, T. *J. Chem. Soc., Perkin Trans* **1990**, *2*, 1085.

---

## 8 Appendix

### 8.1 List of Publications

**Part of the work described in this thesis has been published or is in preparation**

#### Appendix A

(1) Slachtova, V.; Sebel, M.; Torfs, E.; Oorts, L.; Cappoen, D.; Berka, K.; Bazgier, V.; Brulikova, L. *Eur. J. Med. Chem.* **2020**, *185*, 111812.

#### Appendix B

(2) Slachtova, V.; Brulikova, L. *ChemistrySelect* **2018**, *3* (17), 4653–4662.

#### Appendix C

(3) Slachtova, V.; Chasak, J.; Brulikova, L. *ACS Omega* **2019**, *4* (21), 19314–19323.

#### Appendix D

(4) Slachtova, V.; Janovska, L.; Brulikova, L. *J. Mol. Struct.* **2019**, *1183*, 182–189.

#### Appendix E

(5) Chasak, J.; Slachtova, V.; Urban, M.; Brulikova, L. *Eur. J. Med. Chem.* **2021**, *202*, 112872.

#### Appendix F

(6) Urban, M.; Slachtova, V.; Brulikova, L. *Eur. J. Med. Chem.* **2021**, *212*, 113139.

**Contributions in form of an oral presentation**

*Novel Approaches for the Synthesis of 2-Aminobenzoxazoles and Their N-Substituted Derivatives*

XIX. Interdisciplinary Meeting of Young Life Scientists, May 2019, Milovy, Czech Republic



Contents lists available at ScienceDirect

European Journal of Medicinal Chemistry

journal homepage: <http://www.elsevier.com/locate/ejmech>

Research paper

## Novel thiazolidinedione-hydroxamates as inhibitors of *Mycobacterium tuberculosis* virulence factor Zmp1



Veronika Šlachetová<sup>a</sup>, Marek Šebela<sup>b</sup>, Eveline Torfs<sup>c</sup>, Lauren Oorts<sup>c</sup>, Davie Cappoen<sup>c</sup>, Karel Berka<sup>d</sup>, Václav Bazgier<sup>d</sup>, Lucie Brulíková<sup>a,\*</sup>

<sup>a</sup> Department of Organic Chemistry, Faculty of Science, Palacký University, 17. listopadu 12, 771 46, Olomouc, Czech Republic

<sup>b</sup> Department of Protein Biochemistry and Proteomics, Centre of the Region Haná for Biotechnological and Agricultural Research, Faculty of Science, Palacký University, Šlechtitelů 27, 783 71, Olomouc, Czech Republic

<sup>c</sup> Laboratory of Microbiology, Parasitology and Hygiene (LMPH), S7, Faculty of Pharmaceutical, Biomedical and Veterinary Sciences, University of Antwerp, Wilrijk, Belgium

<sup>d</sup> Department of Physical Chemistry, Regional Centre of Advanced Technologies and Materials, Faculty of Science, Palacký University, 17. listopadu 12, 771 46, Olomouc, Czech Republic

### ARTICLE INFO

#### Article history:

Received 2 May 2019

Received in revised form

7 August 2019

Accepted 23 October 2019

Available online 5 November 2019

#### Keywords:

Zmp1

*Mycobacterium tuberculosis*

Thiazolidinediones

Hydroxamates

MALDI-TOF

### ABSTRACT

Zinc metalloprotease 1 (Zmp1) is an extracellular enzyme, which has been found essential for the intracellular survival and pathogenesis of *Mycobacterium tuberculosis*. In this work, we designed and synthesized a series of novel thiazolidinedione-hydroxamates and evaluated *in silico* their drug-likeness behavior. Then, their inhibitory properties towards a recombinant Zmp1 from *Mycobacterium tuberculosis* were analyzed by MALDI-TOF MS. Nine of the tested compounds were found to inhibit the enzymatic reaction more effectively than the generic metalloprotease inhibitor phosphoramidon. Furthermore, the synthesized thiazolidinedione-hydroxamate hybrids were evaluated for their *in vitro* antimycobacterial activity and acute cytotoxicity using whole-cell assays. Results showed that none of the hybrids exhibited acute cytotoxicity against RAW264.7 macrophages. Whereas extracellular antimycobacterial activity was limited, RAW264.7 macrophage infection results showed that a majority of the hybrids inhibited the intracellular growth of *Mycobacterium tuberculosis* at a concentration of 100 and 10  $\mu$ M. The thiazolidinedione-hydroxamate compound **2n** was considered to be the best candidate of the evaluated library.

© 2019 Elsevier Masson SAS. All rights reserved.

### 1. Introduction

Tuberculosis (TB), an infectious disease predominantly caused by the bacillus *Mycobacterium tuberculosis* (*Mtb*) still poses a major and enduring global health threat [1]. The infectious disease remains one of the top 10 causes of death and is, additionally, the leading cause of death due to a single infectious agent. In 2017, approximately 10 million people developed active TB disease and over 1.6 million persons died as a result [2]. Furthermore, the epidemic is fueled by the current HIV/AIDS pandemic and ever-increasing emergence of anti-TB drug resistance [2]. Moreover, there is only a limited number of drugs available on the market for the treatment of multidrug-resistant (MDR) and extensively drug-

resistant (XDR) TB. Additionally, treatment is less efficient and associated with serious side effects [3]. Without doubt, the discovery of entirely new compounds with an alternative mechanism of action to the existing therapeutics and directed towards unknown targets of *Mtb* becomes more and more desirable [4,5].

One attractive mycobacterial target is represented by the promising and validated 20S proteasome protein, which is necessary for persistence in mice and vitality of the bacterium in pathogenesis as it protects *Mtb* against nitrosative stress from the host [6]. More recently, another interesting mycobacterial enzyme with protease activity was identified, i.e. zinc metalloprotease 1 (Zmp1). The enzyme is found to be essential for the intracellular survival and pathogenesis of *Mtb* [7–11]. In 2008, Master et al. illustrated that Zmp1 affects the macrophage phagosome maturation via suppression of inflammasome activation and subsequent phagolysosome formation, desired for the full clearance of the invalid pathogens (Fig. 1). The exact action mechanism of Zmp1 in the

\* Corresponding author.

E-mail address: [lucie.brulikova@upol.cz](mailto:lucie.brulikova@upol.cz) (L. Brulíková).



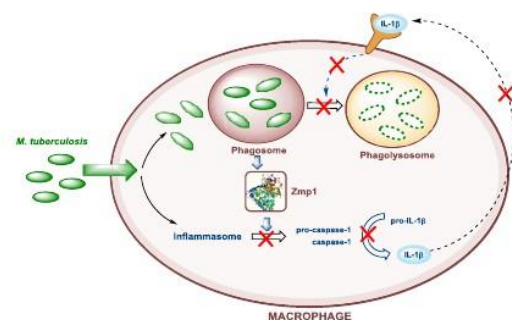


Fig. 1. Inhibition of the phagosome maturation process by mycobacterial Zmp1 (this figure was adopted from Ferraris and Rizzi) [11].

pathogenesis, however, has not been fully elucidated. Though, there is evidence that the zinc metalloprotease, a type of enzyme which can carry out diverse functions in pathogenic microorganisms, may be released from *Mtb* and act on the activation of the caspase-1/interleukin-1 $\beta$  inflammasome, ultimately disrupting phagolysosome formation and *Mtb* clearance [8]. Therefore, Zmp1 and its inhibition leading to virulence attenuation may also represent a potentially useful drug target and are worthy of further investigation.

The molecular structures of the mycobacterial 20S proteasome and Zmp1 are markedly different. Unlike the monomeric Zmp1 [7], 20S proteasome is a large barrel-shaped oligomer: 7  $\alpha$ -subunits are arranged into an  $\alpha$ -ring and 7  $\beta$ -subunits form a  $\beta$ -ring. These rings are stacked to a symmetric complex of  $\alpha_{1-7} \beta_{1-7} \beta_{1-7} \alpha_{1-7}$  [12]. The active site of Zmp1 appears between the two structural domains rich in  $\alpha$ -helices and contains a catalytic zinc ion in tetrahedral coordination. Because of the presence of hydrophobic residues, peptide substrates with a large hydrophobic P1' side chain (e.g. Phe, Leu, Ile) are well accommodated. There is also a secondary binding pocket available at the active site, with arginine residues, which has been suggested a promising docking site for inhibitors [7]. Conversely, the proteolytic mechanism of 20S proteasome involves

the N-terminal threonine residue of each  $\beta$ -subunit [13]. The arrangement of the substrate binding pocket in *M. tuberculosis* 20S proteasome allows versatility in degrading of hydrophobic, basic as well as acidic peptide substrates [12]. The enzyme shows not only a different mechanism but also substrate and cleavage specificity compared to Zmp1. Thus, it is clear that the designing of new inhibitors of these two enzyme targets has to follow unique principles and approaches.

To date, only a few examples of Zmp1 inhibitors are known [14–18]. In 2014, the first selective *Mtb* Zmp1 inhibitors emerged, when the Botta group identified active structures by combining an *in silico* structure-based inhibitor design and biochemical studies (Fig. 2) [14]. Most of the defined structures in their study comprised the rhodanine skeleton that further served as a basic structural motif for the development of other Zmp1 inhibitors [15–18]. The most potent Zmp1 inhibitor to date was identified in the latest study from 2018 [16] when Paolino et al. described a series of 8-hydroxyquinolines modified with a hydroxamate substitution as the zinc-binding group.

In the present study, a protocol for synthetic preparation of thiazolidinedione-hydroxamates was developed. All synthesized compounds were evaluated for their antimycobacterial activity. In addition, the inhibitory properties of the studied compounds towards a recombinant Zmp1 from *Mycobacterium tuberculosis* were analyzed by MALDI-TOF MS.

## 2. Results and discussion

Based on the biological significance of both thiazolidinedione scaffold [19–21] and known hydroxamate-based zinc-binding group (ZBG) [22,23], a new library of thiazolidinedione-hydroxamate hybrids was designed and synthesized (Fig. 3). Two lipophilic hydroxamates as privileged scaffolds in a multitude of medicinally useful agents were selected for our initial studies [23–25]. Thiazolidinedione heterocycle may further be modified by various benzylidene or alkylidene according to various known biologically active structures [19]. Furthermore, the thiazolidinedione and hydroxamate scaffolds are connected via an appropriate linker  $R^2$ , where two simple variants were selected for the initial study.

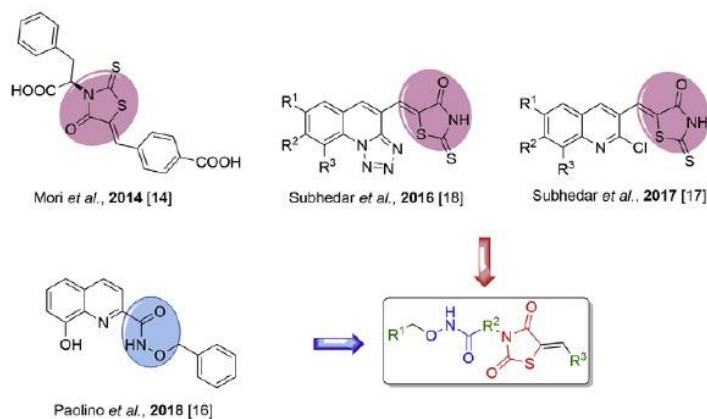
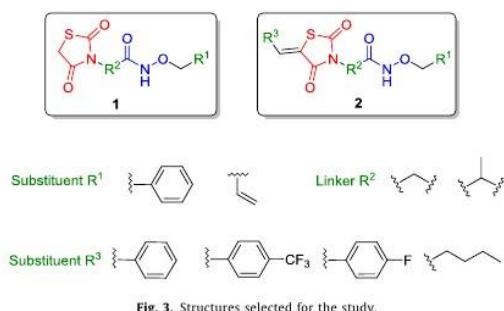


Fig. 2. Examples of known Zmp1 inhibitors and design of novel compounds.



### 3. Chemistry

First, simple thiazolidinedione-unsubstituted hydroxamates **1** were generated (Scheme 1). The initial thiazolidinedione **3** was synthesized according to a previously described procedure [26] and reacted with methyl bromoacetate or methyl 2-bromopropionate giving compounds **4**. This step was followed by the acid-catalyzed hydrolysis resulting in carboxylic acids **5**. The desired compounds **1** were obtained after a coupling reaction of the carboxylic acids **5** with either *O*-allylhydroxylamine hydrochloride or *O*-benzylhydroxylamine hydrochloride using *N*-(3-dimethylaminopropyl)-*N'*-ethyl carbodiimide hydrochloride (EDC.HCl) under aqueous conditions in moderate yields (see Table 1).

Next, hydroxamates **2** were synthesized (Scheme 1). The synthetic procedure was initiated with Knoevenagel condensation of thiazolidinedione **3** with various aldehydes to reach compounds **6**. Then a substitution with methyl bromoacetate or methyl 2-bromopropionate gave compounds **7**. After the acid-mediated hydrolysis of **7**, the resulting carboxylic acids **8** were coupled with either *O*-allylhydroxylamine hydrochloride or *O*-benzylhydroxylamine hydrochloride using EDC.HCl to give hydroxamates **2** in yields ranging from 31 to 75% (see Table 2). The lower yields were caused by losses during column chromatography.

Finally, we assessed the stereochemical outcome of our synthetic protocol. The formation of two geometrical isomers *E* or *Z* after Knoevenagel condensation is possible. These two isomers can easily be distinguished by their <sup>1</sup>H NMR spectral characteristics. It is well known that the benzyldiene proton appears above 7.90 ppm for *Z* isomer and below 7.42 ppm for *E* isomer [27,28]. The measured

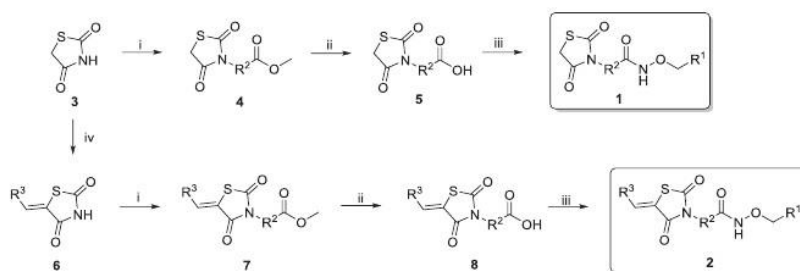
NMR data confirmed the formation of *Z* isomers for all our products. Moreover, the final compounds containing a stereogenic centre were analyzed by supercritical fluid chromatography (SFC). All analyses confirmed the racemic form of both mentioned derivatives (See Supplementary).

#### 3.1. In silico prediction of drug-likeness properties

To select those compounds suitable for further screening, *in silico* physicochemical and pharmacokinetic parameters of the thiazolidinedione-hydroxamates were predicted using the knowledge-based FAFDrugs4 [29] and admetSAR [30] software tools [6,31]. Narrowing the library to a series of compounds with a favourable drug-likeness and no toxicity alerts avoids futile investment in compounds with possible undesirable effects in later stages of the drug discovery and development cascade. For each hybrid, the predicted drug-likeness parameters are shown in Table 3, whereas ranges of such parameters followed by 95% of known drugs are also added in the footnotes [32,33]. The results revealed that the synthesized thiazolidinedione-hydroxamates meet the Lipinski's rule of five as the predicted values of the molecular weight, *n*-octanol, and water partition coefficient, hydrogen bond acceptors and hydrogen-bond donors parameters fall within the prescribed ranges. Furthermore, the number of atoms was also found within the range, improving drug-likeness [29]. Aqueous solubility was forecasted to be good for all thiazolidinedione-hydroxamates, except for **2g**, for which it was predicted to be reduced with a log<sup>S<sub>w</sub></sup> of -5.22. The thiazolidinedione-hydroxamates were also considered to have a good oral bioavailability, based on Verber's rule [34]. All hybrids were designated to class III considering acute oral toxicity, which reveals that the compounds should possess fairly high lethal doses (i.e. LD<sub>50</sub> = 0.5–5 g/kg) and can be considered druggable. As for mutagenicity (Ames test), there were no alerts indicated. In contrast, another rule of thumb such as the GSK 4/400 rule, which anticipates higher risks of toxicity, interactions with off-targets or difficulties during development if the log<sub>P</sub> and the molecular weight is larger than 4 and 400, respectively, suggested that **2e** and **2g** could be less druggable [29]. Though, the overall results indicate that the synthesized thiazolidinedione-hydroxamates generally do possess drug-likeness behavior. Therefore, all derivatives are selected for further investigation, except the compounds **2e** and **2g**.

#### 3.2. Inhibitory activity towards Zmp1

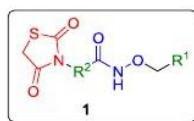
The inhibitory properties of the studied compounds towards a recombinant zinc metalloproteinase (Zmp1) from *Mtb* were



**Scheme 1.** Synthesis of model compounds **1** and **2**.

Reagents and conditions: (i) methyl bromoacetate or methyl 2-bromopropionate, NaH, DMF dry, rt, on; (ii) HBr (40%), reflux, 5 h; (iii) *O*-allylhydroxylamine hydrochloride or *O*-benzylhydroxylamine hydrochloride, EDC.HCl, H<sub>2</sub>O, rt, 2 h; (iv) aldehyde, piperidine, EtOH, reflux, 5 h.

**Table 1**  
Overview of synthesized products 1.



Entry	R <sup>1</sup>	R <sup>2</sup>	Yield <sup>a</sup> [%]
<b>1a</b>			49
<b>1b</b>			55
<b>1c</b>			61
<b>1d</b>			52

<sup>a</sup> Isolated yield after purification.

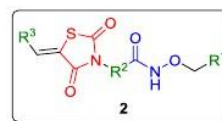
analyzed by matrix-assisted laser desorption/ionization-time of flight mass spectrometry (MALDI-TOF MS). The reaction mixture contained human angiotensin II as a substrate and the respective inhibitor. The proteolytic digestion of angiotensin II ( $m/z$  1046) produced two peptide fragments providing characteristic signals in the mass spectrum, namely DRVY ( $m/z$  552) and IHPF ( $m/z$  513), in accordance with the literature [35] and as confirmed by tandem MS (MS/MS) analyses (not shown). The production of the fragments was accompanied by a simultaneous decrease in the angiotensin II signal (Supplementary Figs. S1–2).

MALDI is generally not considered a robust ionization technique for quantitative measurements, but a growing number of reports have documented its applicability for quantifying peptides [36]. This stems from reduced experimental difficulties because of the ongoing technological improvement of the instruments [37]. In this work, we eliminated both sample-to-sample and shot-to-shot variability of peak intensities by reading intensity ratios of the reaction product at  $m/z$  552 and substrate at  $m/z$  1046 in mass spectra averaged from 1000 laser shots. Finally, the inhibition rate was calculated from the ratio of the determined time-dependence slopes for inhibited and control reaction (Supplementary Table S1). Fig. 4 shows the obtained results. All compounds were found to inhibit the enzymatic reaction but the existing structural differences were reflected in their inhibitory strength. The most potent inhibitors were **2c**, **2k–m**, and **1b** (which inhibited almost completely), whereas **2d** and **2g** inhibited only by less than 20%.

Using the measured inhibition percentages,  $IC_{50}$  (half-maximal inhibitory concentration) values of the inhibitors can be estimated (100% activity for  $[I]=0 \mu M$ ) and they appear in the range of 20–160  $\mu M$ . Experimental  $IC_{50}$  values were obtained with three different inhibitor concentrations for **2n** (18  $\mu M$ ) and **2e** (38  $\mu M$ ), which represent highly efficient and medium-efficient inhibitors from the studied group, respectively. These numbers correspond to inhibition constants described for some other Zmp1 inhibitors [6,14,38].

Supplementary table (Table S2) shows a graphic interpretation of the influence of chemical functional groups on the inhibitory properties. The analyzed hybrid compounds can be divided into five clusters according to the substituent at the thiazolidinedione moiety ( $R^3$ ): without any substitution, with a benzylidene, fluoro-benzylidene, trifluorobenzylidene, and pentyldene substituting group. In each cluster, the presence of either a benzyl or allyl

**Table 2**  
Overview of synthesized products 2.



Entry	R <sup>1</sup>	R <sup>2</sup>	R <sup>3</sup>	Yield <sup>a</sup> [%]
<b>2a</b>				58
<b>2b</b>				51
<b>2c</b>				64
<b>2d</b>				62
<b>2e</b>				49
<b>2f</b>				50
<b>2g</b>				48
<b>2h</b>				31
<b>2i</b>				35
<b>2j</b>				40
<b>2k</b>				60
<b>2l</b>				56
<b>2m</b>				75
<b>2n</b>				75
<b>2o</b>				45
<b>2p</b>				45

<sup>a</sup> Isolated yield after purification.

substitution at the hydroxamate moiety ( $R^1$ ) was considered, plus a possible methyl group in the linker ( $R^2$ ). As can be seen, the benzyl group at the hydroxamate function resulted predominantly in a lower inhibition potency compared to the allyl group at this position for the hybrid compounds with both non-substituted and trifluorobenzylidene-substituted thiazolidinedione ring. An opposite trend was found for those containing the benzylidene-substituted thiazolidinedione ring, whereas no clear trend was observed for the other two clusters. The methyl group presence in



**Table 3**  
*In silico* predicted physicochemical and pharmacokinetic parameters of the thiazolidinedione-hydroxamates.

Compound	MW <sup>a</sup>	LogP <sup>b</sup>	HBD <sup>c</sup>	HBA <sup>d</sup>	No. of atoms <sup>e</sup>	Rotatable bonds <sup>f</sup>	logSw <sup>g</sup>	Solubility Forecast Index	Oral bioavailability (Veber's rule)	4/400	Ames test toxicity	Acute oral toxicity
<b>1a</b>	280.3	1.14	1	6	19	5	-2.11	Good	Good	Good	Non	III
<b>1b</b>	230.24	0.29	1	6	15	5	-1.12	Good	Good	Good	Non	III
<b>1c</b>	294.33	1.54	1	6	20	5	-2.44	Good	Good	Good	Non	III
<b>1d</b>	244.27	0.69	1	6	16	5	-1.46	Good	Good	Good	Non	III
<b>2a</b>	368.41	3.26	1	6	26	6	-3.99	Good	Good	Good	Non	III
<b>2b</b>	318.35	2.41	1	6	22	6	-3.06	Good	Good	Good	Non	III
<b>2c</b>	382.43	3.67	1	6	27	6	-4.32	Good	Good	Good	Non	III
<b>2d</b>	332.37	2.82	1	6	23	6	-3.4	Good	Good	Good	Non	III
<b>2e</b>	436.41	4.15	1	6	30	7	-4.9	Good	Good	Bad	Non	III
<b>2f</b>	386.35	3.30	1	6	26	7	-3.97	Good	Good	Good	Non	III
<b>2g</b>	450.43	4.55	1	6	31	7	-5.22	Reduced	Good	Bad	Non	III
<b>2h</b>	400.37	3.70	1	6	27	7	-4.3	Good	Good	Good	Non	III
<b>2i</b>	386.4	3.36	1	6	27	6	-4.17	Good	Good	Good	Non	III
<b>2j</b>	336.34	2.51	1	6	23	6	-3.23	Good	Good	Good	Non	III
<b>2k</b>	400.42	3.77	1	6	28	6	-4.5	Good	Good	Good	Non	III
<b>2l</b>	350.36	2.92	1	6	24	6	-3.57	Good	Good	Good	Non	III
<b>2m</b>	348.42	3.52	1	6	24	8	-3.79	Good	Good	Good	Non	III
<b>2n</b>	298.36	2.67	1	6	20	8	-2.84	Good	Good	Good	Non	III
<b>2o</b>	362.44	3.92	1	6	25	8	-4.12	Good	Good	Good	Non	III
<b>2p</b>	312.38	3.07	1	6	21	8	-3.18	Good	Good	Good	Non	III

<sup>a</sup> Molecular Weight (MW; 130 to 725).

<sup>b</sup> Log partition coefficient between *n*-octanol and water (-2 to 6.5).

<sup>c</sup> Number of hydrogen bond donors (0-6).

<sup>d</sup> Number of hydrogen acceptors (2-20).

<sup>e</sup> Number of atoms (20-70).

<sup>f</sup> Number of rotatable bonds (0-15).

<sup>g</sup> Log aqueous solubility (-6.5 to 0.5).

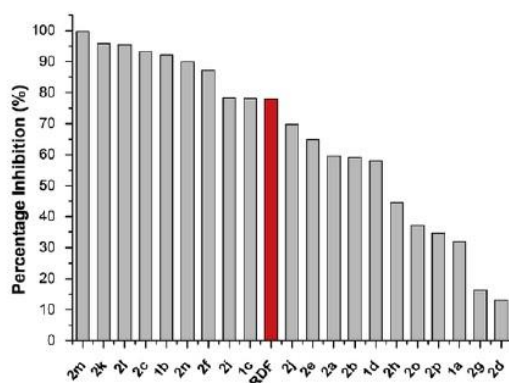


**Fig. 4.** Inhibitory activity toward Zmp1. Inhibition rate at a given inhibitor concentration of 40  $\mu$ M was calculated by inverting the ratio of slopes for inhibited and control reaction. Phosphoramidon (RDF) was used as a reference at a final concentration of 40  $\mu$ M [16].

the linker resulted in lower inhibitory properties when compared to the counterparts without this group, for the compounds with pentylidene and trifluorbenzylidene substitutions at the thiazolidinedione ring. It was the opposite for those with the fluoro-benzylidene substitution. Generally, this interpretation indicates that the measured inhibition data reflect a structure-based interaction with the enzyme molecule as they are not fully random.

### 3.3. *In vitro* biological activity

Following the synthesis and enzymatic assays, the thiazolidinedione-hydroxamate hybrids were evaluated for their

*in vitro* activity against *Mycobacterium tuberculosis* H37Ra using a whole-cell assay. Antimycobacterial potency was assessed using resazurin, as previously reported [39]. The results were expressed as the IC<sub>50</sub>, and also minimal inhibitory concentration (MIC) at which the mycobacterial growth is reduced by 90% (Table 4). In parallel, the acute cytotoxicity of the thiazolidinedione-hydroxamates against the eukaryotic RAW264.7 macrophage cell line was studied using a previously reported neutral red uptake (NRU) assay [40]. The cytotoxic concentration (CC<sub>50</sub>) of a compound is defined as the concentration at which the NRU by the cells is reduced by 50% (Table 4). The selectivity index (SI) of the synthesized compounds was calculated by dividing the CC<sub>50</sub> with the MIC (Table 4). Results showed that most of the thiazolidinedione-hydroxamates showed no significant antimycobacterial activity against extracellular *Mtb* H37Ra, i.e. IC<sub>50</sub> and MIC values > 64  $\mu$ M (Table 4). The hybrids **2f**, **2k**, **2l**, **2m** and **2n** showed a low antimycobacterial potency with IC<sub>50</sub> values of 51.7, 44.4, 60.0, 55.0 and 42.2 respectively. For **2n**, a MIC value of 61.8 could be calculated. Except for **2o**, none of the compounds exhibited acute cytotoxicity against RAW264.7 macrophages, i.e. CC<sub>50</sub> values > 128  $\mu$ M (Table 4). Only **2o** showed a low cytotoxic effect with a CC<sub>50</sub> value of 43.9  $\mu$ M. Though, this effect did not exceed the cytotoxic effect of the reference drug tamoxifen (CC<sub>50</sub> = 11.1  $\mu$ M). As a result, a SI of at least 2.1 and 0.7, respectively, could be calculated for **2n** and **2o**. Although only a low antimycobacterial activity against extracellular *Mtb* H37Ra was present, **2n** showed to be the most potent of the evaluated hybrids. Interestingly, this compound belonged to those providing the strongest inhibitory properties towards the mycobacterial enzyme Zmp1.

As the thiazolidinedione-hydroxamate hybrids were designed as Zmp1-inhibitors, the *in vitro* antimycobacterial activity of the compounds against intracellular residing *Mtb* H37Ra bacilli was assessed as well. The intracellular activity was studied using a luminometric macrophage infection assay [41]. Based on the luminescent signal of the synthesized compounds and untreated control, the obtained results were expressed as inhibition

**Table 4**  
In vitro antimycobacterial activity and acute cytotoxicity results.

Compound	IC <sub>50</sub> (μM) <sup>a</sup>	MIC (μM) <sup>b</sup>	CC <sub>50</sub> (μM) <sup>c</sup>	SI <sup>d</sup>
<b>1a</b>	>64	>64	>128	ND
<b>1b</b>	>64	>64	>128	ND
<b>1c</b>	>64	>64	>128	ND
<b>1d</b>	>64	>64	>128	ND
<b>2a</b>	>64	>64	>128	ND
<b>2b</b>	>64	>64	>128	ND
<b>2c</b>	>64	>64	>128	ND
<b>2d</b>	>64	>64	>128	ND
<b>2e</b>	59.5	>64	>128	ND
<b>2f</b>	51.7	>64	>128	ND
<b>2g</b>	>64	>64	>128	ND
<b>2h</b>	>64	>64	>128	ND
<b>2i</b>	>64	>64	>128	ND
<b>2j</b>	>64	>64	>128	ND
<b>2k</b>	>64	>64	>128	ND
<b>2l</b>	60.0	>64	>128	ND
<b>2m</b>	55.0	>64	>128	ND
<b>2n</b>	42.2	61.8	>128	>2.1
<b>2o</b>	44.4	>64	43.9	>0.7
<b>2p</b>	>64	>64	>128	ND
Isoniazid	0.1	0.3	ND	ND
Tamoxifen	ND	ND	11.1	ND

ND, not done.

<sup>a</sup> Fifty percent inhibitory concentration.

<sup>b</sup> Minimum inhibitory concentration.

<sup>c</sup> Fifty percent cytotoxicity concentration.

<sup>d</sup> Selectivity index (CC<sub>50</sub>/MIC).

percentages. As depicted in Fig. 5, sixteen of the thiazolidinedione-hydroxamates were found antimycobacterial at a final test concentration of 100 μM. Only **2f**, **2h**, **2m** and **2o** completely lacked intracellular activity. Considering a final concentration of 10 μM, eight of the thiazolidinedione-hydroxamates showed an antimycobacterial activity in this experimental arrangement, namely **1b**, **1d**, **2a**, **2c**, **2e**, **2g**, **2i**, and **2k**. The percentage inhibition was 30.2, 21.6, 38.3, 46.9, 48.8, 19.4, 20.6 and 25.1%, respectively. This indicates that the existing structural differences not only influence the enzymatic inhibitory strength towards Zmp1 but also affect less straightforward biological properties such as cell membrane penetration. The hybrid **2n**, which showed only a low antimycobacterial activity against extracellular *Mtb* H37Ra, exhibited intracellular activity at the relatively high 100-μM concentration. In

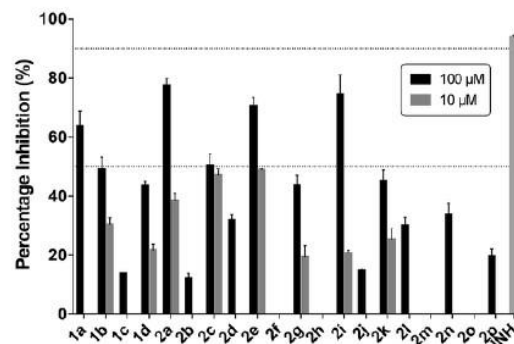


**Fig. 5.** Intracellular antimycobacterial activity of the thiazolidinedione-hydroxamates. The growth inhibition of *Mtb* H37Ra<sup>lux</sup> inside RAW264.7 macrophages upon 24 h of exposure to 100 and 10 μM of the hybrids was expressed as the percentage inhibition. Isoniazid (INH) was used as a reference at a final test concentration of 0.1 μM. Results are presented as the mean ± SD.

contrast, **2e** excels in antimycobacterial activity against intracellular residing *Mtb* H37Ra, even at the lower concentration of 10 μM, whereas it lacks a significant extracellular activity. Structure-activity relationship deductions indicate that the R<sup>2</sup> linker, connecting the thiazolidinedione and hydroxamate moieties, did not influence *in vitro* intracellular activity too much. In contrast, the R<sup>1</sup> substitution appeared largely influential. For example, for the simple thiazolidinedione-unsubstituted hydroxamates **1**, the benzyl-substitution (**1a** and **1c**) reduced intracellular antimycobacterial activity at lower concentrations. In contrast, the R<sup>1</sup> benzyl-substitution of the thiazolidinedione-hydroxamates **2** increased their *in vitro* potency against intracellular residing *Mtb* H37Ra. For the latter group, the R<sup>2</sup> substitution also showed to be important: the presence of an alkyl reduced the antimycobacterial activity at low concentrations, whereas substitution with either an unsubstituted benzyl group or fluorinated benzyl group increased the inhibition percentage in the intracellular test. Hybrid **2e** was selected as the most potent inhibitor of intracellular residing *Mtb* H37Ra, with an inhibition percentage of 70.4 and 48.8% at 100 and 10 μM, respectively. Hybrid **2n**, however, was selected as the most optimal compound considering the overall results, including the *in silico* drug-likeness predictions and target-based enzymatic assays.

#### 3.4. Pose identification with *in silico* molecular docking

In order to explain the inhibitory effect of the thiazolidinedione-hydroxamates, we have employed a molecular docking of **2n** into the internal central cavity of *Mycobacterium tuberculosis* zinc metalloprotease Zmp1 structure (PDB ID: 3ZUK) [7]. The compound mimics the interactions of the indole part of phosphoramidon inhibitor crystal pose as shown in Fig. 6A. Both aromatic moieties, the indole of phosphoramidon and thiazolidinedione of compound **2n**, interact via a π-π interaction with the phenyl ring of F48. They also share the H-bond with R628 and the hydrophobic interactions with the aliphatic chain in the cleft formed by F48 and W604. Phosphoramidon, however, shows a direct interaction with the zinc atom and its surroundings leading towards much stronger inhibition ( $K_i = 35$  nM according to PDBBIND) [42]. Compound **2n** shows additional polar contacts with the cavity entrance at R616. This is in agreement with the previous suggestion of designing such promising inhibitors, which would target the secondary binding pocket at the active site of Zmp1 [7].

The reasons for a good performance of the compound **2n** seem to be i) nonpolar aliphatic chain interaction with the hydrophobic cleft, where larger moieties do not fit, ii) unbranched linker joining the polar moiety of **2n** to the thiazolidinedione ring, which allows more flexibility towards the polar part of the entrance into the cavity and iii) polar interactions with highly populated charged residues within the entrance.

The studied thiazolidinedione-hydroxamates are thus expected to occupy the entrance into the central cavity, approximately 7 Å apart of the zinc-binding catalytic site (Fig. 6B). This is probably the reason for their lower efficiency than it could have been expected from their rational design (combining structural features of previously described potent inhibitors) as they are only gate-keeping the entry/exit of the peptidic substrate and do not further interfere with the reaction on the zinc atom. In contrast, as shown in crystal structures, phosphoramidon interacts directly with the zinc catalytic site and this allows the compound to inhibit also human zinc metalloprotease neprilysin (NEP) structure (PDB ID: 1DMT) [43] as shown in Fig. 6C. NEP is able to cleave peptide bonds between hydrophobic residues in a variety of peptides such as opioid Met- and Leu-enkephalins [44] or angiotensins (e.g. angiotensin II). However, while the cleft surrounding the zinc-binding catalytic site is structurally identical, the entrance into the cavity differs



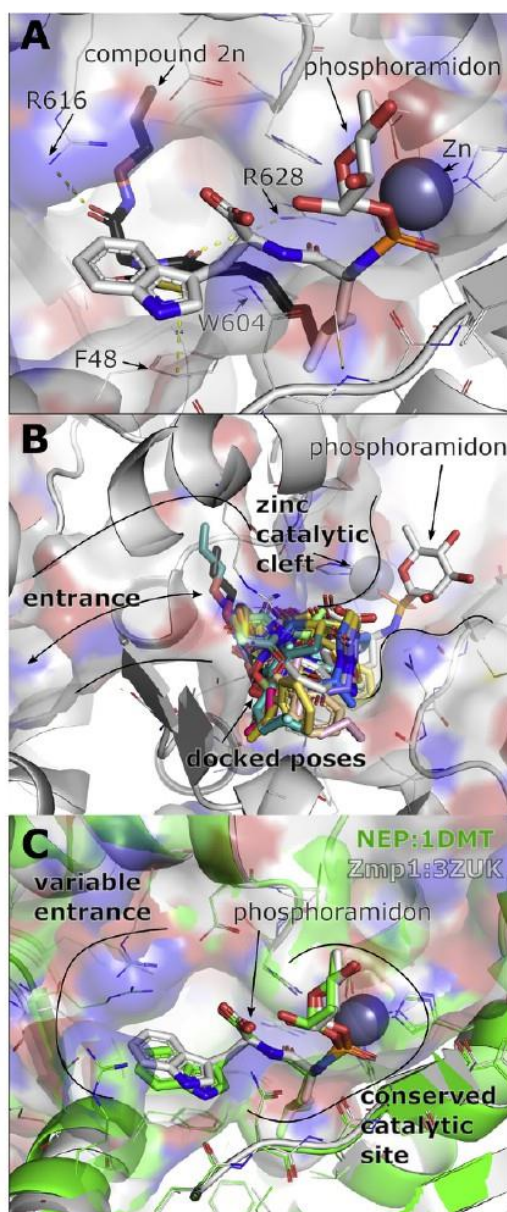


**Fig. 6.** Pose identification with molecular docking. A – a comparison of the docked pose of **2n** with that of phosphoramidon (from the crystal structure, PDB ID: 3ZUK) at the catalytic site of Zmp1; B – the docked poses of thiazolidinedione-hydroxamates in the entrance compared to the crystal structure pose of phosphoramidon blocking the entrance and also occupying the catalytic site of Zmp1; C – a comparison of the binding of phosphoramidon in the cavity of Zmp1 (PDB ID: 3ZUK) and nepriylsin (NEP; PDB ID: 1DMT) [43]. Notice the conserved amino acids around the zinc-binding catalytic site; on the contrary, the entrance shows a variability in the constituting amino acids.

dramatically between the *Mycobacterium* and human zinc metallopeptidases.

#### 4. Conclusion

In conclusion, we have developed an efficient synthetic protocol for the preparation of a series of thiazolidinedione-hydroxamates and assessed their inhibitory properties towards a recombinant Zmp1 from *Mycobacterium tuberculosis* by MALDI-TOF MS. This characterization was completed by whole-cell biological activity and cytotoxicity tests. Results showed that none of the synthesized thiazolidinedione-hydroxamates possessed acute cytotoxic effects against RAW264.7 macrophages. The extracellular antimicrobial activity was rather limited, whereas antimicrobial activity against intracellular residing bacilli was present for the majority of the tested hybrid library. The existing structural differences were reflected in the variability of the *in silico* predicted parameters and biologically determined responses. When looking for a synergic behavior of the studied synthetic compounds in all performed experimental tests, the compound **2n**, which does not contain aromatic R<sup>1</sup> and R<sup>3</sup> substituents as well as a branched R<sup>2</sup> linker, was found the most optimal.

#### 5. Experimental section

##### 5.1. Materials and methods

Solvents and chemicals were purchased from Sigma-Aldrich ([www.sigmaaldrich.com](http://www.sigmaaldrich.com)) and Fluorochem ([www.fluorochem.co.uk](http://www.fluorochem.co.uk)). All reactions were carried out at ambient temperature (21 °C) unless stated otherwise. Analytical thin-layer chromatography (TLC) was performed using aluminum plates precoated with silica gel (silica gel 60 F254).

The LC-MS analyses were carried out on UHPLC-MS system consisting of UHPLC chromatograph Accela with photodiode array detector and triple quadrupole mass spectrometer TSQ Quantum Access (Thermo Scientific, CA, USA), using Nucleodur Gravity C18 column (dimensions 1.8 μm, 2.1 × 50 mm at 30 °C and a flow rate of 800 μl/min (Macherey-Nagel, Germany). The mobile phase was (A) 0.1% ammonium acetate in water, and (B) 0.1% ammonium acetate in acetonitrile, linearly programmed from 10% to 80% B over 2.5 min, kept for 1.5 min. The column was re-equilibrated with 10% of solution B for 1 min. The APCI source operated at a discharge current of 5 μA, vaporizer temperature of 400 °C and a capillary temperature of 200 °C.

NMR 1H/13C spectra were recorded on JEOL ECX-500SS (500 MHz) or JEOL ECA400II (400 MHz) spectrometer at magnetic field strengths of 11.75 T (with operating frequencies 500.16 MHz for 1H and 125.77 MHz for 13C) and 9.39 T (with operating frequencies 399.78 MHz for 1H and 100.53 MHz for 13C) at ambient temperature (-21 °C). Chemical shifts ( $\delta$ ) are reported in parts per million (ppm), and coupling constants ( $J$ ) are reported in Hertz (Hz). NMR spectra were recorded at ambient temperature (21 °C) in DMSO-*d*<sub>6</sub> and referenced to the resonance signal of the solvent.

HRMS analysis was performed with LC-MS and an Orbitrap high-resolution mass spectrometer (Dionex, Ultimate 3000, Thermo Exactive plus, MA, USA) operating in positive full scan mode in the range of 80–1200 *m/z*. The settings for electrospray ionization were as follows: 150 °C oven temperature and 3.6 kV source voltage. The acquired data were internally calibrated with phthalate as a contaminant in methanol (*m/z* 297.15909). Samples were diluted to a final concentration of 0.1 mg/ml in a solution of water and acetonitrile (50:50, v/v). The samples were injected into the mass spectrometer following HPLC separation on a Kinetex C18 column (2.6 μm, 100 Å, 50 × 3.0 mm) using an isocratic mobile

phase of 0.01M acetonitrile/ammonium acetate (80/20) at a flow rate of 0.3 ml min<sup>-1</sup>.

SFC chiral analyses were performed using an Acquity UPC system (Waters) consisting of a binary solvent manager, sample manager, column manager, column heater, convergence manager, PDA detector 2998, QDA mass detector and chiral analytical columns CHIRALPAK IA3, IB3, IC3 and ID3 (4.6 × 100 mm, 3 μm particle size). The chromatographic runs were performed at a flow rate of 2.2 ml min<sup>-1</sup>, column temperature of 38 °C and ABPR 2000 psi.

## 5.2. Chemistry

### 5.2.1. General procedure for Knoevenagel condensation

A mixture of thiazolidinedione **3**, aldehyde (1 eq), piperidine (0.8 eq) and EtOH (130 ml/17 mmol) was refluxed on (16–20 h) and worked up according to *method A* or *B*.

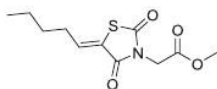
*Method A:* The reaction mixture was poured into H<sub>2</sub>O (200 ml), acidified with AcOH (10 ml) and filtered affording compounds **6**.

*Method B:* The product was concentrated in *vacuum* and purified by column chromatography (mobile phase: hexane/EtOAc 6:2) affording compounds **6**.

### 5.2.2. General procedure for reaction with bromoester

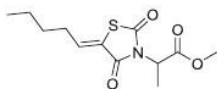
Thiazolidinedione **3** or **6** was dissolved in dry DMF (10 ml/8 mmol). NaH (1 eq) was slowly added to the reaction mixture followed by stirring and stirred for 10 min. Bromoester (1 eq) was added dropwise. After stirring overnight (24 h), the reaction mixture was diluted with water (50 ml). The product was extracted with DCM (5 × 50 ml), organic layers were washed with 5% HCl, brine, dried over Na<sub>2</sub>SO<sub>4</sub> and concentrated in *vacuum*.

### 5.2.3. Methyl 2-(2,4-dioxo-5-pentylidenethiazolidin-3-yl)acetate **7a**



Orange oil. Yield: 81% (822 mg). <sup>1</sup>H NMR (500 MHz, DMSO-*d*<sub>6</sub>): δ 7.12 (t, *J* = 7.7 Hz, 1H), 4.44 (s, 2H), 3.70 (s, 3H), 2.28–2.23 (m, 2H), 1.53–1.47 (m, 2H), 1.32 (dd, *J* = 14.9, 7.4 Hz, 2H), 0.89 (t, *J* = 7.3 Hz, 3H). <sup>13</sup>C NMR (126 MHz, DMSO-*d*<sub>6</sub>): δ 167.17, 166.63, 163.57, 140.10, 123.92, 52.58, 41.83, 31.01, 29.23, 21.74, 13.56. HRMS: *m/z*: calcd for C<sub>11</sub>H<sub>15</sub>NO<sub>4</sub>S: 258.0795 [M+H]<sup>+</sup>; found: 258.0796.

### 5.2.4. Methyl 2-(2,4-dioxo-5-pentylidenethiazolidin-3-yl)propanoate **7b**



Mobile phase: DCM/MeOH 98:2. Brown solid. Yield: 44% (467 mg). <sup>1</sup>H NMR (500 MHz, DMSO-*d*<sub>6</sub>): δ 7.10 (t, *J* = 7.7 Hz, 1H), 5.07 (q, *J* = 7.1 Hz, 1H), 3.65 (s, 3H), 2.24 (dd, *J* = 14.8, 7.5 Hz, 2H), 1.51–1.46 (m, 5H), 1.32 (dd, *J* = 14.9, 7.4 Hz, 2H), 0.89 (t, *J* = 7.3 Hz, 3H). <sup>13</sup>C NMR (126 MHz, DMSO-*d*<sub>6</sub>): δ 169.02, 166.42, 163.42, 140.12, 123.77, 52.57, 49.98, 30.99, 29.24, 21.76, 13.95, 13.57. HRMS: *m/z*: calcd for C<sub>12</sub>H<sub>17</sub>NO<sub>4</sub>S: 272.0951 [M+H]<sup>+</sup>; found: 272.0952.

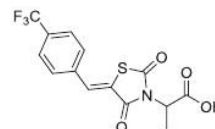
### 5.2.5. Ester hydrolysis

Ester **4/7** was dissolved in HBr 40% (8 ml/5 mmol) and refluxed for 5 h. The mixture was cooled down to rt and diluted with water (50 ml) and worked up according to *method A* or *B*.

*Method A:* The resulting suspension was filtered and washed with water.

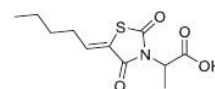
*Method B:* The product was extracted with EtOAc (3 × 50 ml), washed with brine, dried over Na<sub>2</sub>SO<sub>4</sub> and concentrated in *vacuum*.

### 5.2.6. 2-(2,4-Dioxo-5-(4-trifluoromethyl)benzylidene)thiazolidin-3-yl)propanoic acid **8a**



*Method A.* Brown solid. Yield: 55% (734 mg). <sup>1</sup>H NMR (500 MHz, DMSO-*d*<sub>6</sub>): δ 13.28 (s, 1H), 8.06 (s, 1H), 7.91 (d, *J* = 8.4 Hz, 2H), 7.86 (d, *J* = 8.1 Hz, 2H), 5.03 (q, *J* = 7.2 Hz, 1H), 1.52 (d, *J* = 7.2 Hz, 3H). <sup>13</sup>C NMR (126 MHz, DMSO-*d*<sub>6</sub>): δ 169.89, 166.32, 164.63, 136.83, 131.89, 130.63, 130.01 (q, *J* = 32.7 Hz), 126.12, 123.79 (q, *J* = 272.1 Hz), 123.68, 50.49, 13.87. HRMS: *m/z*: calcd for C<sub>14</sub>H<sub>10</sub>F<sub>3</sub>NO<sub>4</sub>S: 346.0355 [M+H]<sup>+</sup>; found: 346.0358.

### 5.2.7. 2-(2,4-Dioxo-5-pentylidenethiazolidin-3-yl)propanoic acid **8b**



*Method B.* Brown solid. Yield: 83% (415 mg). <sup>1</sup>H NMR (500 MHz, DMSO-*d*<sub>6</sub>): δ 13.16 (s, 1H), 7.08 (t, *J* = 7.7 Hz, 1H), 4.93 (q, *J* = 7.2 Hz, 1H), 2.24 (dd, *J* = 14.8, 7.5 Hz, 2H), 1.51–1.45 (m, 5H), 1.32 (dd, *J* = 14.9, 7.4 Hz, 2H), 0.89 (t, *J* = 7.3 Hz, 3H). <sup>13</sup>C NMR (126 MHz, DMSO-*d*<sub>6</sub>): δ 169.97, 166.48, 163.58, 139.59, 123.94, 50.06, 30.96, 29.26, 21.76, 13.91, 13.57. HRMS: *m/z*: calcd for C<sub>11</sub>H<sub>15</sub>NO<sub>4</sub>S: 258.0795 [M+H]<sup>+</sup>; found: 258.0795.

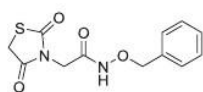
### 5.2.8. Reaction with hydroxylamine.HCl

Carboxylic acid (1 eq) **5/8** was suspended in water (20 ml/1 mmol). Hydroxylamine.HCl (1.5 eq) was dissolved in water (20 ml/1 mmol). The amine mixture was added to the acid mixture and the pH was adjusted to 4.5 with 1M NaOH. THF was added until a homogeneous solution was obtained. EDC.HCl (3 eq) was dissolved in water (10 ml/1 mmol) and added in aliquots (4 ml/1 min) to the reaction mixture. The reaction was stirred for 2 h and worked up according to the *method A* or *B*.

*Method A:* The reaction was filtered and the solid was dried overnight.

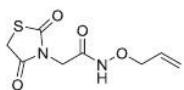
*Method B:* The product was extracted with EtOAc (3 × 40 ml), washed with saturated NaHCO<sub>3</sub>, brine, dried over Na<sub>2</sub>SO<sub>4</sub> and concentrated in *vacuum*.

### 5.2.9. *N*-(benzyloxy)-2-(2,4-dioxothiazolidin-3-yl)acetamide **1a**



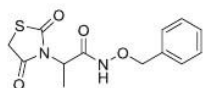
**Method A.** Mobile phase: DCM/MeOH 90:10. White solid. Yield: 49% (277 mg).  $^1\text{H}$  NMR (500 MHz, DMSO- $d_6$ ):  $\delta$  11.22 (s, 1H), 7.42–7.35 (m, 5H), 4.82 (s, 2H), 4.25 (s, 2H), 4.10 (s, 2H).  $^{13}\text{C}$  NMR (126 MHz, DMSO- $d_6$ ):  $\delta$  171.84, 171.46, 162.66, 135.65, 128.87, 128.32, 77.05, 41.14, 33.97. HRMS:  $m/z$ : calcd for  $\text{C}_{12}\text{H}_{12}\text{N}_2\text{O}_4\text{S}$ : 281.0591  $[\text{M}+\text{H}]^+$ ; found: 281.0592.

5.2.10. *N*-(allyloxy)-2-(2,4-dioxothiazolidin-3-yl)acetamide 1b



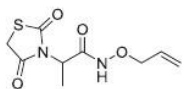
**Method B.** Mobile phase:  $\text{CHCl}_3/\text{MeOH}$  90:10. Yellow oil. Yield: 55% (257 mg).  $^1\text{H}$  NMR (500 MHz, DMSO- $d_6$ ):  $\delta$  11.35 (s, 1H), 5.95–5.87 (m, 1H), 5.31 (d,  $J = 17.3$  Hz, 1H), 5.26 (d,  $J = 10.4$  Hz, 1H), 4.27 (s, 4H), 4.03 (s, 2H).  $^{13}\text{C}$  NMR (126 MHz, DMSO- $d_6$ ):  $\delta$  171.82, 171.44, 162.49, 132.70, 119.48, 76.05, 41.11, 33.96. HRMS:  $m/z$ : calcd for  $\text{C}_8\text{H}_{10}\text{N}_2\text{O}_4\text{S}$ : 231.0434  $[\text{M}+\text{H}]^+$ ; found: 231.0435.

5.2.11. *N*-(benzyloxy)-2-(2,4-dioxothiazolidin-3-yl)propanamide 1c



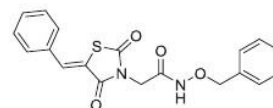
**Method B.** Mobile phase: DCM/MeOH 90:10. Yellow oil. Yield: 61% (342 mg).  $^1\text{H}$  NMR (500 MHz, DMSO- $d_6$ ):  $\delta$  11.35 (s, 1H), 7.40–7.38 (m, 4H), 7.37–7.36 (m, 1H), 4.75 (d,  $J = 7.1$  Hz, 2H), 4.68 (q,  $J = 7.1$  Hz, 1H), 4.16 (s, 2H), 1.40 (d,  $J = 7.2$  Hz, 3H).  $^{13}\text{C}$  NMR (126 MHz, DMSO- $d_6$ ):  $\delta$  171.71, 171.31, 165.08, 135.67, 128.94, 128.28, 76.90, 49.39, 34.03, 13.61. HRMS:  $m/z$ : calcd for  $\text{C}_{13}\text{H}_{14}\text{N}_2\text{O}_4\text{S}$ : 295.0747  $[\text{M}+\text{H}]^+$ ; found: 295.0749.

5.2.12. *N*-(allyloxy)-2-(2,4-dioxothiazolidin-3-yl)propanamide 1d



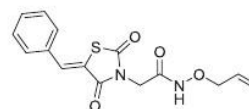
**Method B.** Mobile phase:  $\text{CHCl}_3/\text{MeOH}$  90:10. Yellow oil. Yield: 52% (240 mg).  $^1\text{H}$  NMR (500 MHz, DMSO- $d_6$ ):  $\delta$  11.24 (s, 1H), 5.94–5.86 (m, 1H), 5.30 (dd,  $J = 17.3, 1.6$  Hz, 1H), 5.24 (d,  $J = 10.5$  Hz, 1H), 4.65 (q,  $J = 7.1$  Hz, 1H), 4.25–4.23 (m, 2H), 4.16 (s, 2H), 1.38 (d,  $J = 7.2$  Hz, 3H).  $^{13}\text{C}$  NMR (126 MHz, DMSO- $d_6$ ):  $\delta$  171.66, 171.29, 164.87, 132.80, 119.24, 75.83, 49.33, 34.02, 13.59. HRMS:  $m/z$ : calcd for  $\text{C}_9\text{H}_{12}\text{N}_2\text{O}_4\text{S}$ : 245.0591  $[\text{M}+\text{H}]^+$ ; found: 245.0593.

5.2.13. 2-(5-benzylidene-2,4-dioxothiazolidin-3-yl)-*N*-(benzyloxy)acetamide 2a



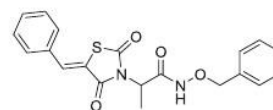
**Method A.** White solid. Yield: 58% (451 mg).  $^1\text{H}$  NMR (500 MHz, DMSO- $d_6$ ):  $\delta$  11.34 (s, 1H), 7.96 (s, 1H), 7.65 (d,  $J = 7.3$  Hz, 2H), 7.56 (t,  $J = 7.3$  Hz, 2H), 7.52 (d,  $J = 7.1$  Hz, 1H), 7.42–7.37 (m, 5H), 4.84 (s, 2H), 4.28 (s, 2H).  $^{13}\text{C}$  NMR (126 MHz, DMSO- $d_6$ ):  $\delta$  166.96, 165.15, 162.54, 135.64, 133.50, 132.83, 130.77, 130.15, 129.39, 128.91, 128.33, 121.00, 77.10, 41.50. HRMS:  $m/z$ : calcd for  $\text{C}_{19}\text{H}_{16}\text{N}_2\text{O}_4\text{S}$ : 369.0904  $[\text{M}+\text{H}]^+$ ; found: 369.0907.

5.2.14. *N*-(allyloxy)-2-(5-benzylidene-2,4-dioxothiazolidin-3-yl)acetamide 2b



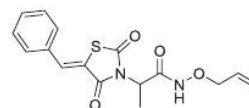
**Method A.** White solid. Yield: 51% (339 mg).  $^1\text{H}$  NMR (500 MHz, DMSO- $d_6$ ):  $\delta$  11.26 (s, 1H), 7.96 (s, 1H), 7.64 (d,  $J = 6.0$  Hz, 2H), 7.58–7.51 (m, 3H), 5.96 (s, 1H), 5.35 (d,  $J = 17.2$  Hz, 1H), 5.28 (d,  $J = 9.2$  Hz, 1H), 4.30 (d,  $J = 28.8$  Hz, 4H).  $^{13}\text{C}$  NMR (126 MHz, DMSO- $d_6$ ):  $\delta$  166.94, 165.13, 162.38, 133.48, 132.82, 132.69, 130.77, 130.14, 129.39, 120.99, 119.54, 76.09, 41.46. HRMS:  $m/z$ : calcd for  $\text{C}_{15}\text{H}_{14}\text{N}_2\text{O}_4\text{S}$ : 319.0747  $[\text{M}+\text{H}]^+$ ; found: 319.0749.

5.2.15. 2-(5-benzylidene-2,4-dioxothiazolidin-3-yl)-*N*-(benzyloxy)propanamide 2c



**Method B.** Mobile phase: DCM/MeOH 98:2. Yellow solid. Yield: 64% (373 mg).  $^1\text{H}$  NMR (500 MHz, DMSO- $d_6$ ):  $\delta$  11.46 (s, 1H), 7.94 (s, 1H), 7.65 (d,  $J = 7.4$  Hz, 2H), 7.58–7.50 (m, 3H), 7.40–7.34 (m, 5H), 4.87 (q,  $J = 7.1$  Hz, 1H), 4.77 (q,  $J = 10.7$  Hz, 2H), 1.50 (d,  $J = 7.2$  Hz, 3H).  $^{13}\text{C}$  NMR (126 MHz, DMSO- $d_6$ ):  $\delta$  166.75, 164.99, 164.90, 135.69, 132.96, 130.63, 130.05, 129.40, 128.97, 128.27, 121.36, 76.92, 49.85, 13.86. HRMS:  $m/z$ : calcd for  $\text{C}_{20}\text{H}_{18}\text{N}_2\text{O}_4\text{S}$ : 383.1060  $[\text{M}+\text{H}]^+$ ; found: 383.1058.

5.2.16. *N*-(allyloxy)-2-(5-benzylidene-2,4-dioxothiazolidin-3-yl)propanamide 2d

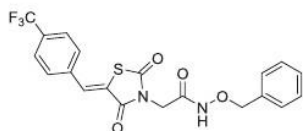


**Method B.** Mobile phase: DCM/MeOH 98:2. Yellow solid. Yield: 62% (314 mg).  $^1\text{H}$  NMR (500 MHz, DMSO- $d_6$ ):  $\delta$  11.36 (s, 1H), 7.94 (s, 1H), 7.64 (d,  $J = 7.4$  Hz, 2H), 7.58–7.51 (m, 3H), 5.91 (dq,  $J = 10.7$ ,



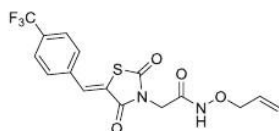
6.1 Hz, 1H), 5.31 (d,  $J = 17.3$  Hz, 1H), 5.24 (d,  $J = 11.7$  Hz, 1H), 4.85 (q,  $J = 7.1$  Hz, 1H), 4.26 (t,  $J = 5.2$  Hz, 2H), 1.48 (d,  $J = 7.2$  Hz, 3H).  $^{13}\text{C}$  NMR (126 MHz,  $\text{DMSO}-d_6$ ):  $\delta$  166.72, 164.98, 164.70, 132.95, 132.82, 130.63, 130.05, 129.39, 121.36, 119.30, 75.87, 49.81, 13.85. HRMS:  $m/z$ : calcd for  $\text{C}_{16}\text{H}_{16}\text{N}_2\text{O}_4\text{S}$ : 333.0904  $[\text{M}+\text{H}]^+$ ; found: 333.0905.

5.2.17. *N*-(benzyloxy)-2-(2,4-dioxo-5-(4-trifluoromethyl)benzylidene)thiazolidin-3-yl)acetamide 2e



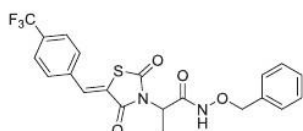
**Method A.** White solid. Yield: 49% (298 mg).  $^1\text{H}$  NMR (500 MHz,  $\text{DMSO}-d_6$ ):  $\delta$  11.35 (s, 1H), 8.04 (s, 1H), 7.87 (dd,  $J = 19.3, 8.2$  Hz, 4H), 7.43–7.37 (m, 5H), 4.85 (s, 2H), 4.29 (s, 2H).  $^{13}\text{C}$  NMR (126 MHz,  $\text{DMSO}-d_6$ ):  $\delta$  166.62, 164.93, 162.45, 136.81, 135.63, 131.67, 129.97 (q,  $J = 31.5$  Hz), 128.92, 128.33, 126.13, 124.00, 123.79 (q,  $J = 273.4$  Hz), 77.11, 41.63. HRMS:  $m/z$ : calcd for  $\text{C}_{20}\text{H}_{15}\text{F}_3\text{N}_2\text{O}_4\text{S}$ : 437.0777  $[\text{M}+\text{H}]^+$ ; found: 437.0775.

5.2.18. *N*-(allyloxy)-2-(2,4-dioxo-5-(4-trifluoromethyl)benzylidene)thiazolidin-3-yl)acetamide 2f



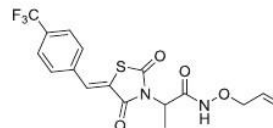
**Method A.** Yellow solid. Yield: 50% (289 mg).  $^1\text{H}$  NMR (500 MHz,  $\text{DMSO}-d_6$ ):  $\delta$  11.27 (s, 1H), 8.03 (s, 1H), 7.89 (d,  $J = 8.4$  Hz, 2H), 7.85 (d,  $J = 8.4$  Hz, 2H), 5.96 (dd,  $J = 16.1, 9.9$  Hz, 1H), 5.35 (d,  $J = 17.2$  Hz, 1H), 5.28 (d,  $J = 10.1$  Hz, 1H), 4.33 (s, 4H).  $^{13}\text{C}$  NMR (126 MHz,  $\text{DMSO}-d_6$ ):  $\delta$  166.60, 164.91, 162.29, 136.81, 132.69, 131.66, 130.63, 129.97 (q,  $J = 31.5$  Hz), 126.16, 124.00, 123.81 (q,  $J = 272.1$  Hz), 119.56, 76.11, 41.59. HRMS:  $m/z$ : calcd for  $\text{C}_{16}\text{H}_{13}\text{F}_3\text{N}_2\text{O}_4\text{S}$ : 387.0621  $[\text{M}+\text{H}]^+$ ; found: 387.0621.

5.2.19. *N*-(benzyloxy)-2-(2,4-dioxo-5-(4-trifluoromethyl)benzylidene)thiazolidin-3-yl)propanamide 2g



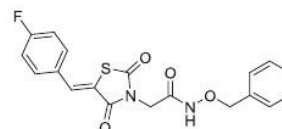
**Method B.** Mobile phase: DCM/MeOH 95:5. White solid. Yield: 48% (126 mg).  $^1\text{H}$  NMR (500 MHz,  $\text{DMSO}-d_6$ ):  $\delta$  11.47 (s, 1H), 8.03 (s, 1H), 7.91 (d,  $J = 8.3$  Hz, 2H), 7.86 (d,  $J = 8.1$  Hz, 2H), 7.41–7.34 (m, 5H), 4.88 (q,  $J = 7.0$  Hz, 1H), 4.77 (q,  $J = 8.4$  Hz, 2H), 1.50 (d,  $J = 7.1$  Hz, 3H).  $^{13}\text{C}$  NMR (126 MHz,  $\text{DMSO}-d_6$ ):  $\delta$  166.41, 164.82, 164.78, 136.94, 135.67, 131.05, 130.53, 129.85 (q,  $J = 32.7$ ), 128.98, 128.28, 126.16, 124.41, 123.80 (q,  $J = 273.4$  Hz), 49.95, 13.82. HRMS:  $m/z$ : calcd for  $\text{C}_{21}\text{H}_{17}\text{F}_3\text{N}_2\text{O}_4\text{S}$ : 451.0934  $[\text{M}+\text{H}]^+$ ; found: 451.0934.

5.2.20. *N*-(allyloxy)-2-(2,4-dioxo-5-(4-trifluoromethyl)benzylidene)thiazolidin-3-yl)propanamide 2h



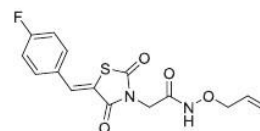
**Method B.** Mobile phase: DCM/MeOH 98:2. White solid. Yield: 31% (127 mg).  $^1\text{H}$  NMR (500 MHz,  $\text{DMSO}-d_6$ ):  $\delta$  11.37 (s, 1H), 8.02 (s, 1H), 7.91 (d,  $J = 8.3$  Hz, 2H), 7.85 (d,  $J = 8.2$  Hz, 2H), 5.91 (qd,  $J = 11.8, 6.1$  Hz, 1H), 5.31 (d,  $J = 17.3$  Hz, 1H), 5.24 (d,  $J = 10.4$  Hz, 1H), 4.86 (q,  $J = 6.9$  Hz, 1H), 4.26 (t,  $J = 5.1$  Hz, 2H), 1.49 (d,  $J = 7.1$  Hz, 3H).  $^{13}\text{C}$  NMR (126 MHz,  $\text{DMSO}-d_6$ ):  $\delta$  166.38, 164.76, 164.62, 136.94, 132.81, 131.04, 130.54, 129.85 (q,  $J = 31.5$  Hz), 126.18, 124.41, 123.80 (q,  $J = 272.1$  Hz), 119.34, 75.89, 49.92, 13.79. HRMS:  $m/z$ : calcd for  $\text{C}_{17}\text{H}_{15}\text{F}_3\text{N}_2\text{O}_4\text{S}$ : 401.0777  $[\text{M}+\text{H}]^+$ ; found: 401.0775.

5.2.21. *N*-(benzyloxy)-2-(5-(4-fluorobenzylidene)-2,4-dioxothiazolidin-3-yl)acetamide 2i



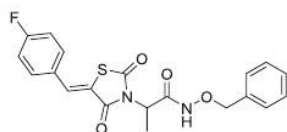
**Method A.** Yellow solid. Yield: 75% (617 mg).  $^1\text{H}$  NMR (500 MHz,  $\text{DMSO}-d_6$ ):  $\delta$  11.33 (s, 1H), 7.97 (d,  $J = 7.0$  Hz, 1H), 7.71 (dd,  $J = 12.5, 6.7$  Hz, 2H), 7.42–7.36 (m, 7H), 4.84 (s, 2H), 4.27 (s, 2H).  $^{13}\text{C}$  NMR (126 MHz,  $\text{DMSO}-d_6$ ):  $\delta$  166.85, 165.11, 164.06, 162.53, 162.06, 135.64, 132.66, 132.47, 129.51, 128.99, 128.82, 128.41, 128.26, 120.70, 116.74, 116.67, 116.43, 77.10, 41.51. HRMS:  $m/z$ : calcd for  $\text{C}_{19}\text{H}_{15}\text{FN}_2\text{O}_4\text{S}$ : 387.0809  $[\text{M}+\text{H}]^+$ ; found: 387.0813.

5.2.22. *N*-(allyloxy)-2-(5-(4-fluorobenzylidene)-2,4-dioxothiazolidin-3-yl)acetamide 2j



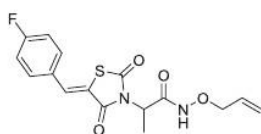
**Method A.** Yellow solid. Yield: 75% (432 mg).  $^1\text{H}$  NMR (500 MHz,  $\text{DMSO}-d_6$ ):  $\delta$  11.25 (s, 1H), 7.97 (s, 1H), 7.74–7.69 (m, 2H), 7.38 (t,  $J = 8.4$  Hz, 2H), 5.95 (s, 1H), 5.35 (d,  $J = 17.1$  Hz, 2H), 5.28 (d,  $J = 9.5$  Hz, 2H), 4.32 (br s, 4H).  $^{13}\text{C}$  NMR (126 MHz,  $\text{DMSO}-d_6$ ):  $\delta$  166.82, 165.10, 162.37, 162.06, 132.70, 132.62, 132.43, 129.50, 119.54, 116.72, 116.61, 116.55, 116.44, 76.09, 41.47. HRMS:  $m/z$ : calcd for  $\text{C}_{15}\text{H}_{13}\text{FN}_2\text{O}_4\text{S}$ : 337.0653  $[\text{M}+\text{H}]^+$ ; found: 337.0653.

5.2.23. *N*-(benzyloxy)-2-(5-(4-fluorobenzylidene)-2,4-dioxothiazolidin-3-yl)propanamide 2k



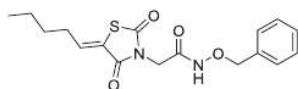
**Method B.** Mobile phase: DCM/MeOH 98:2. Green solid. Yield: 45% (62 mg).  $^1\text{H}$  NMR (500 MHz, DMSO- $d_6$ ):  $\delta$  11.46 (s, 1H), 7.96 (s, 1H), 7.72 (dd,  $J$  = 8.5, 5.5 Hz, 2H), 7.43–7.34 (m, 7H), 4.87 (q,  $J$  = 7.1 Hz, 1H), 4.77 (d,  $J$  = 8.2 Hz, 2H), 1.49 (d,  $J$  = 7.2 Hz, 3H).  $^{13}\text{C}$  NMR (126 MHz, DMSO- $d_6$ ):  $\delta$  166.63, 164.95, 164.89, 163.97, 161.97, 135.69, 132.59, 131.89, 129.62, 128.97, 128.27, 121.07, 116.68, 116.50, 76.92, 49.88, 13.86. HRMS:  $m/z$ : calcd for  $\text{C}_{20}\text{H}_{17}\text{FN}_2\text{O}_4\text{S}$ : 401.0966  $[\text{M}+\text{H}]^+$ ; found: 401.0968.

5.2.24. *N*-(allyloxy)-2-(5-(4-fluorobenzylidene)-2,4-dioxothiazolidin-3-yl)propanamide 2l



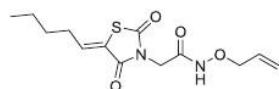
**Method B.** Mobile phase: DCM/MeOH 95:5. Green solid. Yield: 45% (54 mg).  $^1\text{H}$  NMR (500 MHz, DMSO- $d_6$ ):  $\delta$  11.35 (s, 1H), 7.95 (s, 1H), 7.72 (dd,  $J$  = 8.7, 5.4 Hz, 2H), 7.41 (t,  $J$  = 8.8 Hz, 2H), 5.95–5.87 (m, 1H), 5.30 (d,  $J$  = 16.0 Hz, 1H), 5.24 (d,  $J$  = 10.4 Hz, 1H), 4.84 (q,  $J$  = 7.0 Hz, 1H), 4.26 (t,  $J$  = 5.2 Hz, 2H), 1.48 (d,  $J$  = 7.2 Hz, 3H).  $^{13}\text{C}$  NMR (126 MHz, DMSO- $d_6$ ):  $\delta$  166.59, 164.94, 164.69, 161.97, 132.81, 132.59, 132.52, 131.88, 129.64, 121.07, 119.31, 116.67, 116.50, 75.88, 49.84, 13.84. HRMS:  $m/z$ : calcd for  $\text{C}_{16}\text{H}_{15}\text{FN}_2\text{O}_4\text{S}$ : 351.0809  $[\text{M}+\text{H}]^+$ ; found: 351.0811.

5.2.25. *N*-(benzyloxy)-2-(2,4-dioxo-5-pentylidene-thiazolidin-3-yl)acetamide 2m



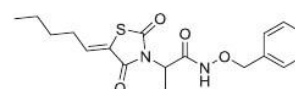
**Method B.** Brown solid. Yield: 35% (174 mg).  $^1\text{H}$  NMR (500 MHz, DMSO- $d_6$ ):  $\delta$  11.29 (s, 1H), 7.43–7.37 (m, 5H), 7.09 (dt,  $J$  = 11.2, 7.6 Hz, 1H), 4.83 (d,  $J$  = 8.5 Hz, 2H), 4.21 (s, 2H), 2.27 (dq,  $J$  = 11.2, 7.4 Hz, 2H), 1.53 (dd,  $J$  = 14.5, 10.9 Hz, 2H), 1.36 (ddd,  $J$  = 14.5, 11.1, 7.5 Hz, 2H), 0.92 (t,  $J$  = 11.3, 7.3 Hz, 3H).  $^{13}\text{C}$  NMR (126 MHz, DMSO- $d_6$ ):  $\delta$  166.79, 163.86, 162.60, 139.33, 135.64, 128.86, 128.33, 124.32, 77.07, 41.19, 30.95, 29.28, 21.75, 13.57. HRMS:  $m/z$ : calcd for  $\text{C}_{17}\text{H}_{20}\text{N}_2\text{O}_4\text{S}$ : 349.1217  $[\text{M}+\text{H}]^+$ ; found: 349.1217.

5.2.26. *N*-(allyloxy)-2-(2,4-dioxo-5-pentylidene-thiazolidin-3-yl)acetamide 2n



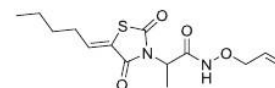
**Method B.** Mobile phase: hex/EtOAc 60:40. Yellow solid. Yield: 40% (178 mg).  $^1\text{H}$  NMR (500 MHz, DMSO- $d_6$ ):  $\delta$  11.40 (s, 1H), 7.08 (t,  $J$  = 7.7 Hz, 1H), 5.91 (ddd,  $J$  = 16.5, 11.3, 6.0 Hz, 1H), 5.32 (d,  $J$  = 17.3 Hz, 1H), 5.26 (d,  $J$  = 10.4 Hz, 1H), 4.35–4.13 (m, 4H), 2.24 (dd,  $J$  = 14.7, 7.4 Hz, 2H), 1.50 (dt,  $J$  = 15.0, 7.4 Hz, 2H), 1.32 (dd,  $J$  = 14.9, 7.4 Hz, 2H), 0.89 (t,  $J$  = 7.3 Hz, 3H).  $^{13}\text{C}$  NMR (126 MHz, DMSO- $d_6$ ):  $\delta$  166.76, 163.85, 162.43, 139.28, 132.70, 124.31, 119.48, 76.06, 41.16, 30.94, 29.27, 21.74, 13.57. HRMS:  $m/z$ : calcd for  $\text{C}_{13}\text{H}_{18}\text{N}_2\text{O}_4\text{S}$ : 299.1060  $[\text{M}+\text{H}]^+$ ; found: 299.1060.

5.2.27. *N*-(benzyloxy)-2-(2,4-dioxo-5-pentylidene-thiazolidin-3-yl)propanamide 2o



**Method B.** Mobile phase: DCM/MeOH 95:5. Yellow oil. Yield: 60% (160 mg).  $^1\text{H}$  NMR (500 MHz, DMSO- $d_6$ ):  $\delta$  11.41 (s, 1H), 7.39–7.34 (m, 5H), 7.04 (t,  $J$  = 7.7 Hz, 1H), 4.76 (t,  $J$  = 8.8 Hz, 3H), 2.23 (q,  $J$  = 7.4 Hz, 2H), 1.51–1.48 (m, 2H), 1.45 (d,  $J$  = 7.2 Hz, 3H), 1.33 (dd,  $J$  = 14.9, 7.4 Hz, 2H), 0.89 (t,  $J$  = 7.3 Hz, 3H).  $^{13}\text{C}$  NMR (126 MHz, DMSO- $d_6$ ):  $\delta$  166.59, 164.94, 163.73, 138.64, 135.68, 128.95, 128.26, 124.51, 76.89, 49.64, 30.87, 29.32, 21.75, 13.85, 13.59. HRMS:  $m/z$ : calcd for  $\text{C}_{18}\text{H}_{22}\text{N}_2\text{O}_4\text{S}$ : 363.1373  $[\text{M}+\text{H}]^+$ ; found: 363.1372.

5.2.28. *N*-(allyloxy)-2-(2,4-dioxo-5-pentylidene-thiazolidin-3-yl)propanamide 2p



**Method B.** DCM/MeOH 85:15. Yellow oil. Yield: 56% (129 mg).  $^1\text{H}$  NMR (500 MHz, DMSO- $d_6$ ):  $\delta$  11.31 (s, 1H), 7.04 (s, 1H), 5.91 (ddd,  $J$  = 17.0, 11.2, 5.9 Hz, 1H), 5.29 (d,  $J$  = 15.8 Hz, 1H), 5.23 (d,  $J$  = 8.8 Hz, 1H), 4.76 (q,  $J$  = 7.1 Hz, 1H), 4.24 (s, 2H), 2.23 (dd,  $J$  = 14.8, 7.4 Hz, 2H), 1.51–1.47 (m, 2H), 1.43 (d,  $J$  = 7.2 Hz, 3H), 1.33 (dd,  $J$  = 14.9, 7.4 Hz, 2H), 0.89 (t,  $J$  = 7.3 Hz, 3H).  $^{13}\text{C}$  NMR (126 MHz, DMSO- $d_6$ ):  $\delta$  166.54, 164.74, 163.71, 138.63, 132.81, 119.25, 75.84, 49.59, 30.87, 29.32, 21.75, 13.84, 13.58. HRMS:  $m/z$ : calcd for  $\text{C}_{14}\text{H}_{20}\text{N}_2\text{O}_4\text{S}$ : 313.1217  $[\text{M}+\text{H}]^+$ ; found: 313.1215.

5.3. *In silico* prediction of drug-likeness properties

Physicochemical and pharmacokinetic parameters of the thiazolidinedione-hydroxamates were *in silico* predicted using the FAFDrugs4 [29] and admetSAR tools [30]. The different parameters predicted were as follows: molecular weight, octanol/water partition coefficient, number of hydrogen donors, number of hydrogen acceptors, number of atoms, number of rotatable bonds, aqueous solubility, Solubility Forecast Index, oral bioavailability via Veber's rule, 4/400 GSK rule, Ames toxicity and acute oral toxicity.

5.4. *Zmp1* inhibition assay

Human angiotensin II (Sigma-Aldrich, Cat. No. A9525) was dissolved in LC-MS-quality water to a concentration of 4 nmol/ml. Aliquots (24  $\mu\text{l}$ ) of the stock solution were mixed with 1  $\mu\text{l}$  of 2M  $\text{NH}_4\text{HCO}_3$  in 0.5-ml test tubes. This was followed by pipetting either

1  $\mu\text{l}$  of neat acetone (control) or 1  $\mu\text{l}$  of 1 mM inhibitor solution in acetone (sample). After pre-incubation in a thermostat at 37 °C for 3 min, the reaction was started by adding 1  $\mu\text{l}$  of a recombinant Zmp1 metalloproteinase from *Mycobacterium tuberculosis* (ProSci, Poway, CA, USA; Cat. No. 90–361; diluted 1:4, v/v, with cold 50 mM  $\text{NH}_4\text{HCO}_3$  and kept on ice during the measurements) and proceeded at 37 °C for 20 min. Aliquots (0.5  $\mu\text{l}$ ) of the reaction mixture were aspirated by a pipette each 2 min, spotted onto the MALDI target (an MSP BigAnchor 96 BC; Bruker Daltonik, Bremen, Germany), immediately overlaid with matrix solution ( $\alpha$ -cyano-4-hydroxycinnamic acid, 5 mg/ml in acetonitrile; 2.5% (v/v) trifluoroacetic acid, 7:3, v/v), and left to dry and crystallize.

MALDI-TOF MS measurements were carried out on a Microflex LRF 20 instrument equipped with a 60-Hz nitrogen laser operating at  $\lambda_{\text{max}} = 337 \text{ nm}$  (Bruker Daltonik). Mass spectra were accumulated from 1000 laser shots in the reflectron positive ion mode using an acceleration voltage (IS1) of 18.0 kV, extraction voltage (IS2) of 15.5 kV, lens voltage of 9.3 kV, reflectron voltage of 19.0 kV, detector voltage of 1590 V and pulsed ion extraction delay time of 350 ns. The instrument was calibrated externally with a peptide mixture (Peptide Calibration Standard II; Bruker Daltonik).

The enzymatic reaction was monitored by the hydrolysis of angiotensin II yielding a peptide DRVY ( $m/z$  552.3), which is accompanied by a simultaneous decrease in the angiotensin II signal (DRVYIHPF;  $m/z$  1046.5). The ratio of  $m/z$  552 versus  $m/z$  1046 signal intensities was plotted against the reaction time to achieve an increasing linear dependence. The inhibition rate at the given inhibitor concentration of 40  $\mu\text{M}$  was finally calculated by inverting the ratio of slopes for inhibited and control reaction. Phosphoramidone (RDF) was used as a reference inhibitor [16]. Three different inhibitor concentrations in the range of 20–80  $\mu\text{M}$  were used to determine the corresponding  $\text{IC}_{50}$  value. The measured responses (percentages of inhibition) were plotted against the respective concentrations. All data points obtained for a single inhibitor were fitted by a straight line (linear regression equation:  $y = a \cdot x + b$ ) and then  $\text{IC}_{50}$  (in  $\mu\text{M}$ ) was obtained as a result of calculating formula  $(50 - b)/a$ .

#### 5.5. In vitro antimycobacterial activity

In vitro activity of the synthesized hybrids against *Mtb* H37Ra (ATCC® 25177™) was evaluated by a resazurin assay. The thiazolidinedione-hydroxamates were solubilized in DMSO (Sigma-Aldrich) at stock concentration of 10 mM. A two-fold serial dilution of each compound was made in liquid Middlebrook 7H9 broth (Sigma-Aldrich) with 10% oleic acid, albumin, dextrose, catalase (OADC) enrichment (BD Biosciences; complete 7H9 broth) with final concentrations ranging from 64 to 0.25  $\mu\text{M}$ . Volumes of 100  $\mu\text{l}$  of the serial dilutions were added in triplicate to flat-bottomed 96-well plates. A mycobacterial suspension was prepared by thawing and dissolving a frozen glycerol-stock of *Mtb* H37Ra and, subsequently, diluting it in complete 7H9 broth to obtain a suspension with an appropriate inoculum size. A volume of 100  $\mu\text{l}$  of the mycobacterial suspension was added to each well of the test plates. Isoniazid was used as a reference drug. Positive (100% growth) and negative (0% growth) controls were included as well. Test plates were incubated at 37 °C for 7 days. After 7 days of exposure, extracellular mycobacterial replication was assessed by resazurin. To each test well, 20  $\mu\text{l}$  of a 0.02% resazurin (Sigma-Aldrich) solution was added. Test plates were incubated at 37 °C until a color change from blue to pink occurred. Fluorescence was measured at  $\lambda_{\text{ex}} = 550 \text{ nm}$  and  $\lambda_{\text{em}} = 590 \text{ nm}$  using a spectrophotometer (Promega Discover). Results were presented as the mean of triplicate values.

#### 5.6. Assessment of acute in vitro cytotoxicity

The 50% cytotoxic concentration towards the RAW264.7 murine macrophage cell line (ATCC® TIB-71™) was determined by a neutral red uptake (NRU) assay. The RAW264.7 cells were cultured in Dulbecco's modified Eagle's medium (DMEM; Thermo Fisher) supplemented with 10% (v/v) heat-inactivated fetal calf serum (iFCS; Thermo Fisher) in a 5%  $\text{CO}_2$  atmosphere at 37 °C until a semi-confluent layer of cells was obtained. Next, the cells were harvested and seeded into transparent, flat-bottomed 96-well plates at a density of 40,000 cells per well and left for recovery at 37 °C and 5%  $\text{CO}_2$ . The following day, twofold serial dilutions of the tested compounds were made in DMEM +10% iFCS with a final starting concentration of 128  $\mu\text{M}$ . As a positive control, tamoxifen (Sigma-Aldrich) was included. The RAW264.7 cells were washed with sterile phosphate-buffered saline (PBS; Thermo Fisher) and exposed to the compounds by adding volumes of 100  $\mu\text{l}$  of the serial dilutions. Tamoxifen was used as a reference drug. Test plates were left for 24 h at 37 °C and 5%  $\text{CO}_2$ . After 24 h exposure to the compounds, the cells were washed two times with sterile PBS and 100  $\mu\text{l}$  neutral red (Sigma-Aldrich) working solution was added per well. Subsequently, the test plates were incubated for 3 h at 37 °C and 5%  $\text{CO}_2$ . The cells were washed again with sterile PBS and 150  $\mu\text{l}$  of a 1:1 ethanol/acetic acid (Merck) mixture was added in each well. The plates were left shaking until the color became homogeneous purple, and the optical density was measured at 530 nm and 620 nm (reference wavelength) using a plate reader (Promega Discover). Results were presented as the mean of triplicate values.

#### 5.7. Macrophage infection assay

The intracellular activity of the thiazolidinedione-hydroxamates was tested by infecting the murine RAW264.7 macrophage cell line with *Mtb* H37Ra<sup>lux</sup>, a laboratory *Mtb* H37Ra strain transformed with a pSMT1 luciferase reporter plasmid. The RAW264.7 cells were cultured, harvested and seeded into transparent, flat-bottomed 96-well plates as described above. Upon recovery, the cells were washed with sterile PBS and infected with H37Ra<sup>lux</sup> at a multiplicity of infection (MOI) of 10 for 2 h at 37 °C. RAW264.7 cells were washed two times with sterile PBS, incubated with 100  $\mu\text{g}/\text{ml}$  gentamicin (Sigma-Aldrich) for 1 h to kill the residual extracellular bacteria and, again, washed with sterile PBS. Then, the infected RAW264.7 cells were treated with the thiazolidinedione-hydroxamates at a final test concentration of 10 and 100  $\mu\text{M}$ . Isoniazid was included as a reference drug at 0.1  $\mu\text{M}$ . Uninfected cells were used as control. At 24 h post-exposure, the infected RAW264.7 cells were washed and lysed with 200  $\mu\text{l}$  of 1% Triton X-100 (Sigma-Aldrich). To assess the intracellular mycobacterial replication, 25  $\mu\text{l}$  of 1% (v/v) *n*-decanol in ethanol was added to 100  $\mu\text{l}$  of the lysate and luminescence was measured using a luminometer (Promega Discover). Results were presented the mean of triplicate values.

#### 5.8. In silico molecular docking

All 3D structures of the designed library of ligands were obtained with Marvin 15.1.5, software which can be used for drawing, displaying and characterization of chemical structure, substructures and reactions. Polar hydrogens were added to all ligands and proteins with the AutoDock Tools program [45]. Docking of the library of the structures into *Mycobacterium tuberculosis* zinc metalloprotease Zmp1 (PDB ID: 3ZUK) was carried out using AutoDock Vina 1.1.2 [46]. A grid box with the edge of 21 Å was centred on the active site of Zmp1 in the crystal structure (grid x: 95.8, y: 93.2, z: 33.0). The exhaustiveness parameter was set to 80 (default: 8).



After docking, we compared the docked poses in bulk and that of the compound **2n** was further analyzed and interpreted.

### Acknowledgements

This work was supported by grant no. JG\_2019\_002 from Palacký University in Olomouc.

### Appendix A. Supplementary data

Supplementary data to this article can be found online at <https://doi.org/10.1016/j.ejmech.2019.111812>.

### References

- M. Pai, M.A. Behr, M. Divangahi, D. Menzies, M. Pai, D. Dowdy, K. Dheda, C.C. Boehme, A. Ginsberg, S. Swaminathan, M. Spigelman, H. Getahun, M. Raviglione, Tuberculosis, Nat. Rev. Dis. Prim. 2 (2016) 16076.
- World Health Organization (WHO), Global Tuberculosis Report 2018, 2018 (Geneva).
- World Health Organization (WHO), WHO Consolidated Guidelines on Drug-Resistant Tuberculosis Treatment, 2019 (Geneva).
- World Health Organization (WHO), Implementing the End TB Strategy: the Essentials, 2015 (Geneva).
- K.C. Chang, C.C. Leung, E. Nuernberger, G. Sotgiu, New drugs and regimens for tuberculosis, Respirology 23 (2018) 978–990.
- R. Mehra, L.A. Khan, A. Nargotra, Anti-tubercular drug discovery: in silico implications and challenges, Eur. J. Pharm. Sci. 104 (2017) 1–15.
- D.M. Ferraris, D. Sbardella, A. Petrer, S. Marini, B. Amstutz, M. Coletta, P. Sander, M. Rizzi, Crystal structure of Mycobacterium tuberculosis zinc-dependent metalloprotease-1 (Zmp1), a metalloprotease involved in pathogenicity, J. Biol. Chem. 286 (2011) 32475–32482.
- S.S. Master, S.K. Rampini, A.S. Davis, C. Keller, S. Ehlers, B. Springer, G.S. Timmins, P. Sander, V. Deretic, Mycobacterium tuberculosis prevents inflammasome activation, Cell Host Microbe 3 (2008) 224–232.
- V. Lazarevic, F. Martinon, Linking inflammasome activation and phagosome maturation, Cell Host Microbe 3 (2008) 199–200.
- D.M. Ferraris, R. Miggiano, F. Rossi, M. Rizzi, Mycobacterium tuberculosis molecular determinants of infection, survival strategies, and vulnerable targets, Pathogens 7 (2018).
- D.M. Ferraris, M. Rizzi, Zinc-dependent Metalloprotease-1 (Zmp1), John Wiley & Sons Ltd., 2013, pp. 1–7.
- G. Hu, G. Lin, M. Wang, L. Dick, R.M. Xu, C. Nathan, H. Li, Structure of the Mycobacterium tuberculosis proteasome and mechanism of inhibition by a peptidyl boronate, Mol. Microbiol. 59 (2006) 1417–1428.
- A.F. Kisselev, Z. Songyang, A.L. Goldberg, Why does threonine, and not serine, function as the active site nucleophile in proteasomes? J. Biol. Chem. 275 (2000) 14831–14837.
- M. Mori, F. Moraca, D. Deodato, D.M. Ferraris, P. Selchow, P. Sander, M. Rizzi, M. Botta, Discovery of the first potent and selective Mycobacterium tuberculosis Zmp1 inhibitor, Bioorg. Med. Chem. Lett 24 (2014) 2508–2511.
- M. Mori, D. Deodato, M. Kasula, D.M. Ferraris, A. Sanna, A. De Logu, M. Rizzi, M. Botta, Design, synthesis, SAR and biological investigation of 3-(carboxymethyl)rhodanine and aminothiazole inhibitors of Mycobacterium tuberculosis Zmp1, Bioorg. Med. Chem. Lett 28 (2018) 637–641.
- M. Paolino, M. Brindisi, A. Vallone, S. Butini, G. Campiani, C. Nannicini, G. Giuliani, M. Anzini, S. Lamponi, G. Giorgi, D. Sbardella, D.M. Ferraris, S. Marini, M. Coletta, I. Palucci, M. Minerva, G. Delogu, I. Pepponi, D. Goletti, A. Cappelli, S. Gemma, S. Brogi, Development of potent inhibitors of the Mycobacterium tuberculosis virulence factor Zmp1 and evaluation of their effect on mycobacterial survival inside macrophages, ChemMedChem 13 (2018) 422–430.
- D.D. Subbedar, M.H. Shaikh, B.B. Shingate, L. Nawale, D. Sarkar, V.M. Khedkar, K.F. Kalam, J.N. Sangshetti, Quinolindene-rhodanine conjugates: facile synthesis and biological evaluation, Eur. J. Med. Chem. 125 (2017) 385–399.
- D.D. Subbedar, M.H. Shaikh, L. Nawale, A. Yeware, D. Sarkar, F.A. Kalam Khan, J.N. Sangshetti, B.B. Shingate, Novel tetrazoloquinoline-rhodanine conjugates: highly efficient synthesis and biological evaluation, Bioorg. Med. Chem. Lett 26 (2016) 2278–2283.
- S. Ponnuchamy, S. Kanchithalaivan, R. Ranjith Kumar, M. Ashraf Ali, T. Soo Choon, Antimycobacterial evaluation of novel hybrid arylidene thiazolidine-2,4-diones, Bioorg. Med. Chem. Lett 24 (2014) 1089–1093.
- N.B. Patel, I.H. Khan, Synthesis of newer 5-benzylidene-2,4-thiazolidinediones as potential antimicrobials, Indian J. Res. Pharm. Biotechnol. 2 (9) (2014) 993–1001.
- F.M. Shaikh, N.B. Patel, D. Rajani, Synthesis of new thiazolidine-2,4-dione derivatives and their antimicrobial and antitubercular activity, Indian J. Res. Pharm. Biotechnol. 1 (2013) 496–503.
- J.A. Jacobsen, J.L. Major Jourden, M.T. Miller, S.M. Cohen, To bind zinc or not to bind zinc: an examination of innovative approaches to improved metalloprotease inhibition, Biochim. Biophys. Acta Mol. Cell Res. 1803 (2010) 72–94.
- M.W. Majewski, S. Cho, P.A. Miller, S.G. Franzblau, M.J. Miller, Syntheses and evaluation of substituted aromatic hydroxamates and hydroxamic acids that target Mycobacterium tuberculosis, Bioorg. Med. Chem. Lett 25 (2015) 4933–4936.
- M. Flipo, T. Beghyn, J. Charton, V.A. Leroux, B.P. Deprez, R.F. Deprez-Poulain, A library of novel hydroxamic acids targeting the metallo-protease family: design, parallel synthesis and screening, Bioorg. Med. Chem. 15 (2007) 63–76.
- Y.M. Lin, M.J. Miller, Practical synthesis of hydroxamate-derived siderophore components by an indirect oxidation method and syntheses of a DIG-siderophore conjugate and a biotin-siderophore conjugate, J. Org. Chem. 64 (1999) 7451–7458.
- K. Kar, U. Krithika, Mithuna, P. Basu, S. Santhosh Kumar, A. Reji, B.R. Prashantha Kumar, Design, synthesis and glucose uptake activity of some novel glitazones, Bioorg. Chem. 56 (2014) 27–33.
- S. Mohanty, A.K. Roy, V.K.P. Kumar, S.G. Reddy, A.C. Karmakar, Acetic anhydride-promoted one-pot condensation of 2,4-thiazolidinedione with bisulfite adducts of aldehydes, Tetrahedron Lett. 55 (2014) 4585–4589.
- U.R. Pratap, D.V. Jawale, R.A. Waghmare, D.L. Lingampalle, R.A. Mane, Synthesis of 5-arylidene-2,4-thiazolidinediones by Knoevenagel condensation catalyzed by Baker's yeast, New J. Chem. 35 (2011) 49–51.
- D. Lagorce, O. Sperandio, J.B. Baell, M.A. Miteva, B.O. Villoutreix, FAF-Drugs3: a web server for compound property calculation and chemical library design, Nucleic Acids Res. 43 (2015) W200–W207.
- F. Cheng, W. Li, Y. Zhou, J. Shen, Z. Wu, G. Liu, P.W. Lee, Y. Tang, admetSAR: a comprehensive source and free tool for assessment of chemical ADMET properties, J. Chem. Inf. Model. 52 (2012) 3099–3105.
- S. Chander, P. Ashok, D. Cappel, P. Cos, S. Murugesan, Design, synthesis and biological evaluation of novel quinoline-based carboxylic hydrazides as anti-tubercular agents, Chem. Biol. Drug Des. 88 (2016) 585–591.
- S. Chander, P. Ashok, D. Cappel, P. Cos, S. Murugesan, Design, synthesis and biological evaluation of novel quinoline-based carboxylic hydrazides as anti-tubercular agents, Chem. Biol. Drug Des. 88 (2016) 585–591.
- W.L. Jorgensen, E.M. Duffy, Prediction of drug solubility from Monte Carlo simulations, Bioorg. Med. Chem. Lett 10 (2000) 1155–1158.
- D.F. Veber, S.R. Johnson, H.Y. Cheng, B.R. Smith, K.W. Ward, R.D. Kopple, Molecular properties that influence the oral bioavailability of drug candidates, J. Med. Chem. 45 (2002) 2615–2623.
- J.A. Carson, T. Ansaï, S. Awano, W. Yu, T. Takehara, A.J. Turner, Characterization of PgpPepO, a bacterial homologue of endothelin-converting enzyme-1, Clin. Sci. (Lond.) 103 (Suppl 48) (2002) 90S–93S.
- M. Bucknall, K.Y.C. Fung, M.W. Duncan, Practical quantitative biomedical applications of MALDI-TOF mass spectrometry, J. Am. Soc. Mass Spectrom. 13 (2002) 1015–1027.
- N.V. Gogichaeva, T. Williams, M.A. Alterman, MALDI TOF/TOF tandem mass spectrometry as a new tool for amino acid analysis, J. Am. Soc. Mass Spectrom. 18 (2007) 279–284.
- Y. Zheng, X. Jiang, F. Gao, J. Song, J. Sun, L. Wang, X. Sun, Z. Lu, H. Zhang, Identification of plant-derived natural products as potential inhibitors of the Mycobacterium tuberculosis proteasome, BMC Complement Altern. Med. 14 (2014) 400–401, 4007.
- E. Torfs, J. Vajs, M. Bidart de Macedo, F. Cools, B. Vanhoutte, Y. Gorbanev, A. Bogaerts, L. Verschaeve, G. Caljon, L. Mies, P. Delputte, P. Cos, J. Kosmrlj, D. Cappel, Synthesis and in vitro investigation of halogenated 1,3-bis(4-nitrophenyl)triazene salts as antitubercular compounds, Chem. Biol. Drug Des. 91 (2018) 631–640.
- R.J. Smets, E. Torfs, F. Lemiere, P. Cos, D. Cappel, K. Abbaspour Tehrani, Synthesis and antitubercular activity of 1- and 3-substituted benzo[g]isoquinoline-5,10-diones, Org. Biomol. Chem. 17 (2019) 2923–2939.
- D. Cappel, P. Claes, J. Jacobs, R. Anthonissen, V. Mathys, L. Verschaeve, K. Huygen, N.D. Kimpe, 1,2,3,4,8,9,10,11-Octahydrobenzo[j]phenanthridine-7,12-diones as New Leads against Mycobacterium tuberculosis, J. Med. Chem. 57 (2014) 2895–2907.
- R. Wang, X. Fang, Y. Lu, C.Y. Yang, S. Wang, The PDBbind database: methodologies and updates, J. Med. Chem. 48 (2005) 4111–4119.
- C. Oefner, A. D'Arcy, M. Hennig, F.K. Winkler, G.E. Dale, Structure of human neutral endopeptidase (neprilysin) complexed with phosphoramidon, J. Mol. Biol. 296 (2000) 341–349.
- A. Wisner, E. Dufour, M. Messaoudi, A. Nejd, A. Marcel, M.N. Ungeheuer, C. Rougeot, Human Opiorphin, a natural antinociceptive modulator of opioid-dependent pathways, Proc. Natl. Acad. Sci. U.S.A. 103 (2006) 17979–17984.
- G.M. Morris, R. Huey, W. Lindstrom, M.F. Sanner, R.K. Belew, D.S. Goodsell, A.J. Olson, AutoDock, AutoDockTools, Automated docking with selective receptor flexibility, J. Comput. Chem. 30 (2009) 2785–2791.
- O. Trott, A.J. Olson, AutoDock Vina, Improving the speed and accuracy of docking with a new scoring function, efficient optimization, and multithreading, J. Comput. Chem. 31 (2010) 455–461.

## Medicinal Chemistry &amp; Drug Discovery

## Benzoxazole Derivatives as Promising Antitubercular Agents

Veronika Šlachtová<sup>[b]</sup> and Lucie Brulíková<sup>\*[a]</sup>

Tuberculosis (TB) is an infectious disease caused predominantly by bacillus *Mycobacterium tuberculosis* (MTB). The increasing prevalence of multidrug-resistant MTB necessitates the discovery and development of alternative drugs against tuberculosis with a new mechanism of action. Over the past years, several benzoxazole derivatives have been synthesized and screened for their biological activity. Interestingly, some of them had

promising antitubercular activity. Despite that, none of the benzoxazole derivatives has entered the phase of the preclinical hit-to-lead optimization step in anti-TB research. In this review, we are summarizing recently published articles that evaluate the potency of benzoxazole heterocycle in the development of novel anti-TB agents and outlined the future aspects of this promising heterocycle.

## 1. Introduction

TB is a bacterial infection caused by *Mycobacterium tuberculosis* (MTB) which belongs to *Mycobacterium tuberculosis complex* (MTC). MTB is a very slow-growing, intracellular organism known for its lipid-rich cell wall. Consequently, the treatment of infected patients requires the use of multiple-drug therapy for several months. Moreover, an increasing number of the MTB strains are becoming resistant to one or more of the standard anti-TB drugs, which complicate treatment and the rise of the number of people affected by drug-resistant TB and latent TB is alarming. Multidrug-resistant (MDR) tuberculosis is defined by its *in vitro* resistance to at least isoniazid (INH) and rifampicin; while extensively drug-resistant (XDR) TB is resistant to at least one fluoroquinolone and one second-line anti-TB drug in addition to INH and rifampicin.<sup>[1–6]</sup> The occurrence of MDR and XDR MTB infections intensified the efforts to discover novel anti-TB agents with a new mode of action and directed at yet unknown targets of MTB.

The current situation and effort to effectively control TB requires development of new antitubercular agents acting on new targets. Overall, new antitubercular drug should meet at least some of these criteria: (1) be more potent than the existing drugs; (2) should have a good safety profile; (3) should be able to reduce the duration of therapy; (4) should be effective to treat multidrug-resistant and extensively drug-resistant tuberculosis; (5) should be compatible with concomitant ART since many patients are co-infected with HIV, and (6) should have no antagonistic activity against other tuberculosis drugs in the treatment regimen. With no doubt, the discovery

of entirely new compounds with an alternative mechanism of action to the existing therapeutics remains challenging.

Over the past years, the benzoxazole skeleton was found to have a wide range of biological activities and it is currently one of the most important scaffolds found in pharmacologically active compounds. As a consequence of this enormous interest, benzoxazole heterocycles and their biological properties have been reviewed many times.<sup>[7–10]</sup> Furthermore, variously substituted benzoxazoles have been found in many natural products such as Boxazomycin A, Calcimycin or Nakijinol B (Figure 1).<sup>[11–13]</sup>

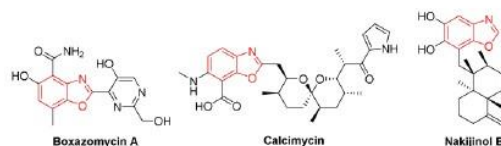


Figure 1. Benzoxazoles as component of natural products.

Inspired by the nature, researchers synthesized a variety of benzoxazole derivatives and screened for their biological activity<sup>[7–9]</sup> which resulted in several marketed drugs (Figure 2).<sup>[14–18]</sup>

Two different synthetic approaches were applied to prepare different benzoxazoles: (a) solution-phase synthetic approach and (b) solid-phase synthetic approach. Both of these approaches have been clearly summarized in 2017.<sup>[19]</sup> A conventional solution-phase synthetic approach (Figure 3) comprises the condensation of *o*-aminophenols with aldehydes<sup>[20–22]</sup> or carboxylic acids.<sup>[23–25]</sup> Benzoxazoles can also be synthesized *via* the condensation of *o*-aminophenols with ortho-esters<sup>[26]</sup> or 1,1-dihaloalkenes.<sup>[27,28]</sup>

Solid-phase synthetic approach covers the efficient methods leading to benzoxazole libraries formed by combinatorial

[a] Dr. L. Brulíková  
Department of Medicinal Chemistry, Institute of Molecular and Translational Medicine, Hněvotínská 5, Olomouc, Czech Republic, 77900  
E-mail: lucie.brulikova@upol.cz

[b] V. Šlachtová  
Department of Organic Chemistry, Faculty of Science, 17. listopadu 12, Olomouc, Czech Republic, 77146



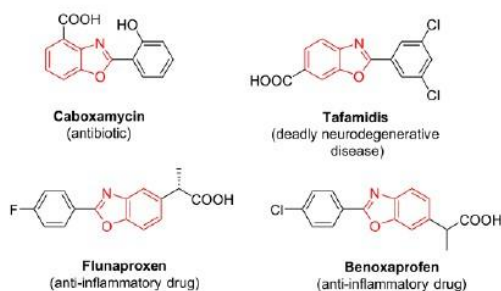


Figure 2. Marketed drugs based on the benzoxazole structure.

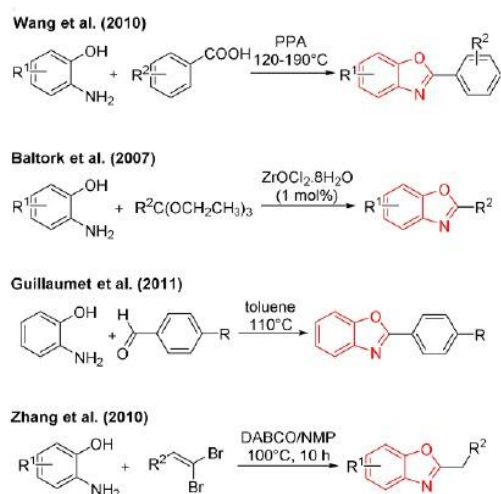


Figure 3. Solution-phase methods leading to benzoxazoles.

assembly (Figure 4). Wang et al. reported the synthesis of benzoxazole using Wang resin,<sup>[29]</sup> Beebe et al. used polystyrene-based linker and 3-nitrotyrosins,<sup>[30]</sup> Chen with coworkers established a strategy on PEG-5000 soluble support.<sup>[31]</sup> Gong

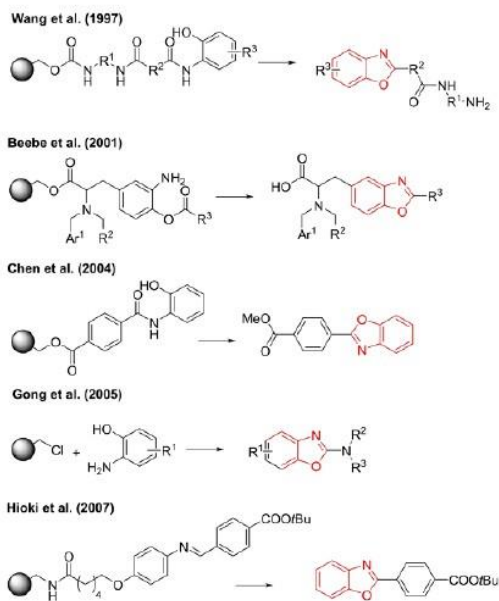


Figure 4. Solid-phase methods leading to benzoxazoles.

and his coworkers described the solid-supported synthesis using Merrifield resin<sup>[32]</sup> and Hioki with his group reported solid-phase synthesis with use of a traceless aniline linker.<sup>[33]</sup>

Both above mentioned approaches produced a number of interesting compounds. The unflagging effort resulted in several above mentioned marketed drugs. Despite that, none of the benzoxazole derivatives has entered the phase of the preclinical hit-to-lead optimization step in anti-TB research.

For this reason, benzoxazole-based compounds remain promising heterocyclic scaffold and the detailed SAR studies might reveal entirely new approach to help with the struggles to find a new treatment against tuberculosis. In this review, we will focus on benzoxazole derivatives as promising antitubercular agents considering the type and position of substitution and also the future aspects in anti-TB research.



Lucie Brulíková received her Ph.D. in Organic Chemistry at Charles University in Prague under supervising of prof. Antonín Holý. After that, she joined prof. Hlaváč group at Department of Organic chemistry, Palacky University in Olomouc, where she is currently working as assistant professor. In 2017 she set up junior research group focused on the design and development of new antituberculars.



Veronika Šlachtová studied at Faculty of Pharmacy in Brno, where she also received her M.Sc degree in 2017. Afterwards, she joined the group of Lucie Brulíková as a doctoral student. Her research interest is solution-phase as well as solid-phase synthesis of biologically active compounds.

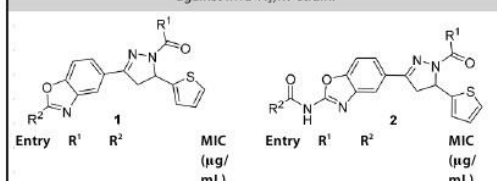
## 2. Benzoxazoles as anti-TB agents

Benzoxazole skeleton has been studied as antitubercular agent since 1949.<sup>[34]</sup> However, this structure has attracted the considerable attention mostly during the last two decades. Different substituents can be incorporated onto the benzene ring to improve the biological activity; especially the substitution at the position 2 and 5 is influential.

### 2.1. Benzoxazole-pyrazoline derivatives

Pyrazoline heterocycle has been found to have an interesting antitubercular activity.<sup>[35–37]</sup> Considering this fact, Soni group designed and synthesized a series of novel pyrazoline based benzoxazole derivatives **1** and **2** (Table 1) and screened for their

**Table 1.** *In vitro* antitubercular activity of pyrazoline-benzoxazoles **1** and **2** against *MTB* H<sub>37</sub>Rv strain.



Entry	R <sup>1</sup>	R <sup>2</sup>	MIC (µg/mL)	Entry	R <sup>1</sup>	R <sup>2</sup>	MIC (µg/mL)
<b>1a</b>	CH <sub>3</sub>	SH	6.25	<b>1m</b>	CH <sub>3</sub>	4-pyridyl	25
<b>1b</b>	CH <sub>3</sub>	NH <sub>2</sub>	6.25	<b>1n</b>	NH <sub>2</sub>	NH <sub>2</sub>	6.25
<b>1c</b>	CH <sub>3</sub>	C <sub>6</sub> H <sub>5</sub>	25	<b>1o</b>	NH <sub>2</sub>	SH	12.5
<b>1d</b>	CH <sub>3</sub>	2-ClC <sub>6</sub> H <sub>4</sub>	25	<b>2a</b>	CH <sub>3</sub>	CH <sub>3</sub>	25
<b>1e</b>	CH <sub>3</sub>	2-OMeC <sub>6</sub> H <sub>4</sub>	25	<b>2b</b>	CH <sub>3</sub>	CH(CH <sub>3</sub> ) <sub>2</sub>	25
<b>1f</b>	CH <sub>3</sub>	3-OMeC <sub>6</sub> H <sub>4</sub>	25	<b>2c</b>	CH <sub>3</sub>	CH <sub>2</sub> CH <sub>2</sub> CH <sub>3</sub>	12.5
<b>1g</b>	CH <sub>3</sub>	4-OMeC <sub>6</sub> H <sub>4</sub>	12.5	<b>2d</b>	CH <sub>3</sub>	CH <sub>2</sub> Cl	6.25
<b>1h</b>	CH <sub>3</sub>	4-OHC <sub>6</sub> H <sub>4</sub>	0.8	<b>2e</b>	CH <sub>3</sub>	C <sub>6</sub> H <sub>5</sub>	6.25
<b>1i</b>	CH <sub>3</sub>	3,4,5-(OMe) <sub>3</sub> C <sub>6</sub> H <sub>2</sub>	25	<b>2f</b>	CH <sub>3</sub>	2-ClC <sub>6</sub> H <sub>4</sub>	25
<b>1j</b>	CH <sub>3</sub>	CH <sub>3</sub> C <sub>6</sub> H <sub>5</sub>	50	<b>2g</b>	CH <sub>3</sub>	2-OMeC <sub>6</sub> H <sub>4</sub>	25
<b>1k</b>	CH <sub>3</sub>	2-pyridyl	25	<b>2h</b>	CH <sub>3</sub>	3-ClC <sub>6</sub> H <sub>4</sub>	12.5
<b>1l</b>	CH <sub>3</sub>	3-pyridyl	25	<b>2i</b>	CH <sub>3</sub>	3-OMeC <sub>6</sub> H <sub>4</sub>	1.6

activity against *MTB* H<sub>37</sub>Rv, MDR-TB and XDR-TB strains.<sup>[38]</sup> Two compounds of these series had interesting activity, even better than all of the standard drugs (Streptomycin (6.25 µg/mL), Pyrazinamide (3.12 µg/mL) and Ciprofloxacin (3.12 µg/mL)) with value 0.8 µg/mL (**1h**) and 1.6 µg/mL (**2i**) against *MTB* H<sub>37</sub>Rv strain.

In 2014 Brahmshatriya group reported two papers focused on combining of the pyrazoline and benzoxazole pharmacophores.<sup>[39,40]</sup> *In vitro* antitubercular activity evaluation of the first group of compounds against *MTB* H<sub>37</sub>Rv, MDR-TB and XDR-TB revealed significant potency of target compounds **3** (Table 2). Most of the prepared compounds had potent activity (MIC value 1.25–25 µg/mL) against H<sub>37</sub>Rv strain. More interestingly, a few compounds showed better antitubercular activity than INH against MDR-TB and XDR-TB strains.<sup>[39]</sup>

The second group of conjugates (Table 3) revealed a few analogues with an activity comparable with INH against H<sub>37</sub>Rv strain (**4a**) and against MDR-TB strain (**4a**, **4k** and **4n**).<sup>[40]</sup>

In 2016, Devi group reported QSAR (Monte Carlo method) and docking studies of benzoxazole-pyrazoline based structures **4**.<sup>[41]</sup> Their computational results indicate that the presence of F or Cl substitution is preferred to Br and I, thiol group is preferred to amino group and OH or CH<sub>3</sub> group are more preferable than OCH<sub>3</sub>. These results might be valuable for the design of further benzoxazole-pyrazoline compounds with potent antitubercular activity.

### 2.2. Benzoxazoles with 2-phenyl/benzyl substitution

Recently, Temiz-Arpaci group published two articles describing a series of 2-phenyl/benzyl substituted benzoxazoles with potent antimicrobial activity.<sup>[42,43]</sup> Firstly, they described the synthesis of series of benzyl substituted benzoxazoles **5** and their antitubercular activity against *MTB* and its isolate (Table 4).<sup>[42]</sup> Further, authors suggested that a [4-(*p*-chloro/fluoro-phenyl)piperazin-1-yl]acetamido moiety in position 5 might permit an easier penetration through the lipophilic mycobacterial cell wall. The series of ten tested compounds revealed certain structure-activity relationships reflected the presence of halogen (F or Cl). On the other hand, all of the tested compounds were less active than the reference drugs (INH and ethambutol).

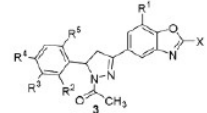
Three years later, Temiz-Arpaci et al. modified the structure **5** with *p*-tert-butylphenyl moiety giving compounds **6** (Table 5).<sup>[43]</sup> Again, they expected that a lipophilic *p*-tert-butylphenyl moiety in the position 2 of the benzoxazole part might improve the penetration through the lipophilic mycobacterial cell wall. Unfortunately, neither this substitution of benzoxazole skeleton brought better results than those from the previous report. The best MIC values were 8 µg/mL.

In 2016, Ertan-Bolelli et al. reported the synthesis and biological evaluation of 5-amino-2-(4-substitutedphenyl)-benzoxazoles **7** and **8** (Table 6).<sup>[44]</sup> Few of the tested compounds had interesting antitubercular activity with MIC value of 8 µg/mL. Moreover, molecular docking of the most active compounds from this series into the active site of InhA revealed interaction with Tyr158 and/or co-factor NAD<sup>+</sup>. For this reason, compounds **7a**, **7c** and **7f** might be considered as promising scaffolds for new potent anti-TB drugs.

### 2.3. Benzylsulfanyl benzoxazoles

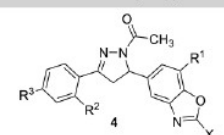
Benzylsulfanyl modification of the benzoxazole skeleton revealed promising results in the field of anti-TB research. In 2002 and subsequently in 2009, Klimešová et al. reported synthesis and biological evaluation of 2-benzylsulfanyl benzoxazole derivatives **9** (Table 7).<sup>[45,46]</sup> Moreover, compounds **9e** and **9i** were tested against MDR *M. tuberculosis* (*MTB* 7357/98, 4166/04, 4977/03 and 550/04). Compound **9e** exhibited significant activity against both sensitive and resistant strains of *MTB* (MIC value 2–4 µmol/L). In contrast, derivative **9i** had activity with MIC value 8–32 µmol/L. Furthermore, benzoxazole **9e**

Table 2. *In vitro* antitubercular activity and cytotoxicity of pyrazoline-benzoxazoles 3.



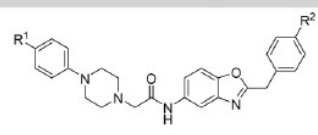
Entry	X	R <sup>1</sup>	R <sup>2</sup>	R <sup>3</sup>	R <sup>4</sup>	R <sup>5</sup>	MIC (µg/mL)		XDR-TB	Cytotoxicity IC50 (µg/mL)
							H <sub>37</sub> Rv	MDR-TB		
3a	SH	H	H	OCH <sub>3</sub>	OCH <sub>3</sub>	H	12.5	12.5	> 100	ND
3b	SH	H	H	H	OCH <sub>3</sub>	H	6.25	6.25	50	ND
3c	SH	H	Cl	H	H	H	6.25	12.5	> 100	ND
3d	SH	H	H	Cl	H	H	3.25	12.5	50	> 62.5
3e	SH	H	H	H	Cl	H	3.25	25	50	32.5
3f	SH	OCH <sub>3</sub>	H	OCH <sub>3</sub>	OCH <sub>3</sub>	H	6.25	12.5	50	ND
3g	SH	OCH <sub>3</sub>	H	H	OCH <sub>3</sub>	H	12.5	12.5	25	ND
3h	SH	OCH <sub>3</sub>	Cl	H	H	H	6.25	50	25	ND
3i	SH	OCH <sub>3</sub>	H	Cl	H	H	25	6.25	50	ND
3j	SH	OCH <sub>3</sub>	H	H	Cl	H	3.25	25	50	> 62.5
3k	SH	OCH <sub>3</sub>	OCH <sub>3</sub>	H	H	OCH <sub>3</sub>	12.5	50	12.5	> 62.5
3l	SH	OCH <sub>3</sub>	H	Br	H	H	1.25	3.25	12.5	> 62.5
3m	SH	OCH <sub>3</sub>	H	H	Br	H	3.25	25	25	32.5
3n	NH <sub>2</sub>	H	H	OCH <sub>3</sub>	OCH <sub>3</sub>	H	6.25	6.25	> 100	ND
3o	NH <sub>2</sub>	H	H	H	OCH <sub>3</sub>	H	12.5	25	50	ND
3p	NH <sub>2</sub>	H	Cl	H	H	H	25	25	50	ND
3q	NH <sub>2</sub>	H	H	Cl	H	H	25	50	> 100	ND
3r	NH <sub>2</sub>	H	H	H	Cl	H	6.25	3.25	> 100	ND
3s	NH <sub>2</sub>	OCH <sub>3</sub>	Cl	H	H	H	12.5	12.5	> 100	ND
3t	NH <sub>2</sub>	OCH <sub>3</sub>	H	H	Br	H	25	3.25	50	ND
INH	-	-	-	-	-	-	0.5	6.25	50	ND

Table 3. *In vitro* antitubercular activity of pyrazoline-benzoxazoles 4.



Entry	X	R <sup>1</sup>	R <sup>2</sup>	R <sup>3</sup>	MIC (µg/mL)	
					H <sub>37</sub> Rv	MDR-TB
4a	NH <sub>2</sub>	OCH <sub>3</sub>	H	H	0.625	6.25
4b	NH <sub>2</sub>	OCH <sub>3</sub>	Cl	Cl	12.5	12.5
4c	NH <sub>2</sub>	OCH <sub>3</sub>	H	F	6.25	25
4d	NH <sub>2</sub>	OCH <sub>3</sub>	Br	H	12.5	25
4e	NH <sub>2</sub>	H	H	H	25	25
4f	NH <sub>2</sub>	H	Br	H	25	12.5
4g	NH <sub>2</sub>	Cl	H	H	25	25
4h	NH <sub>2</sub>	Cl	Br	H	3.25	25
4i	SH	OCH <sub>3</sub>	H	H	6.25	12.5
4j	SH	OCH <sub>3</sub>	Cl	Cl	6.25	12.5
4k	SH	OCH <sub>3</sub>	H	F	12.5	6.25
4l	SH	OCH <sub>3</sub>	Br	H	12.5	25
4m	SH	H	H	H	25	25
4n	SH	H	Br	H	12.5	6.25
4o	SH	Cl	H	H	1.25	25
4p	SH	Cl	Br	H	6.25	12.5
INH	-	-	-	-	0.625	6.25

Table 4. *In vitro* antitubercular activity of benzoxazoles 5.



Entry	R <sup>1</sup>	R <sup>2</sup>	MIC (µg/mL)	
			H <sub>37</sub> Rv	MTB isolate
5a	Cl	Cl	32	8
5b	F	Cl	16	8
5c	Cl	CH <sub>3</sub>	64	32
5d	F	CH <sub>3</sub>	32	16
5e	Cl	H	64	16
5f	F	H	16	64
5g	Cl	F	8	8
5h	F	F	8	32
5i	Cl	Br	64	8
5j	F	Br	16	8
INH	-	-	< 0.25	< 0.25
ethambutol	-	-	2	2

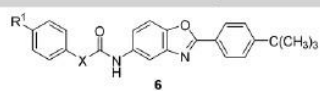
#### 2.4. Benzoxazole alkaloids

In 1999, Rodriguez et al. screened marine natural products from the West Indian gorgonian coral *Pseudopterogorgia elisabethae* with anti-TB properties.<sup>[47]</sup> Their effort resulted in the isolation of two active alkaloids – pseudopteroxazol **10** and its biogenetic precursor seco-pseudopteroxazole **11** (Figure 5). Pseudopteroxazol **10** exhibited potent growth inhibition (97%)

showed the lowest lipophilicity (log *P* = 3.779) and enlarged molar refractivity (MR = 84.365 Å<sup>3</sup>). All these results indicate that the introduction of benzyl moiety and two nitro groups increase the anti-TB activity compared to other substituent.



**Table 5.** *In vitro* antitubercular activity of benzoxazoles **6**.



Entry	R <sup>1</sup>	X	MIC (μg/mL)	
			H <sub>37</sub> Rv	MTB isolate
6a	H	-	8	8
6b	F	CH <sub>2</sub>	8	8
6c	F	-	16	32
6d	Br	-	128	128
6e	C <sub>2</sub> H <sub>5</sub>	-	32	32
6f	NO <sub>2</sub>	-	32	16
6g	H	CH <sub>2</sub>	8	32
6h	CH <sub>3</sub>	-	16	8
6i	Cl	-	64	16
6j	CH <sub>3</sub>	CH <sub>2</sub>	8	8
6k	C <sub>2</sub> H <sub>5</sub>	-	32	16
6l	CN	-	64	32
6m	OCH <sub>3</sub>	CH <sub>2</sub>	64	16
6n	NO <sub>2</sub>	CH <sub>2</sub>	32	32
6o	Br	CH <sub>2</sub>	16	8
INH	-	-	< 0.25	< 0.25
ethambutol	-	-	2	2

of *MTB* H<sub>37</sub>Rv with MIC value 12.5 μg/mL. On the other hand, seco-pseudopteroxazole **11** inhibited only 66% of mycobacterial growth.

Several years later, the same group reported biological evaluation of ileabethoxazole **12** (Figure 5), perhydroacenaphthene-type diterpene alkaloid from *Pseudopterogorgia elisabethae*.<sup>[48]</sup> This novel benzoxazole alkaloid showed interesting activity against *MTB* H<sub>37</sub>Rv at the concentration range of 128–64 μg/mL.

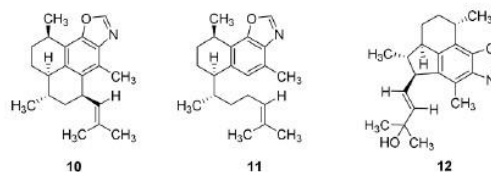


Figure 5. Structure of the benzoxazole alkaloids **10–12**.

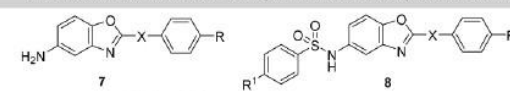
### 2.5. 2-Amino benzoxazoles and related structures

Between 1966–1973 Sycheva and others reported several papers describing various benzoxazoles amino-(or hydrazino)-modified at the position 2 (Figure 6).<sup>[49–53]</sup>

First attempts of Sycheva group at benzoxazole derivatization at the position 2 in order to reach active anti-TB compound led to the synthesis compounds **13** (Figure 6).<sup>[51]</sup> Investigation of anti-TB activity (H<sub>37</sub>Rv strain) of the synthesized compounds revealed that the most interesting activity possessed the thioamide of 6-ethoxy-2-benzoxazole carboxylic acid, 6-ethoxy-2-hydrazinobenzoxazole and 6-ethoxy-2-(thiazolyl-2'-amino)benzoxazole with MIC value 0.5 μg/mL, 4 μg/mL and 8 μg/mL, respectively (in the absence of serum). The presence of serum led to the dramatic decreasing in tuberculostatic activity.

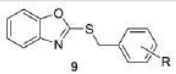
The consecutive *in vitro* tests of derivatives **14** (Figure 6) revealed interesting activity against H<sub>37</sub>Rv strain of thiazoyl compound **14b** with MIC value 0.5 μg/mL in absence of serum and 2 μg/mL in serum.<sup>[49]</sup> On the other hand, 2-pyridyl derivative **14a** showed lower activity (with MIC value 4 μg/mL in absence of serum and 15 μg/mL in serum). Moreover, the

**Table 6.** *In vitro* antitubercular activity of benzoxazole compounds **7** and **8**.



Entry	X	R	R <sup>1</sup>	MIC (μg/mL)		Entry	X	R	R <sup>1</sup>	MIC (μg/mL)	
				H <sub>37</sub> Rv	MTB isolate					H <sub>37</sub> Rv	MTB isolate
7a	-	H	-	8	8	8g	-	OCH <sub>3</sub>	NO <sub>2</sub>	64	16
7b	-	Cl	-	16	8	8h	CH <sub>2</sub>	H	NO <sub>2</sub>	32	16
7c	-	F	-	8	8	8i	CH <sub>2</sub>	Cl	NO <sub>2</sub>	32	16
7d	-	Br	-	8	32	8j	CH <sub>2</sub>	F	NO <sub>2</sub>	32	16
7e	-	C <sub>2</sub> H <sub>5</sub>	-	16	8	8k	CH <sub>2</sub>	Br	NO <sub>2</sub>	32	16
7f	-	CH <sub>3</sub>	-	8	8	8l	CH <sub>2</sub>	CH <sub>3</sub>	NO <sub>2</sub>	32	16
7g	-	OCH <sub>3</sub>	-	64	8	8m	-	H	NH <sub>2</sub>	64	32
7h	CH <sub>2</sub>	H	-	32	32	8n	-	Cl	NH <sub>2</sub>	64	64
7i	CH <sub>2</sub>	Cl	-	16	8	8o	-	F	NH <sub>2</sub>	64	64
7j	CH <sub>2</sub>	F	-	16	32	8p	-	Br	NH <sub>2</sub>	64	64
7k	CH <sub>2</sub>	Br	-	16	16	8q	-	C <sub>2</sub> H <sub>5</sub>	NH <sub>2</sub>	64	16
7l	CH <sub>2</sub>	CH <sub>3</sub>	-	32	64	8r	-	CH <sub>3</sub>	NH <sub>2</sub>	64	64
8a	-	H	NO <sub>2</sub>	64	32	8s	-	OCH <sub>3</sub>	NH <sub>2</sub>	64	64
8b	-	Cl	NO <sub>2</sub>	64	32	8t	CH <sub>2</sub>	H	NH <sub>2</sub>	32	16
8c	-	F	NO <sub>2</sub>	64	64	8u	CH <sub>2</sub>	Cl	NH <sub>2</sub>	16	16
8d	-	Br	NO <sub>2</sub>	64	32	8v	CH <sub>2</sub>	F	NH <sub>2</sub>	32	16
8e	-	C <sub>2</sub> H <sub>5</sub>	NO <sub>2</sub>	64	16	8w	CH <sub>2</sub>	Br	NH <sub>2</sub>	16	16
8f	-	CH <sub>3</sub>	NO <sub>2</sub>	64	64	8x	CH <sub>2</sub>	CH <sub>3</sub>	NH <sub>2</sub>	16	16

**Table 7.** *In vitro* antitubercular activity of benzoxazoles **9a-j**<sup>[46]</sup> and **9k-a**.<sup>[45]</sup>



Entry	R	MTB My 331/88 14 days	21 days
9a	H	250	500
9b	4-NO <sub>2</sub>	> 62	> 125
9c	3-NO <sub>2</sub>	> 62	125
9d	2-NO <sub>2</sub>	> 250	> 250
9e	3,5-NO <sub>2</sub>	8	8
9f	2,4-NO <sub>2</sub>	8	8
9g	4-CN	> 62	> 62
9h	3-CN	125	125
9i	4-CSNH <sub>2</sub>	8	16
9j	3-CSNH <sub>2</sub>	8	16
9k	4-Cl	250	> 500
9l	3-Cl	62	125
9m	2-Cl	> 250	> 250
9n	4-F	250	500
9o	3-F	62	125
9p	4-CH <sub>3</sub>	> 500	> 500
9q	3-CH <sub>3</sub>	250	500
9r	4-OCH <sub>3</sub>	62	125
9s	3-OCH <sub>3</sub>	125	250
9t	2-F	125	250
9u	4-Br	> 62	> 125
9v	3-Br	125	250
9w	2-F, 6-Cl	62	125
9x	3,4-Cl	> 125	> 250
9y	3,4-F	125	125
9z	2-F, 6-NO <sub>2</sub>	> 62	> 62
9aa	4-CF <sub>3</sub>	125	125
9ab	3-CF <sub>3</sub>	62	125
9ac	3,5-CF <sub>3</sub>	62	125
INH	-	0.5	1

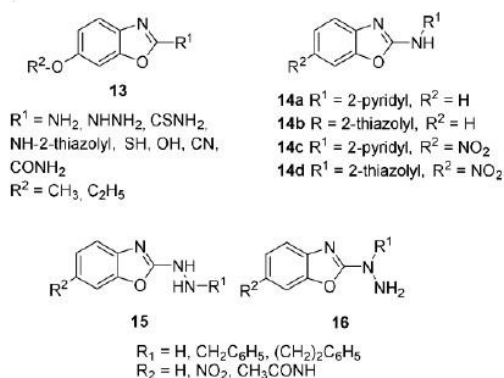


**Figure 6.** Structures of the 2-amino modified benzoxazoles **13–16**.

introduction of nitro group to the position 6 afforded compounds with decreased activity.

In 1967, Sycheva et al. broaden the series of their benzoxazole derivatives with (benzoxazol-2-yl) hydrazines **15** and **16** (Figure 6).<sup>[52]</sup> *In vitro* tuberculostatic activity testing showed 1-

phenyl-2-(benzoxazolyl-2')hydrazine and (6-nitrobenzoxazolyl-2) hydrazine as the most active compounds from this series (MIC = 4 µg/mL, without serum).

Based on the previous promising result showing the potency of 2-(2'-thiazolylamino)-benzoxazole, Sycheva and coworkers reported the synthesis and biological evaluation of 2-(2'-thiazolylamino)benzoxazole analogues **17** (Figure 7).<sup>[53]</sup>

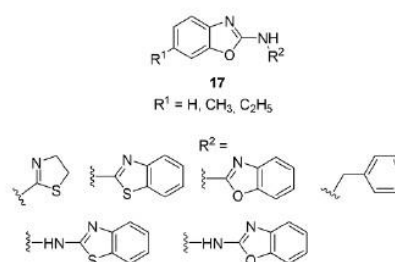


**Figure 7.** Structures of the 2-amino modified benzoxazoles **17**.

Results obtained from anti-TB testing against H<sub>37</sub>Rv strain indicated that the di(benzoxazolyl-2)-amine and *N*-benzothiazolyl-2-benzoxazolyl-2-amine are the most interesting compounds from this study with MIC value 2 and 8 µg/mL without serum, respectively. The presence of an alkoxy group in the position 6 decreases the activity.

Sycheva et al. also described a number of *N*-(benzoxazol-2-yl)-*N'*-phenylthioureas **18** (Figure 8).<sup>[50]</sup> Biological evaluation of

**Figure 8.** Structures of the benzoxazoles **18**.

**18** revealed, that the most active compound from this series, *N*-(2-benzoxazolyl)-*N'*-*p*-ethoxyphenylthiourea, inhibited the growth of *MTB* (strain H<sub>37</sub>Rv) at concentration of 2 µg/mL in the absence of serum (15 µg/mL in the presence of serum). In contrast, benzoxazole without *p*-ethoxy substitution had lower activity (8 µg/mL in the absence of serum, 250 µg/mL in serum), that indicates the importance of an alkoxy group in the *p*-position of the benzene ring. Furthermore, introduction of an alkyl group into the position 6 of the benzoxazole skeleton did not result in an increase in anti-TB activity.

The group of Khazi reported the synthesis and biological evaluation of benzoxazole derivatives of 1,3,4-thiadiazoles and

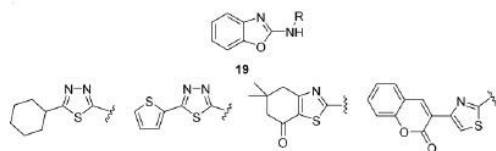


Figure 9. Structures of the benzoxazoles 19.

thiazoles 19 (Figure 9).<sup>[54]</sup> All prepared compounds were tested against *M. tuberculosis*; however, none of the tested compounds had interesting antitubercular activity.

Thiadiazole compounds represent other heterocyclic scaffold having very interesting pharmacological and biological profile. Based on this knowledge, Hegde et al. combined benzoxazole with thiadiazole heterocycle and obtained compounds 20 evaluated for their antitubercular properties against *MTB* H<sub>37</sub>Rv using the BACTEC 460 radiometric system (Figure 10). Both derivatives had a very good inhibitory activity against *MTB* H<sub>37</sub>Rv at < 6.25 µg/mL.<sup>[55]</sup>



Figure 10. Structure of the thiadiazole-based benzoxazoles 20.

## 2.6. 2-Substituted 5,7-di-tert-butylbenzoxazoles

Vinsova et al. paid their attention to the synthesis of lipophilic benzoxazoles, since lipophilic part in molecules may permit their easier penetration through the mycobacterial cell wall. Firstly, they reported the synthesis and biological evaluation of 2-substituted 5,7-di-tert-butylbenzoxazoles.<sup>[56,57]</sup> By the reaction of substituted benzoquinone with amino acids and dipeptides a series of several 5,7-di-tert-butylbenzoxazoles 21 was obtained (Figure 11). Unfortunately, none of the tested compounds had any promising anti-TB activity.<sup>[56]</sup>

After that, Vinsova and coworkers pursued the synthesis and biological evaluation of 2-substituted 5,7-di-tert-butylbenzoxazoles 22 and 23 (Figure 12).<sup>[57]</sup> All of the prepared benzoxazoles were screened for their antitubercular activity against *M. tuberculosis* H<sub>37</sub>Rv strain. Interestingly, 5,7-di-tert-butyl-2-(pyridin-4-yl)benzoxazole and 5,7-di-tert-butyl-2-styrylbenzoxazole exhibited the highest activity in vitro with MIC

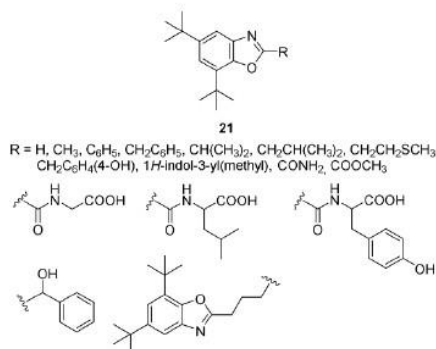


Figure 11. Structure of the tri-substituted benzoxazoles 21.

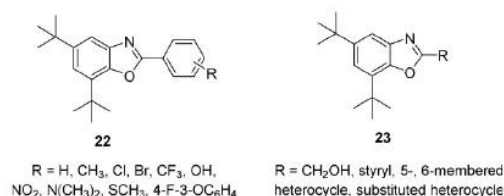


Figure 12. Structure of the tri-substituted benzoxazoles 22 and 23.

value 6.25 and 3.13 µg/mL, respectively (INH as standard – MIC value 0.02 µg/mL).

## 2.7. Others

Imramovsky et al. reported synthesis and biological evaluation of 2-[(*E*)-2-substituted-ethenyl]-1,3-benzoxazoles 24 (Figure 13).<sup>[58]</sup> In spite of the relatively large series of synthesized

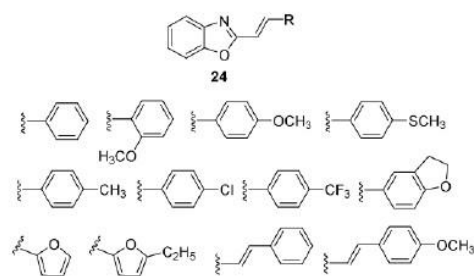


Figure 13. Structure of benzoxazoles 24.

compounds, none of them had any potential based on the anti-TB activity shown. However, derivatives modified with 4-



OMePh, 4-SMePh and 2,3-dihydro-1-benzofuran-5-yl moiety were active against *M. avium* 330/88 (MIC = 32-62.5; 62.5 and 32  $\mu\text{mol/L}$ , respectively). SAR observations also indicate that electron-donor groups (4-OMe) are favorable substituent.

Another promising scaffold was reported by Sycheva et al.<sup>[59]</sup> They designed and synthesized *S*-heterylmercaptoacetic acids comprising also the benzoxazoles **25** (Figure 14) and

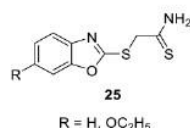


Figure 14. Structure of benzoxazoles **25**.

evaluated their biological activity. Compounds **25** substituted with ethoxy group was active against *MTB* H<sub>37</sub>Rv (MIC = 1  $\mu\text{g/mL}$ , without serum). However, studied benzoxazole **25** did not have appropriate pharmacological properties.

Sankar et al. reported *in silico* design, synthesis and biological evaluation of 1,3-benzoxazole-5-carbohydrazide **26** (Figure 15) that had *in vitro* activity against *MTB* H<sub>37</sub>Rv strain.<sup>[60]</sup> A small substitution in the position 2 enhances biological activity.

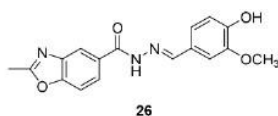


Figure 15. Structure of benzoxazoles **26**.

The group of Westwell published the synthesis and biological evaluation of several 4-hydroxycyclohexa-2,5-dienones.<sup>[61]</sup> Benzoxazole **27** (Figure 16) had potency against *MTB*

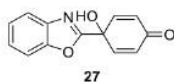


Figure 16. Structure of benzoxazoles **27**.

H<sub>37</sub>Rv with MIC value 1.56  $\mu\text{g/mL}$ . Moreover, benzoxazole **27** showed inhibition of *MTB* Thioredoxin C/Thioredoxin reductase signaling (IC<sub>50</sub> = 50  $\mu\text{M}$ ).

One of the best result to date emerged from a library of more than 60 novel quinolone analogues.<sup>[62]</sup> Compound **28** (Figure 17) showed a MIC value of 5.5  $\mu\text{M}$  and no measurable cytotoxicity. Moreover, this benzoxazole was found to have good blood stability and no hERG affinity.

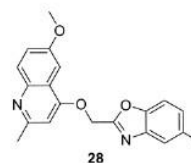


Figure 17. Structure of benzoxazole **28**.

### 3. Potential targets of benzoxazole-based compounds

The most promising approach against tuberculosis is targeting specific mycobacterial enzymes with small molecules. As a consequence of this external intervention, the disruption of some important cellular processes may occur. However, the discovery of novel anti-TB agents with a new mode of action and directed towards unknown targets of *MTB* remains also challenging.

The benzoxazole skeleton offers a number of interactions with the host protein. The planar aromatic heterocycle can act through the  $\pi$ - $\pi$  stacking, nitrogen and oxygen atoms can mediate the hydrogen bonding and lipophilic character may enable the hydrophobic interactions.

*Mycobacterium tuberculosis* enoyl acyl carrier protein reductase (*MtInhA*) is one of the most attractive enzymes to design and develop novel drugs for tuberculosis therapy<sup>[63-66]</sup> and might be a promising target for novel inhibitors active against MDR and XDR *MTB*.<sup>[67]</sup> Several benzoxazoles have been studied in respect to the *MtInhA* inhibition.<sup>[60]</sup> The synthesized benzoxazole-pyrazoline compounds **4** (Table 3) were docked into the enoyl-acyl carrier protein (ACP) reductase, a known molecular target of INH. Reported experiments showed a successful docking into the active site of enoyl-ACP reductase with significant contribution of benzoxazole core over the other two ring nucleus (pyrazoline, aryl). These results might indicate the potential target of benzoxazole-based compounds.

Further, Pauli et al. reported *in silico* approach that might reveal new *InhA* inhibitors.<sup>[66]</sup> Among others, benzoxazole **29** (Figure 18) was selected for *in vitro* evaluation. Pauli group

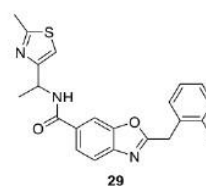


Figure 18. Structure of benzoxazole **29** as potent *InhA* inhibitor.

reported that benzoxazole **29** interacts via hydrogen bond to NADH and several hydrophobic interactions with the protein, including Ala198 (important to tight binding).

One of the other potential target of tuberculosis is *Mycobacterium protein tyrosine phosphatase B* (mPTPB). Zhang with co-workers applied the Diversity-Oriented Synthesis (DOS) strategy in order to find novel and selective drug-like inhibitors of this enzyme and synthesized a range of novel bicyclic salicylic acids as mPTPB inhibitors.<sup>[68]</sup> However, benzoxazoles comprised in this study did not show any interesting specificity to the studied enzyme. Nevertheless, other substitution might be worthy.

#### 4. Conclusion

In this review, we have summarized the available information regarding to benzoxazole scaffold and its antitubercular properties. Benzoxazole moiety has been frequently studied and successfully combined with another promising heterocycle such is pyrazoline. However, none of the reviewed benzoxazole derivatives reached nanomolar concentrations and has entered the phase of the preclinical hit-to-lead optimization in anti-TB research.

Despite this, the search for new benzoxazole-based compounds active against TB remains a challenge. In particular, since the occurrence of MDR and XDR *MTB* infections is alarming and the molecular mechanism involved in the resistance and its possible targets is still not completely understood.

In this review, benzoxazoles several possible targets have been also outlined; however, additional efforts must be made in order to discover novel anti-TB agents with a new mode of action and directed at unknown targets of *MTB*. This review should serve the researchers working in the area of the development of new antituberculotics as a guide through both the successful and less successful research that has been done during the recent past years in order to find new antituberculotics based on benzoxazole scaffold and help them to focus their future research towards the most promising structures.

#### 5. Future perspectives

TB is one of the top 10 causes of deaths worldwide and the first among the mortality caused by bacterial infections. It is estimated that until 2020 nearly 1 billion additional people will be infected with TB, 200 million will become sick, and 35 million will die of this disease. Many *M. tuberculosis* strains are resistant to one or more of the standard TB drugs, which complicates treatment and the rise in number of people affected by drug-resistant TB and latent TB is alarming. The current situation and effort to effectively control TB requires development of new antitubercular agents acting on new targets. With no doubt, the discovery of entirely new compounds with an alternative mechanism of action to the existing therapeutics remains challenging.

The question is, can any benzoxazole serve as a lead for the discovery of new antitubercular agents acting on new targets?

The above literature findings reveal benzoxazoles as a promising scaffold that is in the most cases substituted with other heterocycle contributing to the antitubercular activity. From this point of view, the pyrazoline modification of benzoxazole remains the most promising from all studied substitutions. Several compounds of these series had interesting activity, even better than all of the standard drugs against *MTB* H<sub>37</sub>Rv strain.

All biological studies reported in this review make benzoxazole nucleus highly suitable for discovery of new antitubercular agents. However, detailed SAR studies and additional efforts must be made in order to discover novel anti-TB agents with a new mode of action and directed at unknown targets of *MTB*.

#### Acknowledgement

This work was supported by the Ministry of Education, Youth and Sport of the Czech Republic (projects IGA\_PrF\_2018\_029, IGA\_LF\_2018\_032) and the National Program of Sustainability (project LO1304).

#### Conflict of Interest

The authors declare no conflict of interest.

**Keywords:** antitubercular · benzoxazole · biological activity · *Mycobacterium tuberculosis* · tuberculosis

- [1] G. B. Migliori, M. Dara, C. P. de, H. Kluge, M. C. Raviglione, *Eur. Respir. J.* **2012**, *39*, 1290–1291.
- [2] A. Skrahina, H. Hurevich, A. Zalutskaya, E. Sahalchik, A. Astrauko, G. W. van, S. Hoffner, V. Rusovich, M. Zignol, *Eur. Respir. J.* **2012**, *39*, 1425–1431.
- [3] D. Falzon, N. Gandhi, G. B. Migliori, G. Sotgiu, H. S. Cox, T. H. Holtz, M. G. Hollm-Delgado, S. Keshavjee, K. DeRiemer, R. Centis, L. D'Ambrosio, C. G. Lange, M. Bauer, D. Menzies, *Eur. Respir. J.* **2013**, *42*, 156–168.
- [4] G. B. Migliori, G. Sotgiu, N. R. Gandhi, D. Falzon, K. DeRiemer, R. Centis, M. G. Hollm-Delgado, D. Palmero, C. Perez-Guzman, M. H. Vargas, L. D'Ambrosio, A. Spanevello, M. Bauer, E. D. Chan, H. S. Schaaf, S. Keshavjee, T. H. Holtz, D. Menzies, *Eur. Respir. J.* **2013**, *42*, 169–179.
- [5] M. Zignol, M. Dara, A. Dadu, K. Kremer, A. S. Dean, D. Falzon, K. Floyd, H. Hoffmann, S. Hoffner, *Drug Resist Updat* **2013**, *16*, 108–115.
- [6] N. R. Gandhi, P. Nunn, K. Dheda, H. S. Schaaf, M. Zignol, S. D. van, P. Jensen, J. Bayona, *Lancet* **2010**, *375*, 1830–1843.
- [7] C. S. Demmer, L. Bunch, *Eur. J. Med. Chem.* **2015**, *97*, 778–785.
- [8] M. K. Gautam, Sonal, N. K. Sharma, Priyanka, K. K. Jha, *Int. J. ChemTech Res.* **2012**, *4*, 640–650.
- [9] Maruthamuthu, S. Rajam, P. C. R. Stella, A. G. B. Dileepan, R. Ranjith, *J. Chem. Pharm. Res.* **2016**, *8*, 505–526.
- [10] S. Singh, G. Veeraswamy, D. Bhattarai, J. I. Goo, K. Lee, Y. Choi, *Asian J. Org. Chem.* **2015**, *4*, 1338–1361.
- [11] I. Oren, I. Yalcin, *Ankara Univ. Eczacilik Fak. Derg.* **1993**, *21*, 53–65.
- [12] S. P. B. Ovenden, J. L. Nielson, C. H. Liptrot, R. H. Willis, D. M. Tapiolas, A. D. Wright, C. A. Motti, *J. Nat. Prod.* **2011**, *74*, 65–68.
- [13] T. Kusumi, T. Ooi, M. R. Walchli, H. Kakisawa, *J. Am. Chem. Soc.* **1988**, *110*, 2954–2958.
- [14] C. Hohmann, K. Schneider, C. Bruntner, E. Irran, G. Nicholson, A. T. Bull, A. L. Jones, R. Brown, J. E. M. Stach, M. Goodfellow, W. Beil, M. Kraemer, J. F. Imhoff, R. D. Suessmuth, H. P. Fiedler, *J. Antibiot.* **2009**, *62*, 99–104.
- [15] L. J. Scott, *Drugs* **2014**, *74*, 1371–1378.

- [16] C. Hohmann, K. Schneider, C. Bruntner, E. Irran, G. Nicholson, A. T. Bull, A. L. Jones, R. Brown, J. E. M. Stach, M. Goodfellow, W. Beil, M. Kraemer, J. F. Imhoff, R. D. Suessmuth, H. P. Fiedler, *J. Antibiot.* **2009**, *62*, 99–104.
- [17] D. W. Dunwell, D. Evans, T. A. Hicks, *J. Med. Chem.* **1975**, *18*, 1158–1159.
- [18] E. Marmo, R. Acampora, M. Angrisani, L. Berrino, M. Cazzola, D. De Santis, A. Filippelli, V. Filippelli, V. Guarino, et al, *Riforma Med.* **1986**, *101*, 253–282.
- [19] S. Rajasekhar, B. Maiti, K. Chanda, *Synlett* **2017**, *28*, 521–541.
- [20] A. Kumar, R. A. Maurya, P. Ahmad, *J. Comb. Chem.* **2009**, *11*, 198–201.
- [21] M. B. Madhusudana Reddy, A. Nizam, M. A. Pasha, *Synth. Commun.* **2011**, *41*, 1838–1842.
- [22] Y. Riadi, R. Mamouni, R. Azzalou, M. El Haddad, S. Routier, G. Guillaumet, S. Lazar, *Tetrahedron Lett.* **2011**, *52*, 3492–3495.
- [23] S. Kaul, A. Kumar, B. Sain, A. K. Bhatnagar, *Synth. Commun.* **2007**, *37*, 2457–2460.
- [24] B. Wang, Y. Zhang, P. Li, L. Wang, *Chin. J. Chem.* **2010**, *28*, 1697–1703.
- [25] D. R. Chancellor, K. E. Davies, O. De Moor, C. R. Dorgan, P. D. Johnson, A. G. Lambert, D. Lawrence, C. Lecci, C. Maillol, P. J. Middleton, G. Nugent, S. D. Poignant, A. C. Potter, P. D. Price, R. J. Pye, R. Storer, J. M. Tinsley, R. van Well, R. Vickers, J. Vile, F. J. Wilkes, F. X. Wilson, S. P. Wren, G. M. Wynne, *J. Med. Chem.* **2011**, *54*, 3241–3250.
- [26] I. Mohammadpoor-Baltork, A. R. Khosropour, S. F. Hojati, *Catal. Commun.* **2007**, *8*, 1865–1870.
- [27] K. Tao, J. Zheng, Z. Liu, W. Shen, J. Zhang, *Tetrahedron Lett.* **2010**, *51*, 3246–3249.
- [28] X. Fan, Y. He, X. Zhang, S. Guo, Y. Wang, *Tetrahedron* **2011**, *67*, 6369–6374.
- [29] F. Wang, J. R. Hauske, *Tetrahedron Lett.* **1997**, *38*, 6529–6532.
- [30] X. Beebe, D. Wodka, T. J. Sowin, *J. Comb. Chem.* **2001**, *3*, 360–366.
- [31] C. Chen, Y. J. Chen, *Tetrahedron Lett.* **2004**, *45*, 113–115.
- [32] J. Y. Hwang, Y. D. Gong, *J. Comb. Chem.* **2006**, *8*, 297–303.
- [33] H. Hioki, K. Matsushita, M. Kubo, K. Harada, M. Kodama, Y. Fukuyama, *Tetrahedron* **2007**, *63*, 11315–11324.
- [34] W. H. Wagner, H. Vonderbank, *Z. Gesamte Exp. Med.* **1949**, *115*, 66–81.
- [35] K. Manna, Y. K. Agrawal, *Eur. J. Med. Chem.* **2010**, *45*, 3831–3839.
- [36] M. S. Yar, A. A. Siddiqui, M. A. Ali, *Bioorg. Med. Chem. Lett.* **2006**, *16*, 4571–4574.
- [37] S. Sharma, P. K. Sharma, N. Kumar, R. Dudhe, *Biomed. Pharmacother.* **2011**, *65*, 244–251.
- [38] H. M. Soni, P. K. Patel, M. T. Chhabria, A. K. Patel, D. N. Rana, P. S. Brahmshatriya, *Int. J. Org. Chem.* **2016**, *6*, 157–176.
- [39] D. N. Rana, M. T. Chhabria, N. K. Shah, P. S. Brahmshatriya, *Med. Chem. Res.* **2014**, *23*, 370–381.
- [40] D. N. Rana, M. T. Chhabria, N. K. Shah, P. S. Brahmshatriya, *Med. Chem. Res.* **2014**, *23*, 2218–2228.
- [41] K. Devi, M. Kachroo, L. Pathak, *J. Comput. Methods Mol. Des.* **2016**, *6*, 8–19.
- [42] M. Arisoy, O. Temiz-Arpaci, F. Kaynak-Onurdag, *Ankara Univ. Eczacilik Fak. Derg.* **2010**, *39*, 155–162.
- [43] M. Arisoy, O. Temiz-Arpaci, F. Kaynak-Onurdag, S. Ozgen, *Z. Naturforsch., C: J. Biosci.* **2013**, *68*, 453–460.
- [44] T. Ertan-Bolelli, I. Yildiz, S. Ozgen-Ozgacar, *Med. Chem. Res.* **2016**, *25*, 553–567.
- [45] V. Klimesova, J. Koci, K. Waisser, J. Kaustova, U. Moellmann, *Eur. J. Med. Chem.* **2009**, *44*, 2286–2293.
- [46] J. Koci, V. Klimesova, K. Waisser, J. Kaustova, H. M. Dahse, U. Moellmann, *Bioorg. Med. Chem. Lett.* **2002**, *12*, 3275–3278.
- [47] A. D. Rodriguez, C. Ramirez, I. I. Rodriguez, E. Gonzalez, *Org Lett* **1999**, *1*, 527–530.
- [48] I. I. Rodriguez, A. D. Rodriguez, Y. Wang, S. G. Franzblau, *Tetrahedron Lett.* **2006**, *47*, 3229–3232.
- [49] T. P. Sycheva, I. D. Kiseleva, M. N. Shchukina, *Khim. Geterotsikl. Soedin.* **1966**, 205–211.
- [50] T. P. Sycheva, I. D. Kiseleva, M. N. Shchukina, *Khim. Geterotsikl. Soedin.* **1966**, 687–689.
- [51] T. P. Sycheva, Z. A. Pankina, I. D. Kiseleva, M. N. Shchukina, *Khim. Geterotsikl. Soedin.* **1966**, 4, 506–510.
- [52] T. P. Sycheva, I. D. Kiseleva, M. N. Shchukina, *Khim. Geterotsikl. Soedin.* **1967**, 43–47.
- [53] T. P. Sycheva, T. N. Pavlova, T. N. Zykova, M. N. Shchukina, *Khim. Farm. Zh.* **1973**, *7*, 3–5.
- [54] G. Kolavi, V. Hegde, I. Ahmedkhazi, *J. Sulfur Chem.* **2006**, *27*, 225–231.
- [55] V. S. Hegde, G. D. Kolavi, R. S. Lamani, I. A. Khazi, *Phosphorus, Sulfur Silicon Relat. Elem.* **2007**, *182*, 911–920.
- [56] J. Vinsova, V. Horak, V. Buchta, J. Kaustova, *Molecules* **2005**, *10*, 783–793.
- [57] J. Vinsova, K. Cermakova, A. Tomeckova, M. Ceckova, J. Jampilek, P. Cermak, J. Kunes, M. Dolezal, F. Staud, *Bioorg. Med. Chem.* **2006**, *14*, 5850–5865.
- [58] A. Imramovsky, J. Kozic, M. Pesko, J. Stolarikova, J. Vinsova, K. Kralova, J. Jampilek, *Sci. World J.* **2014**, 705973–1–705973/12.
- [59] T. P. Sycheva, T. N. Pavlova, T. N. Zykova, M. N. Shchukina, *Khim. Farm. Zh.* **1969**, *3*, 18–21.
- [60] S. P. Sankar, A. Mathew, T. Jayakumar, S. Chand, C. Mathew, *Asian J. Pharm. Health Sci.* **2013**, *3*, 661–676.
- [61] M. Shah, G. Wells, T. D. Bradshaw, C. A. Laughton, M. F. G. Stevens, A. D. Westwell, *Letts. Drug Des. Discovery* **2006**, *3*, 419–423.
- [62] E. Pitta, M. K. Rogacki, O. Balabon, S. Huss, F. Cunningham, E. M. Lopez-Roman, J. Joossens, K. Augustyns, L. Ballell, R. H. Bates, P. Van der Veken, *J. Med. Chem.* **2016**, *59*, 6709–6728.
- [63] L. Encinas, H. O'Keefe, M. Neu, M. J. Remuinan, A. M. Patel, A. Guardia, C. P. Davie, N. Perez-Macias, H. Yang, M. A. Convery, J. A. Messer, E. Perez-Herran, P. A. Centrella, D. Alvarez-Gomez, M. A. Clark, S. Huss, G. K. O'Donovan, F. Ortega-Muro, W. McDowell, P. Castaneda, C. C. Arico-Muendel, S. Pajk, J. Rullas, I. Angulo-Barturen, E. Alvarez-Ruiz, A. Mendoza-Losana, L. Ballell Pages, J. Castro-Pichel, G. Evindar, *J. Med. Chem.* **2014**, *57*, 1276–1288.
- [64] O. Holas, P. Ondrejcek, M. Dolezal, *J. Enzyme Inhib. Med. Chem.* **2015**, *30*, 629–648.
- [65] B. Inturi, G. V. Pujar, M. N. Purohit, *Arch. Pharm.* **2016**, *349*, 817–826.
- [66] I. Pauli, R. N. dos Santos, D. C. Rostirolla, L. K. Martinelli, R. G. Ducati, L. F. S. M. Timmers, L. A. Basso, D. S. Santos, R. V. C. Guido, A. D. Andricopulo, O. Norberto de Souza, *J. Chem. Inf. Model.* **2013**, *53*, 2390–2401.
- [67] P. Pan, P. J. Tonge, *Curr. Top. Med. Chem.* **2012**, *12*, 672–693.
- [68] R. He, Y. Bai, Z. H. Yu, L. Wu, A. M. Gunawan, Z. Y. Zhang, *MedChemComm* **2014**, *5*, 1496–1499.

Submitted: March 3, 2018

Revised: April 12, 2018

Accepted: April 16, 2018





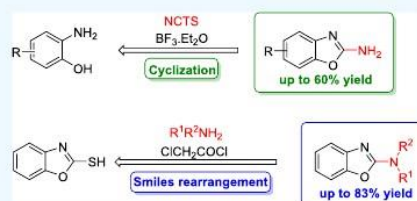
## Synthesis of Various 2-Aminobenzoxazoles: The Study of Cyclization and Smiles Rearrangement

Veronika Šlachtová, Jan Chasák, and Lucie Brulíková\*

Department of Organic Chemistry, Faculty of Science, Palacký University Olomouc, 17. listopadu 12, 771 46 Olomouc, Czech Republic

## Supporting Information

**ABSTRACT:** This study reports two synthetic approaches leading to 2-aminobenzoxazoles and their *N*-substituted analogues. Our first synthetic strategy involves a reaction between various *o*-aminophenols and *N*-cyano-*N*-phenyl-*p*-toluenesulfonamide as a non-hazardous electrophilic cyanating agent in the presence of Lewis acid. The second synthetic approach uses the Smiles rearrangement upon activation of benzoxazole-2-thiol with chloroacetyl chloride. Both developed synthetic protocols are widely applicable, afford the desired aminobenzoxazoles in good to excellent yields, and use nontoxic and inexpensive starting material.



## INTRODUCTION

2-Aminobenzoxazoles and their *N*-substituted analogues play an important role in medicinal chemistry and chemical biology.<sup>1–7</sup> They are described as potential therapeutic agents including various enzyme inhibitors (proteases, chymase, butyrylcholinesterase, topoisomerase II inhibitors, etc.).<sup>4,7,8</sup> They also have applications in materials chemistry.<sup>9</sup> In addition, aminobenzoxazoles serve as positron emission tomography probes.<sup>2</sup> Therefore, the development of effective methods leading to 2-aminobenzoxazoles and their analogues has attracted great attention.

Several methods for synthesis of 2-aminobenzoxazoles have been reported (Scheme 1).<sup>8,10–20</sup> However, most of these methods suffer from specific drawbacks. The most published protocol comprises the cyclization of 2-aminophenols using BrCN as a cyanating agent,<sup>8,14–18,21</sup> but this BrCN reagent is highly toxic. The next reported approach is the direct 2-C amination of benzoxazoles,<sup>22–24</sup> but its drawbacks include the use of transition metal catalysts, high temperatures, nitrogen atmosphere, or co-oxidants. In recent years, many efficient methods have been developed for the synthesis of *N*-substituted aminobenzoxazoles.<sup>25–32</sup> Most of these methods suffer from low yields and use toxic precursors or expensive reagents. *N*-substituted aminobenzoxazoles can be prepared from corresponding hydroxyl/thiol scaffolds through the aryl halides (Scheme 1).<sup>30</sup> Unfortunately, this method requires toxic and acidic halogenating agents. Amination using Rose Bengal as a photocatalyst has been recently reported.<sup>26</sup> Despite being efficient and the low cost of Rose Bengal catalyst, this protocol needs a strong organic base (DBU) and has long reaction time that downgrade its advantages. Microwave-enhanced on-water amination of 2-mercaptobenzoxazoles has also been recently introduced.<sup>29</sup> However, its drawbacks include an inert atmosphere or co-oxidants. In addition, transition metal

catalysts used in this method may be expensive and higher temperatures are sometimes inevitable.

Given the shortcomings of the abovementioned methods, we attempted to develop a new, nontoxic, and efficient protocol relying on an inexpensive starting material. Thus, accordingly, we designed two independent protocols leading to 2-aminobenzoxazoles (Scheme 1, path a) and their *N*-mono or disubstituted analogues (Scheme 1, path b). The first protocol is based on the use of *N*-cyano-*N*-phenyl-*p*-toluenesulfonamide (NCTS) as a nonhazardous electrophilic cyanating agent. It combines operational simplicity, a nontoxic reagent, and wide substrate scope. The second approach is based on the Smiles rearrangement that enables the functionalization of heteroaromatic rings under economic conditions. Both the developed protocols are widely applicable and afford the desired compounds in good yields, thus indicating their efficacy.

## RESULTS AND DISCUSSION

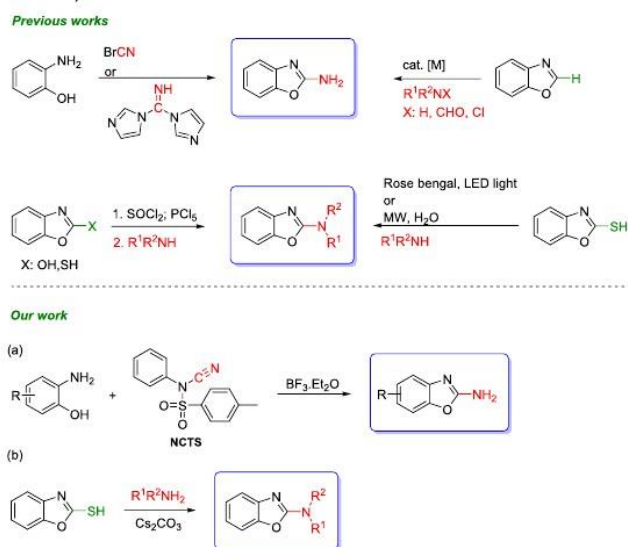
In 2015, Kasthuri et al. reported the synthesis of 2-aminobenzoxazoles using an efficient, air-stable, and nonhazardous electrophilic cyanating agent, i.e., NCTS.<sup>13</sup> NCTS can be easily synthesized from inexpensive and commercially available phenyl urea by dehydrative tosylation in pyridine in high yields.<sup>33</sup> The synthetic protocol described by Kasthuri et al.<sup>13</sup> required 1 equiv of LiHMDS to accomplish the reaction. Unfortunately, despite our efforts to acquire additional optimization, we found the reaction to be irreproducible in our hands as it yielded only up to 11% of the desired product **2a** (Table 1, entry 6).<sup>34</sup> Compound **3** was always detected as the major product according to liquid chromatography–mass spectrometry (LC–MS) traces.

Received: August 21, 2019

Accepted: October 18, 2019

Published: November 5, 2019

Scheme 1. Aminobenzoxazole Synthesis

Table 1. Optimization of the Reaction Conditions<sup>a†</sup>

entry	NCTS (equiv)	LiHMDS (equiv)	T (°C)	results <sup>b</sup> (% of 2a)
1	1	1	0 to rt	9
2	1	3	0 to rt	9
3	1.2	1	0 to rt	6
4	1.5	1	0 to rt	4
5	1.2	3	0 to rt	9
6	1	3	0 to 60	11

<sup>a</sup>Reaction conditions: *o*-aminophenol (0.18 mmol, 20 mg), NCTS, LiHMDS, tetrahydrofuran (THF; 1 mL), 2 h. <sup>b</sup>Conversion estimated from LC–MS traces at 210–500 nm.

Following these results, we changed the reaction conditions keeping NCTS as a cyanating agent. Initial investigations were aimed at the direct use of NCTS without any activation. Unfortunately, NCTS was found to be ineffective in this case. Thus, we suggested that the use of a strong Lewis acid as BF<sub>3</sub>·Et<sub>2</sub>O in combination with NCTS could successfully activate the CN group toward a nucleophilic attack<sup>33</sup> and afford the desired product 2a. Indeed, our expectations met with successful results, and after some optimization (Table 2), the desired product 2a was obtained in good yield. Using these optimal conditions, the reaction can proceed even at a 5 mmol scale. This result suggested that the process might be scaled up with only a slightly lower yield.

With optimum reaction conditions, the substrate scope was explored (Table 3). We found out that the substitution pattern does not affect the reaction yields. Both EWG and EDG substituents yielded the desired products in moderate to good yields (45–60%). Considering the satisfactory LC–MS

Table 2. Optimization of the Reaction Conditions with Lewis Acids<sup>a†</sup>

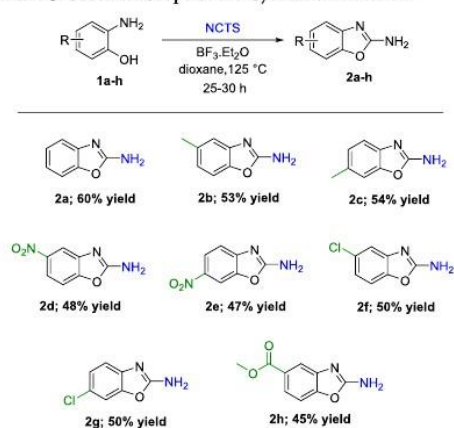
entry	BF <sub>3</sub> ·Et <sub>2</sub> O (equiv)	NCTS (equiv)	T (°C)	results <sup>c</sup> (% of 2a)
1	3	3	reflux	86
2	3	3	100 <sup>b</sup>	39
3	3	2	reflux	75
4	3	1.5	reflux	87
5	3	1.2	reflux	54
6	2	1.5	reflux	90
7	1	1.5	reflux	71

<sup>a</sup>Reaction conditions: *o*-aminophenol (0.18 mmol, 20 mg), NCTS, BF<sub>3</sub>·Et<sub>2</sub>O, 1,4-dioxane (1 mL), 30 h. <sup>b</sup>External temperature of the bath. <sup>c</sup>Conversion estimated from LC–MS traces at 210–500 nm.

conversions, we estimated that the multistep isolation and purification procedure resulted in lowered isolated yields. Hence, different solvents were tried to improve the workup and isolated yield (Supporting Information, Table S1). Unfortunately, none of the used solvents led to a higher yield.

Based on the observations and prevalent literature,<sup>35</sup> the reaction mechanism was proposed (Scheme 2). The reaction is initiated through the Lewis acidic activation of NCTS via the coordination of its cyano group to BF<sub>3</sub>·Et<sub>2</sub>O. The activation facilitates the subsequent nucleophilic attack of the amino group and the elimination of the sulfonamide residue. The hydroxy group then attacks the electron-deficient carbon. Finally, the desired product 2 is formed during the workup. We confirmed the eliminated sulfonamide by mass *m/z* = 246 [M – H], providing the next experimental support for our mechanistic proposal.



Table 3. Substrate Scope of the Cyclization Reaction<sup>a</sup>

<sup>a</sup>Reaction conditions: *o*-aminophenol (0.9 mmol, 100 mg), NCTS (1.5 equiv),  $\text{BF}_3\cdot\text{Et}_2\text{O}$  (2 equiv), 1,4-dioxane (5 mL), reflux, 25–30 h.

We were also interested in the catalyst-free synthesis of *N*-substituted benzoxazole analogues. Recently, the Smiles rearrangement, an intramolecular  $\text{S}_{\text{N}}\text{Ar}$  reaction, has received renewed attention.<sup>36</sup> It enables the functionalization of heteroaromatic rings via breaking a C–X single bond and forming a new C–X or C–C bond under economic conditions. In 2017, Wang et al. published an interesting synthesis of *N*-aryl-2-aminobenzoxazoles from substituted benzoxazole-2-thiol and 2-chloro-*N*-arylacetylides in a KOH–dimethylformamide (DMF) system.<sup>37</sup> However, this method is described only for aromatic substrates. By taking inspiration from the capabilities of the Smiles rearrangement and commercially available heterocyclic thiols, we suggested a synthetic approach to *N*-substituted aminobenzoxazoles.

First, we focused on the reaction of benzoxazole-2-thiol with various aliphatic bromoamines and expected the Smiles rearrangement to result in the desired thiol (Scheme 3). Interestingly, some of the investigated substrates reacted giving the mixture of thiol and disulfide or other unexpected products.

The reaction of benzoxazole-2-thiol **4** with 3-bromopropylamine HBr **5** according to the conditions listed by Abdelazeem

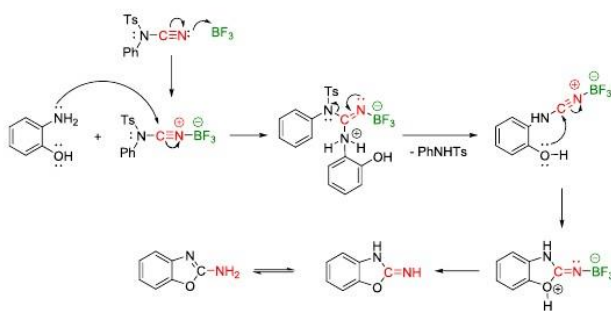
et al.<sup>3</sup> gave a mixture of benzoxazole **6** and disulfide analogue **7** (Scheme 3). The reaction conditions were further optimized concerning the amine and base equivalents (Supporting Information, Table S2). If an excess of the base was used, disulfide was obtained as the main product of the reaction. However, 2 equiv of the amine together with 2 equiv of the base provided compound **6** selectively. Moreover, radical scavenger  $\text{Et}_3\text{N}$  strongly suppressed disulfide **7** formation. Therefore, disulfide **7** might be probably formed by a radical mechanism. On the other hand, there was no effect of oxidation (Supporting Information, Table S2, entry 8).

Subsequently, we explored the reaction of benzoxazole-2-thiol with 2-bromoethylamine HBr (Scheme 3). Surprisingly, we observed a different reactivity compared to bromopropylamine (Supporting Information, Table S3). The reaction of benzoxazole-2-thiol started with 4 equiv of the amine and 3 equiv of  $\text{K}_2\text{CO}_3$ , giving a mixture of products **9** and **10**. Disulfide **10** was formed selectively using just 2 equiv of the amine. The temperature was found to play a key role in the reaction. Heating at 70 °C resulted in a mixture of both compounds, and an increased temperature of 120 °C afforded disulfide **10** selectively. Changing the amount of  $\text{K}_2\text{CO}_3$  did not provide the desired selectivity. Consequently, we tried  $\text{Et}_3\text{N}$  instead and realized that 2 equiv of the amine and 1 equiv of  $\text{Et}_3\text{N}$  are the most convenient conditions for the synthesis of compound **9**.

We also studied the reactivity of benzoxazole-2-thiol with 4-bromobutylamine HBr **11** (Scheme 3, Supporting Information, Table S4). The bromoamine **11** was synthesized from commercially available aminoalcohol according to the previously described procedure followed by ionex workup.<sup>38</sup> Surprisingly, the rapid 5-membered ring closure provided pyrrolidine **14** as the main product regardless of the reaction conditions. This ring-closing reaction is speeded up by negligible ring strain and insignificant entropy change. Lower temperature only slowed all of the conversion down. Finally, 2 equiv of the amine and 2 equiv of  $\text{Et}_3\text{N}$  in refluxing toluene provided compound **14** within 4 h.

The reactivity of 5-bromopentylamine HBr **15** was also explored (Scheme 3, Supporting Information, Table S5). Bromoamine **15** was synthesized from 5-aminopentan-1-ol according to the previously described procedure followed by ionex workup.<sup>38</sup> The substitution leading to product **16** proceeded smoothly after the careful optimizations using 2 equiv of  $\text{Et}_3\text{N}$  in refluxing toluene. Harsher reaction conditions were tried to obtain the rearranged compound **17**, but we

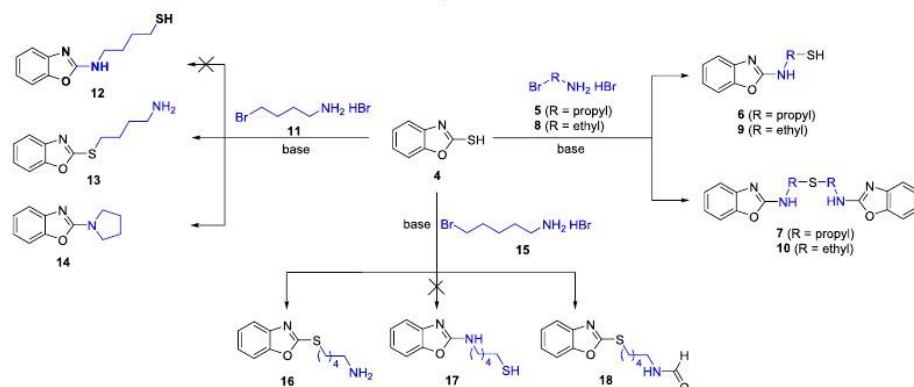
Scheme 2. Proposed Reaction Pathway



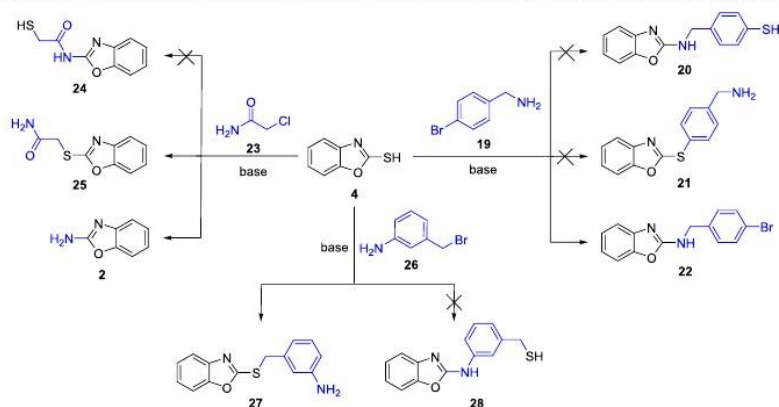
19316

DOI: 10.1021/acsomega.9b02702  
ACS Omega 2019, 4, 19314–19323

Scheme 3. Reaction of Benzoxazole-2-thiol with Various Aliphatic Bromoamines



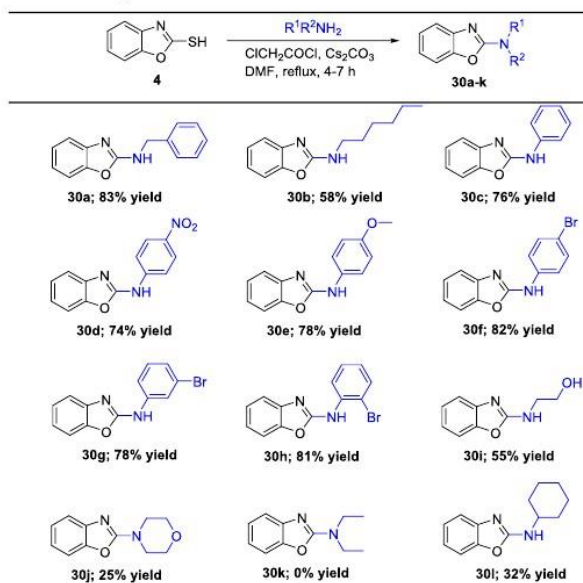
Scheme 4. Reaction of Benzoxazole-2-thiol with 4-Bromobenzylamine/2-Chloroacetamide/3-(Bromomethyl)aniline

Table 4. Optimization of Reaction Conditions with Cyclohexylamine<sup>a</sup>

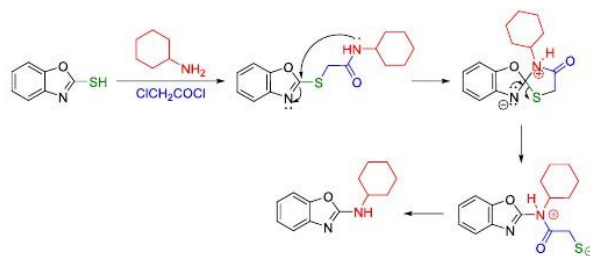
entry	chloride (equiv)	base (equiv)	T (°C)	time (h)	solvent	ratio of 30:31 (%) <sup>b</sup>
1	1.2	Cs <sub>2</sub> CO <sub>3</sub> (3.2)	160 (MW)	1/2	DMF	57:0
2	1.2	Cs <sub>2</sub> CO <sub>3</sub> (3.2)	160	8	DMF	58:0
3	1.7	Cs <sub>2</sub> CO <sub>3</sub> (3.2)	160 (MW)	1/2	DMF	31:0
4	1.2	Cs <sub>2</sub> CO <sub>3</sub> (3.7)	160 (MW)	1/2	DMF	48:0
5	1.2	Cs <sub>2</sub> CO <sub>3</sub> (3.2)	160 (MW)	1/2	N,N-DMA	25:0
6	1.2	Cs <sub>2</sub> CO <sub>3</sub> (3.2)	160 (MW)	1/2	N,N-DMA	47:0
7	1.2	DBU (3.2)	reflux	2	MeCN	0:95
8	1.2	NaH (3.2)	150	2	N,N-DMA	0:42

<sup>a</sup>Reaction conditions: Benzoxazole-2-thiol (0.16 mmol, 25 mg), cyclohexylamine (0.16 mmol), base, ClCH<sub>2</sub>COCl, solvent (1 mL). <sup>b</sup>Conversion estimated from LC-MS traces at 210–500 nm.

Table 5. Substrate Scope of the Rearrangement



Scheme 5. Proposed Reaction Pathway



observed the formylation in DMF instead. As a result, compound **18** was isolated after the microwave irradiation.

We next investigated the behavior of chloroacetamide as well as aromatic substrates in the Smiles reaction (Scheme 4). For this, we studied the reactivity of aromatic 4-bromobenzylamine **19** (Scheme 4, Supporting Information, Table S6). Lower susceptibility to nucleophilic attack usually makes aromatic halides rather unreactive. However, the unexpected reaction occurred on using 2 equiv of  $Et_3N$  in refluxing toluene. Under these conditions, the amino group was found to be sufficiently nucleophilic to substitute the thiol, providing benzoxazolamine **22**.

The investigation of more challenging substrates such as amides and benzylic bromides gave only the expected substitution products. Their rearrangement was probably prevented by sterically and energetically demanding transition states. First, we examined the reactivity of 2-chloroacetamide **23** (Scheme 4, Supporting Information, Table S7). All of the

optimizations gave mostly compound **25** probably due to lower acidic nitrogen nucleophilicity as well as an unfavorable transition state. Moreover, microwave irradiation afforded a mixture of **25** and 2-aminobenzoxazole **2**. We also explored the reactivity of 3-(bromomethyl)aniline (Scheme 4, Supporting Information, Table S8). There was no rearrangement regardless of the reaction conditions. We always obtained only the substitution product **27**. Finally, reactions with various aromatic bromoanilines were attempted, but no reaction occurred as expected.

Since we aimed at a wide substrate scope, a universal method was needed. Thus, a more challenging intramolecular variant of the Smiles rearrangement using chloroacetyl chloride was explored (Table 4). First, reaction conditions described by Tian et al.<sup>39</sup> applied on cyclohexylamine as a model substrate were attempted (Table 4, entry 1). This one-pot reaction was performed under microwave irradiation as well as under conventional heating in an oil bath at 160 °C. The second



reaction provided a slightly better result. Excess chloride or  $\text{Cs}_2\text{CO}_3$ , as well as changing the solvent, prolonged the reaction time, or the higher temperature gave worse conversion. On the other hand, no rearrangement occurred using different bases. Since bromoacetyl bromide showed better activating properties, milder reaction conditions were considered for aniline (Supporting Information, Table S9). The reaction proceeded even at 85 °C without compromising the isolated yield. Different bases provided only the substitution product **31c**. Unfortunately, these milder conditions failed with other amines giving the substitution product **31** only.

With the optimized reaction conditions, we studied the scope of the rearrangement (Table 5). Various types of amines, including aromatic, aliphatic, alicyclic (both primary and secondary), and bisnucleophilic ethanolamine, were tested. Regardless of the electron effects and substitution patterns, the aromatic and primary amines reacted smoothly, giving the desired products **30a–h** in good yields (58–83%). On the other hand, a steric hindrance on the amine lowered the yield significantly. The reaction resulted in a moderate isolated yield of benzoxazole **30i** (32%), while the reaction with morpholine gave low yield of **30j** (25%). The rearrangement of diethylamine completely failed. Finally, we upscaled the reaction of benzoxazole-2-thiol **4** with aniline to 3.5 mmol of **4**, which required a slightly prolonged reaction time (8 h), giving **30c** in a 71% isolated yield. This result suggested that the process also can be upscaled with only a slightly lower yield.

Based on the above observations and the existing literature, the reaction mechanism set out in Scheme 5 was suggested. First, *S*-alkylated thiol undergoes the Smiles rearrangement by the nucleophilic attack of the nitrogen at the benzoxazole ring carbon, forming a new C–N bond to give the spiro intermediate. Second, rearomatization and alkaline hydrolysis in the presence of  $\text{Cs}_2\text{CO}_3$  afford the *N*-substituted benzoxazole **30**.

## CONCLUSIONS

In conclusion, synthetic strategies affording various 2-aminobenzoxazoles and their *N*-substituted analogues from readily available starting materials have been developed. Our first approach to substituted 2-aminobenzoxazoles is based on the nonhazardous cyanating agent NCTS, activated with  $\text{BF}_3 \cdot \text{Et}_2\text{O}$ . This newly developed synthetic protocol combines operational simplicity, a nontoxic and readily available reagent, and wide substrate scope. Moreover, an efficient one-pot amination of benzoxazole-2-thiol by various amines mediated with chloroacetyl chloride via the intramolecular Smiles rearrangement was developed. Our methodology stands out because of the wide amine scope, short reaction time, and a metal-free approach. The obtained results also indicated that the reactions can be scaled up, providing an alternative process for the chemical industry. Finally, we believe that our methodologies represent a straightforward way to various aminobenzoxazoles and their analogues as important building blocks in organic and medicinal chemistry.

## EXPERIMENTAL SECTION

**General Information.** Solvents and chemicals were purchased from Sigma-Aldrich ([www.sigmaaldrich.com](http://www.sigmaaldrich.com)) and Fluorochem ([www.fluorochem.co.uk](http://www.fluorochem.co.uk)). All reactions were carried out at ambient temperature (21 °C) unless stated otherwise. Analytical thin-layer chromatography (TLC) was

performed using aluminum plates precoated with silica gel (silica gel 60 F254).

The LC–MS analyses were carried out on an UHPLC–MS system consisting of UHPLC chromatograph Accela with a photodiode array detector and triple quadrupole mass spectrometer TSQ Quantum Access (Thermo Scientific, CA), using a Nucleodur Gravity C18 column (dimensions 1.8  $\mu\text{m}$ , 2.1  $\times$  50 mm<sup>2</sup> at 30 °C and a flow rate of 800  $\mu\text{L}/\text{min}$  (Macherey-Nagel, Germany)). The mobile phase was (A) 0.1% ammonium acetate in water and (B) 0.1% ammonium acetate in acetonitrile, linearly programmed from 10 to 80% B over 2.5 min, kept for 1.5 min. The column was re-equilibrated with 10% of solution B for 1 min. The APCI source operated at a discharge current of 5  $\mu\text{A}$ , vaporizer temperature of 400 °C, and a capillary temperature of 200 °C.

NMR <sup>1</sup>H/<sup>13</sup>C spectra were recorded on a JEOL ECX-500SS (500 MHz) or JEOL ECA400II (400 MHz) spectrometer at magnetic field strengths of 11.75 T (with operating frequencies 500.16 MHz for <sup>1</sup>H and 125.77 MHz for <sup>13</sup>C) and 9.39 T (with operating frequencies 399.78 MHz for <sup>1</sup>H and 100.53 MHz for <sup>13</sup>C) at ambient temperature (~21 °C). Chemical shifts ( $\delta$ ) are reported in parts per million (ppm), and coupling constants (*J*) are reported in hertz (Hz). NMR spectra were recorded at ambient temperature (21 °C) in DMSO-*d*<sub>6</sub> and referenced to the resonance signal of the solvent.

HRMS analysis was performed with LC–MS and an Orbitrap high-resolution mass spectrometer (Dionex, Ultimate 3000, Thermo Exactive plus, MA) operating in positive full scan mode in the range of 80–1200 *m/z*. The settings for electrospray ionization were as follows: 150 °C oven temperature and 3.6 kV source voltage. The acquired data were internally calibrated with phthalate as a contaminant in methanol (*m/z* 297.15909). Samples were diluted to a final concentration of 0.1 mg/mL in a solution of water and acetonitrile (50:50, v/v). The samples were injected into the mass spectrometer following HPLC separation on a Kinetex C18 column (2.6  $\mu\text{m}$ , 100 Å, 50  $\times$  3.0 mm<sup>2</sup>) using an isocratic mobile phase of 0.01 M MeCN/ammonium acetate (80/20) at a flow rate of 0.3 mL/min.

All reactions carried out under microwave irradiation were performed with the CEM Discover SP microwave synthesizer, using the dynamic mode in the following settings: maximum amount of microwave power (150 W), premixing time (1 min), and stirring speed (high). A simultaneous cooling of the reaction vessel provided by compressed air (24 psi) was applied during the entire experiment (PowerMax option “ON”). All 0.5 mmol scale reactions were performed in a 10 mL borosilicate glass reaction vessel closed with a disposable silicon cap and equipped with a Teflon-coated egg-shaped magnetic stir bar. The temperature was monitored by an external infrared sensor.

**General Procedures and Characterization of Individual Compounds. Cyclization of Aminophenols with NCTS.** *O*-aminophenol **1** (0.9 mmol; 1 equiv) and NCTS (1.35 mmol; 1.5 equiv) were dissolved in 1,4-dioxane (4 mL).  $\text{BF}_3 \cdot \text{Et}_2\text{O}$  (1.8 mmol; 2 equiv) was added dropwise. The mixture was refluxed overnight (monitored by TLC, 24–30 h). After that, the cooled (rt) mixture was quenched with sat.  $\text{NaHCO}_3$  (pH ~ 7), diluted with  $\text{H}_2\text{O}$  (30 mL), and extracted with EtOAc (3  $\times$  30 mL). Combined organic layers were dried over anhydrous  $\text{Na}_2\text{SO}_4$  and concentrated in vacuo. The residue was purified by column chromatography using Hex/EtOAc.

**Benzo[*d*]oxazol-2-amine (2a).** Brown solid. Yield: 60% (72 mg). <sup>1</sup>H NMR (400 MHz, DMSO-*d*<sub>6</sub>):  $\delta$  7.35 (s, 2H), 7.30 (d, *J* = 7.8 Hz, 1H), 7.19 (d, *J* = 7.3 Hz, 1H), 7.08 (t, *J* = 7.2 Hz, 1H),

6.95 (t,  $J = 7.2$  Hz, 1H).  $^{13}\text{C}$  NMR (101 MHz, DMSO- $d_6$ ):  $\delta$  162.70, 147.92, 143.61, 123.45, 119.92, 115.25, 108.38. HRMS:  $m/z$ : calcd for  $\text{C}_7\text{H}_8\text{N}_2\text{O}$ : 135.0553 [M + H] $^+$ ; found: 135.0554.

**5-Methylbenzo[d]oxazol-2-amine (2b).** Brown solid. Yield: 53% (71 mg).  $^1\text{H}$  NMR (400 MHz, DMSO- $d_6$ ):  $\delta$  7.29 (s, 2H), 7.16 (d,  $J = 8.0$  Hz, 1H), 7.00 (s, 1H), 6.75 (d,  $J = 7.9$  Hz, 1H), 2.30 (s, 3H).  $^{13}\text{C}$  NMR (101 MHz, DMSO- $d_6$ ):  $\delta$  162.89, 146.09, 143.78, 132.47, 120.46, 115.69, 107.80, 21.10. HRMS:  $m/z$ : calcd for  $\text{C}_8\text{H}_8\text{N}_2\text{O}$ : 149.0709 [M + H] $^+$ ; found: 149.0709.

**6-Methylbenzo[d]oxazol-2-amine (2c).** Brown solid. Yield: 54% (72 mg).  $^1\text{H}$  NMR (400 MHz, DMSO- $d_6$ ):  $\delta$  7.29 (s, 2H), 7.14 (s, 1H), 7.06 (d,  $J = 7.9$  Hz, 1H), 6.90 (d,  $J = 7.6$  Hz, 1H), 2.32 (s, 3H).  $^{13}\text{C}$  NMR (101 MHz, DMSO- $d_6$ ):  $\delta$  162.30, 148.06, 140.89, 129.38, 124.09, 114.69, 108.9, 20.97. HRMS:  $m/z$ : calcd for  $\text{C}_8\text{H}_8\text{N}_2\text{O}$ : 149.0709 [M + H] $^+$ ; found: 149.0710.

**5-Nitrobenzo[d]oxazol-2-amine (2d).** Yellow solid. Yield: 48% (77 mg).  $^1\text{H}$  NMR (400 MHz, DMSO- $d_6$ ):  $\delta$  7.98–7.96 (m, 1H), 7.95–7.90 (m, 3H), 7.55 (d,  $J = 8.7$  Hz, 1H).  $^{13}\text{C}$  NMR (101 MHz, DMSO- $d_6$ ):  $\delta$  164.80, 152.31, 144.65, 144.36, 116.65, 109.98, 108.64. HRMS:  $m/z$ : calcd for  $\text{C}_7\text{H}_7\text{N}_3\text{O}_3$ : 178.0258 [M – H] $^+$ ; found: 178.0242.

**6-Nitrobenzo[d]oxazol-2-amine (2e).** Yellow solid. Yield: 47% (75 mg).  $^1\text{H}$  NMR (400 MHz, DMSO- $d_6$ ):  $\delta$  8.29–8.17 (m, 3H), 8.10 (dd,  $J = 8.7, 2.3$  Hz, 1H), 7.32 (d,  $J = 8.7$  Hz, 1H).  $^{13}\text{C}$  NMR (101 MHz, DMSO- $d_6$ ):  $\delta$  166.35, 150.99, 147.19, 140.29, 121.09, 114.13, 104.65. HRMS:  $m/z$ : calcd for  $\text{C}_7\text{H}_7\text{N}_3\text{O}_3$ : 178.0258 [M – H] $^+$ ; found: 178.0241.

**5-Chlorobenzo[d]oxazol-2-amine (2f).** Brown solid. Yield: 50% (76 mg).  $^1\text{H}$  NMR (400 MHz, DMSO- $d_6$ ):  $\delta$  7.58 (s, 2H), 7.32 (d,  $J = 8.4$  Hz, 1H), 7.22 (d,  $J = 2.1$  Hz, 1H), 6.97 (dd,  $J = 8.4, 2.2$  Hz, 1H).  $^{13}\text{C}$  NMR (101 MHz, DMSO- $d_6$ ):  $\delta$  163.86, 146.73, 145.30, 127.65, 119.43, 114.88, 109.39. HRMS:  $m/z$ : calcd for  $\text{C}_7\text{H}_5\text{ClN}_2\text{O}$ : 169.0163 [M + H] $^+$ ; found: 169.0165.

**6-Chlorobenzo[d]oxazol-2-amine (2g).** Red solid. Yield: 50% (75 mg).  $^1\text{H}$  NMR (400 MHz, DMSO- $d_6$ ):  $\delta$  7.52 (s, 2H), 7.48 (d,  $J = 1.8$  Hz, 1H), 7.17 (d,  $J = 8.3$  Hz, 1H), 7.12 (dd,  $J = 8.3, 2.0$  Hz, 1H).  $^{13}\text{C}$  NMR (101 MHz, DMSO- $d_6$ ):  $\delta$  163.31, 148.27, 142.80, 123.69, 123.54, 115.85, 109.13. HRMS:  $m/z$ : calcd for  $\text{C}_7\text{H}_5\text{ClN}_2\text{O}$ : 169.0163 [M + H] $^+$ ; found: 169.0164.

**Methyl 2-Aminobenzo[d]oxazol-5-carboxylate (2h).** Yellow solid. Yield: 45% (49 mg).  $^1\text{H}$  NMR (500 MHz, DMSO- $d_6$ ):  $\delta$  7.72 (d,  $J = 1.7$  Hz, 1H), 7.65 (dd,  $J = 8.3, 1.7$  Hz, 1H), 7.63 (s, 2H), 7.43 (d,  $J = 8.3$  Hz, 1H), 3.84 (s, 3H).  $^{13}\text{C}$  NMR (101 MHz, DMSO- $d_6$ ):  $\delta$  166.36, 163.71, 151.30, 144.02, 125.32, 122.17, 115.78, 108.47, 52.05. HRMS:  $m/z$ : calcd for  $\text{C}_9\text{H}_8\text{N}_2\text{O}_3$ : 193.0608 [M + H] $^+$ ; found: 193.0607.

**Cyclization of Aminophenols with LiHMDS.** *O*-Aminophenol **1** (1.61 mmol; 1 equiv) and NCTS were dissolved in THF (dry, 2.5 mL). The mixture was cooled down to 5 °C, and 1 M LiHMDS in hexane (1.61 mmol; 1 equiv) was added dropwise. It was stirred at 5 °C to rt for 1 h. Then, the reaction mixture was poured into ice water (50 mL) and stirred for 15 min. This was followed by an extraction with EtOAc (3  $\times$  50 mL), and the organic layers were washed with brine (1 $\times$ ), dried over anhydrous  $\text{Na}_2\text{SO}_4$ , and concentrated in vacuo. The residue was purified by column chromatography using Hex/EtOAc.

**2-Aminophenyl-4-methylbenzenesulfonate (3).** Brown solid. Yield: 35% (148 mg).  $^1\text{H}$  NMR (500 MHz, DMSO- $d_6$ ):  $\delta$  9.28 (s, 2H), 7.63 (d,  $J = 8.3$  Hz, 2H), 7.30 (d,  $J = 8.2$  Hz, 2H), 7.13 (dd,  $J = 8.0, 1.6$  Hz, 1H), 6.91 (td,  $J = 7.9, 1.6$  Hz, 1H), 6.72 (dd,  $J = 8.0, 1.1$  Hz, 1H), 6.68 (td,  $J = 7.9, 1.4$  Hz, 1H), 2.33 (s, 3H).  $^{13}\text{C}$  NMR (101 MHz, DMSO- $d_6$ ):  $\delta$  150.19, 142.89, 137.82, 129.42, 126.86, 126.15, 124.40, 119.04, 115.59, 21.05.

HRMS:  $m/z$ : calcd for  $\text{C}_{13}\text{H}_{13}\text{NO}_3\text{S}$ : 264.0689 [M + H] $^+$ ; found: 264.0689.

**Smiles Rearrangement with 3-Bromopropylamine HBr.** Benzoxazole-2-thiol **4** (1.61 mmol, 1 equiv),  $\text{K}_2\text{CO}_3$  (3.2 mmol; 2 equiv/4.8 mmol; 3 equiv), and 3-bromopropylamine HBr **5** (3.2 mmol; 2 equiv/1.61 mmol; 1 equiv) were suspended in DMF (10 mL). The reaction mixture was stirred at 70 °C for 2 h. It was followed by dilution with  $\text{H}_2\text{O}$  (50 mL) and extraction with EtOAc (3  $\times$  50 mL). Organic layers were washed with brine (1 $\times$ ), dried over anhydrous  $\text{Na}_2\text{SO}_4$ , and concentrated in vacuo. The residue was purified by column chromatography using Hex/EtOAc.

**3-(Benzo[d]oxazol-2-ylamino)propane-1-thiol (6).** White solid. Yield: 67% (222 mg).  $^1\text{H}$  NMR (500 MHz, DMSO- $d_6$ ):  $\delta$  7.90 (t,  $J = 5.6$  Hz, 1H), 7.32 (d,  $J = 7.8$  Hz, 1H), 7.23 (d,  $J = 7.1$  Hz, 1H), 7.10 (td,  $J = 7.6, 1.0$  Hz, 1H), 6.96 (td,  $J = 7.7, 1.2$  Hz, 1H), 3.39 (dd,  $J = 12.6, 6.7$  Hz, 2H), 2.56 (dd,  $J = 13.8, 6.8$  Hz, 2H), 2.40 (t,  $J = 7.3$  Hz, 1H), 1.86 (p,  $J = 6.9$  Hz, 2H).  $^{13}\text{C}$  NMR (126 MHz, DMSO- $d_6$ ):  $\delta$  162.31, 147.98, 143.24, 123.51, 120.02, 115.36, 108.42, 40.74, 32.96, 21.11. HRMS:  $m/z$ : calcd for  $\text{C}_{10}\text{H}_{12}\text{N}_2\text{OS}$ : 209.0743 [M + H] $^+$ ; found: 209.0743.

***N,N'*-(Disulfanediy)bis(propene-3,1-diy)bis(benzo[d]oxazol-2-amine) (7).** Yellow solid. Yield: 66% (219 mg).  $^1\text{H}$  NMR (500 MHz, DMSO- $d_6$ ):  $\delta$  7.94 (t,  $J = 5.6$  Hz, 2H), 7.31 (d,  $J = 7.8$  Hz, 2H), 7.23 (d,  $J = 7.4$  Hz, 2H), 7.09 (td,  $J = 7.7, 0.9$  Hz, 2H), 6.96 (td,  $J = 7.8, 1.1$  Hz, 2H), 3.39 (dd,  $J = 12.7, 6.6$  Hz, 4H), 2.81 (t,  $J = 7.1$  Hz, 4H), 2.03–1.90 (m, 4H).  $^{13}\text{C}$  NMR (126 MHz, DMSO- $d_6$ ):  $\delta$  162.25, 147.99, 143.23, 123.51, 120.04, 115.39, 108.43, 40.89, 35.02, 28.38. HRMS:  $m/z$ : calcd for  $\text{C}_{20}\text{H}_{22}\text{N}_4\text{O}_2\text{S}_2$ : 415.1257 [M + H] $^+$ ; found: 415.1258.

**Smiles Rearrangement with 2-Bromoethylamine HBr.** Benzoxazole-2-thiol **4** (1.61 mmol, 1 equiv),  $\text{K}_2\text{CO}_3$  (4.8 mmol; 3 equiv), and 2-bromoethylamine HBr **8** (3.2 mmol; 2 equiv) were suspended in DMF (10 mL). The reaction mixture was stirred at 120 °C for 2 h. This was followed by dilution with  $\text{H}_2\text{O}$  (50 mL) and extraction with EtOAc (3  $\times$  50 mL). Organic layers were washed with brine (1 $\times$ ), dried over anhydrous  $\text{Na}_2\text{SO}_4$ , and concentrated in vacuo. The residue was purified by column chromatography using Hex/EtOAc.

***N,N'*-(Disulfanediy)bis(ethane-2,1-diy)bis(benzo[d]oxazol-2-amine) (10).** White solid. Yield: 71% (220 mg).  $^1\text{H}$  NMR (400 MHz, DMSO- $d_6$ ):  $\delta$  8.14 (t,  $J = 5.7$  Hz, 2H), 7.33 (d,  $J = 7.8$  Hz, 2H), 7.25 (d,  $J = 7.6$  Hz, 2H), 7.10 (td,  $J = 7.5, 0.9$  Hz, 2H), 6.97 (td,  $J = 7.7, 1.1$  Hz, 2H), 3.61 (dd,  $J = 12.9, 6.4$  Hz, 4H), 3.01 (t,  $J = 6.7$  Hz, 4H).  $^{13}\text{C}$  NMR (101 MHz, DMSO- $d_6$ ):  $\delta$  162.03, 148.02, 143.08, 123.62, 120.24, 115.56, 108.58, 41.45, 36.86. HRMS:  $m/z$ : calcd for  $\text{C}_{18}\text{H}_{18}\text{N}_4\text{O}_2\text{S}_2$ : 387.0944 [M + H] $^+$ ; found: 387.0944.

**Smiles Rearrangement with 4-Bromobutylamine HBr.** Benzoxazole-2-thiol **4** (0.6 mmol, 1 equiv) and  $\text{Et}_3\text{N}$  (1.2 mmol, 2 equiv) were dissolved in toluene (5 mL) and premixed at rt for 10 min. Subsequently, 4-bromobutylamine HBr **11** (1.2 mmol, 2 equiv) was added. The reaction mixture was refluxed for 4 h. It was cooled to room temperature, diluted with  $\text{H}_2\text{O}$  (20 mL), and extracted with EtOAc (3  $\times$  20 mL). Organic layers were dried over anhydrous  $\text{Na}_2\text{SO}_4$  and concentrated in vacuo. The residue was purified by column chromatography using Hex/EtOAc.

**2-(Pyrrolidin-1-yl)benzo[d]oxazole (14).** White solid. Yield: 54% (60 mg).  $^1\text{H}$  NMR (400 MHz, DMSO- $d_6$ ):  $\delta$  7.37 (dd,  $J = 7.9, 0.5$  Hz, 1H), 7.25 (dd,  $J = 7.8, 0.8$  Hz, 1H), 7.12 (td,  $J = 7.7, 1.1$  Hz, 1H), 6.97 (td,  $J = 7.7, 1.3$  Hz, 1H), 3.54 (ddd,  $J = 6.7, 4.3, 2.6$  Hz, 4H), 2.00–1.93 (m, 4H).  $^{13}\text{C}$  NMR (101 MHz, DMSO-



$d_6$ ):  $\delta$  160.51, 148.54, 143.59, 123.72, 119.77, 115.36, 108.63, 47.16, 25.03. HRMS:  $m/z$ : calcd for  $C_{11}H_{12}N_2O$ : 189.1022  $[M + H]^+$ ; found: 189.1022.

**Smiles Rearrangement with 5-Bromopentylamine HBr.** Benzoxazole-2-thiol **4** (0.6 mmol, 1 equiv) and  $Et_3N$  (1.2 mmol, 2 equiv) were dissolved in toluene (5 mL) and premixed at rt for 10 min. Subsequently, 5-bromopentylamine HBr **15** (1.2 mmol, 2 equiv) was added. The reaction mixture was refluxed for 4 h. It was cooled to room temperature, diluted with  $H_2O$  (20 mL), and extracted with EtOAc ( $3 \times 20$  mL). Organic layers were dried over anhydrous  $Na_2SO_4$  and concentrated in vacuo.

**5-(Benzo[d]oxazol-2-ylthio)pentan-1-amine HBr (16).** White solid. Yield: 95% (134 mg).  $^1H$  NMR (400 MHz,  $DMSO-d_6$ ):  $\delta$  7.68–7.59 (m, 2H), 7.37–7.28 (m, 2H), 3.54 (br s, 3H), 3.37–3.28 (m, 2H), 2.60 (t,  $J = 6.5$  Hz, 2H), 1.85–1.71 (m, 2H), 1.53–1.35 (m, 4H).  $^{13}C$  NMR (101 MHz,  $DMSO-d_6$ ):  $\delta$  164.47, 151.18, 141.31, 124.52, 124.12, 118.15, 110.09, 41.04, 31.77, 31.68, 28.75, 25.30. HRMS:  $m/z$ : calcd for  $C_{12}H_{16}N_2OS$ : 237.1056  $[M + H]^+$ ; found: 237.1056.

**Smiles Rearrangement with 16.** Compound **16** (0.42 mmol, 1 equiv) and  $Et_3N$  (0.84 mmol, 2 equiv) were dissolved in DMF (4 mL). The reaction mixture was stirred under microwave irradiation at 120 °C for 2 h. After that, it was cooled to room temperature, diluted with  $H_2O$  (20 mL), and extracted with EtOAc ( $3 \times 20$  mL). Organic layers were dried over anhydrous  $Na_2SO_4$  and concentrated in vacuo. The residue was purified by column chromatography using Hex/EtOAc.

**N-(5-(Benzo[d]oxazol-2-ylthio)pentyl)formamide (18).** Brown oil. Yield: 58% (64 mg).  $^1H$  NMR (400 MHz,  $DMSO-d_6$ ):  $\delta$  7.99 (s, 1H), 7.97 (br s, 1H), 7.68–7.59 (m, 2H), 7.36–7.28 (m, 3H), 3.35–3.28 (m, 2H, overlapped with  $H_2O$ ), 3.09 (q,  $J = 6.3$  Hz, 2H), 1.84–1.73 (m, 2H), 1.50–1.38 (m, 4H).  $^{13}C$  NMR (101 MHz,  $DMSO-d_6$ ):  $\delta$  164.43, 160.87, 151.18, 141.31, 124.52, 124.12, 118.16, 110.10, 36.83, 31.59, 28.51, 28.39, 25.30. HRMS:  $m/z$ : calcd for  $C_{13}H_{16}N_2O_2S$ : 265.1005  $[M + H]^+$ ; found: 265.1006.

**Smiles Rearrangement with 4-Bromobenzylamine.** Benzoxazole-2-thiol **4** (0.6 mmol, 1 equiv) and  $Et_3N$  (1.2 mmol, 2 equiv) were dissolved in toluene (5 mL) and premixed at rt for 10 min. Subsequently, 4-bromobenzylamine **19** (1.2 mmol, 2 equiv) was added. The reaction mixture was refluxed overnight (monitored by TLC, 18 h). It was cooled to room temperature, diluted with  $H_2O$  (20 mL), and extracted with EtOAc ( $3 \times 20$  mL). Organic layers were dried over anhydrous  $Na_2SO_4$  and concentrated in vacuo. The residue was purified by column chromatography using Hex/EtOAc.

**N-(4-Bromobenzyl)benzo[d]oxazol-2-amine (22).** Brown solid. Yield: 69% (125 mg).  $^1H$  NMR (400 MHz,  $DMSO-d_6$ ):  $\delta$  8.48 (t,  $J = 6.1$  Hz, 1H), 7.56–7.49 (m, 2H), 7.34 (d,  $J = 8.6$  Hz, 3H), 7.24 (dd,  $J = 7.8, 0.6$  Hz, 1H), 7.10 (td,  $J = 7.6, 1.0$  Hz, 1H), 6.98 (td,  $J = 7.7, 1.2$  Hz, 1H), 4.50 (d,  $J = 6.0$  Hz, 2H).  $^{13}C$  NMR (101 MHz,  $DMSO-d_6$ ):  $\delta$  162.29, 148.11, 143.01, 138.54, 131.21, 129.39, 123.61, 120.28, 120.02, 115.58, 108.58, 45.02. HRMS:  $m/z$ : calcd for  $C_{14}H_{11}BrN_2O$ : 303.0128  $[M + H]^+$ ; found: 303.0126.

**Smiles Rearrangement with 2-Chloroacetamide.** Benzoxazole-2-thiol **4** (1.61 mmol, 1 equiv),  $K_2CO_3$  (4.8 mmol; 3 equiv), and 2-chloroacetamide **23** (3.2 mmol; 2 equiv) were suspended in DMF (10 mL). The reaction mixture was stirred at 70 °C for 4 h. It was cooled to room temperature, diluted with  $H_2O$  (50 mL), and extracted with EtOAc ( $3 \times 50$  mL). Organic layers were washed with brine (1 $\times$ ), dried over anhydrous

$Na_2SO_4$ , and concentrated in vacuo. The residue was purified by column chromatography using Hex/EtOAc.

**2-(Benzo[d]oxazol-2-ylthio)acetamide (25).** Yellow solid. Yield: 46% (152 mg).  $^1H$  NMR (400 MHz,  $DMSO-d_6$ ):  $\delta$  7.75 (s, 1H), 7.63 (ddd,  $J = 7.0, 3.1, 1.2$  Hz, 2H), 7.39–7.27 (m, 3H), 4.12 (s, 2H).  $^{13}C$  NMR (101 MHz,  $DMSO-d_6$ ):  $\delta$  168.00, 164.10, 151.28, 141.27, 124.63, 124.25, 118.19, 110.19, 35.82. HRMS:  $m/z$ : calcd for  $C_9H_8N_2O_2S$ : 209.0379  $[M + H]^+$ ; found: 209.0378.

**Smiles Rearrangement with 3-(Bromomethyl)aniline.** Benzoxazole-2-thiol **4** (0.6 mmol, 1 equiv), 3-(bromomethyl)aniline **26** (1.2 mmol, 2 equiv), and  $K_2CO_3$  (1.2 mmol, 2 equiv) were suspended in DMF (5 mL). The reaction mixture was stirred at 70 °C for 2 h. It was cooled to room temperature, diluted with  $H_2O$  (20 mL), and extracted with EtOAc ( $3 \times 20$  mL). Organic layers were dried over anhydrous  $Na_2SO_4$  and concentrated in vacuo. The residue was purified by column chromatography using Hex/EtOAc.

**3-(Benzo[d]oxazol-2-ylthio)methyl)aniline (27).** White solid. Yield: 80% (123 mg).  $^1H$  NMR (400 MHz,  $DMSO-d_6$ ):  $\delta$  7.65 (m, 2H), 7.37–7.29 (m, 2H), 6.97 (t,  $J = 7.7$  Hz, 1H), 6.66 (t,  $J = 1.9$  Hz, 1H), 6.59 (d,  $J = 7.5$  Hz, 1H), 6.47 (m, 1H), 5.13 (br s, 2H), 4.47 (s, 2H).  $^{13}C$  NMR (101 MHz,  $DMSO-d_6$ ):  $\delta$  164.04, 151.22, 148.92, 141.28, 136.52, 129.10, 124.60, 124.27, 118.27, 116.19, 114.01, 113.35, 110.18, 36.00. HRMS:  $m/z$ : calcd for  $C_{14}H_{12}N_2OS$ : 257.0743  $[M + H]^+$ ; found: 257.0742.

**Smiles Rearrangement with Amines.** To a stirred solution of amine **29** (0.48 mmol, 1 equiv) and  $Cs_2CO_3$  (1.54 mmol, 3.2 equiv) in DMF (3 mL) cooled to  $-5$  °C were added chloroacetyl chloride (0.58 mmol, 1.2 equiv) and benzoxazole-2-thiol **4** (0.48 mmol, 1 equiv). The reaction mixture was refluxed (monitored by TLC, 4–7 h). After that, the cooled (rt) mixture was diluted with  $H_2O$  (20 mL), extracted with  $CH_2Cl_2$  ( $3 \times 30$  mL), and washed with brine (50 mL). Combined organic layers were dried over  $Na_2SO_4$  and concentrated in vacuo. The residue was purified by column chromatography using Hex/EtOAc and Tol/MeCN.

**N-Benzylbenzo[d]oxazol-2-amine (30a).** Yellow solid. Yield: 83% (89 mg).  $^1H$  NMR (500 MHz,  $DMSO-d_6$ ):  $\delta$  8.45 (t,  $J = 6.1$  Hz, 1H), 7.41–7.30 (m, 5H), 7.25 (dd,  $J = 15.1, 7.8$  Hz, 2H), 7.10 (td,  $J = 7.7, 1.0$  Hz, 1H), 6.98 (td,  $J = 7.8, 1.2$  Hz, 1H), 4.52 (d,  $J = 6.2$  Hz, 2H).  $^{13}C$  NMR (101 MHz,  $DMSO-d_6$ ):  $\delta$  162.46, 148.13, 143.15, 139.06, 128.39, 127.19, 127.06, 123.64, 120.24, 115.54, 108.60, 45.69. HRMS:  $m/z$ : calcd for  $C_9H_{12}N_2O_2S$ : 225.1022  $[M + H]^+$ ; found: 225.1023.

**N-Hexylbenzo[d]oxazol-2-amine (30b).** Orange solid. Yield: 58% (60 mg).  $^1H$  NMR (400 MHz,  $DMSO-d_6$ ):  $\delta$  7.89 (t,  $J = 5.6$  Hz, 1H), 7.31 (d,  $J = 7.8$  Hz, 1H), 7.22 (d,  $J = 7.6$  Hz, 1H), 7.09 (t,  $J = 7.6$  Hz, 1H), 6.95 (td,  $J = 7.8, 0.9$  Hz, 1H), 3.28 (dd,  $J = 13.0, 6.8$  Hz, 2H), 1.62–1.51 (m, 2H), 1.35–1.25 (m, 6H), 0.86 (t,  $J = 6.7$  Hz, 3H).  $^{13}C$  NMR (101 MHz,  $DMSO-d_6$ ):  $\delta$  162.40, 147.99, 143.40, 123.52, 119.94, 115.32, 108.42, 42.29, 30.98, 28.88, 25.96, 22.10, 13.93. HRMS:  $m/z$ : calcd for  $C_{13}H_{18}N_2O$ : 219.1492  $[M + H]^+$ ; found: 219.1491.

**N-Phenylbenzo[d]oxazol-2-amine (30c).** Yellow solid. Yield: 76% (76 mg).  $^1H$  NMR (400 MHz,  $DMSO-d_6$ ):  $\delta$  10.61 (s, 1H), 7.76 (d,  $J = 7.8$  Hz, 2H), 7.47 (dd,  $J = 13.3, 7.7$  Hz, 2H), 7.37 (t,  $J = 7.9$  Hz, 2H), 7.22 (td,  $J = 7.7, 0.9$  Hz, 1H), 7.13 (td,  $J = 7.8, 1.2$  Hz, 1H), 7.03 (t,  $J = 7.4$  Hz, 1H).  $^{13}C$  NMR (101 MHz,  $DMSO-d_6$ ):  $\delta$  157.97, 146.99, 142.43, 138.73, 129.00, 124.01, 122.12, 121.68, 117.55, 116.62, 108.97. HRMS:  $m/z$ : calcd for  $C_{13}H_{10}N_2O$ : 211.0866  $[M + H]^+$ ; found: 211.0864.

***N*-(4-Nitrophenyl)benzo[d]oxazol-2-amine (30d).** Yellow solid. Yield: 74% (90 mg).  $^1\text{H}$  NMR (400 MHz, DMSO- $d_6$ ):  $\delta$  11.45 (s, 1H), 8.30 (d,  $J$  = 9.1 Hz, 2H), 7.98 (d,  $J$  = 8.8 Hz, 2H), 7.60–7.54 (m, 2H), 7.29 (t,  $J$  = 7.6 Hz, 1H), 7.22 (t,  $J$  = 7.7 Hz, 1H).  $^{13}\text{C}$  NMR (101 MHz, DMSO- $d_6$ ):  $\delta$  156.87, 147.00, 144.93, 141.67, 141.27, 125.37, 124.38, 122.68, 117.30, 117.15, 109.41. HRMS:  $m/z$ : calcd for  $\text{C}_{13}\text{H}_9\text{N}_3\text{O}_3$ : 256.0717 [M + H] $^+$ ; found: 256.0719.

***N*-(4-Methoxyphenyl)benzo[d]oxazol-2-amine (30e).** Orange solid. Yield: 78% (90 mg).  $^1\text{H}$  NMR (500 MHz, DMSO- $d_6$ ):  $\delta$  10.36 (s, 1H), 7.65 (d,  $J$  = 9.1 Hz, 2H), 7.45 (d,  $J$  = 7.8 Hz, 1H), 7.41 (d,  $J$  = 7.1 Hz, 1H), 7.19 (td,  $J$  = 7.6, 1.1 Hz, 1H), 7.09 (td,  $J$  = 7.7, 1.2 Hz, 1H), 6.96 (d,  $J$  = 9.1 Hz, 2H), 3.74 (s, 3H).  $^{13}\text{C}$  NMR (101 MHz, DMSO- $d_6$ ):  $\delta$  158.36, 154.65, 147.08, 142.64, 131.92, 123.91, 121.34, 119.15, 116.34, 114.23, 108.82, 55.25. HRMS:  $m/z$ : calcd for  $\text{C}_{14}\text{H}_{12}\text{N}_2\text{O}_3$ : 241.0972 [M + H] $^+$ ; found: 241.0970.

***N*-(4-Bromophenyl)benzo[d]oxazol-2-amine (30f).** Yellow solid. Yield: 82% (113 mg).  $^1\text{H}$  NMR (500 MHz, DMSO- $d_6$ ):  $\delta$  10.77 (s, 1H), 7.74 (d,  $J$  = 8.9 Hz, 2H), 7.55 (d,  $J$  = 8.9 Hz, 2H), 7.48 (dd,  $J$  = 14.3, 7.7 Hz, 2H), 7.23 (td,  $J$  = 7.7, 1.0 Hz, 1H), 7.15 (td,  $J$  = 7.8, 1.2 Hz, 1H).  $^{13}\text{C}$  NMR (101 MHz, DMSO- $d_6$ ):  $\delta$  157.63, 146.97, 142.19, 138.14, 131.77, 124.11, 121.94, 119.46, 116.77, 113.58, 109.09. HRMS:  $m/z$ : calcd for  $\text{C}_{13}\text{H}_9\text{BrN}_2\text{O}$ : 288.9971 [M + H] $^+$ ; found: 288.9969.

***N*-(3-Bromophenyl)benzo[d]oxazol-2-amine (30g).** Yellow solid. Yield: 78% (108 mg).  $^1\text{H}$  NMR (400 MHz, DMSO- $d_6$ ):  $\delta$  10.82 (s, 1H), 8.11 (t,  $J$  = 1.9 Hz, 1H), 7.67 (dd,  $J$  = 8.2, 1.2 Hz, 1H), 7.51 (d,  $J$  = 8.9 Hz, 2H), 7.33 (t,  $J$  = 8.1 Hz, 1H), 7.23 (m, 2H), 7.16 (td,  $J$  = 7.6, 1.1 Hz, 1H).  $^{13}\text{C}$  NMR (101 MHz, DMSO- $d_6$ ):  $\delta$  157.44, 146.94, 142.07, 140.34, 130.97, 124.66, 124.16, 122.08, 121.93, 119.62, 116.94, 116.46, 109.14. HRMS:  $m/z$ : calcd for  $\text{C}_{13}\text{H}_9\text{BrN}_2\text{O}$ : 288.9971 [M + H] $^+$ ; found: 288.9971.

***N*-(2-Bromophenyl)benzo[d]oxazol-2-amine (30h).** White solid. Yield: 81% (112 mg).  $^1\text{H}$  NMR (400 MHz, DMSO- $d_6$ ):  $\delta$  9.87 (s, 1H), 7.93 (s, 1H), 7.70 (d,  $J$  = 8.0 Hz, 1H), 7.45 (t,  $J$  = 7.2 Hz, 2H), 7.37 (d,  $J$  = 7.6 Hz, 1H), 7.25–7.08 (m, 3H).  $^{13}\text{C}$  NMR (101 MHz, DMSO- $d_6$ ):  $\delta$  133.00, 128.48, 126.53, 125.46, 124.07, 121.55, 117.20, 109.10. HRMS:  $m/z$ : calcd for  $\text{C}_{13}\text{H}_9\text{BrN}_2\text{O}$ : 288.9971 [M + H] $^+$ ; found: 288.9969.

**2-(Benzo[d]oxazol-2-ylamino)ethan-1-ol (30i).** White solid. Yield: 55% (47 mg).  $^1\text{H}$  NMR (400 MHz, DMSO- $d_6$ ):  $\delta$  7.92 (t,  $J$  = 5.7 Hz, 1H), 7.32 (d,  $J$  = 7.8 Hz, 1H), 7.22 (d,  $J$  = 7.4 Hz, 1H), 7.09 (td,  $J$  = 7.7, 0.8 Hz, 1H), 6.96 (td,  $J$  = 7.7, 1.1 Hz, 1H), 4.80 (t,  $J$  = 5.5 Hz, 1H), 3.56 (q,  $J$  = 5.9 Hz, 2H), 3.35 (q,  $J$  = 5.8 Hz, 2H overlapped with  $\text{H}_2\text{O}$ ).  $^{13}\text{C}$  NMR (101 MHz, DMSO- $d_6$ ):  $\delta$  162.49, 148.03, 143.31, 123.56, 120.01, 115.34, 108.47, 59.44, 44.99. HRMS:  $m/z$ : calcd for  $\text{C}_9\text{H}_{10}\text{N}_2\text{O}_2$ : 179.0815 [M + H] $^+$ ; found: 179.0814.

**2-Morpholinobenzo[d]oxazole (30j).** White solid. Yield: 31% (30 mg).  $^1\text{H}$  NMR (400 MHz, DMSO- $d_6$ ):  $\delta$  7.42–7.40 (m, 1H), 7.33–7.28 (m, 1H), 7.16 (td,  $J$  = 7.6, 1.1 Hz, 1H), 7.03 (td,  $J$  = 7.7, 1.3 Hz, 1H), 3.76–3.69 (m, 4H), 3.62–3.55 (m, 4H).  $^{13}\text{C}$  NMR (101 MHz, DMSO- $d_6$ ):  $\delta$  161.85, 148.30, 142.79, 124.02, 120.69, 115.98, 108.98, 65.41, 45.37. HRMS:  $m/z$ : calcd for  $\text{C}_{11}\text{H}_{12}\text{N}_2\text{O}_2$ : 205.0972 [M + H] $^+$ ; found: 205.0972.

***N*-Cyclohexylbenzo[d]oxazol-2-amine (30l).** Orange solid. Yield: 33% (34 mg).  $^1\text{H}$  NMR (400 MHz, DMSO- $d_6$ ):  $\delta$  7.84 (d,  $J$  = 7.7 Hz, 1H), 7.31 (d,  $J$  = 7.8 Hz, 1H), 7.22 (d,  $J$  = 7.7 Hz, 1H), 7.08 (t,  $J$  = 7.6 Hz, 1H), 6.95 (t,  $J$  = 7.7 Hz, 1H), 3.54 (brs, 1H), 1.96 (m, 2H), 1.73 (m, 2H), 1.59 (m, 1H), 1.36–1.23 (m, 4H), 1.21–1.10 (m, 1H).  $^{13}\text{C}$  NMR (101 MHz, DMSO- $d_6$ ):  $\delta$

161.65, 147.85, 143.41, 123.50, 119.90, 115.27, 108.37, 51.56, 32.42, 25.20, 24.55. HRMS:  $m/z$ : calcd for  $\text{C}_{13}\text{H}_{16}\text{N}_2\text{O}$ : 217.1335 [M + H] $^+$ ; found: 217.1337.

**Substitution with Cyclohexylamine.** To a stirred solution of amine **29** (0.48 mmol, 1 equiv) and DBU (1.54 mmol, 3.2 equiv) in MeCN (3 mL) cooled to  $-5^\circ\text{C}$  were added chloroacetyl chloride (0.58 mmol, 1.2 equiv) and benzoxazole-2-thiol **4** (0.48 mmol, 1 equiv). The reaction mixture was refluxed (monitored by TLC, 3 h). After that, the cooled (rt) mixture was diluted with  $\text{H}_2\text{O}$  (20 mL), extracted with  $\text{CH}_2\text{Cl}_2$  (3  $\times$  30 mL), and washed with brine (50 mL). Combined organic layers were dried over  $\text{Na}_2\text{SO}_4$  and concentrated in vacuo. The residue was purified by column chromatography using Hex/EtOAc.

**2-(Benzo[d]oxazol-2-ylthio)-*N*-cyclohexylacetamide (31l).** White solid. Yield: 62% (86 mg).  $^1\text{H}$  NMR (400 MHz, DMSO- $d_6$ ):  $\delta$  8.19 (d,  $J$  = 7.7 Hz, 1H), 7.66–7.58 (m, 2H), 7.38–7.29 (m, 2H), 4.11 (s, 2H), 3.62–3.48 (m, 1H), 1.79–1.63 (m, 4H), 1.53 (m, 1H), 1.32–1.11 (m, 5H).  $^{13}\text{C}$  NMR (101 MHz, DMSO- $d_6$ ):  $\delta$  164.96, 163.94, 151.22, 141.24, 124.61, 124.24, 118.14, 110.12, 48.02, 35.83, 32.14, 25.11, 24.31. HRMS:  $m/z$ : calcd for  $\text{C}_{15}\text{H}_{18}\text{N}_2\text{O}_2\text{S}$ : 291.1162 [M + H] $^+$ ; found: 291.1161.

## ■ ASSOCIATED CONTENT

### Supporting Information

The Supporting Information is available free of charge on the ACS Publications website at DOI: 10.1021/acsomega.9b02702.

Optimization of the reaction conditions with Lewis acids, 3-bromopropylamine HBr, 2-bromoethylamine HBr, 4-bromobutylamine HBr, 5-bromopentylamine HBr, 4-bromobenzylamine, 2-chloroacetamide, 3-(bromomethyl)aniline, and aniline; copies of  $^1\text{H}$  and  $^{13}\text{C}$  NMR spectra (Tables S1–S9) (PDF)

## ■ AUTHOR INFORMATION

### Corresponding Author

\*E-mail: lucie.brulikova@upol.cz.

### ORCID

Lucie Bruliková: 0000-0001-8380-073X

### Notes

The authors declare no competing financial interest.

## ■ ACKNOWLEDGMENTS

This work was supported by the Ministry of Education, Youth and Sport of the Czech Republic (project IGA\_PrF\_2019\_027) and by grant no. JG\_2019\_002 from Palacký University in Olomouc.

## ■ REFERENCES

- Šlachetová, V.; Brulikova, L. Benzoxazole Derivatives as Promising Antitubercular Agents. *ChemistrySelect* **2018**, *3*, 4653–4662.
- Cui, M.; Ono, M.; Kimura, H.; Ueda, M.; Nakamoto, Y.; Togashi, K.; Okamoto, Y.; Ihara, M.; Takahashi, R.; Liu, B.; Saji, H. Novel 18F-Labeled Benzoxazole Derivatives as Potential Positron Emission Tomography Probes for Imaging of Cerebral  $\alpha$ -Amyloid Plaques in Alzheimer's Disease. *J. Med. Chem.* **2012**, *55*, 9136–9145.
- Abdelazeem, A. H.; Khan, S. I.; White, S. W.; Sufka, K. J.; McCurdy, C. R. Design, synthesis and biological evaluation of bivalent benzoxazolone and benzothiazolone ligands as potential anti-inflammatory/analgesic agents. *Bioorg. Med. Chem.* **2015**, *23*, 3248–3259.
- Harmange, J. C.; Weiss, M. M.; Germain, J.; Polverino, A. J.; Borg, G.; Bready, J.; Chen, D.; Choquette, D.; Coxon, A.; DeMelh, T.;



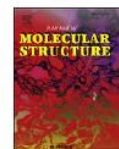
- DiPietro, L.; Doerr, N.; Estrada, J.; Flynn, J.; Graceffa, R. F.; Harriman, S. P.; Kaufman, S.; La, D. S.; Long, A.; Martin, M. W.; Neervannan, S.; Patel, V. F.; Potashman, M.; Regal, K.; Roveto, P. M.; Schrag, M. L.; Starnes, C.; Tasker, A.; Teffera, Y.; Wang, L.; White, R. D.; Whittington, D. A.; Zanon, R. Naphthamides as Novel and Potent Vascular Endothelial Growth Factor Receptor Tyrosine Kinase Inhibitors: Design, Synthesis, and Evaluation. *J. Med. Chem.* **2008**, *51*, 1649–1667.
- (5) Khajondetchairit, P.; Phuangsawai, O.; Suphakun, P.; Rattanabunpong, S.; Choowongkorn, K.; Gleeson, M. P. Design, synthesis, and evaluation of the anticancer activity of 2-amino-aryl-7-aryl-benzoxazole compounds. *Chem. Biol. Drug Des.* **2017**, *90*, 987–994.
- (6) Sweis, R. F.; Hunt, J. A.; Sinclair, P. J.; Chen, Y.; Eveland, S. S.; Guo, Q.; Hyland, S. A.; Milot, D. P.; Cumiskey, A. M.; Latham, M.; Rosa, R.; Peterson, L.; Sparrow, C. P.; Anderson, M. S. 2-(4-Carbonylphenyl)benzoxazole inhibitors of CETP: Attenuation of hERG binding and improved HDLc-raising efficacy. *Bioorg. Med. Chem. Lett.* **2011**, *21*, 2597–2600.
- (7) Potashman, M. H.; Bready, J.; Coxon, A.; DeMelfi, T. M., Jr; DiPietro, L.; Doerr, N.; Elbaum, D.; Estrada, J.; Gallant, P.; Germain, J.; Gu, Y.; Harmange, J. C.; Kaufman, S. A.; Kendall, R.; Kim, J. L.; Kumar, G. N.; Long, A. M.; Neervannan, S.; Patel, V. F.; Polverino, A.; Rose, P.; Van der Plas, S.; Whittington, D.; Zanon, R.; Zhao, H. Design, Synthesis, and Evaluation of Orally Active Benzimidazoles and Benzoxazoles as Vascular Endothelial Growth Factor-2 Receptor Tyrosine Kinase Inhibitors. *J. Med. Chem.* **2007**, *50*, 4351–4373.
- (8) Chikhale, R.; Thorat, S.; Choudhary, R. K.; Gadewal, N.; Khedekar, P. Design, synthesis and anticancer studies of novel aminobenzazolyl pyrimidines as tyrosine kinase inhibitors. *Bioorg. Chem.* **2018**, *77*, 84–100.
- (9) Ko, C. W.; Tao, Y. T.; Danel, A.; Krzeminska, L.; Tomasik, P. Organic Light-Emitting Diodes Based on 2-(Stilbene-4-yl)benzoxazole Derivatives: An Implication on the Emission Mechanism. *Chem. Mater.* **2001**, *13*, 2441–2446.
- (10) Grytsai, O.; Druzhenko, T.; Demange, L.; Ronco, C.; Benhida, R. Cyanoguanidine as a versatile, eco-friendly and inexpensive reagent for the synthesis of 2-aminobenzoxazoles and 2-guanidinobenzoxazoles. *Tetrahedron Lett.* **2018**, *59*, 1642–1645.
- (11) Nagano, T.; Itoh, M.; Matsumura, K. Preparation of certain derivatives of benzoxazole. *J. Am. Chem. Soc.* **1953**, *75*, 2770–2771.
- (12) Wu, Y. Q.; Limburg, D. C.; Wilkinson, D. E.; Hamilton, G. S. Formation of nitrogen-containing heterocycles using di(imidazole-1-yl)methanimine. *J. Heterocycl. Chem.* **2003**, *40*, 191–193.
- (13) Kasthuri, M.; Babu, H. S.; Kumar, K. S.; Sudhakar, C.; Kumar, P. V. N. A Facile Synthesis of 2-Aminobenzoxazoles and 2-Amino-benzimidazoles Using N-Cyano-N-phenyl-p-toluenesulfonamide (NCTS) as an Efficient Electrophilic Cyanating Agent. *Synlett* **2015**, *26*, 897–900.
- (14) Glotz, G.; Lebl, R.; Dallinger, D.; Kappe, C. O. Integration of Bromine and Cyanogen Bromide Generators for the Continuous-Flow Synthesis of Cyclic Guanidines. *Angew. Chem., Int. Ed.* **2017**, *56*, 13786–13789.
- (15) Reddy, L. M.; Prakash, T. B.; Padmaja, A.; Padmavathi, V. Synthesis and antimicrobial activity of pyrazolyl benzoxazoles, benzothiazoles and benzimidazoles. *Med. Chem. Res.* **2015**, *24*, 970–979.
- (16) Gudipati, R.; Anreddy, R. N. R.; Manda, S. Synthesis, anticancer and antioxidant activities of some novel N-(benzo[d]oxazol-2-yl)-2-(7- or 5-substituted-2-oxindolin-3-ylidene) hydrazinecarboxamide derivatives. *J. Enzyme Inhib. Med. Chem.* **2011**, *26*, 813–818.
- (17) Kaupp, G.; Schmeyers, J.; Boy, J. Quantitative gas-solid reactions with ClCN and BrCN: synthesis of cyanamides, cyanates, thiocyanates, and their derivatives. *Chem. - Eur. J.* **1998**, *4*, 2467–2474.
- (18) Schuart, J.; Mueller, H. K. Reactions with 2-aminobenzoxazoles. 8. 2-Amino-oxazole and 2-imino-oxazoline. *Pharmazie* **1975**, *30*, 155–157.
- (19) Liu, J.; Hoover, J. M. Cobalt-Catalyzed Aerobic Oxidative Cyclization of 2-Aminophenols with Isonitriles: 2-Aminophenol Enabled O<sub>2</sub> Activation by Cobalt(II). *Org. Lett.* **2019**, *21*, 4510–4514.
- (20) Lee, S.; Lee, Y. Copper-Catalyzed Electrophilic Amination of Benzoxazoles via Magnesiation. *Eur. J. Org. Chem.* **2019**, *2019*, 3045–3050.
- (21) Wu, Y. Q.; Limburg, D. C.; Wilkinson, D. E.; Hamilton, G. S. Formation of nitrogen-containing heterocycles using di(imidazole-1-yl)methanimine. *J. Heterocycl. Chem.* **2003**, *40*, 191–193.
- (22) Kim, J. Y.; Cho, S. H.; Joseph, J.; Chang, S. Cobalt- and Manganese-Catalyzed Direct Amination of Azoles under Mild Reaction Conditions and the Mechanistic Details. *Angew. Chem., Int. Ed.* **2010**, *49*, 9899–9903.
- (23) Cho, S. H.; Kim, J. Y.; Lee, S. Y.; Chang, S. Silver-mediated direct amination of benzoxazoles: tuning the amino group source from formamides to parent amines. *Angew. Chem., Int. Ed.* **2009**, *48*, 9127–9130.
- (24) Wang, J.; Hou, J. T.; Wen, J.; Zhang, J.; Yu, X. Q. Iron-catalyzed direct amination of azoles using formamides or amines as nitrogen sources in air. *Chem. Commun.* **2011**, *47*, 3652–3654.
- (25) Cioffi, C. L.; Lansing, J. J.; Yuksel, H. Synthesis of 2-Aminobenzoxazoles Using Tetramethyl Orthocarbonate or 1,1-Dichlorodiphenoxymethane. *J. Org. Chem.* **2010**, *75*, 7942–7945.
- (26) Liu, B.; Yin, M.; Gao, H.; Wu, W.; Jiang, H. Synthesis of 2-Aminobenzoxazoles and 3-Aminobenzoxazines via Palladium-Catalyzed Aerobic Oxidation of o-Aminophenols with Isocyanides. *J. Org. Chem.* **2013**, *78*, 3009–3020.
- (27) Liu, M.; Zeng, M. T.; Xu, W.; Wu, L.; Dong, Z. B. Selective synthesis of 2-aminobenzoxazoles and 2-mercaptobenzoxazoles by using o-aminophenols as starting material. *Tetrahedron Lett.* **2017**, *58*, 4352–4356.
- (28) Rattanangkool, E.; Sukwattanasinit, M.; Wacharasindhu, S. Organocatalytic Visible Light Enabled SNAr of Heterocyclic Thiols: A Metal-Free Approach to 2-Aminobenzoxazoles and 4-Aminoquinazolines. *J. Org. Chem.* **2017**, *82*, 13256–13262.
- (29) Tankam, T.; Srisa, J.; Sukwattanasinit, M.; Wacharasindhu, S. Microwave-Enhanced On-Water Amination of 2-Mercaptobenzoxazoles To Prepare 2-Aminobenzoxazoles. *J. Org. Chem.* **2018**, *83*, 11936–11943.
- (30) Wang, G.; Peng, Z.; Wang, J.; Li, J.; Li, X. Synthesis, biological evaluation and molecular docking study of N-arylbenzo[d]oxazol-2-amines as potential  $\alpha$ -glucosidase inhibitors. *Bioorg. Med. Chem.* **2016**, *24*, 5374–5379.
- (31) Zhang, X.; Jia, X.; Wang, J.; Fan, X. An economically and environmentally sustainable synthesis of 2-aminobenzothiazoles and 2-aminobenzoxazoles promoted by water. *Green Chem.* **2011**, *13*, 413–418.
- (32) Zhou, Y.; Liu, Z.; Yuan, T.; Huang, J.; Liu, C. The synthesis of 2-aminobenzoxazoles using reusable ionic liquid as a green catalyst under mild conditions. *Molecules* **2017**, *22*, 576/1–576/9.
- (33) Mo, S. N-Cyano-N-phenyl-p-toluenesulfonamide. *Synlett* **2014**, *25*, 1337–1338.
- (34) Yang, Y.; Zhang, Y.; Wang, J. B. Lewis Acid Catalyzed Direct Cyanation of Indoles and Pyrroles with N-Cyano-N-phenyl-p-toluenesulfonamide (NCTS). *Org. Lett.* **2011**, *13*, 5608–5611.
- (35) Nagata, T.; Matsubara, H.; Kiyokawa, K.; Minakata, S. Catalytic Activation of 1-Cyano-3,3-dimethyl-3-(1H)-1,2-benziodoxole with B(C<sub>6</sub>F<sub>5</sub>)<sub>3</sub> Enabling the Electrophilic Cyanation of Silyl Enol Ethers. *Org. Lett.* **2017**, *19*, 4672–4675.
- (36) Holden, C. M.; Greaney, M. F. Modern Aspects of the Smiles Rearrangement. *Chem. - Eur. J.* **2017**, *23*, 8992–9008.
- (37) Wang, G.; Wang, J.; Li, L.; Chen, S.; Peng, Y.; Xie, Z.; Chen, M.; Deng, B.; Li, W. Synthesis of N-aryl-2-aminobenzoxazoles from substituted benzoxazole-2-thiol and 2-chloro-N-arylacetylides in KOH-DMF system. *Heterocycles* **2017**, *94*, 1257–1268.
- (38) Minin, P. L.; Walton, J. C. Radical Ring Closures of 4-Isocyanato Carbon-Centered Radicals. *J. Org. Chem.* **2003**, *68*, 2960–2963.
- (39) Tian, X.; Wu, R. M.; Liu, G.; Li, Z. B.; Wei, H. L.; Yang, H.; Shin, D. S.; Wang, L. Y.; Zuo, H. Smiles rearrangement for the synthesis of diarylamines. *ARKIVOC* **2011**, 118–126.





Contents lists available at ScienceDirect

Journal of Molecular Structure

journal homepage: <http://www.elsevier.com/locate/molstruc>

## Solid phase synthesis of new thiazolidinedione-pyrimidine conjugates and their antibacterial properties

Veronika Šlachťová<sup>a</sup>, Lucie Janovská<sup>b, c</sup>, Lucie Brulíková<sup>d, \*</sup>

<sup>a</sup> Department of Organic Chemistry, Faculty of Science, Palacký University, 17. Listopadu 12, Olomouc, 77146, Czech Republic

<sup>b</sup> Department of Chemical Biology and Genetics, Centre of the Region Haná for Biotechnological and Agricultural Research, Faculty of Science, Palacký University, Šlechtitělská 27, Olomouc, 783 71, Czech Republic

<sup>c</sup> Department of Microbiology, Faculty of Medicine and Dentistry, Palacký University, Hněvotínská 3, Olomouc, 775 15, Czech Republic

<sup>d</sup> Department of Medicinal Chemistry, Institute of Molecular and Translational Medicine, Hněvotínská 5, Olomouc, 77900, Czech Republic



### ARTICLE INFO

#### Article history:

Received 18 December 2018

Received in revised form

23 January 2019

Accepted 24 January 2019

Available online 29 January 2019

#### Keywords:

Solid-phase synthesis

Pyrimidine

Thiazolidinedione

Conjugates

Antimicrobial

Antibacterial

### ABSTRACT

The polymer-supported synthetic protocol for preparation of thiazolidinedione-pyrimidine hybrids was developed and applied for rapid and effective synthesis of a library of variously substituted conjugates. Reported synthetic methodology is based on easy accessible building blocks and very simple chemical operations enabling effective development of potent experimental therapeutics of this type via a combinatorial manner. Synthesized model compounds were tested for their antitubercular activity against *Mycobacterium tuberculosis* H37Rv, antimicrobial activity against several Gram-positive and Gram-negative strains such as *Staphylococcus aureus*, *Pseudomonas aeruginosa*, *Escherichia coli* and *Enterococcus faecalis* and two fungal strains (*Candida albicans* and *Aspergillus niger*). Slight activity was found for some of them.

© 2019 Elsevier B.V. All rights reserved.

### 1. Introduction

The thiazolidine-2,4-diones (glitazones) are well-known pharmacophores introduced in the late 1990's for the treatment of type 2 diabetes mellitus [1]. Thiazolidinediones are found to exhibit a broad spectrum of biological activities [2] that can be antidiabetic [2,3], antimicrobial [2,4–15], anti-HIV [11,16] or anti-inflammatory [17–20]. Several thiazolidinediones have been synthesized and screened for their antitubercular activity against *M. tuberculosis* H37Rv that showed promising results indicating the potential of this scaffold in the development of novel anti-TB agents [2,3,10–15,21–24]. For example, several hybrid arylidene thiazolidinediones synthesized by Kumar et al. in 2014 [23] exhibited moderate to good activity with MIC value < 50 μM. To date, the best result in this field has been described by Khan et al. [25] Screening of 700 compounds, known to be active against the whole cell of *M. tuberculosis* led to the selection of one thiazolidinedione showing excellent anti-TB activity with MIC value 1.4 μM.

Subsequently, they validated mycobacterial ATP synthase as the target for the selected thiazolidinedione.

Pyrimidine pharmacophore plays an important role in several biological active substances and was found to possess a range of diverse biological activities such as anticancer [26], anti-inflammatory [27], anti-hepatitis [28], anti-diabetic [29] and many others. Moreover, variously modified pyrimidines were successfully studied as antibacterial agents [30–39].

Since the combination of two pharmacophores is a well-established approach for designing more potent drugs with a significant increase in biological activity [40,41], we decided to combine two known pharmacophores - thiazolidinedione scaffold and 5-nitropyrimidine (Fig. 1) primarily as novel potent antitubercular agents.

Herein, we introduce the solid-phase synthesis protocol for the preparation of thiazolidinediones conjugated with 5-nitropyrimidine that does not require isolation/purification of intermediates and uses relatively inexpensive starting materials. Our methodology is based on easy access to structural diversity from abundant and easily available building blocks with minimal synthetic operations. Very few papers have described the solid-phase synthetic approach using Merrifield resin for the construction of

\* Corresponding author.

E-mail address: [lucie.brulikova@upol.cz](mailto:lucie.brulikova@upol.cz) (L. Brulíková).

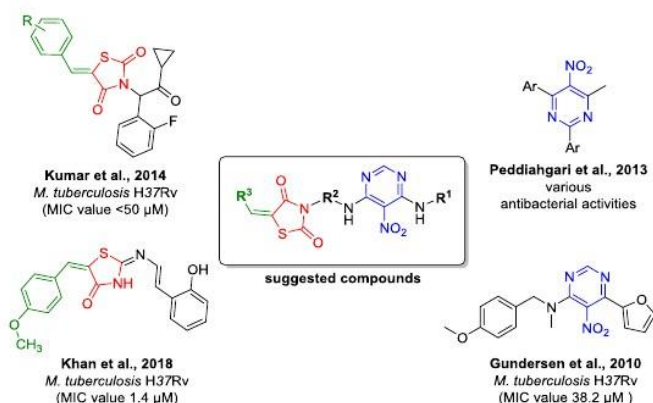


Fig. 1. Design of novel thiazolidinediones.

novel thiazolidinediones [42–44]. To the best of our knowledge, none of the reported solid-phase synthetic approaches have been used for rapid and effective preparation of the chemical library of thiazolidinediones-pyrimidine conjugates.

## 2. Materials and methods

Solvents, chemicals and the polystyrene resins were purchased from Sigma-Aldrich (St. Louis, Missouri, USA). Synthesis was carried out on Domino Blocks in disposable polypropylene reaction vessels (Torviq, Niles, MI).

All reactions were carried out at ambient temperature (21 °C) unless stated otherwise. The volume of wash solvent was 10 mL per 1 g of resin. For washing, resin slurry was shaken with the fresh solvent for 1 min before changing the solvent. After adding the individual reagents, the resin slurry was shaken vigorously to break any potential resin clumps. Resin-bound intermediates were dried by a stream of nitrogen for prolonged storage and/or quantitative analysis.

For LC-MS analysis, a sample of the resin (~5 mg) was treated with trifluoroacetic acid (TFA) in dichloromethane (DCM), the cleavage cocktail was evaporated by a stream of nitrogen, and cleaved compounds extracted into 1 mL of MeOH. The LC-MS analyses were carried out on UHPLC-MS system consisting of UHPLC chromatograph Accela with photodiode array detector and triple quadrupole mass spectrometer TSQ Quantum Access (Thermo Scientific, CA, USA), using Nucleodur Gravity C18 column (dimensions 1.8 μm, 2.1 × 50 mm) at 30 °C and flow rate of 800 μL/min (Macherey-Nagel, Germany). Mobile phase was (A) 0.1% ammonium acetate in water, and (B) 0.1% ammonium acetate in acetonitrile, linearly programmed from 10% to 80% B over 2.5 min, kept for 1.5 min. The column was re-equilibrated with 10% of solution B for 1 min. The APCI source operated at a discharge current of 5 μA, vaporizer temperature of 400 °C and a capillary temperature of 200 °C.

Purification was carried out on C18 column 19 × 100 mm for 5 μm particles; gradient was formed from 10 mM aqueous ammonium acetate and acetonitrile with a flow rate 15 mL/min. For lyophilization of residual solvents at –110 °C the ScanVac Coolsafe 110–4 was used.

NMR <sup>1</sup>H/<sup>13</sup>C spectra were recorded on JEOL ECX500 spectrometer at magnetic field strengths of 11.75 T (with operating frequencies 500.16 MHz for <sup>1</sup>H and 125.77 MHz for <sup>13</sup>C). Chemical

shifts (δ) are reported in parts per million (ppm), and coupling constants (*J*) are reported in Hertz (Hz). NMR spectra were recorded at ambient temperature (21 °C) in DMSO-*d*<sub>6</sub> or CD<sub>3</sub>OD solutions and referenced to the resonance signal of the solvent. Acetate salts exhibited singlet at 1.7–1.9 ppm in the <sup>1</sup>H NMR spectrum and two resonances at 173 and 23 ppm in <sup>13</sup>C spectrum. In some cases, residual signal for DMF appeared at 2.54 ppm; 1 carbon from diamine linker is overlapped with DMSO.

HRMS analysis was performed with LC-MS and an Orbitrap high-resolution mass spectrometer (Dionex Ultimate 3000, Thermo Exactive plus, MA, USA) operating in positive full scan mode in the range of 80–1200 *m/z*. The settings for electrospray ionization were as follows: 150 °C oven temperature and 3.6 kV source voltage. The acquired data were internally calibrated with phthalate as a contaminant in methanol (*m/z* 297.15909). Samples were diluted to a final concentration of 0.1 mg/mL in a solution of water and acetonitrile (50:50, v/v). The samples were injected into the mass spectrometer following HPLC separation on a Kinetex C18 column (2.6 μm, 100 Å, 50 × 3.0 mm) using an isocratic mobile phase of 0.01 M MeCN/ammonium acetate (80/20) at a flow rate of 0.3 mL/min.

### 2.1. General synthetic methods

#### 2.1.1. Synthesis of resins 1

Wang resin (loading 1.0 mmol/g, ~1 g) was washed three times with DCM. A solution consisting of Fmoc-amino acid (2 mmol), HOBt (2 mmol), DMAP (0.5 mmol) and DIC (2 mmol) in DMF/DCM (1:1, v/v, 10 mL) was added to the resin. The resin slurry was shaken at rt for 16 h. The resin was washed three times with DMF and three times with DCM.

#### 2.1.2. Reaction with 4,6-dichloro-5-nitropyrimidines (resins 2)

Firstly, Fmoc protecting group of resins 1 (~1 g) was removed by exposure to 50% piperidine in DMF (v/v 10 mL) for 15 min, and then, the resin was washed three times with DMF and three times with DCM. Further, resins were washed three times with dry DMF and reacted with a solution consisting of 4,6-dichloro-5-nitropyrimidine (5 mmol) and DIEA (5 mmol) in dry DMF (10 mL) at rt for 2 h. The resin was washed five times with DMF and three times with DCM.

### 2.1.3. Reaction with amino alcohols (resins 3)

Resins **2** (~500 mg) were each washed three times with dry DMF and reacted with a solution consisting of amino alcohol (2.5 mmol) and DIEA (2.5 mmol) in dry DMF (5 mL) at rt for 2 h. The resin was washed three times with DMF and three times with DCM.

### 2.1.4. Fukuyama-Mitsunobu reaction with thiazolidinedione (resins 4)

Resins **3** (~500 mg) were each washed three times with anhydrous THF. A solution consisting of thiazolidine-2,4-dione (1.25 mmol) and PPh<sub>3</sub> (1.25 mmol) in anhydrous THF (5 mL) was added. The resin was stored in a freezer for 30 min followed by reaction with DIAD (1.25 mmol) at rt for 1 h. The resin was washed three times with THF and five times with DCM.

### 2.1.5. Knoevenagel condensation with aldehydes (resins 5)

Resins **4** (~250 mg) were each washed three times with DMF and reacted with a solution consisting of aldehyde (0.62 mmol) and piperidine (0.25 mmol) in DMF (2.5 mL) at 70 °C for 20 h. The resin was washed three times with DMF and three times with DCM.

### 2.1.6. Cleavage from resin with TFA (compounds 6 and 7)

Resins **4** and **5** (~250 mg) were each treated with 2 mL of a solution consisting of TFA/DCM (1:1, v/v) for 1 h. The cleavage cocktail was collected, and the resin was washed three times with 50% TFA in DCM. The combined extracts were evaporated by a stream of nitrogen, and the crude products were purified by reversed-phase HPLC.

## 2.2. Analytical data of individual compounds

### 2.2.1. (6-((2-(2,4-Dioxothiazolidin-3-yl)ethyl)amino)-5-nitropyrimidin-4-yl)valine **6a**

Orange solid. Yield: 27%. <sup>1</sup>H NMR (500 MHz, DMSO-*d*<sub>6</sub>): δ 9.64 (d, *J* = 7.7 Hz, 1H), 9.52 (t, *J* = 4.9 Hz, 1H), 8.06 (s, 1H), 4.63 (dd, *J* = 7.8, 4.3 Hz, 1H), 4.08 (s, 2H), 3.75 (s, 4H), 2.28–2.22 (m, 1H), 0.97 (d, *J* = 6.9 Hz, 3H), 0.90 (d, *J* = 6.9 Hz, 3H). <sup>13</sup>C NMR (126 MHz, DMSO-*d*<sub>6</sub>): δ 172.44, 172.01, 159.23, 157.11, 156.14, 112.10, 59.45, 40.73, 38.80, 33.77, 30.52, 18.75, 18.16. HRMS: *m/z*: calcd for C<sub>14</sub>H<sub>18</sub>N<sub>6</sub>O<sub>6</sub>S: 399.1081 [M+H]<sup>+</sup>; found: 399.1085.

### 2.2.2. (6-((3-(2,4-Dioxothiazolidin-3-yl)propyl)amino)-5-nitropyrimidin-4-yl)valine **6b**

Orange solid. Yield: 58%. <sup>1</sup>H NMR (500 MHz, DMSO-*d*<sub>6</sub>): δ 9.97 (d, *J* = 7.6 Hz, 1H), 9.51 (t, *J* = 6.0 Hz, 1H), 8.01 (s, 1H), 4.40 (dd, *J* = 7.6, 3.8 Hz, 1H), 4.17 (s, 2H), 3.57–3.50 (m, 4H), 2.19 (qd, *J* = 10.8, 6.8 Hz, 1H), 1.81 (p, *J* = 6.8 Hz, 2H), 0.95 (d, *J* = 6.9 Hz, 3H), 0.83 (d, *J* = 6.9 Hz, 3H). <sup>13</sup>C NMR (126 MHz, DMSO-*d*<sub>6</sub>): δ 172.58, 172.23, 159.40, 156.63, 156.44, 112.29, 59.03, 38.26, 30.33, 26.82, 18.71, 18.00. HRMS: *m/z*: calcd for C<sub>15</sub>H<sub>20</sub>N<sub>6</sub>O<sub>6</sub>S: 413.1238 [M+H]<sup>+</sup>; found: 413.1241.

### 2.2.3. (6-((2-(2,4-Dioxothiazolidin-3-yl)ethyl)amino)-5-nitropyrimidin-4-yl)phenylalanine **6c**

Orange solid. Yield: 51%. <sup>1</sup>H NMR (500 MHz, DMSO-*d*<sub>6</sub>): δ 9.59 (d, *J* = 6.7 Hz, 1H), 9.47 (t, *J* = 5.1 Hz, 1H), 8.07 (s, 1H), 7.21 (t, *J* = 7.2 Hz, 2H), 7.15 (t, *J* = 7.2 Hz, 1H), 7.10 (d, *J* = 6.9 Hz, 2H), 4.75 (dd, *J* = 11.9, 5.5 Hz, 1H), 4.07 (s, 2H), 3.75 (s, 4H), 3.28 (dd, *J* = 13.5, 5.4 Hz, 1H), 3.18 (dd, *J* = 13.5, 5.4 Hz, 1H). <sup>13</sup>C NMR (126 MHz, DMSO-*d*<sub>6</sub>): δ 172.42, 172.08, 171.88, 159.15, 157.15, 155.42, 137.49, 129.41, 127.96, 126.23, 111.93, 56.28, 40.78, 38.71, 36.86, 33.77. HRMS: *m/z*: calcd for C<sub>18</sub>H<sub>18</sub>N<sub>6</sub>O<sub>6</sub>S: 447.1081 [M+H]<sup>+</sup>; found: 447.1085.

### 2.2.4. (6-((3-(2,4-Dioxothiazolidin-3-yl)propyl)amino)-5-nitropyrimidin-4-yl)phenyl-alanine **6d**

Brown solid. Yield: 74%. <sup>1</sup>H NMR (500 MHz, DMSO-*d*<sub>6</sub>): δ 9.48 (dd, *J* = 14.1, 6.6 Hz, 2H), 8.08 (s, 1H), 7.24 (t, *J* = 7.2 Hz, 2H), 7.17 (dd, *J* = 17.5, 7.1 Hz, 3H), 4.91 (dd, *J* = 12.3, 6.0 Hz, 1H), 4.17 (s, 2H), 3.53 (dt, *J* = 11.1, 6.7 Hz, 4H), 3.27 (dd, *J* = 13.7, 5.2 Hz, 1H), 3.19 (dd, *J* = 13.7, 6.2 Hz, 1H), 1.81 (p, *J* = 6.8 Hz, 2H). <sup>13</sup>C NMR (126 MHz, DMSO-*d*<sub>6</sub>): δ 172.57, 172.22, 171.94, 159.32, 156.60, 155.81, 136.99, 129.33, 128.14, 126.49, 112.12, 55.67, 38.84, 38.25, 36.73, 33.96, 26.82. HRMS: *m/z*: calcd for C<sub>19</sub>H<sub>20</sub>N<sub>6</sub>O<sub>6</sub>S: 461.1238 [M+H]<sup>+</sup>; found: 461.1239.

### 2.2.5. (6-((2-(2,4-Dioxothiazolidin-3-yl)ethyl)amino)-5-nitropyrimidin-4-yl)proline **6e**

Yellow solid. Yield: 50%. <sup>1</sup>H NMR (500 MHz, DMSO-*d*<sub>6</sub>): δ 8.38 (t, *J* = 5.6 Hz, 1H), 7.98 (s, 1H), 4.56 (s, 1H), 4.06 (s, 2H), 3.71 (s, 4H), 3.07 (d, *J* = 59.0 Hz, 2H), 2.26–2.18 (m, 1H), 2.01–1.93 (m, 1H), 1.88–1.79 (m, 2H). <sup>13</sup>C NMR (126 MHz, DMSO-*d*<sub>6</sub>): δ 172.95, 172.37, 172.06, 156.59, 156.03, 154.42, 113.78, 62.90, 49.97, 40.95, 38.63, 33.75, 24.46, 21.25. HRMS: *m/z*: calcd for C<sub>14</sub>H<sub>16</sub>N<sub>6</sub>O<sub>6</sub>S: 397.0925 [M+H]<sup>+</sup>; found: 397.0928.

### 2.2.6. (6-((3-(2,4-Dioxothiazolidin-3-yl)propyl)amino)-5-nitropyrimidin-4-yl)proline **6f**

Yellow solid. Yield: 84%. <sup>1</sup>H NMR (500 MHz, DMSO-*d*<sub>6</sub>): δ 8.40 (t, *J* = 6.0 Hz, 1H), 7.98 (s, 1H), 4.57 (s, 1H), 4.18 (s, 2H), 3.53 (t, *J* = 6.8 Hz, 2H), 3.46 (dt, *J* = 9.3, 6.8 Hz, 2H), 3.15 (s, 1H), 3.03 (s, 1H), 2.28–2.18 (m, 1H), 2.02–1.92 (m, 1H), 1.91–1.83 (m, 2H), 1.82–1.75 (m, 2H). <sup>13</sup>C NMR (126 MHz, DMSO-*d*<sub>6</sub>): δ 172.91, 172.56, 172.21, 156.80, 155.78, 154.65, 113.62, 62.96, 50.17, 38.90, 38.20, 33.95, 27.05. HRMS: *m/z*: calcd for C<sub>15</sub>H<sub>18</sub>N<sub>6</sub>O<sub>6</sub>S: 411.1081 [M+H]<sup>+</sup>; found: 411.1084.

### 2.2.7. (Z)-6-((2-(2,4-dioxo-5-(4-(trifluoromethyl)benzylidene)thiazolidin-3-yl)ethyl)amino)-5-nitropyrimidin-4-yl)valine **7a**

Brown solid. Yield: 36%. <sup>1</sup>H NMR (500 MHz, DMSO-*d*<sub>6</sub>): δ 9.66 (d, *J* = 7.8 Hz, 1H), 9.60 (t, *J* = 6.1 Hz, 1H), 7.98 (s, 1H), 7.95 (s, 1H), 7.88 (d, *J* = 8.4 Hz, 2H), 7.81 (d, *J* = 8.3 Hz, 2H), 4.57 (dd, *J* = 7.8, 4.2 Hz, 1H), 3.94 (ddd, *J* = 13.7, 6.4, 3.3 Hz, 2H), 3.87–3.78 (m, 2H), 2.22–2.15 (m, 1H), 0.91 (d, *J* = 6.9 Hz, 3H), 0.84 (d, *J* = 6.9 Hz, 3H). <sup>13</sup>C NMR (126 MHz, DMSO-*d*<sub>6</sub>): δ 171.98, 167.15, 165.60, 159.12, 157.16, 156.02, 136.97, 130.53, 130.48, 129.86 (q, *J* = 28.75 Hz), 126.11, 126.09, 124.56, 123.81 (q, *J* = 271.25 Hz), 112.05, 59.52, 41.27, 30.58, 18.68, 18.14. HRMS: *m/z*: calcd for C<sub>22</sub>H<sub>21</sub>F<sub>3</sub>N<sub>6</sub>O<sub>6</sub>S: 555.1268 [M+H]<sup>+</sup>; found: 555.1272.

### 2.2.8. (Z)-6-((2-(5-(4-fluorobenzylidene)-2,4-dioxothiazolidin-3-yl)ethyl)amino)-5-nitropyrimidin-4-yl)valine **7b**

Brown solid. Yield: 42%. <sup>1</sup>H NMR (500 MHz, DMSO-*d*<sub>6</sub>): δ 9.60 (t, *J* = 7.7 Hz, 2H), 7.99 (s, 1H), 7.88 (s, 1H), 7.67 (dd, *J* = 8.8, 5.4 Hz, 2H), 7.38 (t, *J* = 8.8 Hz, 2H), 4.62 (dd, *J* = 7.8, 4.3 Hz, 1H), 3.92 (ddd, *J* = 13.3, 6.4, 3.2 Hz, 2H), 3.83 (ddd, *J* = 16.4, 8.4, 4.7 Hz, 2H), 2.23–2.16 (m, 1H), 0.92 (d, *J* = 6.9 Hz, 3H), 0.85 (d, *J* = 6.9 Hz, 3H). <sup>13</sup>C NMR (126 MHz, DMSO-*d*<sub>6</sub>): δ 171.98, 167.39, 165.79, 163.90, 161.91, 159.12, 157.12, 156.16, 132.53, 131.35, 129.69, 121.23, 116.60, 116.42, 112.11, 59.25, 41.14, 30.51, 18.68, 18.05. HRMS: *m/z*: calcd for C<sub>21</sub>H<sub>21</sub>FN<sub>6</sub>O<sub>6</sub>S: 505.1300 [M+H]<sup>+</sup>; found: 505.1302.

### 2.2.9. (Z)-6-((2-(5-benzylidene-2,4-dioxothiazolidin-3-yl)ethyl)amino)-5-nitropyrimidin-4-yl)valine **7c**

White solid. Yield: 49%. <sup>1</sup>H NMR (500 MHz, DMSO-*d*<sub>6</sub>): δ 9.60 (t, *J* = 7.5 Hz, 2H), 7.99 (s, 1H), 7.87 (s, 1H), 7.60 (d, *J* = 7.2 Hz, 2H), 7.53 (t, *J* = 7.4 Hz, 2H), 7.49 (t, *J* = 7.2 Hz, 1H), 4.63 (dd, *J* = 7.8, 4.3 Hz, 1H), 3.95–3.90 (m, 1H), 3.83 (ddd, *J* = 15.9, 8.3, 4.7 Hz, 2H), 2.24–2.17 (m, 1H), 0.93 (d, *J* = 6.9 Hz, 3H), 0.86 (d, *J* = 6.9 Hz, 3H). <sup>13</sup>C NMR



(126 MHz, DMSO- $d_6$ ):  $\delta$  171.94, 167.51, 165.83, 159.12, 157.11, 156.20, 133.00, 132.42, 130.50, 130.01, 129.33, 121.52, 112.13, 59.16, 41.10, 30.47, 18.67, 18.04. HRMS:  $m/z$ : calcd for  $C_{21}H_{22}N_6O_6S$ : 487.1394  $[M+H]^+$ ; found: 487.1399.

2.2.10. (Z)-6-((2-(5-(4-methoxybenzylidene)-2,4-dioxothiazolidin-3-yl)ethyl)amino)-5-nitropyrimidin-4-yl)valine 7d

White solid. Yield: 39%.  $^1H$  NMR (500 MHz, DMSO- $d_6$ ):  $\delta$  9.59 (dd,  $J = 10.7, 5.0$  Hz, 2H), 7.99 (s, 1H), 7.82 (s, 1H), 7.56 (d,  $J = 8.8$  Hz, 2H), 7.10 (d,  $J = 8.9$  Hz, 2H), 4.64 (dd,  $J = 7.8, 4.3$  Hz, 1H), 3.94–3.88 (m, 2H), 3.88–3.79 (m, 5H), 2.24–2.18 (m, 1H), 0.93 (d,  $J = 6.9$  Hz, 3H), 0.87 (d,  $J = 6.9$  Hz, 3H).  $^{13}C$  NMR (126 MHz, DMSO- $d_6$ ):  $\delta$  171.98, 167.59, 165.95, 161.07, 159.11, 157.10, 156.23, 132.46, 132.13, 125.48, 118.24, 114.94, 112.15, 59.11, 55.48, 41.00, 30.47, 18.67, 18.02. HRMS:  $m/z$ : calcd for  $C_{22}H_{24}N_6O_7S$ : 517.1500  $[M+H]^+$ ; found: 517.1500.

2.2.11. (Z)-6-((2-(2,4-dioxo-5-(pyridin-4-ylmethylene)thiazolidin-3-yl)ethyl)amino)-5-nitropyrimidin-4-yl)valine 7e

Orange solid. Yield: 39%.  $^1H$  NMR (500 MHz, DMSO- $d_6$ ):  $\delta$  9.60 (dd,  $J = 12.3, 6.9$  Hz, 2H), 8.72 (d,  $J = 6.1$  Hz, 2H), 7.99 (s, 1H), 7.84 (s, 1H), 7.53 (d,  $J = 6.1$  Hz, 2H), 4.61 (dd,  $J = 7.8, 4.3$  Hz, 1H), 3.99–3.90 (m, 2H), 3.87–3.77 (m, 2H), 2.25–2.17 (m, 1H), 0.92 (d,  $J = 6.9$  Hz, 3H), 0.85 (d,  $J = 6.9$  Hz, 3H).  $^{13}C$  NMR (126 MHz, DMSO- $d_6$ ):  $\delta$  172.05, 166.94, 165.47, 159.15, 157.13, 156.15, 150.63, 140.04, 129.42, 126.62, 123.32, 112.11, 59.32, 41.31, 30.54, 18.71, 18.07. HRMS:  $m/z$ : calcd for  $C_{20}H_{21}N_7O_6S$ : 488.1347  $[M+H]^+$ ; found: 488.1350.

2.2.12. (E)-6-((Z)-2,4-dioxo-5-((E)-3-phenylallylidene)thiazolidin-3-yl)ethyl)amino)-5-nitropyrimidin-4-yl)valine 7f

Yellow solid. Yield: 31%.  $^1H$  NMR (500 MHz, DMSO- $d_6$ ):  $\delta$  9.59 (t,  $J = 7.0$  Hz, 2H), 8.01 (s, 1H), 7.66 (d,  $J = 7.0$  Hz, 2H), 7.56 (d,  $J = 11.2$  Hz, 1H), 7.45–7.36 (m, 3H), 7.30 (d,  $J = 15.2$  Hz, 1H), 6.96 (dd,  $J = 15.2, 11.4$  Hz, 1H), 4.66 (dd,  $J = 7.8, 4.3$  Hz, 1H), 3.91–3.86 (m, 2H), 3.85–3.76 (m, 2H), 2.26–2.20 (m, 1H), 0.94 (d,  $J = 6.8$  Hz, 3H), 0.89 (d,  $J = 6.8$  Hz, 3H).  $^{13}C$  NMR (126 MHz, DMSO- $d_6$ ):  $\delta$  171.97, 167.33, 165.31, 159.13, 157.09, 156.27, 143.82, 135.53, 132.81, 129.76, 128.90, 127.84, 123.20, 122.70, 112.16, 59.08, 40.93, 30.45, 18.69, 18.02. HRMS:  $m/z$ : calcd for  $C_{23}H_{24}N_6O_6S$ : 513.1551  $[M+H]^+$ ; found: 513.1555.

2.2.13. (Z)-6-((2-(2,4-dioxo-5-pentylidenethiazolidin-3-yl)ethyl)amino)-5-nitropyrimidin-4-yl)valine 7g

White solid. Yield: 29%.  $^1H$  NMR (500 MHz, DMSO- $d_6$ ):  $\delta$  9.57 (t,  $J = 5.9$  Hz, 1H), 9.51 (d,  $J = 7.8$  Hz, 1H), 7.99 (s, 1H), 6.96 (t,  $J = 7.7$  Hz, 1H), 4.72 (dd,  $J = 7.8, 4.4$  Hz, 1H), 3.85 (d,  $J = 5.0$  Hz, 2H), 3.82–3.76 (m, 2H), 2.29–2.24 (m, 1H), 2.17 (q,  $J = 7.4$  Hz, 2H), 1.49–1.42 (m, 2H), 1.30 (dt,  $J = 14.7, 7.3$  Hz, 2H), 0.97 (d,  $J = 6.9$  Hz, 3H), 0.93 (d,  $J = 6.8$  Hz, 3H), 0.87 (t,  $J = 7.3$  Hz, 3H).  $^{13}C$  NMR (126 MHz, DMSO- $d_6$ ):  $\delta$  171.97, 167.36, 164.53, 159.11, 157.04, 156.44, 138.03, 124.77, 112.18, 58.76, 40.87, 30.82, 30.35, 29.31, 21.71, 18.68, 17.91, 13.56. HRMS:  $m/z$ : calcd for  $C_{19}H_{26}N_6O_6S$ : 467.1707  $[M+H]^+$ ; found: 467.1706.

2.2.14. (Z)-6-((3-(2,4-Dioxo-5-(4-(trifluoromethyl)benzylidene)thiazolidin-3-yl)propyl)amino)-5-nitropyrimidin-4-yl)valine 7h

Yellow solid. Yield: 55%.  $^1H$  NMR (500 MHz, DMSO- $d_6$ ):  $\delta$  9.85 (d,  $J = 7.7$  Hz, 1H), 9.54 (t,  $J = 6.0$  Hz, 1H), 8.00 (d,  $J = 9.7$  Hz, 2H), 7.89 (d,  $J = 8.4$  Hz, 2H), 7.83 (d,  $J = 8.4$  Hz, 2H), 4.49 (dd,  $J = 7.7, 4.0$  Hz, 1H), 3.72 (t,  $J = 6.7$  Hz, 2H), 3.58 (dt,  $J = 16.2, 6.8$  Hz, 2H), 2.23–2.17 (m, 1H), 1.93 (t,  $J = 6.8$  Hz, 2H), 0.94 (d,  $J = 6.9$  Hz, 3H), 0.84 (d,  $J = 6.9$  Hz, 3H).  $^{13}C$  NMR (126 MHz, DMSO- $d_6$ ):  $\delta$  172.06, 167.20, 165.63, 159.36, 156.85, 155.75, 136.97, 130.88, 130.54, 129.81 (q,  $J = 32.50$  Hz), 126.13, 126.10, 124.49, 123.81 (q,  $J = 271.25$  Hz), 112.02, 60.38, 38.25, 30.80, 26.78, 18.77, 18.50. HRMS:  $m/z$ : calcd for  $C_{23}H_{23}F_3N_6O_6S$ : 569.1425  $[M+H]^+$ ; found: 569.1440.

2.2.15. (Z)-6-((3-(5-(4-Fluorobenzylidene)-2,4-dioxothiazolidin-3-yl)propyl)amino)-5-nitropyrimidin-4-yl)valine 7i

Yellow solid. Yield: 55%.  $^1H$  NMR (500 MHz, DMSO- $d_6$ ):  $\delta$  9.90 (d,  $J = 7.7$  Hz, 1H), 9.54 (t,  $J = 6.0$  Hz, 1H), 8.00 (s, 1H), 7.93 (s, 1H), 7.69 (dd,  $J = 8.8, 5.4$  Hz, 2H), 7.38 (t,  $J = 8.8$  Hz, 2H), 4.44 (dd,  $J = 7.7, 3.9$  Hz, 1H), 3.71 (t,  $J = 6.6$  Hz, 2H), 3.56 (ddt,  $J = 19.7, 13.3, 6.5$  Hz, 2H), 2.24–2.15 (m, 1H), 1.95–1.89 (m, 2H), 0.94 (d,  $J = 6.9$  Hz, 3H), 0.84 (d,  $J = 6.9$  Hz, 3H).  $^{13}C$  NMR (126 MHz, DMSO- $d_6$ ):  $\delta$  172.00, 167.42, 165.81, 163.94, 161.95, 159.35, 156.88, 155.60, 132.59, 131.74, 129.67, 121.14, 116.62, 116.44, 111.96, 60.66, 38.22, 30.88, 26.86, 18.78, 18.64. HRMS:  $m/z$ : calcd for  $C_{22}H_{23}FN_6O_6S$ : 519.1457  $[M+H]^+$ ; found: 519.1457.

2.2.16. (Z)-6-((3-(5-Benzylidene-2,4-dioxothiazolidin-3-yl)propyl)amino)-5-nitropyrimidin-4-yl)valine 7j

White solid. Yield: 40%.  $^1H$  NMR (500 MHz, DMSO- $d_6$ ):  $\delta$  9.67 (d,  $J = 7.8$  Hz, 1H), 9.54 (t,  $J = 6.0$  Hz, 1H), 8.04 (s, 1H), 7.92 (s, 1H), 7.62 (d,  $J = 7.2$  Hz, 2H), 7.54 (t,  $J = 7.4$  Hz, 2H), 7.49 (t,  $J = 7.2$  Hz, 1H), 4.63 (dd,  $J = 7.8, 4.3$  Hz, 1H), 3.72 (t,  $J = 6.7$  Hz, 2H), 3.58 (dt,  $J = 13.0, 6.7$  Hz, 2H), 2.28–2.21 (m, 1H), 1.96–1.89 (m, 2H), 0.95 (d,  $J = 6.9$  Hz, 3H), 0.89 (d,  $J = 6.9$  Hz, 3H).  $^{13}C$  NMR (126 MHz, DMSO- $d_6$ ):  $\delta$  171.99, 167.55, 165.85, 159.36, 156.70, 156.22, 132.98, 132.82, 130.58, 130.06, 129.35, 121.41, 112.21, 59.44, 38.32, 30.49, 26.83, 18.73, 18.14. HRMS:  $m/z$ : calcd for  $C_{22}H_{24}N_6O_6S$ : 501.1551  $[M+H]^+$ ; found: 501.1553.

2.2.17. (Z)-6-((3-(5-(4-Methoxybenzylidene)-2,4-dioxothiazolidin-3-yl)propyl)amino)-5-nitropyrimidin-4-yl)valine 7k

Yellow solid. Yield: 63%.  $^1H$  NMR (500 MHz, DMSO- $d_6$ ):  $\delta$  9.63 (d,  $J = 7.8$  Hz, 1H), 9.54 (t,  $J = 6.0$  Hz, 1H), 8.04 (s, 1H), 7.87 (s, 1H), 7.58 (d,  $J = 8.9$  Hz, 2H), 7.10 (d,  $J = 8.9$  Hz, 2H), 4.65 (dd,  $J = 7.8, 4.3$  Hz, 1H), 3.83 (s, 3H), 3.70 (t,  $J = 6.6$  Hz, 2H), 3.61–3.53 (m, 2H), 2.27–2.21 (m, 1H), 1.91 (p,  $J = 6.8$  Hz, 2H), 0.96 (d,  $J = 6.9$  Hz, 3H), 0.90 (d,  $J = 6.9$  Hz, 3H).  $^{13}C$  NMR (126 MHz, DMSO- $d_6$ ):  $\delta$  172.03, 167.60, 165.96, 161.14, 159.36, 156.67, 156.29, 132.90, 132.20, 125.44, 118.06, 114.95, 112.24, 59.29, 55.48, 38.33, 30.45, 26.88, 18.72, 18.08. HRMS:  $m/z$ : calcd for  $C_{23}H_{26}N_6O_7S$ : 531.1656  $[M+H]^+$ ; found: 531.1656.

2.2.18. (Z)-6-((3-(2,4-Dioxo-5-(pyridin-4-ylmethylene)thiazolidin-3-yl)propyl)amino)-5-nitropyrimidin-4-yl)valine 7l

Brown solid. Yield: 50%.  $^1H$  NMR (500 MHz, DMSO- $d_6$ ):  $\delta$  9.54 (dd,  $J = 14.1, 7.0$  Hz, 2H), 8.73 (d,  $J = 6.1$  Hz, 2H), 8.06 (s, 1H), 7.87 (s, 1H), 7.55 (d,  $J = 6.1$  Hz, 2H), 4.69 (dd,  $J = 7.8, 4.4$  Hz, 1H), 3.72 (t,  $J = 6.6$  Hz, 2H), 3.59 (dd,  $J = 13.6, 6.8$  Hz, 2H), 2.30–2.22 (m, 1H), 1.93 (dt,  $J = 12.0, 5.9$  Hz, 2H), 0.96 (d,  $J = 6.9$  Hz, 3H), 0.91 (d,  $J = 6.9$  Hz, 3H).  $^{13}C$  NMR (126 MHz, DMSO- $d_6$ ):  $\delta$  172.01, 167.00, 165.50, 159.39, 156.63, 156.49, 150.64, 140.04, 129.75, 126.53, 123.34, 112.34, 58.95, 38.37, 30.32, 26.71, 18.70, 17.96. HRMS:  $m/z$ : calcd for  $C_{21}H_{23}N_7O_6S$ : 502.1503  $[M+H]^+$ ; found: 502.1503.

2.2.19. (E)-6-((Z)-2,4-dioxo-5-((E)-3-phenylallylidene)thiazolidin-3-yl)propyl)amino)-5-nitropyrimidin-4-yl)valine 7m

Yellow solid. Yield: 41%.  $^1H$  NMR (500 MHz, DMSO- $d_6$ ):  $\delta$  9.54 (d,  $J = 7.2$  Hz, 2H), 8.06 (s, 1H), 7.67 (d,  $J = 7.1$  Hz, 2H), 7.61 (d,  $J = 11.4$  Hz, 1H), 7.46–7.36 (m, 3H), 7.33 (d,  $J = 15.2$  Hz, 1H), 6.99 (dd,  $J = 15.2, 11.4$  Hz, 1H), 4.72 (dd,  $J = 7.7, 4.5$  Hz, 1H), 3.68 (t,  $J = 6.5$  Hz, 2H), 3.57 (dt,  $J = 9.9, 6.8$  Hz, 2H, overlapped with water), 2.26 (dd,  $J = 11.4, 6.8$  Hz, 1H), 1.90 (t,  $J = 6.6$  Hz, 2H), 0.96 (d,  $J = 6.9$  Hz, 3H), 0.93 (d,  $J = 6.8$  Hz, 3H).  $^{13}C$  NMR (126 MHz, DMSO- $d_6$ ):  $\delta$  172.01, 167.35, 165.32, 159.37, 156.60, 156.56, 144.02, 135.52, 133.21, 129.81, 128.90, 127.87, 123.24, 122.52, 112.35, 58.83, 38.40, 30.27, 26.87, 18.70, 17.92. HRMS:  $m/z$ : calcd for  $C_{24}H_{26}N_6O_6S$ : 527.1707  $[M+H]^+$ ; found: 527.1706.

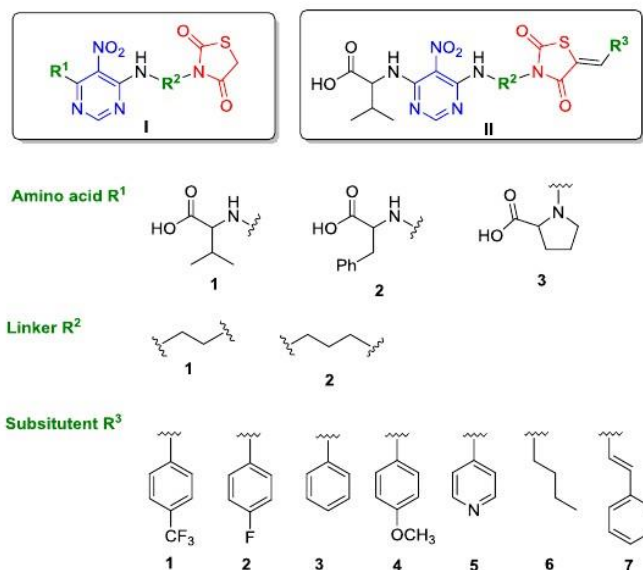


Fig. 2. Structures selected for this study.

2.2.20. (Z)-6-((3-(2,4-Dioxo-5-pentylidene-3-thiazolidin-3-yl)propyl)amino)-5-nitropyrimidin-4-yl)valine **7n**

Yellow solid. Yield: 47%.  $^1\text{H NMR}$  (500 MHz,  $\text{DMSO-}d_6$ ):  $\delta$  9.62 (d,  $J = 7.8$  Hz, 1H), 9.51 (t,  $J = 6.0$  Hz, 1H), 8.04 (s, 1H), 7.02 (t,  $J = 7.7$  Hz, 1H), 4.68 (dd,  $J = 7.8, 4.3$  Hz, 1H), 3.64 (t,  $J = 6.7$  Hz, 2H), 3.54 (dt,  $J = 10.5, 6.7$  Hz, 2H), 2.29–2.23 (m, 1H), 2.21 (dd,  $J = 14.8, 7.4$  Hz, 2H), 1.87 (p,  $J = 6.7$  Hz, 2H), 1.48 (dt,  $J = 14.9, 7.4$  Hz, 2H), 1.31 (dq,  $J = 14.4, 7.3$  Hz, 2H), 0.97 (d,  $J = 6.9$  Hz, 3H), 0.92 (d,  $J = 6.9$  Hz, 3H).  $^{13}\text{C NMR}$  (126 MHz,  $\text{DMSO-}d_6$ ):  $\delta$  172.00, 167.34, 164.55, 159.35, 156.64, 156.35, 138.50, 124.62, 112.25, 59.17, 38.37, 30.91, 30.42, 29.33, 26.79, 21.74, 18.72, 18.04, 13.57. HRMS:  $m/z$ : calcd for  $\text{C}_{20}\text{H}_{28}\text{N}_6\text{O}_6$ : 481.1864  $[\text{M}+\text{H}]^+$ ; found: 481.1867.

### 2.3. Antimycobacterial activity

Antimycobacterial activity of the pyrimidines against *M. tuberculosis* H37Rv (NCTC 7416) was evaluated in duplicates by determining their minimum inhibitory concentration (MIC) in 96-well microtitre plates. Stock solutions of the drugs and their subsequent 2-fold serial dilutions were prepared in 5% DMSO. Isoniazid was used as the drug control. *M. tuberculosis* H37Rv was cultured in Middlebrook 7H9 broth (Himedia, Mumbai) supplemented with 10% OADC (Himedia, Mumbai). The inoculums were prepared by diluting the mycobacterial culture in 7H9 broth. The controls consisted of drug-free media for sterility check and the media inoculated with *M. tuberculosis* H37Rv for the growth patterns in drug-inoculated tubes. The tubes were incubated for 1–2 weeks at 37 °C. The MICs were defined as the lowest concentration of the compound at which no visible bacterial growth was observed and evaluated by Resazurin microtiter assay [45,46].

### 2.4. Antimicrobial activity

The antimicrobial activities of the final compounds against

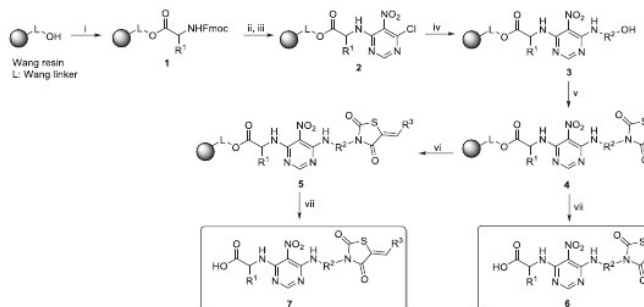
*Staphylococcus aureus* (CCM 3953), *Pseudomonas aeruginosa* (CCM 3955), *Escherichia coli* (CCM 3954), *Candida albicans* (ATCC 90028), *Aspergillus niger* (CCM 8189), and *Enterococcus faecalis* (CCM 4224) were determined by their MIC as described earlier [47]. Gentamicin was used as the drug control for bacteria, and amphotericin B for yeast and mould.

Antimicrobial activities of the synthesized compounds were assessed using the standard dilution micromethod in duplicates. Disposable microtitration plates were used for the tests. The stock solution of compounds in 5% DMSO (1024  $\mu\text{g}/\text{mL}$ ) were diluted 2–16 times with an additional Breath heart infusion broth (50  $\mu\text{L}$ ) inoculated with the tested bacteria/yeast at a concentration of  $10^5$ – $10^6$  CFU  $\text{mL}^{-1}$ . Tested concentrations of compounds were 512–0.015  $\mu\text{g}/\text{mL}$ .

The minimum inhibitory concentration (MIC) of aerobic bacteria was read after 24 h of incubation at 37 °C as the minimum inhibitory concentration (MIC) of the tested substance that inhibited the growth of the bacterial strain. The MIC of anaerobic bacteria, yeast and mould was read after 48 h of incubation at 30 °C.

The minimum bactericidal concentration (MBC) or minimum fungicidal concentration (MFC) may be characterized as the minimum concentration of the sample required to achieve irreversible inhibition, i.e., killing the bacteria/yeast after a defined period of incubation. The MBC was examined by a modified imprint method. With an applicator, ~5  $\mu\text{L}$  of the tested samples with defined concentrations were transferred from the microplate wells and imprinted on the surface of blood agar for bacteria or Sabouraud agar without antimicrobial agents for yeast. The MBC was determined as the lowest concentration that inhibited the visible growth of the used bacterium.

The minimum bacteriostatic concentration (MBS) may be characterized as the minimum concentration of the sample required to achieve reversible inhibition, i.e., the bacteria growth after removing the effects of the antimicrobial compound.



**Scheme 1.** Solid-phase synthesis of model compounds 6 and 7<sup>a</sup>.

### 3. Results and discussion

In view of the biological significance of thiazolidinedione and 5-nitropyrimidine scaffolds, we designed and synthesized a library of novel hybrids depicted in Fig. 2.

The two scaffolds (thiazolidinedione and 5-nitropyrimidine) are connected via an appropriate linker. For primary screening and the development of synthetic protocol, we selected ethylenediamine and propylenediamine linkers. The whole system was built on the Wang resin via the immobilization of various amino acids that are known for their ability to tune optimal pharmacokinetic and pharmacodynamics properties of potential drugs [48–50]. Since all novel compounds were designed primarily as promising antitubercular agents (more than 60% of the mycobacterial cell wall are lipids), the central part of amino acid linker was selected considering its lipophilicity. For the first group of novel thiazolidinediones (structures I) three different amino acids were selected (with respect to their lipophilicity) to test the impact of amino acid on resulting biological activity. For the second group of compounds (structures II) only valine linker containing lipophilic central part was chosen. Furthermore, thiazolidinedione scaffold was modified with variously substituted benzylidenes or alkylidenes. Some benzylidenes have already been found to be involved in the construction of biologically active structures (see Fig. 1) [23,25].

#### 3.1. Solid-phase synthesis of the model compounds

Solid-phase synthesis of the desired compounds commenced with the immobilization of amino acids on Wang resin to give corresponding resin **1** (Scheme 1). Subsequent deprotection of amino group and substitution with 4,6-dichloro-5-nitropyrimidine afforded resin **2**. The chlorine atoms of resin **2** are very reactive and can be easily hydrolyzed as we had described earlier [51]. For this reason, resin **2** was immediately modified with aminoethanol or aminopropanol giving resin **3**. Desired precursor **4** was obtained after Fukuyama-Mitsunobu reaction where thiazolidinedione was easily prepared from thiourea and chloroacetic acid according to previously described procedure [10]. Here, thiazolidinedione was allowed to react with resin **3** for 16 h; however, subsequent optimization studies showed that 99% conversion was possible in 1 h.

<sup>a</sup> Reagents and conditions: (i) Fmoc-amino acid, *N*-hydroxybenzotriazole (HOBT), DMAP, DIC, DMF/DCM (1:1), 16 h; (ii) 50% piperidine, DMF, 15 min; (iii) 4,6-dichloro-5-nitro-pyrimidine, DIEA, dry DMF, 2 h; (iv) amino alcohol, DIEA, dry DMF, rt, 2 h; (v) thiazolidine-2,4-dione, PPh<sub>3</sub>, DIAD, dry THF, rt, 1 h; (vi) aldehyde, piperidine, DMF, 60 °C, 20 h; (vii) 50% TFA in DCM, rt, 1 h.

Further, Knoevenagel condensation of resin **4** with variously substituted aldehydes afforded polymer-bound intermediate **5**. When thiazolidinedione-resin **4** reacted with aldehyde in the presence of *N,N*-diisopropylethylamine (DIEA) as a base in DCM at room temperature, conversion of **4** to resin **5** was only about 30% according to LC-MS traces at 210–500 nm. Then, trials with various bases, solvents and reaction temperature were carried out; the optimal reaction conditions were aldehyde, piperidine, DMF, 70 °C, 20 h. The reaction occurred smoothly with aromatic aldehydes bearing electron-withdrawing or electron-donating groups as well as aliphatic aldehydes in crude purity between 58 and 91%. Finally, the resulting derivatives **6** and **7** were isolated by standard cleavage and HPLC purification (Tables 1 and 2). Overall yields ranged from 29 to 63% and the lower yields were caused with some losses during HPLC purification procedure.

After Knoevenagel condensation, formation of two geometrical isomers *E* or *Z* is possible. These two isomers can be easily distinguished by the <sup>1</sup>H NMR spectral characteristics. It is well known

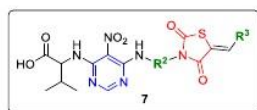
**Table 1**  
Overview of synthesized products 6.



Entry	R <sup>1</sup>	R <sup>2</sup>	Yield [%]
6a			27
6b			58
6c			51
6d			74
6e			50
6f			84



**Table 2**  
Overview of synthesized products 7.



Entry	R <sup>2</sup>	R <sup>3</sup>	Yield [%]
7a			36
7b			42
7c			49
7d			39
7e			39
7f			31
7g			29
7h			55
7i			55
7j			40
7k			63
7l			50
7m			41
7n			47

that benzylidene proton appears above 7.90 ppm in *Z* isomer and below 7.42 ppm in *E* isomer [52,53]. The NMR elucidation confirmed the formation of *Z* isomers for all our products.

### 3.2. In vitro evaluation of antitubercular activity against *M. tuberculosis* H37Rv and antimicrobial activity against other strains

The final compounds 6 and 7 were tested for their antimicrobial activity against reference Gram-positive and Gram-negative bacterial strains (*Staphylococcus aureus* CCM 3953, *Pseudomonas aeruginosa* CCM 3955, *Escherichia coli* CCM 3954, *Enterococcus faecalis* CCM 4224), against two fungal strains (*Candida albicans* ATCC 90028, *Aspergillus niger* CCM 8189) and against *Mycobacterium tuberculosis* H37Rv.

Thiazolidinediones 6 exhibited no significant activities and none of the derivatives showed activity against *E. Coli*, *P. aeruginosa*, *C. albicans* and *A. niger*. On the contrary, compounds 7 showed more interesting results. Thiazolidinedione 7h (see Table 3) showed the highest antimicrobial activity against *S. aureus* CCM 3953 (MIC = 128 µg/mL) and antitubercular activity against *M. tuberculosis* H37Rv (MIC = 256 µg/mL). *Mycobacterium* has a similar cell wall construction as Gram-positive bacteria. The compounds that had an antimicrobial effect on Gram-positive bacteria (like 7f or 7h) may have a bacteriostatic or inhibitory effect on the

**Table 3**  
Minimum inhibition concentrations (MIC; µg/mL), minimum bacteriostatic concentrations (MBS) or minimum bactericidal concentrations (MBC) of synthesized compounds 7.

Entry	<i>Mycobacterium tuberculosis</i>	<i>Staphylococcus aureus</i>		<i>Enterococcus faecalis</i>	
	MIC	MIC	MBS/ MBC	MIC	MBS/ MBC
7a	–	256	256/-	1024	1024/-
7b	–	1024	1024/-	–	–
7c	–	1024	1024/-	–	–
7f	1024	256	256/-	256	256/-
7g	–	–	–	1024	1024/-
7h	256	128	128/ 1024	256	256/-
7i	–	1024	1024/-	–	–
7j	–	1024	-/1024	–	–
7k	–	512	512/-	–	–
7l	–	1024	1024/-	1024	1024/-
isoniazid	0.125	x	x	x	x
gentamicine	x	16	-/16	64	-/64

strain *Mycobacterium tuberculosis* H37Rv.

Moreover, we observed certain structure-activity dependence for compounds 7. While derivative 7h with propylenediamine linker between two pharmacophores exhibited the most interesting activities, compounds 7a with ethylenediamine linker showed only slight antimicrobial activity against *S. aureus* and *P. aeruginosa*.

## 4. Conclusion

In summary, we have developed a rapid and effective approach to the synthesis of novel thiazolidinedione-pyrimidine conjugates by employing an efficient solid-phase synthetic protocol. Our methodology is based on easy access to structural diversity from abundant and easily available building blocks with minimal synthetic operations and was validated in synthesis of model chemical library prepared *via* a combinatorial manner. Although the design of our library was motivated by testing the reactivity of various building blocks, some of the prepared derivatives exhibited slight antimicrobial and antitubercular activity mainly against *S. aureus* CCM 3953 (MIC = 128 µg/mL) and moderate activity against *M. tuberculosis* H37Rv (MIC = 256 µg/mL). The developed synthetic protocol can be used for fast and efficient synthesis of a chemical library designed with use of sophisticated methods in the future.

## Acknowledgement

This work was supported by the Ministry of Education, Youth and Sport of the Czech Republic (projects IGA\_PrF\_2018\_029, IGA\_LF\_2018\_032) and the National Program of Sustainability (project LO1304).

## Appendix A. Supplementary data

Supplementary data to this article can be found online at <https://doi.org/10.1016/j.molstruc.2019.01.073>.

## References

- [1] M.J. Nanjan, M. Mohammed, B.R. Prashantha Kumar, M.J.N. Chandrasekar, Thiazolidinediones as antidiabetic agents: a critical review, *Bioorg. Chem.* 77 (2018) 548–567.
- [2] S. Sucheta, P. Tahlán, K. Verma, Biological potential of thiazolidinedione derivatives of synthetic origin, *Chem. Cent. J.* 11 (2017) 130.
- [3] S. Pattan, M. Kedar, J. Pattan, S. Dengale, M. Sanap, U. Gharate, et al., Synthesis and evaluation of some novel 2,4-thiazolidinedione derivatives for

- antibacterial, antitubercular and antidiabetic activities, *Indian J. Chem. Sect. B Org. Chem. Incl. Med. Chem.* 51B (2012) 1421–1425.
- [4] S. Bondock, W. Khalifa, A.A. Fadda, Synthesis and antimicrobial evaluation of some new thiazole, thiazolidinone and thiazoline derivatives starting from 1-chloro-3,4-dihydro-2H-pyridin-2-one, *Eur. J. Med. Chem.* 42 (2007) 948–954.
- [5] N.C. Desai, A.M. Dodiya, A.H. Makwana, Antimicrobial screening of novel synthesized benzimidazole nucleus containing 4-oxo-thiazolidine derivatives, *Med. Chem. Res.* 21 (2012) 2320–2328.
- [6] N.C. Desai, A.M. Dodiya, P.N. Shihora, A clubbed quinazolinone and 4-thiazolidinone as potential antimicrobial agents, *Med. Chem. Res.* 21 (2012) 1577–1586.
- [7] N.K. Fuloria, V. Singh, M.S. Yar, M. Ali, Synthesis, characterization and antimicrobial evaluation of novel imines and thiazolidinone derivatives, *Acta Pol. Pharm.* 66 (2009) 141–146.
- [8] S. Ozkirimli, F. Kazan, Y. Tunali, Synthesis, antibacterial and antifungal activities of 3-(1,2,4-triazol-3-yl)-4-thiazolidinones, *J. Enzym. Inhib. Med. Chem.* 24 (2009) 447–452.
- [9] N.B. Patel, S.D. Patel, Synthesis and antimicrobial study of fluoroquinolone-based 4-thiazolidinones, *Med. Chem. Res.* 19 (2010) 757–770.
- [10] N.M. Parekh, K.V. Juddhawala, B.M. Rawal, Antimicrobial activity of thiazolyl benzensulfonamide-condensed 2,4-thiazolidinediones derivatives, *Med. Chem. Res.* 22 (2013) 2737–2745.
- [11] F.M. Shaikh, N.B. Patel, G. Sanna, B. Busonera, P. La Colla, D.P. Rajani, Synthesis of some new 2-amino-6-thiocyanato benzothiazole derivatives bearing 2,4-thiazolidinediones and screening of their in vitro antimicrobial, antitubercular and antiviral activities, *Med. Chem. Res.* 24 (2015) 3129–3142.
- [12] S.S. Purohit, A. Alman, J. Shewale, Synthesis and antimicrobial activity of a new series of 3,5-disubstituted thiazolidine-2,4-diones, *Int. J. Pharm. Pharmacol. Sci.* 4 (2012) 273–276.
- [13] N.B. Patel, A.C. Purohit, D. Rajani, Design and synthesis of newer thiazolidinediones incorporated with pyridine and 1,3,4-oxadiazole moieties as antimicrobial agents, *Int. J. Drug Des. Discovery* 5 (2014) 1342–1351.
- [14] N.B. Patel, I.H. Khan, Synthesis of newer 5-benzylidene-2,4-thiazolidinediones as potential antimicrobials, *Indian J. Res. Pharm. Biotechnol.* 2 (9) (2014) 993–1001.
- [15] F.M. Shaikh, N.B. Patel, D. Rajani, Synthesis of new thiazolidine-2,4-dione derivatives and their antimicrobial and antitubercular activity, *Indian J. Res. Pharm. Biotechnol.* 1 (2013) 496–503.
- [16] M.L. Barreca, A. Chimiri, L. De Luca, A.M. Monforte, P. Monforte, A. Rao, et al., Discovery of 2,3-diaryl-1,3-thiazolidin-4-ones as potent anti-HIV-1 agents, *Bioorg. Med. Chem. Lett* 11 (2001) 1793–1796.
- [17] A. Deep, S. Jain, P.C. Sharma, P. Phogat, M. Malhotra, Synthesis of 2-(aryl)-5-(arylidene)-4-thiazolidinone derivatives with potential analgesic and anti-inflammatory activity, *Med. Chem. Res.* 21 (2012) 1652–1659.
- [18] A.A. Geronikaki, A.A. Lagunin, D.I. Hadjipavlou-Litina, P.T. Eleftheriou, D.A. Filimonov, V.V. Porokov, et al., Computer-aided discovery of anti-inflammatory thiazolidinones with dual cyclooxygenase/lipoxygenase inhibition, *J. Med. Chem.* 51 (2008) 1601–1609.
- [19] A. Kumar, C.S. Rajput, Synthesis and anti-inflammatory activity of newer quinazolin-4-one derivatives, *Eur. J. Med. Chem.* 44 (2009) 83–90.
- [20] R. Ottana, R. Maccari, M.L. Barreca, G. Bruno, A. Rotondo, A. Rossi, et al., 5-Arylidene-2-imino-4-thiazolidinones: design and synthesis of novel anti-inflammatory agents, *Bioorg. Med. Chem.* 13 (2005) 4243–4252.
- [21] S.G. Kucukguzel, E.E. Oruc, S. Rollas, F. Sahin, A. Ozbek, Synthesis, characterization and biological activity of novel 4-thiazolidinones, 1,3,4-oxadiazoles and some related compounds, *Eur. J. Med. Chem.* 37 (2002) 197–206.
- [22] G. Kucuekguzel, A. Kocatepe, E. De Clercq, F. Sahin, M. Guelluec, Synthesis and biological activity of 4-thiazolidinones, thiosemicarbazides derived from difluoral hydradize, *Eur. J. Med. Chem.* 41 (2006) 353–359.
- [23] S. Ponnuchamy, S. Kanchithalaivan, R. Ranjith Kumar, M. Ashraf Ali, T. Soo Choon, Antimicrobial evaluation of novel hybrid arylidene thiazolidine-2,4-diones, *Bioorg. Med. Chem. Lett* 24 (2014) 1089–1093.
- [24] N. Babu, K.K. Rajasekhar, T. Singirisetty, V.S. Synthesis, Characterisation and Anti-tubercular Activity of Some New 3,5-Disubstituted-2,4-Thiazolidinediones, 6 ed, 2013.
- [25] S. Kumar, R. Mehra, S. Sharma, N.P. Bokolia, D. Raina, A. Nargotra, et al., Screening of antitubercular compound library identifies novel ATP synthase inhibitors of *Mycobacterium tuberculosis*, *Tuberculosis* 108 (2018) 56–63.
- [26] S. Prachayasittikul, R. Pingsaw, A. Worachartcheewan, N. Sinthupoom, V. Prachayasittikul, S. Ruchirawat, et al., Roles of pyridine and pyrimidine derivatives as privileged scaffolds in anticancer agents, *Mini Rev. Med. Chem.* 17 (2017) 869–901.
- [27] A.P. Keche, G.D. Hatnapure, R.H. Tale, A.H. Rodge, S.S. Birajdar, V.M. Kamble, A novel pyrimidine derivatives with aryl urea, thiourea and sulfonamide moieties: synthesis, anti-inflammatory and antimicrobial evaluation, *Bioorg. Med. Chem. Lett* 22 (2012) 3445–3448.
- [28] N. Shakya, S. Vedi, C. Liang, F. Yang, B. Agrawal, R. Kumar, 4'-Substituted pyrimidine nucleosides lacking 5'-hydroxyl function as potential anti-HCV agents, *Bioorg. Med. Chem. Lett* 24 (2014) 1407–1409.
- [29] Z. Yang, Y. Fang, T.A. Pham, J. Lee, H. Park, Synthesis and biological evaluation of 5-nitropyrimidine analogs with azabicyclic substituents as GPR119 agonists, *Bioorg. Med. Chem. Lett* 23 (2013) 1519–1521.
- [30] T. Wang, G. Bemis, B. Hanzelka, H. Zuccola, M. Wynn, C.S. Moody, et al., Mtb PKNA/PKNB dual inhibition provides selectivity advantages for inhibitor design to minimize host kinase interactions, *ACS Med. Chem. Lett.* 8 (2017) 1224–1229.
- [31] N.H. Bhuvu, P.K. Talpara, P.M. Singala, V.K. Gothaliya, V.H. Shah, Synthesis and biological evaluation of pyrimidinyl sulphonamide derivatives as promising class of antitubercular agents, *J. Saudi Chem. Soc.* 21 (2017) 517–527.
- [32] C.R. Wilson, R.K. Gessner, A. Moosa, R. Seldon, D.F. Warner, V. Mizrahi, et al., Novel antitubercular 6-dialkylaminopyrimidine carboxamides from phenotypic whole-cell high throughput screening of a SoftFocus library: structure-activity relationship and target identification studies, *J. Med. Chem.* 60 (2017) 10118–10134.
- [33] E.V. Verbitskiy, S.A. Baskakova, M.A. Kravchenko, S.N. Skorniyakov, G.L. Rusinov, O.N. Chupakhin, et al., Synthesis and evaluation of antitubercular activity of fluorinated 5-aryl-4-(hetero)aryl substituted pyrimidines, *Bioorg. Med. Chem.* 24 (2016) 3771–3780.
- [34] D. Seenaiyah, P.R. Reddy, G.M. Reddy, A. Padmaja, V. Padmavathi, N. Siva Krishna, Synthesis, antimicrobial and cytotoxic activities of pyrimidinyl benzoxazole, benzothiazole and benzimidazole, *Eur. J. Med. Chem.* 77 (2014) 1–7.
- [35] L. Ballell, R.H. Bates, R.J. Young, D. Alvarez-Gomez, E. Alvarez-Ruiz, V. Barroso, et al., Fueling open-source drug discovery: 177 small-molecule leads against tuberculosis, *ChemMedChem* 8 (2013) 313–321.
- [36] M.R. Sura, V.G.R. Peddiahari, R.P.R. Bhoomireddy, R.K. Vadde, Synthesis of new 2,4-diaryl-6-methyl-5-nitropyrimidines as antibacterial and antioxidant agents, *J. Heterocycl. Chem.* 50 (2013) 1395–1399.
- [37] C. Kishor, T. Arya, R. Reddi, X. Chen, V. Sattanapu, A.K. Marapaka, et al., Identification, biochemical and structural evaluation of species-specific inhibitors against type I methionine aminopeptidases, *J. Med. Chem.* 56 (2013) 5295–5305.
- [38] M.L. Read, M. Braendvang, P.O. Miranda, L.L. Gundersen, Synthesis and biological evaluation of pyrimidine analogs of antimycobacterial purines, *Bioorg. Med. Chem.* 18 (2010) 3885–3897.
- [39] D.S. Reddy, K.M. Hosamani, H.C. Devarajegowda, Design, synthesis of benzocoumarin-pyrimidine hybrids as novel class of antitubercular agents, their DNA cleavage and X-ray studies, *Eur. J. Med. Chem.* 101 (2015) 705–715.
- [40] C.H. Zhou, Y. Wang, Recent researches in triazole compounds as medicinal drugs, *Curr. Med. Chem.* 19 (2012) 239–280.
- [41] A. Campanico, R. Moreira, F. Lopes, Drug discovery in tuberculosis. New drug targets and antimycobacterial agents, *Eur. J. Med. Chem.* 150 (2018) 525–545.
- [42] K.M. Brummond, J. Lu, Solid-phase synthesis of BRL 49653, *J. Org. Chem.* 64 (1999) 1723–1726.
- [43] N.C.O. Tomkinson, A.M. Seifler, K.D. Plunket, S.G. Blanchard, D.J. Parks, T.M. Willson, Solid-phase synthesis of hybrid thiazolidinedione-fatty acid PPAR $\alpha$ -ligands, *Bioorg. Med. Chem. Lett* 7 (1997) 2491–2496.
- [44] D.L. Mohler, G. Shen, A.K. Dotse, Solution- and solid-phase synthesis of peptide-substituted thiazolidinediones as potential PPAR ligands, *Bioorg. Med. Chem. Lett* 10 (2000) 2239–2242.
- [45] J.C. Palomino, A. Martin, M. Camacho, H. Guerra, J. Swings, F. Portaels, Resazurin microtiter assay plate: simple and inexpensive method for detection of drug resistance in *Mycobacterium tuberculosis*, *Antimicrob. Agents Chemother.* 46 (2002) 2720–2722.
- [46] P.C. Nguyen, A. Madani, P. Santucci, B.P. Martin, R.R. Paudel, S. Delattre, et al., Cyclophostin and Cyclophostin analogues, new promising molecules to treat mycobacterial-related diseases, *Int. J. Antimicrob. Agents* 51 (2018) 651–654.
- [47] Z. Ozdemir, U. Bildizuevich, D. Saman, L. Havlicek, L. Rarova, L. Navratilova, et al., Amphiphilic derivatives of (3 $\beta$ ,17 $\beta$ )-3-hydroxyandrost-5-ene-17-carboxylic acid, *Steroids* 128 (2017) 58–67.
- [48] S. Majumdar, S. Duvvuri, A.K. Mitra, Membrane transporter/receptor-targeted prodrug design: strategies for human and veterinary drug development, *Adv. Drug Deliv. Rev.* 56 (2004) 1437–1452.
- [49] V.K. Singh, B.B. Subudhi, Development of reversible glutamine conjugate of methotrexate for enhanced brain delivery, *Med. Chem. Res.* 24 (2015) 624–635.
- [50] I.S. Krylov, B.A. Kashemirov, J.M. Hilfinger, C.E. McKenna, Evolution of an amino acid based prodrug approach: stay tuned, *Mol. Pharm.* 10 (2013) 445–458.
- [51] L. Brulikova, S. Krupkova, M. Labora, K. Motyka, L. Hradilova, M. Mistrik, et al., Synthesis and study of novel pH-independent fluorescent mitochondrial labels based on Rhodamine B, *RSC Adv.* 6 (2016) 23242–23251.
- [52] S. Mohanty, A.K. Roy, V.K.P. Kumar, S.G. Reddy, A.C. Karmakar, Acetic anhydride-promoted one-pot condensation of 2,4-thiazolidinedione with bisulfite adducts of aldehydes, *Tetrahedron Lett.* 55 (2014) 4585–4589.
- [53] U.R. Pratap, D.V. Jawale, R.A. Waghmare, D.L. Lingampalle, R.A. Mane, Synthesis of 5-arylidene-2,4-thiazolidinediones by Knoevenagel condensation catalyzed by Baker's yeast, *New J. Chem.* 35 (2011) 49–51.





Contents lists available at ScienceDirect

European Journal of Medicinal Chemistry

journal homepage: <http://www.elsevier.com/locate/ejmech>



Review article

## Squaric acid analogues in medicinal chemistry

Jan Chasák<sup>a,1</sup>, Veronika Šlachťová<sup>a,1</sup>, Milan Urban<sup>b</sup>, Lucie Brulíková<sup>a,\*</sup>



<sup>a</sup> Department of Organic Chemistry, Faculty of Science, Palacký University Olomouc, 17. listopadu 12, 771 46, Olomouc, Czech Republic

<sup>b</sup> Medicinal Chemistry, Institute of Molecular and Translational Medicine, Faculty of Medicine and Dentistry, Palacký University in Olomouc, Hněvotínská 5, 779 00, Olomouc, Czech Republic

### ARTICLE INFO

#### Article history:

Received 18 August 2020  
Received in revised form  
12 September 2020  
Accepted 21 September 2020  
Available online 2 October 2020

#### Keywords:

Squaric acid  
Squarate  
Squaramide  
Biological activity

### ABSTRACT

In this review, we summarize the published data on squaric acid analogues with a special focus on their use in medicinal chemistry and as potential drugs. Squaric acid is an interesting small molecule with an almost perfectly square shape, and its analogues have a variety of biological activities that are enabled by the presence of significant H-bond donors and acceptors. Unfortunately, most of these compounds also exhibit reactive functionalities, and this deters the majority of medicinal chemists and pharmacologists from trying to use them in drug development. However, this group of compounds is experiencing a renaissance, and large numbers of them are being tested for antiprotozoal, antibacterial, antifungal, and antiviral activities. The most useful of these compounds exhibited IC<sub>50</sub> values in the nanomolar range, which makes them promising drug candidates. In addition to these activities, their interactions with living systems were intensively explored, revealing that squaric acid analogues inhibit various enzymes and often serve as receptor antagonists and that the squaric acid moiety may be used as a non-classical isosteric replacement for other functional groups such as carboxylate. In summary, this review is focused on squaric acid and its analogues and their use in medicinal chemistry and should serve as a guide for other researchers in the field to demonstrate the potential of these compounds based on previous research.

© 2020 Elsevier Masson SAS. All rights reserved.

### Contents

1. Introduction .....	2
1.1. Physicochemical properties .....	2
1.2. Pharmacological profile .....	2
2. Squaric acid analogues in medicinal chemistry .....	4
2.1. Antiprotozoal activity .....	4
2.2. Antibacterial activity .....	6
2.3. Cytotoxic activity .....	7
2.4. Antiviral activity .....	11
2.5. CXCR2 receptor antagonists .....	12
2.6. Bioisosteres .....	13
2.7. Vaccines .....	14
2.8. Various receptor antagonists .....	15
2.9. Various enzyme inhibitors .....	17
3. Conclusions and future perspectives .....	20
Declaration of competing interest .....	20
Acknowledgement .....	20
References .....	20

\* Corresponding author.  
E-mail address: [lucie.brulikova@upol.cz](mailto:lucie.brulikova@upol.cz) (L. Brulíková).

<sup>1</sup> These authors contributed equally.

## 1. Introduction

The squaric acid scaffold (Fig. 1) represents a unique moiety that has received considerable attention, especially during the last decade, due to its numerous synthetic [1–10], pharmaceutical [1–3,11,12], and other applications [1,2,13–17]. Squaric acid **1** (also known as quadratic acid; 3,4-dihydroxycyclobut-3-ene-1,2-dione) is a planar aromatic framework that received its special name because of its extraordinary, almost perfect square shape. The first cyclobutenediones were synthesized in the 1950s [18–20] and triggered this area of unique and versatile synthons in organic chemistry [10]. In the medicinal chemistry field, however, the squaric acid scaffold only came to the forefront in the last decade due to earlier concern about the risk of *in vivo* toxicity because of the scaffold's rather reactive functional groups. Squaric acid itself as well as its analogues features several unique physicochemical and pharmacokinetic properties described in more detail further.

### 1.1. Physicochemical properties

Squaric acid is a symmetrical planar diprotic four-membered oxocarbon compound that possesses unique  $2\pi$ -pseudo-aromaticity [21]. Consequently, squaric acid features unusual high double acidity ( $pK_{a1} = 0.54$ ;  $pK_{a2} = 3.58$ ) due to the resonance stabilized squarate dianion (Fig. 1) [22]. Several physicochemical methods were employed to confirm the aromatic character of the squarate dianion (Fig. 1) by geometric (bond length, bond order), energetic (aromatic stabilization energies) and magnetic parameters ( $^{17}\text{O}$ -chemical shifts, nucleus-independent chemical shifts) [23,24].

Among the most common squaric acid analogues (Fig. 2), squaramides **5** have received considerable attention especially because of their interesting molecular structure capable of multiple interactions with biological targets *via* specific molecular recognition [2]. Squaramides can bind selectively through the four hydrogen bonds, acting both as hydrogen bond donors and acceptors. The potential of secondary squaramides to participate in hydrogen bonding is another significant feature which is one of the reasons for their high melting points of 275–300 °C and their low solubility in water [3]. Studies of squaramide-based artificial receptors used for the recognition of cations described that the capability to serve as a hydrogen bond acceptor is modulated by the increase in aromaticity [25]. The ability of squaramides to act as hydrogen bond donors to anionic species was investigated as well [26]. Squaramide-based artificial receptors designed to bind carboxylate anions proved hydrogen bond donor ability also due to enhanced aromaticity. Furthermore, electrostatic potentials suggest that the combined effect of two carbonyls enables squaramides

to form strong acceptor interactions more efficiently in comparison with ureas [2].

Despite certain similarities between amides and squaramides, the rigid and planar structure of squaramides containing two coplanar carbonyls makes them a distinctive feature.  $sp^2$ -Hybridised nitrogens make this arrangement stable by providing their lone pairs to conjugation with the  $\pi$ -system orthogonal to the plane [2]. The mutual influence of a NH and carbonyl oxygen contributes to the formation of zwitterionic structures. Moreover, the dipole presented by a zwitterionic squaramide form is known to mimic the  $\alpha$ -ammonium carboxylate motif and thus represents  $\alpha$ -amino acid bioisosteres [27]. Amide-like restricted rotation around the C–N bonds forces a bis-secondary squaramide having two C–N bonds to prefer anti/anti conformation [2].

### 1.2. Pharmacological profile

In general, the main core of the squaric acid derivatives is chemically stable in water environment which these compounds encounter in the organism. Some studies revealed, that squaramides used as isosteres of amino acids may be more resistant against decarboxylases because they do not contain nucleophilic nitrogen important for the decarboxylation [2,27].

Although many derivatives were designed as potential drugs, the pharmacological profile was evaluated only in several of them and only the most promising lead compounds were selected for these advanced studies. As a result, several candidates have entered various stages of clinical trials (Fig. 3). Among them, perzinfotel **8**, discovered in 1999 [27] as a unique NMDA antagonist, had a favourable preclinical profile and therefore seemed to be a suitable lead structure for the development of a drug for the treatment of neurological disorders such as stroke and head trauma. In Ref. [27], the authors tried to improve its low bioavailability by synthesizing tetrazole analogue, which unfortunately failed in *in vivo* experiment designed to show neuroprotective potency (focal ischemia model involving occlusion of the middle cerebral artery in rats). Further attempts to modify perzinfotel **8** [28] afforded prodrug **9** that was adsorbed much better, it was enzymatically transformed to parent compound **8** and this significantly improved the perzinfotel half-life and potency *in vivo* (oral administration in a rodent model of inflammatory pain) [28].

Navarixin **10**, squaric acid dibutyl ester **11**, pibutidine **12** and BMY-25368 **13** (Fig. 3) are other examples of SQ analogues that entered clinical trials. Navarixin **10** (SCH527123, MK-7123) acts as an antagonist of the cysteine chemokine receptor (interleukin 8A receptor) and is under Phase II clinical trials for the treatment of solid tumours (combination therapy, late-stage disease, metastatic

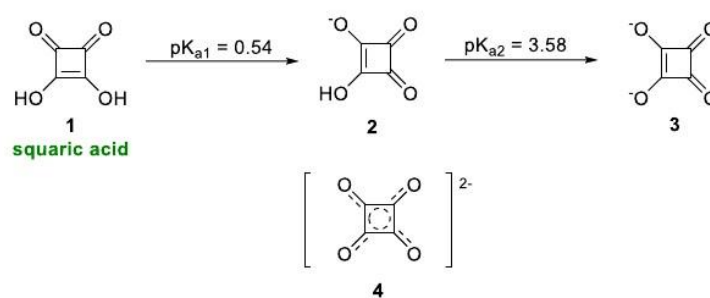


Fig. 1. Resonance stabilized squarate dianion.

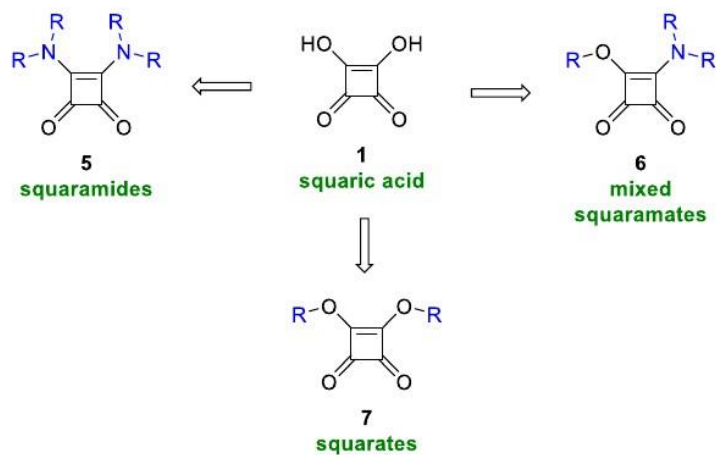


Fig. 2. Squaric acid analogues.

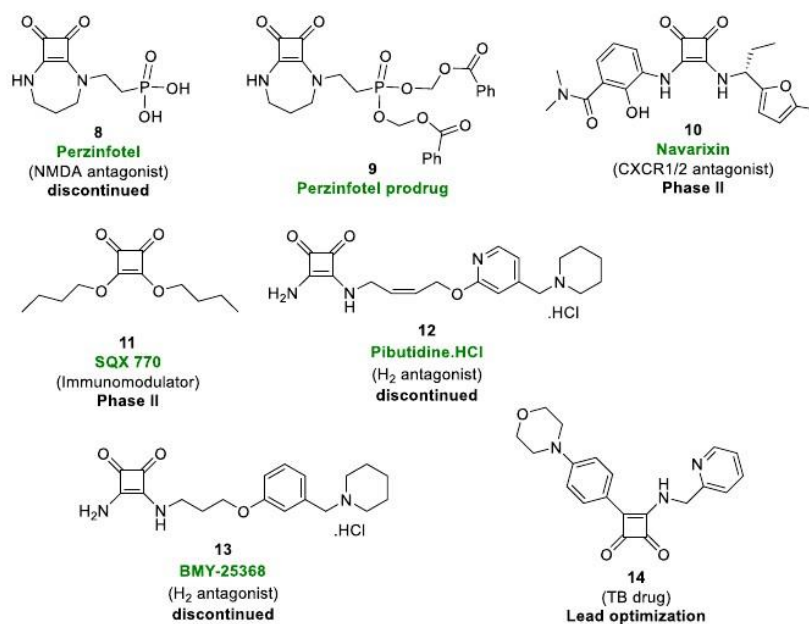


Fig. 3. Clinical/preclinical candidates containing a modified squaramide scaffold.

disease, second-line therapy or greater) in the USA and Israel [29]. Navarixin has also been investigated for the treatment of asthma, chronic obstructive pulmonary disease and psoriasis [30]. It was thought to reduce neutrophil migration to the diseased lung what should improve a participant's symptoms. However, this assumption was not proved, and this research has been discontinued. Squaric acid dibutyl ester **11** (SQX 770) was evaluated for its safety

and efficacy for the treatment of herpes labialis in a clinical trial containing 54 patients and it was found that the compound is slightly effective in reducing the number of the disease outbreaks per year but it had non-serious adverse effects in more than 50% of the treated patients (mostly non-serious itching, redness, or swelling) [31,32]. Pibutidine **12** exhibited an H<sub>2</sub> antagonistic effect and was investigated as a gastrointestinal agent for ulcers [33–35]



by Taisho Pharmaceutical. In 2000, however, it was discontinued in Phase I due to cardiotoxicity and gastrointestinal toxicity [36]. BMY-25368 **13**, developed by Bristol-Myers Squibb, advanced as far as phase III clinical studies for duodenal and gastric ulcers. This compound acts as a histamine H<sub>2</sub> receptor antagonist [37,38].

Another example of pharmacokinetic and pharmacodynamic profiling for SA analogue was done in Ref. [39], where an anti-tuberculous compound **14** (Fig. 3) was developed. In **14**, high metabolic clearance was observed, which was likely caused by cytochromes. Therefore, the authors used pan CYP inhibitor (amino-benzotriazole, ABT) together with **14** in *in vivo* experiment (peroral administration in mice) and this caused a 300-fold increase in free plasma concentration when administered along with 100 mg/kg ABT. This provided plasma concentration above MIC for 15 h which was considered sufficient for further evaluation of pharmacodynamic profile in the acute model of tuberculosis infection. In general, it seems that some SA analogues may be enzymatically stable and other may be metabolized by various enzymes and therefore it is advisable to investigate the metabolic clearance for the most promising lead structures before they enter more expensive clinical trials.

Despite the importance of squaric acid analogues as privileged scaffolds in drug discovery, only two reviews have been published recently on this topic, both about squaramides [40,41]. The first [40] is a very comprehensive review about squaramides, their use in chemical biology, and especially their supramolecular properties. The second review [41] summarizes the synthetic approaches to squaramides. Older reviews on squaramides and squaric acid conjugates exist [2,3]. In contrast, this article presents an overview of squaric acid derivatives in general and focuses predominantly on their potential applications in drug development. The main purpose of this review is to provide an overview of the squaric scaffold-based derivatives as agents with remarkable potential in the medicinal chemistry field. Considerable attention is given to structure-activity relationship (SAR) studies and mechanism of action studies.

## 2. Squaric acid analogues in medicinal chemistry

Squaric acid analogues are significant in medicinal chemistry for many reasons. First, unlike many other compounds designed as potential drugs, they usually do not suffer from high lipophilicity and low solubility in water. Especially when squaric acid or the squaramide scaffold is combined with amine and carboxylic groups, the resulting compounds show increased solubility, and this makes them suitable therapeutic agents [42,43]. In addition, squaric acid analogues may serve as non-classical isosteres for carboxylates and amino acids during drug development [2]. For example, *N*-(hydroxydioxyclobutenyl)-containing analogues of gamma-amino-butyric acid and L-glutamate were successfully used as analogues of compounds that are active towards amino acid receptors (AMPA and NMDA) in neurons [44].

Mono-amides of squaric acid (squaramates) are often used for bioconjugation with Lys and other amines. Diamides (squaramides) have been used as a phosphate group surrogate in nucleotide [45–47] or oligonucleotide (ON) analogues [48,49]. A chemically synthesized 2'-sugar-linked squaramate–RNA conjugate, prepared by the reaction of 2'-amino-modified RNA with diethyl squarate, was reported to cross-link to aminoacyl-transferase FemXWv [50], and this is the only example of the use of a squaric acid analogue in nucleic acid conjugation. Within the research aimed at base-functionalized nucleic acids for applications in chemical biology, the authors designed [51,52,123] novel squaramate-linked cytosine 2'-deoxyribonucleoside triphosphate (dNTP) for the enzymatic synthesis of modified DNA and cross-linking with proteins.

The use of squaric acid analogues in chemical biology is mostly represented by their bioconjugation to proteins or carbohydrates and by their use as ion receptors. In contrast, in medicinal chemistry, these compounds have numerous biological effects, including antiplasmodial, antichagasic, anticancer, and antibacterial activity, which makes them promising agents in drug development. In this chapter, various activities of squaric acid analogues will be summarized, and the advances towards their therapeutic use will be critically reviewed.

### 2.1. Antiprotozoal activity

Protozoans are unicellular eukaryotic organisms responsible for several serious human diseases, such as malaria, human African trypanosomiasis (HAT, sleeping sickness), leishmaniasis, and Chagas disease [53]. These four tropical diseases are endemic in many countries worldwide and together affect approximately 226 million people, particularly in developing countries [54]. Moreover, protozoal infections are among the most common life-threatening secondary infections in immunocompromised patients, e.g., patients with HIV or undergoing cancer chemotherapy. There are many antiparasitic compounds available; however, their use is often limited due to the emergence of drug resistance. An urgent need for novel efficient drugs that act by different mechanisms encourages global antiparasitic drug discovery. Squaric acid analogues might help to overcome the increasing antiparasitic drug resistance because many of these analogues have promising antiparasitic activities [42,55–58].

The first squaric acid analogues with activity against *Plasmodium falciparum*, the causative agent of malaria, appeared in 2013 [57]. The Santos group followed in their previous works [59,60] and synthesized a series of conjugates containing a squaric moiety and heterocycles of general structure **15** and **17** derived from known antimalarials (Fig. 4). Three compounds had nanomolar potency against chloroquine-resistant *P. falciparum* and approximately two-fold higher potency than the parent drug chloroquine. Moreover, they were not cytotoxic against NIH 3T3 or HEK 293T cells. The most interesting derivative **16** from this series is depicted in Fig. 4. Encouraged by these promising results, Ribeiro et al. synthesized other squaramides modified with aminoquinoline (Fig. 4) and tested them against liver-stage malaria parasites using human hepatoma cells (Huh7) infected by *Plasmodium berghei*. Compound **18** (Fig. 4) showed a 7.3-fold greater effect compared to the standard drug primaquine (the only available drug active against all *Plasmodium* exoerythrocytic forms). Overall, both papers by the Santos group [57,58] were focused on finding the most favourable linker between the substituted quinoline and squaramide parts. They tested various flexible alkyl chains, a rigid piperazine linker, and the direct binding of the heterocycle to the squaramide moiety. However, the rigid alkyl chain proved to be the most effective linker within the selected library. The direct binding of squaramide and aminoquinoline resulted in reduced activity [57]. Considering these interesting results, squaramide-modified aminoquinolines might represent a new class of antiplasmodial agents.

Squaramide-based compounds were also tested for their anti-leishmanial activity [55]. Leishmaniasis is a parasitic disease endemic in 98 countries worldwide. More than 1 million new cases are reported per year, and 350 million people are at risk of being infected [61]. The substances currently available for the treatment of this illness are pentavalent antimonials, paromomycin, amphotericin B, and miltefosine. Because these compounds are becoming less efficient due to the emergence of protozoal resistance, there are no effective substances to cure this parasitic disease. Considering the widespread resistance, there is an urgent need to identify new highly active antileishmanial drugs. Due to their interesting biological activity, modified squaramides have been explored as

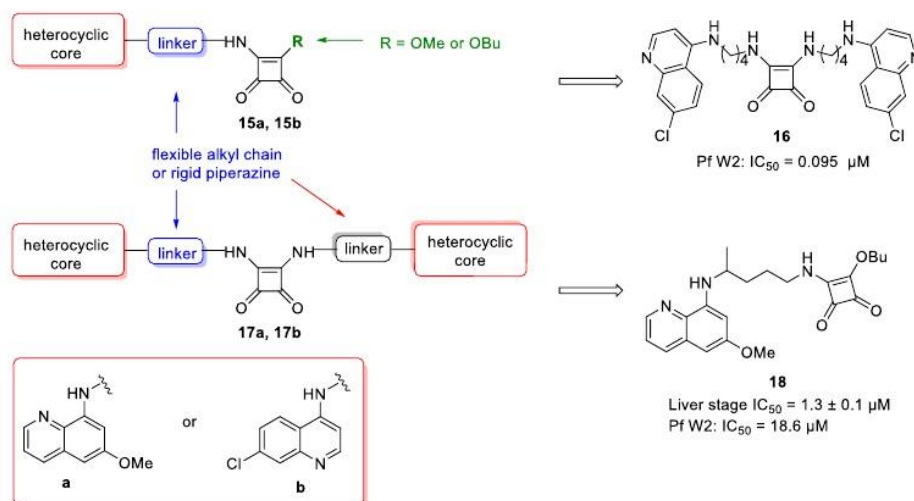


Fig. 4. Squaramides with antiplasmodial activity [57,58].

antileishmanial agents [55]. In 2016, the Sánchez-Moreno group reported the synthesis of variously substituted squaramides of general structures **19–21** (Fig. 5) and their antileishmanial activity on promastigote and amastigote forms of *Leishmania donovani*, *Leishmania infantum*, and *Leishmania braziliensis*. Three of the prepared compounds exhibited higher activity than the standard drug glucantime and were less toxic (Fig. 5). Among them, compound **23** (Fig. 5) was the most effective. Moreover, the authors observed certain alterations in the excretion products of all species indicating the leishmanicidal activity of the studied squaramides.

Of note, squaramide-based compounds have already been explored as highly efficient antichagasic agents [42,56]. Chagas disease (also known as American trypanosomiasis) is an insect-transmitted protozoal infection caused by *Trypanosoma cruzi*. The World Health Organization (WHO) has stated that an estimated 8 million people are infected with *Trypanosoma cruzi* worldwide, especially in Latin America, causing more than 10,000 deaths per year [62]. Current treatment is based on the use of nifurtimox (NFX) and benznidazole (BZN), compounds developed more than 40 years ago. Moreover, their mechanism of action is still under debate

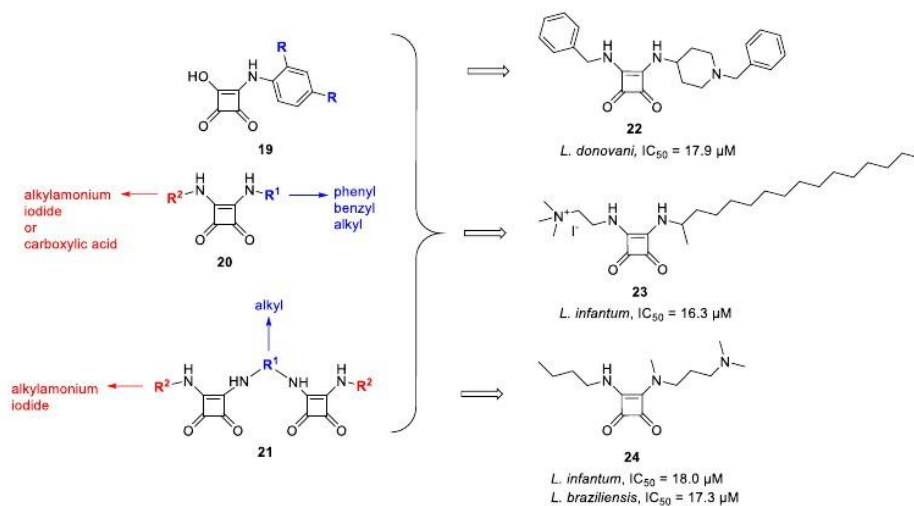


Fig. 5. Squaramides with antileishmanial activity [55].

[63,64]. Unfortunately, both agents are limited in their ability to eliminate *T. cruzi* from the body and have severe side effects such as vomiting, anorexia, and peripheral polyneuropathy due to their high toxicity [42]. For this reason, it is necessary to overcome the serious drawbacks of current antichagasic drugs and develop less toxic and more selective compounds.

During their research with novel squaramides, Olmo et al. found that some of the tested compounds of general structures **25** and **26** exhibited interesting antichagasic properties (Fig. 6) [42]. *In vitro* and *in vivo* studies of various structurally simple amino-squaramides revealed compound **27** (Fig. 6) to be the most active from the selected library in both the acute and chronic phases of Chagas disease. In immunosuppression experiments in a mouse model, the monitoring of total Ig-G in response to *T. cruzi* infection showed comparatively low levels in treated mice and confirmed compound **27** as an ideal candidate for preclinical studies.

The obtained knowledge triggered a study of similar squaramides of general structures **28** and **29** reported by Martín-Escolano et al., in 2019 (Fig. 6) [56]. Among various substitutions, a longer alkyl chain and a dimethylamino substituent showed efficacy against *T. cruzi* [42]. Therefore, the subsequent survey focused on the study of squaramides with longer alkyl chains [56]. To perform an SAR study, they evaluated derivatives with an increasing length of the linear aliphatic chain (C0–C16), compounds with different

heteroatoms, and squaramides containing two or three basic nitrogens (Fig. 6). Based on the *in vitro* and *in vivo* studies, compound **30** was identified as the most potent form of the studied library. Interestingly, the authors attempted to determine the mechanism of action and suggested that compound **30** can depolarize the mitochondrial membrane, resulting in an energetic deficit and subsequent cell death by necrosis. Because selected compound **30** exhibited better trypanocidal properties *in vitro* and lower toxicity compared to the standard drug BZN, it is worth further investigation in the preclinical phase.

## 2.2. Antibacterial activity

Bacterial infections represent one of the greatest public health problems, especially when we consider the increasing antibiotic resistance. This rapid emergence of resistant bacteria is occurring worldwide; therefore, it is essential to extend the spectrum of existing antibiotics. From this point of view, many compounds derived from squaric acid have been studied.

The first reports of antibacterial activity associated with the squarate scaffold associated emerged in 1996 [65] when the Kojima group noted that several squaramides of general structure **31** could act as H<sub>2</sub> antagonists (Fig. 7). Moreover, some of the tested derivatives such as **32** exhibited moderate to weak inhibitory activity

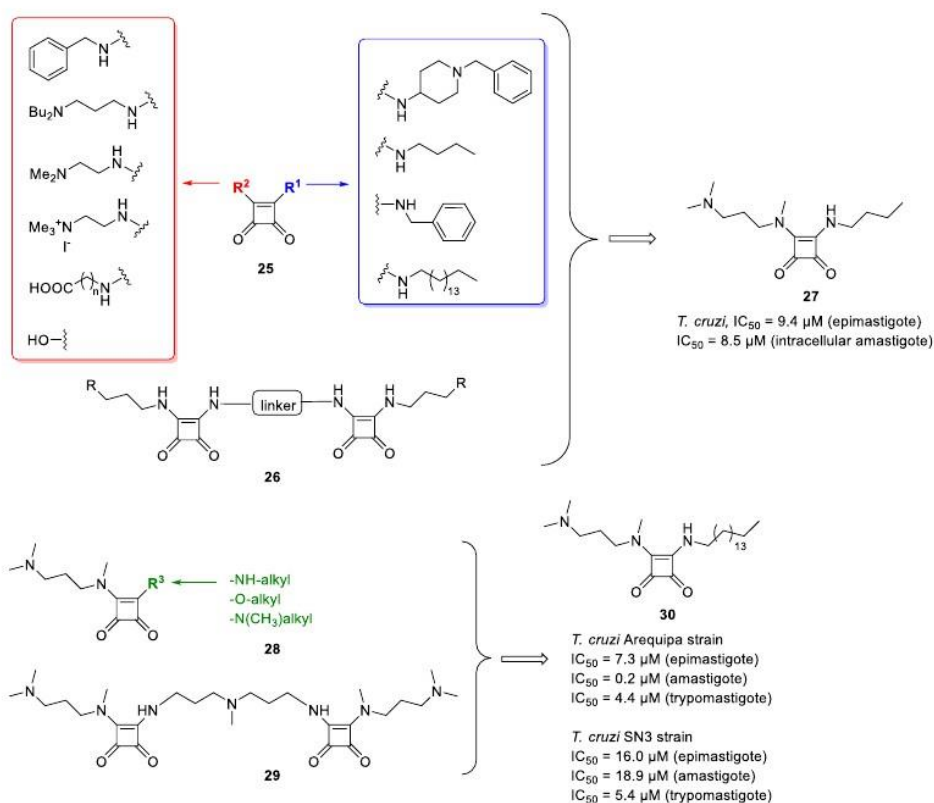
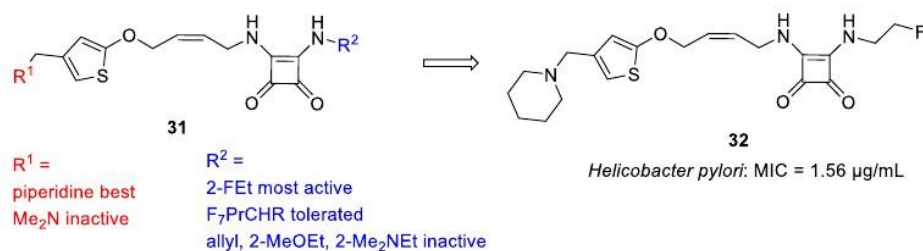


Fig. 6. Squaramides with antichagasic activity [42,56].



Fig. 7. Squaramides acting as H<sub>2</sub> antagonists [65,66].

against *Helicobacter pylori*. Later, this observation resulted in the synthesis of other potent H<sub>2</sub> antagonists and their progression to human clinical trials (as mentioned above with Pibutidine and BMY-25368, Fig. 3) [66].

Lindhorst and co-workers described the interesting behaviour of mannosidic squaric acid monoamides **33** and **34** (Fig. 8) [67,68]. Bacteria use fimbriae (also known as pili) to connect to the host cell [69], and synthetic mannosides based on the squarate structure can inhibit type 1 fimbriae-mediated mannose-specific bacterial adhesion that normally proceeds through the lectin FimH. Synthetic squarate **33** showed high affinity to FimH and exhibited ~50-fold greater inhibitory potency than the standard agent pNPMan [67].

The high potency of squaramides within the medicinal chemistry field was recently confirmed by work published in *J. Med. Chem.* [70]. During the search for novel antibacterial agents, the Murakami team focused on the large antibacterial target, RNA polymerase, which is essential for gene expression, cell growth, and viability [71]. Using a high-throughput screening of a corporate compound library, the Murakami team identified a highly active novel structural framework of general structure **35** based on the squaramide moiety (Fig. 9). This squaramide was shown to bind to the RNA polymerase switch region and result in the dysfunction of the region with consequent transcriptional inhibition. Detailed SAR studies indicated that the terminal isoxazole and benzyl rings are essential for specific binding to pockets in the switch region. Nevertheless, there are further structural modifications to be explored.

Recently, the groups of Gupta and Ravishankar reported one of the most active compounds against *Mycobacterium tuberculosis* (*Mtb*) based on the unique squaramide feature acting as a mycobacterial ATP synthase inhibitor (Fig. 10) [39]. ATP synthase is a ubiquitous key enzyme in the energetics and metabolism of

bacteria that utilizes the energy stored in as transmembrane electrochemical potential for the production of ATP [72]. ATP synthase in *Mtb* has recently been validated as a highly promising target of antibacterial compounds. It is noteworthy that these research groups screened approximately 900,000 compounds in cooperation with AstraZeneca to identify hits and proceed with lead optimization (Fig. 10). The lead series of squaramides **37** was very specific and selective while lacking cytotoxicity [73]. Interestingly, a comparison of squaramide **14** with bedaquiline (an approved drug for tuberculosis treatment that acts as an ATP synthase inhibitor) showed the absence of cross-resistance in bedaquiline-resistant mutants. This finding suggests that squaramide **14** interacts with an ATP synthase site distinct from that with which bedaquiline interacts. These observations indicate the high potency of squaramide **14** in the identification of novel drug candidates active against drug-resistant mutants of *Mtb*.

### 2.3. Cytotoxic activity

The treatment of cancer remains a hot topic. Many researchers explore how to reduce the inherent toxicity of currently used drugs, limit adverse effects on the human body, and improve drug targeting. The most commonly used chemotherapeutics (many approved more than 40 years ago) suffer from low bioavailability due to low water solubility or poor membrane permeability and thus require high dosage. Furthermore, the majority of these compounds have led to the development of multidrug resistance along with fatal side effects. Therefore, the discovery of novel effective anticancer agents with different mechanisms of action has become one of the main research goals worldwide.

Squaric acid analogues have received special attention as potent anticancer agents especially in the last decade [45,74–79]. However, the first report on cytotoxic squaramides appeared as early as 2005 [80], when Grabner et al. studied the complex compound [Pt<sub>3</sub>(μ<sub>2</sub>-C<sub>4</sub>O<sub>4</sub>)<sub>3</sub>(H<sub>2</sub>NPr<sup>f</sup>)<sub>6</sub>·3H<sub>2</sub>O **38** (Fig. 11) obtained by the reaction of cis-[Pt(H<sub>2</sub>O)<sub>2</sub>(H<sub>2</sub>NPr<sup>f</sup>)<sub>2</sub>]SO<sub>4</sub> with barium squarate in a 1:1 M ratio and found that it exhibited interesting cytotoxic properties. In this complex, platinum atoms are joined by squarate ligands that occupy a rather significant distance (approximately 2 Å) between platinum atoms (so-called trinuclear complex); the distance between oxygen atoms is relatively short in comparison (approximately 3.1–3.2 Å). 3D structure is deposited in the published paper as Supplementary data [80]. The cytotoxicity of this compound was tested on T24 cells, which exhibited slightly reduced size after exposure to this compound. This complex has not achieved cytotoxicity similar to cisplatin; however, future studies with squarate complexes might help to overcome the inherent cytotoxicity of platinum complexes.

In 2012, Villalonga et al. reported the synthesis of oligosquaramide-based macrocycles with anticancer properties of

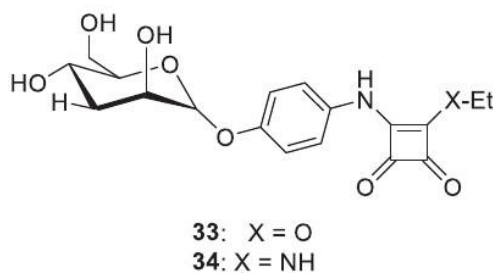


Fig. 8. Squarates as inhibitors of bacterial adhesion [67].

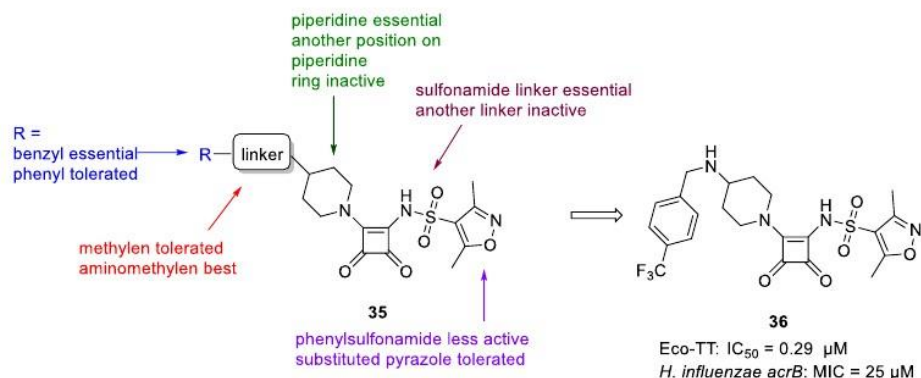


Fig. 9. Squaramides as RNA polymerase inhibitors [70].

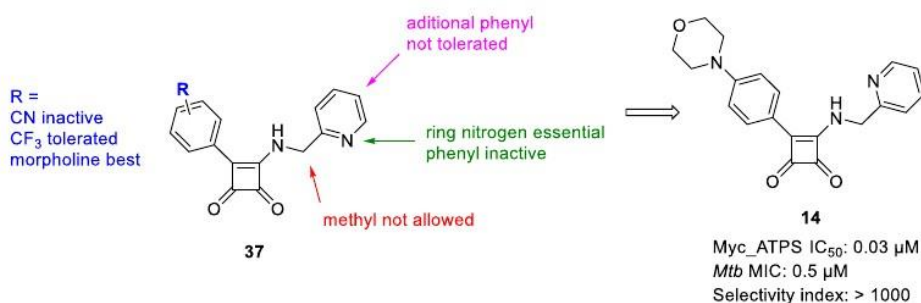


Fig. 10. Squaramides acting as mycobacterial ATP synthase inhibitors [39].

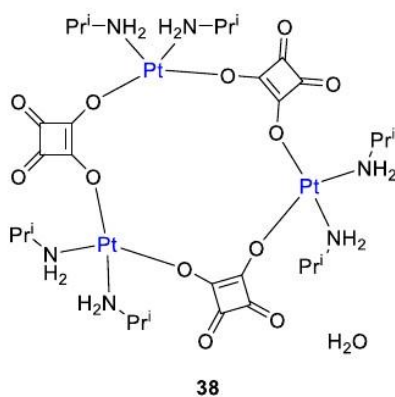


Fig. 11. Structure of trinuclear complex.

general structure **39** (Fig. 12) [79]. They prepared various oligomer cyclosquaramides and acyclic oligosquaramides and tested their

anticancer activity primarily on mantle cell lymphoma (MCL) cell lines Jeko-1 and Z-138. Interestingly, the appropriate size of the macrocycle was crucial for antiproliferative activity. The most interesting oligomer comprises five squaramide scaffolds (**40**,  $n = 3$ ) connected with appropriate linkers (Fig. 12) and displays a well-defined structure with a certain level of conformational pre-organization and flexibility that is very important for ligand binding on the desired target. In contrast, corresponding acyclic oligosquaramides and smaller cyclosquaramides containing 2–4 squaramides did not show any anticancer activity. The oligosquaramide **40** exhibited significant antiproliferative activity against both Jeko-1 and Z-138 cells and was subsequently tested against the NCI-60 human tumour cell line panel. Moreover, oligosquaramide **40** did not show toxicity against controlled nontransformed NIH3T3 fibroblasts. Although the biological target of cyclosquaramides remains unknown to date, the authors speculated that target proteins may include kinases. However, determining the exact mechanism of action will require more information and consistent studies in the future.

The anticancer SAR of squaric acid analogues inspired by the structure of the known antimitotic agent combretastatin A4 (CA4) demonstrated the potency of this motif (Fig. 13) [75]. Liu et al. synthesized various 3,4-diaryl squaric acid analogues **43** as CA4 mimetics incorporating the squaric scaffold as a *cis*-restricted linker and studied their cytotoxicity. All the compounds were tested



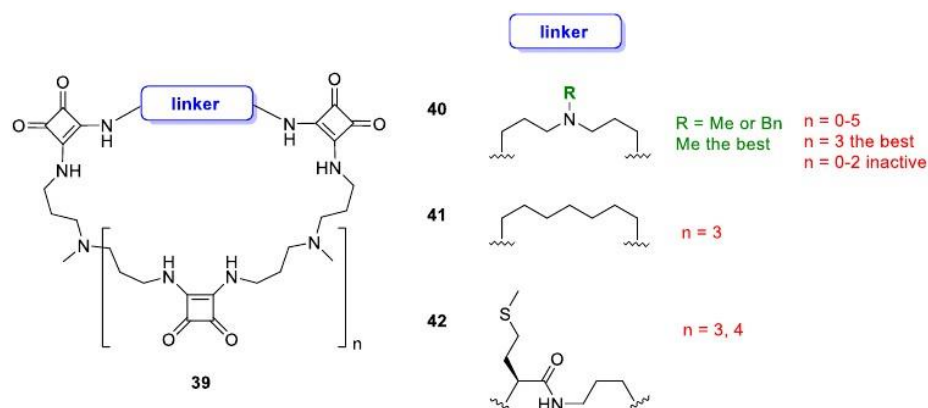


Fig. 12. Cyclosquaramides with antiproliferative activity [79].

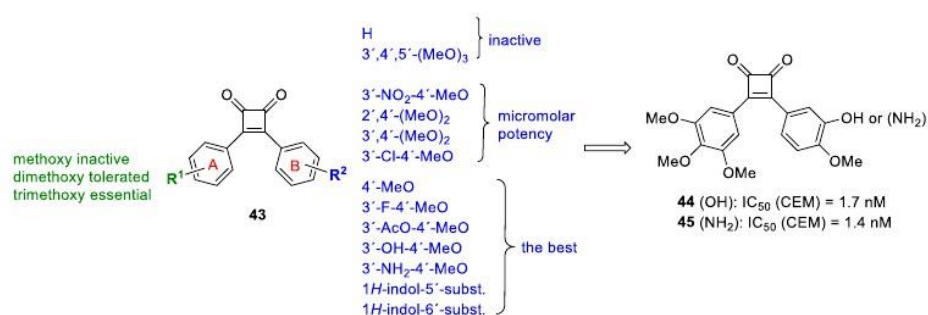


Fig. 13. Squaric acid analogues with antimetabolic activity [75].

against the non-solid human CEM cell line and further evaluated against a panel of human tumour cell lines, including Bel-7402, HepG2, and SMMC-7221 human liver cancer cells, MCF-7 human breast cancer cells, SW-1990 human pancreatic cancer cells, HCT116 human colon adenocarcinoma cells, and CEM human leukaemia cells, with CA4 employed as a positive control. The extended SAR study revealed that some of the tested compounds exhibited nanomolar activities against human leukaemia cells and potent activities against a panel of human tumour cell lines. Of note, compounds **44** and **45** exhibited activities comparable to the standard drug CA4 (IC<sub>50</sub> (CEM) = 1.6 nM). Moreover, the reported SAR study showed that all three methoxy groups of the A ring are essential, whereas the substitution of the B ring can be more varied. The authors also reported preliminary mechanism of action studies revealing that compounds **44** and **45** cause cell cycle arrest tumour cells in G2-M phase and interact with the colchicine binding site on microtubules.

In 2016, Quintana et al. reported the cytotoxicity of various squaramates and squaramides of general structure **46** (Fig. 14) evaluated on different tumour cell lines (especially HeLa, cervical carcinoma, and HGC-27, gastric carcinoma) [78]. The reported anticancer SAR of all hybrids depicted in Fig. 14 demonstrates the necessity of both NH groups (squaramates did not show any significant activity). Interestingly, squaramides with cinchona-based

substituents exhibited micromolar potency with IC<sub>50</sub> values of 3–12 μM in HGC-27 or HeLa cells. The best candidate from the evaluated library was compound **47** with an IC<sub>50</sub> value of 1.81 μM in HGC-27 cells and 34.63 μM in HeLa cells. Squaramide **47** was further tested on different cell lines such as T98 and U87 glioblastoma cells (the most aggressive cell type causing brain cancer), HEK293 transformed human kidney cells, MDCK cells (epithelial cells) and Vero (African green monkey kidney cell). The results confirm cell type-dependent toxicity (IC<sub>50</sub> values of 60.25 μM and 7.15 μM for glioblastoma cell lines U87 and T98, respectively, 9.03 μM for HEK293, 70.20 μM for MDCK, and 33.40 μM for Vero). Furthermore, the authors found out that the inhibitory effect of **47** is associated with cell cycle arrest at the G1 phase and the induction of caspase-dependent apoptosis. Based on these results, squaramide **47** could act as a hit for further optimization.

In 2016, Soukarié et al. designed novel cap-binding inhibitors of 4E factor (eIF4E) based on the squaramide scaffold [45]. The factor eIF4E is a component of the eukaryotic translation initiation factor 4F complex, which recognizes the 7-methylguanosine cap structure at the 5' end of messenger RNAs and is a key player in the regulation of translation. eIF4E activity is implicated in mitosis, embryogenesis, and apoptosis. Interestingly, eIF4E is overexpressed in numerous human tumours, which makes it an interesting target for anticancer therapy. Based on the known crystal structure of

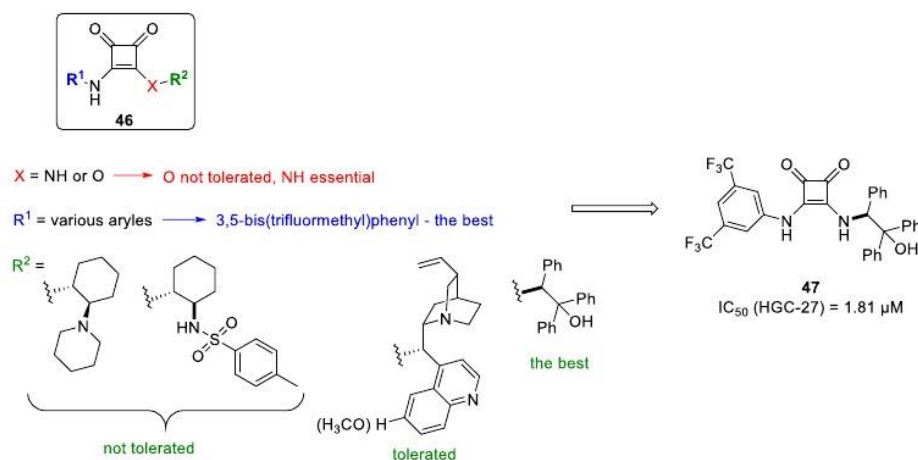


Fig. 14. Squaramates and squaramides evaluated for their cytotoxicity [78].

eIF4E and in consideration of the cellular bioavailability of potent drugs, Soukariéh et al. designed and synthesized novel eIF4E cap-binding inhibitors, some of which contain the squaramate scaffold (Fig. 15). Most of the tested squaramates did not show any significant activity; only compounds **49** and **50** exhibited modest inhibitory effects (Fig. 15). Moreover, these two depicted squaramates were co-crystallized with eIF4E. The obtained crystal structures showed similar binding modes to cap derivatives reported previously.

Carbocyclic nucleosides **51–53** incorporating the squaric acid scaffold synthesized by Lu et al. (Fig. 16) were examined for their anticancer activity in a National Cancer Institute battery of human tumour cell lines [77]. All three derivatives exhibited modest anticancer activity against non-small cell lung cancer (NCI–H522) at 10 μM. Squaramide **51** and squaramate **52** showed micromolar potency against renal cancer (UO-31). Moreover, compound **51** exhibited modest anticancer activity against ovarian cancer (OVCAR-8) and leukaemia (CCRF-CEM), whereas compound **52** was potent against colon cancer (KM12) and melanoma (UACC-257) at 10 μM. Interestingly, derivative **53** showed moderate growth

inhibition of CNS cancer (SF-295) at 10 μM. Furthermore, all three analogues were tested for toxicity to HeLa cells. However, none of the tested compounds showed better inhibitory effects compared with the standard drug cisplatin. Overall, the tested squaric acid analogues exhibited moderate anticancer activity with a selective effect on some of the tested cell lines. However, more studies are needed to demonstrate the potency of the presented carbocyclic nucleosides as non-classical bioisosteres for the heterocyclic base in cancer treatment.

The squaric acid scaffold was also incorporated into the structure of nucleosides designed as inhibitors of SNM1A [81]. SNM1A (sensitive to nitrogen mustard 1A) is a DNA repair enzyme that plays a crucial role in the repair of interstrand crosslinks. The enzyme is considered a potential therapeutic target for the treatment of cancer that is resistant to DNA crosslinking agents. Because the active site of SNM1A contains a zinc atom, Doherty et al. proposed that a molecule modified with a zinc-binding group might block this enzyme and inhibit the repair of interstrand crosslinks. Because squarate or the squaramide ring can selectively bind through hydrogen bonds acting as hydrogen bond donors or

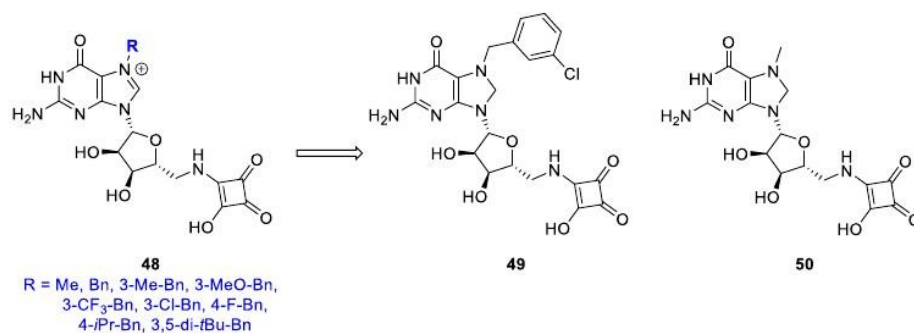


Fig. 15. Squaramates as eIF4E inhibitors [45].

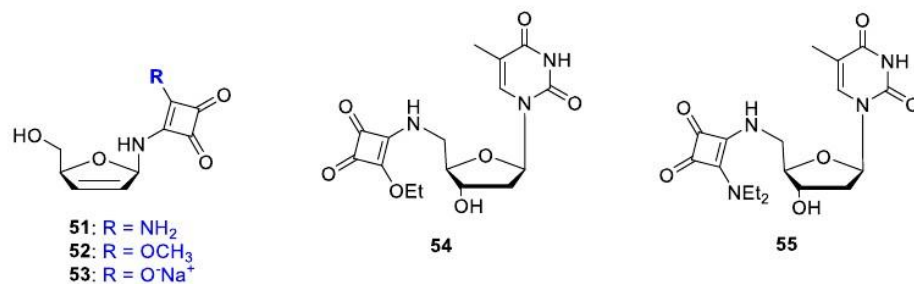


Fig. 16. Carbocyclic nucleosides incorporating the squarimate scaffold [77] and nucleosides designed as inhibitors of SNM1A [81].

acceptors, this nucleoside modification was selected as a suitable zinc-binding group (Fig. 16). Unfortunately, neither squarate **54** nor squaramide **55** showed any activity in the performed assay.

Squaric acid derivatives as cytotoxic agents were further described by Fernández-Moreira et al. [74]. They studied several squarates and squaramides for their cytotoxicity against HeLa cervical cancer cells (Fig. 17). Compound **57** exhibited the greatest cytotoxicity (IC<sub>50</sub> = 0.88 μM). Moreover, the cyclobutenedione ring was modified with various fluorophores for potential application in cell imaging studies, and the novel luminescent compounds were visualized using fluorescence cell microscopy. The authors observed lysosomal and nuclear localization. Squarate compound **58** was the most promising candidate from the evaluated library. Compound **58** enters the cell and accumulates in the nucleus. These

results indicate the high potential of squaramide-based transporters, which merit further investigation.

#### 2.4. Antiviral activity

Among all the viral diseases, acquired immunodeficiency syndrome (AIDS) caused by the human immunodeficiency virus (HIV) continues to be a major global health issue, having claimed almost 33 million lives. Due to gaps in HIV services, 690,000 people died from HIV-related causes in 2019, and 1.7 million people were newly infected [82]. The emergence of resistance and/or a lack of tolerability in individual patients requires a wider range of treatment options. As a result, the development of new anti-HIV agents with improved safety, better resistance profiles, and new mechanisms of

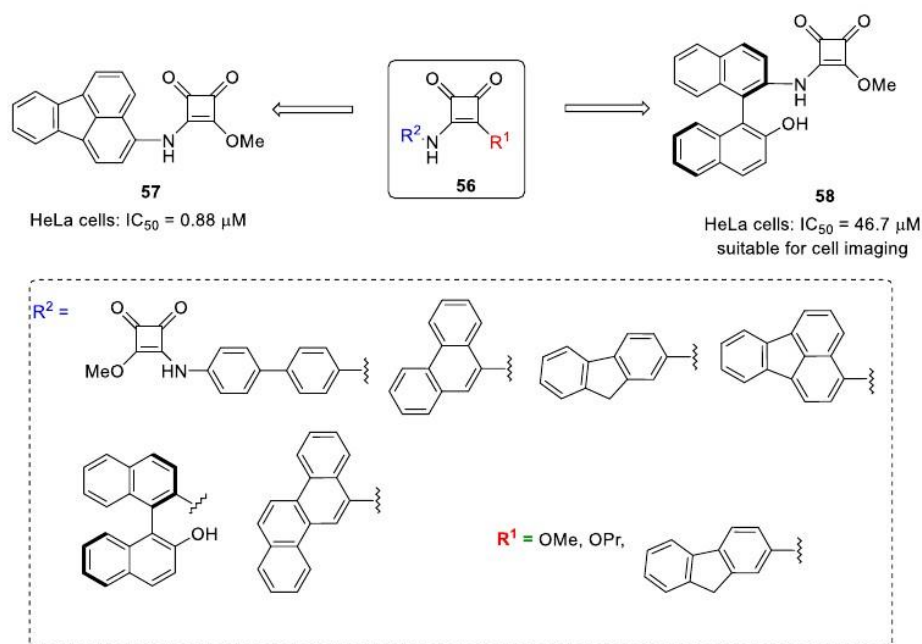


Fig. 17. Luminescent derivatives studied for their cytotoxicity against HeLa cells [74].



action is gaining attention [83]. Squaric acid analogues offer interesting opportunities within this research area.

In contrast to their significant antibacterial properties, the antiviral activity of squaric acid analogues has not been explored extensively. Most attention has been paid to analogues with anti-HIV activity. In 2005, Lee et al. screened a novel series of peptidomimetics containing a squaramide scaffold of general structure **59** (Fig. 18) as bioisosteric replacement for guanidine. These compounds were studied for their ability to inhibit the Tat-TAR interaction required for the conversion of arrested RNA polymerase II into a form needed for successful viral transcription. Derivative **60** was able to bind TAR RNA with high affinity ( $K_D = 7.7 \mu\text{M}$ ) [84].

Another series of anti-HIV squaramides of general structure of **61** was synthesized and studied by Ghosh et al., in 2019 [85]. All the HIV-1 protease inhibitors contain a squaramide-derived scaffold as the P2 ligand combined with an (*R*)-hydroxyethylamine sulfonamide isostere (Fig. 18). Compound **62** with an *N*-methyl-3-(*R*)-aminotetrahydrofuranyl squaramide P2 ligand exhibited the best HIV-1 protease inhibitory  $K_i$  value of 0.51 nM. To explain the inhibitory potency, an energy-minimized active site model of inhibitor **62** was employed, and this model revealed several key interactions with Asp29 and Asp30 [85].

Previously mentioned carbocyclic nucleosides **51–53** incorporating the squaric acid scaffold synthesized by Lu et al. (Fig. 16) were examined for their antiviral activity [77]. However, no antiviral activity was observed for any of the analogues against a National Institute of Allergy and Infectious Diseases (NIAID) panel of 25 viruses [77].

### 2.5. CXCR2 receptor antagonists

CXCR1 and CXCR2 receptors are G protein-coupled receptors activated by growth-related protein- $\alpha$  (CXCL1) and interleukin-8 (CXCL8) [86]. These receptors are expressed on many different

inflammatory and structural cells, where they regulate pulmonary functions. Therefore, CXCR2 is involved in the pathology of various lung diseases such as chronic obstructive pulmonary disease (COPD), asthma, acute respiratory distress syndrome, and cystic and pulmonary fibrosis [87–89]. Due to the key role of CXCR2 in a number of inflammatory disorders, potent selective CXCR2 antagonists have been developed over the past decade as promising anti-inflammatory agents [90].

In 2007, Gonsiorek et al. confirmed the pharmacological specificity of Sch527123 as a novel, potent, and allosteric CXCR2 antagonist with potential therapeutic utility in a variety of inflammatory conditions (Fig. 19) [91]. To measure compound affinity, [ $^3\text{H}$ ] Sch527123 was characterized in both equilibrium and nonequilibrium binding analyses. Its binding to CXCRs was both saturable and reversible. Although Navarixin **10** bound to CXCR1 with good affinity ( $K_d = 3.9 \pm 0.3 \text{ nM}$ ), the compound is CXCR2-selective ( $K_d = 0.049 \pm 0.004 \text{ nM}$ ). The extraordinary picomolar potency of Sch527123 binding to hCXCR2 arises from slow (approximately 24 h at room temperature) dissociation from the receptor [91].

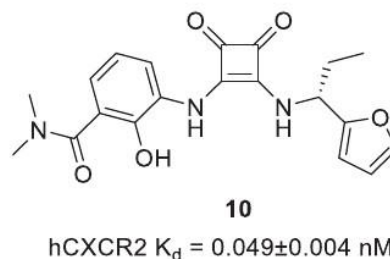


Fig. 19. Navarixin (Sch527123) [91].

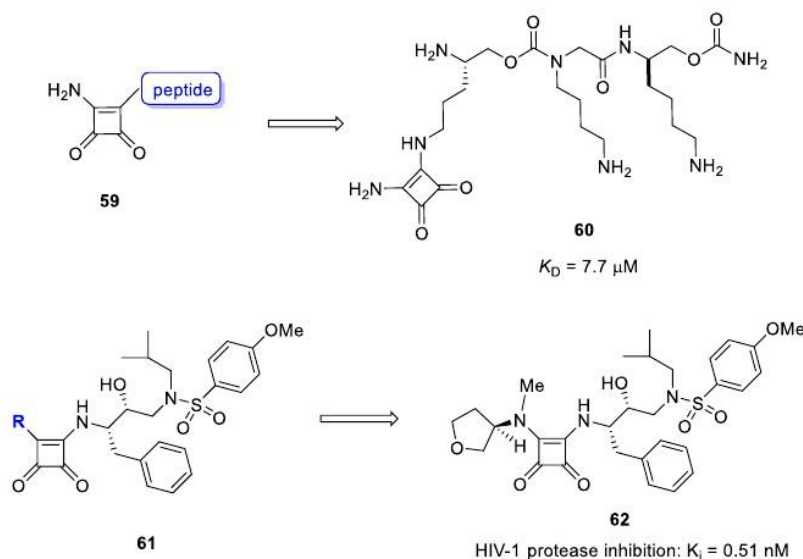


Fig. 18. Anti-HIV peptidomimetics containing squaramide scaffold [84] and squaramides as HIV-1 protease inhibitors [85].

*N,N'*-diarylsquaramides **63** were identified by McClelland and co-workers as selective and potent CXCR2 antagonists (Fig. 20) [92]. They studied squaramides as bioisosteric replacements of previously synthesized *N,N'*-diarylureas and *N,N'*-diaryl (cyano)guanidine-type CXCR2 antagonists. Based on SAR, NHs and the phenolic group are essential. In contrast, diarylsquaramides are insensitive to the ionization state of the phenol. The 3-position adjacent to the phenol is tolerant to the modulation of physicochemical parameters by the introduction of solubilizing sulfonamides and amides. All the other aromatic substituents have limited effects on solubility. Within the series, squaramide **64** (Fig. 20) displays the best activity and most desirable pharmacokinetic profile [92].

Another isosteric urea replacement by *N,N'*-diarylsquaramide moiety, which has received an increased attention, was disclosed in three patents by Glaxo-SmithKline in 2001 and 2002 (Fig. 21) [93]. Additionally, there was a joint application from Pharmacopeia and Schering-Plough in 2002 covering phenol-containing squaramides such as compound **65** with the typical aryl right-hand side, compound **69** bearing a branched alkyl group, and compound **70** containing a benzyl-type group (Fig. 21). The preference of a 3-(*N,N*-dimethylcarboxamido)-2-hydroxyphenyl left-hand side indicates this as an optimal group for this class of squaramides. All these phenol-containing CXCR2 antagonists play an important role in the resurgence of chemokine receptor antagonists and demonstrate efficacy in complex chronic diseases such as COPD and cystic fibrosis [93].

Extended SAR studies conducted with the diaryl cyclobutenedione series comprising general structures **71** resulted in compound **72** (Fig. 22), which demonstrated significant affinity in the CXCR2 binding assay ( $IC_{50} = 36$  nM) [94]. Due to concerns about the metabolic fate of the 4-NO<sub>2</sub> group, the 3-dimethylcarboxamide derivative **73** (Fig. 22) was created and showed excellent *in vitro* potency (CXCR2  $IC_{50} = 15$  nM) and good functional activity in a CXCR2 chemotaxis assay ( $IC_{50} = 19$  nM). Moreover, compound **73** showed improved organic solubility and better predicted absorption. Further SAR studies focused on the exploration of the right-hand benzylic functionality. The (*R*)-ethyl analogue **74** (Fig. 22) demonstrated superior binding affinities (CXCR2  $IC_{50} = 6.8$  nM) and a high level of oral bioavailability. However, the best potency (CXCR2  $IC_{50} = 2.6$  nM) was observed upon replacement of the phenyl ring of **74** with heterocyclic rings affording the previously mentioned clinical candidate Sch527123 (Fig. 19) [94].

Novartis is developing the CXCR2 selective antagonist **75** (Fig. 23) with the potential to become the first anti-inflammatory treatment for COPD. Recently, Martin and co-workers developed a manufacturing concept for the choline salt of a nonsymmetric squaramide as a potent CXCR2 antagonist to increase drug

substance quality [95]. Progress was outlined in terms of yield improvement as well as purging strategies for key impurities. Furthermore, an alternative sequence has been explored to avoid the switching of the phenolate salt from triethylammonium to free acid to a choline salt, providing significant cost reduction [95].

## 2.6. Bioisosteres

The concept of isosterism between relatively simple chemical entities was originally contemplated by James Moir in 1909 [96]. The term "bioisostere" was introduced in 1950 by Harris Friedman, who defined bioisosteres as compounds eliciting a similar biological effect [97]. Bioisosteres are usually less than exact structural mimetics and are often more alike in biological rather than physical properties. Consequently, bioisosteres introduce structural changes that can be beneficial for the design and development of drug candidates, and thus they have become a fundamental tactical approach in medicinal chemistry [98]. In this context, squaric acid derivatives were also explored as non-classical bioisosteres.

First, squaric acids were identified as useful isosteres of carboxylic acids and tetrazoles in angiotensin II antagonists due to their high intrinsic acidity. Squarate **76** (Fig. 24) reduced blood pressure in Goldblatt hypertensive rats, although efficacy was lower than the analogous tetrazole [99].

In an elegant example of isostere design, diaminosquaric acid derivatives **77** were conceived as achiral mimetics of glutamic acid [100]. Some of these molecules exhibited modest affinity for the *N*-methyl-D-aspartate (NMDA) glutamate receptor. The phosphonate derivative **78** (Fig. 24) was the most potent NMDA ligand, although it showed lower affinity than glutamic acid with an  $IC_{50} = 70$  nM [100].

Butera et al. studied bioisosteric replacement of *N*-cyanoquinidine with a squaramide moiety to identify structurally novel adenosine 5'-triphosphate-sensitive potassium ( $K_{ATP}$ ) channel openers of general structure **79** to treat urge urinary incontinence (UUI) [101]. A systematic SAR study on aryl and alkylamide groups produced definitive trends summarized in Fig. 24. Mechanistic studies were performed within the series, and compound **80** (Fig. 24) showed significant  $K_{ATP}$  hyperpolarization and thus represents an attractive development candidate for the treatment of UUI [101].

Additionally, squaramide-type nucleotide analogues **81** and **82** were evaluated as phosphate isosteres. NMR analysis of compound **83** (Fig. 25) revealed its *N*-type form of ribose puckering identical to that in cAMP and cGMP. Due to their acidity ( $pK_a = 2.3$ ) and conformational properties, they are interesting as potential antiviral and anticancer agents [102].

R<sup>2</sup>: high tolerability: H, sulfonamides or amides  
sulfonamides best

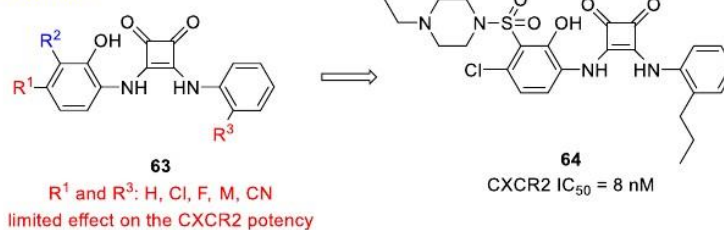
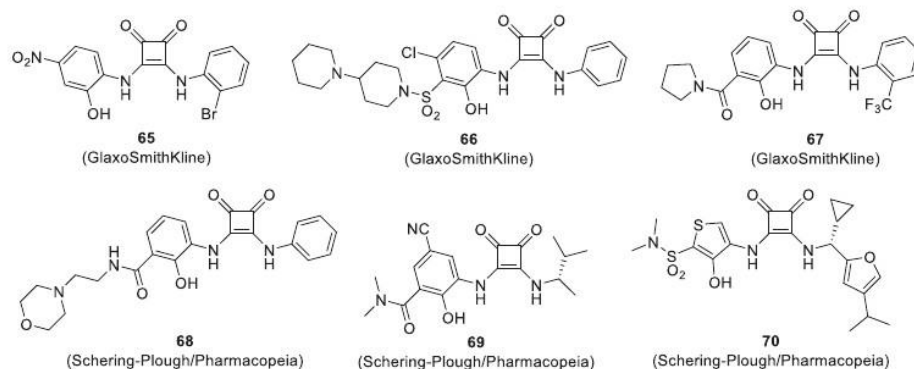
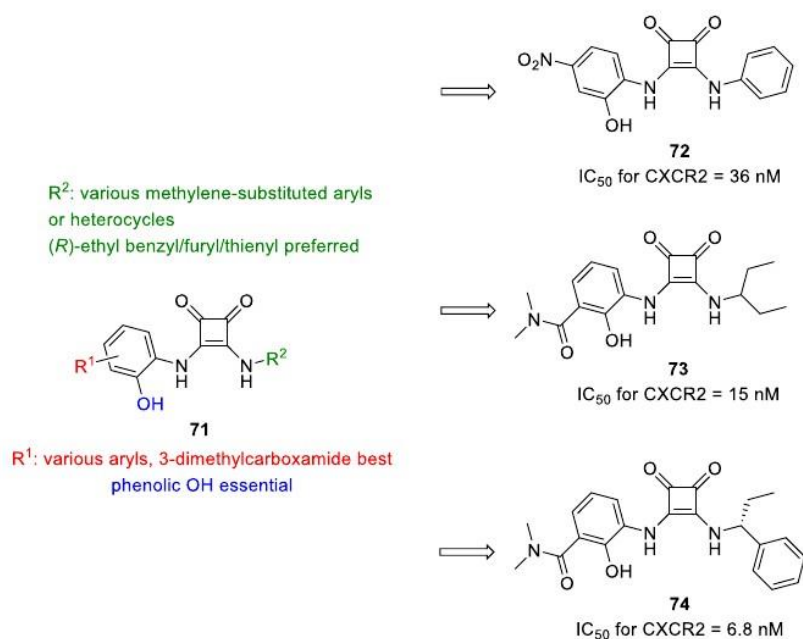


Fig. 20. *N,N'*-diarylsquaramides as antagonists of CXCR2 receptor [92].

Fig. 21. *N,N'*-diarylsquaramide CXCR2 antagonists [93].Fig. 22. Phenol-containing *N,N'*-squaramide CXCR2 antagonists [94].

Additional squaramide-based phosphate bisosteres **84** were described by Xie et al. [103]. They showed that the squaric acid moiety could be incorporated in protein tyrosine phosphatase inhibitors as a phosphate bisostere. As a result, compounds **85** and **86** (Fig. 26) were developed and showed moderate inhibitory activity against *Yersinia pestis* protein tyrosine phosphatase with IC<sub>50</sub>s at pH 5.5 of 120 ± 20 and 350 ± 40 μM, respectively [103].

## 2.7. Vaccines

The introduction of vaccination against bacterial infections represents a breakthrough in human medicine [104]. Instead of a curing effect, an immunological memory is installed. In the field of vaccine development, the squaric acid moiety was initially used to prepare glycoconjugates from synthetic linker-equipped carbohydrates [105,106].



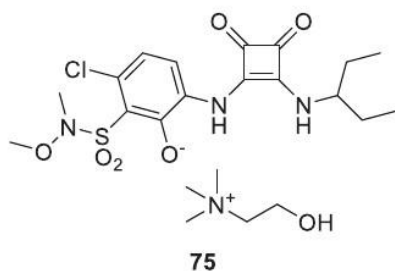
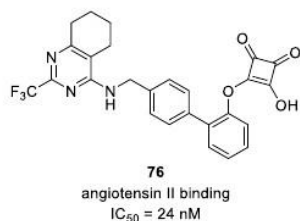


Fig. 23. A selective CXCR2 antagonist in development at Novartis [95].

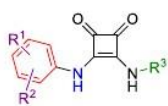
In the context of cancer immunotherapy, Palitzsch et al. synthesized mucin MUC1-glycopeptide vaccines with TTox as the immune-stimulating carrier and analysed their SAR in immunizations. Diethyl squarate has been used to couple glycopeptide antigens to carrier proteins. As a result, a synthetic glycopeptide vaccine inducing tumour-associated MUC1-specific IgG monoclonal antibodies that differentiate between normal and tumour mammary cells has been generated [105].



$R^1$  and  $R^2$ : *p*-cyano substitution optimal  
*o*-Et/CH<sub>3</sub>/Br/Cl substitution best

various heteroaryls tolerated  
phenyl preferred

*N*-alkylation essential  
*N*-acylation tolerated



$R^3$ : (*R*)-3,3-dimethyl-2-butyl/1-methylbenzyl/*t*-butyl optimal

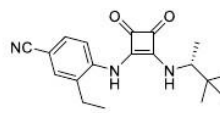
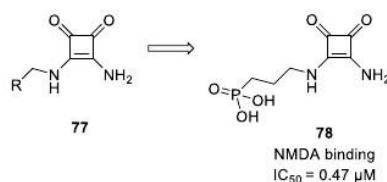


Fig. 24. Squaric acid isostere **76** as angiotensin II receptor antagonist [99], diaminosquaric acid-based NMDA antagonists **78** [100], and *N*-cyanoguanidine bisosteres **80** as K<sub>ATP</sub> channel openers [101].

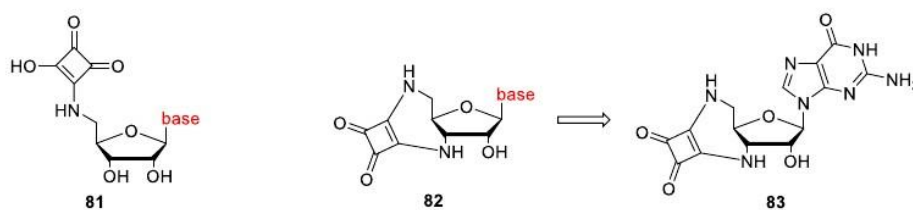


Fig. 25. Squaramide-type nucleotide analogues [102].

Peng and co-workers studied factors affecting the conjugation of bacterial polysaccharides to protein carriers employing squaric acid chemistry. Based on the identification of efficient conjugation to bovine serum albumin (BSA) and recombinant tetanus toxin fragment C (rTT-Hc) at pH 8.5, 9.0, and 9.5, higher-quality labelling of the O-SP-core (O-SPcNH<sub>2</sub>) polysaccharide antigen with methyl squarate has been achieved. The novelty of the described approach is based primarily on the direct conjugation without the introduction of linkers to the molecule. Overall, the results indicate an increased efficiency of conjugation of the *Vibrio cholerae* O1 lipopolysaccharide (LPS) to BSA from 25% to 51% [106].

## 2.8. Various receptor antagonists

In 1992, Kinney et al. described a series of squaramide-based NMDA antagonists. These compounds inhibit excitatory amino acids (EAAs) such as a glutamic acid neurotransmitter that can lead to neuronal cell death [100]. Therefore, NMDA antagonists have been considered for the treatment of epilepsy, stroke, and neurodegenerative disorders [107]. Among all the studied isosteres, phosphonic acid **87** provided protection against NMDA-induced lethality in mice (Fig. 27) [100].

The squarate scaffold has also been used as a carboxylic acid bisostere for the design of a potent, non-peptidic, non-tetrazole

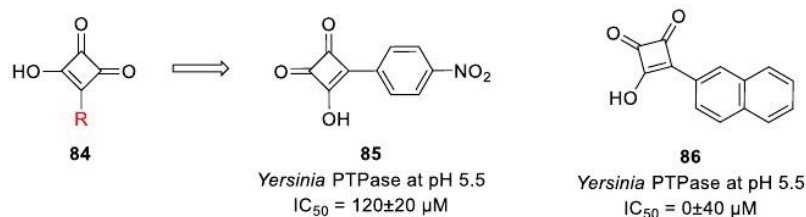


Fig. 26. Squaric acid-based protein tyrosine phosphatase inhibitors [103].

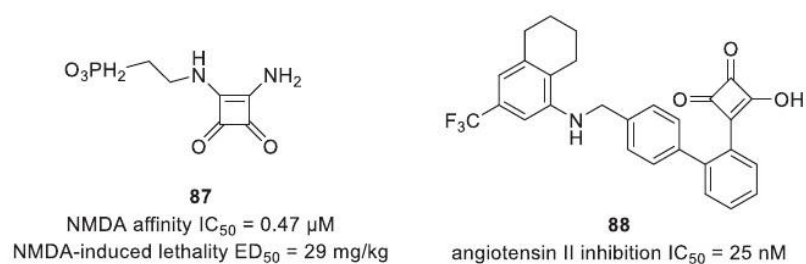
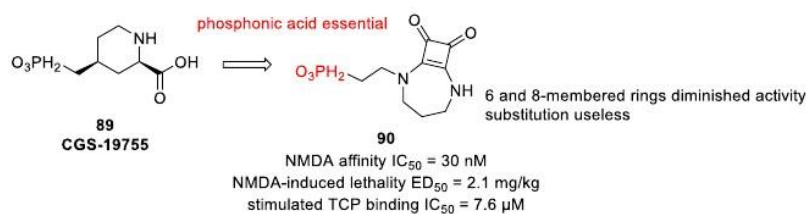
Fig. 27. Phosphonoalkyl squaramide-based NMDA antagonist **87** [100] and squarate-derived angiotensin II inhibitor **88** [99].

Fig. 28. Fused phosphonoalkyl squaramides as NMDA antagonists [27].

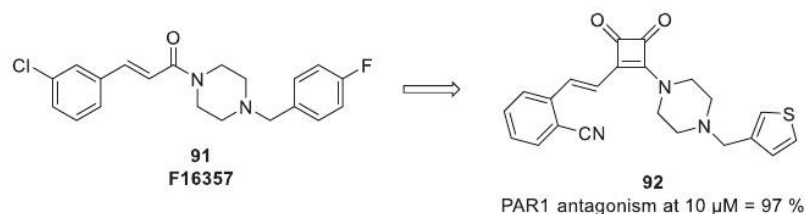


Fig. 29. Squarate-type cinnamoylpiperazine PAR1 antagonists [108].

angiotensin II antagonist [99]. The main purpose of this study was to assess *in vitro* potency as angiotensin II antagonists and the *in vivo* antihypertensive profile of various carboxylic acid bioisosteres including squarates compared with losartan. Unfortunately, squarate **88** was less potent in lowering blood pressure than losartan (Fig. 27) [99].

In another series of NMDA antagonists, the diazabicyclic amino acid phosphonate **90** was found to have equivalent potency as GCS-

19755 **89** in the [<sup>3</sup>H]CPP binding assay, the stimulated [<sup>3</sup>H]TCP binding assay, and the NMDA-induced lethality model in mice [27]. Compound **90** is a unique NMDA antagonist with a favourable preclinical profile offering an opportunity for the treatment of several neurological disorders (Fig. 28). Extensive SAR exploration indicated that the 6- or 8-membered ring compounds possessed diminished activity and revealed that a 2-carbon side chain is optimal for NMDA receptor affinity. Substitution on the ring was



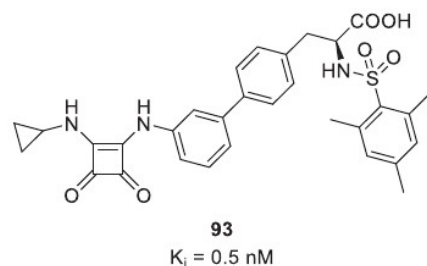


Fig. 30. Biphenyl squaramide as a vitronectin receptor antagonist [109].

not beneficial, and replacement of the phosphonic acid group was also ineffective [27].

Planty and co-workers synthesized squarate-type cinnamoylpiperazines as new protease activated receptor 1 (PAR1) antagonists [108]. Because human PAR1 is involved in thrombin-induced platelet aggregation, its antagonism should result in novel antiplatelet drugs. Additionally, PAR1 antagonists do not affect thrombin's role in the coagulation cascade and thus have a limited impact on bleeding. All the reported squarate analogues were derived from the cinnamoylpiperazine PAR1 inhibitor F16357 **91** (Fig. 29). Replacement of the carbonyl scaffold by a squarate bioisostere led to very potent PAR1 antagonists such as compound **92**, which showed 97% antagonism at  $10 \mu\text{M}$  (Fig. 29). In contrast, no anti-aggregant properties were detected in an *in vitro* human platelet model [108].

In 2007, other squaramides were investigated as arginine mimetic moieties acting as vitronectin receptor ( $\alpha_v\beta_3$ ) antagonists by Klaus et al. [109]. Squaramide **93** proved to be a subnanomolar  $\alpha_v\beta_3$  antagonist ( $K_i$  of 0.5 nM) and could be used as a new treatment of restenosis after balloon angioplasty (Fig. 30) [109].

Finally, phosphoglycolipid analogues modified by the squaryl group were studied by Ding and co-workers for their modulatory activity towards the class A G-protein coupled receptor (GPR) 55 [110]. Localized in spinal cord sensory axons, GPR55 plays a key role in neuropathic pain, cancer, and inflammation [111]. In this study, the endogenous ligand lyso-phosphatidyl- $\beta$ -D-glucoside (LPGlc)-derived analogues with a squaryl diamide group were developed as GPR55 modulators. Compound **95** showed LPGlc-like behaviour and repelled dorsal root ganglion (DRG) nociceptive axons (Fig. 31) [110].

### 2.9. Various enzyme inhibitors

The first enzyme to highlight in association with squaric acid inhibitors is histone deacetylase (HDAC) [112]. HDAC catalyses the deacetylation of the lysine residues, thereby affecting the chromatin remodelling process, and its inhibition has antiproliferative

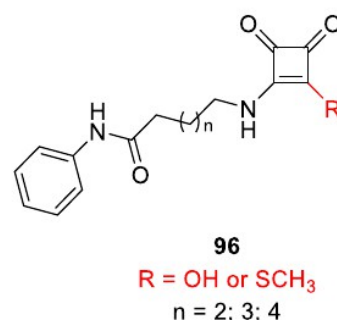


Fig. 32. Squaric acid derivatives as potential HDAC inhibitors [112].

effects. To prepare suberoylanilide hydroxamic acid (SAHA) analogues as HDAC inhibitors, Hannesian et al. replaced the Zn-binding group (ZBG) with squaric acid, N-hydroxyurea, and 4-hydroxymethyl oxazoline moieties (Fig. 32). Subsequently, they tested the inhibitory activity against HDAC. Unfortunately, no inhibitory activity against HDAC was observed at concentrations less than  $1.0 \mu\text{M}$ , and no cytotoxicity to tumour cell lines was observed below  $20 \mu\text{M}$  [112].

Another series of squaramide-based hydroxamic acids of general structure **97** were studied as novel class I and IIB HDAC inhibitors for the topical treatment of cutaneous t-cell lymphoma (CTCL) [113]. Fournier et al. targeted *mycosis fungoides*, an early form of CTCL, by a topical approach with HDAC inhibitors with an improved safety profile. As a result, a novel scaffold binding to class I, IIB, and IV HDACs include a hydroxamic acid as ZBG and a squaramide that pinches the Asp104 carboxylate. SAR studies revealed that a *para*-substituted phenyl improves potency and metabolic clearance, whereas a benzylic side chain decreases potency. Additionally, aliphatic branching with small substituents improves organic and aqueous solubility and further increases metabolic clearance. Docking studies also predicted that 5- or 6-carbon linkers would provide the best inhibitory activity. Lead compound **98** showed good potency with an  $\text{IC}_{50}$  of 7.3 nM in the Hut78 cell line, which was comparable to those of approved drugs (Fig. 33) [113].

The second potential target for tacrine-squaramide inhibitors is acetylcholinesterase (AChE) [114]. This serine protease catalyses the hydrolysis of the acetylcholine (ACh) neurotransmitter to produce choline and acetic acid, which are associated with cognitive impairment and dementia. Because tacrine is a central reversible AChE inhibitor marketed in 1993 for Alzheimer's disease treatment, a series of tacrine-squaramide homodimers was evaluated for their

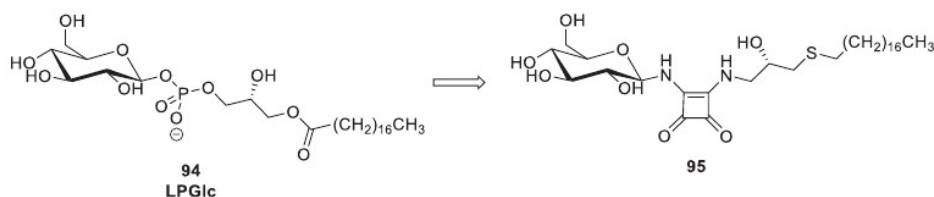


Fig. 31. Squaramide analogue of LPGlc as a GPR55 modulator [110].

$R^2/R^3$ : methyl substitution essential

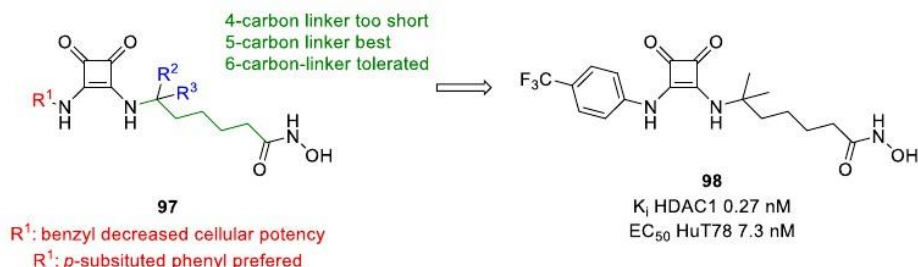


Fig. 33. Squaramide-type inhibitors of class I and IIB HDAC [113].

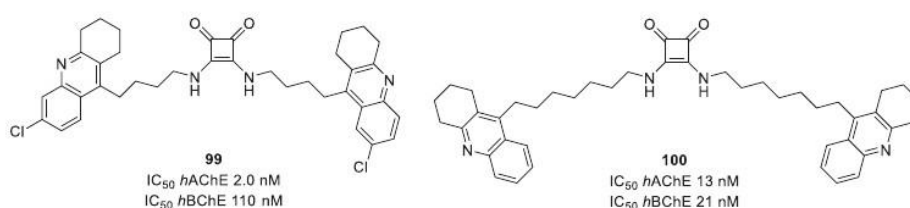


Fig. 34. Tacrine-squaramide cholinesterase inhibitors [114].

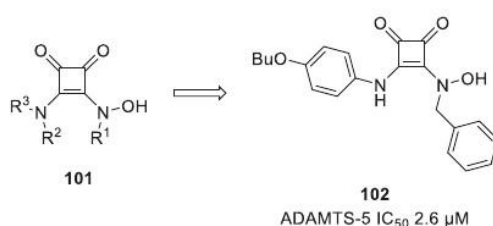


Fig. 35. Squaric acid *N*-hydroxylamide amides as ADAMTS-5 inhibitors [115].

anti-cholinesterase activity to find less toxic analogues. Compounds **99** and **100** exhibited the best inhibition of hAChE of 2.0 and 13 nM, respectively, and inhibition of hBChE of 110 and 21 nM,

respectively (Fig. 34). Moreover, both inhibitors possessed the lowest cytotoxicity to HepG2 cells [114].

In 2018, the parallel synthesis of 200 squaric acid *N*-hydroxylamide amides was performed by Charton et al. [115]. Subsequently, the library was screened against the zinc metalloenzyme ADAMTS-5, thus allowing the identification of the totally new micromolar inhibitor **102** with an IC<sub>50</sub> of 2.6 μM (Fig. 35) [115].

A series of squaric acid-peptide conjugates of general structures **103** was synthesized and studied as matrix metalloprotease-1 (MMP-1) inhibitors [116]. In general, MMPs are structurally related endopeptidases remodelling the extracellular matrix. Their over-expression is associated with a wide range of pathological conditions such as multiple sclerosis [117], rheumatoid arthritis [118], angiogenesis [119], and metastasis [120]. The squaric acid moiety of all the studied compounds was substituted in the 3-position with various zinc-binding functional groups, and the 4-position was modified with mono-peptides or dipeptides interacting with S1' and

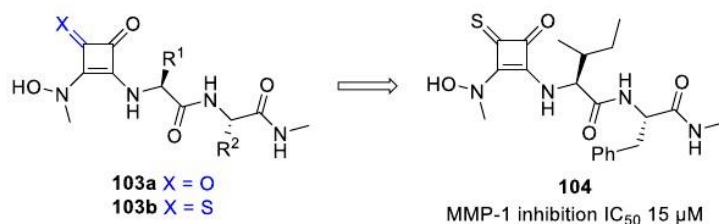


Fig. 36. Squaric acid-based peptidic inhibitors of MMP-1 [116].

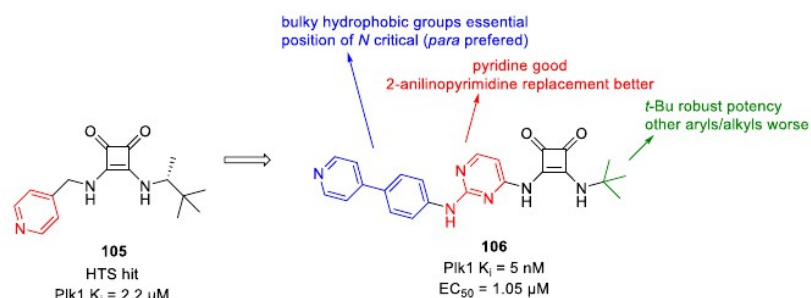


Fig. 37. Squarate-containing polo-like inhibitors [121].

**Table 1**  
The most potent squaric acid analogues with submicromolar biological activity.

Compound	Target(s)	$\text{IC}_{50}$ or $K_i$ value(s)
	<i>Mtb</i> ATP synthase (Myc_ATPS)	$\text{IC}_{50} = 30 \text{ nM}$
	<i>P. falciparum</i> (PW2)	$\text{IC}_{50} = 95 \text{ nM}$
	Human leukaemia cells (CEM)	$\text{IC}_{50} = 1.7$ or $1.4 \text{ nM}$
	HIV-1 protease	$K_i = 0.51 \text{ nM}$
	CXCR2	$\text{IC}_{50} = 8 \text{ nM}$
	Angiotensin II	$\text{IC}_{50} = 25 \text{ nM}$
	Human acetylcholinesterase (hAChE)	$\text{IC}_{50} = 2.0 \text{ nM}$



S2' enzymatic subsites. Positional scanning revealed that the combination of an -N (Me)OH chelating group and Leu-Tle-NHMe peptide was the best (Fig. 36). Moreover, the conversion of one carbonyl to thiocarbonyl resulted in an 18-fold increase in potency, providing compound **104** with an IC<sub>50</sub> of 15 μM (Fig. 36) [116].

The last enzyme group known to be influenced by squarate-containing inhibitors are polo-like kinases (Plks) [121]. Plks are serine/threonine kinases involved in the regulation of cell cycle via G2 and mitosis, thus controlling cell proliferation. Recently, ATP-competitive Plk1 inhibitors have inspired Zhang et al. to perform hit-to-lead optimization of an initial HTS hit **105** (Fig. 37). Molecular modelling revealed the importance of a hydrophobic aromatic amine side chain that enables H-binding. However, the incorporation of a 2-anilinepyrimidine moiety as a replacement for the 4-pyridyl significantly improved kinase affinity. Considering the substitution of the 2-aniline pyrimidine scaffold, hydrophobic aromatic cores interacting along the sidechain of Arg136 were beneficial. To attain acceptable pharmacokinetic properties, a simple *t*-butyl aliphatic right-hand side chain showed robust potency. Moreover, the position of the pyridine nitrogen was a critical parameter with the *para* position preferred. Finally, extensive SAR studies led to inhibitor **106** with Plk1 K<sub>i</sub> = 5 nM and ED<sub>50</sub> = 1.05 μM and moderate efficacy at 100 mpk in a MiaPaCa tumour model [121].

### 3. Conclusions and future perspectives

Squaric acid derivatives, squaramides, squaramines, and squarates are very simple, yet highly useful molecules. Despite these structures being discovered many decades ago by synthetic organic chemists, their use as potential therapeutics has only been explored quite recently. The main reason for this was their appearance; the structures include highly reactive functionalities that are usually associated with negative side-effects, such as toxicity, lack of selectivity, and promiscuity towards various molecular targets. Such compounds are generally not appreciated by pharmaceutical companies and regulatory organizations despite their superior pharmacological activity, because they often fail in late phases of drug development after large investments have been made and, in some of the worst cases, after they cause severe damage to the health of the first patients. However, such a strict selection of compounds entering the primary screening along with growing drug resistance emerging for the majority of infectious agents, cancers, etc. has resulted in a lack of effective drugs for some of the most prevalent illnesses. This environment has led to renewed attention to some of the previously overlooked compounds, including derivatives of squaric acid. These compounds have a variety of biological activities in low concentrations (often sub-micromolar), such as antiparasitic, antibacterial, cytotoxic, and antiviral activity, and some have known mechanisms of action (they inhibit certain receptors, enzymes, etc.), which makes them potentially useful in drug development. Ongoing research covering diverse fields of medicinal chemistry has revealed several small squaric acid analogues with significant biological activity; the most potent scaffolds from each group are summarized in Table 1.

Therefore, several compounds have passed clinical trials, and although none are on the market yet, it is very likely that this will change soon. Squaric acid analogues have been overlooked by medicinal chemists for some time but this has changed. In the future, all of the synthesized analogues of squaric acid should be tested for possible biological activities, and if they are selected for the development of a potential new drug, their toxicity should be carefully evaluated using *in vitro* experiments initially. Advanced *in vivo* toxicology experiments should follow as soon as possible to distinguish between compounds with selective activity to a drugable target and compounds with toxic side effects.

### Declaration of competing interest

The authors declare that they have no known competing financial interests or personal relationships that could have appeared to influence the work reported in this paper.

### Acknowledgement

This work was supported by grant no. JG\_2019\_002 and by an internal grant (IGA\_PřF\_2020\_012) from Palacký University in Olomouc, Czech Republic.

### References

- [1] X. Han, H. Zhou, C. Dong, Applications of chiral squaramides: from asymmetric organocatalysis to biologically active compounds, *Chem. Rec.* 16 (2016) 897–906.
- [2] R.I. Storer, C. Aciro, L.H. Jones, Squaramides: physical properties, synthesis and applications, *Chem. Soc. Rev.* 40 (2011) 2330–2346.
- [3] F.R. Wurm, H.-A. Klok, Be squared: expanding the horizon of squaric acid-mediated conjugations, *Chem. Soc. Rev.* 42 (2013) 8220–8236.
- [4] A. Mukkanti, M. Periasamy, Methods of synthesis of cyclobutenediones, *Arkivoc* 11 (2005) 48–77.
- [5] S. Sopena, E. Martín, E.C. Escudero-Adán, A.W. Kleij, Pushing the limits with squaramide-based organocatalysts in cyclic carbonate synthesis, *ACS Catal.* 7 (2017) 3532–3539.
- [6] D.E. Lynch, D.G. Hamilton, Microreview: pyrrol-3-yl squaramines (including indol-3-yl squaramines), *J. Heterocycl. Chem.* 55 (2018) 1249–1262.
- [7] J.P. Malerich, K. Hagihara, V.H. Rawal, Chiral squaramide derivatives are excellent hydrogen bond donor catalysts, *J. Am. Chem. Soc.* 130 (2008) 14416–14417.
- [8] A. Rouf, C. Tanyeli, Squaramide based organocatalysts in organic transformations, *Curr. Org. Chem.* 20 (2016) 2996–3013.
- [9] S. Karahan, C. Tanyeli, Squaramide catalyzed  $\alpha$ -chiral amine synthesis, *Tetrahedron Lett.* 59 (2018) 3725–3737.
- [10] P. Chen, G. Dong, Cyclobutenones and benzocyclobutenones: versatile synthons in organic synthesis, *Chemistry* 22 (2016) 18290.
- [11] T.S. Elliott, A. Slowey, Y. Ye, S.J. Conway, The use of phosphate bioisosteres in medicinal chemistry and chemical biology, *Med. Chem. Comm.* 3 (2012) 735–751.
- [12] P. Kováč, P. Xu, Controlled and highly efficient preparation of carbohydrate-based vaccines: squaric acid chemistry is the way to go, *Carbohydr. Chem.* 42 (2017) 83–115.
- [13] M.D. Laramie, A. Levitz, M. Henary, Cyanine and squaric acid metal sensors, *Sensor. Actuator. B Chem.* 243 (2017) 1191–1204.
- [14] C. Tong, T. Liu, V. Saez Talens, W.E.M. Noteborn, T.H. Sharp, M.M.R.M. Hendrix, I.K. Voets, C.L. Mummery, V.V. Orlova, R.E. Kieleyka, Squaramide-based supramolecular materials for three-dimensional cell culture of human induced pluripotent stem cells and their derivatives, *Biomacromolecules* 19 (2018) 1091–1099.
- [15] X. Qian, C. Jin, X. Zhang, Y. Jiang, C. Lin, L. Wang, Squaramide derivatives and their applications in ion recognition, *Prog. Chem.* 26 (2014) 1701.
- [16] I. Castro, M.L. Calatayud, J. Sletten, M. Julve, F. Lloret, Squarate and croconate in designing one- and two-dimensional oxamidato-bridged copper (II) complexes: synthesis, crystal structures and magnetic properties of [Cu<sub>2</sub>(apox)(C<sub>4</sub>O<sub>4</sub>)(H<sub>2</sub>O)<sub>2</sub>]<sub>n</sub> · nH<sub>2</sub>O and [Cu<sub>2</sub>(apox)<sub>2</sub>(C<sub>4</sub>O<sub>4</sub>)<sub>2</sub>] · 6H<sub>2</sub>O, *Comptes Rendus l'Académie Des Sci. IIC-Chimie* 4 (2001) 235–243.
- [17] W. Chequepán, J. Martínez-Olivares, A. Rodes, J.M. Orts, Squaric acid adsorption and oxidation at gold and platinum electrodes, *J. Electroanal. Chem.* 819 (2018) 178–186.
- [18] E.J. Smutny, J.D. Roberts, Phenylcyclobutadienoquinone, *J. Am. Chem. Soc.* 77 (1955) 3420.
- [19] M. Julia, A. Rouault, Synthesis of cyclobutanecarboxylic acids, *Bull. Soc. Chim. Fr.* (1959) 1833–1840.
- [20] S. Cohen, J.R. Lacher, J.D. Park, Diketocyclobutenediol, *J. Am. Chem. Soc.* 81 (1959) 3480.
- [21] S.L. Kitson, Squaryl molecular metaphors-application to rational drug design and imaging agents, *J. Diagnostic Imaging Ther* 4 (2017) 35–75.
- [22] L.M. Schwartz, L.O. Howard, Conductance study of squaric acid aqueous dissociation, *J. Phys. Chem.* 75 (1971) 1798–1803.
- [23] P. von R. Schleyer, C. Maerker, A. Dransfeld, H. Jiao, N.J.R. van Eikema Hommes, Nucleus-independent chemical shifts: a simple and efficient aromaticity probe, *J. Am. Chem. Soc.* 118 (1996) 6317–6318.
- [24] P. von R. Schleyer, K. Najafian, B. Kiran, H. Jiao, Are oxocarbon dianions aromatic? *J. Org. Chem.* 65 (2000) 426–431.
- [25] D. Quiñero, A. Frontera, P. Ballester, P.M. Deyà, A theoretical study of aromaticity in squaramide and oxocarbons, *Tetrahedron Lett.* 41 (2000) 2001–2005.
- [26] C. Garau, A. Frontera, P. Ballester, D. Quiñero, A. Costa, P.M. Deyà, A theoretical ab initio study of the capacity of several binding units for the



- molecular recognition of anions, *Eur. J. Org. Chem.* 2005 (2005) 179–183.
- [27] W.A. Kinney, M. Abou-Gharbia, D.T. Garrison, J. Schmid, D.M. Kowal, D.R. Bramlett, T.L. Miller, R.P. Tasse, M.M. Zaleska, J.A. Moyer, Design and synthesis of [2-(8,9-Dioxo-2,6-diazabicyclo[5.2.0]non-1(7)-en-2-yl)-ethyl] phosphonic acid (EAA-090), a potent *N*-Methyl-D-aspartate antagonist, via the use of 3-cyclobutene-1, 2-dione as an achiral  $\alpha$ -amino acid bioisostere, *J. Med. Chem.* 41 (1998) 236–246.
- [28] R.B. Baudy, J.A. Butera, M.A. Abou-Gharbia, H. Chen, B. Harrison, U. Jain, R. Magolda, J.Y. Sze, M.R. Brandt, T.A. Cummons, Prodrugs of perzinfotel with improved oral bioavailability, *J. Med. Chem.* 52 (2009) 771–778.
- [29] K. Jaeger, S. Bruenle, T. Weinert, W. Guba, J. Muehle, T. Miyazaki, M. Weber, A. Furrer, N. Haenggi, T. Tetaz, Structural basis for allosteric ligand recognition in the human CC chemokine receptor 7, *Cell* 178 (2019) 1222–1230.
- [30] S.I. Rennard, D.C. Dale, J.F. Donohue, F. Kanniss, H. Magnusson, E.R. Sutherland, H. Watz, S. Lu, P. Stryszak, E. Rosenberg, CXCR2 antagonist MK-7123. A phase 2 proof-of-concept trial for chronic obstructive pulmonary disease, *Am. J. Respir. Crit. Care Med.* 191 (2015) 1001–1011.
- [31] M.A. Palli, H. McTavish, A. Kimball, T.D. Horn, Immunotherapy of recurrent herpes labialis with squaric acid, *JAMA Dermatol.* 153 (2017) 828–829.
- [32] A.L.S. Chang, G. Honari, L. Guan, L. Zhao, M.A. Palli, T.D. Horn, A.Z. Dudek, H. McTavish, A phase 2, Multi-center, Placebo-controlled study of single dose squaric acid dibutyl ester (SADBE) to reduce frequency of outbreaks in subjects with recurrent herpes labialis, *J. Am. Acad. Dermatol.* (2020), <https://www.sciencedirect.com/science/article/abs/pii/S0190962220305612>.
- [33] S. Okabe, T. Nishida, H. Igata, K. Takagi, Effects of IT-066, a new histamine H<sub>2</sub>-receptor antagonist, on gastric acid secretion and experimental gastric ulcers in rats and dogs, *Nihon Yakurigaku Zasshi* 95 (1990) 247.
- [34] Y. Naito, T. Yoshikawa, K. Matsuyama, N. Yagi, M. Arai, Y. Nakamura, T. Kaneo, N. Yoshida, M. Kondo, Effect of a novel histamine H<sub>2</sub> receptor antagonist, IT-066, on acute gastric injury induced by ischemia-reperfusion in rats, and its antioxidative properties, *Eur. J. Pharmacol.* 294 (1995) 47–54.
- [35] K. Kato, S. Jingu, N. Ogawa, S. Higuchi, Development and validation of a liquid chromatographic–tandem mass spectrometric method for the determination of pibutidine in human urine, *J. Chromatogr. B Biomed. Sci. Appl.* 740 (2000) 187–193.
- [36] T. Oshima, Repeated dose toxicity study of 3-amino-4-[[[2]-4-[4-(piperidinomethyl)-2-pyridyl]oxy]-2-butenyl]amino]-3-cyclobutene-1, 2-dione monohydrochloride (Pibutidine hydrochloride) in rats (1): 13-week oral toxicity study with 4-week recovery test, *Jpn. Pharmacol. Ther.* 27 (1999) 331–345.
- [37] C.J. Gavey, J.T.L. Smith, C.U. Nwokolo, R.E. Pounder, The effect of SK&F 94482 (BMV-25368) on 24-hour intragastric acidity and plasma gastrin concentration in healthy subjects, *Aliment. Pharmacol. Ther.* 3 (1989) 557–564.
- [38] R.L. Cavanagh, J.P. Buyinski, Effect of BMV-25368, a potent and long-acting histamine H<sub>2</sub>-receptor antagonist, on gastric secretion and aspirin-induced gastric lesions in the dog, *Aliment. Pharmacol. Ther.* 3 (1989) 299–313.
- [39] S.J. Tantry, S.D. Markkar, V. Shinde, J. Bhat, G. Balakrishnan, A.K. Gupta, A. Ambady, A. Ratchurkar, C. Kedari, S. Sharma, N.V. Mudgal, A. Narayan, C.N. Naveen Kumar, R. Nanduri, S. Bharath, J. Reddy, V. Panduga, K.R. Prabhakar, K. Kandaswamy, R. Saralaya, P. Kaur, N. Dinesh, S. Gupta, K. Rich, D. Murray, H. Plant, M. Preston, H. Ashton, D. Plant, J. Walsh, P. Alcock, K. Naylor, M. Collier, J. Whiteaker, R.E. McLaughlin, M. Mallya, M. Panda, S. Rudrapatna, V. Ramachandran, R. Shandil, V.K. Sambandamurthy, K. Mdluli, C.B. Cooper, H. Rubin, T. Yano, P. Iyer, S. Narayanan, S. Kavanagh, K. Mukherjee, V. Balasubramanian, V.P. Hosagahara, S. Solapure, S. Ravishankar, S. Hameed, P. discovery of imidazo[1,2-*a*]pyridine ethers and squaramides as selective and potent inhibitors of mycobacterial adenosine triphosphate (ATP) synthesis, *J. Med. Chem.* 60 (2017) 1379–1399, <https://doi.org/10.1021/acs.jmedchem.6b01358>.
- [40] L.A. Marchetti, L.K. Kumawat, N. Mao, J.C. Stephens, R.B.P. Elmes, The versatility of squaramides: from supramolecular chemistry to chemical biology, *Chem.* 5 (2019) 1398–1485.
- [41] S. Nagy, P. Kisszekelyi, J. Kupai, Synthesis and application of thiosquaramides and their derivatives: a review, *period. Polytech. Chem. Eng.* 62 (2018) 467–475.
- [42] F. Olmo, C. Rotger, I. Ramirez-Macias, L. Martinez, C. Marin, L. Carreras, K. Urbanova, M. Vega, G. Chaves-Lemaun, A. Sampedro, Synthesis and biological evaluation of *N*, *N'*-squaramides with high *in vivo* efficacy and low toxicity: toward a low-cost drug against Chagas disease, *J. Med. Chem.* 57 (2014) 987–999.
- [43] D. Cui, D. Prashar, P. Sejwal, Y.-Y. Luk, Water-driven ligations using cyclic amino squarates: a class of useful SN1-like reactions, *Chem. Commun.* 47 (2011) 1348–1350.
- [44] P.C.M. Chan, R.J. Roon, J.F. Koerner, N.J. Taylor, J.F. Honek, A 3-Amino-4-hydroxy-3-cyclobutene-1, 2-dione-Containing glutamate analog exhibiting high affinity to excitatory amino acid receptors, *J. Med. Chem.* 38 (1995) 4433–4438.
- [45] F. Soukari, M.W. Nowicki, A. Bastide, T. Pöyry, C. Jones, K. Dudek, G. Patwardhan, F. Meulenet, N.J. Oldham, M.D. Walkinshaw, Design of nucleotide-mimetic and non-nucleotide inhibitors of the translation initiation factor eIF4E: synthesis, structural and functional characterisation, *Eur. J. Med. Chem.* 124 (2016) 200–217.
- [46] S. Niewiadomski, Z. Beebejaun, H. Denton, T.K. Smith, R.J. Morris, G.K. Wagner, Rationally designed squaryldiamides—a novel class of sugar-nucleotide mimics? *Org. Biomol. Chem.* 8 (2010) 3488–3499.
- [47] Y. Zhang, M. Jumppanen, M.M. Maksimainen, S. Auno, Z. Awol, L. Ghemtio, H. Venkannagari, L. Lehtio, J. Yli-Kauhaluoma, H. Xhaard, Adenosine analogs bearing phosphate isosteres as human MDO1 ligands, *Bioorg. Med. Chem.* 26 (2018) 1588–1597.
- [48] E. Dürr, W. Doherty, S.Y. Lee, A.H. El-Sagheer, A. Shivalingam, P.J. McHugh, T. Brown, J.F. McGouran, Squaramide-based 5'-phosphate replacements bind to the DNA repair exonuclease SNM1A, *ChemistrySelect* 3 (2018) 12824–12829.
- [49] K. Sato, K. Seo, M. Sekine, Squaryl group as a new mimic of phosphate group in modified oligodeoxynucleotides: synthesis and properties of new oligodeoxynucleotide analogues containing an internucleotide squaryldiamide linkage, *J. Am. Chem. Soc.* 124 (2002) 12715–12724.
- [50] M. Fonville, N. Sakkas, L. Iannazzo, C. Le Fournis, D. Mengin-Lecreux, A. El-Sagheer, E. Braud, S. Cardon, T. Brown, Electrophilic RNA for peptidyl-RNA synthesis and site-specific cross-linking with tRNA-binding enzymes, *Angew. Chemie* 128 (2016) 13751–13755.
- [51] M. Hocek, Synthesis of base-modified 2'-deoxyribonucleoside triphosphates and their use in enzymatic synthesis of modified DNA for applications in bioanalysis and chemical biology, *J. Org. Chem.* 79 (2014) 9914–9921.
- [52] M. Hocek, Enzymatic synthesis of base-functionalized nucleic acids for sensing, cross-linking, and modulation of protein–DNA binding and transcription, *Acc. Chem. Res.* 52 (2019) 1730–1737.
- [53] K.T. Andrews, G. Fisher, T.S. Skinner-Adams, Drug repurposing and human parasitic protozoan diseases, *Int. J. Parasitol. Drugs Drug Resist* 4 (2014) 95–111.
- [54] W.H. Organization, Chagas disease in Latin America: an epidemiological update based on 2010 estimates, *Wkly. Epidemiol. Rec. Rev. Epidemiologique Hebd* 90 (2015) 33–44.
- [55] C. Marin, M. Ximenis, I. Ramirez-Macias, C. Rotger, K. Urbanova, F. Olmo, R. Martín-Escolano, M.J. Rosales, R. Cañas, R. Gutierrez-Sánchez, Effective anti-leishmanial activity of minimalist squaramide-based compounds, *Exp. Parasitol.* 170 (2016) 36–49.
- [56] R. Martín-Escolano, C. Marin, M. Vega, Á. Martín-Montes, E. Medina-Carmona, C. López, C. Rotger, A. Costa, M. Sánchez-Moreno, Synthesis and biological evaluation of new long-chain squaramides as anti-chagas agents in the BALB/c mouse model, *Bioorg. Med. Chem.* 27 (2019) 865–879.
- [57] C.J.A. Ribeiro, S.P. Kumar, J. Gut, L.M. Gonçalves, P.J. Rosenthal, R. Moreira, M.M.M. Santos, Squaric acid/4-aminoquinoline conjugates: novel potent antiparasitic agents, *Eur. J. Med. Chem.* 69 (2013) 365–372.
- [58] C.J.A. Ribeiro, M. Espadinha, M. Machado, J. Gut, L.M. Gonçalves, P.J. Rosenthal, M. Prudêncio, R. Moreira, M.M.M. Santos, Novel squaramides with *in vitro* liver stage antiparasitic activity, *Bioorg. Med. Chem.* 24 (2016) 1786–1792.
- [59] S.P. Kumar, P.M.C. Clória, L.M. Gonçalves, J. Gut, P.J. Rosenthal, R. Moreira, M.M.M. Santos, Squaric acid: a valuable scaffold for developing antimalarials? *Med. Chem. Comm.* 3 (2012) 489–493.
- [60] P.M.C. Clória, J. Gut, L.M. Gonçalves, P.J. Rosenthal, R. Moreira, M.M.M. Santos, Aza vinyl sulfones: synthesis and evaluation as antiparasitic agents, *Bioorg. Med. Chem.* 19 (2011) 7635–7642.
- [61] A.S. Nagle, S. Khare, A.B. Kumar, F. Supek, A. Buchynskyy, C.J.N. Mathison, N.K. Chennamaneni, N. Pendem, F.S. Buckner, M.H. Gelb, Recent developments in drug discovery for leishmaniasis and human African trypanosomiasis, *Chem. Rev.* 114 (2014) 11305–11347.
- [62] W.H. Organization, Chagas disease-epidemiology, WHO, 2018, WHO. Available. <https://www.who.int/Chagas/Epidemiology/En/>. (Accessed 1 August 2019).
- [63] J.D. Maya, B.K. Cassels, P. Iturriga-Vásquez, J. Ferreira, M. Faúndez, N. Galanti, A. Ferreira, A. Morello, Mode of action of natural and synthetic drugs against *Trypanosoma cruzi* and their interaction with the mammalian host, *Comp. Biochem. Physiol. Part A Mol. Integr. Physiol.* 146 (2007) 601–620.
- [64] S.R. Wilkinson, C. Bot, J.M. Kelly, B.S. Hall, Trypanocidal activity of nitroaromatic prodrugs: current treatments and future perspectives, *Curr. Top. Med. Chem.* 11 (2011) 2072–2084.
- [65] K. Kojima, K. Nakajima, H. Kurata, K. Tabata, Y. Utsui, Synthesis of a piperidinomethylthiophene derivative as H<sub>2</sub>-antagonist with inhibitory activity against *Helicobacter pylori*, *Bioorg. Med. Chem. Lett* 6 (1996) 1795–1798.
- [66] H. Kijima, Y. Isobe, M. Muramatsu, S. Yokomori, M. Suzuki, S. Higuchi, Structure–activity characterization of an H<sub>2</sub>-receptor antagonist, 3-Amino-4-[4-[(1-piperidinomethyl)-2-pyridyloxy]-cis-2-butenylamino]-3-cyclobutene-1, 2-dione hydrochloride (IT-066), involved in the insurmountable Antagonism against histamine-induced P, *Biochem. Pharmacol.* 55 (1998) 151–157.
- [67] C. Grabosch, M. Hartmann, J. Schmidt-Lassen, T.K. Lindhorst, Squaric acid monoamide mannosides as ligands for the bacterial lectin FimH: covalent inhibition or not? *ChemBiochem* 12 (2011) 1066–1074.
- [68] T.K. Lindhorst, K. Bruegge, A. Fuchs, O. Sperling, A bivalent glycopeptide to target two putative carbohydrate binding sites on FimH, *Beilstein J. Org. Chem.* 6 (2010) 801–809.
- [69] K. Ohlsen, T.A. Oelschlaeger, J. Hacker, A.S. Khan, Carbohydrate receptors of bacterial adhesins: implications and reflections, in: *Glycosci. Microb. Adhes.*, Springer, 2008, pp. 17–65.
- [70] V. Molodtsov, P.R. Fleming, C.J. Eyermann, A.D. Ferguson, M.A. Foulk, D.C. McKinney, C.E. Masse, E.T. Buurman, K.S. Murakami, X-ray crystal



- structures of *Escherichia coli* RNA polymerase with switch region binding inhibitors enable rational design of squaramides with an improved fraction unbound to human plasma protein, *J. Med. Chem.* 58 (2015) 3156–3171.
- [71] E.T. Buurman, M.A. Foulk, N. Gao, V.A. Laganas, D.C. McKinney, D.T. Moustakas, J.A. Rose, A.B. Shapiro, P.R. Fleming, Novel rapidly diversifiable antimicrobial RNA polymerase switch region inhibitors with confirmed mode of action in *Haemophilus influenzae*, *J. Bacteriol.* 194 (2012) 5504–5512.
- [72] K. Andries, P. Verhasselt, J. Guillemont, H.W.H. Göhlmann, J.-M. Neefs, H. Winkler, J. Van Gestel, P. Timmerman, M. Zhu, E. Lee, A diarylquinoline drug active on the ATP synthase of *Mycobacterium tuberculosis*, *Science* (80- ) 307 (2005) 223–227.
- [73] C. Geadas, S.K. Stoszek, D. Sherman, B.B. Andrade, S. Srinivasan, C.D. Hamilton, J. Ellner, Advances in basic and translational tuberculosis research: proceedings of the first meeting of RePORT international, *Tuberculosis* 102 (2017) 55–67.
- [74] V. Fernández-Moreira, J.V. Alegre-Requena, R.P. Herrera, I. Marzo, M.C. Gimeno, Synthesis of luminescent squaramide monoesters: cytotoxicity and cell imaging studies in HeLa cells, *RSC Adv.* 6 (2016) 14171–14177.
- [75] Z. Liu, Y. Wang, Y. Han, L. Liu, J. Jin, H. Yi, Z. Li, J. Jiang, D.W. Boykin, Synthesis and antitumor activity of novel 3, 4-diaryl squaric acid analogs, *Eur. J. Med. Chem.* 65 (2013) 187–194.
- [76] K.A. López, M.N. Pina, R. Alemay, O. Vögler, F. Barcelo, J. Morey, Antifolate-modified iron oxide nanoparticles for targeted cancer therapy: inclusion vs. covalent union, *RSC Adv.* 4 (2014) 19196–19204.
- [77] M. Lu, Q.-B. Lu, J.F. Honek, Squarate-based carbocyclic nucleosides: syntheses, computational analyses and anticancer/antiviral evaluation, *Bioorg. Med. Chem. Lett.* 27 (2017) 282–287.
- [78] M. Quintana, J.V. Alegre-Requena, E. Marqués-López, R.P. Herrera, G. Triola, Squaramides with cytotoxic activity against human gastric carcinoma cells HGC-27: synthesis and mechanism of action, *Med. Chem. Comm.* 7 (2016) 550–561.
- [79] P. Villalonga, S.F. de Mattos, G. Ramis, A. Obrador-Hevia, A. Sampedro, C. Rotger, A. Costa, Cyclo-squaramides as kinase inhibitors with anticancer activity, *ChemMedChem* 7 (2012) 1472–1480.
- [80] S. Grabner, B. Modec, M. Cemažar, N. Bukovec, Crystal structures and cytotoxicity of isopropylamine Pt(II) complexes: a trinuclear squarato-bridged [Pt<sub>3</sub>(μ<sub>2</sub>-C4O4)3(μ<sub>2</sub>-NH<sub>2</sub>)<sub>2</sub>] 3H<sub>2</sub>O and a mononuclear cis-[Pt(II)(NO<sub>3</sub>)<sub>2</sub>(H<sub>2</sub>NPr)] 2], *J. Inorg. Biochem.* 99 (2005) 1465–1471.
- [81] W. Doherty, E.-M. Dürr, H.T. Baddock, S.Y. Lee, P.J. McHugh, T. Brown, M.D. Sengle, E.M. Scanlan, J.F. McGouran, A hydroxamic-acid-containing nucleoside inhibits DNA repair nuclease SNM1A, *Org. Biomol. Chem.* 17 (2019) 8094–8105.
- [82] W.H. Organization, *Hiv/Aids Key Facts, 2018, 2018. Available Online WHO, <https://www.who.int/news-room/fact-sheets/detail/hiv-aids>. (Accessed 5 August 2019).*
- [83] T. Ghilar, M. Fordyce, Current status and prospects of HIV treatment, *Curr. Opin. Virol.* 18 (2016) 50–56.
- [84] C.-W. Lee, H. Cao, K. Ichihama, T.M. Rana, Design and synthesis of a novel peptidomimetic inhibitor of HIV-1 Tat–TAR interactions: squaryldiamide as a new potential bioisostere of unsubstituted guanidine, *Bioorg. Med. Chem. Lett.* 15 (2005) 4243–4246.
- [85] A.K. Ghosh, J.N. Williams, S. Kovela, J. Takayama, H.M. Simpson, D.E. Walters, S. Hattori, M. Aoki, H. Mitsuya, Potent HIV-1 protease inhibitors incorporating squaramide-derived P2 ligands: design, synthesis, and biological evaluation, *Bioorg. Med. Chem. Lett.* 29 (2019) 2565–2570.
- [86] R. Fentger-Barish, I. Yron, T. Meshel, E. Matityahu, A. Ben-Baruch, IL-8-induced migratory responses through CXCR1 and CXCR2: association with phosphorylation and cellular redistribution of focal adhesion kinase, *Biochemistry* 42 (2003) 2874–2886.
- [87] R.W. Chapman, J.E. Phillips, R.W. Hipkin, A.K. Curran, D. Lundell, J.S. Fine, CXCR2 antagonists for the treatment of pulmonary disease, *Pharmacol. Ther.* 121 (2009) 55–68.
- [88] D.J. Nicholls, N.P. Tomkinson, K.E. Wiley, A. Brammall, L. Bowers, C. Grahames, A. Gaw, P. Meghani, P. Shelton, T.J. Wright, Identification of a putative intracellular allosteric antagonist binding-site in the CXCR2 chemokine receptors 1 and 2, *Mol. Pharmacol.* 74 (2008) 1193–1202.
- [89] K. Salchow, M.E. Bond, S.C. Evans, N.J. Press, S.J. Charlton, P.A. Hunt, M.E. Bradley, A common intracellular allosteric binding site for antagonists of the CXCR2 receptor, *Br. J. Pharmacol.* 159 (2010) 1429–1439.
- [90] L.E. Donnelly, P.J. Barnes, Chemokine receptors as therapeutic targets in chronic obstructive pulmonary disease, *Trends Pharmacol. Sci.* 27 (2006) 546–553.
- [91] W. Gonsiorek, X. Fan, D. Hesik, J. Fossetta, H. Qiu, J. Jakway, M. Billah, M. Dwyer, J. Chao, G. Deno, Pharmacological characterization of Sch527123, a potent allosteric CXCR1/CXCR2 antagonist, *J. Pharmacol. Exp. Therapeut.* 322 (2007) 477–485.
- [92] B.W. McClelland, R.S. Davis, M.R. Palovich, K.L. Widdowson, M.L. Werner, M. Burman, J.J. Foley, D.B. Schmidt, H.M. Sarau, M. Rogers, Comparison of N, N'-diarylsquaramides and N, N'-diarylureas as antagonists of the CXCR2 chemokine receptor, *Bioorg. Med. Chem. Lett.* 17 (2007) 1713–1717.
- [93] J. Busch-Petersen, Y. Wang, Phenol-containing antagonists of the CXCR2 receptor, *Expert Opin. Ther. Pat.* 18 (2008) 629–637.
- [94] M.P. Dwyer, P. Biju, Discovery of 3, 4-diaminocyclobut-3-ene-1, 2-dione-based CXCR2 receptor antagonists for the treatment of inflammatory disorders, *Curr. Top. Med. Chem.* 10 (2010) 1339–1350.
- [95] B. Martin, X. Lai, U. Baettig, E. Neumann, T. Kuhnle, D. Porter, R. Robinson, J. Hatto, A.-M. D'Souza, O. Steward, Early process development of a squaramide-based CXCR2 receptor antagonist, *Org. Process Res. Dev.* 19 (2015) 1038–1043.
- [96] N.A. Meanwell, Synopsis of some recent tactical application of bioisosteres in drug design, *J. Med. Chem.* 54 (2011) 2529–2591.
- [97] H.L. Friedman, Influence of isosteric replacements upon biological activity, *Nasrns* 206 (1951) 295–358.
- [98] L.M. Lima, E.J. Barreiro, Bioisosterism: a useful strategy for molecular modification and drug design, *Curr. Med. Chem.* 12 (2005) 23–49.
- [99] R.M. Soll, W.A. Kinney, J. Primeau, L. Garrick, R.J. McCaully, T. Colatsky, G. Oshiro, C.H. Park, D. Hartupey, V. White, 3-hydroxy-3-cyclobutene-1, 2-dione: application of novel carboxylic acid bioisostere to an in-vivo active non-tetrazole angiotensin-II antagonist, *Bioorg. Med. Chem. Lett.* 3 (1993) 757–760.
- [100] W.A. Kinney, N.E. Lee, D.T. Garrison, E.J. Podlesny Jr., J.T. Simmonds, D. Bramlett, R.R. Notvest, D.M. Kowal, R.P. Tasse, Bioisosteric replacement of the alpha-amino carboxylic acid functionality in 2-amino-5-phosphonopentanoic acid yields unique 3, 4-diamino-3-cyclobutene-1, 2-dione containing NMDA antagonists, *J. Med. Chem.* 35 (1992) 4720–4726.
- [101] J.A. Butera, M.M. Antane, S.A. Antane, T.M. Argentieri, C. Freedren, R.F. Graceffa, B.H. Hirth, D. Jenkins, J.R. Lennox, E. Matelan, Design and SAR of novel potassium channel openers targeted for urge urinary incontinence. 1. N-Cyanoguanidine bioisosteres possessing in vivo bladder selectivity, *J. Med. Chem.* 43 (2000) 1187–1202.
- [102] K. Seo, T. Miyashita, K. Sato, M. Sekine, Synthesis and properties of new nucleotide analogues possessing squaramide moieties as new phosphate isosters, *Eur. J. Org. Chem.* 2005 (2005) 5163–5170.
- [103] J. Xie, A.B. Comeau, C.T. Seto, Squaric acids: a new motif for designing inhibitors of protein tyrosine phosphatases, *Org. Lett.* 6 (2004) 83–86.
- [104] E. Von Behring, S. Kitasato, The mechanism of diphtheria immunity and tetanus immunity in animals, 1890, *Mol. Immunol.* 28 (1991) 1317–1319.
- [105] B. Palitzsch, N. Gaidzik, N. Stergiou, S. Stahn, S. Hartmann, B. Gerlitzki, N. Teusch, P. Flemming, E. Schmitt, H. Kunz, A synthetic glycopeptide vaccine for the induction of a monoclonal antibody that differentiates between normal and tumor mammary cells and enables the diagnosis of human pancreatic cancer, *Angew. Chemie Int. Ed.* 55 (2016) 2894–2898.
- [106] P. Xu, M. Kelly, W.F. Vann, F. Qadri, E.T. Ryan, P. Kováč, Conjugate vaccines from bacterial antigens by squaric acid chemistry: a closer look, *ChemBiochem* 18 (2017) 799–815.
- [107] B. Engelsen, Neurotransmitter glutamate: its clinical importance, *Acta Neurol. Scand.* 74 (1986) 337–355.
- [108] B. Planty, C. Pujol, M. Lamothe, C. Maraval, C. Horn, B. Le Grand, M. Perez, Exploration of a new series of PAR1 antagonists, *Bioorg. Med. Chem. Lett.* 20 (2010) 1735–1739.
- [109] K. Urbahns, M. Härter, M. Albers, D. Schmidt, B. Stelte-Ludwig, U. Brüggemeier, A. Vaupel, C. Gerdes, Biphenyls as potent vitronectin receptor antagonists, *Bioorg. Med. Chem. Lett.* 12 (2002) 205–208.
- [110] F. Ding, A.T. Guy, P. Greimel, Y. Hirabayashi, H. Kamiguchi, Y. Ito, Squaryl group modified phosphoglycolipid analogs as potential modulators of GPR55, *Chem. Commun.* 54 (2018) 8470–8473.
- [111] A.T. Guy, Y. Nagatsuka, N. Ooashi, M. Inoue, A. Nakata, P. Greimel, A. Inoue, T. Nabetani, A. Murayama, K. Ohta, Glycero-phospholipid regulation of modality-specific sensory axon guidance in the spinal cord, *Science* 349 (2015) 974–977.
- [112] S. Hanessian, V. Vincí, L. Auzzas, M. Marzi, G. Giannini, Exploring alternative Zn-binding groups in the design of HDAC inhibitors: squaric acid, N-hydroxyurea, and oxazoline analogues of SAHA, *Bioorg. Med. Chem. Lett.* 16 (2006) 4784–4787.
- [113] J.-F. Fournier, Y. Bhuruth-Alcor, B. Musicki, J. Aubert, M. Aurely, C. Bouix-Peter, K. Bouquet, L. Chantalat, M. Delorme, B. Drean, Squaramides as novel class I and II histone deacetylase inhibitors for topical treatment of cutaneous T-cell lymphoma, *Bioorg. Med. Chem. Lett.* 28 (2018) 2985–2992.
- [114] B. Svobodova, E. Mezeiova, V. Hepnarova, M. Hrabanova, L. Muckova, T. Kobrlova, D. Jun, O. Soukup, M.L. Jimeno, J. Marco-Contelles, Exploring structure-activity relationship in tacrine-squaramide derivatives as potent cholinesterase inhibitors, *Biomolecules* 9 (2019) 379.
- [115] J. Charton, B.P. Déprez, R.F. Déprez-Poulain, Synthesis of a 200-member library of squaric acid N-hydroxylamide amides, *Bioorg. Med. Chem. Lett.* 18 (2008) 4968–4971.
- [116] M.B. Onaran, A.B. Comeau, C.T. Seto, Squaric acid-based peptidic inhibitors of matrix metalloproteinase-1, *J. Org. Chem.* 70 (2005) 10792–10802.
- [117] W. Liedtke, B. Cannella, R.J. Mazzacaro, J.M. Clements, K.M. Miller, K.W. Wucherpfennig, A.J.H. Gearing, C.S. Raine, Effective treatment of models of multiple sclerosis by matrix metalloproteinase inhibitors, *Ann. Neurol. Off. J. Am. Neurol. Assoc. Child Neurol. Soc.* 44 (1998) 35–46.
- [118] C. Jackson, M. Nguyen, J. Arkell, P. Sambrook, Selective matrix metalloproteinase (MMP) inhibition in rheumatoid arthritis-targeting gelatinase A activation, *Inflamm. Res.* 50 (2001) 183–186.
- [119] C. Fisher, S. Gilbertson-Beadling, E.A. Powers, G. Petzold, R. Poorman, M.A. Mitchell, Interstitial collagenase is required for angiogenesis in vitro, *Dev. Biol.* 162 (1994) 499–510.
- [120] M. Whittaker, C.D. Floyd, P. Brown, A.J.H. Gearing, Design and therapeutic application of matrix metalloproteinase inhibitors, *Chem. Rev.* 99 (1999)

- 2735–2776.
- [121] Q. Zhang, Z. Xia, M.J. Mitten, L.M. Lasko, V. Klinghofer, J. Bouska, E.F. Johnson, T.D. Penning, Y. Luo, V.L. Giranda, Hit to Lead optimization of a novel class of squarate-containing polo-like kinases inhibitors, *Bioorg. Med. Chem. Lett* 22 (2012) 7615–7622.
- [123] Ivana Ivancová, et al., Squaramate-Modified Nucleotides and DNA for Specific Cross-Linking with Lysine-Containing Peptides and Proteins, *Angewandte Chemie* (2019), <https://doi.org/10.1002/anie.201906737>.



Contents lists available at ScienceDirect

European Journal of Medicinal Chemistry

journal homepage: <http://www.elsevier.com/locate/ejmech>

Review article

## Small organic molecules targeting the energy metabolism of *Mycobacterium tuberculosis*

Milan Urban<sup>a,1</sup>, Veronika Šlachťová<sup>b,1</sup>, Lucie Brulíková<sup>b,\*</sup><sup>a</sup> Institute of Molecular and Translational Medicine, Medicinal Chemistry, Faculty of Medicine and Dentistry, Palacky University in Olomouc, Hněvotínská 5, 779 00, Olomouc, Czech Republic<sup>b</sup> Department of Organic Chemistry, Faculty of Science, Palacky University Olomouc, 17. Listopadu 12, 771 46, Olomouc, Czech Republic

## ARTICLE INFO

## Article history:

Received 11 July 2020  
 Received in revised form  
 22 December 2020  
 Accepted 23 December 2020  
 Available online 29 December 2020

## Keywords:

*Mycobacterium tuberculosis*  
 Oxidative phosphorylation  
 ATP synthase  
 QcrB  
 Inhibitors

## ABSTRACT

Causing approximately 10 million incident cases and 1.3–1.5 million deaths every year, *Mycobacterium tuberculosis* remains a global health problem. The risk is further exacerbated with latent tuberculosis (TB) infection, the HIV pandemic, and increasing anti-TB drug resistance. Therefore, unexplored chemical scaffolds directed towards new molecular targets are increasingly desired. In this context, mycobacterial energy metabolism, particularly the oxidative phosphorylation (OP) pathway, is gaining importance. Mycobacteria possess primary dehydrogenases to fuel electron transport; *aa<sub>3</sub>*-type cytochrome *c* oxidase and *bd*-type menaquinol oxidase to generate a protonmotive force; and ATP synthase, which is essential for both growing mycobacteria as well as dormant mycobacteria because ATP is produced under both aerobic and hypoxic conditions. Small organic molecules targeting OP are active against latent TB as well as resistant TB strains. FDA approval of the ATP synthase inhibitor bedaquiline and the discovery of clinical candidate Q203, which both interfere with the cytochrome *bc<sub>1</sub>* complex, have already confirmed mycobacterial energy metabolism to be a valuable anti-TB drug target. This review highlights both preferable molecular targets within mycobacterial OP and promising small organic molecules targeting OP. Progressive research in the area of mycobacterial OP revealed several highly potent anti-TB compounds with nanomolar-range MICs as low as 0.004 μM against *Mtb* H37Rv. Therefore, we are convinced that targeting the OP pathway can combat resistant TB and latent TB, leading to more efficient anti-TB chemotherapy.

© 2020 Elsevier Masson SAS. All rights reserved.

## Contents

1. Introduction	2
2. Druggable molecular targets within the ETC in <i>Mtb</i>	2
2.1. Mycobacterial primary dehydrogenases	3
2.1.1. NADH dehydrogenases	3
2.1.2. Succinate dehydrogenase	3
2.1.3. Inhibitors of mycobacterial primary dehydrogenases	4
2.2. Mycobacterial cytochrome oxidases	5
2.2.1. The <i>aa<sub>3</sub></i> -type cytochrome <i>c</i> oxidase	5
2.2.2. Cytochrome <i>bd</i> -type oxidase	5
2.2.3. Inhibitors of mycobacterial cytochrome oxidases	5
2.3. Mycobacterial ATP synthase	8
2.3.1. Characterization and function of mycobacterial ATP synthase	8

\* Corresponding author.

E-mail address: [lucie.brulikova@upol.cz](mailto:lucie.brulikova@upol.cz) (L. Brulíková).<sup>1</sup> These authors contributed equally.<https://doi.org/10.1016/j.ejmech.2020.113139>

0223-5234/© 2020 Elsevier Masson SAS. All rights reserved.



2.3.2. Inhibitors of mycobacterial ATP synthase .....	9
2.3.3. Small molecules influencing ATP homeostasis .....	11
3. Author's insight on the topic .....	11
4. Conclusion .....	11
5. Future directions .....	13
Declaration of competing interest .....	14
Acknowledgements .....	14
Abbreviations .....	14
References .....	14

## 1. Introduction

Tuberculosis (TB) is a communicable disease associated with the bacillus *Mycobacterium tuberculosis* (*Mtb*), and it is the most common cause of death among patients with a single infectious agent [1]. Worldwide, there are approximately 1.3–1.5 million deaths associated with this disease every year, and it is estimated that approximately 10 million people fall ill with TB annually [1]. Moreover, an estimated 1.7 billion people have latent TB infection (LTBI), defined as the state of persistent immune response to stimulation by MT antigens without clinically manifested active TB disease. Considering the very large reactivation risk, LTBI-infected people represent a dangerous reservoir for new, active TB cases. In particular, patients coinfecting with HIV are at high risk for the development of active TB from its latent phase [2]. Targeted LTBI treatment is, therefore, a key part of the End TB Strategy. Despite rapid development in the pharmaceutical industry and health care systems in many countries during the past few decades, it seems that treatment options for TB have reached their limits for several reasons. First, at the end of the boom of new antibiotics, it seemed that the library of antibacterial drugs was highly diverse to treat almost all bacterial infections, including the complicated superinfections associated with attacks by multiple bacterial strains. At that time, there was no need for the development of new structures with alternative mechanisms of action, and the development of antibacterial drugs was significantly reduced. At the same time, antibiotics became a prevalent cure for most bacterial infections, and in many cases, these drugs were misused for the treatment of illnesses not associated with bacteria, including improvement in animal husbandry, etc. As a result, most of the antibiotics polluted the environment, influencing the naturally occurring bacteria. Some of the bacterial pathogens have evolved in environments loaded with antibiotics and become resistant. Other routes of resistance development occurred in patients treated by antibiotics who, for one reason or another, did not obey the prescription directions, interrupted treatment sooner than they were supposed to, or took subtherapeutic doses. In all cases, the bacteria encountered antibiotics in low enough concentrations for the development of drug resistance. On the molecular level, the main force driving drug resistance is the acquisition of mutations in genes coding the drug target or drug-activating enzymes. These mutations usually originate in the form of insertion, deletion or single-nucleotide polymorphism [3]. TB drug resistance appears *via* two main mechanisms. The first one is primary or transmitted drug resistance which forms when resistant strains are transmitted to a new host. On the contrary, secondary or acquired drug resistance is mediated by the acquisition of drug resistance mutations to one or more drugs [4–6]. Currently, these resistant bacterial strains represent a major health threat to the world's population, and among them, multidrug resistant (MDR) or extensively resistant (XDR) TB is probably the most serious problem. Their treatment requires the use of several drugs, many of which are toxic and have various side

effects. For example, aminoglycosides such as amikacin, kanamycin and streptomycin cause ototoxicity due to effects to the eighth cranial nerve [7]. Secondly, Capreomycin induces tubular neuropathy resulting in renal side effects and alkalosis [8]. Also, isoniazid-mediated hepatotoxicity *via* a choline deficiency is often observed [9]. Linezolid, as a reversible nonselective monoamine oxidase inhibitor, interacts with adrenergic and serotonergic agents increasing the risk of serotonin syndrome [10]. Finally, rifamycins induce CYP3A4 and thus interact with azole compounds leading to subtherapeutic serum concentrations while CYP2D6 isozyme is included in the metabolism of thioridazine resulting in elevated levels and enhanced cardiotoxicity when the compound is administered in combination with CYP2D6 inhibitors such as fluoxetine or propranolol [11,12]. All the side effects make the treatment expensive and, even worse, to take a long time and often fail. For the abovementioned reasons, research on new anti-tubercular agents has been resurrected, and its main area of focus is new compounds with a new mechanism of action that would allow for the treatment of resistant TB strains and the latent phase of the disease.

There are several mechanisms by which *Mycobacterium tuberculosis* acquires resistance. *Mtb* may develop a thick, waxy, hydrophobic cell envelope that is impenetrable to antibiotics, it may express enzymes that degrade the antibiotic or modify their molecular targets to reduce their affinity to the drug. Commonly, *Mtb* starts the expression of diverse multidrug transporters encoded by their DNA that transport various xenobiotics from the bacteria into their surroundings [13]. The effectiveness of multidrug resistance is often provided by the combination of several mechanisms, and the efflux systems probably serve as a stepping stone for the development of high-level multidrug resistance [13]. These transporters are predominantly dependent on proton motive force or ATP availability [14]. Small compounds that would interfere with the bacterial electron transport chain are therefore promising candidates for the treatment of MDR or XDR TB. Additionally, *Mtb* uses its electron transport chain (ETC) for energy production *via* oxidative phosphorylation during both replicating and latent (dormant) persistence [15–18]. As a result, small molecules inhibiting energy metabolism possess remarkable potential for LTBI, MDR TB, and XDR TB treatment. This review is focused on the description of new antitubercular drugs targeting bacterial energetics in these main areas: 1. NADH, 2. QcrB, and 3. ATP synthase and homeostasis.

## 2. Druggable molecular targets within the ETC in *Mtb*

In bacteria, the ETC is integrally involved in energy production *via* oxidative phosphorylation. During oxidative phosphorylation, various ETC protein complexes establish a transmembrane proton motive force (PMF). PMF energy is subsequently used for the ATP synthase-mediated production of ATP (Fig. 1) [19]. Energetic metabolism and the ETC in *Mtb* are rather complicated, having multiple side pathways and alternative mechanisms that have been

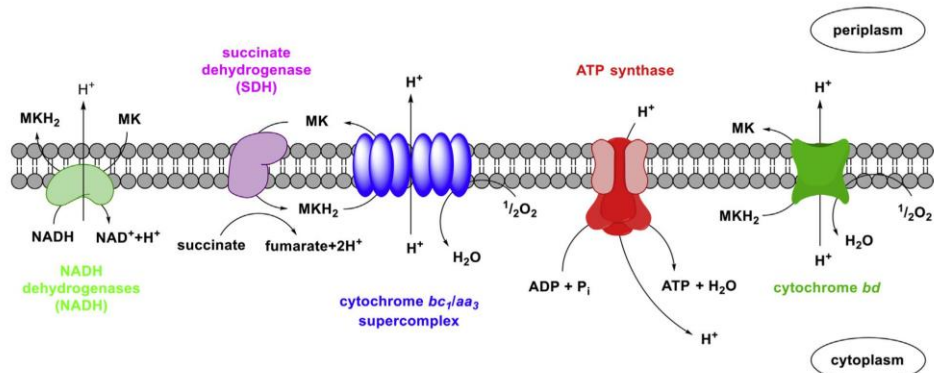


Fig. 1. Oxidative phosphorylation in *Mtb* (this figure was drawn according to Bald and Koul) [26].

reported multiple times [14,19,20]. To briefly summarize all mycobacterial ETCs, *Mtb* harbors multiple primary dehydrogenases to transport electrons to the lipophilic redox carrier menaquinone. Alternatively, *Mtb* possesses several reducing equivalents (e.g., nitrate reductase and fumarate reductase) to facilitate turnover under anaerobic conditions [21,22]. Depending on oxygen availability, electrons are then passed to terminal oxidases, an *aa*<sub>3</sub>-type cytochrome *c* oxidase and cytochrome *bd*-type menaquinol reductase, for dioxygen reduction [23]. Such a process is coupled to the generation of a PMF, thus powering ATP synthase to synthesize ATP [14,24]. Individual roles of the main components of the ETC are detailed below.

Recently, a very informative review article was published summarizing the proteins and members of the ETC that may serve as potential targets for drug development [25]. The review mostly focuses on the biological aspects of the proteins and includes a table with the eight most promising small molecules targeting these proteins. These derivatives are all at advanced stages of drug development towards resistant *Mtb* [25]. Additionally, there were two more reviews published earlier as a summary of clinical candidates and approved drugs targeting mycobacterial metabolism [14,26]. However, there are no more recent and comprehensive overviews of early-stage research and development of small molecules interacting with mycobacterial energetics published. Therefore, the main scientific contribution and novelty of our review consist of the focus on basic research in medicinal chemistry and early-stage development of small molecules targeting the ETC. Furthermore, the review contains not only the most promising lead compounds but summarizes all of the research.

## 2.1. Mycobacterial primary dehydrogenases

Mycobacteria harbor multiple primary dehydrogenases to fuel the electron transport chain. The NADH dehydrogenase complex (complex I) accepts electrons from NADH and passes them to the electron carrier menaquinone [27]. NADH I dehydrogenase is preferred under aerobic conditions, while NADH II predominates in an anaerobic environment with menaquinone connecting electron-donating and electron-accepting reactions [28]. Succinate dehydrogenase forms complex II of the respiratory chain and couples oxidative phosphorylation to central carbon metabolism via the tricarboxylic acid cycle (TCA). Mycobacterial type-II NADH dehydrogenase (NDH-2) as a promising target for the treatment of

tuberculosis was reviewed in 2017 [29]. The review mostly focused on the biological properties of the enzyme and the methods of its evaluation as a reasonable target. Therefore, in our review, we will be more oriented towards small molecules as inhibitors and on the newest articles on this topic.

### 2.1.1. NADH dehydrogenases

In prokaryotes, NADH is produced in the cytosol by glycolytic enzymes (glyceraldehyde, 3-phosphate dehydrogenase, pyruvate dehydrogenase) and enzymes in the tricarboxylic acid cycle (isocitrate,  $\alpha$ -ketoglutarate, malate dehydrogenases) [30]. X-ray structural determination of the bacterial NADH dehydrogenase complex revealed that it is L-shaped and composed of a hydrophobic membrane arm and a hydrophilic matrix arm (Fig. 1) [27]. Mycobacteria were identified to contain two types of respiratory NADH dehydrogenases. First, proton-pumping NADH I dehydrogenase transfers electrons to menaquinone [31]. Coupled with the downhill electron transfer, there is uphill proton or sodium translocation across the membranes with concomitant generation of a membrane potential enabling ATP synthesis [32]. Electron transfer occurs in the matrix arm via iron-sulfur clusters, while transmembrane  $\alpha$ -helices form proton pumping modules in the membrane arm. Every two-electron menaquinone reduction causes four protons to be pumped into the crista space, generating approximately half of the total proton motive force in mitochondria [27]. On the other hand, nonproton pumping NADH II dehydrogenase does not conserve energy, and its specific role is still unclear. Since NADH II inhibitors are bactericidal towards nonreplicating *M. tuberculosis*, they are probably essential for the recycling of NADH under hypoxic conditions [33]. A more detailed description of *Mtb* NADH dehydrogenases, their properties, their role in virulence, and their possible use as therapeutic targets may be found in Ref. [34].

### 2.1.2. Succinate dehydrogenase

Although embedded in the crista membrane, succinate dehydrogenase does not contribute to proton motive force by pumping protons. Therefore, it is not considered an integral part of the respiratory chain. Succinate dehydrogenase transfers two electrons directly to menaquinone, bypassing NADH dehydrogenase [27]. Most mycobacteria possess two succinate dehydrogenases, SDH1 and SDH2 [35]. Observations have indicated that SDH1 could be dedicated to succinate dehydrogenase and that SDH2 catalyzes



fumarate reductase activity, which is important for survival under hypoxia [36]. SDH1 is a key regulator of oxidative phosphorylation, catalyzing the oxidation of succinate to fumarate with a simultaneous interchange of menaquinone to menaquinol, while fumarate reductase catalyzes the reverse reaction vital for proton motive force maintenance [37,38]. However, the structure of both of these mycobacterial enzymes remains experimentally unresolved [25]. Remodeling of the TCA confirmed that the activity of SDH is essential for mycobacterial persistence and therefore represents a potential novel drug target [14].

### 2.1.3. Inhibitors of mycobacterial primary dehydrogenases

Phenothiazine derivatives (Fig. 2) have been used as therapeutics for a long time. Among them, thioridazine **1**, chlorpromazine **2**, and trifluoperazine **3** are commonly used antipsychotic agents. Promethazine **4**, on the other hand, is used to treat various symptoms of allergies. The possibility of the use of these compounds in antitubercular treatment was reviewed by Singh and coworkers [39]. In addition to their primary use, the compounds were investigated because of their significant anti-TB activity *in vitro*. The review article summarizes all of the results from the antitubercular research of phenothiazine derivatives and concludes that their main target is *Mtb* type II NADH dehydrogenase, a key component of the *Mtb* respiratory chain that helps the bacterium survive under stress conditions [39,40]. Importantly, this protein is not a part of the mammalian genome; therefore, it is a promising target for selective inhibition. Therefore, targeting this component of the ETC seems to be a promising strategy against latent *Mtb*. Thioridazine **1** was one of the most promising derivatives for potential antitubercular drug development, even showing effectiveness against phagocytosed *Mtb*. Compound **1** is not a single target inhibitor since it also inhibits bacterial efflux pumps, thereby helping to increase the efficacy of other drugs [39]. In addition, the fact that all of these compounds are currently used as drugs would simplify their

development into commercial drugs and reduce research costs during the late stages of clinical trials.

In 2012, a primary article was published on quinolinyl pyridines with the general formula **5** along with their significant anti-TB activity [41]. Their activity was associated with the inhibition of NADH II. A small SAR study showed that compound **6** had an MIC = 1.91  $\mu$ M, while the IC<sub>50</sub> against NADH II = 43 nM.

Additionally, advanced *in silico* experiments were performed [42]. Tethering fragment-based drug discovery revealed disulfide **7** as the most potent NADH II inhibitor. Its aromatic ring was predicted to bind within a hydrophobic clamp formed by GLN317 and ILE379 deep in the quinone binding pocket. Moreover, there are three predicted hydrogen bonds, between the carbonyl oxygen of compound **7** and THR349 as well as between the backbone carbonyl of ILE379 to the nitrogen in the fragment tail responsible for the high binding affinity [42].

Wang and coauthors identified two types (**8** and **9**) of selective NADH II inhibitors using multicomponent high-throughput screening [43]. Altogether, they investigated 800 000 compounds, obtained 7000 primary hits, and after multiple advanced screenings (e.g., removing cytotoxic compounds), they ended up with structures **8** and **9**. These compounds showed the highest potency against both *Msmeg* and *Mtb* NADH II (IC<sub>50</sub> 10.7 nM and 64.7 nM, respectively). Their activity against *Mtb* NADH A was similarly potent [43].

A series of 2-mercaptoquinoxalines was prepared by Boshoff et al. [44]. Whole-cell SARs for this series of identified compounds with the general formula **10** were the most active. The authors screened for pharmacological parameters, toxicity, and other properties of the compounds related to drug development, and compounds **10a** – **10c** were identified as the most potent. They exhibit MIC values = 0.3–0.8  $\mu$ M against *Mtb*, while microsomal clearance was reasonable in the range of 1.4–4.7 mL/min/g and the kinetic solubility was high enough (83–250  $\mu$ M). Additionally, **10a**

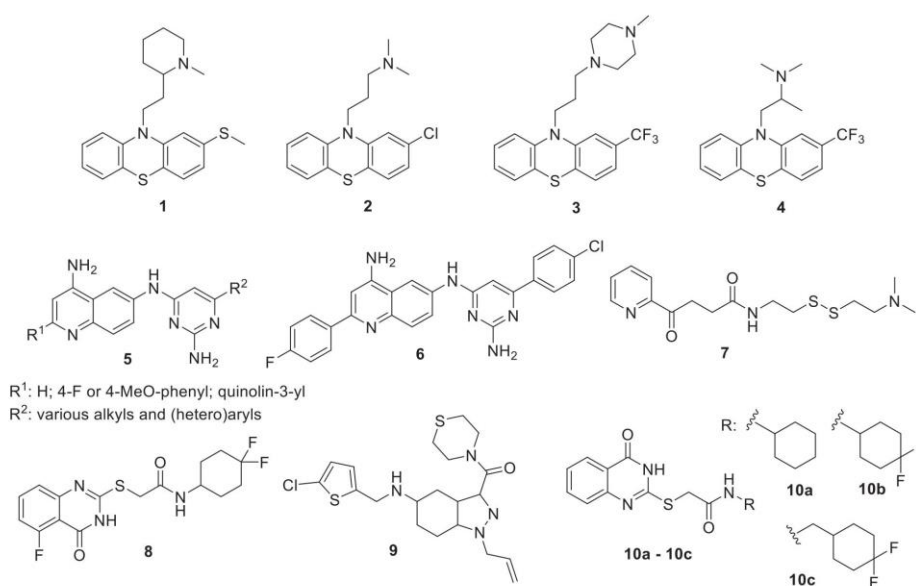


Fig. 2. Structures of antitubercular agents that inhibit NADH reductases.

– **10c** were indicated to inhibit NADH II noncompetitively in an enzyme kinetic study [44].

A series of 7-phenyl benzoxaborole derivatives was prepared and found to be active against *Mtb* with  $IC_{50}$  values as low as 5.1  $\mu$ M by Sacchetti and coworkers [45]. Resistant mutants towards the most active 7-phenyl benzoxaborole were isolated and characterized, and mutations were found in the genes for NADH dehydrogenase (NADH) or the regulatory protein Mce3R, which suggests that Ndh may be the target of this series of compounds [45].

Other molecules that are known to inhibit the growth of *Mtb* are quinoline quinones [46]. Therefore, Cook and coauthors focused on the elucidation of the mechanism of action and found that quinoline quinones target *Mtb* NADH II, which activates NADH oxidation and generates a bactericidal level of ROS in a similar but more efficient manner compared to the anti-*Mtb* drug clofazimine [47]. The most recent work on quinoline quinones was published by Timmer et al. in which a large series of compounds were prepared and evaluated; however, the best derivative, 7-chloro-6-propargylamino-quinoline-5,8-dione, had only a moderate MIC = 8  $\mu$ M [48].

## 2.2. Mycobacterial cytochrome oxidases

Mycobacteria display a branched respiratory chain with two terminal oxidases,  $aa_3$ -type Cu-heme cytochrome *c* oxidase encoded by *ctaB*, *ctaC*, *ctaD* and *ctaF* genes and cytochrome *bd* menaquinol oxidase, which are both present for dioxygen reduction coupled to proton motive force generation (Fig. 3). The cross-membrane potential provides energy for various cellular components, such as ATP synthase. The  $aa_3$ -type cytochrome *c* oxidase, which forms a supercomplex with cytochrome *bc\_1* reductase, is the major respiratory route under aerobic conditions [49,50]. On the other hand, the bioenergetically less efficient cytochrome *bd* branch is synthesized at low oxygen concentrations. Their expression is regulated according to an oxygen supply, but the molecular mechanisms remain unknown [24,51].

### 2.2.1. The $aa_3$ -type cytochrome *c* oxidase

The cytochrome *c* route consists of menaquinol-cytochrome *c* oxidoreductase termed the  $bc_1$  complex and an  $aa_3$ -type cytochrome *c* oxidase [20]. This pathway represents the main mycobacterial respiratory route under standard aerobic conditions. The  $bc_1$  complex is composed of redox groups, including a 2Fe/2S center located on a Rieske protein (QcrA), a single polypeptide bearing low and high potential *b*-type hemes (QcrB) and cytochrome *c*<sub>1</sub> heme (QcrC). Cytochrome oxidase *c* functions as a proton pump [52].

**2.2.1.1. Structural organization of the  $bc_1$  complex.** The overall structure of the  $bc_1$  complex can be divided into three regions: the membrane-spanning, the intermembrane space, and the matrix regions (Fig. 3). The subunit composition of  $bc_1$  complexes varies significantly from 13 transmembrane helices in human mitochondria to 10 or 11 helices in bacteria [53]. Despite such structural diversity, all  $bc_1$  complexes have three redox subunits in common: a cytochrome *b* protein containing two *b*-type hemes with high ( $b_h$ ) and low ( $b_l$ ) potential, a *c*-type heme and an iron-sulfur protein (ISP) with a high-potential 2Fe–2S iron-sulfur cluster. Furthermore, the purified  $bc_1$  complex contains ubiquinone and phospholipids. All additional (supernumerary) subunits do not have a well-established cellular function, and they are believed to contribute to the enhanced overall stability [54,55].

**2.2.1.2. Functions of the  $bc_1$  complex.** The cytochrome  $bc_1$  complex is essential in the respiratory chain for electron transport across the membrane from menaquinol to cytochrome *c* [56,57]. The cytochrome *b* protein forms the hydrophobic core, enabling further interactions within the complex [58]. There are two identical *b*-type hemes,  $b_h$  and  $b_l$ , located on the cytoplasmatic and exterior faces of the membrane, respectively [53]. Subunit  $b_h$  contributes to menaquinone reduction ( $Q_N$ ), whereas  $b_l$  engages in menaquinol oxidation ( $Q_p$ ). The  $bc_1$  complex transfers  $H^+$  to the coupled  $aa_3$  cytochrome *c* oxidase that carries out oxygen reduction [59].

### 2.2.2. Cytochrome *bd*-type oxidase

Cytochrome *bd* oxidase has been investigated to a lesser extent, and its function may be complex. Although not required for aerobic growth, cytochrome *bd* plays an important role in the response to antibacterial stress and adaptation to a reduced oxygen environment [60]. The cytochrome *bd* complex generates charge separation via electron transport instead of translocating  $H^+$  [61,62]. The mycobacterial cytochrome  $bc_1$  complex has already been validated as a promising drug target. It displays two substrate (quinone/quinol) binding sites that may be able to accommodate a variety of small-molecule inhibitors. Moreover, targeting cytochrome *bd* appears highly efficient, but further structural and functional analysis is needed to explore this enzyme [26].

### 2.2.3. Inhibitors of mycobacterial cytochrome oxidases

Imidazo[1,2- $\alpha$ ]pyridines were synthesized as potent lead anti-TB molecules from a high-throughput screen [63]. The most promising compounds, **14** and **15**, had notable antitubercular potency in various *Mtb* strains with MICs = 0.03  $\mu$ M–5  $\mu$ M and acceptable pharmacokinetic profiles. Furthermore, a dose-response

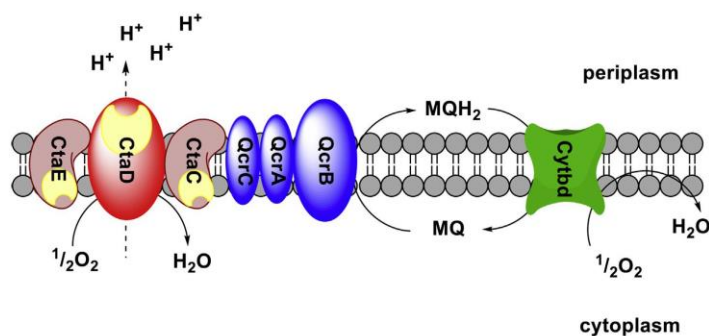


Fig. 3. Mycobacterial cytochrome oxidases.



efficacy study in an acute murine model revealed bacteriostatic behavior *in vivo*, demonstrating a 2 log CFU reduction with respect to nontreated controls. Resistant mutants were generated to find the molecular target of the best derivative (**14**), which was identified as QcrB by genome sequencing [63]. Additional proof of this target was given when the MIC of compound **14** increased significantly (from 0.5  $\mu\text{M}$  to 8  $\mu\text{M}$ ) in bacteria with significantly over-expressed QcrB. This is one of the earliest studies showing QcrB as a promising anti-TB target.

A set of five chemically diverse heterocyclic compounds was investigated [64]. Among them, compounds **16–18** were the most interesting, with imidazo[1,2-*a*]pyridine **16** being the most active against *M. tuberculosis* H37Rv, inhibiting its visible growth with MIC >50  $\mu\text{M}$  and more than 90% resazurin reduction under MABA conditions of 0.15  $\mu\text{M}$ . Imidazo[1,2-*a*]pyridine **16** exhibited an inability to inhibit *Mtb* H37Rv while inhibiting the transfer of electrons followed by resazurin reduction as well as the final ATP production with kinetics similar to BDQ. Such an inability was probably caused by the upregulation of cytochrome *bd* oxidase as an alternative respiratory complex. Indeed, the cytochrome *bd* oxidase mutant (cydKO) was found to be highly susceptible to imidazo[1,2-*a*]pyridines with a MIC of less than 0.024  $\mu\text{M}$  and MABA less than 0.024  $\mu\text{M}$  [64].

Surprisingly, another imidazopyridine, zolpidem (**19**, used for the treatment of insomnia), was found to have anti-TB activity (*M. tuberculosis* H37Rv, MIC 10–50  $\mu\text{M}$ ) [61]. A rationally designed set of zolpidem analogs was subsequently synthesized, and their antitubercular potency was evaluated. Among them, compound **20** had an MIC = 0.004  $\mu\text{M}$ . Since the target was of great interest, screening against a panel of *qcrB*-resistant mutants revealed that all the tested imidazopyridines were *bc<sub>1</sub>* complex inhibitors, as demonstrated by their loss of potency [61]. Another zolpidem analog was studied in Ref. [65]. The authors rationally designed a large library of the analogs and anagrams with the main scaffold imidazopyridine and tested them against *Mtb*. The most potent derivatives had MICs as low as 0.004  $\mu\text{M}$  and reasonable selectivity, which made them potential therapeutics.

Other imidazo[1,2-*a*]pyridines were subjected to target elucidation. Compounds **21a–21c** showed the best potency against intracellular *Mtb* and were therefore chosen for the next experiments. They exhibited significant inhibition of *M. tuberculosis* R37Rv with an  $\text{IC}_{50}$  of 0.15–0.39  $\mu\text{M}$ . As the *Mtb* QcrBT<sub>3131</sub> mutant strain showed resistance to the tested compounds with at least 8-fold shifts in MICs (MIC<sub>90</sub> 6.5–>20  $\mu\text{M}$ ), QcrB was proposed to be their molecular target. Disrupted pH homeostasis and depleted ATP levels provided further evidence of an effect on the electron transport chain. Protein Rv1339, a member of the  $\beta$ -lactamase superfamily, was established as the secondary target. This protein could affect cell wall structure, thereby impacting compound permeation. Finally, none of the tested compounds was cytotoxic against THP1 cells, making them potential drug candidates [66].

A set of more than fifty pyrrolo[3,4-*c*]pyridine-1,3(2*H*)-diones was prepared by Westhuyzen et al. [67], and their HTS identified hit pyrrolopyridine **22** that was active against *Mtb* (*M. tuberculosis* H37RvMa, MIC<sub>90</sub> 0.132  $\mu\text{M}$ ). Unfortunately, pharmacological parameter tests showed that its ester moiety undergoes microsomal hydrolysis (only 35% of **22** remained in solution after 40 min of incubation). Subsequently, bioisosteric replacements of the labile ester were investigated. The 1,2,4-oxadiazole moiety was identified as biologically active and metabolically stable. *In vivo* pharmacokinetic studies of **23** in mice indicated high clearance and low plasma exposure ( $C_{\text{max}}$  = 0.033  $\mu\text{M}$ ), but the metabolic stability was highly improved (97% of **23** remained in solution after 40 min of exposure to microsomes). Codosing **23** with aminobenzotriazole (ABT) improved the unfavorable parameters. To determine the

mechanism of action, target identification studies were performed. Hypersensitivity of the cydKO deletion mutant and the cross-resistance of the cydKO/QcrBA317T mutant strongly indicated that these compounds target the QcrB subunit of the *bc<sub>1</sub>* complex [67].

Novel phenoxyalkylbenzimidazoles were prepared to expand the SAR studies. Observed key determinants for antimycobacterial activity were methyl groups at both the C-6 of the benzimidazole and the C-4 of the terminal phenyl, a three-carbon atom linker, and a nitrogen heteroatom on the alkyl chain. One of the most potent compounds against *Mtb* H37Rv, **24**, had MIC = 0.47  $\mu\text{M}$ , improved derivative **25** had an MIC = 0.061–0.070  $\mu\text{M}$ . First, QcrB targeting was confirmed by testing the MIC. All tested compounds showed a 5-fold lower MIC against the resistant mutant QcrB<sub>M342T</sub> compared to the parental strain. The benzene ring may be responsible for QcrB targeting since the QcrB<sub>M342T</sub> mutant was not resistant to the imidazole analogs. Second, ATP depletion together with decreased intracellular pH provided further evidence for QcrB as a target [68].

A phenotypic screen by GSK identified 2-(quinoline-4-yl)oxy acetamides as potent *Mtb* growth inhibitors. A preliminary SAR investigation of the antitubercular activity identified five analogs, **26a–26b** and **27a–27b** (Fig. 4; MIC<sub>90</sub> *Mtb* H37Rv, 0.3–3.3  $\mu\text{M}$ ). Based on the SAR, another set of compounds was prepared with the best compounds, **27c–27e**, showing activity of 0.62–0.45  $\mu\text{M}$  against *M. tuberculosis* H37Rv determined by MABA and thus showing improved potency compared with the original hits, with an activity of 1.11  $\mu\text{M}$  under the same conditions. In general, bulky, lipophilic substituents at R improved the potency, while a methoxy at C-6 was critical for activity. In addition, the tested compounds exhibited enhanced MICs of 0.12–<0.063  $\mu\text{M}$  towards the *Mtb* cydKO strain. Based upon the magnitude of MIC enhancement, these compounds were established as cytochrome *bc<sub>1</sub>* oxidase inhibitors [69].

The next promising antitubercular agents are imidazo[2,1-*b*]thiazole-5-carboxamides, which are endowed with nanomolar potency (*Mtb* H37Rv MIC < 0.05  $\mu\text{M}$ ). Moreover, compounds **28a–28c** were exceptionally potent against mono-drug resistant strains (MIC<sub>RMP</sub> less than 0.04–0.201  $\mu\text{M}$ , MIC<sub>INH</sub> less than 0.04–0.506  $\mu\text{M}$ ). Antituberculosis assays revealed two unsuitable modifications, namely, a trifluoromethyl group in the ortho position and a biaryl ether aniline compared to the biaryl ether benzylamine. To suggest the molecular target, compounds **28a–28c** were screened against six QcrB mutants. As a result, their QcrB selectivity was confirmed [70,71].

The synergistic effects between phenoxyalkylbenzimidazoles (PABs, e.g., **29**) and other compounds targeting the bacterial respiratory chain, such as clofazimine and bedaquiline, were investigated [72]. It was found that the combination of PABs with clofazimine led to strong synergistic killing of both replicating and nonreplicating *Mtb*. On the other hand, the combination of PABs with bedaquiline showed antagonism, which disappeared within three weeks, and as a result, the PAB-bedaquiline combination became strongly bactericidal.

A new series of antimycobacterial 4-amino-thieno[2,3-*d*]pyrimidines targeting cytochrome *bc<sub>1</sub>* oxidoreductase was discovered. From 78 screened small molecule nucleotide mimetics, **30** exhibited the highest growth inhibition with an  $\text{IC}_{50}$  of  $2.7 \pm 0.84$   $\mu\text{M}$ . Finally, enhanced activity against *qcrB* mutants and depletion of ATP levels confirmed cytochrome *bc<sub>1</sub>* as a target [73].

Four derivatives, **31–34** (Fig. 5), within a larger 2-ethylthio-4-methylaminoquinazoline chemical library showed good activity ranging from 0.02 to 0.09  $\mu\text{g/mL}$  against *Mtb* H37Rv and HepG2 cells, respectively, and low toxicity ( $\text{TD}_{50}$  > 5  $\mu\text{g/mL}$ ) *in vitro*. Quinazoline **32** was the most selective from this series. Considering the SAR, fluorine atoms at positions 6 and 8 and ethyl thioalkyl chains

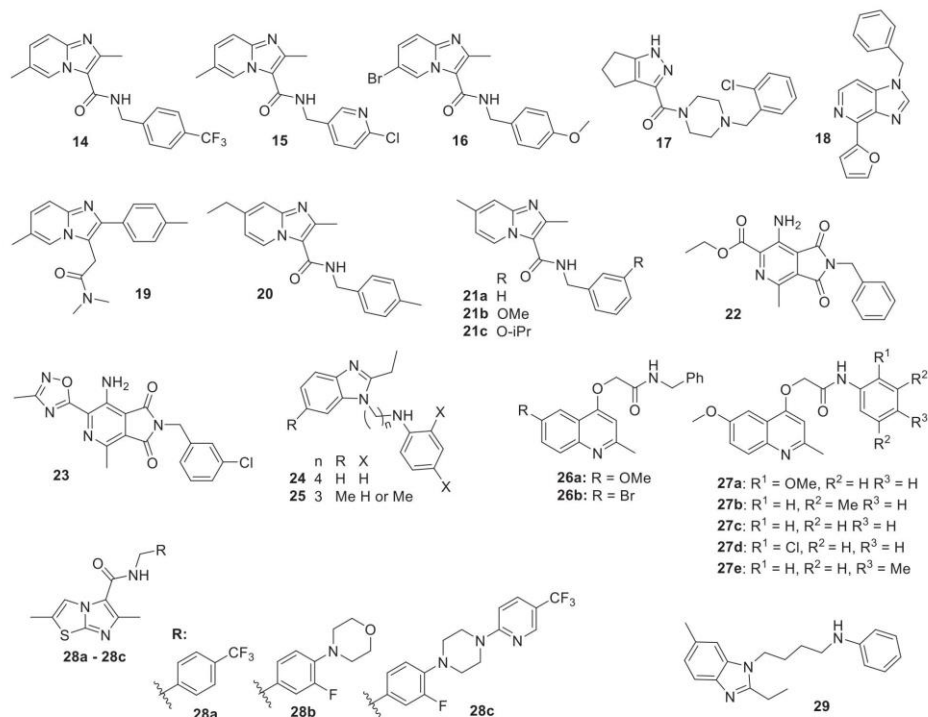


Fig. 4. Inhibitors of mycobacterial cytochrome oxidases.

were found to be preferable. Moreover, the smallest substitution in position 4 was observed to enhance the antitubercular activity. Quinazolines were revealed to target cytochrome *bc<sub>1</sub>* by whole-genome sequencing [74].

The 2-(quinoline-4-yloxy)acetamides (QOAs) of general formula 35 (Fig. 5) were reported to be promising antitubercular agents. These molecules have intracellular activity similar to INH and RMP (MIC = 0.01–0.08 µg/mL) and great efficacy against resistant *M. tuberculosis* isolates (MIC = 0.01–0.08 µg/mL). Target identification based on genome sequencing and MIC indicated two targets: DNA gyrase and the cytochrome *bc<sub>1</sub>* complex. Docking experiments revealed that the *b*-subunit of the cytochrome, namely, protein residues THR313, MET342 and LEU167, are responsible for the main interactions. Firstly, the hydroxyl group of the THR313 mediates polar interaction essential to inhibitor stabilization in the protein active site. Secondly, MET342 and LEU167 are involved in hydrophobic interactions with the Q<sub>b</sub> quinol oxidation site, which is vital for cell survival [75].

Whole-cell screening identified morpholinothiophene analogs as potential antitubercular scaffolds. Initial hit 36 (Fig. 5) showed good antitubercular activity against *Mtb* H37Rv (MIC = 0.72 µM). Moreover, compound 36 showed acceptable physicochemical and pharmacokinetic properties. Therefore, many more morpholinothiophenes with the general formula 37 (Fig. 5) were synthesized for the SAR study. Since the SAR suggested that the phenethyl linker and the amide carbonyl were critical aspects of the pharmacophore,

it appeared that the whole series shared a similar pharmacophore to scaffolds that target QcrB. To confirm the molecular target, ATP and growth were monitored in the same experiment. As a result, ATP depletion occurred in a dose-dependent manner, similar to Q203 (a known QcrB inhibitor) [76].

As potent antitubercular agents *in vitro*, arylvinylpiperazine amides were studied intensively. The investigated arylvinylpiperazine amides demonstrated potent antitubercular activity against *Mtb* H37Rv *in vitro* (MIC 0.05–0.1 µM), and the IC<sub>50</sub> for *Mtb*-infected TFP-1 macrophages ranging from 0.1 to 0.3 µg/mL reflects the potent *ex vivo* activity of these molecules. In addition, all compounds had low cytotoxicity. Compounds 38a and 38c (Fig. 5) proved the *in vivo* activity determined in a mouse model of acute TB. Both compounds significantly reduced the bacterial loads in mouse lungs by 0.4 and 0.6 log<sub>10</sub>, respectively, compared to the vehicle control. A cross-resistance study revealed different interactions with the quinol binding pocket of the cytochrome *bc<sub>1</sub>*-aa3 oxidase QcrB subunit compared to Q203. Additionally, transcriptomic and bioenergetic flux studies confirmed QcrB as the primary target [77].

Various commercial chemical libraries were screened by Cechetto and coworkers to find diverse anti-tubercular compounds [78]. As a result, imidazopyridine amide derivative 39a was identified as the best inhibitor. Compound 39a was synthesized and fully screened *in vitro* to find that its activity against MDR and XDR *Mtb* is in the nanomolar range, and subsequent experiments found



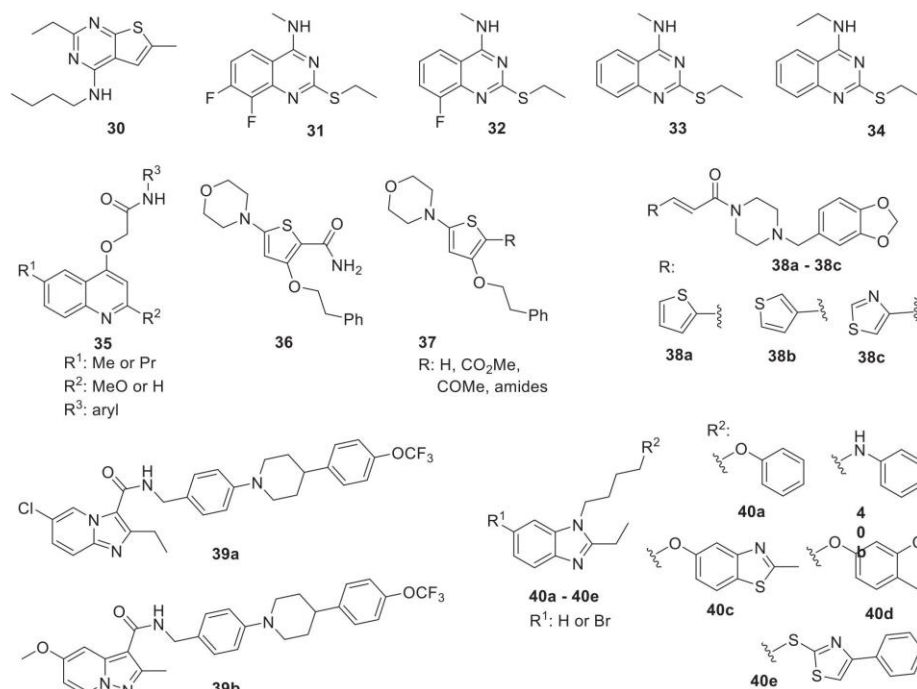


Fig. 5. Inhibitors of mycobacterial cytochrome oxidases.

it to have *in vivo* activity at doses lower than 1 mg per 1 kg body weight. The mechanism of action was elucidated and it was shown that nanomolar concentrations significantly lower the levels of ATP, which led to the suggestion that the compound inhibits cytochrome *bc1* activity [78]. Based on the structure of **39a**, bioisosteric pyrazolo[1,5-*a*]pyridine-3-carboxamide analogs were prepared and identified as potential new antitubercular agents with high activity against *Mtb* H37Rv (MIC<sub>90</sub> = 0.125 µg/mL) [79]. More importantly, lead compound **39b** (Fig. 5) had remarkable activity against 56 *Mtb* isolates, including 37 MDR and 2 XDR strains. Moreover, a lack of toxicity combined with high oral bioavailability was reported. Docking studies of **39b** in the Q<sub>p</sub> binding site revealed  $\pi$ - $\pi$  interactions with the aromatic side chains of TYR321 and PHE156, similar to the interactions observed with Q203. Surprisingly, **39b** exhibited a strong synergy with subtherapeutic concentrations of PZA and RMP, causing a 4- and 5-fold reduction in lung CFU [79].

High-throughput screening identified phenoxallybenzimidazoles as very adaptable scaffolds with nanomolar MICs (MIC<sub>50</sub> = 0.34–5.3 µM) against *Mtb*. They inhibit *Mtb* growth inside macrophages with insignificant cytotoxicity. These compounds likely target QcrB, a component of the cytochrome *bc1* complex. However, *Mtb* is able to reroute its ETC to provide resistance to therapy. Considering these factors, combinations of ETC-targeting compounds with synergistic activity are needed. Such synergistic killing was achieved with compounds **40a-40e** (Fig. 5) in combination with CFZ under both replicating and nonreplicating conditions [72].

### 2.3. Mycobacterial ATP synthase

#### 2.3.1. Characterization and function of mycobacterial ATP synthase

ATP synthase is a ubiquitous enzyme present in mitochondria, chloroplasts, or plasmatic membranes. Resembling a turbine, the structure of ATP synthase consists of two components: a rotor (F<sub>0</sub>) and a stator (F<sub>1</sub>) connected through a central stalk, reversibly coupling proton flow to either ATP synthesis or hydrolysis [27,80]. Oxidative phosphorylation is the source of energy that drives ATP synthase to convert the electrochemical potential energy into chemical energy in the form of ATP by the reaction of ADP with inorganic phosphate (P<sub>i</sub>) [14,81].

Considering the mycobacterial ATP synthase (Fig. 6A), three  $\alpha$  and three  $\beta$  subunits alternate to form the hydrophilic stator (F<sub>1</sub>), which extends into the cytoplasm. The membrane-embedded rotor (F<sub>0</sub>) includes one *a*, two *b*, and a ring of more than ten *c* subunits. Rotor and stator connection via the central stalk containing  $\gamma$ ,  $\delta$  and *e* subunits has specific fusion between one *b* and one  $\delta$  subunit [82]. The resulting *b*/ $\delta$  fusion protein improves the bonding interaction between ATP precursors and the  $\alpha_3\beta_3$  hexamer, while the free *b* subunit increases power transmission within the ATP synthase complex. As a result, the presence of two different *b* subunits probably enhances their overall mutual interaction [83].

Compared to mycobacterial ATP synthase, bacterial ATP synthase (Fig. 6B) shows structural differences, such as relaxed junctions between the *b* and  $\delta$  subunits. Moreover, bacterial ATP synthase usually contains exactly ten *c* subunits with proton-binding sites. A lower number of monomers per subunit of the *c*

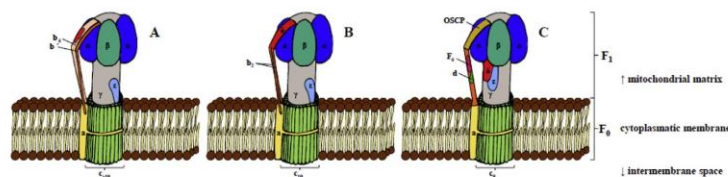


Fig. 6. Mycobacterial (A), bacterial (B), and human (C) ATP synthases (this figure was drawn according to Lu and Bald) [80].

oligomer may decrease the  $H^+$ /ATP ratio and thus complicate ATP synthesis under low proton motive force conditions [84]. On the other hand, eukaryotic ATP synthase (Fig. 6C) contains homologous oligomycin sensitivity-conferring protein (OSCP) instead of the  $\delta$  subunit, with only one  $b$  subunit accompanied by minor  $d$  and  $F_6$  subunits and eight monomers in the  $c$  ring [85,86]. Finally, in ATP synthase in chloroplasts, the  $b$  homodimer is replaced by two homologous  $b$  and  $b'$  subunits [87].

ATP synthase is strongly evolutionarily conserved among prokaryotes and eukaryotes. *M. tuberculosis*, an obligate aerobic bacterium, is dependent on oxidative phosphorylation to produce ATP for growth and survival. Apart from replicating mycobacteria, ATP synthase is also essential in the dormant state, carrying specific features facilitating survival under nonreplicating conditions, including oxygen insufficiency, nutrient limitation, and acidic pH [88].

As such, mycobacterial ATP synthase features several functional adaptations. First, mycobacterial ATP synthase lacks the ATP hydrolysis function to prevent ATP from being wasted. Suppression of the hydrolytic activity may be caused by inhibitory binding of Mg-ADP, subunit  $\epsilon$  dysregulation, or by the inhibitory protein subunit  $\zeta$  [89]. The second specific feature to mention is the ability to synthesize ATP under low proton motive force ( $-110$  mV), which is closely linked to the structure of subunit  $c$ . A large  $c$  oligomer causes increased  $H^+$ /ATP turnover, resulting in promoted ATP formation. Even an unusual stiffness of the stator stalk or highly lipophilic cytoplasmic membrane may speed up ATP synthesis [35,90].

All of the aforementioned differences compared to human ATP synthase may be crucial to understand the design and development of selective ATP synthase inhibitors.

### 2.3.2. Inhibitors of mycobacterial ATP synthase

One of the first compounds found to target *Mtb* ATP synthase, especially its subunit  $c$ , was bedaquiline **41** (Fig. 7) [91–95]. The compound was efficient even against MDR *Mtb* and developed by Jansen Pharmaceuticals [96]. Despite its high potency, compound **41** has several drawbacks, such as a long half-life, high lipophilicity, and low solubility; therefore, several research groups have focused on analogs with better pharmacological profiles. Palmer and co-authors synthesized 26 analogs with the naphthalene unit replaced with pyridines were to reduce the lipophilicity and half-life [96]. Compounds **42** and **43** (Fig. 7) significantly inhibited bacterial growth of *Mtb* H37Rv under both replicating (MABA) and non-replicating (LORA) conditions. Specifically, derivative **42** had an  $MIC_{90}$  of 0.01  $\mu\text{g/mL}$  under MABA conditions and 0.06  $\mu\text{g/mL}$  under LORA conditions, and derivative **43** had an  $MIC_{90}$  of 0.02  $\mu\text{g/mL}$  under MABA conditions and 0.02  $\mu\text{g/mL}$  under LORA conditions. Both compounds were also effective *in vivo* (CFU reduction) and noncytotoxic ( $IC_{50}$  values  $> 10$   $\mu\text{g/mL}$  in the Vero assay). Both compounds have notably lower hERG potencies than bedaquiline, resulting in reduced cardiovascular toxicity [96].

A luciferin-based ATP assay selected thiazolidinone derivative **44** for further studies. Compound **44** showed excellent anti-TB

activity (*Mtb* H37Rv,  $MIC_{90} = 0.5$   $\mu\text{g/mL}$ , and intracellular  $MIC_{90}$  in macrophages = 4.0  $\mu\text{g/mL}$ ) and low cytotoxicity (therapeutic window 80). Additionally, **44** exhibited a 2–8-fold higher MIC in RMP<sup>R</sup> and MDR isolates of *Mtb*. Considering the molecular target, screening against *M. smegmatis* ATP synthase on an inverted membrane was performed ( $IC_{50}$  0.312  $\mu\text{M}$ ). Docking analysis showed that residue LEU59 of *Mtb* ATP synthase was involved in H-bond interactions with the phenyl ring of **44**. Finally,  $\pi$ - $\pi$  interactions between TYR64 and the abovementioned phenyl ring were detected [97].

*In silico* methods such as homology modeling and virtual screening can find various molecules that effectively inhibit *Mtb*  $F_1F_0$  ATPase. In this quest, four virtual hits, **45–48**, were obtained and showed better binding affinity compared to bedaquiline **41**. Molecular docking revealed key interactions with GLU61 and ARG186 [98].

Simplification to the structure of bedaquiline used a fragment-based approach and resulted in 4 series of 3-(4-(*N,N*-dimethylaminomethyl)phenyl)quinolines. Among these compounds, **49** and **50** were found to be the most potent candidates against *Mtb* H37Rv with  $MICs = 0.43$  and 0.44  $\mu\text{g/mL}$  and against DR isolates ( $MIC$  0.48–0.94  $\mu\text{g/mL}$ ). Therefore, **49** and **50** were assayed for their capacity to inhibit *Mtb* ATP synthase, showing a direct impact with  $IC_{50}$  values of 20.3  $\pm$  1.0 and 38.8  $\pm$  1.0  $\mu\text{M}$ , respectively. Compound **49** was the best candidate with an improved  $\log P$  of 5.55, which is beneficial for pharmacokinetic properties [99].

A very large SAR study of squaramides resulted in compounds with nanomolar potencies in an ATP synthase inhibition assay [100]. The most active was derivative **51**. Complete stasis after two weeks of treatment with a 200 mg/kg dose established the *in vivo* efficacy of **51** in a mouse model of acute TB, and the activity against *Mtb* H37Rv showed an  $MIC = 0.43$   $\mu\text{M}$ . SAR exploration revealed that 2-pyridylmethyl substitution is critical for achieving good potency. On the left-hand side of the molecule, a morpholinophenyl moiety was found to be the best. ATP synthase was suggested as a molecular target based on a membrane-based biochemical assay (Myc-ATPS  $IC_{50}$  0.03  $\mu\text{M}$ ) measuring ATP synthesis through oxidative phosphorylation. This result was confirmed by spontaneous resistant mutant characterization. To understand the binding mode, **51** was docked into *Mtb* ATP synthase. The pyridine nitrogen of **51** forms  $\pi$ - $\pi$  interactions and H-bonds with ARG186 of subunit  $\alpha$ . Furthermore, the morpholine oxygen interacts with PHE69 of subunit  $c$  through H-bonding [100].

The novel scaffold 6,7-dihydropyrazolo[1,5-a]pyrazin-4-one was identified by screening using *M. smegmatis* ATP synthase. A scaffold hopping approach revealed compounds **52** with improved activity against *Mtb* H37Rv with  $MIC$  2–4  $\mu\text{M}$ . They do not inhibit any of the CYP450 enzymes and could be a starting point for anti-TB drug discovery [101].

Novel *Mtb* ATP synthase inhibitors derived from neuroleptic phenothiazines were synthesized. Compounds **53a** and **53b** with the strongest *Mtb* H37Rv growth inhibition ( $MIC = 6.25$   $\mu\text{g/mL}$ ) were screened for ATP synthase inhibition using inverted



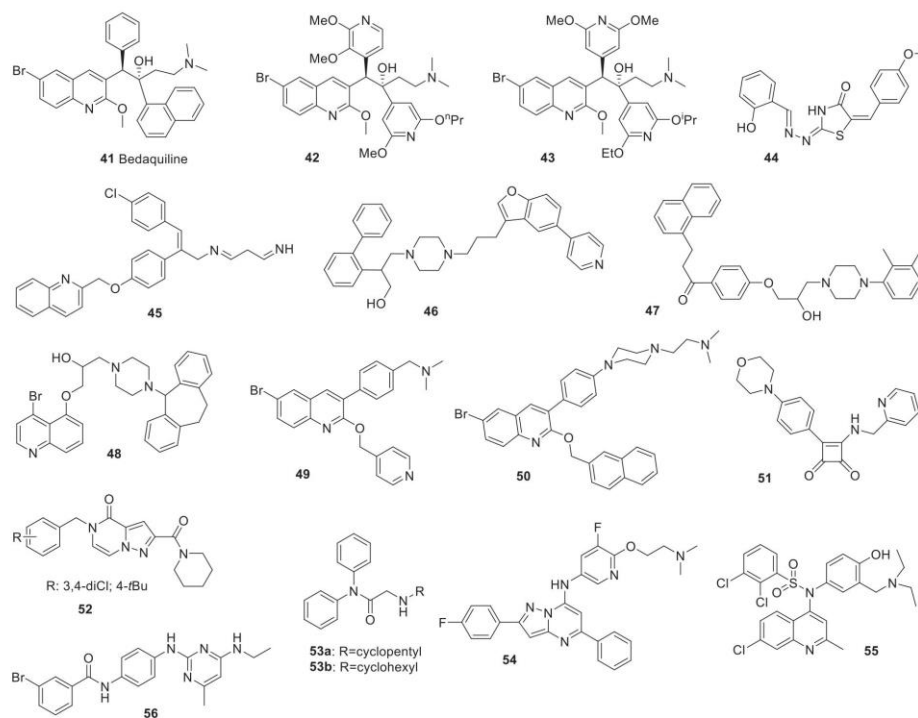


Fig. 7. Inhibitors of mycobacterial ATP synthase.

membrane *M. smegmatis* vesicles ( $IC_{50}$  values of 14 and 10.4  $\mu\text{M}$ , respectively). The blood-brain barrier crossing ability ( $Pe$   $2.7 \times 10^{-6}$  and  $3.0 \times 10^{-6}$  cm/s) was reduced compared to chlorpromazine, indicating diminished CNS side effects. Docking studies showed  $\pi$ - $\pi$  interactions between the phenyl rings of 53 and PHE69. Since PHE69 is absent in human enzymes, compounds 53 tended to be safe and efficacious [102].

First, HTS resulted in the identification of 2,4-diaminoquinazolines as ATP synthase inhibitors. Second, scaffold hopping led to pyrazolopyrimidines with over 100-fold improved selectivity for *Mtb* ATP synthase ( $Myc\_ATPS$   $IC_{50} = 0.5 \mu\text{M}$ ;  $SI = 20$ ). Compound 54 docked into the bedaquiline binding site showed a 4-fluorophenyl group responsible for the blocking capacity between the Atp-a and Atp-c subunits. However, the absence of cross-resistance against bedaquiline-resistant strains suggested that pyrazolopyrimidines interact with ATP synthase differently than bedaquiline despite binding at the same site [103]. Compound 54 had antitubercular activity against *Mtb* H37Rv with an  $MIC = 6.2 \mu\text{M}$ .

A large study of potential antitubercular compounds was performed [104]. First, a large virtual library of compounds was screened *in silico*, and then a set of compounds was prepared from the most promising hit. Among them, chloroquinolines of general formula 55 with cytotoxicity above the detection limit ( $CC_{50} \geq 300 \mu\text{g/mL}$ ) and excellent ATPase inhibitory activity and selectivity ( $IC_{50}$   $0.51 \pm 0.030 \mu\text{M}$ ;  $SI \geq 200$ ) were identified as lead compounds. Compound 55a was the best compound and exhibited bactericidal

effects in the hypoxic *Mtb* culture (more than 2.3  $\log_{10}$  reductions in CFU). In a murine model of chronic TB, compound 55a showed 2.12  $\log_{10}$  reductions in CFU in both the lung and spleen at a dose of 173  $\mu\text{mol/kg}$ . Pharmacokinetic studies on 55a indicated quick absorption, high distribution volume ( $V_{ss}$  0.41 L/kg), moderate clearance (0.06 L/h/kg), and a long half-life (4.2 h). These results suggest that 55a is a promising drug candidate (activity against *Mtb* H37Rv,  $MIC$  3.12  $\mu\text{g/mL}$ ) [104]. Another study on six new chloroquinoline derivatives containing the same scaffold 55 was published in Ref. [105], the activity against *Mtb* was  $MIC_{50} = 3.12$ – $6.25 \mu\text{g/mL}$ , and the  $IC_{50}$  against ATP synthase was 0.36– $1.83 \mu\text{M}$ . Compound 55b was selected as the best compound with an  $MIC_{50}$  of 3.12  $\mu\text{g/mL}$  against *Mtb* and an  $IC_{50}$  against ATP synthase of 0.39  $\mu\text{M}$ .

To overcome the clinical resistance and long terminal half-life of BDQ, a new generation of 3,5-dialkoxypyridine analogs is currently under investigation. Among them, compound 56 had remarkable properties and activity against *Mtb* H37Rv with a  $MIC_{50} = 33 \mu\text{M}$ . An inverted membrane vesicle (IMV) assay was used to confirm mycobacterial ATP synthase inhibition ( $IC_{50}$  of  $0.5 \pm 0.1 \mu\text{M}$  against *M. smegmatis* and  $5.2 \pm 1.1 \mu\text{M}$  against *M. bovis* BCG). Biochemical and NMR studies showed that 56 inhibits ATP synthase by binding to the  $\gamma$  subunit loop. Preliminary *in vitro* ADME profiling revealed that 56, with a  $clogP$  of 4.37, is less lipophilic than BDQ and metabolically stable in mouse liver microsomes. Finally, *in vitro* ATP synthesis experiments indicated a synergistic effect with BDQ [106].

### 2.3.3. Small molecules influencing ATP homeostasis

Small molecules interfering with energy metabolism may not be restricted just to ATP synthase inhibitors, but they may influence ATP homeostasis by the activation of latent ATP hydrolytic activity or by rerouting electron flow to reactive electron species. Since the results are similar to those of ATP synthase inhibitors, we are adding them to this chapter (Fig. 8).

New amino lipopeptides named trichodermins were isolated from the marine-derived fungus *Trichoderma* sp. These compounds were tested for their antimycobacterial activities, and among them, trichodermin A (**56**) was the most potent with activity against *Mtb* H37Rv (MIC 0.12 µg/mL). This sparked interest in identifying its molecular target by influencing gene expression. It was found that mycobacteria with the highly overexpressed genes *atpB*, *atpE*, *atpF*, *atpH*, and parts of *atpA* coding mycobacterial ATP synthase became resistant to Trichodermin A (**56**), which is indirect proof that compound **56** targets ATP synthase. In addition, **56** reduced the intracellular ATP concentration in *M. bovis* BCG [107].

The low level of bacterial respiration is an important point of *Mtb* metabolic vulnerability. Therefore, a hypoxic ATP depletion model has been developed to carry out HTS campaigns. Among 60 000 screened compounds, thiophenes were identified to significantly disrupt ATP homeostasis (hypoxic ATP IC<sub>50</sub> 3.4 µM, aerobic MIC<sub>50</sub> 1.7 µM for compound **57**) [108].

A cellular screen and subsequent lead optimization provided various anti-TB pyrimidine-imidazoles (PIs). Mechanism of action studies linked their activity to glycerol metabolism. PIs cause the accumulation of glycerol phosphate coupled with ATP depletion, thereby impairing *Mtb* growth. Compound **58** strongly affected carbon metabolism, leading to the highest anti-TB activity against within a PI series with an MIC = 0.036 µM against *Mtb* H37Rv [109].

### 3. Author's insight on the topic

Due to the ever-increasing risk of drug-resistant and latent TB, searching for alternative molecular targets is becoming a hot topic. Since energy metabolism represents a fundamental feature in mycobacterial adaptation, targeting various ETC protein complexes is a promising way to generate new anti-TB drugs. Progressive research in the field of mycobacterial energy metabolism has identified several small organic molecule inhibitors with significant anti-TB potency, as summarized in Table 1. Considering the most active scaffolds, some promising QcrB inhibitors, such as imidazopyridine **20** [61], phenoxyalkylbenzimidazoles **25** [68], imidazo [2,1-*b*]thiazole-5-carboxamides **28** [70], and arylvinylpiperazine

amides **38** [77], showed nanomolar MICs against *Mtb* H37Rv. Nanomolar MICs against *Mtb* H37Rv were also found among ATP synthase inhibitors, including C-pyridyl analogs **42** and **43** [96] and pyrimidine-imidazole **58** [110].

To highlight the efficacy of targeting OP, there are already various clinical candidates and approved drugs that have been identified among small molecules targeting mycobacterial energy metabolism. Their structures, current status, and targeted protein components of the mycobacterial ETC pathway are summarized in Table 2. Such therapeutic potential reinforces the importance of OP as a promising drug target. Furthermore, these ETC-targeted drugs combined with other drugs acting via different mechanisms lead to synergistic killing, enabling more effective treatment of drug-susceptible and drug-resistant TB [19,25].

### 4. Conclusion

This review summarizes the efforts in the development of a new type of antitubercular drug focused on energetic metabolism inhibitors. Such compounds are very promising for the treatment of MDR, XDR, and latent stage tuberculosis, especially in combination with other drugs. In this review, we focused mostly on inhibitors of NADH dehydrogenase, *Mtb* cytochrome oxidases, and ATP synthase.

NADH dehydrogenase is a promising molecular target for *Mtb* infection since the protein is not a part of the mammalian genome, and thus, its selective inhibition may selectively kill *Mtb*. Since this enzyme is important for bacteria even in the latent stage, compounds targeting *Mtb* NADH dehydrogenase may be advantageous over compounds that are only effective against the active form. However, the amount of literature on this topic is rather limited. This may be because it is rather complicated to find compounds that selectively target just this protein or due to the fact that it is time-consuming and complicated to prove that NADH dehydrogenase is the target since similar effects, such as ATP depletion, may be reached by targeting different proteins. Up to date, compound **8** (Fig. 2) exhibited the highest potency against *Msmeg* as well as *Mtb* NADH II with IC<sub>50</sub> of 10.7 nM and thus was identified as a primary hit [43]. In our opinion, there is remarkable room for the development of new small molecules targeting this part of the ETC.

A number of articles were published on inhibitors of *Mtb* cytochrome oxidases. Some of them have nanomolar MIC values, which probably makes them the most promising small molecules for the future treatment of tuberculosis. Herein, imidazopyridines tuned out to represent the key heterocyclic cores. Among them, imidazopyridine **20**, derived from zolpidem **19** (Fig. 4), possess

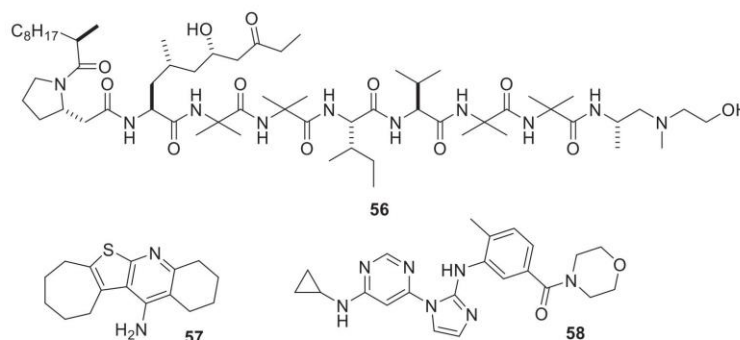
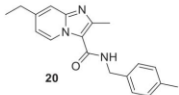
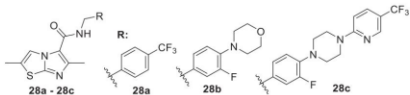
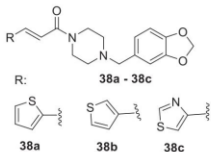
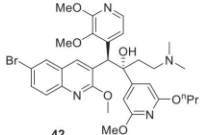
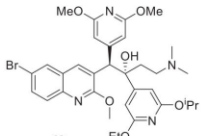
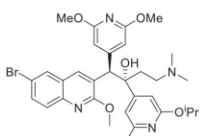
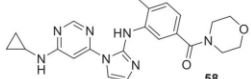


Fig. 8. Compounds disrupting mycobacterial ATP homeostasis.

**Table 1**  
The most potent small organic molecules targeting mycobacterial energy metabolism with nanomolar MICs.

Compound	Target(s)	MIC value(s)
 20	Cytochrome <i>bc</i> <sub>1</sub> complex	0.004 μM
 28a - 28c	Cytochrome <i>bc</i> <sub>1</sub> complex	0.061–0.070 μM
 38a - 38c	Cytochrome <i>bc</i> <sub>1</sub> complex	<0.05 μM
 42	Cytochrome <i>bc</i> <sub>1</sub> complex	0.05–0.1 μM
 43	ATP synthase	0.01 μg/mL
 43	ATP synthase	0.02 μg/mL
 58	ATP homeostasis	0.036 μM

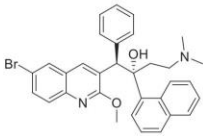
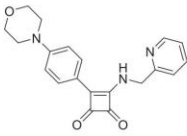
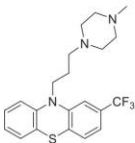
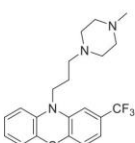
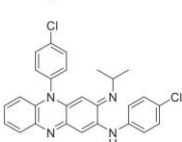
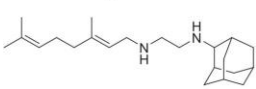
outstanding inhibitory potency on the *bc*<sub>1</sub> complex with MIC as low as 0.004 μM [61]. In addition, several compounds with the highest activity have been used for a long time as treatments for other diseases. Given that, their pharmacological parameters, toxicity, adverse effects, and other important properties are known, which would significantly speed up anti-*Mtb* drug development while reducing the price.

It is well known that mycobacterial ATP synthase carries idiosyncratic features that contribute to efficient ATP production. Therefore, elucidating the exact mechanism of how ATP synthase works can add to the understanding of its general function and reveal specific molecular adaptations. A better insight into all these

processes may provide key input for the rational design of new small molecule entities acting as ATP synthase inhibitors. Moreover, mycobacterial ATP synthase exhibits critical differences compared with human ATP synthase and thus reinforces the design and development of selective ATP synthase inhibitors as anti-tubercular agents. The most promising ATP synthase inhibitors **42** and **43** were derived from bedaquiline **41** (Fig. 7) by Palmer and coworkers [96] by replacing the naphthalene unit with pyridines to achieve reduced cardiotoxicity, lipophilicity and half-life. Both compounds inhibited bacterial growth of *Mtb* H37Rv under MABA with MIC<sub>90</sub> of 0.01 and 0.02 μg/mL as well as LORA conditions with MIC<sub>90</sub> of 0.06 and 0.02 μg/mL, respectively.



**Table 2**  
Clinical candidates and approved drugs within small molecules targeting the mycobacterial ETC pathway.

Name	Structure	Target	Current status
Bedaquiline <b>41</b>		ATP synthase (subunit <i>c</i> )	Approved
Squaramide <b>51</b>		ATP synthase (subunit <i>a</i> )	Preclinical
Q203 <b>39a</b>		Cytochrome <i>bc<sub>1</sub></i> complex ( <i>Q<sub>b</sub></i> site)	Phase 1
Thioridazine <b>3</b>		NADH II (ROS-mediated oxidation) <sup>a</sup>	Approved
Clofazimine		NADH II	Approved
SQ109		Proton motive force (Mmpl3 inhibitor) <sup>b</sup>	Phase 2

<sup>a</sup> Reactive oxygen species.

<sup>b</sup> Mycobacterial membrane protein Large 3.

This review summarizes all literature published about targeting of energy metabolism of *Mtb* in order to find new therapeutics. This article should be useful, especially for medicinal chemists that are focused on the development of compounds with antitubercular activity, since it shows the best structures from the majority of the research articles published on this topic.

### 5. Future directions

Tuberculosis is one of the most prevalent infectious diseases, and despite the long-term existence of antitubercular drugs, this infection kills millions of people. The major problems are resistance to mycobacterial strains and *Mtb* in the latent stage, which can become reactivated when the immune system of the infected person weakens due to various conditions, such as HIV infection, cancer, or immunosuppressive treatment. Targeting *Mtb* energy metabolism is a recent approach to overcome these problems with old-fashioned antituberculars. First, resistance is often caused by

overexpression of efflux pumps that need energy in the form of ATP to drive xenobiotics (including antituberculars) out of the bacterial cell. Decreasing the level of cellular ATP by inhibiting bacterial energy metabolism likely impedes drug efflux and makes the bacteria more vulnerable to the drug. It is advisable to use inhibitors of the ETC in combination with other antitubercular drugs to shorten the time of treatment and to treat MDR, XDR, and latent tuberculosis [111].

The previous research of *Mtb* has resulted in several druggable targets and a number of small molecules that are capable of inhibiting *Mtb* growth. The main goal – full eradication of this infectious disease, however, remains unresolved for the future research and it seems that reaching this goal will be very difficult if not impossible. Therefore, several easier goals should be achieved in the meantime. First of all, it is important to use all tools of molecular and chemical biology to identify alternative targets and more molecules that inhibit the infection. These are important for overcoming the bacterial resistance. Especially functional genomic

may be useful in components that are critical for *Mtb* to survive in the human body. Secondly, more focus should be given to the full understanding of the biology of *Mtb* and especially to the mechanism of the development of the latent infection and its transition into active phase. Such knowledge should result in either prevention of this transition or possibility to completely cure the *Mtb* in latent phase. Third, alternative drug regimens should be established that would allow for more efficient usage of existing and new drugs, shortening the duration of the cure, limiting the side effects, reducing costs, and allowing for an effective treatment of immunodeficient patients and patients with co-morbidities. Last not least, new methods for fast and reliable diagnostics are of a high interest, new biochemical assays should be developed that would be compatible with the majority of the *in vivo* microenvironments.

#### Declaration of competing interest

The authors declare that they have no known competing financial interests or personal relationships that could have appeared to influence the work reported in this paper.

#### Acknowledgements

This work was supported by grant no. JG\_2019\_002 from Palacký University in Olomouc. Authors are grateful to Milan Dak, Tereza Šlitrová and Jan Chasák, who contributed to this review with Figures of OP, mycobacterial cytochrome oxidases and ATP synthases.

#### Abbreviations

TB	tuberculosis
<i>Mtb</i>	<i>Mycobacterium tuberculosis</i>
LTBI	latent tuberculosis infection
MDR	multi-drug resistant
XDR	extensively drug-resistant
DNA	deoxyribonucleic acid
ATP	adenosine triphosphate
ETC	electron transport chain
NADH	nicotinamide adenine dinucleotide
QcrB	subunit b of the cytochrome <i>bc<sub>1</sub></i> complex
PMF	proton motive force
TCA	tricarboxylic acid cycle
SDH	succinate dehydrogenase
MIC	minimal inhibitory concentration
ROS	reactive oxygen species
ISP	iron-sulfur protein
CFU	colony-forming units
MABA	microplate Alamar Blue assay
BDQ	bedaquiline
HTS	high-throughput screening
ABT	aminobenzotriazole
GSK	GlaxoSmithKline
SAR	structure-activity relationship
PAB	phenoxy alkyl benzimidazole
INH	isoniazid
RMP	rifampicin
PZA	pyrazinamide
CFZ	clofazimine
ADP	adenosine diphosphate
OSCP	oligomycin-sensitivity-conferring protein
LORA	Low-oxygen recovery assay
IMV	inverted membrane vesicles
PI	pyrimidine-imidazoles

#### References

- [1] W.H. Organization, Global Tuberculosis Report 2019, World Health Organization; 2019, Geneva (Switzerland), 2019.
- [2] S. Kiazky, T.B. Ball, Tuberculosis (TB): latent tuberculosis infection: an overview, *Can. Comm. Dis. Rep.* 43 (2017) 62.
- [3] N. Dookie, S. Rambaran, N. Padayatchi, S. Mahomed, K. Naidoo, Evolution of drug resistance in *Mycobacterium tuberculosis*: a review on the molecular determinants of resistance and implications for personalized care, *J. Antimicrob. Chemother.* 73 (2018) 1138–1151.
- [4] S.H. Gillespie, Evolution of drug resistance in *Mycobacterium tuberculosis*: clinical and molecular perspective, *Antimicrob. Agents Chemother.* 46 (2002) 267–274.
- [5] J.C. Palomino, A. Martin, Drug resistance mechanisms in *Mycobacterium tuberculosis*, *Antibiotics* 3 (2014) 317–340.
- [6] P.E. Almeida Da Silva, J.C. Palomino, Molecular basis and mechanisms of drug resistance in *Mycobacterium tuberculosis*: classical and new drugs, *J. Antimicrob. Chemother.* 66 (2011) 1417–1430.
- [7] C.A. Peloquin, S.E. Berning, A.T. Nitta, P.M. Simone, M. Goble, G.A. Huit, M.D. Iseman, J.L. Cook, D. Curran-Everett, Aminoglycoside toxicity: daily versus thrice-weekly dosing for treatment of mycobacterial diseases, *Clin. Infect. Dis.* 38 (2004) 1538–1544.
- [8] G. Di Perri, S. Bonora, Which agents should we use for the treatment of multidrug-resistant *Mycobacterium tuberculosis*? *J. Antimicrob. Chemother.* 54 (2004) 593–602.
- [9] W.E. Sanders Jr., C.C. Sanders, Toxicity of antibacterial agents: mechanism of action on mammalian cells, *Annu. Rev. Pharmacol. Toxicol.* 19 (1979) 53–83.
- [10] A.C. Go, L.K. Golightly, G.R. Barber, M.A. Barron, Linezolid interaction with serotonin reuptake inhibitors: report of two cases and incidence assessment, *Drug Metab. Pers. Ther.* 25 (2010) 41–47.
- [11] W.J. Burman, K. Gallicano, C. Peloquin, Comparative pharmacokinetics and pharmacodynamics of the rifamycin antibacterials, *Clin. Pharmacokinet.* 40 (2001) 327–341.
- [12] W.A. Daniel, M. Syrek, A. Haduch, J. Wójcikowski, Pharmacokinetics and metabolism of thioridazine during co-administration of tricyclic antidepressants, *Br. J. Pharmacol.* 131 (2000) 287–295.
- [13] S.M. Gygli, S. Borrell, A. Trauner, S. Gagneux, Antimicrobial resistance in *Mycobacterium tuberculosis*: mechanistic and evolutionary perspectives, *FEMS Microbiol. Rev.* 41 (2017) 354–373.
- [14] P.A. Black, R.M. Warren, G.E. Louw, P.D. van Helden, T.C. Victor, B.D. Kana, Energy metabolism and drug efflux in *Mycobacterium tuberculosis*, *Antimicrob. Agents Chemother.* 58 (2014) 2491–2503, <https://doi.org/10.1128/AAC.02293-13>, 14 pp.
- [15] N. Kamariah, P. Raganathan, J. Shin, W.-G. Saw, C.-F. Wong, T. Dick, G. Grüber, Unique structural and mechanistic properties of mycobacterial F-ATP synthases: implications for drug design, *Prog. Biophys. Mol. Biol.* 152 (2020) 64–73.
- [16] A. Harikishore, S.S.M. Chong, P. Raganathan, R.W. Bates, G. Grüber, Targeting the menaquinol binding loop of mycobacterial cytochrome *bd* oxidase, *Mol. Divers.* (2020) 1–8.
- [17] V. Patil, V. Jain, Insights into the physiology and metabolism of a mycobacterial cell in an energy-compromised state, *J. Bacteriol.* 201 (2019) e00219.
- [18] G.S. Shetye, S.G. Franzblau, S. Cho, New tuberculosis drug targets, their inhibitors, and potential therapeutic impact, *Transl. Res.* 220 (2020) 68–97.
- [19] D. Bald, A. Koul, Respiratory ATP synthesis: the new generation of mycobacterial drug targets? *FEMS Microbiol. Lett.* 308 (2010) 1–7.
- [20] H.I.M. Boshoff, C.E. Barry III, Tuberculosis: metabolism and respiration in the absence of growth, *Nat. Rev. Microbiol.* 3 (2005) 70–80, <https://doi.org/10.1038/nrmicro1065>.
- [21] R.K. Dhiman, S. Mahapatra, R.A. Slayden, M.E. Boyne, A. Lenaerts, J.C. Hinshaw, S.K. Angala, D. Chatterjee, K. Biswas, P. Narayanasamy, M. Kurosu, D.C. Crick, Menaquinone synthesis is critical for maintaining mycobacterial viability during exponential growth and recovery from non-replicating persistence, *Mol. Microbiol.* 72 (2009) 85–97, <https://doi.org/10.1111/j.1365-2958.2009.06625.x>.
- [22] K. Hards, C. Adolph, L.K. Harold, M.B. McNeil, C.-Y. Cheung, A. Jinich, K.Y. Rhee, G.M. Cook, Two for the price of one: attacking the energetic-metabolic hub of mycobacteria to produce new chemotherapeutic agents, *Prog. Biophys. Mol. Biol.* 152 (2020) 35–44.
- [23] B.S. Lee, E. Sviriaeva, K. Pethe, Targeting the cytochrome oxidases for drug development in mycobacteria, *Prog. Biophys. Mol. Biol.* (2020).
- [24] G.M. Cook, K. Hards, C. Vilcheze, T. Hartman, M. Berney, Energetics of respiration and oxidative phosphorylation in mycobacteria, *Microbiol. Spectr.* 2 (2014) 20, <https://doi.org/10.1128/microbiolspec.MGM2-0015-2013>, MGM200152013/1-MGM200152013/20.
- [25] K.K. Roy, M.A. Wani, Emerging opportunities of exploiting mycobacterial electron transport chain pathway for drug-resistant tuberculosis drug discovery, *Expet Opin. Drug Discov.* 15 (2020) 231–241, <https://doi.org/10.1080/17460441.2020.1696771>.
- [26] D. Bald, C. Villellas, P. Lu, A. Koul, Targeting energy metabolism in *Mycobacterium tuberculosis*, a new paradigm in antimycobacterial drug discovery, *mBio* 8 (2017), <https://doi.org/10.1128/mBio.00272-17> e00272-17/1-e00272-17/11.



- [27] B. Alberts, J. Alexander, J. Lewis, M. Raff, K. Roberts, P. Walter, *Molecular Biology of the Cell*, fourth ed., Wiley, 2004.
- [28] L. Shi, C.D. Sohaskey, B.D. Kana, S. Dawes, R.J. North, V. Mizrahi, M.L. Gennaro, Changes in energy metabolism of *Mycobacterium tuberculosis* in mouse lung and under in vitro conditions affecting aerobic respiration, *Proc. Natl. Acad. Sci. U.S.A.* 102 (2005) 15629–15634, <https://doi.org/10.1073/pnas.0507850102>.
- [29] S. Sellamuthu, M. Singh, A. Kumar, S.K. Singh, Type-II NADH Dehydrogenase (NDH-2): a promising therapeutic target for antitubercular and antibacterial drug discovery, *Expert Opin. Ther. Targets* 21 (2017) 559–570.
- [30] T. Yagi, Bacterial NADH-quinone oxidoreductases, *J. Bioenerg. Biomembr.* 23 (1991) 211–239, <https://doi.org/10.1007/BF00762218>.
- [31] E.A. Weinstein, T. Yano, L.-S. Li, D. Avarbock, A. Avarbock, D. Helm, A.A. McCollm, K. Duncan, J.T. Lonsdale, H. Rubin, Inhibitors of type II NADH: menaquinone oxidoreductase represent a class of antitubercular drugs, *Proc. Natl. Acad. Sci. U.S.A.* 102 (2005) 4548–4553, <https://doi.org/10.1073/pnas.0500469102>.
- [32] A.M.P. Melo, T.M. Bandejas, M. Teixeira, New insights into type II NAD(P)H: quinone oxidoreductases, *Microbiol. Mol. Biol. Rev.* 68 (2004) 603–616, <https://doi.org/10.1128/MMBR.68.4.603-616.2004>.
- [33] S.P.S. Rao, S. Alonso, L. Rand, T. Dick, K. Pethe, The protonmotive force is required for maintaining ATP homeostasis and viability of hypoxic, non-replicating *Mycobacterium tuberculosis*, *Proc. Natl. Acad. Sci. U. S. A.* 105 (2008) 11945–11950, <https://doi.org/10.1073/pnas.0711697105>.
- [34] C. Vilcheze, B. Weinrick, L.W. Leung, W.R. Jacobs, Plasticity of *Mycobacterium tuberculosis* NADH dehydrogenases and their role in virulence, *Proc. Natl. Acad. Sci. Unit. States Am.* 115 (2018) 1599–1604.
- [35] M. Berney, G.M. Cook, Unique flexibility in energy metabolism allows mycobacteria to combat starvation and hypoxia, *PLoS One* 5 (2010), <https://doi.org/10.1371/journal.pone.0008614>. No pp. given.
- [36] J.E. Griffin, J.D. Gawronski, M.A. DeJesus, T.R. Iøerger, B.J. Akerley, C.M. Sasseti, High-resolution phenotypic profiling defines genes essential for mycobacterial growth and cholesterol catabolism, *PLoS Pathog.* 7 (2011), e1002251, <https://doi.org/10.1371/journal.ppat.1002251>.
- [37] T. Hartman, B. Weinrick, C. Vilcheze, M. Berney, J. Tufariello, G.M. Cook, W.R. Jacobs Jr., Succinate dehydrogenase is the regulator of respiration in *Mycobacterium tuberculosis*, *PLoS Pathog.* 10 (2014) 15, <https://doi.org/10.1371/journal.ppat.1004510>, e1004510/1-e1004510/15.
- [38] S. Watanabe, M. Zimmermann, M.B. Goodwin, U. Sauer, C.E. Barry III, H.J. Boshoff, Fumarate reductase activity maintains an energized membrane in anaerobic *Mycobacterium tuberculosis*, *PLoS Pathog.* 7 (2011), e1002287, <https://doi.org/10.1371/journal.ppat.1002287>.
- [39] S. Sharma, A. Singh, Phenothiazines as anti-tubercular agents: mechanistic insights and clinical implications, *Expert Opin. Invest. Drugs* 20 (2011) 1665–1676, <https://doi.org/10.1517/13543784.2011.628657>.
- [40] M.G. Nizi, J. Desantis, Y. Nakatani, S. Massari, M.A. Mazzarella, G. Shetye, S. Sabatini, M.L. Barreca, G. Manfroni, T. Felicetti, Antitubercular poly-halogenated phenothiazines and phenoselenazine with reduced binding to CNS receptors, *Eur. J. Med. Chem.* (2020) 112420.
- [41] P.S. Shirude, B. Paul, N. Roy Choudhury, C. Kedari, B. Bhandodkar, B.G. Ugarkar, Quinolonyl pyrimidines: potent inhibitors of NDH-2 as a novel class of anti-TB agents, *ACS Med. Chem. Lett.* 3 (2012) 736–740, <https://doi.org/10.1021/ml300134b>.
- [42] A. Heikal, Y. Nakatani, W. Jiao, C. Wilson, D. Rennison, M.R. Weimar, E.J. Parker, M.A. Brimble, G.M. Cook, “Tethering” fragment-based drug discovery to identify inhibitors of the essential respiratory membrane protein type II NADH dehydrogenase, *Bioorg. Med. Chem. Lett.* 28 (2018) 2239–2243, <https://doi.org/10.1016/j.bmcl.2018.05.048>.
- [43] M.B. Harbut, B. Yang, R. Liu, T. Yano, C. Vilcheze, B. Cheng, J. Lockner, H. Guo, C. Yu, S.G. Franzblau, H.M. Petrassi, W.R.J. Jacobs, H. Rubin, A.K. Chatterjee, F. Wang, Small molecules targeting *Mycobacterium tuberculosis* type II NADH dehydrogenase exhibit antimycobacterial activity, *Angew. Chem. Int. Ed.* 57 (2018) 3478–3482, <https://doi.org/10.1002/anie.201800260>.
- [44] D. Murugesan, P.C. Ray, T. Bayliss, G.A. Prosser, J.R. Harrison, K. Green, C. Soares de Melo, T.-S. Feng, L.J. Street, K. Chibale, D.F. Warner, V. Mizrahi, O. Epemolu, P. Scullion, L. Ellis, J. Riley, Y. Shishikura, L. Ferguson, M. Osuna-Cabello, K.D. Read, S.R. Green, D.A. Lamprecht, P.M. Finin, A.J.C. Steyn, T.R. Iøerger, J. Sacchettini, K.Y. Rhee, K. Arora, C.E. Barry III, P.G. Wyatt, H.I.M. Boshoff, 2-Mercapto-Quinazolinones as inhibitors of type II NADH dehydrogenase and *Mycobacterium tuberculosis*: structure-activity relationships, mechanism of action and absorption, distribution, metabolism, and excretion characterization, *ACS Infect. Dis.* 4 (2018) 954–969, <https://doi.org/10.1021/acinfedcis.7b00275>.
- [45] A. Korkegian, T. O'Malley, Y. Xia, Y. Zhou, D.S. Carter, B. Sunde, L. Flint, D. Thompson, T.R. Iøerger, J. Sacchettini, The 7-phenyl benzoxaborole series is active against *Mycobacterium tuberculosis*, *Tuberculosis* 108 (2018) 96–98.
- [46] B.J. Mulchin, C.G. Newton, J.W. Batty, C.H. Grasso, W.J. Martin, M.C. Walton, E.M. Dangerfield, C.H. Plunkett, M.V. Berridge, J.L. Harper, The anti-cancer, anti-inflammatory and tuberculostatic activities of a series of 6, 7-substituted-5, 8-quinolinequinones, *Bioorg. Med. Chem.* 18 (2010) 3238–3251.
- [47] A. Heikal, K. Hards, C.-Y. Cheung, A. Menorca, M.S.M. Timmer, B.L. Stocker, G.M. Cook, Activation of type II NADH dehydrogenase by quinolinequinones mediates antitubercular cell death, *J. Antimicrob. Chemother.* 71 (2016) 2840–2847.
- [48] K.T. Santoso, A. Menorca, C.-Y. Cheung, G.M. Cook, B.L. Stocker, M.S.M. Timmer, The synthesis and evaluation of quinolinequinones as antimycobacterial agents, *Bioorg. Med. Chem.* 27 (2019) 3532–3545.
- [49] L.G. Matsoso, B.D. Kana, P.K. Crellin, D.J. Lea-Smith, A. Pelosi, D. Powell, S.S. Dawes, H. Rubin, R.L. Coppel, V. Mizrahi, Function of the cytochrome bc<sub>1</sub>-aa3 branch of the respiratory network in *Mycobacteria* and network adaptation occurring in response to its disruption, *J. Bacteriol.* 187 (2005) 6300–6308, <https://doi.org/10.1128/JB.187.18.6300-6308.2005>.
- [50] J.L. Small, S.W. Park, B.D. Kana, T.R. Iøerger, J.C. Sacchettini, S. Ehr, Perturbation of cytochrome c maturation reveals adaptability of the respiratory chain in *Mycobacterium tuberculosis*, *mBio* 4 (2013).
- [51] B.D. Kana, E.A. Weinstein, D. Avarbock, S.S. Dawes, H. Rubin, V. Mizrahi, Characterization of the cydAB-encoded cytochrome bd oxidase from *Mycobacterium smegmatis*, *J. Bacteriol.* 183 (2001) 7076–7086, <https://doi.org/10.1128/JB.183.24.7076-7086.2001>.
- [52] J.A. Megehee, J.P. Hosler, M.D. Lundrigan, Evidence for a cytochrome bcc-aa3 interaction in the respiratory chain of *Mycobacterium smegmatis*, *Microbiology* 152 (2006) 823–829, <https://doi.org/10.1099/mic.0.28723-0>.
- [53] D. Xia, L. Esser, W.-K. Tang, F. Zhou, Y. Zhou, L. Yu, C.-A. Yu, Structural analysis of cytochrome bc<sub>1</sub> complexes: implications to the mechanism of function, *Biochim. Biophys. Acta Bioenerg.* 1827 (2013) 1278–1294, <https://doi.org/10.1016/j.bbabi.2012.11.008>.
- [54] P.O. Ljungdahl, J.D. Pennoyer, D.E. Robertson, B.L. Trumppower, Purification of highly active cytochrome bc<sub>1</sub> complexes from phylogenetically diverse species by a single chromatographic procedure, *Biochim. Biophys. Acta Bioenerg.* 891 (1987) 227–241, [https://doi.org/10.1016/0005-2728\(87\)90218-0](https://doi.org/10.1016/0005-2728(87)90218-0).
- [55] C.-A. Yu, L. Yu, Structural role of phospholipids in ubiquinol-cytochrome c reductase, *Biochemistry* 19 (1980) 5715–5720, <https://doi.org/10.1021/bi00566a008>.
- [56] Y. Ko, I. Choi, Putative 3D structure of QcrB from *Mycobacterium tuberculosis* cytochrome bc<sub>1</sub> complex, a novel drug-target for new series of antituberculosis agent Q203, *Bull. Kor. Chem. Soc.* 37 (2016) 725–731, <https://doi.org/10.1002/bkcs.10765>.
- [57] M. Blaise, L. Kremer, Self-control of QcrB from *Mycobacterium tuberculosis* in the crystal, *J. Biol. Chem.* 295 (2020) 3771–3772.
- [58] Z. Pan, Y. Wang, X. Gu, J. Wang, M. Cheng, Refined homology model of cytochrome bc<sub>1</sub> complex B subunit for virtual screening of potential anti-tuberculosis agents, *J. Biomol. Struct. Dyn.* 38 (2020) 4733–4745.
- [59] B.L. Trumppower, Cytochrome bc<sub>1</sub> complexes of microorganisms, *Microbiol. Rev.* 54 (1990) 101–129, <https://doi.org/10.1128/mmr.54.2.101-129.1990>.
- [60] S.T. Cole, R. Brosch, J. Parkhill, T. Garnier, C. Churcher, D. Harris, S.V. Gordon, K. Eiglmeier, S. Gas, C.E. Barry III, F. Tekaia, K. Badoock, D. Basham, D. Brown, T. Chillingworth, R. Connor, R. Davies, K. Devlin, T. Feltwell, S. Gentles, N. Hamlin, S. Holroyd, T. Hornsby, K. Jagels, A. Krogh, J. McLean, S. Moule, L. Murphy, K. Oliver, J. Osborne, M.A. Quail, M.-A. Rajandream, J. Rogers, S. Rutter, K. Seeger, J. Skelton, R. Squares, S. Squares, E.J. Sultson, K. Taylor, S. Whitehead, B.G. Barrell, Deciphering the biology of *Mycobacterium tuberculosis* from the complete genome sequence. [Erratum to document cited in CA129:77224], *Nature* 396 (1998) 190–198, <https://doi.org/10.1038/24206>.
- [61] I. Bown, S.K. Srivastava, B.M. Piercey, C.K. McIsaac, K. Tahlan, Mycobacterial membrane proteins QcrB and AtpE: roles in energetics, antibiotic targets, and associated mechanisms of resistance, *J. Membr. Biol.* 251 (2018) 105–117, <https://doi.org/10.1007/s00232-017-9957-3>.
- [62] C.V. Holyoake, R.K. Poole, M. Shepherd, The CydDC family of transporters and their roles in oxidase assembly and homeostasis, *Adv. Microb. Physiol.* 66 (2015) 1–53, <https://doi.org/10.1016/bs.ampbs.2015.04.002>.
- [63] K.A. Abrahams, J.A.G. Cox, V.L. Spivey, N.J. Loman, M.J. Pallen, C. Constantinidou, R. Fernandez, C. Alemparte, M.J. Remuani, D. Barros, L. Ballell, G.S. Besra, Identification of novel imidazo[1,2-a]pyridine inhibitors targeting *M. tuberculosis* QcrB, *PLoS One* 7 (2012), e25951, <https://doi.org/10.1371/journal.pone.0052951>.
- [64] K. Arora, B. Ochoa-Montano, P.S. Tsang, T.L. Blundell, S.S. Dawes, V. Mizrahi, T. Bayliss, C.J. MacKenzie, L.A.T. Cleghorn, P.C. Ray, P.G. Wyatt, E. Uh, J. Lee, C.E. Barry, H.I. Boshoff, Respiratory flexibility in response to inhibition of cytochrome c oxidase in *Mycobacterium tuberculosis*, *Antimicrob. Agents Chemother.* 58 (2014) 6962–6965, <https://doi.org/10.1128/AAC.03486-14.5> pp.
- [65] G.C. Moraski, P.A. Miller, M.A. Bailey, J. Ollinger, T. Parish, H.I. Boshoff, S. Cho, J.R. Anderson, S. Mulugeta, S.G. Franzblau, Putting tuberculosis (TB) to rest: transformation of the sleep aid, Ambien, and “anagrams” generated potent antituberculosis agents, *ACS Infect. Dis.* 1 (2015) 85–90.
- [66] T. O'Malley, T. Alling, J. V. Early, H.A. Westcott, A. Kumar, G.C. Moraski, M.J. Miller, T. Masquelin, P.A. Hipskind, T. Parish, Imidazopyridine compounds inhibit mycobacterial growth by depleting ATP levels, *Antimicrob. Agents Chemother.* 62 (2018), <https://doi.org/10.1128/aac.02439-17> e02439-17/1-e02439-17/8.
- [67] R. van der Westhuyzen, S. Winks, C.R. Wilson, G.A. Boyle, R.K. Gessner, C. Soares de Melo, D. Taylor, C. de Kock, M. Njoroge, C. Brunschwig, N. Lawrence, S.P.S. Rao, F. Sirgel, P. van Helden, R. Seldon, A. Moosa, D.F. Warner, L. Arista, U.H. Manjunatha, P.W. Smith, L.J. Street, K. Chibale, Pyrrolo[3,4-c]pyridine-1,3(2H)-diones: a novel antimycobacterial class targeting mycobacterial respiration, *J. Med. Chem.* 58 (2015) 9371–9381,



- <https://doi.org/10.1021/acs.jmedchem.5b01542>.
- [68] N.S. Chandrasekera, B.J. Berube, G. Shetye, S. Chettiar, T. O'Malley, A. Manning, L. Flint, D. Awasthi, T.R. Ioerger, J. Sacchetti, T. Masquelin, P.A. Hipskind, J. Odingo, T. Parish, Improved phenoxyalkylbenzimidazoles with activity against *Mycobacterium tuberculosis* appear to target QcrB, *ACS Infect. Dis.* 3 (2017) 898–916, <https://doi.org/10.1021/acsinfecdis.7b00112>.
- [69] N. Phummarin, H.I. Boshoff, P.S. Tsang, J. Dalton, S. Wiles, C.E. Barry 3rd, B.R. Copp, SAR and identification of 2-(quinolin-4-yl)oxyacetamides as *Mycobacterium tuberculosis* cytochrome bc1 inhibitors, *Med. Chem. Comm.* 7 (2016) 2122–2127, <https://doi.org/10.1039/C6MD00236F>.
- [70] G.C. Moraski, N. Seeger, P.A. Miller, A.G. Oliver, H.I. Boshoff, S. Cho, S. Mulgetta, J.R. Anderson, S.G. Franzblau, M.J. Miller, Arrival of imidazo[2,1-b]thiazole-5-carboxamides: potent anti-tuberculosis agents that target QcrB, *ACS Infect. Dis.* 2 (2016) 393–398, <https://doi.org/10.1021/acsinfecdis.5b00154>.
- [71] G.C. Moraski, N. Deboosère, K.L. Marshall, H.A. Weaver, A. Vandeputte, C. Hastings, L. Woolhiser, A.J. Lenaerts, P. Brodin, M.J. Miller, Intracellular and in vivo evaluation of imidazo [2, 1-b] thiazole-5-carboxamide anti-tuberculosis compounds, *PLoS One* 15 (2020), e0227224.
- [72] B.J. Berube, T. Parish, Combinations of respiratory chain inhibitors have enhanced bactericidal activity against *Mycobacterium tuberculosis*, *Antimicrob. Agents Chemother.* 62 (2018) 1–10, <https://doi.org/10.1128/aac.01677-17>.
- [73] G.A. Harrison, A.E.M. Bridwell, M. Singh, K. Jayaraman, L.A. Weiss, R.L. Kinsella, J.S. Aneke, K. Flentie, M.E. Schene, M. Gaggioli, S.D. Solomon, S.A. Wildman, M.J. Meyers, C.L. Stallings, Identification of 4-Amino-Thieno [2,3-d]Pyrimidines as QcrB inhibitors in *Mycobacterium tuberculosis*, *mSphere* 4 (2019), <https://doi.org/10.1128/mSphere.00606-19> e00606-19/e00606-19/14.
- [74] A. Lupien, C.S.-Y. Foo, S. Savina, A. Vocat, J. Piton, N. Monakhova, A. Benjak, D.A. Lamprecht, A.J.C. Steyn, K. Pethe, V.A. Makarov, S.T. Cole, New 2-ethylthio-4-methylaminoquinazoline derivatives inhibiting two subunits of cytochrome bc1 in *Mycobacterium tuberculosis*, *PLoS Pathog.* 16 (2020), <https://doi.org/10.1371/journal.ppat.1008270> e1008270/19.
- [75] F.T. Subtil, A.D. Villela, B.L. Abbadi, V.S. Rodrigues-Junior, C.V. Bizarro, L.F.S.M. Timmers, O. Norberto de Souza, K. Pissinate, P. Machado, A. Lopez-Gavin, G. Tudo, J. Gonzalez-Martin, L.A. Basso, D.S. Santos, Activity of 2-(quinolin-4-yl)oxyacetamides in *Mycobacterium tuberculosis* clinical isolates and identification of their molecular target by whole-genome sequencing, *Int. J. Antimicrob. Agents* 51 (2018) 378–384, <https://doi.org/10.1016/j.ijantimicag.2017.08.023>.
- [76] L.A.T. Cleghorn, P.C. Ray, J. Odingo, A. Kumar, H. Wescott, A. Korkegian, T. Masquelin, A. Lopez Moure, C. Wilson, S. Davis, M. Huggett, P. Turner, A. Smith, O. Epemolu, F. Zuccotto, J. Riley, P. Scullion, Y. Shishikura, L. Ferguson, J. Rullas, L. Guijarro, K.D. Read, S.R. Green, P. Hipskind, T. Parish, P.G. Wyatt, Identification of morpholino thiophenes as novel *Mycobacterium tuberculosis* inhibitors, targeting QcrB, *J. Med. Chem.* 61 (2018) 6592–6608, <https://doi.org/10.1021/acs.jmedchem.8b00172>.
- [77] C.S. Foo, A. Lupien, M. Kienle, A. Vocat, A. Benjak, A.R. Sommer, D.A. Lamprecht, A.J.C. Steyn, K. Pethe, J. Piton, K.-H. Altmann, S.T. Cole, Arylvinylpiperazine amides, a new class of potent inhibitors targeting QcrB of *Mycobacterium tuberculosis*, *mBio* 9 (2018), <https://doi.org/10.1128/mBio.01276-18> e01276-18/1-10/1276-18/13.
- [78] K. Pethe, P. Bifani, J. Jang, S. Kang, S. Park, S. Ahn, J. Jiricek, J. Jung, H.K. Jeon, J. Cechetto, Discovery of Q203, a potent clinical candidate for the treatment of tuberculosis, *Nat. Med.* 19 (2013) 1157–1160.
- [79] X. Lu, Z. Williams, K. Hards, J. Tang, C.-Y. Cheung, H.L. Aung, B. Wang, Z. Liu, X. Hu, A. Lenaerts, L. Woolhiser, C. Hastings, X. Zhang, Z. Wang, K. Rhee, K. Ding, T. Zhang, G.M. Cook, Pyrazolo[1,5-a]pyridine inhibitor of the respiratory cytochrome bcc complex for the treatment of drug-resistant tuberculosis, *ACS Infect. Dis.* 5 (2019) 239–249, <https://doi.org/10.1021/acsinfecdis.8b00225>.
- [80] P. Lu, H. Lill, D. Bald, ATP synthase in mycobacteria: special features and implications for a function as drug target, *Biochim. Biophys. Acta Bioenerg.* 1837 (2014) 1208–1218, <https://doi.org/10.1016/j.bbabi.2014.01.022>.
- [81] M. Berney, G.M. Cook, Respiration and oxidative phosphorylation in mycobacteria, *Adv. Photosynth. Respir.* 39 (2014) 277–293, [https://doi.org/10.1007/978-94-017-8742-0\\_15](https://doi.org/10.1007/978-94-017-8742-0_15).
- [82] C.S. Gajadeera, J. Weber, *Escherichia coli* F1Fo-ATP synthase with a b/δ fusion protein allows analysis of the function of the individual b subunits, *J. Biol. Chem.* 288 (2013) 26441–26447.
- [83] P.A. Del Rizzo, Y. Bi, S.D. Dunn, ATP synthase b subunit dimerization domain: a right-handed coiled coil with offset helices, *J. Mol. Biol.* 364 (2006) 735–746, <https://doi.org/10.1016/j.jmb.2006.09.028>.
- [84] T. Meier, N. Morgner, D. Matthies, D. Pogoryelov, S. Keis, G.M. Cook, P. Dimroth, B. Brutschy, A tridecameric c ring of the adenosine triphosphate (ATP) synthase from the thermoalkaliphilic *Bacillus* sp. strain TA2.A1 facilitates ATP synthesis at low electrochemical proton potential, *Mol. Microbiol.* 65 (2007) 1181–1192, <https://doi.org/10.1111/j.1365-2958.2007.05857.x>.
- [85] I.M. Willis, R.D. Moir, Integration of nutritional and stress signaling pathways by MafI, *Trends Biochem. Sci.* 32 (2007) 51–53, <https://doi.org/10.1016/j.tibs.2006.12.001>.
- [86] W. Jiang, J. Hermlin, R.H. Fillingame, The preferred stoichiometry of c subunits in the rotary motor sector of *Escherichia coli* ATP synthase is 10, *Proc. Natl. Acad. Sci. U.S.A.* 98 (2001) 4966–4971, <https://doi.org/10.1073/pnas.081424898>.
- [87] A.L. Cozens, J.E. Walker, The organization and sequence of the genes for ATP synthase subunits in the cyanobacterium *Synechococcus* 6301. Support for an endosymbiotic origin of chloroplasts, *J. Mol. Biol.* 194 (1987) 359–383, [https://doi.org/10.1016/0022-2836\(87\)90667-X](https://doi.org/10.1016/0022-2836(87)90667-X).
- [88] A. Koul, L. Vranckx, N. Dendouga, W. Balemans, I. Van den Wyngaert, K. Vergauwen, H.W.H. Goehlmann, R. Willebrords, A. Poncelet, J. Guillemont, D. Bald, K. Andries, Diarylquinolines are bactericidal for dormant mycobacteria as a result of disturbed ATP homeostasis, *J. Biol. Chem.* 283 (2008) 25273–25280, <https://doi.org/10.1074/jbc.M803899200>.
- [89] A.C. Haagsma, N.N. Driessen, M.-M. Hahn, H. Lill, D. Bald, ATP synthase in slow- and fast-growing mycobacteria is active in ATP synthesis and blocked in ATP hydrolysis direction, *FEMS Microbiol. Lett.* 313 (2010) 68–74, <https://doi.org/10.1111/j.1574-6968.2010.02123.x>.
- [90] P. Lu, H. Lill, D. Bald, ATP synthase in mycobacteria: special features and implications for a function as drug target, *Biochim. Biophys. Acta Bioenerg.* 1837 (2014) 1208–1218, <https://doi.org/10.1016/j.bbabi.2014.01.022>.
- [91] A. Koul, N. Dendouga, K. Vergauwen, B. Molenberghs, L. Vranckx, R. Willebrords, Z. Ristic, H. Lill, I. Dorange, J. Guillemont, Diarylquinolines target subunit c of mycobacterial ATP synthase, *Nat. Chem. Biol.* 3 (2007) 323–324.
- [92] K. Andries, P. Verhasselt, J. Guillemont, H.W.H. Goehlmann, J.-M. Neefs, H. Winkler, J. Van Gestel, P. Timmerman, M. Zhu, E. Lee, A diarylquinoline drug active on the ATP synthase of *Mycobacterium tuberculosis*, *Science* (80) 307 (2005) 223–227.
- [93] M. Lakshmanan, A.S. Xavier, Bedaquiline—The first ATP synthase inhibitor against multi drug resistant tuberculosis, *J. Young Pharm.* 5 (2013) 112–115.
- [94] M.J. Lobo, R. Ray, G.G. Shenoy, Gaining deeper insights into the surface binding of bedaquiline analogues with the ATP synthase subunit C of *Mycobacterium tuberculosis* using molecular docking, molecular dynamics simulation and 3D-QSAR techniques, *New J. Chem.* 44 (2020) 18831–18852.
- [95] H. Guo, G.M. Courbon, S.A. Bueler, J. Mai, J. Liu, J.L. Rubinstein, Structure of mycobacterial ATP synthase bound to the tuberculosis drug bedaquiline, *Nature* (2020) 1–5.
- [96] A. Blaser, H.S. Sutherland, A.S.T. Tong, P.J. Choi, D. Conole, S.G. Franzblau, C.B. Cooper, A.M. Upton, M. Lotlikar, W.A. Denny, B.D. Palmer, Structure-activity relationships for unit C pyridyl analogues of the tuberculosis drug bedaquiline, *Bioorg. Med. Chem.* 27 (2019) 1283–1291, <https://doi.org/10.1016/j.bmc.2019.02.025>.
- [97] S. Kumar, R. Mehra, S. Sharma, N.P. Bokolia, D. Raina, A. Nargotra, P.P. Singh, L.A. Khan, Screening of antitubercular compound library identifies novel ATP synthase inhibitors of *Mycobacterium tuberculosis*, *Tuberculosis* (Oxford, United Kingdom) 108 (2018) 56–63, <https://doi.org/10.1016/j.tube.2017.10.008>.
- [98] R.K. Munnaluri, V. Manga, In silico Quest guided by physico-chemical descriptors of bedaquiline for new scaffolds with potential inhibitory capacity against homology model of mycobacterium F1Fo ATP synthase, *Asian J. Chem.* 30 (2018) 904–912, <https://doi.org/10.14233/ajchem.2018.21145>.
- [99] C. He, L. Preiss, B. Wang, L. Fu, H. Wen, X. Zhang, H. Cui, T. Meier, D. Yin, Structural simplification of bedaquiline: the discovery of 3-(4-(N,N-Dimethylaminomethyl)phenyl)quinoline-Derived antitubercular lead compounds, *ChemMedChem* 12 (2017) 106–119, <https://doi.org/10.1002/cmdc.201600441>.
- [100] S.J. Tantry, S.D. Markad, V. Shinde, J. Bhat, G. Balakrishnan, A.K. Gupta, A. Ambady, A. Raichurkar, C. Kedari, S. Sharma, N.V. Mudugal, A. Narayan, C.N. Naveen Kumar, R. Nanduri, S. Bharath, J. Reddy, V. Panduga, K.R. Prabhakar, K. Kandaswamy, R. Saralaya, P. Kaur, N. Dinesh, S. Guptha, K. Rich, D. Murray, H. Plant, M. Preston, H. Ashton, D. Plant, J. Walsh, P. Alcock, K. Naylor, M. Collier, J. Whiteaker, R.E. McLaughlin, M. Mallya, M. Panda, S. Rudrapatna, V. Ramachandran, R. Shandil, V.K. Sambandamurthy, K. Mdluli, C.B. Cooper, H. Rubin, T. Yano, P. Iyer, S. Narayanan, S. Kavanagh, K. Mukherjee, V. Balasubramanian, V.P. Hosagrahara, S. Solapure, S. Ravishanker, S. Hameed P, Discovery of imidazo[1,2-a]pyridine ethers and squaramides as selective and potent inhibitors of mycobacterial adenosine triphosphate (ATP) synthesis, *J. Med. Chem.* 60 (2017) 1379–1399, <https://doi.org/10.1021/acs.jmedchem.6b01358>.
- [101] Y.B. Surase, K. Samby, S.R. Amale, R. Sood, K.P. Purnapatre, P.K. Pareek, B. Das, K. Nanda, S. Kumar, A.K. Verma, Identification and synthesis of novel inhibitors of mycobacterium ATP synthase, *Bioorg. Med. Chem. Lett.* 27 (2017) 3454–3459, <https://doi.org/10.1016/j.bmcl.2017.05.081>.
- [102] S. Sellamuthu, A.H. Asseri, H.G. Goojani, G. Nath, S.K. Singh, Preliminary studies on ligand-based design and evaluation of new mycobacterial ATP synthase inhibitors, *Curr. Drug Ther.* 13 (2018) 56–73, <https://doi.org/10.2174/1574885512666170911144732>.
- [103] S.J. Tantry, V. Shinde, G. Balakrishnan, S.D. Markad, A.K. Gupta, J. Bhat, A. Narayan, A. Raichurkar, L.K. Jena, S. Sharma, N. Kumar, R. Nanduri, S. Bharath, J. Reddy, V. Panduga, K.R. Prabhakar, R. Kandaswamy, P. Kaur, N. Dinesh, S. Guptha, R. Saralaya, M. Panda, S. Rudrapatna, M. Mallya, H. Rubin, T. Yano, K. Mdluli, C.B. Cooper, V. Balasubramanian, V.K. Sambandamurthy, V. Ramachandran, R. Shandil, S. Kavanagh, S. Narayanan, P. Iyer, K. Mukherjee, V.P. Hosagrahara, S. Solapure, S. Hameed P, S. Ravishanker, Scaffold morphing leading to evolution of 2,4-diaminoquinolines and aminopyrazolopyrimidines as inhibitors of the ATP synthesis pathway, *Med. Chem. Comm.* 7 (2016) 1022–1032, <https://doi.org/10.1039/c5md00000a>.



- 10.1039/C5MD00589B.
- [104] S. Singh, K.K. Roy, S.R. Khan, V.K. Kashyap, A. Sharma, S. Jaiswal, S.K. Sharma, M.Y. Krishnan, V. Chaturvedi, J. Lal, S. Sinha, A. Dasgupta, R. Srivastava, A.K. Saxena, Novel, potent, orally bioavailable and selective mycobacterial ATP synthase inhibitors that demonstrated activity against both replicating and non-replicating *M. tuberculosis*, *Bioorg. Med. Chem.* 23 (2015) 742–752, <https://doi.org/10.1016/j.bmc.2014.12.060>.
- [105] S.R. Khan, S. Singh, K.K. Roy, M.S. Akhtar, A.K. Saxena, M.Y. Krishnan, Biological evaluation of novel substituted chloroquinolines targeting mycobacterial ATP synthase, *Int. J. Antimicrob. Agents* 41 (2013) 41–46.
- [106] A. Hotra, P. Seankongsuk, A. Harikishore, P. Sae-Lao, R.W. Bates, P. Ragunathan, S.W. Geok, J. Shin, C.N. Pradeep, H. Makhija, P. Droge, K. Pethe, P.S. Ng, J.P. Sarathy, T. Dick, U. Lakshmanan, A. Poulsen, J.H.L. Tan, N.P. Kalia, R. Kalyanasundaram, S. Anbarasu, K. Parthasarathy, G. Gruber, Discovery of a novel Mycobacterial F-ATP synthase inhibitor and its potency in combination with diarylquinolines, *Angew Chem. Int. Ed. Engl.* (2020).
- [107] P. Pruksakorn, M. Arai, L. Liu, P. Moodley, W.R. Jacobs Jr., M. Kobayashi, Action-mechanism of trichoderin A, an anti-dormant mycobacterial aminolipopeptide from marine sponge-derived *Trichoderma* sp, *Biol. Pharm. Bull.* 34 (2011) 1287–1290, <https://doi.org/10.1248/bpb.34.1287>.
- [108] P.A. Mak, S.P.S. Rao, M. Ping Tan, X. Lin, J. Chyba, J. Tay, S.H. Ng, B.H. Tan, J. Cherian, J. Duraiswamy, P. Bifani, V. Lim, B.H. Lee, N. Ling Ma, D. Beer, H.I. Boshoff, C.E. Barry 3rd, T. Dick, K. Pethe, L.R. Camacho, A high-throughput screen to identify inhibitors of ATP homeostasis in non-replicating *Mycobacterium tuberculosis*, *ACS Chem. Biol.* 7 (2012) 1190–1197, <https://doi.org/10.1021/cb2004884>.
- [109] K. Pethe, P.C. Sequeira, S. Agarwalla, K. Rhee, K. Kuhen, W.Y. Phong, V. Patel, D. Beer, J.R. Walker, J. Duraiswamy, J. Jiricek, T.H. Keller, A. Chatterjee, M.P. Tan, M. Ujjini, S.P.S. Rao, L. Camacho, P. Bifani, P.A. Mak, I. Ma, S.W. Barnes, Z. Chen, D. Plouffe, P. Thayalan, S.H. Ng, M. Au, B.H. Lee, B.H. Tan, S. Ravindran, M. Nanjundappa, X. Lin, A. Goh, S.B. Lakshminarayana, C. Shoen, M. Cynamon, B. Kreiswirth, V. Dartois, E.C. Peters, R. Glynn, S. Brenner, T. Dick, A chemical genetic screen in *Mycobacterium tuberculosis* identifies carbon-source-dependent growth inhibitors devoid of in vivo efficacy, *Nat. Commun.* 1 (2010), <https://doi.org/10.1038/ncomms1060>. Pet1/1-Pet1/8SPet1/1-SPet1/2.
- [110] K. Pethe, P.C. Sequeira, S. Agarwalla, K. Rhee, K. Kuhen, W.Y. Phong, V. Patel, D. Beer, J.R. Walker, J. Duraiswamy, J. Jiricek, T.H. Keller, A. Chatterjee, M.P. Tan, M. Ujjini, S.P.S. Rao, L. Camacho, P. Bifani, P.A. Mak, I. Ma, S.W. Barnes, Z. Chen, D. Plouffe, P. Thayalan, S.H. Ng, M. Au, B.H. Lee, B.H. Tan, S. Ravindran, M. Nanjundappa, X. Lin, A. Goh, S.B. Lakshminarayana, C. Shoen, M. Cynamon, B. Kreiswirth, V. Dartois, E.C. Peters, R. Glynn, S. Brenner, T. Dick, A chemical genetic screen in *Mycobacterium tuberculosis* identifies carbon-source-dependent growth inhibitors devoid of in vivo efficacy, *Nat. Commun.* 1 (2010), <https://doi.org/10.1038/ncomms1060>. Pet1/1-Pet1/8SPet1/1-SPet1/2.
- [111] B.S. Lee, N.P. Kalia, X.E.F. Jin, E.J. Hasenoehrl, M. Berney, K. Pethe, Inhibitors of energy metabolism interfere with antibiotic-induced death in mycobacteria, *J. Biol. Chem.* 294 (2019) 1936–1943.